Comparative molecular physiology of novel P2X receptors: identification, cloning and functional characterisation

Stuart Boyd Hanmer

A thesis submitted in requirements for
the degree of PhD

Molecular Biosciences Division
School of Biosciences
Cardiff University

September 2014

Declaration

This work has not been submitted in substance for any other degree or award at this or any other university or place of learning, nor is being submitted concurrently in candidature for any degree or other award.

Signed …… (candidate) Date: 17 September 2014

STATEMENT 1

This thesis is being submitted in partial fulfillment of the requirements for the degree of PhD

Signed …… (candidate) Date: 17 September 2014

STATEMENT 2

This thesis is the result of my own independent work/investigation, except where otherwise stated. Other sources are acknowledged by explicit references. The views expressed are my own.

Signed …… (candidate) Date: 17 September 2014

STATEMENT 3

I hereby give consent for my thesis, if accepted, to be available for photocopying and for inter-library loan, and for the title and summary to be made available to outside organisations.

Signed …… (candidate) Date: 17 September 2014

STATEMENT 4: PREVIOUSLY APPROVED BAR ON ACCESS

I hereby give consent for my thesis, if accepted, to be available for photocopying and for inter-library loans **after expiry of a bar on access previously approved by the Academic Standards & Quality Committee.**

Signed …… (candidate) Date: 17 September 2014

Summary

P2X receptors are ATP-gated ion channels with myriad roles in humans and other higher vertebrates. Research over the past decade has described the cloning, pharmacology, and physiological role of this receptor family in a number of invertebrate organisms, as well as in unicellular amoeba and algae. However, questions remain regarding the extant of P2X receptor phylogeny and function in many invertebrates. A greater understanding of invertebrate P2X receptor pharmacology and function may provide insights into structure-function relationships in "higher" homologues, as well as novel roles for this ligand-gated ion channel family.

This thesis investigated P2X receptor expression and function within eukaryotic phylogeny, with particular emphasis on invertebrate animals. Homology searching of transcriptomic and genomic datasets identified a number of candidate P2X receptor sequences across a range of phyla.

Notably, homologues were bioinformatically identified within orders of the class Insecta, where they had been previously thought to be absent. Homologous sequences were also identified in a multicellular alga of the Charophycea, a class of the Viridiplantae division Charophyta, considered to represent the closest extant taxon to terrestrial plants.

Following the identification of a P2X receptor homologue in the cnidarian *Hydra vulgaris* (AEP) ('aepP2X') by bioinformatics approaches, total RNA preparations were used for cDNA synthesis to generate templates for PCR to yield aepP2X clones. These clones encoded proteins that exhibited concentration-dependent ATP-evoked inward currents when expressed heterologously in HEK293 cells (EC_{50} ca. 120 μM; holding potential of -60 mV). Co-application of the classic P2 receptor antagonists pyridoxalphosphate-6-azophenyl-2', 5'-disulphonic acid (PPADS) and suramin was ineffective, as were phenol red and brilliant blue G (BBG). The synthetic ATP analogues α,β-methylene ATP and β,γ-methylene ATP (1 mM) did not evoke currents at aepP2X. Consistent with most mammalian homologues, aepP2X was found to be a non-selective cation channel with negligible chloride ion permeability. Immunohistochemistry using a custom polyclonal antiserum raised against a C-terminal epitope of aepP2X suggested the expression of this receptor occurs in developing and late-stage nematocysts in whole *Hydra* polyps.

A P2X receptor from the microcrustacean *Daphnia pulex* (*Dpu*P2XB) was also expressed heterologously in HEK293 cells, and was found to be largely insensitive to extracellular ATP (EC_{50} > 1 mM), although reduction of total divalent cation concentration of perfusing extracellular solution partially restored ATP sensitivity in *Dpu*P2XB. Whilst a P2X receptor homologue from the placazoan, *Trichoplax adhaerens* (*Tad*P2XA) did not respond to extracellular ATP in HEK293 cells, a P2X receptor from the lancelet *Branchiostoma floridae* (*Bflo*P2X) does respond in a concentration-dependent manner to ATP. Currents evoked through *Bflo*P2X displayed rundown with repeated 1 mM ATP applications.

Acknowledgements

Firstly, I would like to thank the Biotechnology and Biological Research Council (BBSRC) for providing financial support for this project. Thanks also to The Welsh Livery Guild and The Physiological Society (UK) for providing financial support to for techniques training and attending conferences, respectively.

I would like to thank my supervisors, Dr Wynand van der Goes van Naters and Prof. Paul Kemp, for their help, support, and understanding over the past years. It has been a wonderful privilege to have been a PhD student with you both. Wynand, I especially look forward to your inventing phosphorescent tulips.

My heartfelt appreciation goes to all members of the Kemp and Riccardi research groups (Alex, Becky, Belinda, Bill, Charlie G, Craig A., Craig R., Dani, Dave, Harry, Jules, João B., João G., Jules, Lydia, Martin, Polly, Sarah, Seva, Rach, and Tom D.). Thank you for all your help, in whatever way it may have been. Special thanks also goes to Bec, Dan, Mel, Shelley and Matt, Tim "The Voice" Nelson, and Tom P. Thank you also to members of the 'Fly Groups' for stimulating discussions, despite the wingless nature of members of the zoo. Thank you to Dr Mark Young and Leanne for their guidance with Western blotting.

I am very grateful to those who have provided me with the organisms and materials used in the current thesis (Prof. Leo Buss (Yale University, USA); Dr Dieter Ebert (Universität Basal, Switzerland); and Dr Dave Ferrier (Scottish Oceans Institute, University of St Andrews, Scotland, UK). Many thanks to Prof. Dr Thomas Bosch (Zoologisches Institüt, Christian-Albrechts Universität zu Kiel, Germany) and his research group for allowing me to spend a (very memorable!) stint with them in 2010. Thank you especially to Kostya and Jörg for their assistance with *Hydra* embryo microinjection.

Finally I would like to thank my parents, Jinny and Pete, as well as my sister Charlie, for their unending support throughout the PhD - thank you!

Tho' much is taken, much abides; and tho'
We are not now that strength which in old days
Moved earth and heaven, that which we are, we are;
One equal temper of heroic hearts,
Made weak by time and fate, but strong in will
To strive, to seek, to find, and not to yield.

Ulysses
Alfred, Lord Tennyson

Table of contents

SUMMARY ..... **III**

ACKNOWLEDGEMENTS ..... **IV**

LIST OF ABBREVIATIONS ..... **XIII**

LIST OF FIGURES ..... **XVII**

LIST OF TABLES ..... **XXII**

1 GENERAL INTRODUCTION **2**

1.1 AN INTRODUCTION TO PURINERGIC SIGNALLING 2

1.1.1 Purinergic signalling in whole organisms 4

1.2 THE PURINERGIC REPONSE 4

1.2.1 Introduction 4

1.2.2 Release of purines and pyrimidines 6

1.2.3 Purinergic receptors 7

1.2.4 Extracellular metabolism of purines 8

1.3 STRUCTURE AND FUNCTION OF P2X RECEPTORS 10

1.4 INTRODUCTION 11

1.4.1 Transmembrane domains 13

1.4.2 Pore formation and gating 14

1.4.3 Ion permeability 15

1.4.4 Extracellular loop domain 16

1.4.5 N- and C-termini 19

1.4.6 Modulation of P2X receptor responses 20

1.4.7 P2X receptors as therapeutic targets 28

1.5 PHYLOGENY OF P2X RECEPTORS 30

1.6 EUKAYROTIC PHYLOGENY 32

1.6.1 The Animalia kingdom 35

1.6.2 The Plantae kingdom 37

1.6.3 Purinergic signalling in unicellular eukaryotes 38

1.6.4 P2X receptors in Amoebozoa 38

1.6.5 The Bacteria kingdom 40

1.7 HYDRA – A MEMBER OF THE EARLY METAZOAN CNIDARIA PHYLUM 40

1.7.1 *Hydra* and its place in metazoan phylogeny 41

1.7.2 *Hydra* as a model system 42
1.7.3 General morphology of *Hydra* 43
1.7.4 Cell types of *Hydra* 44
1.7.4.1 Epithelial stem cells 44
1.7.4.2 Interstitial stem cells and their derivatives 45
1.7.4.3 Nematocytes – a phylum-restricted cell type in the Cnidaria 48
1.7.5 The life cycle of Hydra 54
1.1.1 Purinergic signalling in Cnidaria and Ctenophora 55
1.8 DAPHNIA PULEX – A MICROCRUSTACEAN AND TOXOLOGICAL MARKER 55
1.8.1 Purinergic signalling in Crustacea 57
1.9 TRICHOPLAX – AN EARLY DIVERGING METAZOAN 58
1.10 AMPHIOXUS – A MODERN PROXY OF AN EARLY CHORDATE 59
1.11 AIMS OF THE THESIS 60
2 MATERIALS AND METHODS 63
2.1 SOLUTIONS AND REAGENTS 63
2.2 BIOINFORMATIC ANALYSIS 63
2.2.1 Homology searching of genomic and transcriptomic sequence databases 64
2.2.2 Multiple sequence alignment of primary amino acid sequences 66
2.2.3 Protein topology prediction 67
2.3 EXPERIMENTAL ANIMALS 68
2.3.1 Culture of *Hydra vulgaris* (AEP) 68
2.3.1.1 *Artemia franciscana* culture 68
2.3.2 Culture of *Daphnia pulex* (TCO) 69
2.3.2.1 *Scendesmus quadricauda* algae culture 69
2.3.3 Culture of *Trichoplax adhaerens* 69
2.3.3.1 *Pyrenomonas salina* algae culture 70
2.4 MOLECULAR BIOLOGY TECHNIQUES 70
2.4.1 Isolation of genomic DNA from whole organisms 70
2.4.2 Isolation of total RNA from whole organisms 71
2.4.3 First-strand cDNA synthesis 72
2.4.4 Assessing purity and yield of nucleic acids 72
2.4.5 Polymerase chain reaction (PCR) 72
2.4.5.1 Primer design 72
2.4.5.2 PCR reactions 73

2.4.6 TAE agarose gel electrophoresis 77
2.4.6.1 Purification of DNA from agarose gels 78
2.4.6.2 Automated DNA sequencing 79
2.4.7 Sub-cloning techniques 79
2.4.7.1 Cloning of PCR products into TA cloning vectors 79
2.4.7.2 Preparation of chemically competent Z-competent™ DH5α E. coli 80
2.4.7.3 Transformation of Z-competent™ chemically competent DH5α E. coli 80
2.4.7.4 Stocks of antibiotics 81
2.4.7.5 Preparation of bacterial agar plates 81
2.4.7.6 Glycerol stocks of bacteria 82
2.4.7.7 Plasmid amplification and isolation 82
2.4.7.8 Purification of plasmid DNA 83
2.4.7.9 Verification of insert DNA 83
2.4.7.10 Preparation of plasmid for ligation 84
2.4.8 Ligation reactions 85
2.4.9 Western blot analysis 85
2.4.9.1 Sample preparation 85
2.4.9.2 Determination of protein concentration by Bradford assay 86
2.4.9.3 Solutions 86
2.5 CELL CULTURE 88
2.5.1 Culture of Human Embryonic Kidney 293 (HEK293) cells 88
2.5.2 Cryopreservation of HEK293 cells 88
2.6 WHOLE-CELL PATCH-CLAMP ELECTROPHYSIOLOGY 89
2.6.1 Transient transfection of HEK293 cells 89
2.6.2 Solutions for whole-cell voltage electrophysiology 90
2.6.2.1 Standard extracellular solution for whole-cell electrophysiology 90
2.6.2.2 Standard intracellular solution for whole-cell electrophysiology 91
2.6.2.3 Low divalent cation extracellular solution (ldECS) 91
2.6.2.4 Extracellular solutions for analysis of ionic permeability of aepP2X 91
2.6.2.5 ATP stock solution 92
2.6.2.6 Agonist and antagonist solutions 92
2.6.3 Recording microelectrodes 93
2.6.4 Experimental protocol 93
2.6.4.1 Cell-attached configuration of the patch-clamp technique 94
2.6.4.2 Whole-cell configuration of the patch-clamp technique 95

2.6.5 Electrophysiology data analysis and presentation 96
2.6.5.1 ATP concentration-response curves 97
2.6.5.2 aepP2X mono- and divalent cation permeability 97
2.6.5.3 aepP2X chloride ion permeability 98
2.7 IMMUNOHISTOCHEMISTRY 98
2.7.1 Polyclonal antibody generation and choice of antigenic region 99
2.7.1.1 Concentration of affinity-purified antibody solution 101
2.7.1.2 Preparation of Mowiol 4-88 mounting solution 102
2.7.2 IHC protocol 102
2.8 GENERATION OF TRANSGENIC *H. VULGARIS* (AEP) POLYPS 103
2.8.1.1 Construction of plasmids for microinjection 103
2.8.1.2 Microinjection of *H. vulgaris* (AEP) embryos 105
3 CROSS-PHYLUM ANALYSIS OF PREDICTED INVERTEBRATE P2X RECEPTORS 108
3.1 AIMS OF THE CURRENT CHAPTER 108
3.2 INTRODUCTION 108
3.2.1 P2X receptor motifs and key residues 110
3.3 RESULTS 111
3.3.1 P2X receptors in the Deuterostomia superphylum 111
3.3.2 P2X receptors in the Chordata 111
3.3.3 P2X receptors in the Echinodermata and Hemichordata 112
3.3.4 P2X receptors in Arthropoda 114
3.3.4.1 P2X receptors in the Eucheliceratа 114
Fig. 3.2: MSA of candidate spider P2X receptors proteins 118
3.3.4.2 P2X receptors in Myriapoda 119
3.3.4.3 P2X receptors in Crustacea 121
3.3.4.4 P2X receptors in Hexapoda 122
3.3.5 P2X receptors in the Insecta class 131
3.3.5.1 The Archaeognatha 131
3.3.5.2 Pterygota 134
3.3.6 Predicted P2X receptors in Cnidaria and Ctenophora 143
3.3.7 P2X receptors in the Platyhelminthes 149
3.3.8 Incomplete conservation of candidate P2X receptors in Nematoda 154
3.3.9 P2X receptors in Mollusca 157
3.3.10 P2X receptors in Porifera and Placazoa 161

3.3.11 P2X receptors in Choanoflagellata 164
3.3.12 P2X receptors in Amoebozoa 166
3.3.13 Fungal P2X receptors 170
3.3.14 Candidate P2X receptors in the unicellular Bikonta 174
3.3.15 Candidate P2X receptors in the Excavata kingdom 181
3.3.16 A candidate P2X receptor in a member of the Streptophyta 183
3.3.17 P2X receptors are seemingly absent from Bacteria and Archaea 189
3.4 DISCUSSION 189
3.4.1 Defining a P2X receptor: is there an early molecular component? 192
3.4.2 Expansion of knowledge of P2X receptor within the Metazoa 195
3.4.3 A coleopteran P2X receptor? 196
3.4.4 P2X receptors are predicted to be expressed in non-neopteran insects 198
3.4.5 Tissue-specific transcriptomes: linking form and function? 199
3.4.6 P2X receptors in socioeconomically important organisms: a clinical target? 200
3.5 CONCLUSIONS 201
4 CLONING, ELECTROPHYSIOLOGICAL ANALYSIS AND LOCALISATION OF A NOVEL P2X RECEPTOR FROM HYDRA 204
4.1 AIMS OF THE CHAPTER 204
4.2 INTRODUCTION 204
4.2.1 Cloning of mammalian and non-mammalian P2X receptors 205
4.2.2 Putative ion channels in *Hydra* 206
4.2.2.1 GABAergic and glutamatergic transmission 207
4.2.2.2 Glycinergic transmission 208
4.2.2.3 NMDA receptors 209
4.2.2.4 Cloning of novel ion channels in *Hydra* 209
4.3 RESULTS 211
4.3.1 Primary sequence analysis of aepP2X 211
4.3.2 Pharmacological and biophysical characterisation of aepP2X 213
4.3.2.1 aepP2X functions as an ATP-gated ion channel in HEK293 cells 213
4.3.2.2 Predicted N-linked glycosylation sites in aepP2X-$(His)_6$ 215
4.3.2.3 Activation and deactivation kinetics of aepP2X-$(His)_6$ to synthetic ATP analogues 216
4.3.2.4 Agonist insensitivity of aepP2X-$(His)_6$ 216

4.3.2.5 Co-application of the P2 antagonists suramin and PPADS are ineffective at aepP2X-$(His)_6$ 217
4.3.2.6 Ivermectin potentiates ATP-evoked currents through aepP2X-$(His)_6$ .. 220
4.3.2.7 aepP2X is a cation permeable channel 222
4.3.2.8 Estimation of aepP2X receptor channel pore diameter 224
4.3.3 Staining of nematocyst cells with anti-aepP2X antiserum 224
4.3.4 Quinacrine staining of nematocysts in live *Hydra* polyps 229
4.3.5 Mutually exclusive staining of non-nematocyst cells following antiserum polyclonal antibody staining 231
4.3.6 *H. magnipapillata* promoter-driven expression of eGFP in *H. vulgaris* (AEP) embryos 233
4.3.7 Actin-driven expression of a P2X::eGFP fusion protein in endodermal epithelial cells of *Hydra* 235
4.4 DISCUSSION 236
4.4.1 Agonist sensitivity at aepP2X-$(His)_6$ 236
4.4.2 Antagonist insensitivity at aepP2X-$(His)_6$ 238
4.4.3 Ivermectin activity at aepP2X-$(His)_6$ 239
4.4.4 Ion permeability through aepP2X-$(His)_6$ 241
4.4.5 aepP2X immunohistochemistry: localisation of a P2X receptor in a phylum-specific structure? 242
4.5 CONCLUSIONS 248

5 CLONING AND ELECTROPHYSIOLOGICAL ANALYSIS OF NOVEL P2X RECEPTORS FROM REPRESENTATIVE MEMBERS OF THREE INVERTEBRATE PHYLA 251

5.1 AIMS OF THE CHAPTER 251
5.2 INTRODUCTION 251
5.2.1 Ion channels in *Daphnia* 252
5.2.2 Ion channels in Trichoplax 253
5.2.3 Ion channels in *Branchisotoma* 255
5.3 RESULTS 256
5.3.1 Cloning of *Daphnia* P2X receptors 256
5.3.2 Cloning of a *Branchiostoma* P2X receptor 259
5.3.3 Cloning of *Trichoplax* P2X receptors 261
5.3.4 Heterologous expression of cloned P2X receptors in HEK293 cells 264
5.3.5 Pharmacological profile of *Dpu*P2X receptors 265

5.3.5.1 *Dpu*P2XB-$(His)_6$ is largely insensitive to extracellular ATP 265
5.3.5.2 Activation and deactivation kinetics of *D. pulex* P2XB receptors 267
5.3.5.3 Recovery of *Dp*uP2XB ATP sensitivity in low divalent cation conditions 268
5.3.6 *Bflo*P2X functions as an ATP-gated ion channel in HEK293 cells 271
5.3.7 *Tad*P2XA is insensitive to extracellular ATP in HEK293 cells 273
5.4 DISCUSSION 273
5.4.1 *Daphnia pulex* P2XA receptor 273
5.4.2 Low sensitivity of *D. pulex* P2XB to extracellular ATP 276
5.4.3 Putative roles for *Daphnia* P2X receptors 279
5.4.4 P2X receptor from an early chordate 281
5.4.5 Expression of P2X receptors in HEK293 cells: Western blot analysis 282
5.4.6 Metazoan P2X receptors in Placazoa 284
5.5 CONCLUSIONS 286
6 CONCLUSIONS AND FUTURE DIRECTIONS 288
6.1 P2X RECEPTORS IN EUKARYOTIC PHYLOGENY 288
6.2 HYDRA EXPRESS A FUNCTIONAL ATP-GATED ION CHANNEL 289
6.3 FURTHER CHARACTERISATION OF NOVEL P2X RECEPTORS 291
7 REFERENCES 295
8 APPENDIX 333

List of abbreviations

5-HT	5-hydroxytryptamine (serotonin)
ACh	Acetylcholine
ADaM	Aachener Daphnien Medium
Ado	Adenosine
ADP	Adenosine 5'-diphosphate
α,β-meATP	α,β-methylene ATP
AMP	Adenosine 5'-monophosphate
AMPA	α-Amino-3-hydroxy-5-methyl-4-isoxazolepropionic acid
ANOVA	Analysis of variance
APS	Ammonium persulphate
ASIC	Acid-sensing ion channel
ASW	Artificial seawater
ATP	Adenosine 5'-triphosphate
BBG	Brilliant blue G
β,γ-meATP	β,γ-methylene ATP
BLAT	BLAST-like alignment tool
BLAST	Basic Local Alignment Search Tool
BLOSUM	BLOcks SUbstitution Matrix
bp	Base pair
BSA	Bovine serum albumin
cAMP	Cyclic-AMP
cDNA	Complementary DNA
CDS	Coding region sequence
CFA	Complete Freund's adjuvant
CHAPS	3-[3-Cholamidopropyl)dimethylammonio]-1-propanesulphonate
CIAP	Calf intestinal alkaline phosphatase
CORM-2	Carbon monoxide releasing molecule-2
CNG	Cyclic nucleotide-gated
CTP	Cytidine 5'-triphosphate
DAPI	4',6-diamidino-2-phenylindole
D-AP5	D-2-amino-5-phosphonopentanoic acid
dH_2O	Distilled water
ddH_2O	Bi-distilled water
DDM	n-dodecyl-β-D-maltoside
DEPC	Diethylpyrocarbonate
DMEM/F12	Dulbecco's Modified Eagle Medium/F-12
DMSO	Dimethyl sulphoxide
DNA	Deoxyribosenucleic acid
dNTP	Deoxyribonucleotide
D-PBS	Dulbecco's phosphate buffered saline
DTT	Dithiothreitol
ECD	Extracellular domain
ECS	Extracellular solution
ENaC	Epithelial sodium channel
EST	Expressed sequence tag
EtOH	Ethanol
***E*-value**	Expect-value
EDTA	Ethylenediaminetetraacetic acid
eGFP	Enhanced green fluorescent protein

EGTA	Ethylene glycol tetraacetic acid
ELISA	Enzyme-linked immunosorbent assay
E_{rev}	Reversal potential
FBS	Foetal bovine serum
GABA	γ-aminobutyric acid
GPCR	G protein-coupled receptor
GSH	Reduced glutathione
GSP	Gene-specific primer
HCl	Hydrochloric acid
HEK293	Human embryonic kidney 293 cell line
HEPES	N-(2-Hydroxyethyl)piperazine-N'-(2-ethanesulfonic acid
HMM	Hidden Markov model
HRP	Horseradish peroxidase
HSP	High-scoring segment pair
iGluR	Ionotropic glutamate receptor
IHC	Immunohistochemistry
IPTG	Isopropyl β-D-1-thiogalactopyranoside
IVM	Ivermectin
kbp	Kilobase pair
LB	Lysogeny broth
LUCA	Last universal common ancestor
ldECS	Low divalent cation concentration extracellular solution
LGIC	Ligand-gated ion channel
LJP	Liquid junction potential
MAST	Motif Alignment and Search Tool
Mbp	Mega base pairs
MCS	Multiple cloning site
MEME	Multiple EM for Motif Elicitation
MeOH	Methanol
mGluR	Metabotropic glutamate receptor
mRNA	Messenger RNA
MSA	Multiple sequence alignment
MUSCLE	MUltiple Sequence Comparison by Log-Expectation
MYA	Million years ago
NaN_3	Sodium azide
NaOH	Sodium hydroxide
NMDA	N-methyl-D-aspartate
NMDG	N-methyl-D-glucamine
PAGE	Polyacrylamide gel electrophoresis
PAPAb	Peptide affinity-purified antibody
PBS	Phosphate buffered saline
PCA	Peptide competition assay
PCR	Polymerase chain reaction
PFA	Paraformaldehyde
PLC	Phospholipase C
PPADS	Pyridoxal phosphate-6-azo(benzene-2,4-disulfonic acid
PSA	Pairwise sequence alignment
PVDF	Polyvinylidene difluoride
rBLAST	Reciprocal BLAST
RIPA	Radioimmunoprecipitation assay
RNA	Ribonucleic acid
rpm	Revolutions per minute

rRNA	Ribosomal RNA
R_s	Series resistance
RT-PCR	Reverse transcription-polymerase chain reaction
SDS	Sodium dodecyl sulphate
sECS	Standard extracellular solution
SEM	Standard error of the mean
SNARE	SNAP (Soluble NSF Attachment Protein) REceptor
SOC	Super optimal broth (with catabolite repression)
TAE	Tris-acetate/EDTA
Tax ID	Taxonomy ID
T-Coffee	Tree-based Consistency Objective Function For alignment Evaluation
TE	Tris-EDTA
TEMED	Tetramethylethylenediamine
TES	N-[tris(hydroxymethyl)methyl]- 2-aminoethanesulfonic acid
TMD	Transmembrane domain
T_m	Melting temperature
TMD	Transmembrane domain
TM1	Transmembrane domain 1
TM2	Transmembrane domain 2
UDP	Uridine 5'-diphosphate
UTP	Uridine 5'-triphosphate
UV	Ultraviolet (light)
VGIC	Voltage-gated ion channel
WB	Western blot
WT	Wild-type
X-gal	5-bromo-4-chloro-3-indolyl-beta-D-galacto-pyranoside
YSB	Yeast sample buffer

Nucleotide bases

A	Adenine
T	Thymine
G	Guanine
C	Cytosine

Single-letter amino acid code

G	Glycine
P	Proline
A	Alanine
V	Valine
L	Leucine
I	Isoleucine
M	Methionine
C	Cysteine
F	Phenylalanine
Y	Tyrosine
W	Tryptophan
H	Histidine
K	Lysine
R	Arginine
Q	Glutamine
N	Asparagine
E	Glutamic acid
D	Aspartic acid
S	Serine
T	Threonine

Species abbreviations

Aau	*Aurelia aurita*
Aca	*Acanthamoeba castellanii*
Acal	*Aplysia californica*
Adi	*Acropora digitifera*
aep	*Hydra vulgaris* (AEP)
Age	*Acanthoscurria geniculata*
Ama	*Allomyces macrogynus*
Ata	*Alexandrium tamarense*
Aqu	*Amphimedon queenslandica*
Bde	*Batrachochytrium dendrobatidis*
Bflo	*Branchiostoma floridae*
Bm	*Boophilus microplus*
Bna	*Bigelowella natans*
Cow	*Capsaspora owczarzaki*
Cte	*Capitella telata*
Dd	*Dictyostelium discoideum*
Dpu	*Daphnia pulex*
Egr	*Echinococcus granulosus*
Emu	*Ephydatia muelleri*
Emult	*Echinococcus multilocularis*
Fca	*Folsomia candida*
Gpu	*Glomeris pustulata*
h	*Homo sapiens*
Hd	*Hypsidbius dujardini*
Hma	*Hydra magnipapillata*
Hmi	*Hymenolepis microstoma*
Isc	*Ixodes scapularis*
Lgi	*Lottia gigantea*
Lhe	*Latrodectus hesperus*
Lst	*Lymnaea stagnalis*
Lpo	*Lingilodinium polyedrum*
Mbr	*Monosiga brevicollis*
Nve	*Nematostella vectensis*
Oca	*Osceralla carmela*
Oci	*Orchesella cincta*
Ota	*Ostreococcus tauri*
Pba	*Pleurobrachei bachei*
Pbah	*Pyrodinium bahamense*
Ppa	*Polysphondylium pallidum*
Rir	*Rhizophagus irregularis*
Sko	*Saccoglossus kowalevskii*
Sm	*Schistosoma mansoni*
Sme	*Schmidtea mediterranea*
Smi	*Stegodyphus mimosarum*
Spu	*Spiezellomyces punctatus*
Spur	*Strongylocentrotus purpuratus*
Sro	*Salpingoeca rosetta*
Sym	*Symbiodinium* sp.
Tad	*Trichoplax adhaerens*
Tso	*Taenia solium*

List of figures

CHAPTER 1: GENERAL INTRODUCTION

Fig. 1.1: structure of adenosine 5'-triphosphate (ATP) illustrating component moieties 2

Fig. 1.2: summary of the action of ATP against purinergic receptors in a "model cell" 10

Fig. 1.3: conformational changes in trimeric zfP2X4.1 crystal structure in response to ATP binding.....12

Fig. 1.4: coordination of ATP binding in the extracellular domain of zfP2X4.1.....18

Fig. 1.5: P2X receptor modulation by subunit arrangement, alternative splicing of nascent P2X mRNA and endogenous factors……..24

Fig. 1.6: cladogram illustrating extant Eukaryota phylogeny 34

Fig. 1.7: gross morphology of *H. vulgaris* (AEP) polyp 44

Fig. 1.8: stem cells in *Hydra* and schematic diagram of a cross-section of the two cell layers of a *Hydra* polyp body column 47

Fig. 1.9: schematic diagrams of the four types of nematocysts found in *Hydra* species 49

Fig. 1.10: hypoxia-induced increase in haemoglobin gene transcription in *Daphnia*..... 56

Fig. 1.11: Darkfield micrographs of *Daphnia*, *Trichoplax* and *Branchiostoma* 60

CHAPTER 2: MATERIALS AND METHODS

Fig. 2.1: flow diagram illustrating steps underlying bioinformatic analyses detailed in chapter 3.....64

Fig. 2.2: voltage ramp and step protocol used in the recording of current-voltage relationships in aepP2X 96

Fig. 2.3: prediction of a suitable antigenic region for generation of a custom polyclonal antibody……100

CHAPTER 3: CROSS-PHYLUM ANALYSIS OF PREDICTED INVERTEBRATE P2X RECEPTORS

Fig. 3.1: multiple sequence alignment (MSA) of contiguous partial candidate *S. mimosarum* P2X receptor sequences 116

Fig. 3.2: MSA of candidate spider P2X receptors proteins 118

Fig. 3.3: MSA of candidate P2X receptors from the millipedes *G. pustulata* and *S. maritima* 120
Fig. 3.4: MSA of predicted *Daphnia pulex* P2X receptor homologues 122
Fig. 3.5: Hexapoda phylogeny 123
Fig. 3.6: MSA of partial *F. candida* candidate P2X receptor protein sequences 126
Fig. 3.7: MSA of a candidate *O. cincta* candidate P2X receptor protein sequence 128
Fig. 3.8: MSA of a translated partial EST sequences from *A. maritima* and *O. arcticus* 130
Fig. 3.9: MSA of the partial protein sequence of a candidate P2X receptor from an archaeognathan insect 133
Fig. 3.10: MSA of candidate P2X receptor protein fragments from *E. danica* 136
Fig. 3.11: MSA of candidate P2X receptor protein fragments from *I. elegans* 138
Fig. 3.12: MSA of candidate P2X receptor protein fragments from *L. fulva* 140
Fig. 3.13: MSA of candidate P2X receptor protein fragments from *D. virgifera* ... 143
Fig. 3.14: MSA of predicted Cnidaria P2X receptor protein sequences with hP2X1 and hP2X4 receptors 146
Fig. 3.15: topology and primary sequence analysis of candidate Ctenophora P2X receptors 148
Fig. 3.16: predicted protein topology of candidate full-length Cestoda P2X receptors 151
Fig. 3.17: MSA of candidate Platyhelminthes P2X receptor protein sequences with human P2X receptor subunits 153
Fig. 3.18: MSA of protein sequences translated from partial ESTs from *H. contortus* and *X. index* 156
Fig. 3.19: MSA of putative full-length *A. californica* P2X receptors 159
Fig. 3.20: MSA of non-redundant candidate P2X receptor protein sequences from a number of molluscs 160
Fig. 3.21: MSA of candidate P2X receptors from Porifera 163
Fig. 3.22: MSA of Choanoflagellata and Filasterea P2X receptors 166
Fig. 3.23: MSA of retrieved candidate amoeboid P2X receptor protein sequences 169
Fig. 3.24: fungal divisions in which transcripts encoding for candidate P2X receptor proteins were identified 171
Fig. 3.25: MSA of putative fungal P2X receptor protein sequences with hP2X1 and hP2X4 subunits 173
Fig. 3.26: MSA of three candidate *B. natans* P2X receptors 176

Fig. 3.27: topology analysis of non-redundant candidate P2X protein sequences of *Aplanochytrium kerguelense* 178
Fig. 3.28: MSA of candidate P2X receptors from two Stramenopiles 179
Fig. 3.29: MSA of candidate Alveolata P2X receptors 181
Fig. 3.30: MSA of candidate Excavata P2X receptors 183
Fig. 3.31: MSA of putative partial candidate P2X receptors from *N. hyalina* 185
Fig. 3.33: expanded cladogram of illustrating P2X receptors identified in the Eukaryota domain……191

CHAPTER 4: CLONING, ELECTROPHYSIOLOGICAL ANALYSIS AND LOCALISATION OF A NOVEL P2X RECEPTOR FROM *HYDRA*

Fig. 4.1: multiple sequence alignment (MSA) of cloned aepP2X, rP2X4 and hP2X1-7 subunits 212
Fig. 4.2: extracellular ATP application evokes inward currents at aepP2X 214
Fig. 4.3: predicted *N*-linked glycosylation sites in aepP2X-$(His)_6$ 215
Fig. 4.4: aepP2X-$(His)_6$ does not respond to α,β-meATP or β,γ-meATP 217
Fig. 4.5: effects of P2 receptor antagonists at aepP2X-$(His)_6$ 219
Fig. 4.6: ivermectin potentiates ATP-evoked currents at aepP2X-$(His)_6$ 221
Fig. 4.7: ion permeation properties of aepP2X in HEK293 cells 223
Fig. 4.8: immunostaining of whole *H. vulgaris* (AEP) polyps with day 72 PA5619 anti-P2X antiserum 226
Fig. 4.9: immunostaining of nematocysts in whole *Hydra* polyps using anti-P2X antiserum 229
Fig. 4.10: staining of whole polyps using quinacrine 230
Fig. 4.11: mutually exclusive staining of whole fixed *H. vulgaris* (AEP) polyps with affinity-purified PA5619 anti-P2X antibody 232
Fig. 4.12: expression of eGFP, driven by a *H. magnipapillata* P2X receptor promoter and terminator 234
Fig. 4.13: expression of a P2X::eGFP fusion protein in *H. vulgaris* (AEP) polyps 235

CHAPTER 5: CLONING AND ELECTROPHYSIOLOGICAL ANALYSIS OF NOVEL P2X RECEPTORS FROM REPRESENATIVE MEMBERS OF THREE INVERTEBRATE PHYLA

Fig. 5.1: illustration of position of *D. pulex* P2X receptors in the context of a genomic scaffold 256

Fig 5.2: position of priemrs used in the attempted amplification of the predicted *Dpu*_p2xA nucleotide sequence 257

Fig. 5.3: multiple sequence alignment (MSA) of protein sequences predicted and cloned forms of *DpuP*2XB receptors with hP2X1-7 subunits..... 258

Fig. 5.4: MSA of predicted and cloned protein sequences of *Bflo*P2X with hP2X1-7 subunits 260

Fig. 5.5: MSA of protein sequences predicted and cloned forms of *T. adhaerens* P2X receptors with hP2X1-7 subunits..... 263

Fig. 5.6: total protein lysate isolated from P2X receptor-expressing HEK293 cells 265

Fig. 5.7: ATP concentration-response data for *D. pulex* P2XB receptor forms..... 256

Fig. 5.8: scatterplot illustrating grouping of *D. pulex* P2XB receptor and endogenous receptor activity based on peak current and rise time..... 268

Fig. 5.9: improved ATP sensitivity of *Dpu*P2XB receptors in low divalent cation conditions..... 270

Fig. 5.10: concentration-dependent responses of *Bflo*P2X to ATP in HEK293 cells 272

Fig. 5.11: wFleaBase screenshot illustrating expression levels of predicted *Dpu*_p2xA and *Dpu*_p2xB genes..... 275

List of tables

CHAPTER 1: GENERAL INTRODUCTION

Tables 1.1 and 1.2: pharmacology of mammalian and non-mammalian homomeric and known mammalian heteromeric P2X receptor subunits……..……26 & 27

CHAPTER 2: MATERIALS AND METHODS

Table 2.1: sequences used in the analysis of retrieved protein sequences.....67

Table 2.2: components required in standard PCR reactions used for routine applications.....74

Table 2.3: components required in high-fidelity PCR reactions used for applications requiring low error rate, such as cloning.....75

Table 2.5: compositions of stacking and separating gels.....86

Table 2.6: washing solutions used in Western blot protocols.....87

Table 2.7: compositions of extracellular solutions used in the recording of permeabilities of monovalent and divalent cation and anion species.....92

Table 2.8: agonist, antagonist and modulatory compounds used in pharmacological profiling experiments of cloned P2X receptors.....93

Table 2.9: Primary (1°) and secondary (2°) antibodies used in IHC and WB protocols ……...103

CHAPTER 3: CROSS-PHYLUM ANALYSIS OF PREDICTED INVERTEBRATE P2X RECEPTORS

Table 3.1: molluscan species in which searches for P2X receptor homologues were performed..... 157

Table. 3.2: summary table of retrieved putative P2X receptor sequences identified in chapter 3……..187 & 188

CHAPTER 4: CLONING, ELECTROPHYSIOLOGICAL ANALYSIS AND LOCALISATION OF A NOVEL P2X RECEPTOR FROM *HYDRA*

Table 4.1: ionic permeability data for aepP2X in HEK293 cells 224

CHAPTER 5: CLONING AND ELECTROPHYSIOLOGICAL ANALYSIS OF NOVEL P2X RECEPTORS FROM REPRESENATIVE MEMBERS OF THREE INVERTEBRATE PHYLA

Table 5.1: predicted phosphorylation sites in *Bflo*P2X..... 283

APPENDIX

Table A1: list of species and associated genomic or transcriptomic database within which homology searches were performed 334

Table A2: list of retrieved hits identified through homology searching of eukaryotic species..... 339

Table A3: pGEM-T® Easy and pcDNA3.1$^{(+)}$ plasmid construct MCS (multiple cloning site) sequencing primers 357

Table A4: invertebrate P2X receptor amplification primers..... 357

Table A5: primers used for the addition of C-terminal hexahistidine tag to cloned invertebrate P2X receptors, and subsequent subcloning into pcDNA3.1$^{(+)}$ expression vector 358

Table A6: adaptor primers used in 3' RACE of cloned invertebrate P2X receptors 359

Table A7: gene-specific primers used in 3' RACE of cloned invertebrate P2X receptors..... 359

Table A8: primers used in the attempted amplification of *Dpu*_p2xA from complementary DNA (cDNA) or genomic DNA template 360

Table A9: primers combinations (from Table A8) used in the attempted amplification of the candidate *Daphnia pulex* P2XA receptor subtype (*Dpu*_p2xA) from complementary DNA (cDNA) or genomic DNA (gDNA) templates 361

Table A10: Primers used in the amplification of 5' and 3' flanking regions for synthesis of *Hmp2xp-egfp* plasmid construct 362

Table A11: primers used to sequence *Hmp2xp-egfp* plasmid construct 362

Table A12: primers used in the amplification of *aepp2x* for synthesis of *actin-aepp2x::egfp* plasmid construct..... 363

Table A13: primers used to sequence *actin-aepp2x::egfp* plasmid construct 364

Chapter 1:

General Introduction

1 General Introduction

1.1 AN INTRODUCTION TO PURINERGIC SIGNALLING

'Purinergic signalling' is the broad term used to describe the interaction of purine-based molecules with specific receptors and their function in a cellular context. Central to the idea of purinergic signalling is the ubiquitous energy molecule adenosine 5'-triphosphate (ATP) composed of an adenine base (the purine) linked *via* its 1' carbon atom to a pentose sugar. In turn, this ribose sugar moiety is attached to three phosphate (PO_3^-) groups by its 5' carbon atom (Fig. 1.1).

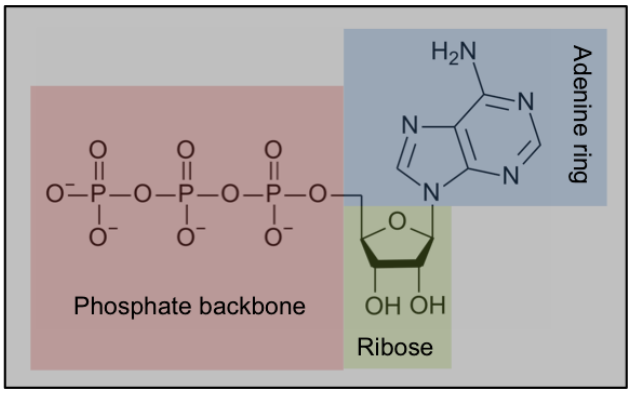

Fig. 1.1: structure of adenosine 5'-triphosphate (ATP) illustrating component moieties.

ATP consists of 3 major component moieties: a triphosphate moiety (red) covalently bound to a ribose sugar (green) at C4, which is in turn bound to an adenine ring (blue) at C1. The latter two components constitute the purine adenosine.

ATP is essential to all eukaryotic and prokaryotic cells and for many years was thought to have a purely intracellular localisation where its roles include: i) acting as the primary energy transfer molecule within cells through successive hydrolysis of its phosphate groups; ii) involvement in signal transduction pathways by phosphorylation of protein and lipid molecules and as a precursor for adenosine 3'5'-cyclic monophosphate (cAMP); and (iii) incorporation into nucleic acids in the conversion of the ribose sugar moiety to deoxyribose. However, the purely intracellular role of ATP was challenged in 1929 when it was found intravenous

injection of crude extracts from a number of tissues (including heart, brain and spleen) produced profound physiological effects including a negative chronotropic effect, bradycardia and coronary artery vasodilation in dogs, guinea pigs rabbits and cats (Drury and Szent-Györgyi, 1929). Further to this finding, intravenous injection of purified adenosine 5'-monophosphate (AMP) and adenosine were able to mimic the effects of crude organ extracts, suggesting that these compounds were the causative agents of these physiological events (Drury and Szent-Györgyi, 1929). In the 30 years following this seminal study, these findings were developed on to include more organ systems and the full range of purines. The first suggestion that ATP could act as a neurotransmitter in the peripheral nervous system came in 1954 when antidromic stimulation of the great auricular nerve caused release of ATP from sensory nerves and vasodilation of the auricular artery of rabbits (Holton and Holton, 1954). Some years later, Pamela Holton used the firefly luciferase method of ATP detection to illustrate that stimulation of the rabbit great auricular nerve resulted in a translation rise in extracellular ATP levels, leading her to conclude that when noradrenaline is liberated from sympathetic nerve endings following nerve stimulation, ATP is also released (Holton, 1959). This was the first description of the concept of 'purinergic co-transmission'. However it wasn't until the early 1970s that firm evidence for ATP as a co-transmitter emerged following the recognition of 'non-adrenergic, non-cholinergic' (NANC) neurotransmission, challenging the erroneous 'Dale's Principle' that each nerve utilized only one neurotransmitter (Dale, 1934). The presence of NANC neurotransmission was initially described in 1963 when blockade of adrenergic and cholinergic neurotransmission failed to ablate contractile responses in guinea pig taenia coli smooth muscle; the rapid hyperpolarisations and relaxation that remained was thought to be due to NANC neurotransmission (Burnstock *et al.*, 1963). ATP was identified to be the transmitter responsible for NANC neurotransmission after it satisfied the criteria to be considered a neurotransmitter: synthesis and storage in nerve terminals; release by a Ca^{2+}-dependent mechanism; and activation of post-synaptic receptors specific for the compound (Burnstock *et al.*, 1970). The purinergic neurotransmission hypothesis was later formulated in an article in *Pharmacological Reviews* (Burnstock, 1972) and although met with some scepticism from the scientific community, has become widely accepted as a major advance in our understanding of purine biology.

The cloning of members of two families of membrane proteins activated by

extracellular nucleotides (the metabotropic, G-protein coupled P2Y receptor (Webb *et al.*, 1993) and the ionotropic ligand-gated ion channel (LGIC) P2X receptor) in the 1990s (Valera *et al.*, 1994) represented a major advance in the purinergic field.

1.1.1 Purinergic signalling in whole organisms

Although initially described as an modulator of cardiovascular activity (Drury and Szent-Györgyi, 1929), extracellular purinergic signalling has important roles in auto- and paracrine systems where it is able to influence and modulate both fast and slow cellular events. These range from fast neuronal responses and responses to cell damage (Hejl *et al.*, 2013), to slower responses that may result from chronic inflammation (such as in arthrosclerosis) and exo- and endocrine signalling (Khakh and North, 2012). This diversity in physiological and pathophysiological function as well as localisation in a number of cell types makes purinergic receptors a potentially propitious clinical target. To date, only one pharmacotherapy is currently in use in the clinic; Clopidogrel, a $P2Y_{12}$ receptor antagonist and platelet inhibitor used as a treatment for many cardiovascular pathologies (Hollopeter *et al.*, 2001; Savi *et al.*, 2001). The publication of crystal structures of a P2X receptor in both the closed (Kawate *et al.*, 2009) and open/ATP-bound state (Hattori and Gouaux, 2012) represents a major advance in purinergic signalling research and will play a vital role in rational drug design and the development of compounds for the treatment of conditions in which malfunction of P2X receptors is implicated.

1.2 THE PURINERGIC REPONSE

1.2.1 Introduction

P2X receptors form one of the three 'superfamilies' of the Cys-loop LGICs, which includes the nicotinic ACh, $GABA_A$ and glycine receptors, and the glutamate-activated cation channels (which includes the AMPA, NMDA and kainate receptors). The recent publications of apo, closed- (Kawate *et al.* 2009) and open-state crystal structures for the zebrafish P2X4.1 receptor (zfP2X4.1) (Hattori *et al.*, 2012)

represents a significant step-change in our understanding of these membrane-bound ion channels. Kawate and colleagues originally presented a 3.1Å resolution 3-dimensional (3D) crystal structure of zfP2X4.1 in its closed state (Kawate *et al.*, 2009). A further advance in P2X receptor structure was provided by Hattori and Gouaux in 2012 when the crystal structure of an acutely modified form of zfP2X4.1 was presented in its open, ATP-bound state at 2.8Å resolution, in addition to a higher resolution 3D structure of the closed state at 2.9Å (Hattori and Gouaux, 2012). The findings that have arisen from these structures have confirmed many of the findings from site-directed mutagenesis of specific residues and regions of P2X receptors and have enabled the development of homology-based structures of other P2X receptors (Cao *et al.*, 2009). These corroborations will be highlighted in the following sections where appropriate.

In mammalian species there are seven P2X receptor subunits (P2X1-7), encoded by a separate genes from which (for some subunits, such as human P2X2 and P2X7) can exist alternative splice variants (North, 2002). Each subunit possesses two transmembrane domains with an intracellular amino- (N-) and carboxyl (C-) termini and a large extracellular loop domain that accounts for the majority of the protein's size. Although P2X receptors share topology with other LGICs, such as acid-sensing ion channels (Jasti *et al.*, 2007; Gonzales *et al.*, 2009), the two do not share amino acid sequence similarity. Functional P2X receptors arise from the association of three individual monomers that can group as either homomers or heteromers from different combinations of subunit. Evidence for this trimeric confirmation comes from a range of data employing various techniques. Stoop and colleagues illustrated that, using concatamers consisting of P2X2 receptor subunits, a positional dependence on the position of a threonine to cysteine mutation at position 336 (T336C) existed. This mutation, which allows the selective inhibition of current flow following exposure to methanethiosulphonate (MTS) derivatives was most effective in receptor complexes consisting of no more than three subunits, consisted with the notion of a trimeric configuration of P2X receptors (Stoop *et al.*, 1999). Indeed, initial work in rat and bullfrog sensory neurons in 1990 had already hinted at the trimeric organisation of the functional receptor, whereby three ATP molecules bind at non-interacting sites to induce pore formation (Bean, 1990). Further experiments were also performed using blue native polyacrylamide gel electrophoresis (PAGE) where the band produced on a gel corresponds to the sum of three individual subunits (Nicke *et al.*, 1998; Aschrafi

et al., 2004). In both these studies, the addition of chemical cross-linking agents allows for the formation of dimer and trimer receptor combination, but not of larger confirmations, further adding to the body of evidence to suggest a trimeric organisation of P2X receptor subunits. Direct imaging of purified P2X receptors using atomic force microscopy has also revealed that the average angle between N-terminal-coupled antibodies is 123°, close to the expected 120° for a trimeric receptor (Barrera *et al.*, 2005). Although a trimeric topology is shared with ASIC channels (Jasti *et al.*, 2007), other LGICs that also possess two TM domains per subunit display a trimeric topology, such as in the epithelial sodium channel (ENaC) (Stewart *et al.*, 2011) and *Streptomyces lividans* potassium channel (KcsA) (Uysal *et al.*, 2009).

1.2.2 Release of purines and pyrimidines

Under physiological conditions ATP exists as ATP^{4-} (Melchoir, 1954) and is an efficient chelator of both Ca^{2+} and Mg^{2+} ions (Wilson and Chin, 1991b). Due to both its size and net negative charge, ATP does not diffuse across cell membranes, but can be released in an uncontrolled fashion into the surrounding extracellular milieu during cell damage or injury (reviewed in Praetorius and Leipziger, 2009) (Fig. 1.2). This release is facilitated by a large initial concentration gradient of ATP between the cell interior and extracellular regions - intracellular ATP concentrations are typically in the millimolar range (Imamura *et al.*, 2009), whereas extracellular concentrations are in the nanomolar range (Lee *et al.*, 2012). The net negative charge of ATP necessitates the need for a controlled method of its diffusion from intracellular compartments to the extracellular space. As such many cells possess specialised granules where ATP is present at millimolar concentrations (Pankratov *et al.*, 2006). These granules can fuse with the cell membrane by exocytosis, whereupon ATP can act in an auto- and/or paracrine fashion. At nerve terminals, ATP is often co-released with neurotransmitters including acetylcholine (ACh) (Whittaker *et al.*, 1972), dopamine, γ-amino butyric acid (GABA) (Jo and Schlichter, 1999), glutamate (Gu and MacDermott, 1997) and noradrenaline (von Kügelgen *et al.*, 1994), in addition to being able to act as a neurotransmitter in its own right.

The controlled release of ATP across intact membranes has been shown in a variety of both excitable and non-excitable cells, from epithelial cells, hepatocytes,

keratinocytes and inflammatory neutrophils and macrophages to glial and nerve cells (Abbracchio *et al.*, 2006; Yegutkin, 2008). ATP-containing vesicles are present in a number of cell types, consistent with an exocytotic-type mode of release from the cell. However, other cell types do not possess these vesicles suggesting an alternative mode of release. Evidence supporting these alternatives includes the movement of ATP through transmembrane channels by diffusion, such as through connexin (Stout *et al.*, 2002) and pannexin (Bao *et al.*, 2004) hemichannels, ATP-binding cassette (ABC) transporters (Abraham *et al.*, 1993) and anion-selective ATP channels (Sabirov and Okada, 2005).

The release of ATP can also be caused by mechanical and chemical stimuli. Chemical stimuli can include the exposure of cells to serotonin (Kreda *et al.*, 2010), bradykinin and phenylephrine (Ostrom *et al.*, 2000) and thrombin (Beigi *et al.*, 1999). Mechanical stimulation and resulting ATP release can result from osmotic stress (Feranchak *et al.*, 2000) and shear stress (Yegutkin *et al.*, 2000). This latter stimulus is of particular importance in endothelial cells that undergo laminar flow stress due to blood flow and through integral tissue movement.

Although total extracellular ATP concentrations is present at the nanomolar concentration range, the use of highly sensitive ATP biosensors (such as the firefly luciferase complex) has revealed that pericellular concentrations are within concentration limits required to activate purinergic receptors (typically 10^{-6} to 10^{-5} M) (Beigi *et al.*, 1999). Constitutive release of ATP *via* the endoplasmic reticulum and Golgi apparatus, although poorly understood with respect to its role in physiological function, has also been described and maintains a basal ATP concentration in the nanomolar range as a result of a balance between release and ATP catabolism (Guillen and Hirschberg, 1995; Lazarowski, 2012).

1.2.3 Purinergic receptors

In a manner analogous to the neurotransmitters ACh, GABA and serotonin (), ATP can act at both ionotropic and metabotropic receptors: P2X and P2Y receptors, respectively (North 2002). Seven P2X receptor subunits have been identified to date (P2X1-7) whilst eight P2Y receptor subunits are currently known ($P2Y_{1, 2, 4, 6, 11, 12,}$

13 and 14). According to convention, the 'P' in both P2X and P2Y donates the sensitivity of these receptors to purines, '2' differentiates the two receptor families from the metabotropic P1 adenosine receptor family and 'X' and 'Y' differentiates the two families as either a LGIC or GPCR, respectively. P2X receptors display different sensitivities to ATP with P2X1-5 receptors activated by low micromolar concentrations whilst P2X7 requires ATP concentrations ca. 10-fold larger (North 2002). In contrast P2Y receptors are activated by a diverse range of purine ligands, primarily ATP, ADP, uridine 5-diphosphate (UDP) and uridine 5-triphosphate (UTP) (Abbrachio *et al.,* 2006). Following their activation by ATP, P2X receptors permit the non-selective passage of cations down their electrochemical gradient. The diffusion of these cations (Na^+, K^+ and Ca^{2+}) results in membrane depolarization and also the activation of voltage-caged Ca^{2+} channels that result in a further increase in intracellular Ca^{2+} concentration. This increase in Ca^{2+} ion concentration can further modulate intracellular processes. P2Y receptors coupled in a subunit-specific manner to the heteromeric G proteins α_i, α_s and/or α_q, resulting in modulation of adenylate cyclase or phospholipase C (PLC) and release of Ca^{2+} from intracellular stores (Abbrachio *et al*., 2006) (Fig. 1.2). P2Y receptors can also directly modulate both voltage-gated ion channels (VGICs) and LGICs, including voltage-gated Ca^{2+} channels (Vartian and Boehm, 2001) and NMDA receptors (Wirkner *et al.*, 2002; Luthardt *et al.*, 2003). Through the diversity of the ligands with which they are activated the downstream effects that result from their activation, the P2 receptors have the potential to modulate a cell's intracellular environment.

1.2.4 Extracellular metabolism of purines

Following the release of ATP into extracellular compartments, there must exist efficient methods by which a system can hydrolyse or remove ATP to reduce prolonged effects at effectors when not required. Three enzyme system families for the sequential digestion of phosphate groups from ATP to yield ADP, AMP and adenosine exist: the ectonucleotide pyrophosphatase/phosphohydrolase (E-NPP) family (Goding *et al.*, 2003); ecto-nucleoside triphosphate diphosphohydrolase (E-NTPDase/CD39) family (Robson *et al.*, 2006); and ecto-5'-nucleotidase (CD73) family (Colgan *et al.*, 2006) (Fig 1.2). Adenosine deaminase (ADA) can further catalyse adenosine into inosine (Barankiewicz and Cohen, 1985), which terminates activation of adenosine receptors (Gomez and Sitkovsky, 2003) and can itself be

metabolised to hypoxathine by the action of purine nucleoside phosphorylases (PNPs) (Bzowska *et al.*, 2000). This array of enzymes capable of metabolising ATP plays a considerable role in its effect at P1 and P2 receptors and subsequent downstream events. Under normal, physiological conditions, the action of these enzymes can account, in part, for the short-term P2X receptor currents seen upon ATP activation. Receptor desensitisation and the limited release of ATP through exocytosis also play an integral part in this short-term activity. However, under conditions of extreme cell stress (such as trauma or inflammation), the activity of these enzymes is not sufficient to maintain a graded and controlled response of a cell to a high concentration of ATP (Yegutkin, 2008).

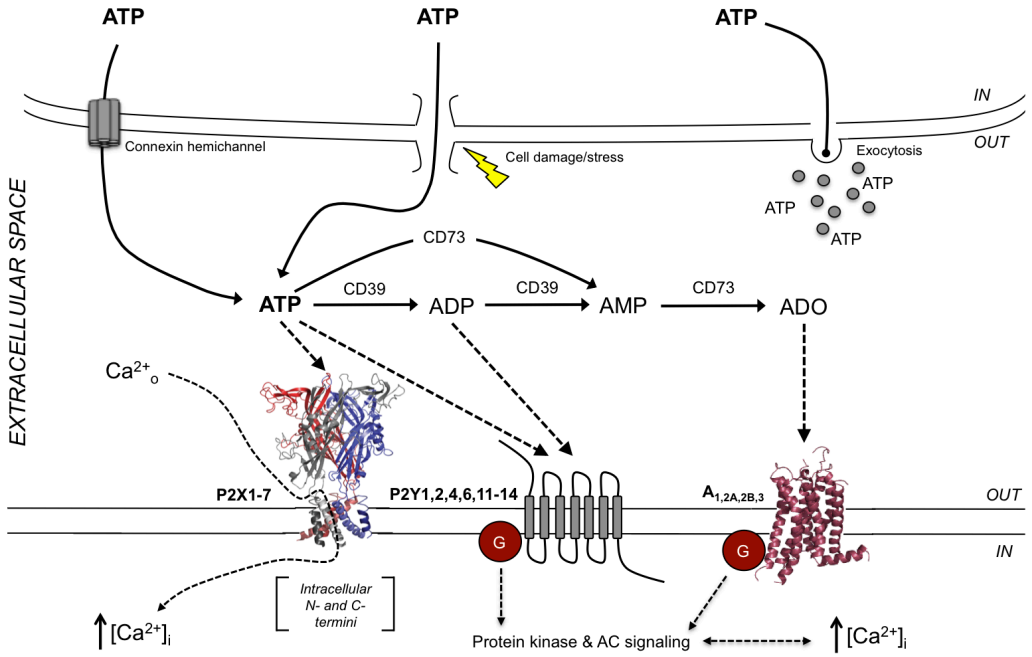

Fig. 1.2: summary of the action of ATP against purinergic receptors in a "model cell"

Cartoon illustrating the release, purinoceptor sites of action, and degradation of ATP within a model cell. Following release from an adjacent cell, either through connexin hemichannels, cell damage and stress or exocytosis, ATP can act at a number of purinergic P2 receptors or adenosine (P1) receptor effectors. ATP acting at P2X receptors can result in direct depolarisation of a host cell through increase in intracellular cation concentration, or indirect modulation of intracellular Ca^{2+}-dependent processes *via* an increase in intracellular Ca^{2+} ion concentration. The action of ATP or ADP at metabotropic P2Y receptors can also activate G-proteins, as well as the action of adenosine at metabotropic P1 receptors. ADP, ADP and AMP hydrolysis by membrane-bound CD39 and CD73 receptors also limits the timecourse of effect of these compounds at their respective effectors. Adenosine can be further metabolised into inosine and hypoxanthine but is omitted in the schematic for clarity. The crystal structure illustrating a membrane-bound P2X receptor is taken from Hattori and Gouaux (2012) under license from Nature Publishing Group. The crystal structure illustrating a membrane-bound P1 receptor is taken from Jaakola *et al.* (2008), under license from the American Association for the Advancement of Science (AAAS).

1.3 STRUCTURE AND FUNCTION OF P2X RECEPTORS

In investigating novel P2X receptors from new species it is important to be aware of the molecular basis of P2X receptor structure and function, gleaned from studies in other organisms. The following sections aim to give a brief overview of our current

understanding of these, particularly in light of the availability of both closed- and open-state (Kawate *et al.*, 2009; Hattori and Gouaux, 2012) structures for a P2X receptor. The imagination of the authors led them to describe the monomeric structure of the closed- and open-state structures as adopting a 'dolphin-like' shape with the head and upper body regions deemed to constitute the ectodomain and the flukes akin to the transmembrane domains. Crystal structures of the intracellular N- and C-termini are not available; these regions had to be excluded from expression constructs to produce viable crystals for analysis (Hattori and Gouaux, 2012).

1.4 INTRODUCTION

P2X receptors form one of the three 'superfamilies' of the Cys-loop LGICs, which includes the nicotinic ACh, $GABA_A$ and glycine receptors, and the glutamate-activated cation channels (which includes the AMPA, NMDA and kainate receptors). The recent publications of apo, closed- and open-state crystal structures for the zebrafish P2X4.1 receptor (zfP2X4.1) represents a significant step-change in our understanding of these membrane-bound ion channels. Kawate and colleagues originally presented a 3.1Å resolution 3-dimensional (3D) crystal structure of zfP2X4.1 in its closed state (Kawate *et al.*, 2009). A further advance in P2X receptor structure was provided by Hattori and Gouaux in 2012 when the crystal structure of an acutely modified form of zfP2X4.1 was presented in its open, ATP-bound state at 2.8Å resolution, in addition to a higher resolution 3D structure of the closed state at 2.9Å (Hattori and Gouaux, 2012). The findings that have arisen from these structures have confirmed many of the findings from site-directed mutagenesis of specific residues and regions of P2X receptors and have enabled the development of homology-based structures of other P2X receptors (Young, 2010).

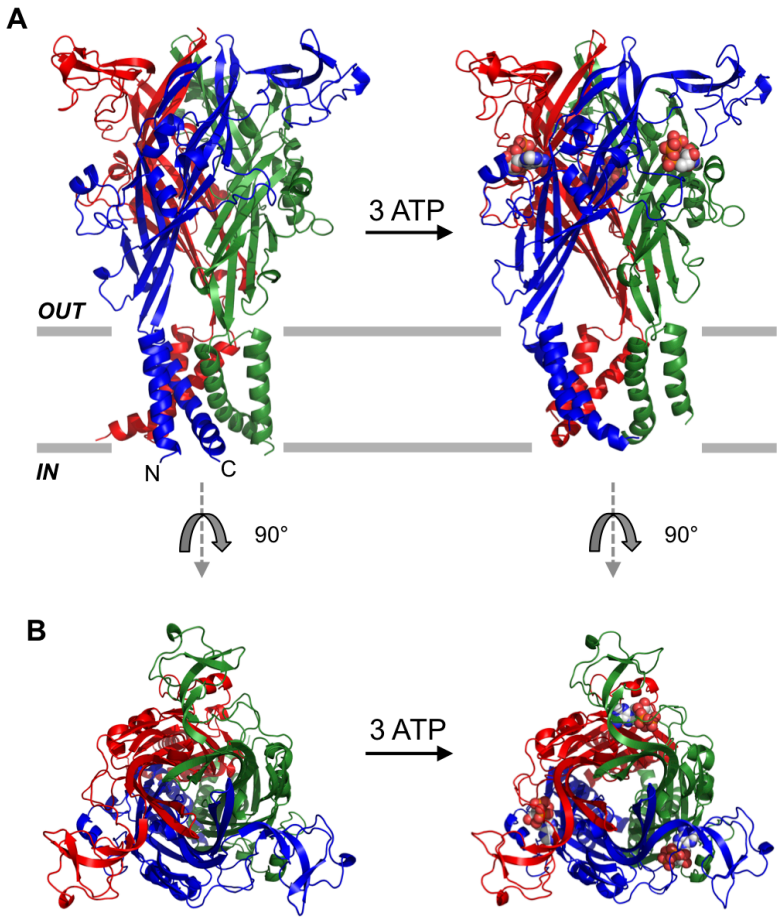

Fig 1.3: conformational changes in trimeric zfP2X4.1 crystal structure in response to ATP binding

A, Crystal structure of trimeric zfP2X4.1, illustrated as a ribbon structure with each monomer depicted in a different colour. Following cooperative binding of 3 ATP molecules (depicted in spacefill form) (top right structure), the rotation of TM1 and TM2 about a central vestibule perpendicular to the membrane, results in the opening of a central pore and expansion of lateral fenestrations above the membrane surface. ***B***, A top-down view of the same conformational change illustrates the expansion of the central pore/vestibule in response to binding of 3 ATP molecules. Figure inspired by Hattori and Gouaux (2012).

In mammalian species there are seven P2X receptor subunits (P2X1-7), encoded by separate genes for which (for some subunits, such as human P2X2 and P2X7) can exist alternative splice variants (North, 2002). Each subunit possesses two transmembrane domains with an intracellular amino- (N-) and carboxyl (C-) termini and a large extracellular loop domain that accounts for the majority of the protein's bulk. Although P2X receptors share topology with other LGICs, such as acid-sensing ion channels (ASIC) (Jasti *et al.*, 2007; Gonzales *et al.*, 2009), the two do not share

amino acid sequence similarity. Functional P2X receptors arise from the association of three individual monomers that can group as either homomers or heteromers from different combinations of subunit. Evidence for this trimeric confirmation comes from a range of data employing various techniques. Stoop and colleagues illustrated that, using concatamers consisting of P2X2 receptor subunits, a positional dependence on the position of a threonine to cysteine mutation at position 336 (T336C) existed. This mutation, which allows the selective inhibition of current flow following exposure to methanethiosulphonate (MTS) derivatives was most effective in receptor complexes consisting of no more than three subunits, consisted with the notion of a trimeric configuration of P2X receptors (Stoop *et al.*, 1999). Indeed, initial work in rat and bullfrog sensory neurons in 1990 had already hinted at the trimeric organisation of the functional receptor, whereby 3 ATP molecules bind at non-interacting sites to induce pore formation (Bean, 1990). Further experiments using blue native polyacrylamide gel electrophoresis (PAGE) where the band produced on a gel corresponds to the sum of three individual subunits (Nicke *et al.*, 1998; Aschrafi *et al.*, 2004). In both these studies, the addition of chemical cross-linking agents allows for the formation of dimer and trimer receptor combination, but not of larger confirmations. Direct imaging of purified P2X receptors using atomic force microscopy has also revealed that the average angle between N-terminal-coupled antibodies is 123°, close to the expected 120° for a trimeric receptor (Barrera *et al.*, 2005). Although a trimeric topology is shared with ASIC channels (Jasti *et al.*, 2007), other LGICs that also possess two TM domains per subunit display a trimeric topology, such as in the epithelial sodium channel (ENaC) (Stewart *et al.*, 2011) and *Streptomyces lividans* potassium channel (KcsA) (Uysal *et al.*, 2009).

1.4.1 Transmembrane domains

Prior to the availability of a crystal structures for a P2X receptors, the α-helical configuration of the TM domains was originally suggested using site-directed mutagenesis. Indeed, the identification of the pore region of the receptor using modulation of introduced cysteine residues along this region using Ag^{+} ions and MTS derivative compounds (where any residues exposed to the aqueous environment (and therefore contribute to the pore) are susceptible to modulation) has also enabled an α-helical topology for the TM domains to be suggested (Rassendren *et al.*, 1997; Egan

et al., 1998; Haines *et al.*, 2001). In these studies a pattern of every 3rd to 4th residue in the predicted TM domain regions appeared to be affected by its mutation to cysteine (or, in analogous studies, alanine) suggesting an α-helical arrangement of the domains. Furthermore, the close proximity of TM1 and 2 between different subunits has been investigated through the mutagenesis of residues at the apical and basal portions of the two domains to cysteine. This allows the formation of disulphide bonds through chemical modification and demonstrated the close association between TM1 and TM2 within the functional trimeric P2X receptor (Jiang *et al.*, 2003).

1.4.2 Pore formation and gating

To allow passage of cations from adjacent compartments, a pore must be present in the P2X receptor. The two transmembrane (TM) domains in each subunit of a functional trimer adopt an α-helical configuration, angled at approximately 45° to the cell's membrane and at an antiparallel orientation to each other (Kawate *et al.*, 2009; Hattori and Gouaux, 2012). The α-helix arrangement of the TM domains was confirmed by crystal structure, but had already been suggested by a number of research groups following site-directed mutagenesis of residues at defined positions in TM1 resulting in current inhibition (Rassendren *et al.*, 1997; Egan *et al.*, 1998). Residues in TM1 mutated every third/fourth position, as cysteine-modifying compounds such as MTSEA were unable to alter ATP-induced currents. Although not as clear as those data gathered for TM1, similar data has been found for TM2 and identified a number of residues that appeared to contribute to a pore structure in rP2X2 (328, 333 and 336 through to 345) (Rassendren *et al.*, 1997; Egan *et al.*, 1998; Haines *et al.*, 2001).

A role for TM1 in rP2X2 in forming the pore has been suggested through studies in which Y43A and F44A mutations result in the formation of a constitutively active receptor with delayed kinetics of activation (Li *et al.*, 2004). Although both transmembrane (TM) domains contribute to the formation of the pore, it is believed that the second TM domains play the dominant role in ion transduction. TM1 and TM2 cross each other at approximately the mid-point of each domain, forming a constriction that was originally thought to constitute the channel pore. In the closed/apo state of the zfP2X4.1 receptor there appears to be two pathways through

which ions may pass through the receptor (through the central vestibule of the channel along its three-fold axis of symmetry, and a lateral pathway through fenestrations situated above the channel pore) (Kawate *et al.*, 2009; Hattori and Gouaux, 2012). However the open state form of the receptor suggests that the former pathway is too narrow to permit the flow of ions and therefore the lateral pathways allow hydrated ions to enter and exit cells (Kawate *et al.*, 2011; Hattori and Gouaux, 2012)

1.4.3 Ion permeability

P2X receptors are described as being 'non-selective cation channels' whereby, upon binding of ATP, a conformational change occurs that allows the diffusible passage of cations through lateral fenestrations in the trimeric structure (situated above the cell membrane) that lead to a pore-structure formed by the transmembrane domains (Mio *et al.*, 2009; Hattori and Gouaux, 2012). Once hydrated ions have passed through these lateral fenestrations, the highly acidic environment of the central vestibule of the channel attracts cations and repels anions (Samways *et al.*, 2011). This is in agreement with the myriad biophysical studies that have demonstrated that P2X receptors are equally permeable to Na^+ and K^+, but also display a significant permeability to Ca^{2+} ions, a key feature of P2X receptors amongst other LGICs (Khakh, 2001). This Ca^{2+} permeability, and subsequent increase in intracellular Ca^{2+} concentration is associated with many physiological and pathophysiological processes involving P2X receptors. Although P2X receptors are largely cation permeable, hP2X5 and chick P2X5 (cP2X5) subunit homologues display some Cl^- permeability (Bo *et al.*, 2000; Ruppelt *et al.*, 2001). Many residues have been implicated in endowing Ca^{2+} permeability of P2X receptors, particularly in those regions that form the channel pore, particularly polar residues lying in TM2 at its narrowest part (Migita *et al.*, 2001b). Equally, acidic residues in the TM domains of receptor subunits P2X1 through to P2X4, when mutated, yield a channel with decreased fractional Ca^{2+} currents (*Pf%*). For instance, mutation of E52 in TM1 of rat P2X1 significantly reduced *Pf%* (Samways and Egan, 2007). The pore structure defined in the crystal structure of zfP2X4.1 agrees well with the data garnered from structure-function studies prior to its availability.

1.4.4 Extracellular loop domain

The large extracellular domain (ECD) of a P2X receptor represents the bulk of a P2X receptor. As well as being the site for agonist and antagonist binding, including modulation by non-purine compounds, the extracellular domain is also subject to post-translational modification through a variety of mechanisms.

Prior to the availability of a crystal structure of a P2X receptor, much of the information regarding the extracellular domain (ECD) came from amino acid substitution experiments. Mammalian P2X receptors possess ten conserved cysteine residues that form disulphide bonds which, if numbered '1-10', were predicted to be paired in order: 1-6, 2-4, 3-5, 7-8 and 9-10. These predictions (determined through selective mutagenesis of these residues both individually and in combination) (Ennion and Evans, 2002a; Clyne *et al.*, 2002b) were corroborated by the crystal structures of zfP2X4.1 (Kawate *et al.*, 2009; Hattori and Gouaux, 2012). These cysteine residues maintain the tertiary structure of the ECD, but are not necessary for function as an ATP-gated ion channel in all receptors as evidenced by the cloning and functional expression of a P2X receptor from *D. discoideum* that shares only five of the 10 conserved residues that are found in mammalian homologues (Fountain *et al.*, 2007). P2X receptors do not possess ATP-binding motifs found in other ATP-binding proteins such as the Walker motif (Walker *et al.*, 1982) and, equally, lack any significant structural homology to ATP-binding proteins.

Prior to the availability of a P2X receptor crystal structure, site-directed mutagenesis had revealed that 8 residues located in the ECD of the receptor play a predominant role in coordinating ATP binding. The negatively charged triphosphate moiety as well as the aromatic ring portions of the ATP molecule are all involved in its binding to the P2X receptor ECD. Of the eight residues identified in playing a role in this binding, positively charged lysine residues are believed to coordinate binding to the triphosphate moiety (Jiang *et al.*, 2000b) and arginine, asparagine, threonine and phenylalanine residues are involved in binding to the adenine and ribose ring moiety of ATP (Roberts and Evans, 2004). The eight conserved residues implicated in ATP binding (hP2X1 numbering) are: K68, K70, F185, T186 (of one subunit) and N290, F291, R292 and K309 of another subunit (Fig 1.4A), the zfP2X4.1 crystal structure (zfP2X4.1 numbering). Mutation of these residues alters the sensitivity of a P2X

receptor to ATP (Ennion *et al.*, 2000; Roberts and Evans, 2004; Wilkinson *et al.*, 2006) although in *Dictyostelium discoideum*, importantly, many of these regions are absent in its P2XA paralogue yet the receptor still retains sensitivity to ATP (Fountain *et al.*, 2007). In the zfP2X4.1 ATP-bound crystal structure ($\Delta P2X_4$-C) (Hattori and Gouaux, 2012), the inter-subunit binding site for ATP is lined with positive residues with the β- and γ phosphate groups of ATP partially exposed to what would be the extracellular milieu. The adenine base is embedded within the binding pocket interacting with T189 and K70, residues previously identified as being important for the potency of ATP at P2X receptors and adenine base specificity (Roberts *et al.*, 2009a). Further hydrophobic interactions with L191 (situated in the lower 'body' of the structure) and I232 (in the 'dorsal fin') and the adenine base of ATP are also apparent and are consistent with site-directed mutagenesis of L186 in rP2X2 which had previously been implicated in the gating of rP2X2 in response to ATP binding (Jiang *et al.*, 2011). Finally, the triphosphate moiety of ATP is exposed to the extracellular environment (Fig. 1.4A and B) and appears to interact hydrophobically with L217; the exposure of this ribose moiety is consistent with ribose-modified analogues of ATP that are known to modulate ATP-induced currents (Bianchi *et al.*, 1999; Virginio *et al.*, 1998b).

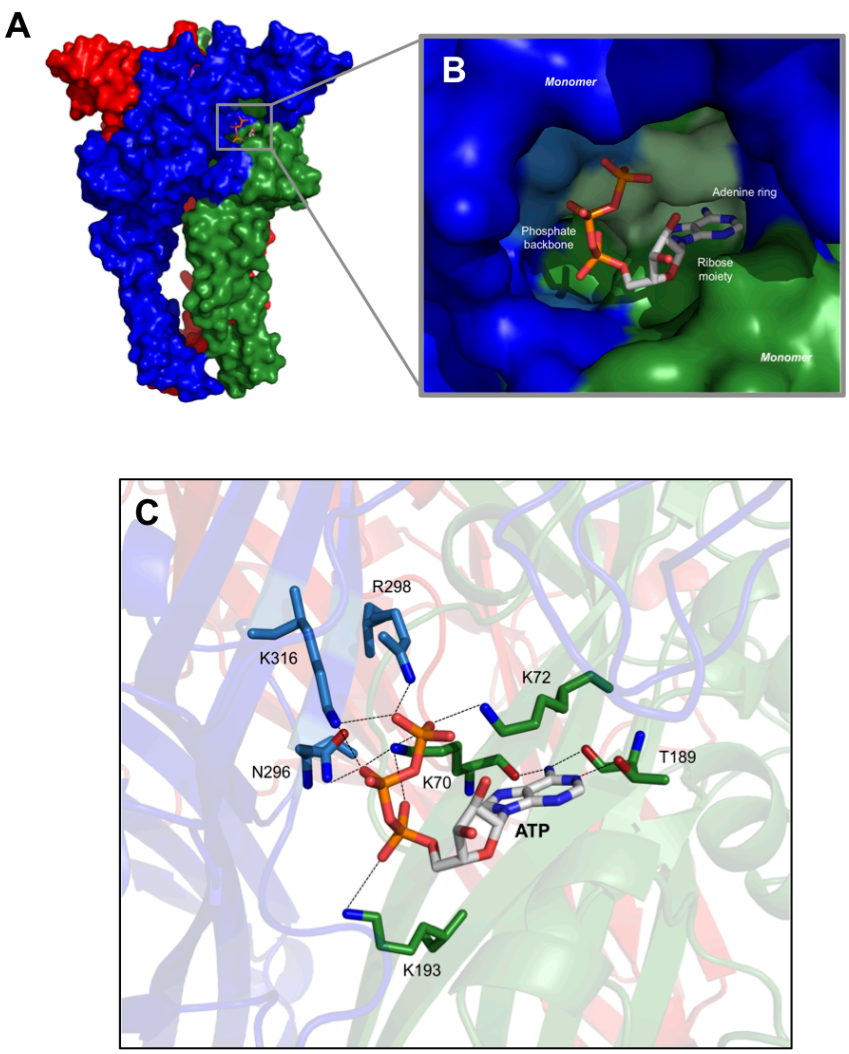

Fig. 1.4: coordination of ATP binding in the extracellular domain of zfP2X4.1

A, Space-filling model of ATP-bound zfP2X4.1 crystal structure (PDB ID: 4DW1) with an ATP molecule positioned in one of the three inter-subunit binding pockets located in the ECD of the receptor. ***B***, Confirmation of ATP in crystal structure with the adenine ring buried inside the binding pocket. ***C***, A more detailed view of the binding site and residues involved in the coordination of ATP binding. Dashed lines illustrate hydrogen bonding between atoms in P2X receptor residues and ATP. Residues from two separate monomers contributing to binding are illustrated in light blue or green, respectively whilst those atoms which contribute to hydrogen bonding are highlighted in blue (hydrogen) and red (oxygen). Figures generated using MolProbity (Chen *et al.*, 2010) and inspired by Hattori and Gouaux (2012). For clarity, phenylalanine residues have not been included.

Glycosylation modification of the ECD is another important form of P2X receptor processing and function. All P2X receptors cloned to date possess the consensus sequence for *N*-linked glycosylation (Nx(S/T)), where x constitutes any amino acid

residue except proline). Through site-directed mutagenesis of these regions or chemical modification such that glycosylation in these receptors is impaired or inhibited entirely, the region's contribution to receptor cell surface expression and function has been investigated. Although not necessary for complete receptor function, as many glycosylation sites are redundant in some P2X subunits (Rettinger *et al.*, 2000), it appears that there is a requirement of at least two sites as mutation of these sites severely reduces or ablates receptor cell surface expression, such as in the rat P2X1 (Rettinger *et al.*, 2000) and P2X2 forms (Torres *et al.*, 1998).

1.4.5 N- and C-termini

Although the conformational structure of N- and C-termini of P2X receptors are absent from the crystal structures of zfP2X4.1, site-directed mutagenesis and generation of chimeras of P2X receptors in which termini have been interchanged between receptor subunits have revealed a role for these domains in heterologous systems. Both intracellular, the N- and C-termini of P2X receptors range from approximately 20 to 30 residues and approximately 25 to 240 residues in length, respectively (North, 2002). The C-terminus of P2X7 receptor isoforms has been the subject of numerous studies attempting to elucidate potential functions this unusually large domain has in P2X function within cells. P2X7 receptor activation has been implicated in a range of intracellular events including caspase activation and induction of cell death (Kahlenberg and Dubyak, 2004), regulation of the cell cycle (Bianco *et al.*, 2006) and the release of pro-inflammatory cytokines such as IL-1β (Clark *et al.*, 2010). The complexity of P2X7 activity is furthered by the observation that prolonged stimulation of the receptor by extracellular ATP results in a progressive increase in ion permeability and pore diameter that permits the passage of larger molecular weight molecules from the extracellular milieu into the cell (Chessell *et al.*, 1998). The exact nature and cause of this phenomenon is unclear with some studies suggesting that the P2X7 pore may allow the initial passage of smaller diameter cations in the early phase of ATP-induced activation followed by a further conformational change to the integral pore that permits larger molecules to pass such as $NMDG^+$ and the fluorescent dyes ethidium bromide and YO-PRO-1. A second mechanism is the activation of a distinct protein partner that is responsible for the passage of higher molecular weight molecules independent of the P2X7 receptor

pore. Many such P2X7 receptor protein partners have been suggested, including pannexin-1 hemichannel (Pelegrin and Suprenant, 2006) and members of the epithelial membrane protein family (Wilson *et al.*, 2002). Although pannexin channels are permeable to larger diameter ions, recent evidence suggests that the P2X7 channel can allow the passage of molecules up to 1.4 nm in diameter, including N-methyl D-glucamine ($NMDG^+$) (Browne *et al.*, 2013). Analysis of the P2X7 C-terminus has suggested putative motifs required for interaction with numerous proteins such as an SRC Homology 3 (SH3) domain that may play a role in LPS-mediated apoptotic pathways (Denlinger *et al.*, 2001).

The P2X receptor N-terminus possesses a highly conserved protein kinase C (PKC) site, truncation of which to remove this site in P2X2 receptors increases the rate of current desensitisation. Conversely, activation of PKC by phorbol esters restores the normal slower desensitisation phenotype to that of a non-truncated, wild-type P2X2 receptor (Boué-Grabot *et al.*, 2000). Further evidence for modulation of P2X receptors has been illustrated by disruption of the PKC motif in the N-terminus of hP2X1 by mutation of T18 in hP2X1 ablated ATP-evoked currents (Ennion and Evans, 2002b). In the C-terminus, further evidence for post-translation processing via a basic amino acid motif is now known to be required for phosphoinositide products of phosphorylation by wortmannin-sensitive phosphatidylinositol 4-kinases and phosphatidylinositol 3-kinases) modulation (Bernier *et al.*, 2012) following the finding that these lipids are capable of acting as a partial agonist at P2X1 (Bernier *et al.*, 2008b) and P2X4 receptors (Bernier *et al.*, 2008a).

1.4.6 Modulation of P2X receptor responses

The hydrolysis of ATP by various ectonucleotidases can prolong or reduce its availability as an activator of P2X receptors. As a result, changes in the inherent desensitisation of many P2X receptors may occur due to the maintained or limited presence of ATP in the vicinity of a cell.

When expressed heterologously P2X receptors display a range of desensitisation rates. P2X1 and P2X3 subtype receptors desensitize within milliseconds of ATP application, whereas P2X2, P2X4 and P2X7 receptors display little desensitisation over the course

of maximal agonist application. At the cellular level these variations in kinetic profile can contribute to the diverse physiological functions played by P2X receptors. For instance, the rapid currents seen through P2X1 and P2X3 are associated with synaptic neurotransmission (Jarvis, 2003) and may prevent over-excitation of neural inputs to sensory systems. In contrast, P2X7 receptors are often implicated in longer term inflammatory signalling seen in cells such as macrophages (Hickman *et al.*, 1994; Falzoni *et al.*, 1995) and ATP-mediated cell lysis (Pizzo *et al.*, 1992). The molecular basis of desensitisation of P2X receptors has been of great interest to researchers and, as a complex property of these receptors, many regions are thought to contribute. The identification of an alternatively spliced variant of P2X2 (P2X2b) presented a clear role for the C-terminus, whereby the truncated P2Xb form (loss of residues V370 to Q438) results in a more rapid desensitisation rate in this receptor. Specifically, a six amino acid region of R371 to P376 P2X2, was found to be responsible for desensitisation rate differences in these two receptors (Koshimizu *et al.*, 1998; Koshimizu *et al.*, 1999). Further contributions of D349 (Zhou *et al.*, 1998) and the finding that mutation of the penultimate arginine in the C-terminus of a P2X receptor from cattle tick *B. microplus* to a positively-charged lysine residue (R413K) endows the mutant receptor with a faster rate of desensitisation relative to its wild-type form (Bavan *et al.*, 2011) illustrated a complex role of the C-terminus in endowing desensitisation in P2X receptors. A form of cross-talk between the ECD and C-terminus was also suggested from the link between ECD binding of agonists and desensitisation rate, a phenomenon suggested by the authors to contribute to modulation of P2X receptor signalling efficacy (He *et al.*, 2002). Within the N-terminus lies a protein kinase C phosphorylation site (YxTx(K/R)), where 'x' is any amino acid residue) that is conserved across mammalian and non-mammalian P2X receptors. Mutation of residues within this site in P2X2 results in a receptor with faster desensitisation (Boué-Grabot *et al.*, 2000), as does mutation of the threonine residue that forms part of this site in P2X1 (Ennion and Evans, 2002b). Although a role for direct phosphorylation of a P2X receptor has not yet been described (Vial *et al.*, 2004), P2X receptors may be phosphorylated basally, with subsequent dephosphorylation modulating receptor function *in vivo* (Boué-Grabot *et al.*, 2000).

Desensitisation is dependent on the availability of an agonist and its binding to a P2X receptor. Heterologously-expressed P2X1 receptors can undergo internalisation following prolonged exposure to ATP (Dutton *et al.*, 2000; Ennion and Evans, 2000).

Constitutive recycling of P2X4 between the plasma membrane and lysosomes has also been described (Bobanović *et al.*, 2002; Royle *et al.*, 2002; Qureshi *et al.*, 2007), with an involvement of the clathrin adaptor protein complex AP2 recognised (Royle *et al.*, 2005). A conserved tyrosine and lysine residue immediately below TM2 (within the N-terminus) form the canonical 'YxxxK' membrane stabilisation motif, where 'x' is any amino acid residue (Chaumont *et al.*, 2004). Its disruption leads to the rapid internalization of P2X2-6 receptor subunits, although it is not necessary in all monomers of the trimeric receptor for stabilization to occur. Recent evidence suggests that expression of a non-functioning Rab5 (an endosome-specific GTPase) mutant in HEK293 cells stably expressing P2X4 abolishes both constitutive and agonist-induced receptor internalisation, further adding to the various means by which this receptor subunit can be trafficked to the membrane (Stokes, 2013). Although constitutive and agonist-dependent internalization is well documented for P2X1 and P2X4, it does not appear to impact P2X2 expression at the cell membrane (Bobanović *et al.*, 2002). Finally, depletion of cholesterol in lipid rafts of HEK293 cells stably expressing P2X1 or in rat tail artery smooth muscle cells reduces ATP-induced currents by over 90 and 50%, respectively following activation using α,β-meATP (Vial and Evans, 2005). Furthermore, ATP-induced currents through P2X1 to P2X4 respond differentially to cholesterol depletion. P2X2 and P2X3 currents are not affected by its depletion, whereas P2X1 currents are inhibited and P2X4 currents are substantially increased (Allsopp *et al.*, 2010). Generation of chimeras between P2X1 and P2X2 revealed a contribution by the N-terminus of the receptor to cholesterol sensitivity, where replacement of the P2X1 N-terminus with that of P2X2 abolished any current reduction following cholesterol depletion in HEK293 cells using 10 μM methyl-β-cyclodextrin (mβ-CD). Further analysis highlighted a role for residues 16-30 in hP2X1 which also contains the consensus Tx(K/R) (where x is any amino acid) sequence (Allsopp *et al.*, 2010) in lipid modulation of this receptor.

The extracellular and intracellular environment in which a P2X receptor resides can drastically alter the biophysical properties of the receptor. Fluctuations in local H^+ concentration, and thus pH, that may occur due to inflammation or change in cellular metabolic state are known to either inhibit or potentiate ATP-induced currents (fig 1.5) depending on the subtype and whether or not the receptor forms homo- or heteromeric trimers. In addition, ions known to be permeable through a P2X receptor can also modulate the ATP-induced current to which it has contributed. For instance,

although the physiological range of Ca^{2+} ion concentration is 1.1 to 1.3 mM the local accumulation of Ca^{2+} ions in the immediate vicinity of the P2X receptor results in the millimolar concentration that is sufficiently high to inhibit many P2X receptor subunits. Finally, trace metal ions such as Zn^{2+} can be seen to have a biphasic effect depending on the receptor subtype that could be fundamental to nervous function in certain brain regions (North, 2002). These modulating factors have been well described for many mammalian subunits and are summarised in Fig. 1.5.

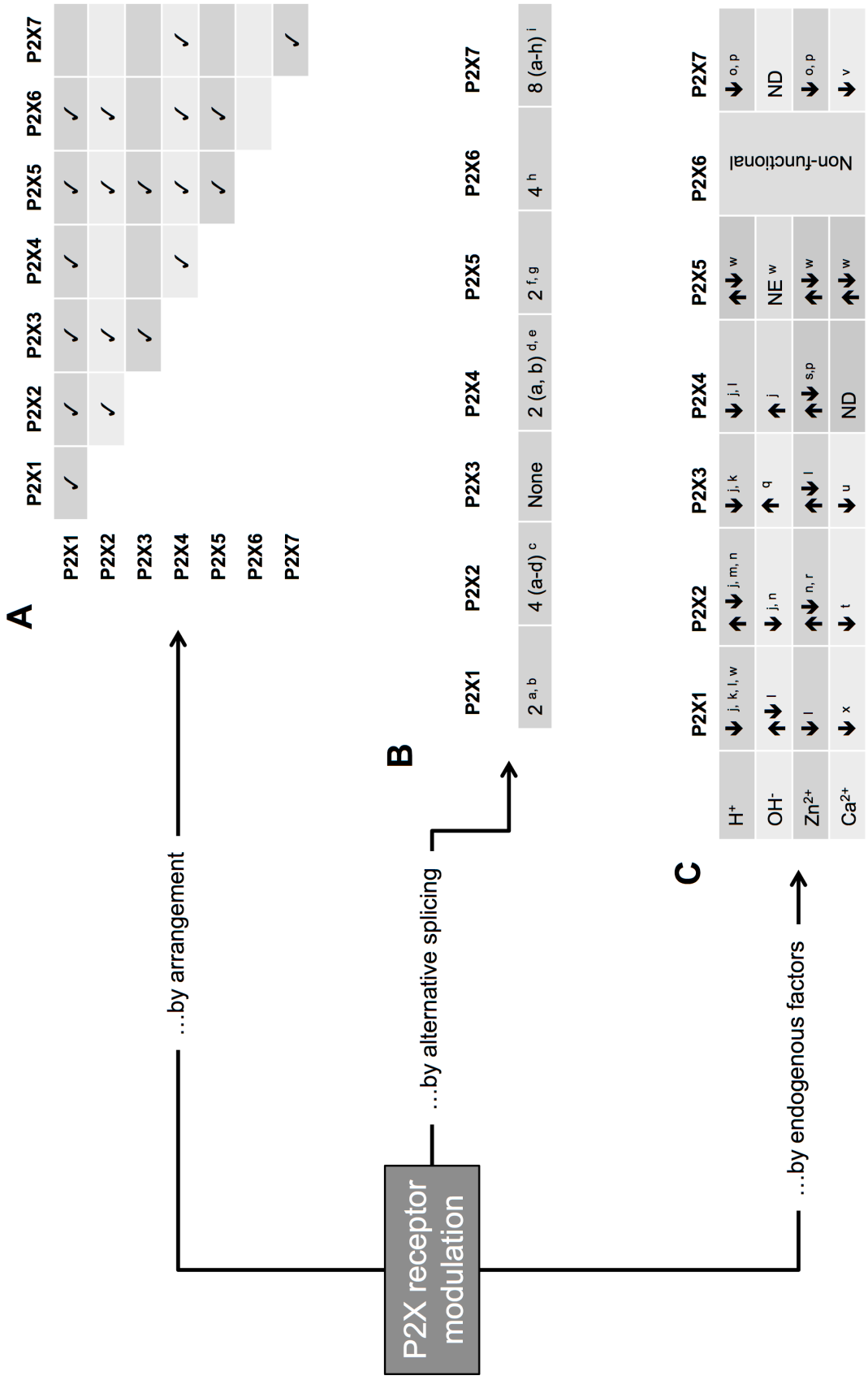
A
P2X1 P2X2 P2X3 P2X4 P2X5 P2X6 P2X7
P2X1 ✓ ✓ ✓ ✓ ✓ ✓ ✓
P2X2 ✓ ✓ ✓ ✓ ✓ ✓
P2X3 ✓ ✓ ✓ ✓ ✓
P2X4 ✓ ✓ ✓ ✓
P2X5 ✓ ✓ ✓
P2X6 ✓ ✓
P2X7 ✓
...by arrangement
B
P2X1 P2X2 P2X3 P2X4 P2X5 P2X6 P2X7
2 a, b 4 (a-d) c None 2 (a, b) d, e 2 f, g 4 h 8 (a-h) i
...by alternative splicing
C
P2X1 P2X2 P2X3 P2X4 P2X5 P2X6 P2X7
H+ ↓ j, k, l, w ↓↑ j, m, n ↓ j, k ↓ j, l ↓↑ w Non-functional ↓ o, p
OH- ↓↑ l ↓ j, n ↑ q ↑ j NE w ND
Zn2+ ↓ l ↓↑ n, r ↓↑ l ↓↑ s,p ↓↑ w ↓ o, p
Ca2+ ↓ x ↓ t ↓ u ND ↓↑ w ↓ v
...by endogenous factors
P2X receptor modulation

Fig. 1.5: P2X receptor modulation by subunit arrangement, alternative splicing of nascent P2X mRNA and endogenous factors

A, *in vivo*, P2X receptor subunits can form homomeric and heteromeric trimers with differing sensitivity to endogenous purines and biophysical properties that can in turn profoundly affect their function in a cell. **B**, alternatively spliced variants of P2X receptor mRNA are well-described in humans and are shown. The large C-terminal tail of hP2X7 (and other P2X7 genes from other species) gives rise to a number of splice variants. Although splice variants for some subunits have been described in other species (reviewed in North 2002), they are seemingly absent in humans (such as P2X3). ***C***, the modulation of P2X receptors by endogenous factors by an increase in acidic conditions (< physiological pH (7.3-7.4) or an alkali environment (> pH 7.3-7.4), and increase in the extracellular Zn^{2+} or Ca^{2+} ion concentration. This table is by no means exhaustive and does not describe the modulation of extracellular heavy metals ions and other trace ions, or indeed synthetically derived agonists and antagonists such as suramin or PPADS.

References detailed in tables: **a**, Hardy *et al.*, 2000; **b**, Greco *et al.*, 2001; **c**, Lynch *et al.*, 1999; **d**, Dhulipala *et al.*, 1998; **e**, Carpenter *et al.*, 1999; **f**, Lê *et al.*, 1997; **g**, Kotnis *et al.*, 2010; **h**, Urano *et al.*, 1997; **i**, Cheewatrakoolpong *et al.*, 2005; **j**, Stoop *et al.*, 1999; **k**, Wildman *et al.*, 1999b; **l**, Brown *et al.*, 2002; **m**, King *et al.*, 1997; **n**, Clyne *et al.*, 2002a; **o**, Virginio *et al.*, 1997; **p**, Acuna-Castillo *et al.*, 2007; **q**, Wirkner *et al.*, 2008; **r**, Lorca *et al.*, 2005; **s**, Coddou *et al.*, 2005; **t**, Evans *et al.*, 1996; **u**, Virginio *et al.*, 1998a; **v**, Virginio *et al.*, 1997; **w**, Wildman *et al.*, 2002; **x**, Evans *et al*., 1995. ND = not determined; NE = no effect. The arrows ↑ and ↓ denote potentiation and inhibition, respectively. In cells containing both arrows, a biphasic effect of specific modulatory factor is seen.

The potency of a number of agonists, modulators and antagonists has been assessed at both against both homomeric and heteromeric forms of mammalian receptors, as well as non-mammalian subunits. Compounds used in the current thesis and their described effects at known P2X receptor subunits are described in Tables 1. ___ and 2. ____, below

Table 1.1: P2X receptor agonists and modulators						
Species	**Subunit**	**ATP**	**α,β-meATP**	**β,γ-meATP**	**Ivermectin**	**CORM-2**
Mammalian	P2X1	1	0.1-1	2	ND	ND
	P2X2	1-30	>100	>300	No effect (10 μM)	3 (weak inhibition > 100 μM)
	P2X3	1	1-2	ND	No effect (10 μM)	No effect (30 μM)
	P2X4	1-20	4-300	>300	Potentiates (3 μM)	Weak inhibition (30 μM)
	P2X5	0.5-4	1-12	10	ND	ND
	P2X6	10	>100	ND	ND	ND
	P2X7	100	>300	>300	>30	ND
	P2X1/5	0.05-5	3	ND	ND	ND
	P2X2/3	1	1-10	>100	No effect (10 μM)	Weak inhibition (30 μM)
	P2X2/6	30	No effect (100 μM)	No effect (100 μM)	ND	ND
	P2X4/6	6	12	ND	Potentiates (15 μM)	ND
S. mansoni	*Sm*P2X	22	0.5 (partial > 100 μM)	ND	Potentiates (10 μM)	ND
O. tauri	*Ot*P2X	250	> 5,000	ND	ND	ND
D. discoideum	*Dd*P2XA	97	95	ND	ND	ND
	*Dd*P2XB	266	No block (100 μM)	ND	ND	ND
	*Dd*P2XC			ND	ND	ND
	*Dd*P2XD			ND	ND	ND
	*Dd*P2XE	511	No block (100 μM)		ND	ND
H. dujardini	*Hd*P2X	45	15	ND	Potentiates (3 μM; 224%)	ND
B. microplus	*Bm*P2X	67	ND	ND	No effect (10 μM)	ND
L. stagnalis	*Lym*P2X	6	8	ND	No effect (10 μM)	ND

Table 1.2: P2X receptor antagonists					
Species	**Subunit**	**Suramin**	**PPADS**	**BBG**	**Phenol red**
Mammalian	P2X1	1	1	>500	3
	P2X2	10	1	1	52
	P2X3	3	1	>10	24
	P2X4	>500	>500	>10	No block (100 μM)
	P2X5	4	3	ND	ND
	P2X6	>100	>100	ND	ND
	P2X7	>300	15-250 nM	10-45	ND
	P2X1/5	1.6	6.6	>10	ND
	P2X2/3	30-100	3-300	>10	No effect
	P2X2/6	6	ND	ND	ND
	P2X4/6	10	10	ND	ND
S. mansoni	*Sm*P2X	10	0.5 (partial > 100 μM)	ND	ND
O. tauri	*Ot*P2X	No block (100 μM)	No block (100 μM)	ND	ND
D. discoideum	*Dd*P2XA	No block (100 μM)	No block (100 μM)	ND	ND
	*Dd*P2XB	No block (100 μM)	No block (100 μM)	ND	ND
	*Dd*P2XC	ND	ND	ND	ND
	*Dd*P2XD	ND	ND	ND	ND
	*Dd*P2XE	No block (100 μM)	No block (100 μM)		ND
H. dujardini	*Hd*P2X	23	15	ND	ND
B. microplus	*Bm*P2X	5 (partial > 300 μM)	ND	ND	ND
L. stagnalis	*Lym*P2X	27 (partial > 300 μM)	8	ND	ND

Tables 1.1 and 1.2: pharmacology of mammalian and non-mammalian homomeric and known mammalian heteromeric P2X receptor subunits

For P2X receptor agonists and the channel modulators ivermectin and CORM-2, EC_{50} values are presented. For antagonists, IC_{50} values are presented. Where data are not available, this is indicated as 'ND' (Not Determined). The table is based on the following references: Brake *et al.*, 1994; Chen *et al.*, 1995; Evans *et al.*, 1995; Lewis *et al.*, 1995; Wildman *et al.*, 1999a; Buell *et al.*, 1996; Collo *et al.*, 1996; Suprenant *et al.*, 1996; Soto *et al.*, 1996b; Lê *et al.*, 1998; Bianchi *et al.*, 1999; Haines *et al.*, 1999; Khakh *et al.*, 1999b; Jiang *et al.*, 2000a; Jones *et al.*, 2000; King *et al.*, 2000; Eickhorst *et al.*, 2002b; Wildman *et al.*, 2002; Agboh *et al.*, 2004; Jones *et al.*, 2004; King *et al.*, 2004; Fountain *et al.*, 2009; Priel and Silberberg, 2004; Zemkova *et al.*, 2004; King *et al.*, 2005; Silberberg *et al.*, 2007; Fountain *et al.*, 2008; Jelínkova *et al.*, 2008; Bavan *et al.*, 2009; Ludlow *et al.*, 2009; Roberts *et al.*, 2009a; Wilkinson *et al.*, 2009; Bavan *et al.*, 2011; Yan *et al.*, 2011; Wilkinson and Kemp, 2011; Bavan *et al.*, 2012.

1.4.7 P2X receptors as therapeutic targets

Given the widespread expression of P2X receptors in myriad tissues in the human body, their potential as targets for the treatment of disease has been of great interest. The availability of subunit-specific P2X receptor knockout models has revealed physiological roles for this receptor in a variety of tissues. P2X1 knockout mice ($P2X1^{-/-}$) have, for instance, revealed that this subtype is involved in vas deferens smooth muscle contraction and that absence of the receptor reduces this contractility and sperm count in males (Mulyran *et al.*, 2000). Further roles for P2X1 in smooth muscle have also been illustrated, including arterial thrombosis (Hechler *et al.*, 2003) and feedback regulatory mechanisms in response to increased blood pressure in the renal microvasculature (Inscho *et al.*, 2003). For P2X2, ablation of the subunit blunts the physiological response to hypoxic challenges (Rong *et al.*, 2003) and reduces synaptic neurotransmission in the gut (Ren *et al.*, 2003). Similarly, reduction in neuronal activity, specifically in sensory afferent neurons of the gut, has been found in $P2X3^{-/-}$ mice (Bian *et al.*, 2003), with other sensory neuron phenotypes also having been found dorsal root ganglia and nodose neurons (Zhong *et al.*, 2001) and in mechanosensory transduction in the bladder (Vlaskovska *et al.*, 2001), the latter study finding a resultant reduction in pelvic afferent nerve activity in response to release of ATP from a distended bladder. A double knockout of the heteromeric P2X2/P2X3 also displays deficiencies in sensory nerve activity (Cockayne *et al.*, 2005). P2X4 receptor ablation has revealed functions for the subunit in both neuronal and non-neuronal tissues, most notably in the hippocampus where it appears to be involved in long-term potentiation at Schaffer collateral synapses (Sim *et al.*, 2006) and longer term synaptic strengthening via NMDA receptors (Baxter *et al.*, 2011). Furthermore, a role for P2X4 in nitric oxide (NO)-dependent vasodilatation has been described based on the findings that $P2X4^{-/-}$ knockout mice display reduced NO production and increased blood pressure (Yamamoto *et al.*, 2006). A resultant feedback increase in vessel diameter following increased flow rate was also ablated. An observation that intraspinal administration of P2X4 antisense deoxyoligonucleotides attenuated the increase in P2X4 receptor expression that is normally seen following induction nerve injury provided the first evidence for the receptor's role in neuropathic pain (Tsuda *et al.*, 2003). Additionally, pharmacological inhibition of the receptor using trinitrophenol-ATP (TNP-ATP) or suramin by intrathecal administration mimicked the effects of receptor knockdown and also suppressed tactile allodynia after nerve

injury (Tsuda *et al.*, 2003). As with knockdown, an attenuation of tactile allodynia due to nerve injury was seen suggesting that P2X4 could represent an important target for neuropathic pain. Conversely, the introduction of microglia in which P2X4 receptors had been stimulated resulted in tactile allodynia in mice (Tsuda *et al.*, 2003). Interestingly, P2X4 receptor expression following spinal injury increases only in microglia expressed in the ipsilateral spinal cord. The use of $P2X4^{-/-}$ mice supports these findings and also demonstrates a dramatic reduction in pain threshold following peripheral nerve injury (Ulmann *et al.*, 2008; Tsuda *et al.*, 2009). Most recently, a disinhibition of pain pathways as a result of P2X4 receptor activation has been described in which P2X4-expressing microglia are stimulated ATP resulting in the release of brain-derived neurotropic factor (BDNF). In inflammation, P2X4 has been implicated in a number of tissues, including in vascular endothelium where stimulation of an inflammatory response by interferon-γ results in feed-forward activation of P2X4 receptor-mediated Ca^{2+} influx (Tang *et al.*, 2008) and in cyclooxygenase-2-dependent release of prostaglandin E2 in macrophages (Ulmann *et al.*, 2010).

Finally, multiple roles for the P2X7 subunit have been described ranging from in inflammatory responses, bone tissue and cancer. Using a $P2X7^{-/-}$ mouse line it has revealed the role for receptor in processing of IL-β in peritoneal macrophages and resultant induction of the cytokine cascade (Solle *et al.*, 2001). Another inflammatory role for P2X7 has been described in leukocytes where absence of the receptor blunts the leukocyte-specific inflammatory response (Labasi *et al.*, 2002), as well as in the accumulation of amyloid-β plaques, a known marker and cause of Alzheimer's disease (Sanz *et al.*, 2009). The P2X7 receptor has been further identified as being a key component of neuropathic and inflammatory pain (Chessell *et al.*, 2005) and cancer (Fu *et al.*, 2009). Other roles for P2X receptors have subsequently been described, including in sleep (Krueger *et al.*, 2010), bone formation and resorption (Ke *et al.*, 2003; Korcok *et al.*, 2004), Alzheimer's disease (Parvathenani *et al.*, 2003) and neuroinflammation (Choi *et al.*, 2007).

Despite the numerous roles for P2X receptors in humans, relatively few clinical trials have been performed on disease states in which this family of LGICs has been implicated. P2X7 has been the subject of two recent clinical trials, where antagonists of the receptor have been shown to provide no significant benefit over the treatment

of placebos or current treatments available for rheumatoid arthritis (Stock *et al.*, 2012; Keystone *et al.*, 2012). At the time of writing, three phase 2 clinical trials are recruiting to investigate the potential of a P2X3-specific antagonist (AF-219) in the treatment of patients with idiopathic or treatment-resistant chronic cough (Afferent Pharmaceuticals, 2012), osteoarthritis of the knee (Afferent Pharmaceuticals, 2013a), and interstitial cystitis/bladder pain syndrome (Afferent Pharmaceuticals, 2013b). It is hoped that the recent publications of a crystal structure for a P2X receptor (Kawate *et al.*, 2009; Hattori and Gouaux, 2012) will aid in the development of specific agonists and antagonists for the treatment of diseases involving P2X receptors.

1.5 PHYLOGENY OF P2X RECEPTORS

Purines have been found to elicit responses in organisms throughout the prokaryotic and eukaryotic domains, from single-cell bacteria, protists and amoeba, to higher mammals and members of the Plantae kingdom. This has led some to suggest that ATP and other purines constitute one of the most primordial signalling molecules throughout the Animal and Plant kingdoms (Burnstock, 1996; Fountain and Burnstock, 2009). Despite many reports of the effects of purines in invertebrate organisms (reviewed in Burnstock, 1996; Fountain and Burnstock, 2009), Agboh and colleagues presented the first molecular evidence for a purinoceptor in this group of organisms in 2004 by cloning and characterising an ionotropic P2X receptor from the parasitic trematode *Schistosoma mansoni* (Agboh *et al.*, 2004). Since this first documentation of an invertebrate P2X receptor, further evidence for the early emergence of purinergic signalling was provided by the cloning of receptors from a number of organisms, including the social amoeba *Dictyostelium discoideum* (Fountain *et al.*, 2007), the tardigrade *Hypsibius dujardini* (Bavan *et al.*, 2008), and the snail *Lymnaea stagnalis* (Bavan *et al*., 2012). A physiological role for a P2X receptor has also been described from the planarian *Dugesia japonica* (Sakurai *et al*., 2012), although this homologue is yet to be pharmacologically characterised.

Understanding the molecular and physiological function of P2X receptors from invertebrate organisms has many potential ramifications in the purinergic field. Firstly, residues in evolutionarily early P2X receptors that are conserved through species in different phyla supports the hypothesis that these residues may contribute

to the key pharmacological properties found in P2X receptors and, as such, have been retained through evolution. As such, cloning and site-directed mutagenesis studies can aid greatly in our understanding of structure-function relationship for this class of receptors, particularly when combined with mutagenesis of conserved residues between higher organisms. Secondly, the reasons for the 'evolutionary flux' of purinergic receptors in a variety of species throughout the 'evolutionary tree' are unclear and determination of *in vivo* functions of P2X receptors from lower organisms will advance this area of purinergic research, and may also highlight the origins of known functions for P2X receptors in higher organisms. Conversely, functions that may not necessarily have been considered in higher organisms may be found. The increasing availability of genomic and transcriptomic databases in numerous species, has enabled us to identify putative homologues of P2X receptors in scientifically and clinically important organisms. Interestingly, using this approach has revealed that despite the presence of P2X receptors in many members of the Animal kingdom, certain organisms do not appear to possess P2X receptors. These include some members of the Insecta class of hexapods, such as *Anopheles gambiae* (mosquito), *Apis mellifera* (European honey bee) and *Drosophila melanogaster* (common fruit fly) (Littleton and Ganetzky, 2000), as well as the nematode *Caenorhabditis elegans* (Agboh *et al.*, 2004). Despite evidence for purinergic signalling in higher members of the Plantae kingdom and bacteria (Fountain and Burnstock 2009), P2X receptors are also seemingly absent from those that have had their genomes completely sequenced. Finally, purinergic signalling in clinically pertinent organisms may provide a novel avenue of treatment for certain conditions. For instance, the identification of a P2X receptor from the trematode *S. mansoni* may suggest a potential target for future treatment of schistosomiasis. Current treatment of the condition often uses the antiparasitic agent ivermectin - the sensitivity of this P2X receptor when expressed heterologously may suggest that this receptor is the target *in vivo*, but this is yet to be fully determined (Agboh *et al.*, 2004). Equally, the cloning of a P2X receptor from the cattle tick *Boophilus microplus* (Bavan *et al.*, 2011) could also represent a new target for the treatment of tickborne disease although Bavan and colleagues found that ivermectin did not potentiate ATP-induced currents in the receptor when expressed in *Xenopus* oocytes, despite the compound's use in the treatment of tick infestation in humans and other mammals (Bavan *et al.*, 2011). A role for a P2X receptor in the proliferation of multipotent stem cells (neoblasts) of the planarian *Dugesia japonica* was proposed where the receptor is

responsible for suppression of neoblast proliferation, a unique role that was confirmed through the use of RNAi knockdown of the receptor *in vivo* (Sakurai *et al.*, 2012). Most recently, a P2X receptor has been cloned from the mollusc *Lymnaea stagnalis*, where mRNA appears to be ubiquitously expressed throughout the organism's CNS (Bavan *et al.*, 2012).

The purpose of the following sections is to describe briefly our current understanding of eukaryotic phylogeny, and the placement of P2X receptors within constituent phyla of this domain. Further consideration is given to roles for ATP in the Bacteria domain, within which P2X receptors appear to be absent.

1.6 EUKAYROTIC PHYLOGENY

The Eukaryota (= Eukarya) domain encompasses organisms whose cells possess both a nucleus and mitochondrion, and includes animals, plants, fungi, and protists. Formally, the Eukaryota are divided into six 'supergroups': Opisthokonta, Amoebozoa, Archaeplastida, Rhizaria, Chromalveolata, and Excavata. Eukaryotes can be further divided into the Amorphea (= Unikonta) (Animalia, Fungi, and Amobozoa), the Diphoretickes (plants (Archaeplastida) and other eukaryotes capable of photosynthesis), and the Stramenopile-Alveolata-Rhizaria (SAR) supergroup (Burki *et al.*, 2007) (Adl *et al.*, 2012). The Bilateria are a division the Animalia that display bilateral symmetry, and include humans, molluscs, and nematodes. The Cnidaria phylum is considered to be the most likely sister group to the Bilateria (Collins, 1998; Medina *et al.*, 2001) (Fig. 1.6).

The plants and excavates can be further grouped in a sister taxon to Unikonta, termed the Bikonta (Cavalier-Smith, 2002). Further groupings of these taxa are numerous, and include a formal division into the Holozoa (Ichthyosporea, Choanoflagellata, and Metazoa) (Lang *et al.*, 2002) and Holomycota (Nucleariids and Fungi) (Liu *et al.*, 2009b), which together form the Opistholonta (Cavalier-Smith, 1987; Wainright *et al.*, 1993) (Fig. 1.6). The Archaeplastida (Plantae *sensu lato*) includes the divisions Glaucophyta, Rhodophyta, and Chloroplastida (Adl *et al.*, 2005; Adl *et al*., 2012). Higher plants are placed within the Charophyta division of the Chlorplastida (within the Streptophyta ranking). The Excavata (Cavalier-Smith, 2002) are composed of six

phyla: Euglenozoa; Heterolobosea; Jakobea Preaxostyla; Fornicata; and Parabasalia (Adl *et al*., 2012). The phylogeny of the Malawimonas genus, composed of two known species (*M. californiana* and *M. jakobiformis*) is unclear, but is considered to be an excavate genus (Adl *et al*., 2012) (Fig. 1.6).

The 'mosaicism' of Eukaryota physiology and cellular biology has drawn much attention regarding the origins of this domain, which remains unresolved. Previous phylogenetic and phylogenomic analyses have suggested a number of positions from which eukaryotic lineages diverged and evolved from: within the Unikonta (Katz *et al.*, 2012); between the Unikonta and Bikonta (Derelle and Lang, 2012); between the Plantae (Archaeplastida) kingdom (Rogozin *et al.*, 2009); and within the Excavata (Cavalier-Smith, 2010; Cavalier-Smith *et al.*, 2014).

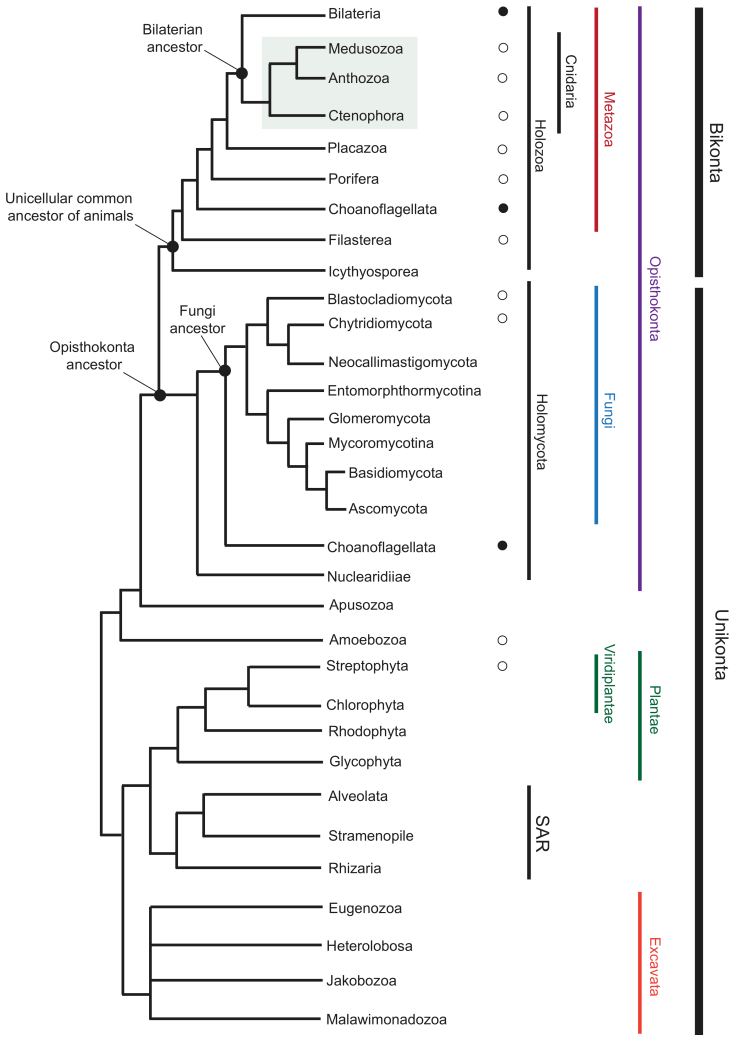

Fig. 1.6: cladogram illustrating extant Eukaryota phylogeny

The eukaryotes include a diverse number of taxa, including unicellular protists, algae, multicellular plants, and animals. The unrooted cladogram was drawn based on phylogenetic data combined from a number of sources, with a broad Bikonta-Unikonta division based on the guidelines posited by Adl *et al.* (2012). Metazoan phylogeny is adapted from Philippe *et al*. (2009) and Pick *et al.* (2010), with early metazoans taken from Ruiz-Trillo *et al.* (2007). The relationship between Ctenophora and Cnidaria is highlighted in green, referring to the Coelenterate hypothesis of divergence of these two phyla from a common ancestor. Fungi phylogeny is adapted from Ebersberger *et al*. (2012) and Gryganskyi *et al.* (2013), and broad Plantae kingdom phylogeny is based on the description summarised in Leliaert *et al.* (2012). Filled circles indicate taxa in which P2X receptors have been cloned, whilst empty circles indicate candidate P2X receptors that have been identified previously using homology searching and described in the literature.

1.6.1 The Animalia kingdom

The Animalia (= Metazoa) kingdom represents a large kingdom of eukaryotic, multicellular organisms and is comprised of five groups of vertebrates: mammals; amphibians; birds; reptiles and fish (further sub-divided into the superclasses of Osteichthyes (bony fish), Chrondrichthyes (sharks and rays), and Agnatha (jawless fish)). Forms of purinergic signalling have been demonstrated in all these groups with P2X receptors having been cloned from the bullfrog (*Rana catesbeiana*) (Jensik *et al.*, 2001), chicken (*Gallus gallus*) (Soto *et al.*, 2003; Fodor *et al.*, 2009; Bo *et al.*, 2000; Ruppelt *et al.*, 2001) and zebrafish (*Danio rerio*) (Egan *et al.*, 2000; Diaz-Hernandez *et al.*, 2002; Kucenas *et al.*, 2003). The availability of genomic data for a variety of species also enables the identification of putative P2X receptors in other vertebrate species, including Atlantic salmon (*Salmo salar*) (Davidson *et al.*, 2010) and the domestic dog (*Canis familiaris*) (Galliot and Quiquand, 2011). Although a P2X receptor has not yet been cloned from the Reptilia class a P2X receptor homologue appears to be present in the genome of the Carolina anole lizard (*Anolis carolinensis*) (Alföldi *et al.*, 2011).

Although descriptions of purinergic signalling has been described largely in vertebrate organisms (as members of the Deuterostome superphylum (Telford, 2006)), there is little description of it in the superphylum Ecdysozoa (Aguinaldo *et al.*, 1997). This superphylum, so named due to the periodic moulting (or 'ecdysis') found in members of all phyla within this group consists of: Arthropoda; Onychophora; Tardigrada; Kinorhyncha; Priopulida; Loricifera; Nematoda; and Nematomorpha. Arthropoda can be further subdivided into other subphyla from which P2X receptors have been cloned. From the Chelicerates (including mites, scorpions and ticks) and Crustacea (including lobsters, crabs and shrimps), a P2X receptor has been cloned from the *B. microplus* (Bavan *et al.*, 2011) and *D. pulex* (as described in the current thesis), respectively. However, an apparent absence of a P2X receptor homologue in the Hexapoda subphylum that is comprised of the large insect group of organisms represents a major peculiarity in our understanding of P2X receptor evolution (Fountain and Burnstock, 2009). It is not known whether P2X receptors are present in the Myriapoda (millipedes, centipedes and others) or indeed the Trilobita. The availability of a genome from a member of the Myriapoda may resolve this, although as the Trilobita subphylum is extinct, a complete understanding of P2X receptor

evolution in the Arthropoda will not be possible. Although it appears that many insects lack a gene homologous to known P2X receptor subunits, forms of purinergic signalling have been described in many species. The release of ATP from erythrocytes is known to stimulate the gorging process found in a number of haematophagus insects, such as the mosquito *Aedes aegypti* (Hosoi, 1958; Galun *et al.*, 1985) and the tsetse fly (Mitchell, 1976). Using electrophysiological recordings of the apical sensilla of mouthparts of haematophagus insects, the rank order of potency for purine compounds in *Culex pipiens* resembles most closely that of P2 type purinoceptors (ADP = ATP > β,γ-meATP >> AMP) but differs slightly in the related species *Culex inornata* (ADP > ATP > β,γ-meATP >> AMP) (Galun *et al.*, 1988). Further support for P2 subtype purinoceptors has been seen in the tsetse fly *G. palpalis* where the rank order of potency for purines is similar to that of P2Y receptors (Galun and Kabayo, 1988). In contrast, ATP-induced electrophysiological and gorging responses could be antagonised by arylazido aminopropionyl ATP ($ANAPP_3$), a photoaffinity analogue of adenosine 5'-triphosphate and P2 receptor antagonist in *in vivo* preparations (Hogaboom *et al.*, 1980; Fedan *et al.*, 1982), in the stable fly *Stomoxys calcitrans* (Ascoli-Christensen *et al.*, 1991). Furthermore, the rank order of potency for purines in *S. calcitrans* resembles that of a P2X receptor-type effector (ATP > ADP >AMP > adenosine) (Ascoli-Christensen *et al.*, 1991). At the behavioural level, when presented when a source of erythrocytes, ATP released into host blood plasma from damaged erythrocytes and platelets following wounding can induce the gorging process in a number of species. In certain species, ATP may be acting as a modulator of existing sensory units responsible for responding to NaCl, and mono- and disaccharide sugars such as in the common blowfly (*Pharmia regina*) whereupon ATP enhances taste neuron responses to glucose and sucrose but reduces responses to NaCl and fructose (Liscia, 1985). Interestingly, components of the ATP metabolism pathway have been cloned from members of the Insecta; apyrase has been cloned from the bed bug *Cimex lectularius* (Valenzuela *et al.*, 1998) and the cat flea *Ctenocephalides fleis* (Cheeseman, 1998). Additionally NTPDase6, an intracellular member of the E-NTPDase family of nucleotidase enzyme has been identified in *Drosophila melanogaster* (Knowles, 2009). Although P2 receptors appear to be absent in many higher members of the class Insecta, a P1 adenosine receptor has been cloned from *D. melanogaster* and is suggested to be involved in cAMP synthesis and the mobilisation of cytosolic Ca^{2+} (Dolezelova *et al.*, 2007)

1.6.2 The Plantae kingdom

Despite the apparent absence of P2X receptor gene homologues from the sequenced genomes of a number of higher plant species, including *Arabidopsis thaliana* (thale cress) (Arabidopsis Genome Initiative, 2000; Kim *et al.*, 2006), *Glycine max* (soybean) (Schmutz *et al.*, 2010) and *Solanum lycopersicum* (tomato) (Tomato Genome Consortium, 2012), purinergic signalling has been documented in many members of the Plantae kingdom. Ectopyrase enzymes are present in *A. thaliana*, particularly in regions of growth (root tips, for instance) (Wu *et al.*, 2007). A role for extracellular ATP and apyrase in growth of plant tissues has also been found in *Arabidopsis*, where a double knockout mutant of two apyrase enzyme genes (APY1 and APY2) results in inhibition of pollen germination (Steinebrunner *et al.*, 2003; Kim *et al.*, 2006) and disruption of plant growth (Wu *et al.*, 2007). A biphasic effect of purines in *Arabidopsis* on stromal function has also been demosntrated, where low concentrations of the synthetic purines adenosine 5'-[γ-thio]triphosphate (ATPγS) or adenosine 5'-[β-thio] diphosphate (ADP-β-S) induce stromal opening whilst higher concentrations inhibit it (Clark *et al.*, 2011).

A response of plants to stress analogous to that of the mammalian immune response involving P1- and P2-type receptors is known. As with many cell types, cell damage results in the uncontrolled release of ATP (Song *et al.*, 2006). Extracellular ATP can also induce a ROS-dependent response in wounding in *A. thaliana* which was mimicked by the purine nucleotides ADP, AMP, cytidine 5'-triphosphate (CTP), guanosine 5'-triphosphate (GTP) and UTP (Song *et al.*, 2006). Significantly, the development of an *Arabidopsis* mutant, *dorn1,* deficient in lectin receptor kinase I.9 has identified as DORN1 as an ATP receptor (Choi *et al.*, 2014). Calcium assays using *dorn1* mutant whole seedlings show decreased calcium responses to the extracellular application of numerous adenine nucleotides (including ATP), independent of exogenous abiotic and biotic stressors (Choi *et al.*, 2014). Furthermore, molecular cloning of DORN1 reveals that the receptor does not share a protein topology consistent with that of P2X receptors, leading the authors to define a new group of extracellular purine receptors termed 'P2K', with that termed $P2K_1$ constituting the founding member (Choi *et al.*, 2014).

1.6.3 Purinergic signalling in unicellular eukaryotes

Evidence for purinergic signalling in unicellular eukaryotes is relatively sparse, although a P2X receptor homologue has been cloned and characterised from *Ostreococcus tauri* (a green algae and the smallest known free-living eurkaryote) (Fountain *et al.*, 2008). Despite the successful expression of the coding region of the *O. tauri* P2X receptor gene (*Ot*P2X) in HEK293 cells, an *in vivo* functional role of *Ot*P2X (using sodium green to monitor ATP-induced Na^+ ion influx) could not be determined (Fountain *et al*., 2008). As a result, the role of this evolutionarily early P2X receptor *in vivo* remains unclear. The authors also reported the functional expression of a P2X receptor from the choanoflagellate *Monosiga brevicollis* but, as with *O. tauri*, its physiological role is yet to be determined (Fountain *et al.*, 2008). Analysis of the genomes of three basal fungi: *Allomyces macrogynus*; *Spizellomyces punctatus*; and *Batrachochytrium dendrobatidis* has further highlighted the presence of P2X homologues at the base of multicellularity (Ruiz-Trillo *et al.*, 2007; Cai, 2012). One potential role for P2X receptors (or indeed, metabotropic P2Y receptors) in algae could be in signalling in response to ATP release from wounds, as has been seen in *Acetabularis acetabulum* and *Dasycladus vermicularis* (Torres *et al.*, 2008), although whether a similar response is seen in algae that do, or appear to express, a P2X receptor homologue remains to be seen. Interestingly, P2X receptors are seemingly absent from the protist *Thecamonas trahens*, which raises questions as to the origins of P2X receptors in multicellular organisms due to its position as an ancestor to the Choanoflagellata (Ruiz-Trillo *et al.*, 2007).

1.6.4 P2X receptors in Amoebozoa

Within the Amoebozoa is a large group of organisms. In other motile Protozoa (which the Amoebozoa phylum), ATP has been demonstrated to elicit inhibitory effects on movement (Zimmerman *et al.*, 1958) and on the activity of the intracellular contractile vacuole in *Amoeba proteus* (Pothier *et al.*, 1987). Extracellular ATP can also cause cell membrane depolarisation of the amoeboid 'slime mould' *Dictyostelium discoideum*, as well as the influx of Ca^{2+} ions (Parish and Weibel, 1980). Importantly, this influx was inhibited by suramin, which was postulated by the authors to be negatively modulating Mg^{2+}-dependent ecto-ATPases. Fountain and

colleagues demonstrated the expression of one of five P2X receptor homologues in the contractile vacuole of *D. discoideum* (AX4 strain), an organelle involved in osmoregulation under conditions of hyposmostic stress (Fountain *et al.*, 2007). Disruption of this *p2xA* gene by homologous recombination resulted in cells unable to respond to hyposmotic conditions by a regulatory volume decrease. In contrast, Ludlow *et al.*, 2008 have provided evidence that deletion of all five P2X receptor paralogues in the AX2 strain of *D. discoideum* does not have any detrimental effect on its ability to osmoregulate, despite its similar expression in contractile vacuoles. When expressed heterologously, the AX4 *Dd*P2XA receptor (Fountain *et al.*, 2007) and AX2 *Dd*P2XA, *Dd*P2XB and *Dd*P2XE paralogues but not P2XC and P2XD (Ludlow *et al.*, 2009), form ATP-gated ion channels. As in mammalian homologues, these receptors respond in a concentration-dependent manner to extracellular ATP and are insensitive to other nucleotides, such as ADP, CTP, UTP or cAMP. However, in HEK293 cells, the ATP analogue β,γ-imidoATP was ten times more potent than ATP at *Dd*P2XA (AX2 strain) (Fountain *et al.*, 2007), and an analogous effect was seen at the *Dd*P2XB paralogue from the AX4 strain when expressed in *Xenopus* oocytes (Ludlow *et al.,* 2009). An apparent 'functional redundancy' in some *Dd*P2X receptors when expressed in *Xenopus* oocytes and HEK293 cells was recently challenged by modulation of extracellular and intracellular ionic conditions to better reflect conditions seen inside the *Dictyostelium* acid, K^+-rich contractile vacuole (Baines *et al.*, 2013). In the Na^+-rich external (Na^+_o-rich)/K^+-rich internal (K^+_i-rich) conditions employed by Fountain *et al.* (2007) and K^+_o-rich conditions of Ludlow *et al*. (2009) in which, of the five *DdP2X* paralogues A, B and E gave robust currents in response to ATP. However Baines *et al*. (2013) have now demonstrated that recording ATP-induced currents through *Dd*P2X receptor channels expressed in HEK293 cells under bi-ionic K^+ conditions with the intracellular pipette solution acidified to pH 6.2 from 7.3 increases the sensitivity of *Dd*P2XA, B, D and E to ATP. Although *Dd*P2XC was expressed at the HEK293 membrane surface (as illustrated through bioitinylation studies) it was not activated by ATP in any ionic condition tested (Baines *et al.*, 2013). These combined data show that *Dictyostelium* posess at least one functional P2X receptor that is adapted to the ionic conditions of the intracellular contractile vacuole. Although it appears that the function described in one strain of *Dictyostelium* may not be conserved across strains, investigation of an intracellular role of a P2X receptor in a mammalian system may identify a novel clinical target.

Recently, it has emerged that the phenotypic differences between the AX2 and AX4 strains in hypotonic conditions arises from a reduced release of Ca^{2+} ions from the intracellular contractile vacuole following exposure to ATP (Sivaramakrishnan and Fountain, 2012a), suggesting that P2X receptor-mediated Ca^{2+} release as a mechanism underlying regulatory volume decrease is redundant in the AX2 strain.

1.6.5 The Bacteria kingdom

Despite the apparent absence of P2X receptors in the genome of many single-celled organisms, including Bacteria (Blattner *et al.*, 1997), there is substantial evidence for roles of purines and pyrimidines in a variety of processes. Effects include the inhibition of spore germination in *Streptomysces gailaeus* when exposed to nucleoside polyphosphates such as adenosine-5'-triphosphate-3'-diphosphate (pppApp) (Hamagishi *et al.*, 1980) and the stimulation of growth and differentiation in *Streptomyces coelicolor* (A3 strain) by both ATP and its analogues (Li *et al.*, 2008). Interestingly, the effects seen in *S. coelicolor* A3 are biphasic, with a lower ATP concentration of 10 μM stimulating growth, whilst a higher concentration of 100 μM retards growth. Despite this evidence and further evidence across other members of this vast kingdom, the exact nature of purinergic signalling in bacteria remains elusive, although authors have suggested that ATP-binding domains in F- and P-type ATPases in *Thermophilae bacillus* PC3 and other species (Kato *et al.*, 2007; Hakansson, 2009) may represent an ancestral origin for an ATP receptor in single-celled organisms (Burnstock and Verkhratsky, 2012).

1.7 HYDRA – A MEMBER OF THE EARLY METAZOAN CNIDARIA PHYLUM

The current thesis presents data from the identification, cloning and pharmacological characterisation of P2X receptors in the cnidarian *Hydra vulgaris* (AEP). As such, a description of *Hydra* anatomy and physiology is useful.

The freshwater polyp *Hydra* was first described in the 18th century by the Dutch naturalist Anton van Leeuwenhoek in a letter to the Royal Society in 1702: "*[...] Further, I discovered a little animal whose body was at times long, at times drawn up*

short, and to the middle of whose body (where I imagined the undermost part of its belly was) a still lesser animalcule of the same make seemed to be fixed fast by its hinder end ..." (van Leeuwenhoek, 1702). In 1744, further studies of *Hydra* by the Swiss naturalist Abraham Trembley (published in his book "Mémoires pour server à l'histoire d;un genre de polypes d'eau douce, à bras en forme des cornes") (Trembley, 1744) revealed the capacity of *Hydra* to regenerate following bisection. Trembley also demonstrated that *Hydra* are able to regenerate a whole animal from a dissected piece of tissue and that this piece of tissue can also be grafted from one polyp to another (Trembley, 1744). In the mid-20th century, this apparently simple freshwater organism was studied further and has made an impact on numerous biological disciplines.

1.7.1 *Hydra* and its place in metazoan phylogeny

Hydra belong to the Cnidaria phylum that, besides the Porifera (sponges) and Ctenophora (comb jellies), represent the most basal group of metazoan animals in the evolutionary 'tree of life'. The Cnidaria are thought to have emerged at the time of the Cambrian explosion around 550 million years ago and contains four classes of organism: Cubozoa (box jellyfish); Scyphozoa (true jellyfish); Anthozoa (sea anemones and corals); and Hydrozoa (which includes *Hydra*). Although the majority of members of the Cnidaria phylum are marine, *Hydra* are unique in that they are inhabit freshwater ecosystems. Common and unique to all cnidarians are the eponymous cnidocytes (or nematocytes, as they are also known). These 'stinging cells' have a number of functions across the phylum, but are predominantly associated with prey capture. Molecular phylogenetics has provided considerable evidence to place cnidarians as a sister group to the bilatiera (Kim *et al.*, 1999; Medina *et al.*, 2001; Philippe *et al.*, 2009) and, as such, analysis of members of this phylum is of great use in the understanding of many shared bilaterian genomic and phenotypic traits. Within the Cnidaria, the Anthozoa are the most basal class, with the Hydrozoa constituting a sister group that appears to have diverged from the Anthozoa approximately 560 million years ago (Chen *et al.*, 2002). The Anthozoa, in contrast to the radially symmetrical Medusozoa (Scyphozoa, Cubozoa and Hydrozoa), display bilateral symmetry. The current thesis makes use of a laboratory strain of the *vulgaris* group of *Hydra* (*H. vulgaris* (AEP)), although three other species groups

exist (*braueri*, *viridissima* and *oligactis*) (Campbell, 1989; Kawaida *et al.*, 2010). Despite its nomenclature, *H. vulgaris* (AEP) has been phylogenetically closer to *H. carnea* and differs significantly in the morphology of its nematocysts (a phylum-defining structure) from the *vulgaris* species of *Hydra* (Hemmrich *et al.*, 2007).

1.7.2 *Hydra* as a model system

In the past 40 years molecular techniques have been married with previous knowledge of *Hydra* physiology. Within biology, *Hydra* has had a significant impact in a variety of different research areas. In the study of aging, the initial observation of an apparent lack of cell senescence in the 1950s (Brien, 1953) that *Hydra* do not seem to deteriorate or lose cellular integrity when surveyed over many years, in addition to a further study on mortality rates (Martinez, 1998) that corroborated these findings. Proponents of this theory have suggested though that, although when dividing asexually, *Hydra* display little (if any) senescence, but display a decrease in budding rate and the capacity of polyps to capture food following sexual differentiation (Yoshida *et al.*, 2006). The remarkable regenerative capacity of *Hydra* has also lent its use to the study of tissue morphogenesis and the induction of tissue growth in transplantation studies of section polyps (Galliot, 2012). The conserved features that govern multipotency in stem cell populations of multicellular organisms have also been the subject of numerous investigations in *Hydra* biology. In an initial analysis of gene homologues that govern multipotency in higher metazoans, *sox2* was identified as being present in the *H. vulgaris* (AEP) transcriptome genome but neither *nanog* or *oct3/4* were found (Hemmrich and Bosch, 2008). This poses interesting questions as to the origin of multipotency in higher organisms and, importantly, helps define this term at its most fundamental level; what are the basic components of "stemness" that enables its differentiation into multiple cell types. Finally there has been great recent interest in the study of the ancient origins of innate and acquired immune systems in the metazoan lineage. Animal epithelia are colonised by microbial communities; *Hydra* is no exception. Different species of *Hydra* have varying levels and composition of bacteria, with *H. vulgaris* harbouring a greater number of colonies compared to *H. oligactis* and many of them forming an endosymbiotic relationship with their cnidarian host (Fraune and Bosch, 2007). Further investigations have uncovered Toll-like receptors in *Hydra* (Franzenburg *et*

al., 2012) as well as the ability of *Hydra* secrete antimicrobial peptides from ectodermal epithelial cells to maintain bacterial numbers below those that would cause harm to the polyp (Jung *et al.*, 2009). These findings are rapidly developing *Hydra* as a model to investigate bacteria-host interactions in a more complex, experimentally tractable organism.

However in comparison to better-known model organisms, such as *Drosophila*, *Xenopus* and *C. elegans*, there are disadvantages in using *Hydra* in functional studies. For instance, despite having proved beneficial in the study of various biological processes in *Hydra*, the development of stable transgenic lines is a laborious process, taking many months with some lines (Wittlieb *et al.*, 2002; Boehm *et al.*, 2012; Franzenburg *et al.*, 2012).

1.7.3 General morphology of *Hydra*

Species of the freshwater polyp *Hydra* range from around 0.5 to 2 cm in length and display a relatively simple body plan (Fig. 1.8) consisting of a closed diploblastic body column with an oral-aboral axis with two epithelial cell layer (endodermal and ectodermal) separated by an acellular matrix called the mesoglea, secreted by both epithelial layers. This matrix is analogous to the basement membrane found underlying vertebrate cells and contains components found in an extracellular matrix (ECM), including major proteins such collagen, laminin and heparin sulphate proteoglycans (Sarras, 2012). The axis of a polyp can be divided into a distal 'head' region, consisting of a domed mouth (the hypostome) around which surrounds a ring of tentacles, and a body column which can be subdivided into a gastric region, budding region and the peduncle (moving successfully basal). Fully-grown, adult polyps typically have 4 to 6 tentacles and, at the peduncle, there is a basal disc that is considered to be the 'foot' of *Hydra*. This 'foot' can secrete a mucous from specialised ectodermal epithelial cells that allow the polyp to adhere to a substrate (Dübel *et al.*, 1987). Furthermore, a gas bubble can be formed at the foot, allowing the polyp to float to the water surface to be carried along in the prevailing water current (Łomnicki and Slobodkin, 1966). This behaviour has been suggested to occur in poorly fed or starved polyps and may constitute a method by which *Hydra* can

enter a new area of their habitat that may populated by a greater number of prey organisms (Łomnicki and Slobodkin, 1966).

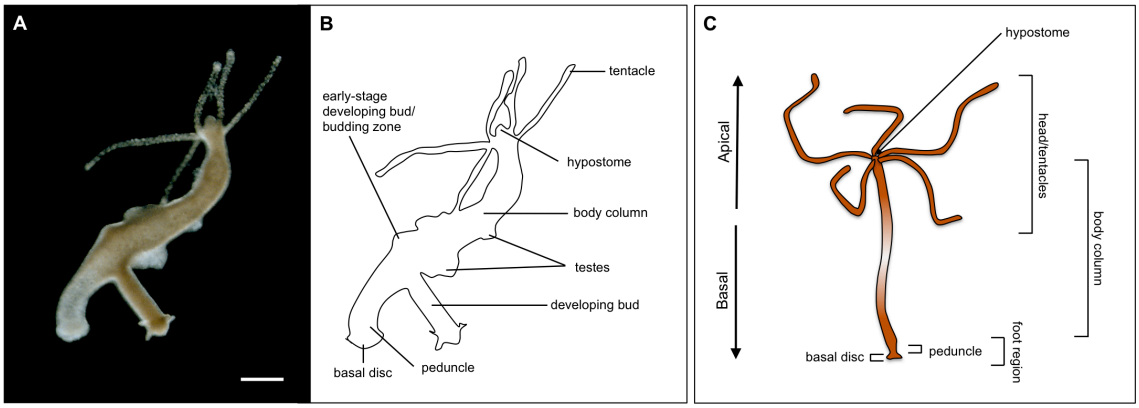

Fig. 1.7: gross morphology of *H. vulgaris* (AEP) polyp

***A*, *B*,** darkfield micrograph illustrating live *H. vulgaris* (AEP) polyp with asexual developing bud and testes. Major anatomical landmarks of polyp shown in A (scale bar = 1 mm) are illustrated in panel B. ***C*,** *Hydra* polyps display an axial body plan with tentacles and hypostome at the axial portion of the polyp and the anchoring foot region positioned basally.

1.7.4 Cell types of *Hydra*

Hydra have three main stem cell lineages: endodermal epithelial stem cells; ectodermal epithelial stem cells; and interstitial stem cells, all of which are capable of proliferation and self-renewal. These cells differentiate to form specific cell types within the polyp and often have defined spatial expression patterns.

1.7.4.1 Epithelial stem cells

Epithelial stem cells of *Hydra* are continuously proliferating by mitosis (Dübel *et al.*, 1987), generating a flow of cells in a distal (towards the head and tentacles) and proximal direction (towards the foot) regions of the polyp. Once at these terminal regions, cells are sloughed off and replaced by more epithelial cells. There are two forms of epithelial cells in *Hydra*: ectodermal and endodermal (Fig. 1.8), with ectodermal epithelial cells being responsible for osmoregulation (Prusch *et al.*, 1976) and endodermal epithelial cells used in digestion of ingested material by phago- or

pinocytosis. These endodermal epithelial cells possess two flagella to assist in digestion of food particles in the gastric cavity. Both endo- and ectodermal epithelial cell lineages have muscular protrusions at their apical (endodermal cells) or basal (ectodermal cells): these protrusions are essential for contraction of the polyp (Müller, 1950). The continual proliferation of epithelial cells in *Hydra* generates a flow of cells from its body column to the distal and proximal ends of the animal, as well as into its budding zone (Campbell, 1967; Otto and Campbell, 1977) where a new polyp is developing, with a mean cell cycle time of approximately three days (David and Campbell, 1972). Once at extremities, ectodermal epithelial cells can terminally differentiate into basal disc cells in the foot region of the polyp and 'battery cells' of the tentacles whereas endodermal epithelial cells can differentiate into tentacle endodermal cells and foot endodermal cells.

1.7.4.2 Interstitial stem cells and their derivatives

Interstitial stem cells ('I-cells') are multipotent stem cells that proliferate and differentiate continuously into many of the specialised cell types found in *Hydra*. They can either undergo germline differentiation in sperm or oocytes, or somatic differentiation into the specialised cells of *Hydra* (nematocytes, nerve cells, gland cells and gametes) (Campbell and David, 1974**;** David and Gierer, 1974; Bode *et al.*, 1976). Gland cells are present between endodermal epithelial cells (Fig. 1.8) and secrete proteolytic enzymes for digestion (Haynes and Burnett, 1963**;** Schmid and David, 1986). I-cells can be either large (occurring as single cells, pairs or in clusters of four) or small (clusters of eight or more) (David, 1973) (Fig 1.8) and are exclusively present in the body column/gastric region of a polyp in contiguous 'bunches' (Bosch and David, 1990) but absent from the foot and head regions of the animal (David and Plotnick, 1980). Although I-cells remain largely in the same position throughout the growth and development of a polyp, differentiating cells such as nematoblasts and neuroblasts seem to migrate rapidly to their final destinations (Bosch and David, 1990; Khalturin *et al.*, 2007).

Clusters of nematocyte precursors (nematoblasts) disperse into single cells that migrate rapidly (differentiating in the process) towards tentacles to become mounted as groups of 10-20 nematocytes in specialised tentacle-specific epithelial cells called

battery cells (David and Gierer, 1974; Campbell, 1987). Neuronal cell precursors (neuroblasts) give rise to nerve cells of two classes: ganglion cells and neurosensory cells (Davies, 1969, Davies, 1971). Ganglionic nerve cells are bi- or multipolar and form the diffuse nerve net of *Hydra* that lies throughout the polyp's body column and tentacles (Fig 1.9) whereas neurosensory cells are unipolar and are found in the body column. Following commitment to a neural cell lineage, half of the cells migrate towards the distal and proximal regions whereas the other half remains at their original position and are integrated into the polyp's diffuse nerve net (Bode and David, 1978; Heimfeld and Bode, 1985; Koizumi and Bode, 1986; Koizumi *et al.*, 1988; Koizumi *et al.*, 1989). Although the exact mechanisms underlying neural cell differentiation are not entirely clear, neuropeptides such as Hym-355 (Takahashi *et al.*, 2000; Takahashi *et al.*, 2009) and members of the FRFamide family of peptides (Hayakawa *et al.*, 2007) can modulate the patterning of neurons in *Hydra* species.

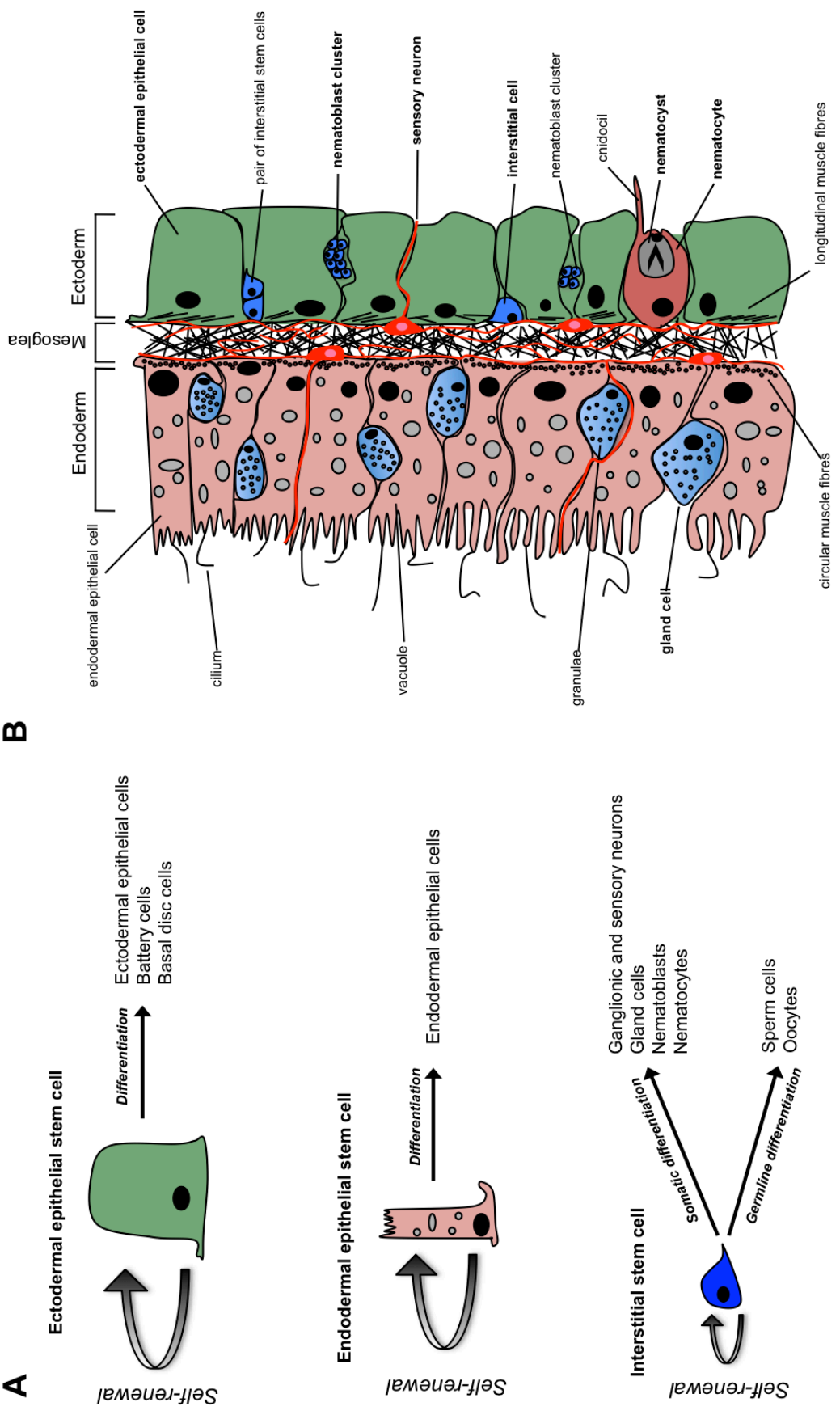
A
Ectodermal epithelial stem cell
Differentiation
Ectodermal epithelial cells
Battery cells
Basal disc cells
Self-renewal
Endodermal epithelial stem cell
Differentiation
Endodermal epithelial cells
Self-renewal
Interstitial stem cell
Somatic differentiation
Ganglionic and sensory neurons
Gland cells
Nematoblasts
Nematocytes
Germline differentiation
Sperm cells
Oocytes
Self-renewal
B
Ectoderm
Mesoglea
Endoderm
ectodermal epithelial cell
pair of interstitial stem cells
nematoblast cluster
sensory neuron
interstitial cell
nematoblast cluster
cnidocil
nematocyst
nematocyte
longitudinal muscle fibres
endodermal epithelial cell
cilium
vacuole
granulae
gland cell
circular muscle fibres

Fig. 1.8: stem cells in *Hydra* and schematic diagram of a cross-section of the two cell layers of a *Hydra* polyp body column

***A*,** endodermal and epithelial stem cells are capable of self-renewal with a population differentiating into epithelial cells that form the two layers of *Hydra*. Interstitial stem cells are also capable of self-renewal, but terminally differentiate into the specialised somatic or germline cells of *Hydra*. ***B*,** schematic cross-section of the inner endodermal and outer ectodermal epithelial layers in *Hydra* separated by the acellular mesoglea. Interspersed amongst the epithelial cells in both layers can be found the specialised cell types of *Hydra* derived from interstitial stem cells.

1.7.4.3 Nematocytes – a phylum-restricted cell type in the Cnidaria

Nematocysts are a defining feature of the Cnidarian phylum, required for prey capture, defence and locomotion; it is these organelle-derived structures that are the bane of swimmers who encounter marine jellyfish and come into contact with tentacles on which large numbers of nematocysts can be found. Nematocysts in hydrozoans can be found embedded in the apical surface of nematocytes (Figs 1.8 and 1.9), with the apical end of the nematocyst facing into the external environment. There are four types of nematocyst: stenoteles; desmonemes; atrichous isorhizas; holotrichous isorhizas, the former two of which are used in prey capture, and latter two are used in active locomotion (Chapman and Tilney, 1959a; Chapman and Tilney, 1959b). Of the nematocysts, stenoteles are the most morphologically striking. Undischarged they display an oval shape within which, under phase contrast microscopy, a 'style-like' object (the 'stylet') is present (Fig. 1.9). This stylet undergoes eversion following stimulation of its associated nematocyte, releasing the stylet along with the penetrating tubule with a distinctive barb that allows for penetration of prey at close range. This long (approximately 0.5 mm) and hollow tubule also enables the rapid delivery of toxin (Lotan *et al.*, 1995; Özbek *et al.*, 2009a) into the captured prey to render it immobilised. The atrichous isorhiza is used primarily for attachment to a substrate during locomotion and when discharged displays a tube devoid of spinules, whereas the holotrichous isorhiza does have a tube with spinules, but is largely used for defence. Finally, the desmonemes possess tubes that coil and wrap around prey upon discharge.

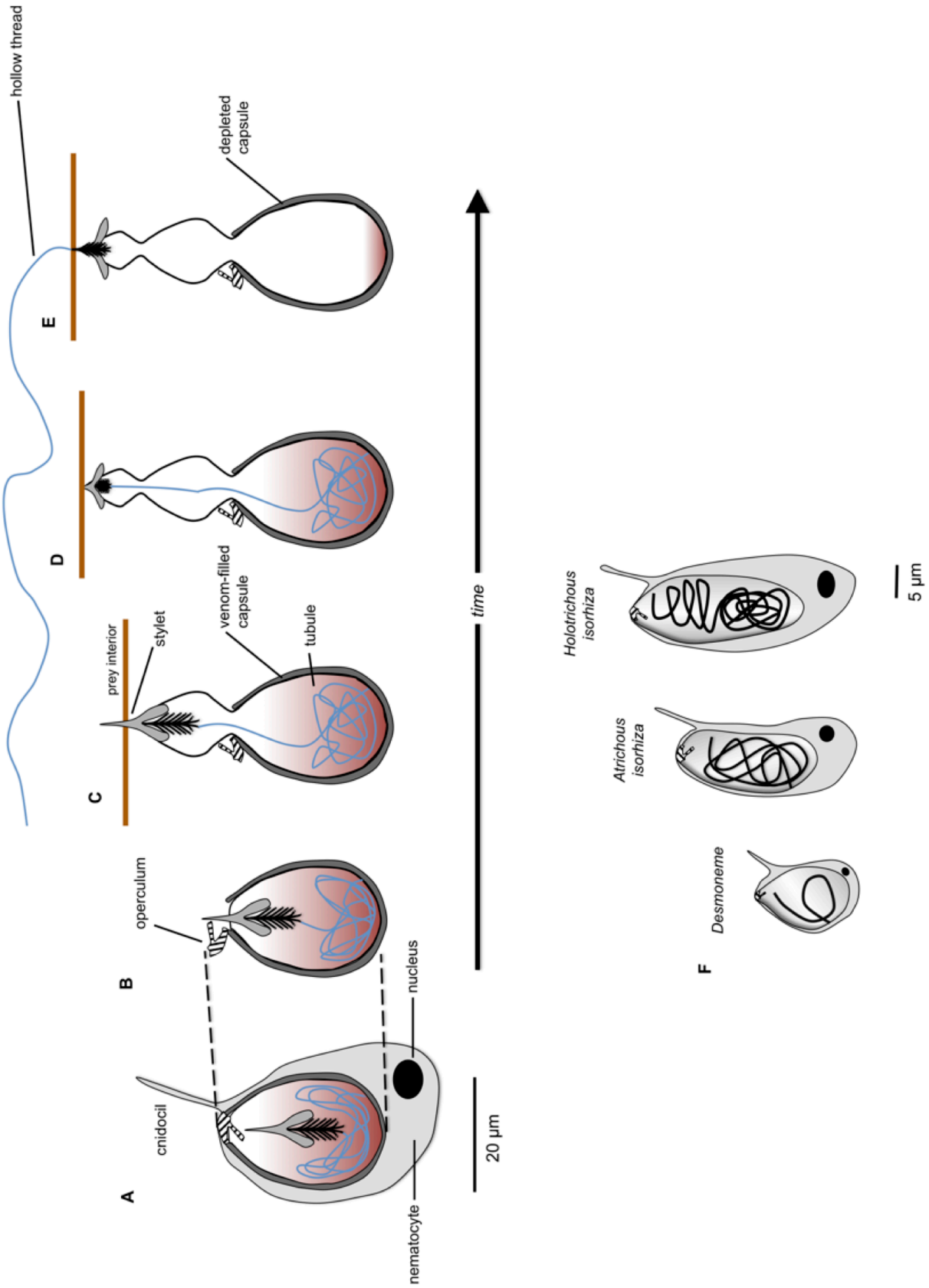
hollow thread
depleted capsule
E
D
venom-filled capsule
tubule
prey interior
stylet
C
operculum
B
cnidocil
nucleus
A
nematocyte
20 µm
time
Holotrichous isorhiza
Atrichous isorhiza
F
Desmoneme
5 µm

Fig. 1.9: schematic diagrams of the four types of nematocysts found in *Hydra* species

A, a stenotele nematocyst housed within a nematocyte cell. The operculum, contiguous with the nematocyst capsule, is situated at the apex of the capsule and opens in response to chemical and mechanical stimuli. The nematocyte cnidocil is exposed to the external environment and is responsible for transducing mechanical stimuli to operculum opening (***B***) and nematocyst firing (***C-E***). Operculum opening (***B***) results in the rapid eversion of the nematocyst capsule inner wall and exocytosis of the stylet (***B,C***). The impact and penetration of the stylet with the prey's exterior (***C***) surface is rapidly followed by the projection of the hollow thread/tubule that permits the transfer of venom contained with the nematocyst capsule to enter and immobilise the prey (***D***). In addition to stenotele nematocysts, *Hydra* also possess desmoneme, and atrichous and holotrichous isorhiza nematocysts (***F***) which are smaller in size and devoid of a barbed stylet.

The majority of nematocytes are found in the polyp tentacles (although a much reduced number can still be found in the body column) and can be regarded as mechano- or chemosensory neural cells (Hausmann and Holstein, 1985). I-cell-derived nematocyte precursors (nematoblasts) divide into clusters of 4, 8, 16 or 32, with the cells within these clusters connected by cytoplasmic bridges (David and Gierer, 1974). Following capsule formation, cell clusters break up and cells migrate towards the tentacles where they are engulfed by specialised ectodermal epithelial cells containing numerous nematocytes with their associated nematocysts and, in doing so, form the 'battery cells'. The nematocysts themselves are not cells, *per se* but are a product of a giant post-Golgi vesicle that forms within the nematocyte (Slautterback and Fawcett, 1959; Holstein, 1981). The nematocyst consists of an outer capsule with a double-layered wall that surrounds an inner matrix. A portion of the outer capsule is inverted and lies within the matrix, housing an inverted spiny tubule. During the five stages of nematocyst development, there is an early growth phase where vesicles are added to a large primordial capsule to form what will become the inverted tubule and stylet. Further addition of vesicles forms a continuous structure of the tubule wall and capsule wall, with the form structure become invaginated into the capsule. Condensation of the protein spinalin forms the distinctive spine structures on the stylet (Koch *et al.*, 1998), following which a final maturation phase occurs in which poly-γ-glutamate is synthesised within the capsule matrix. Two layers form the capsule wall, with the major component of the inner wall being very short mini-collagens of approximately 12-18 units (Kurz *et al.*, 1991) that polymerise to form an insoluble, high-strength layer (Engel *et al.*, 2001). The

outer layer consists primarily of another protein termed Nowa which provides the organisational cue for minicollagen assembly and forms disulphide bonds with the inner capsule minicollagens to stabilise the final nematocyst structure (Engel *et al.*, 2002). Recent analysis of the proteome of nematocysts of *Hydra magnipapillata* has also lead to the identification of Cnidoin, an outer wall protein thought to contribute to the high elastic energy stored in the nematocyst capsule, allowing the rapid discharge of the inner stylet (Balasubramanian *et al.*, 2012).

Nematocyst development proceeds the division of I-cells into nematocytes in the body column. It is understood that I-cells undergo five cycles of synchronous cell divisions, developing into mature nematocytes within about 5 to 7 (for desmonemes and isorhizas nematocysts) or 7 to 8 (for stenoteles nematocysts) days (David and Gierer, 1974). Once mature, nematocytes migrate to the ectoderm of their final position whether it be the body column of the polyp or, more frequently and in greater number, to the ectoderm of the polyp's tentacles. An elegant study by Jakob Weber using TRITC (Tetramethyl Rhodamine Iso-Thiocyanate) labeling of nematocysts *in vivo* has shown that, once mature, desmoneme nematocytes migrate immediately to the tentacles and have a rapid turnover rate of only 0.5 day before being replaced by new ones (Weber, 1995). Atrichous isorhiza nematocytes appear to behave similarly to desmonemes, but are difficult to observe *in vivo* due to their relatively low number. Holotrichous isorhiza nematocytes are largely found in the body column, but do not have the capacity to migrate to the tentacles until much later (approximately 10 to 15 hours post-maturation). Finally, in contrast to the rapid mounting of the other nematocytes, stenotele nematocytes are not mounted in the tentacles until approximately 2 days post-maturation; this may be reflective of the greater degree of structural complexity seen in the nematocysts that may require longer to develop prior to their mounting. However, the turnover rate at which stenotele nemateocysts are replaced is much higher than other nematocysts, potentially indicative of either their greater use as a defence mechanism by *Hydra* (Weber, 1995).

Due to its distinctive morphology and size, the majority of studies investigating the development and function of nematocysts have focused on that of stenotele nematocysts. Exocytosis of the hollow tubule contained within nematocysts is an extremely rapid event due to the fascinating structure of these vesicles. Within the

nematocyst capsule is a 2M concentration of negative charges due to the presence of anionically charged poly-γ-glutamate (PGG) molecules in the capsule matrix (Weber, 1989; Weber, 1990) that bind cations and cause the osmotically-driven uptake of water. This high concentration of PGG within the capsule provides a constant internal osmotic pressure of approximately 12.5 MPa (Weber, 1989). This large internal pressure underpins the extreme forces that result upon stimulation of the nematocyte and the resultant exocytosis of the nematocyst stylet that penetrates the exoskeleton of near-passing prey. The capsule wall itself appears to display a large tensile strength with an estimated elasticity modulus of 1 GPa (Weber, 1989), which further provides support for the high internal osmotic pressure seen in nematocysts and prevents its structural deformation. Upon stimulation, the stylet is extruded at an acceleration in excess of 15,000,000 x *g* in 0.7 ns, with an estimated pressure of 7.7 GPa at the impact site due to the very small surface area at the tip of the pointed barb (Nüchter *et al.*, 2006). This force is sufficient to penetrate the thick cuticle of crustaceans (Tardent, 1995). Although it is clear that nematocyst exocytosis is a rapid event, the processes underlying the discharge of their contents are not so clear. Mechano- and chemosensory factors certainly appear to play a key role in nematocyst exocytosis with the cnidocil, a sensory apparatus situated on the apical surface of nematocytes, acting as a key orchestrator. The cnidocil is exposed to the external environment, and is therefore subject to a number of physical and chemical cues that may initiate exocytosis. In nematocytes of the Anthozoan *Aiptasia mutabilis*, deflection of the cnidocil leads to rapid discharge of the nematocyst which is Ca^{2+} ion-dependent, as demonstrated by blockage of putative voltage-gated Ca^{2+} channels on the nematocyte apical surface (Santoro and Salleo, 1991). It is widely accepted that a combination of the internal osmotic pressure and the high elastic energy stored within the nematocyst capsule contributes to the rapid discharge of the tubule (Szczepanek *et al.*, 2001; Özbek *et al.*, 2009a). The Ca^{2+}-dependence and voltage-dependence of nematocyst discharge has also been demonstrated not only in *Hydra* (Nüchter *et al.*, 2006; Gitter *et al.*, 1994), but also in the marine hydroid polyp *Stauridiosarsia producta* (Brinkmann *et al.*, 1996), leading many authors to suggest that mechanical stimulation of the cnidocil initiates a depolarizing action potential at the apical pole of the nematocyte which activates voltage-gated Ca^{2+} channels and subsequent Ca^{2+} into the cell. Further support for this hypothesis has been provided by the observation that depolarisation stimuli provided to excised tentacle preparations bathed in a reduced extracellular Ca^{2+} ion concentration environment

significantly delays nematocyst discharge, even to the point of inhibition (Nüchter *et al.*, 2006). Nervous control of nematocyst exocytosis has also been described in *Hydra* whereby ganglionic neuron axon projections link battery cell complexes. These associated axons express components of the phototransduction pathway in higher organisms, such as cyclic nucleotide-gated ion (CNG) channels and opsin, which was found to be expressed in axon projections that are in direct proximity to battery cell complexes (Plachetzki *et al.*, 2012). Furthermore, exposure of stenotele nematocytes to intense blue light (470 nm; 2.8 W/cm^2) appeared to reduce the propensity for firing suggesting of an inhibitory effect of intense light conditions that is neuronally modulated and could be reversed by inhibition of CNG channels by *cis*-diltiazem (Plachetzki *et al.*, 2012). Functionally this mechanism could serve as a "nematocyst saving mechanism". During the intense sunlight seen during the day when prey is scarce this mechanism would prevent the discharge of nematocysts unnecessarily. As such, low-light dusk or night time conditions when prey is more plentiful would release this light-induced inhibition and increase the chance of successful prey capture (Plachetzki *et al*., 2012).

The rapid discharge of the nematocyst is preceded by the opening of the operculum, which lies at the apical pole of the nematocyst (Fig. 1.9). The opening of the operculum is followed by the rapid ejection of the stylet process from within the capsule (Fig. 1.9), however the exact mechanism that causes this ejection is disputed. High-speed microcinematographical studies both in *in situ* preparations of *Hydra* tentacles (Robson, 1973; Holstein and Tardent, 1984) and isolated *Pelegia* nematocysts (Salleo *et al.*, 1986) suggest that the capsule volume increases immediately prior to evagination of its tubule followed by an approximately 40-50% decrease in volume following discharge (Tardent and Holstein, 1982; Holstein and Tardent, 1984). This volume change, thought to be as a result of the presence of poly-anionic PGG molecules within the capsule matrix (Szczepanek *et al.*, 2001) has been disputed by Berking and Hermann (2006) who have suggested that positive ions present within the matrix dissociate from the carboxyl groups of the PGG matrix after triggering of discharge. The electrostatic repulsion that occurs as a result of this dissociation creates a rapid pressure, and therefore volume, change (Berking and Hermann, 2006). This theory does not account for the initial increase in volume seen prior to discharge, but may provide a basis for *initiation* of discharge. From the current literature regarding the mechanics underlying nematocyst discharge, it is not

clear how stimulation of the anchoring nematocyte is coupled to expulsion of the nematocyst stylet.

1.7.5 The life cycle of Hydra

Hydra has the capacity to divide both sexually (through the development of oocytes and testes) and asexually (through the growth of new clonal polyps in the basal third of the body column of a larger mature polyp). This so-called 'budding region' can bear more than one polyp at a time, with the oldest polyp situated closest to the peduncle (Holstein *et al.*, 1991). The growth of a new polyp during the process of asexual proliferation involves the simultaneous evagination of endo- and ectodermal epithelial tissue by morphallaxis. This process, referred to as 'budding' is governed by the epithelial stem cell population of a polyp, as animals with no complement of interstitial stem cells are able to bud normally (Campbell, 1976; Sugiyama and Fujisawa, 1978). Under standard conditions where there is a plentiful food source, asexual reproduction is the predominant way by which *Hydra* proliferate. However, sexual reproduction is also possible. In higher metazoans, a separate germline exist but this does not appear to be the case in *Hydra* with the interstitial stem cell lineage giving rise to both somatic and germ cells (Bosch and David, 1987) – it is therefore the I-cell population that is responsible for the determination of the sexual phenotype of *Hydra* (Bosch and David, 1986). Indeed, analysis of differentiation products of the I-cell lineage in *H. oligactis* has revealed subpopulations of these stem cells that can only differentiate into sperm (Littlefield, 1985) and oocytes (Littlefield, 1991). The continual proliferation of stem cells within *Hydra* has lead some to suggest that this organism is "immortal" – the lack of cell senescence and mortality over a period of years in budding polyps has been the primary basis for this assumption (Martinez, 1998). This theory has been challenged by the finding that older polyps have a reduced capacity for prey capture, contraction and sexual reproduction (Yoshida *et al.*, 2006; Estep, 2010).

1.1.1 Purinergic signalling in Cnidaria and Ctenophora

There is relatively little evidence for purinergic signalling in Cnidaria (or indeed, the Ctenophora, which together were formerly classified as the Coelenterates). Adenosine, ADP and ATP have been illustrated to trigger circular muscle contraction in the pedal disc of *Actinia equina* with ATP displaying the greatest potency. However, synthetic analogues, such as α,β-meATP did not elicit an effect. Interestingly, the P2 receptor antagonist brilliant blue G (BBG) caused concentration-dependent contractions suggesting a form of negative modulation of P2 receptors under standard conditions (Hoyle *et al.*, 1989). In sea anemones, ATP enhances the repair of hair bundles, structures analogous to the vertebrate acousticolateralis system, following damage (Watson *et al.*, 1999). Although the authors postulated that ATP in this scenario is acting at ATPases, ATP appears to be stored and released from sensory neurons. In the comb jelly, ATP causes beating of ciliary structures most likely due to increasing the intracellular Ca^{2+} ion concentration as bathing comb jellies in Ca^{2+}-free artificial seawater causes reversal of ciliary movement (Nakamura and Tamm, 1985; Tamm and Tamm, 1989). Finally, in the Scyphozoan *Pelagia noctiluca* (a jellyfish commonly known as the mauve stinger due to its distinctive colouring), incubation of dissected tentacles in solutions of 0.1 or 1 mM ATP causes an increase in the number of discharged nematocytes in response to mechanical stimulation (Morabito *et al.*, 2012). Cyclic AMP (cAMP) also elicited a similar response at the same concentrations and moreover, depletion of Ca^{2+} ions in the bathing solution (in the absence of sensitising compounds) reduced the number of discharge nematocytes upon mechanical stimulation (Morabito *et al.*, 2012), hinting towards a potential role for ionotropic purinergic signalling in these cells in this phylum.

1.8 DAPHNIA PULEX – A MICROCRUSTACEAN AND TOXOLOGICAL MARKER

Daphnia are planktonic crustaceans 1 to 5 mm long (Fig. 1.12A) that filter-feed on small, suspended particles in a variety of freshwater ecosystems around the world (Ebert, 2005). The lifecycle of *Daphnia* is largely asexual during the growth season, with populations dividing by apomixis – offspring are formed without the need of meiosis or fertilisation, producing daughters that are genetic clones of the mothers.

During this lifecycle, females develop diploid parthenogenetic (amictic) eggs enclosed in a protective shell (the ephippia) in a dorsal brooding chamber following each moulting period, when the carapace is shed and replaced. These asexual eggs can develop either into female daphnids under optimal environmental conditions but develop into males when conditions are not optimal, such as in high density populations (Banta, 1919; Banta and Brown, 1929). The same females can also produce haploid eggs that require fertilisation by males. The genome of *D. pulex* ('The Chosen One' (TCO) strain) has been termed 'ecoresponsive' due to its ability to adapt to changes in its ecosystem (Colbourne *et al.*, 2011). Prior to the availability of this genome, one such change well described alteration in gene expression is the increase in haemoglobin production under hypoxic stress, resulting in a characteristic red colouration of *Daphnia* (Kimura *et al.*, 1999; Zeis *et al.*, 2003; Zeis *et al.*, 2009) (Fig. 1.11). Furthermore, ad been illustrated in daphnids inhabiting ecosystems with high (up to 5 M) salt concentrations (termed 'halophilic' daphnids). In contrast to similar organisms inhabiting freshwater environments, halophilic daphnids display a greater rate of molecular evolution as evidenced by an increased rate of sequence changes in nucleotide insertions and deletions in nuclear and mitochondrial genomes and several ribosomal RNA (rRNA) genes (Hebert *et al.*, 2002).

Fig. 1.10: hypoxia-induced increase in haemoglobin gene transcription in *Daphnia*

Two *D. magna* specimens cultured under laboratory conditions in normoxic and hypoxic environments. As an adaptation to low pO_2, the right daphnid displays a greater level of haemoglobin in its haemolymph as seen by an increase in red colouration. Image taken from Colbourne *et al.* (2011), under license from The American Association for the Advancement of Science (AAAS).

Crustacea appear to be the closest major clade to the much large Insecta class (Nardi *et al.*, 2003). Indeed, further phylogenetic analysis has confirmed previous paleontological (Briggs and Fortey, 1989) and comparative morphological/developmental studies (Cook *et al.*, 2001; Duman-Scheel and Patel, 1999; Emerson and Schram, 1997) placing Crustacea as sister group to the Insecta (Meusemann *et al.*, 2010; Regier *et al.*, 2010) raises interesting questions as to the origin of purinergic signalling in pancrustacean lineage. As discussed in previous sections, no P2X receptor has yet been identified or cloned from genomic or transcriptomic data derived from members of the Insecta class. Investigation of P2X gene homologues present in the Crustacea may provide insights as to the loss of this gene family in Insecta.

1.8.1 Purinergic signalling in Crustacea

Crustacea is a large subphylum within the Arthropoda phylum and includes primarily aquatic (both freshwater and marine) organisms such as crabs, crayfish and barnacles. Purinergic signalling in this subphylum is well-documented, particularly in regards to olfaction and gustation in the spiny lobster (Carr *et al.*, 1986; Zimmer-Faust *et al.*, 1988). Receptors for AMP, ADP and ATP are present on chemosensitive neurons present in sensilla of external antennules. Spiny lobsters are known to be scavenger feeders and it is these purinergic chemoreceptors that have been suggested to act as effectors for ATP released from recently deceased prey tissue (Zimmer-Faust *et al.*, 1988). Although the order of potency for purines in some sensilla is suggestive of the presence of P1 type purinoceptors (Carr *et al.*, 1986; Carr *et al.*, 1987), the activation of receptors by ATP analogues such as α,β-meATP also suggests an involvement of P2 type purinoceptors (Carr *et al.*, 1986; Zimmer-Faust *et al.*, 1988). Whilst ATP can act as a stimulant for lobsters, AMP has been demonstrated to elicit an inhibitory effect on some lobster species. As AMP is a breakdown product of ATP, this may serve to direct lobsters towards only the most recently deceased prey (Gleeson *et al.*, 1989; Zimmer-Faust *et al.*, 1988).

1.9 TRICHOPLAX – AN EARLY DIVERGING METAZOAN

In addition to the data presented in the current thesis regarding the cloning and characterisation of P2X receptors in *Hydra* and *Daphnia*, an initial study on P2X receptor genes in the placazoan *Trichoplax adhaerens* was also performed.

Trichoplax is an enigmatic organism that has been found in various tropical and subtropical marine environments. Despite their broad geographical distribution, only one member of the Placazoa phylum has been described to date; *T. adhaerens* (Schulze, 1883). However genetic diversity amongst specimens of the apparent same species is great, suggesting that there may be underlying species differences that may not necessarily manifest as a morphological difference (Srivastava *et al.*, 2008). *Trichoplax* appear as small (2-3 mm diameter) flat discs (fig 1.12B) consisting of two epithelial cell layers that 'sandwich' multinucleate fibre cells (Smith *et al.*, 2014). Only four somatic cell types have been described so far; upper and lower epithelial cells; gland cells; and contractile fibre cells. Sensory cells, nerve cells and muscle cells are absent from *Trichoplax* (Srivastava *et al.*, 2008; Smith *et al.*, 2014).

The Placazoa phylum has been the subject of much controversy regarding its place in the phylogenetic 'tree of life'. Initial studies suggested that they were closely related to Cnidarians (Bridge *et al.*, 1992) but analyses of ribosomal RNA units have placed the phylum as a sister group to the Bilateria (Collins, 1998) or as an earlier branch to the origin of Bilateria (da Silva *et al.*, 2006). The publication of the ca. 98 Mbp genome of *T. adhaerens* has sought to clarify the position of placazoans and agrees with the finding that this phylum is to be placed as a sister group to the Bilateria and the Cnidaria (Srivastava *et al.*, 2008). Although a number of P2X receptors have been cloned from multicellular organisms close to the base of the 'tree of life, including those discussed herein, investigation of P2X receptors from the Placazoa phylum will give a further dimension to the field, extending our knowledge of the penetrance of P2X receptors in evolution and the origin of established role in higher organisms.

1.10 AMPHIOXUS – A MODERN PROXY OF AN EARLY CHORDATE

Amphioxus ('lancelets') are small (5-7 cm), jawless worm-like organisms (Fig. 1.11C) found in temperate to tropical marine habitats (Putnam *et al.*, 2008). Their importance as a model organism comes from their sharing a number of features with higher vertebrates. The Russian embryologist Alexander described the remarkable similarities between amphioxus and higher vertebrates and tunicates (a subphylum of the bilaterian Chorata phylum), including the shared hollow neural tube and the more ventral notochord as well as the shared development of segmented muscle (Kowalevsky, 1866). Tunicates, vertebrates and lancelets together constitute the subphylum Cephalochordata, which is believed to share a common ancestor of the vertebrate phenotype that first arose over 500 million years ago (Putnam *et al.*, 2008). Owing to similarities between modern lancelets and putative Cambrian period chordate fossils, lancelets are considered to be a modern representative of the early chordates. The shared developmental timepoints between *Branchiostoma* and other lancelets, such as the development of the pancreas, pituitary gland and brain have helped shed light on the same organs in higher vertebrates. In addition, genomic studies into the evolutionary origins of genes involved in establishment of a body plan in vertebrates, such as the *Hox* gene cluster (Garcia-Fernàndez and Holland, 1994), as well as in the mechanisms involved in early embryonic patterning (reviewed in Yu *et al.*, 2007).

The publication of the genome of *Branchiostoma floridae* (Putnam *et al.*, 2008) allows researchers to identify candidate genes for further analysis. The 'proto-vertebrate' phenotype of lancelets is an intriguing feature in the study of the early origins of purinergic signalling when considering the multiple neuronal functions of ionotropic signalling. As such investigation of channel-mediated ionotropic signalling may represent a potential model for understanding early P2X receptor signalling in the chordate lineage.

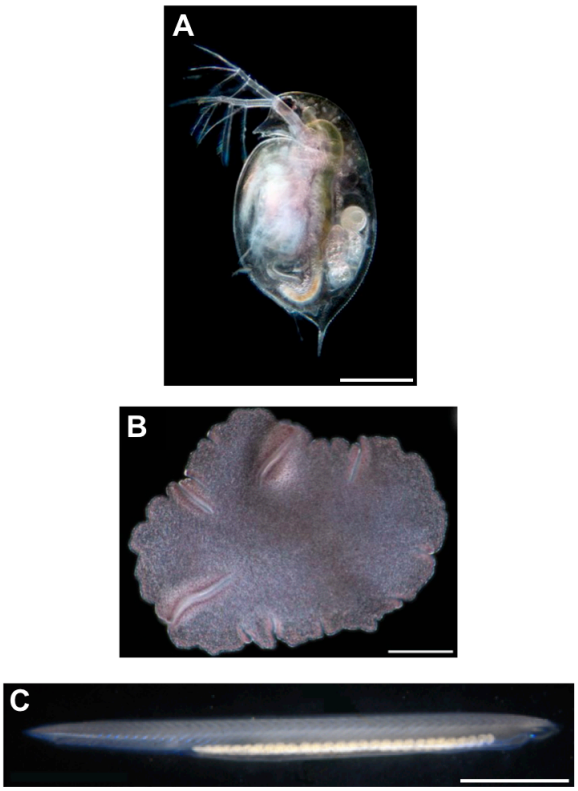

Fig. 1.11: Darkfield micrographs of *Daphnia*, *Trichoplax* and *Branchiostoma*

Darkfield images of organisms that, although discussed as part of the current thesis are not the major focus. **A**, The antero-posterior oriented gut, filled with green algae, is visible in this *D. pulex* (TCO strain) specimen (scale bar = 0.5 mm), as are developing eggs in the rostral brooding chamber. The head is situated ventral to the anterior portion of the gut. **B**, *T. adhaerens* appears as a flat, amoeboid-like disc (scale bar = 1 mm). **C**, The striated muscle segments that lie at the dorsal (top) view of *B. floridae* are clearly visible as well as the pharynx, which appears as a segmented organ in the ventral region. The specimen shown in C is in a caudal-rostral position from left to right (scale bar = 1 mm). Images are taken from: (A), http://genome.jgi-psf.org/Dappu1/Dappu1.home.html (B), Srivastava *et al.* (2008), under license from Nature Publishing Group; (C), http://genome.jgi-psf.org/Brafl1/Brafl1.home.html.

1.11 AIMS OF THE THESIS

Broadly, the aim of the current thesis is to expand our understanding of invertebrate ionotropic signalling via P2X receptors.

1. BLAST homology searching of a number of eukaryotic and prokaryotic genomic and transcriptomic datasets will be performed in order to gain a greater understanding of the predicted expression of P2X receptors within these groups of organisms. Furthermore, the level of conservation of key

motifs and residues known to be important in the function of previous characterized P2X receptor will also be assessed within the primary protein sequences of 'candidate' P2X receptors These aims form the basis of chapter 3.

2. To select and clone a number of candidate P2X receptors, chosen on the basis of the experimental tractability of the organisms within which they are expressed, and their and position within eukaryote phylogeny. This aim forms the basis of chapters 4 and 5.
3. To pharmacologically characterise cloned P2X receptors from the cnidarian *Hydra vulgaris* (AEP), the crustacean *Daphnia pulex*, and the placazoan *Trichoplax adhaerens*. This aim forms the basis of part of chapter 4
4. To examine the expression of a P2X receptor from *H. vulgaris* (AEP) using a whole-mount immunohistochemistry, with a view to hypothesise a potential role for this cnidarian P2X receptor *in vivo*. This aims forms the basis of part of chapter 4

Chapter 2:

Materials and Methods

2 Materials and Methods

2.1 SOLUTIONS AND REAGENTS

Unless otherwise indicated, general reagents were purchased from Fisher Scientific UK Ltd (Loughborough, Leicestershire, UK) and molecular biology reagents were obtained from Life Technologies Ltd (Paisley, Scotland, UK). Purinergic receptor-modulating compounds used in electrophysiological analysis were purchased from Sigma-Aldrich (Poole, Dorset, UK) and were of minimum 99% purity.

In applications requiring in excess of 10 ml of nuclease-free water, double-distilled water (dH_2O) was treated with diethylpyrocarbonate (DEPC) at a concentration of 0.1% (v/v). DEPC covalently modifies histidine, lysine, cysteine and tyrosine residues, rendering protein structures (most importantly in this scenario, DNases and RNases) inactive (Mantiatis *et al.*, 1982). Water containing DEPC was incubated overnight at room temperature (RT) (or for a minimum of 2 hours at 37 °C) and autoclaved to remove the DEPC before use.

2.2 BIOINFORMATIC ANALYSIS

A number of bioinformatics techniques were used in the current study to identify candidate P2X receptor sequences in a range of organisms, analyse retrieved primary protein sequences, and determine the predicted protein topology of retrieved sequences. Major steps in the retrieval and analysis of candidate P2X receptor nucleotide and proteins sequences are detailed in Fig. 2.1.

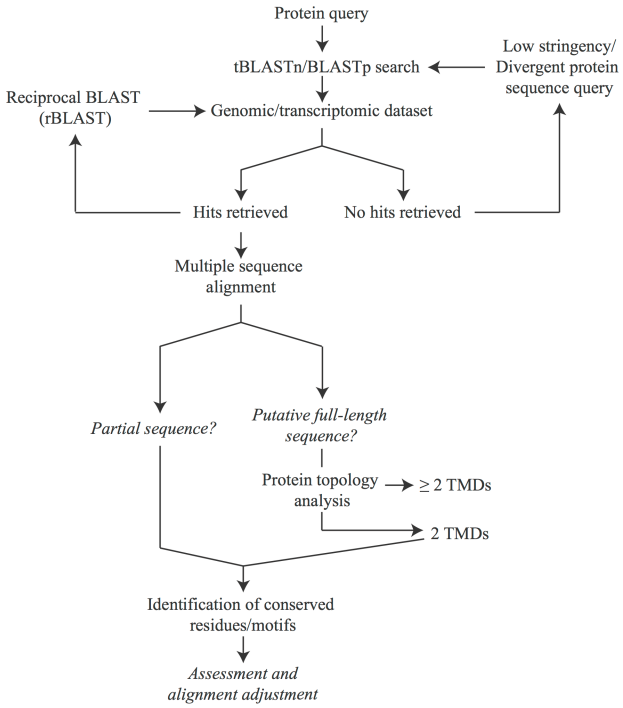

Fig. 2.1: flow diagram illustrating steps underlying bioinformatic analyses detailed in chapter 3

A number of criteria were used during the course of the current study in the assessment of retrieved hits following homology/BLAST searches of available genomic and transcriptomic datasets. Following sequence retrieval, a number of post-retrieval techniques were used during the study to assess conserved amino acid residues of putative P2X receptors from a range of phyla. Assessment of retrieved protein sequences includes the analysis of protein topology and conservation of residues and motifs known to be required for activation and modulation of higher P2X receptors.

2.2.1 Homology searching of genomic and transcriptomic sequence databases

Full-length amino acid sequences of cloned receptors were retrieved from either NCBI or the Universal Protein Resources (UniProt) database (Bairoch *et al.*, 2005), unless otherwise stated. Of these sequences, human P2X4 (hP2X4; Q99571) and *D. dictyostelium* P2XA (*Dd*P2XA; Q86JM7) were typically used as queries in tBLASTn, BLASTp, or BLAT (Kent, 2002) homology searches, as appropriate to the subject database.

Retrieved hits were annotated according to the Latin naming of the organism investigated, in order of Expect-value (*E*-value), with sequences believed to represent

a candidate P2X receptor are annotated as '_p2x'. For instance, a candidate P2X receptor from the sponge *Amphimedon queenslandica* would be annotated as '*Aqu*_p2x'. Species in which multiple, unique candidate P2X receptors were identified are distinguished from each other according to the form '*Aqu*_p2xA; *Aqu*_p2xB, etc.'.

The 'Basic Local Alignment Search Tool' (BLAST) was used to identify homologous gene, transcript and protein sequences in a number of genomic and transcriptomic datasets. BLAST databases are available for many species, with many genomes made publically accessible via the National Center for Biological Institute (NCBI)/GenBank (Benson *et al.*, 2014). Species searched, the phylum to which they belong, and the database at which genomic or transcriptomic data was maintained are provided in the Appendix (Table A1). Primary amino acid sequences of cloned and pharmacologically characterized P2X receptors used in multiple sequence alignment are provided in the Appendix (Table #). Both *E-value* and score were and taken into consideration when performing BLAST searches, with high scoring segment pairs (HSPs) with a low *E*-value and high score considered to be most probably P2X receptor homologues.

BLAST searches were performed using a BLOSUM62 and default word size of 3. Amino acid sequences were used as queries in BLAST searches, against a nucleotide sequence database (translated in all six frames) (tBLASTn), predicted protein database (BLASTp). In the event of no homologous sequence being identified in a database (termed 'hits'), a second BLAST search was performed using *Dd*P2XA as a query due to its low sequence homology. Furthermore, a lower stringency BLOSUM45 matrix could also be used (with a word size of 2) to also aid in the identification of divergent P2X receptor homologues. Hits with an *E*-value ≤1e-3 were retrieved for further analysis. Reciprocal BLAST (rBLAST) searches were performed for some organisms to confirm the orthology of retrieved sequences with mammalian P2X receptor subunits (i.e. that identified sequences diverged after a speciation event – a similar P2X receptor sequence in a different organism that has likely retained its function (Moreno-Hagelsieb and Latimer, 2008)). The quality of the database was also considered during bioinformatics analysis of sequence data, with draft genomes assembled from whole genome shotgun (WGS) sequencing techniques often of lower quality in eukaryotic genomes.

To ensure fidelity of retrieved hits during homology searching of databases, strict criteria were employed in the assessment of retrieved sequences before subsequent inclusion in further analysis. The topology of P2X receptors includes two TMDs, a large ECD and two intracellular termini. For further analysis, sequences must include these regions. In cases where only a portion of this topology appeared to be present, sequences were assessed and regions with significant homology with described P2X receptors included in primary sequence alignment, where appropriate.

2.2.2 Multiple sequence alignment of primary amino acid sequences

Retrieved amino acid sequences were typically aligned using the 'MUltiple Sequence Comparison by Log-Expectation' (MUSCLE) algorithm (Edgar, 2004) and the MacVector sequence analysis program (MacVector, Inc., Cary, NC, USA). The MUSCLE algorithm was chosen over more established alignment algorithms such as ClustalW (Chenna *et al.*, 2003) due to its increased accuracy and speed. For MUSCLE alignment, a maximum number of 16 iterations were considered using a log-expectation profile. The T-Coffee ('Tree-based Consistency Objective Function For alignment Evaluation') (Notredame *et al.*, 2000) algorithm was preferred over MUSCLE in some instances due to its increased accuracy in the aligning shorter fragments to longer sequences. For T-Coffee alignments, standard gap open and gap extension probabilities of -50 were used. Multiple sequence alignments (MSAs) were adjusted by eye when clear misalignments arose. For MSA of retrieved amino acid sequences of cloned P2X receptors, publically available primary full-length amino acid sequences were retrieved from a number of sources, and are detailed in the Table 2.1.

Receptor	Accession ID	Source	Reference
Human P2X1	P51575	UniProt	Valera *et al.*, 1994
Human P2X2 (isoform A)	Q9UBL9	UniProt	Lynch *et al.*, 1999
Human P2X3	P56373	UniProt	Garcia-Guzman *et al.*, 1997b
Human P2X4 (isoform 1)	Q99571	UniProt	Garcia-Guzman *et al.*, 1997a
Human P2X5	Q93086	UniProt	Bo *et al.*, 1995; Collo *et al.*, 1996; Bo *et al.*, 1995
Human P2X6 (isoform 1)	O15547	UniProt	Collo *et al.*, 1996
Human P2X7 (isoform A)	Q99572	UniProt	Rassendren *et al.* 1997
*Dd*P2XA	Q86JM7	UniProt	Fountain *et al.*, 2007
*Dd*P2XB	Q553Y1	UniProt	Ludlow *et al.*, 2009
*Dd*P2XC	Q553Y0	UniProt	Ludlow *et al.*, 2009
*Dd*P2XD	Q54J33	UniProt	Ludlow *et al.*, 2009
*Dd*P2XE	Q54JH4	UniProt	Ludlow *et al.*, 2009
*Ota*P2X	Q015E0	Uniprot	Fountain *et al.*, 2008
*Sma*P2X	AJ83803.1	GenBank	Agboh *et al.*, 2004
*Hd*P2X	EU979525	GenBank	Bavan *et al.*, 2008
*Bm*P2X	HQ333533.1	GenBank	Bavan *et al.*, 2011
*Lym*P2X	JX524180.1	GenBank	Bavan *et al.*, 2012

Table 2.1: sequences used in the analysis of retrieved protein sequences.

UniProt accession numbers of amino acid sequences used in the comparison primary sequence derived from homology sequences with pharmacologically characterised P2X receptors. *Dd*, *Dictyostelium discoideum*; *Ota*, *Ostreococcus tauri*; *Sma*, *Schistosoma mansoni*; *Hd*, *Hypsibius dujardini*; *Bm*, *Boophilus microplus*; *Lym, Lymnaea stagnalis*.

2.2.3 Protein topology prediction

Protein topology and transmembrane helix prediction was performed using the TMHMM Server v2.0 (http://www.cbs.dtu.dk/services/TMHMM-2.0/) (Krogh *et al.*, 2001). TMHMM combines identification of extended regions of hydrophobicity, a classic method for predicted the presence of TMDs in primary protein sequences, and 'charge bias analysis' of residues with predicted TMDs. As a greater abundance of positively charged amino acid residues is associated with the cytoplasmic face of TMDs (von Heijne, 1986), TMHMM is able to predict the orientation of TMDs in relation to the membrane (Krogh *et al.*, 2001). This allows greater information to be

gleaned regarding predicted protein topology with respect to extracellular and intracellular domains. Protein topology plots are presented using MacVector.

2.3 EXPERIMENTAL ANIMALS

A number of freshwater and marine organisms were cultured during the course of the current study. Whilst *Hydra vulgaris* and *Daphnia pulex* are freshwater invertebrates, *Trichoplax* is found in marine ecosystems. As such, culture conditions reflected the difference in salinity seen in the natural ecosystem of each organism.

2.3.1 Culture of *Hydra vulgaris* (AEP)

An 'starter' population of *H. vulgaris* (AEP strain) polyps were a kind gift from the research group of Prof. Dr Thomas Bosch (Zoologisches Institut, Christian-Albrechts Universität zu Kiel, Germany). Polyps were clonally propagated in artificial springwater ('S-medium') consisting of (in mM): 0.29 $CaCl_2$; 0.33 $MgSO_4$; 0.50 $NaHCO_3$; and 0.08 K_2CO_3 (pH 8.0) and maintained at a temperature of 16-18 °C and 12:12 light:dark cycle provided *via* an incandescent light source. S-medium was prepared in dH_2O and *Hydra* cleaned 4-8 hours after feeding with 1-2 day-old *Artemia* nauplii.

2.3.1.1 *Artemia franciscana* culture

Cultures of *Artemia franciscana* (Premium Grade; Brine Shrimp Direct, Ogden, UT, USA) were prepared 24 hours prior to feeding by addition of approx. 0.2 g diapausal cysts to 200 ml of artificial seawater (ASW) prepared from 36 g/L Kent Marine Reef Salt (Kent Marine, Franklin, WI, USA), dissolved in dH_2O. Newly hatched nauplii are weak swimmers. As such, cultures were aerated continuously via a small aquarium pump to prevent settling of nauplii at the bottom of the culture flask and dying. For feeding to *H. vulgaris* (AEP) polyps, *Artemia* were collected using a stripette, rinsed gently in cool tap water using an '*Artemia* sieve' (Brine Shrimp Direct) and resuspended in approximately 100 ml of S-medium. Nauplii were

cultivated at room temperature (RT), and typically emerged 12-18 hours after immersion in ASW.

2.3.2 Culture of *Daphnia pulex* (TCO)

Daphnia pulex (*arenata*; "The Chosen One" (TCO) strain) were a kind gift of Dr Jean-Claude Walser (Zoologisches Institut, Universität Basel, Switzerland) and maintained in Aachener Daphnien Medium (ADaM) containing (in mM): 800 $CaCl_2$, 300 $NaHCO_3$ and 0.63 SeO_2 (pH 8.0) and supplemented with 0.33 g/l of artificial sea salt (Kent Marine 'Reef Salt Mix', Franklin, Wisconsin) (Klüttgen *et al.*, 1994) at 16-18 °C and 12:12 hour light:dark cycle from an incandescent light source. *Daphnia* were fed weekly with a concentrated solution of *Scendesmus* algae and ADaM medium replaced half weekly.

2.3.2.1 *Scendesmus quadricauda* algae culture

S. quadricauda algae were cultured in a modified form of medium from the lab of Dr Dieter Ebert (Zoologisches Institut, Universität Basel, Basel, Switzerland) (Web-guide to *Daphnia* parasites) containing (in mM): 0.25 $CaCl_2$, 1.25 K_2HPO_4, 0.42 $MgSO_4$, 0.42 $NaHCO_3$, 0.063 $NaNO_3$, 0.63 $NaSiO_3$ and 5.06 x 10^{-4} TES (N-[tris(hydroxymethyl)methyl]- 2-aminoethanesulfonic acid) buffer (pH 8.0), dissolved in bi-distilled H_2O (ddH_2O). Algal cultures (500 ml in glass conical flasks) were maintained at room temperature and continuously aerated to reduce sedimentation of algae with new cultures established every 1-2 weeks and the preceding culture stored at 4 °C.

2.3.3 Culture of *Trichoplax adhaerens*

T. adhaerens were a kind gift from Prof. Leo Buss (Department of Ecology and Evolutionary Biology, Yale University, CT, USA). Groups of 20-30 organisms were cultured at room temperature in approximately 100 ml of ASW in 10 cm diameter glass Petri dishes, seeded with *Pyrenomonas salina* algae. *T. adhaerens* cultures

were fed *ad libitum* on *P. salina* and monitored regularly for signs of death, including lack of movement and poorly defined margins. Culture medium was prepared as required by dissolving 36 g of Kent Marine Reef Salt (Kent Marine, Franklin, WI, USA) in 1 litre dH_2O. The resultant ASW was filtered through grade 1 Whatman filter paper to remove insoluble impurities and supplemented with 1 ml Modified, enhanced Guillard's F/2 marine enrichment solution (Guillard, 1975) (Micro Algae Grow™; Florida Aqua Farms, Inc., Florida, USA) per litre of ASW. The resulting ASW was filtered through sterile 0.22 µm syringe-mounted filter (Sarstedt AG & Co., Nümbrecht, Germany) and stored at room temperature until required.

2.3.3.1 *Pyrenomonas salina* algae culture

Monocultures of *P. salina* were maintained at room temperature in the same medium used to culture *T. adhaerens* (section 2.3.3) in 10 cm Petri dishes with natural sunlight.

2.4 MOLECULAR BIOLOGY TECHNIQUES

2.4.1 Isolation of genomic DNA from whole organisms

Genomic DNA (gDNA) from *D. pulex* was used as a template in PCR reactions designed to amplify genomic regions of *Dpu*P2XA (section 5.3.1). Genomic DNA was isolated using the Wizard® SV Genomic DNA Purification System (Promega, Southampton, Hampshire, UK) according to the maunfacturer's protocol. Briefly, a single, clonally propagated adult daphnid was placed in a 1.5 ml tube and rinsed three times with nuclease-free H_2O. Following homogenisation in chilled 'Nuclei Lysis Buffer' using a bevelled pestle, tissue was incubated at 65 °C for 30 mins. Following addition of RNase solution and incubation at 37 °C for a further 30 mins to remove any remaining RNA template, protein was precipitated and centrifuged at 16,000 x *g* for 4 mins. The supernatant was transferred to a fresh 1.5 ml tube and the DNA precipitated using 100% isopropanol. After centrifugation for 1 min at 16,000 x *g*, a white pellet of DNA was easily visible and was washed with 100% ethanol (EtOH) before centrifugation for 1 min at 16, 000 x *g*. EtOH was aspirated and the pellet air

dried for 15 minutes. The resultant DNA pellet was resuspended in 100 µl of 'DNA rehydration solution' and incubated at 65 °C for 1 hour to allow full rehydration of the DNA sample, which was stored at 4 °C or -20 °C for later use. Rehydrated gDNA could be used directly in PCR reactions (section 2.4.5.2).

2.4.2 Isolation of total RNA from whole organisms

For use as a template in RT-PCR reactions, total RNA was isolated from *Hydra*, *Daphnia*, or *Trichoplax* by phenol-chloroform extraction (Chomczynski and Sacchi, 1987) using TRIzol® Reagant (Life Technologies). Prior to treatment with TRIzol reagent, organisms were transferred to fresh solution 2 days prior to RNA isolation to minimise contamination of total samples with RNA from food sources.

Briefly, 10-20 individuals were transferred to a 1.5 ml tube and rinsed thoroughly in nuclease-free H_2O. Due to their chitin exoskeleton, daphnids were homogenized using an RNase-free pestle, whilst a 20G syringe needle was used when homogenizing *Hydra* polyps and *Trichoplax*. Homogenate was incubated for 5 mins at RT to allow complete dissociation of protein complexes associated with nucleic acids. Lysate was transferred to an RNase-free 1.5 ml tube and molecular grade chloroform added. Addition of chloroform and subsequent centrifugation for 15 mins at 4 °C and 12,000 x *g* results in phase separation of the lysate, with RNA present in the liquid supernatant and protein and large cellular debris forming a loose pellet at the bottom of the tube. The supernatant was carefully removed and placed into a new RNase-free tube. An equal volume of 70% EtOH was added to precipitate nucleic acids contained in the solution. This solution was then purified using the PureLink™ RNA Mini Kit (Life Technologies) as per the manufacturer's instructions. A final elution step using nuclease-free water into a clean 1.5 ml RNase-free tube provided a 30 µl sample of total RNA. Samples were processed immediately following isolation, although could be stored at -80 °C until required.

2.4.3 First-strand cDNA synthesis

Following the isolation of total RNA from *Hydra*, *Daphnia*, or *Trichoplax* (section 2.4.2), cDNA was synthesised for downstream PCR reactions using SuperScript® III Reverse Transcriptase (Life Technologies). Approximately 5 µg total RNA (in a maximum volume of 11 µl) was incubated at 65 °C for 5 mins with 1 µl (50 µM) oligo-d$(T)_{18}$ primer (Fermentas Thermo Scientific, Loughborough, Leicestershire, UK) and 1 µl (10 mM) dNTP mix (Fermentas Thermo Scientific). After cooling the reaction mixture on wet ice for 1-2 mins, 2 µl 10x restriction transcriptase buffer, 1 µl 0.1M DTT, 1 µl (40 U/µl) RNasin (Promega, Southampton, Hants., UK), and 1 µl of SuperScript™ III RT (200 units/µl). The reaction mixture was heated at 25 °C for 5 mins, 50 °C for 1 hour, and the reverse transcriptase inactivated at 70 °C for 15 mins. To remove RNA complementary to cDNA, 2 units *E. coli* RNase H (New England Biolabs (NEB) (UK), Ltd, Hitchin, Hertfordshire, UK) was added to the reaction and incubated for a further 20 mins for 37 °C. The resultant cDNA was used diluted at 1/10 in TE buffer when required in downstream PCR reactions.

2.4.4 Assessing purity and yield of nucleic acids

Following extraction and elution, the purity and yield of DNA or RNA samples was determined using a NanoDrop 1000 spectrophotometer (Thermo Fisher Scientific Ltd, Leicester, UK). The absorbance ratios 260/280 nm and 260/230 nm were recorded, with values of ~1.8 (for 260/280 ratio) and ~2.0 (for 260/230 ratio) considered to be relatively free of protein and phenolic contaminants, respectively.

2.4.5 Polymerase chain reaction (PCR)

2.4.5.1 Primer design

To amplify a region of a gene of interest, two primers (short single-stranded nucleotide strands) were designed. When designing primers, a number of factors can play an important role in the successful amplification of a product. Firstly, primers were designed to be between 18 and 24 nucleotides in length, with base composition

ranging between 50 and 60% G+C where possible. A melting temperature (T_m) between 50 and 60 °C, ideally equal between sense and antisense primers, is also highly desirable. Repetitive sequences (e.g. ATATAT) or single nucleotide repeats (e.g. AAAAA) were also avoided where possible. Except where specified, primers were of desalted-level purity and synthesised at 25 to 50 nmole scale (Life Technologies) and resuspended in nuclease-free water 50 μM. A working stock of 5 μM was prepared from this for PCR reactions.

2.4.5.2 PCR reactions

PCR reactions were performed in an MJ Mini Thermal Cycler (Bio-Rad Laboratories, Hemel Hempstead, Hertfordshire, UK). Standard reactions (using Platinum® *Taq* DNA polymerase; Life Technologies) refer to those used for routine procedures that did not require high fidelity of amplicons to target sequence. In contrast, cloning require proofreading activity to generate amplicons faithful to a target sequence (for heterologous expression of receptors, for instance) used Platinum® *Taq* High Fidelity DNA polymerase (Life Technologies). Primers sequences used in the current thesis for the amplification of gene regions are detailed in Appendix (Tables A4 to A8, A10 and A12).

2.4.5.2.1 Standard PCR reactions

Standard PCR reactions refer to those performed for routine applications that did not require the highest fidelity of amplicon cloning. For such reactions, Platinum® *Taq* DNA polymerase was used as PCR cycling conditions required little or no optimisation when the same amplicon also had to be cloned using a high fidelity *Taq* polymerase (section 2.4.5.2). Platinum® *Taq* DNA polymerase incorporates a propriety antibody that blocks polymerase enzyme activity at ambient temperatures. Following denaturation at 94 °C, enzyme activity is restored thereby providing a "hot start", which increases specificity of amplification, yield of product, and reduces the error rate of mutations introduced in PCR reactions (Sharkey *et al.*, 1994). Primer sequences used in standard PCR reactions are detailed in the Appendix, Tables A3, A8 and A9.

In a reaction volume of 50 µl, the following components were combined:

Table 2.2: components required in standard PCR reactions used for routine applications.

Component	Stock concentration	Final concentration	Volume
PCR Buffer (without $MgCl_2$)	10x	1x	5 µl
$MgCl_2$	50 mM	1.5 mM	1.5 µl
Deoxyribonucleotide (dNTP) mix	10 mM	0.2 mM	1 µl
Forward/sense primer	5 µM	0.2 µM	2 µl
Reverse/antisense primer	5 µM	0.2 µM	2 µl
Template	-	-	1-2 µl
Platinum® *Taq* DNA Polymerase	5 units/µl	0.2 µM	1 µl
Nuclease-free water	-	-	To 50 µl

2.4.5.2.2 High-fidelity PCR reactions

In some applications, the number of mutations introduced in a PCR reaction must be minimised. In the current thesis, these reactions included cloning of P2X receptors for functional assays, the generation of constructs for heterologous expression and transgenesis. In such reactions, PCR reactions designed to amplify a P2X receptor or other coding region were repeated three times to account for error rates in PCR reactions. For such 'high-fidelity' PCR reactions, the Platinum® *Taq* DNA Polymerase High Fidelity (Life Technologies) enzyme mixture was used. This mixture combines recombinant *Taq* DNA polymerase, *Pyrococcus* species GB-D polymerase, and Platinum® *Taq* Antibody. *Pyrococcus* species GB-D polymerase possesses a proofreading ability by virtue of its 3' to 5' exonuclease activity (Tindell and Kunkel, 1988). This property, in combination with the hot start activity exhibited by the Platinum® *Taq* DNA polymerase, results in lower error rates and higher yields of high fidelity reactions which makes them well-suited in cloning applications.

Reactions requiring high-fidelity *Taq* polymerase enzyme were the cloning of the predicted CDS of invertebrate P2X receptors, 3' RACE (section 2.4.5.2.3), addition of C-terminal hexahistidine tags to cloned invertebrate P2X receptors for subsequent Western blot analysis (section 2.4.9), and the amplification of gene regions for the synthesis of plasmid constructs for generating transgenic variants of *H. vulgaris*

(AEP) (section 2.8.1.1). Primer sequences for cloning of predicted P2X receptor CDS', 3' RACE, addition of C-terminal hexahistidine tag, and amplification of gene regions for transgenic construct sequences can be found in the Appendix (Tables A4 to A10, and A12).

In reactions requiring a cDNA clone for expression studies, such as in the cloning of novel P2X receptors, PCR reactions were performed in triplicate. Following subcloning of PCR reactions into an appropriate vector and transformation into chemically competent *E. coli*, 6-8 bacterial colonies were picked for subsequent miniprep scale plasmid preparations.

In a reaction volume of 50 µL, the following components were combined:

Table 2.3: components required in high-fidelity PCR reactions used for applications requiring low error rate, such as cloning.

Component	Stock concentration	Final concentration	Volume
High Fidelity PCR Buffer	10x	1x	5 µl
$MgSO_4$	50 mM	2.0 mM	2 µl
dNTP mix	10 mM	0.2 mM	1 µl
Forward primer	5 µM	0.2 µM	2 µl
Reverse primer	5 µM	0.2 µM	2 µl
Template	-	-	As required
Platinum® *Taq* High Fidelity DNA Polymerase	5 units/µl	0.2 µM	1 µl
Nuclease-free water	-	-	To 50 µl

2.4.5.2.3 3' RACE reactions

Errors in genomic and transcriptomic sequence data are possible and may not accurately represent the correct 3' sequence of a gene of interest. The non-coding terminal 3' sequence of a cDNA can regulate mRNA stability and subcellular localisation. Furthermore, sequence variations at the 3' end of mRNA transcripts can result in alternative splice variants and, resultantly, proteins of varying length and function. To identify potential splice variants, and confirm the predicted C-terminal protein sequence of candidate P2X receptors, 3' 'Rapid Amplification of cDNA Ends (3' RACE) was performed. 3' RACE (Rapid Amplification of cDNA Ends) is a form

of PCR that takes advantage of the natural poly-(A) tail of mRNA transcripts as a generic priming site for an oligo-d(T) primer, provided a portion of the cDNA sequence upstream of the poly-(A) tail is known, to determine the 3' sequence of a cDNA (Loh *et al.*, 1989; Ohara *et al.*, 1989).

3' RACE was performed as described previously (Scotto-Lavino *et al.*, 2006). Primer sequences for use in 3' RACE reactions are detailed in the Appendix (Tables A6 and A7). Briefly, 5 µg of total RNA extracted from either *Hydra*, *Daphnia* or *Trichoplax* was denatured (in a volume of 11.25 µl) at 80 °C for 3 mins and cooled rapidly on wet ice for at least 1 minute before combining the following components in a final reaction volume of 20 µl: 1x First-Strand buffer (50 mM Tris-HCl (pH 8.3), 75 mM KCl, 3 mM $MgCl_2$); 1.3 mM dNTPs; 12.9 mM DTT; 50 ng Q_T primer; 10 U RNasin (Promega); and 200 U SuperScript III reverse transcriptase (Life Technologies). The reaction was incubated at 25 °C for 5 mins, followed by 1 hour at 50 °C. The reverse transcriptase enzyme was inactivated at 70 °C for 15 mins before removal of RNA template by addition of 2 U RNase H (NEB) at 37 °C for 20 mins. The reaction volume was increased to 1 ml with Tris-EDTA (pH 8.0) (Sigma-Aldrich); this '3' cDNA pool' could be stored indefinitely at 4 °C before nested PCR was performed to amplify the 3' region of a P2X cDNA.

Two rounds of PCR were performed to isolate the 3' region of a P2X cDNA, both with a high fidelity, proofreading *Taq* polymerase. The use of two rounds increases the specificity of the final amplicon, ensuring the final product is specific to the P2X gene of interest. In a reaction volume of 50 µl, the first round of PCR consisted of the following components: 1x High Fidelity PCR buffer; dNTPs (0.2 mM each); 2 mM $MgSO_4$; 25 pmol GSP (gene-specific primer) 1 primer (25 µM stock); 72 ng Q_O (100 ng/µl stock), 1 U Platinum® *Taq* High Fidelity DNA polymerase (Life Technologies); and 1 µl 3' cDNA pool. The reaction mixture was cycled through the following temperatures (where *x* °C denotes the annealing temperature for GSP1, presented in table 1.#): an initial round of 94 °C for 5 mins, *x* °C for 2 mins, 68 °C for 40 mins; 30 cycles of: 94 °C for 10 s, *x* °C for 10 s, 68 °C for 30 mins; and a final round of 94 °C for 10 s, *x* °C for 10 s and 68 °C for 15 mins. This reaction was diluted 1:20 in TE buffer (pH 8.0) and 1 µl used in the second round of PCR. Reaction components did not differ, with exception of the use of 25 pmol GSP2 and 69 ng of Q_I primers in lieu of GSP1 and Q_O. Annealing temperature was modified according to the melting

temperature of GSP2. Q_O, Q_I, and organism-specific GSP1 and GSP2 primer sequences (and their appropriate annealing temperatures) are provided in Appendix Table A7.

The final PCR product from the second round of amplification was subcloned into pGEM-T easy and sequenced using T7 and SP6 (Appendix, Table A3).

2.4.5.2.4 Synthesis of cloned cDNA

Differences between the codon usage of cloned cDNA and a host system can hamper their efficient expression in heterologous systems (Gustafsson *et al.*, 2004). It has been shown previously that modification of codon usage of a cloned cDNA so as to reflect that used in a heterologous system improves its expression and the subsequent yield of translated protein, such as seen in the heterologous expression of *S. mansoni* cDNA in the mammalian HEK293 cell line (Hamdan *et al.*, 2002). So as to improve yield of cloned P2X receptors when expressed heterologously in HEK293 cells, cDNA clones with a modified codon usage reflecting the GC-rich usage seen in humans were synthesised. A representative cDNA clone identified from PCR reactions (section 2.4.5.2.2) from *H. vulgaris* (AEP) cDNA P2X receptor was synthesised with a modified codon usage reflecting the GC-rich usage seen in humans. These 'Codon usage modified' clones (Mr. Gene GmBH, Regensburg, Germany) included 5' *Kpn*I and 3' *Not*I restriction sites for subsequent subcloning into pcDNA3.1$^{(+)}$. A 3' fifteen nucleotide sequence (5'- CACCATCATCATCAT-3') (preceding the 3' *Not*I restriction site), encoding a pentahistidine epitope tag was included to allow Western blot analysis of aepP2X in whole cell lysate samples (see section 2.4.9.1).

2.4.6 TAE agarose gel electrophoresis

PCR reaction and restriction digest products were visualised by TAE agarose gel electrophoresis. Gels contained between 1-2% (w/v) DNase- and RNase-free agarose (Appleton Woods Ltd, Birmingham, W. Midlands, UK), 1x TAE (4 mM Tris-acetate, 1 mM EDTA, pH 8.3) (Fisher Scientific). SYBR® Safe DNA Gel Stain (Life

Technologies) (Evenson *et al.*, 2012) added when the agarose had cooled to below 60 °C to a final dilution of 1 µl SYBR® Safe DNA gel Stain per 10 ml of molten agarose. Gels were cast with an appropriate comb (8- or 12-well) according to the number of samples to be analysed. Prior to loading into the gel, DNA samples were mixed with an appropriate volume of 5x DNA loading buffer (Bioline Reagents Ltd, London, UK). Electrophoresis was carried out in a Bio-Rad Mini-Sub Cell GT Cell electrophoresis tank (Bio-Rad Laboratories, Hemel Hempstead, Herts., UK) with 1x TAE at 70 V (7 $V.cm^{-1}$). SYBR® Safe DNA Gel Stain fluoresces under ultraviolet (UV) light (302 nm) and when bound to DNA present in the loaded samples allowed visualization of DNA under UV transillumination. Images of gels were acquired using a ChemiDoc XRS+ System (Bio-Rad). DNA fragment size was determined by comparison with markers of known size run alongside the samples in the same gel. Two markers were typically used in the current study: Quick-Load® 100 bp marker (NEB) (giving sizes of 100, 200, 300, 400, 500, 600, 700, 800, 900, 1000, 1200 and 1517 bp) and a Quick-Load® 1 kb marker (NEB) (giving sizes of 0.5 kb, 1.0 kb, 1.5 kb, 2 kb, 3 kb, 4 kb, 5 kb, 6 kb, 8 kb and 10.0 kb). 250 ng of each marker were loaded per gel.

2.4.6.1 Purification of DNA from agarose gels

The GeneJET™ Gel Kit (Fermentas GmBH, Sankt Leon-Rot, Germany) was used to purify fragments ranging from 100 to 4000 bp using a tabletop microcentrifuge prior to sequencing or ligation into an appropriate vector. This kit allowed removal of excess primers, salt, template or enzyme used initially to amplify or digest a DNA template. Under blue light (Dark Reader DR46B Transilluminator; Clare Chemical Research Inc., Denver, CO, USA), individual DNA bands were cut from the agarose gel using a sterile scalpel blade and transferred to a DNase-free 1.5 ml microcentrifuge tube. The agarose block was melted at 55 °C for 10 mins and bound to silica columns according to the manufacturer's instructions. DNA was eluted in 30 to 50 µl of DNase-free TE buffer (10 mM Tris, 1 mM EDTA; pH 8.0).

2.4.6.2 Automated DNA sequencing

DNA was sequenced by Eurofins MWG Operon (Ebersberg, Germany) using ABI 3730xl 96-capillary DNA Analyzers. Sequencing reads typically gave reliable data between 700 and 850 bp in length. Primer sequences for the sequencing of multiple cloning sites of the subcloning pGEM-T® Easy and expression pcDNA3.1$^{(+)}$ vectors are provided in the Appendix, Table A3.

2.4.7 Sub-cloning techniques

Cloned PCR products were inserted into a plasmid vector for further processing, or heterologous expression in HEK293 cells.

2.4.7.1 Cloning of PCR products into TA cloning vectors

Initial cloning of a new P2X receptor gene, or gene region required for the development of a new plasmid DNA construct, utilised the pGEM®-T easy vector (Promega). DNA polymerase enzymes from *Thermus aquaticus* add a single adenine (A) base overhang to the 3' terminal end of amplified products (Mezei and Storts, 1994). This property of the enzyme is useful as it allows its (albeit bidirectional) ligation into linearized pGEM®-T easy vector, which possess complementary 5' thymine (T) overhangs adjacent to its multiple cloning site. A standard pGEM®-T easy ligation reaction consisted of 1 to 3 µl of purified PCR reaction, 1 µl pGEM®-T easy (50 ng), 5 µl 2x Rapid Ligation Buffer (60 mM Tris-HCl (pH 7.8), 20 $MgCl_2$, 20 mM DTT, 2 mM ATP, 10% polyethylene glycol), 1 µl T4 DNA Ligase (3 U/µl), and DNase-free water to a final volume of 10 µl. The ligation reaction was incubated at 4 °C overnight (12-16 hours), but could also be incubated at RT for 2 hours (the latter temperature and incubation largely resulted in a greater number of positive clones following the vector's transformation into chemically competent *E. coli*).

2.4.7.2 Preparation of chemically competent Z-competent™ DH5α E. coli

Z-competent™ DH5α *E. coli* (Zymo Research Corps, Irvine, CA, USA) (genotype: F– Φ80*lac*ZΔM15 Δ(*lac*ZYA-*arg*F) U169 *rec*A1 *end*A1 *hsd*R17 (rK–, mK+) *pho*A *sup*E44 λ– *thi*-1 *gyr*A96 *rel*A1) were prepared according to manufacturer's instructions and used for standard transformation of plasmid DNA during the course of this study. These chemically competent *E. coli* allow for more rapid transformation of foreign DNA compared to standard transformation protocols (5 mins compared to 90 mins), without loss of transformation efficiency. If required, these *E. coli* can be heatshocked for 1 min at 42 °C and recovered in Super Optimal broth (with Catabolite suppression) (SOC) *as per* standard procedures should low transformation efficiencies be seen after the 5 min protocol. Briefly, stocks of *E. coli* were made 'Z-competent™', and thus amenable to rapid chemical transformation, by the following protocol. A single colony of DH5α *E. coli* was used to inoculate 5 ml of LB medium without antibiotic selection and the inoculation shaken for overnight at 37 °C and 225 rpm. Of this overnight culture, 0.5 ml was used to inoculate 50 ml ZymoBroth™ (Zymo Research Corps) and the culture shaken at 225 rpm at a reduced temperature of 18 °C, as reduced temperatures have been cited to improve the competency of *E. coli* cultures (Inoue *et al.*, 1990). Once the OD_{600} of the culture reacheed between 0.4 to 0.6, the culture was placed on wet ice for 10 mins and pelleted at 3,000 rpm for 10 mins at 4 °C. The supernatant was removed and the cells resuspended gently in 5 ml ice cold 2x Wash Buffer (final concentration of 1x) and re-pelleted again at 4 °C for 10 mins and 3,000 rpm. Cells were resuspended gently in 5 ml ice-cold 1x Competent Buffer and 50 µl working aliquots in sterile 1.5 ml microcentrifuge tubes stored at -80 °C.

2.4.7.3 Transformation of Z-competent™ chemically competent DH5α E. coli

For standard cloning and transformations, previously prepared Z-competent DH5α *E.coli* were used. For any one ligation reaction (one PCR amplicon into one vector), a 50 µl aliquot of cells was thawed on wet ice and 1-3 µl of ligation reaction added to the cells. The cells were gently mixed and then incubated on ice for 5 mins before plating 30 µl of the cell mixture on to pre-warmed agar plates containing 100 µg/ml carbenicillin. Plates were upturned and incubated at 37 °C for 12-16 hours

(overnight), allowing antibiotic selection of transformed cells. For lacZ selection (when using pGEM®-T easy vector), 50 mg/ml X-gal, and 0.1 mM isopropyl β-D-1-thiogalactopyranoside (IPTG) was also added to agar plates. Following incubation overnight these plates were transferred to 4 °C for a minimum of 1 hour to allow the blue colour in untransformed cells to intensify, for easier selection of positive clones.

Error rates of nucleotide incorporation during transcription in *E. coli* are in the order of 10^{-5} per nucleotide (Blank *et al.*, 1986; Rosenberger and Hilton, 1983). To account for random mutations in plasmids transformed into *E. coli* for the cloning of P2X receptors, transformations were performed in triplicate for each PCR product.

2.4.7.4 Stocks of antibiotics

Stocks of the penicillin antibiotic carbenicillin (disodium salt) (Melford Laboratories, Ltd, Ipswich, Suffolk, UK) were prepared at a 10 mg/ml in 50% (v/v) EtOH/ddH_2O at -20 °C (filtered through a 0.2 μm filter) and used at a final concentrations of 100 μg/ml for agar plates or 50 μg/ml for liquid medium. In low pH conditions and higher temperatures, carbenicillin is a more stable than its analogue ampicillin, lending to its use in long-term culture of bacteria in protein expression studies (Butler *et al.*, 1970).

2.4.7.5 Preparation of bacterial agar plates

Plates were generally made on the day of transformation, but could be stored for up to a month at 4 °C. The plates were made by mixing 4 g of LB granular agar (Fisher Scientific, UK) in 100 ml dH_2O and autoclaved. The agar mix was allowed to cool to around 50 °C and carbenicillin added to a final concentration of 100 μg/μl. The resultant antibiotic/agar mixture (20-25 ml) was poured gently into 100 ml Petri dishes (approx. 25 ml/dish) and allowed to cool and solidify under aseptic conditions. For LacZ selection, 250 ng of X-gal (50 mg/ml stock) (Promega) was spread over the plate using a sterile spreader. The solution was allowed to diffuse in to the plate at room temperature for 20-30 mins before use.

2.4.7.6 Glycerol stocks of bacteria

To negate the need for repeated transformation of bacteria, glycerol stocks of a single transformed bacteria colony were prepared and stored at -80 °C. 5 ml LB with 50 μg/ml carbenicillin antibiotic was inoculated with 5 μl of a previously obtained culture of *E. coli* transformed with a DNA construct of interest. The inoculation was shaken overnight (approx. 12-18 hours) at 37 °C and 225 rpm. 5 ml of sterile 80% (v/v) glycerol (final concentration of 40% v/v) was added to the overnight culture and the mixture briefly vortexed before 1 ml aliquots were stored at -80 °C in sterile screwtop tubes (VWR). Stocks were recovered by scraping the surface of the frozen stock with a sterile pipette tip and inoculating 5 ml LB broth with 50 μg/ml carbenicillin, shaking overnight at 37 °C and 225 rpm.

2.4.7.7 Plasmid amplification and isolation

Small-scale plasmid DNA extractions ('Minipreps') were performed using the alkaline lysis method of DNA isolation using the QIAprep Spin Miniprep kit (Qiagen UK, Surrey, UK) following the manufacturer's instructions. Yields were typically between 15-20 μg (high-copy number plasmid), giving samples of high enough purity to perform downstream restriction digests and automated sequencing analyses.

Individual inoculated *E. coli* colonies were selected using a sterile pipette tip and used to inoculate 5 ml of LB medium supplemented with carbenicillin (to a final concentration of 50 μg/ml). Inoculations were incubated overnight (12-16 hours) at 37 °C in a rotary shaking incubator at 225 rpm. 4.5 ml of culture was pelleted at 5,400 x *g* for 10 mins at 4 °C and the supernatant removed. The pellet was resuspended in 250 μl P1 resuspension buffer (containing 100 μg/ml RNase A to remove RNA contaminants) and lysed for 5 mins in 250 μl P2 buffer before the reaction was neutralized with 350 μl N3 neutralisation buffer. Crude bacterial membrane was separated from extracted DNA by centrifugation at 16,000 x *g* for 10 mins at RT. The supernatant (containing plasmid DNA) was bound to silica columns, washed with 70% EtOH before eluting in 50 μl EB buffer (10 mM Tris-HCl, pH 8.5). Plasmids were stored at -20 °C until further use.

Larger scale plasmid extractions ('Midipreps') were performed using the Qiagen HiSpeed Plasmid Midi Kit (Qiagen UK), as per the manufacturer's instructions with minor modifications with regards to final precipitation of plasmid DNA (section 1.4.6.8). Midiprep extractions were used to obtain high-quality, high volume plasmid samples for both HEK293 cell transient transfection (section 2.6.1) and *H. vulgaris* (AEP) embryo microinjection (section 2.8).

2.4.7.8 Purification of plasmid DNA

Following elution in 5 ml buffer QF (Qiagen UK), plasmid DNA was precipitated by addition of 3.5 ml (0.7 volumes) 100% isopropanol and centrifugation at 4 °C at 2,000 x *g* for 30 mins. The resultant pellet was washed with 2 ml 70% EtOH and centrifuged again for a further 10 mins. The pellet was air-dried for 5-10 mins and resuspended in 200 µl nuclease-free, sterile H_2O (for *Hydra* embryo microinjection), or Tris-EDTA (TE) buffer (1 mM EDTA, 10 mM Tris, pH 8.0) (for HEK293 cell transfection). A second round of precipitation was performed to obtain high purity constructs for downstream transfections and microinjections. Briefly, 20 µl (1/10 volume) 3M sodium acetate (pH 5.2) and 600 µl RT 100% EtOH (3x volume) was added to the resuspended plasmid solution and gently mixed until the DNA had precipitated. The mixture was then centrifuged at 15,000 x *g* for 15 mins and the resultant pellet washed in 200 µl 70% EtOH before centrifuging again at 15,000 x *g* for 15 mins. After air-drying for 5-10 mins, the pellet was resuspended in 200-400 µl TE buffer (pH 8.0) and incubated at 4 °C overnight to allow the pellet to dissolve. The final plasmid solution was incubated at 65 °C for 10 mins to inactivate nucleases and, if necessary, aid resuspension. A 1 µg/µl working stock of plasmids for transfection was aliquotted and stored at -20 °C until required.

2.4.7.9 Verification of insert DNA

There are a variety of methods for analysing and verifying the presence and orientation of insert DNA within plasmid constructs. Plasmids were either digested using restriction endonucleases, or diluted in DNase-free water and amplified using PCR using either gene- or plasmid-specific primers.

2.4.7.9.1 Digestion of plasmid DNA with restriction endonucleases

Restriction endonucleases, also called restriction enzymes, recognise and cleave at specific base sequences in double stranded DNA. This cleavage can either leave 'blunt-ended' cuts (which leave no overhanging bases between sense and antisense DNA strands), or 'sticky-ended' cuts (which do leave overhanging bases). These enzymes have been used in this investigation to analyse gene orientation within a larger DNA construct and in the subcloning of genes between one vector to another. Restriction enzyme nomenclature consists of a 3-letter abbreviation (e.g. *Not* for *Nocardia otitidis*) followed by a strain designation (if required) and Roman numerals if more than one variant of the enzyme exists. Double digests, where two restriction enzymes were required to digest DNA, were either performed concurrently (when the two enzymes shared the same buffer conditions), or sequentially (when one reaction was performed, then buffer conditions adjusted to provide optimal conditions for the second enzyme). Restriction endonuclease enzymes were purchased from New England Biolabs UK Ltd (Hitchin, Hertfordshire, UK).

Standard reactions consisted of 1 µg of plasmid DNA, 10 units of restriction enzyme(s), 100 ng/µl bovine serum albumin (BSA), 2 µl 10x restriction enzyme buffer and DNase-free water to a final volume of 20 µl. The reaction was incubated at the appropriate temperature (typically 37 °C) for 2-3 hours and the reaction inactivated at 60-70 °C for 20 mins. The restriction digest mixture was analysed by TAE agarose gel electrophoresis and, where a digested fragment was required for downstream ligation, the fragment of interest was excised and purified (see section 2.4.6.1.).

2.4.7.10 Preparation of plasmid for ligation

For ligation between two DNA ends to occur, a covalent phosphodiester bone must form between the 3' hydroxyl group of one nucleotide and the 5' phosphate of another. Without the removal of 5' phosphate groups, the digested plasmid can recircularise, reducing the efficiency of incorporation of DNA into the cut vector. Removal of the 5' phosphate groups was performed using calf intestinal alkaline phosphatase (CIAP) (NEB). CIAP remains active in restriction endonuclease buffers

also purchased from NEB UK Ltd. and, as a result, could be added directly to restriction digest mixtures. Following plasmid digestion for 2 hours, a further 10 units of CIAP (10 U/µl) (Promega) was added to the reaction and incubated at 37 °C for a 30 mins according to the manufacturer's instructions. Digests were analysed by TAE agarose gel electrophoresis and the band of interest excised using a clean scalpel blade and purified according to section 2.4.3.1.

2.4.8 Ligation reactions

Inserts were ligated into appropriate vectors at a 3:1 molar ratio. The amount of insert relative to that of vector were calculated according to the formula:

$$\frac{\text{Mass of vector (ng)} \times \text{kb size of insert}}{\text{kb size of vector}} \times \text{Molar ratio of } \frac{\text{insert}}{\text{vector}} = \text{ng of insert required}$$

CIAP-treated vector and insert DNA treated with the same restriction enzyme(s) were ligated using T4 DNA Ligase (Promega) in a reaction containing a 3:1 molar ratio of insert to vector. A standard 10 µl reaction consisted of 5 µl 2x Rapid Ligation buffer (60 mM Tris-HCl (pH 7.8), 20 mM $MgCl_2$, 20 mM dithiothreitol (DTT), 2 mM ATP and 10% polyethylene glycol), 1 µl T4 DNA Ligase (3 Weiss units/µl). Volumes of insert and vector were added accordingly. The reaction was mixed and incubated at 4 °C overnight, but could also be incubated at RT (20-22 °C) for 1 hour.

2.4.9 Western blot analysis

For analysis of protein expression in HEK293 cells, Western blots were performed.

2.4.9.1 Sample preparation

Following transient transfection of HEK293 cells as described in section 2.6.2, cells were washed gently in PBS, triturated in fresh PBS and transferred to a 1.5 ml microcentrifuge tube. Cells were pelleted at 4,000 x *g* for 3 mins at RT before resuspending in 50 µl RIPA (radioimmunoprecipitation assay) buffer (20 mM Tris-HCl, pH 7.6; 150 mM NaCl; 1 mM $CaCl_2$; 1 mM $MgCl_2$) supplemented with 10% *n*-

Dodecyl β-maltopyranoside (DDM) detergent (final concentration of 1% (v/v)) and 1x (v/v) Protease Inhibitor Cocktail (cOmplete EDTA-free Cocktail Tablets; Roche Applied Sciences, Burgess Hill, West Sussex, UK). The resuspension was incubated on wet ice for 30 mins before centrifugation at 14,000 x *g* for 2 mins at RT to separate the crude membrane fraction from solubilised protein. The supernatant (containing total extracted protein) was transferred to a new 1.5 ml tube. Protein concentration was determined by Bradford assay at a wavelength of 595 nm (Bradford, 1976) (section 2.4.9.2).

2.4.9.2 Determination of protein concentration by Bradford assay

The protein concentration of whole cell and whole tissue lysates was determined according to Bradford, 1976. The Bradford protein assay is a colourimetric assay based on the shift in absorbance of the dye coomassie G-250 upon binding to protein, where the difference in maximal absorbance between the non-bound and bound forms of the dye are at 465 nm and 610 nm, respectively. The extant of this spectral shift directly relates to protein concentration in the sample.

2.4.9.3 Solutions

Table 2.5: compositions of stacking and separating gels

Solution	Component	Volume required
Stacking gel (4%)	H_2O 30% acrylamide/bis-acrylamide 1 M Tris-HCl (pH 6.8) 10% SDS 30% ammonium persulphate (APS) TEMED	1.4 ml 0.35 ml 0.25 ml 20 µl 6.5 µl 2 µl
Separating gel (10%)	H_2O 30% acrylamide/bis-acrylamide 1.5 M Tris-HCl (pH 8.8) 10% SDS 30% APS TEMED	4.1 ml 3.3 ml 2.6 ml 100 µl 33 µl 8 µl

Table 2.6: washing solutions used in Western blot protocols.

Solution	Component
TBS	20 mM Tris-HCl, pH 7.5 150 mM NaCl
TBST	20 mM Tris-HCl, pH 7.5 150 mM NaCl 0.2% Tween-20
TTTBS	20 mM Tris-HCl, pH 7.5 150 mM NaCl 0.05% Tween-20 0.2% Triton X-100

Total protein samples were denatured at 100 °C for 2 mins in 1x (v/v) Yeast Sample Buffer (YSB) (Drew *et al.*, 2008) (50 mM Tris-HCl, pH 7.6; 5 mM ethylenediaminetetraacetic acid (EDTA); 10% glycerol, 0.005% bromophenol blue) and separated on a 4% (stacking)/10% (separating) SDS-PAGE gel (table 2.5), initially at 100V for 15 mins before increasing the voltage to 200V for approx. 1 h as the protein moves through the stacking and separating gels, respectively. Protein was transferred to polyvinylidene fluoride (PVDF) membrane (Bio-Rad, UK) and washed 3x in TTTBS, 1x in TBS and blocked for 1 hour in 3% (w/v) BSA in TBS. Blots were incubated overnight at 4 °C with mouse tetra-His (Qiagen) (anti-His) or mouse anti-β-actin (Abcam, Cambridge, Cambs., UK) primary antibody (1:2000 and 1:600 dilution, respectively, in TBS, 3% (w/v) BSA). Unbound antibody was removed by washing 3x in TTTBS before incubation with HRP (horseradish peroxidase)-conjugated, anti-mouse IgG secondary antibody (1:2000 dilution) (Cell Signalling Technology, Inc., Danvars, MA, USA). Blots were subsequently analysed using the Amersham ECL™ Plus™ detection reagent kit (GE Healthcare, Little Chalfont, Bucks., UK) according to the manufacturer's instructions, whereby a 1:1 ratio of propriety solutions A (luminol; 5-amino-2,3-dihydro-1,4-phthalazinedione) and B (peroxide) are combined and applied immediately to the blot, and incubated for approximately 1-2 mins before visualisation under UV light using a Chemi-Doc™ Bio-Rad XRS+ System (Bio-Rad).

2.5 CELL CULTURE

Cell culture reagents were purchased from Life Technologies Ltd (Paisley, Strathclyde, UK), unless otherwise stated.

2.5.1 Culture of Human Embryonic Kidney 293 (HEK293) cells

Human Embryonic Kidney 293 (HEK293) cells were cultured in Dulbecco's Modified Eagle Medium/F-12 (DMEM/F-12) (1:1) (Gibco, Life Technologies Ltd, Paisley, Strathclyde, UK) supplemented with foetal calf serum (FCS) (Sigma-Aldrich) to a final concentration of 10% (v/v), 2 mM L-glutamine, 100 $U.ml^{-1}$ penicillin and 10 $mg.ml^{-1}$ streptomycin. Cells were grown in monolayer in 25 cm^2 vent-capped BD Falcon cell culture flasks (VWR International Ltd, Leicestershire, UK) in a humidified incubator in 95% air/5% CO_2 atmosphere at 37 °C and passaged every 5-7 days with medium being replaced for fresh every 2-3 days. Cells were passaged at 70-80% confluency, when cells were washed with 2 ml Ca^{2+}- and Mg^{2+}-free Dulbecco's Phosphate Buffered Saline (D-PBS) and 2 ml of 1x trypsin (in Ca^{2+}- and Mg^{2+}-free D-PBS). After 2-3 mins incubation at 37 °C in a humidified incubator, 5 ml of pre-warmed (37 °C) DMEM/F-12 (1:1) medium was added and the resultant cell suspension pelleted by centrifugation at 150 x *g* for 1 min at RT. The supernatant was decanted and the cell pellet resuspended in 10 ml pre-warmed medium and reseeded into 25 cm^2 cell culture flasks at varying densities with 5 ml fresh, pre-warmed medium.

2.5.2 Cryopreservation of HEK293 cells

For long-term storage, HEK293 cells were stored in liquid nitrogen in 1 ml aliquots and thawed when required. For freezing, cells were grown to 70-80% confluency in 75 cm^2 vent-capped BD Falcon cell culture flasks (VWR International Ltd), pelleted and resuspended in 3 ml DMEM/F-12 (1:1) supplemented with 10% foetal calf serum, 2 mM L-glutamine, and 10% (v/v) DMSO. 1 ml aliquots of this suspension were transferred to sterile 2 ml screw-top vials (VWR) and frozen slowly to -80 °C at a rate of 1 °C/minute before transferring to liquid nitrogen using a Mr. Frosty™ Freezing Container (Thermo Fisher Scientific Inc., Rockford, IL, USA) filled with

approximately 100 ml 100% methanol. Cells were recovered by warming the aliquot in a 37 °C water bath and resuspending gently in standard pre-warmed DMEM/F-12 (1:1). Cells were pelleted and resuspended twice to remove residual DMSO before being seeded into a 25 cm^2 vent-capped cell culture flask and incubated as described in section 2.5.1.

2.6 WHOLE-CELL PATCH-CLAMP ELECTROPHYSIOLOGY

All recordings presented in the current thesis are whole-cell patch-clamp in voltage-clamp mode, as first developed by Neher and Sakmann (Neher and Sakmann, 1976; Hamill *et al.*, 1981). In this configuration, the user has access to, and control of, the intracellular contents of a cell as its surrounding extracellular solution in order to investigate biophysical properties of the cell.

2.6.1 Transient transfection of HEK293 cells

Two methods of transient transfection of plasmid constructs of cloned P2X receptors were used during the course of this study. For analysis of ATP-evoked currents using patch-clamp electrophysiology, cells were transfected by nucleofection. Lipofection was used for transfection of plasmid constructs into HEK293 cells for subsequent analysis of protein monomer expression by SDS-PAGE.

HEK293 cells were grown to 70-90% confluency in 25 cm^2 vent-capped flask, trypsinised and pelleted as described in section 2.5.1. Cells were transfected with 5 µg of P2X receptor-pcDNA3.1$^{(+)}$ plasmid construct (1 µg/µl in TE buffer) using the Amaxa Nucleofector® Kit V (catalogue number: VCA-1003) (Lonza Group Ltd, Basal, Switzerland, UK). Briefly, 82 µl of 'Nucleofector® Solution' was combined with 18 µl of 'supplement solution' (total volume of 100 µl), and the resultant 'transfection solution' allowed to warm to room temperature. Following centrifugation in a 15 ml tube, excess DMEM/F:12 medium was gently aspirated from pellet cells, and the 100 µl transfection solution added. Cells were gently agitated to produce a homogenous suspension, and 5 µg plasmid DNA construct subsequently added. Cells were transferred to an electroporation cuvette using a fine

Pasteur pipette and transfected using the 'Q-001' HEK293 cell elctroporation programme and Amaxa Nucleofector™ 2b Device (Lonza Group Ltd). Transfected cells were gently resuspended in 2 ml of warm DMEM/F:12 (1:1) medium and 250 µl plated onto sterile 13 mm glass coverslips (VWR) in 35 mm Petri dishes and incubated at 37°C/5% CO_2 in a humidified incubator for 12-18 hours prior to use.

For Western blot analysis (section 2.4.9), HEK293 cells were transiently transfected with plasmid constructs using Lipofectamine® 2000 (Life Technologies). 3-5 µg of plasmid (1 µg/µl) was mixed with 100 µl Opti-MEM medium, whilst 3-5 µl of Lipofectamine reagent was mixed with a further 100 µl Opti-MEM medium. Following a 5 mins incubation at RT, Lipofectamine® 2000 and plasmid mixtures were combined and incubated for a further 20 mins at RT before transferring to a 35 mm Petri dish of HEK293 cells (70-80% confluency) for a final volume of approximately 2 ml. Cells were harvested 18-24 hours post-transfection and prepared according to section 2.4.9.1.

2.6.2 Solutions for whole-cell voltage electrophysiology

Standard salts were purchased from Fisher Scientific UK Ltd (Loughborough, Leicestershire, UK) with the exception of 1M solutions of $CaCl_2$, KCl and $MgCl_2$ (Sigma-Aldrich, Poole, Dorset, UK) and HEPES (VWR International Ltd, East Grinstead, West Sussex, UK). Transition metal salts were purchased from Sigma-Aldrich and were of minimum 95% purity.

2.6.2.1 Standard extracellular solution for whole-cell electrophysiology

For standard recording of P2X receptor currents, a standard extracellular solution (sECS) consisting of (in mM): 145 NaCl, 2 KCl, 2 $CaCl_2$, 1 $MgCl_2$, 13 D-glucose, and 10 HEPES was used. The pH of the solution was adjusted to 7.3 using NaOH and stored at RT (20-25 °C) during the course of recording.

2.6.2.2 Standard intracellular solution for whole-cell electrophysiology

For standard recording of P2X receptor currents, an intracellular solution consisting of (in mM): 145 NaCl, 10 HEPES, and 10 EGTA was used. The pH of the solution was adjusted to 7.3 using NaOH. Aliquots of 2 ml were stored at -20 °C and thawed on the day of recording.

2.6.2.3 Low divalent cation extracellular solution (ldECS)

For investigation of the effect of the divalent cations Mg^{2+} and Ca^{2+} on ATP-evoked currents evoked at *Dpu*P2XB-$(His)_6$ receptors, a modified form of sECS was used which contained reduced concentrations of divalent cations. This low divalent cation ECS (ldECS) contained 0.2 mM $CaCl_2$ and 0 mM $MgCl_2$. Note that in Ca^{2+}-free solutions, GΩ seals were unstable, leading to the inclusion of 0.2 mM Ca^{2+} in ldECS. All other ldECS components were of the same concentration of sECS (section 2.6.2.3). For recording in low divalent cation conditions, an intracellular solution described in section 2.6.2.2 was used.

2.6.2.4 Extracellular solutions for analysis of ionic permeability of aepP2X

Extracellular solutions used in the analysis of monovalent cation, calcium ion, and chloride ion permeability of aepP2X in HEK293 cells are described below (Table 2.7).

Table 2.7: compositions of extracellular solutions used in the recording of permeabilities of monovalent and divalent cation and anion species.

Ion of interest	Component	Concentration (mM)	pH
Na^+	NaCl HEPES $MgCl_2$	145 10 1	7.3 with NaOH
K^+	KCl HEPES $MgCl_2$	145 10 1	7.3 with NaOH
$NMDG^+$	NMDG HEPES $MgCl_2$	145 10 1	7.3 with HCl
$Tris^+$	Tris HEPES $MgCl_2$	145 10 1	7.3 with NaOH
Ca^{2+}	NMDG $CaCl_2$ HEPES $MgCl_2$	145 5 10 1	7.3 with HCl
Cl^-	Na.gluconate HEPES $MgCl_2$	145 10 1	7.3 with NaOH

2.6.2.5 ATP stock solution

100 mM stocks of ATP (disodium salt) (Sigma-Aldrich) were made in ECS and pH re-adjusted to 7.3. Aliquots of 1 ml were stored at -20 °C and diluted accordingly in ECS on the day of recordings.

2.6.2.6 Agonist and antagonist solutions

Agonist and antagonist compounds stock solutions were prepared in ECS (pH 7.3) (with the exception of ivermectin, which was dissolved in DMSO) and stored at -20 °C. Compounds, the solvents used to resuspend them at a specified concentration are provided in Table 2.8.

Table 2.8: agonist, antagonist and modulatory compounds used in pharmacological profiling experiments of cloned P2X receptors.

Compound	Supplier	Catalogue number	Stock concentration
ATP (disodium salt)	Sigma-Aldrich	A7699	100 mM
α,β-meATP (trisodium salt)	Tocris Bioscience	3209	100 mM
β,γ-meATP (disodium salt)	Sigma-Aldrich	M7510	100 mM
Suramin (sodium salt)	Sigma-Aldrich	S2671	100 mM
PPADS (tetrasodium salt)	Tocris Bioscience	0625	100 mM
Brilliant blue G (BBG)	Sigma-Aldrich	B0770	100 mM
Phenol red (sodium salt)	Sigma-Aldrich	P4758	100 mM
CORM-2	Sigma-Aldrich	288144	100 mM
Ivermectin	Sigma-Aldrich	I8898	10 mM

2.6.3 Recording microelectrodes

Glass microelectrodes for whole-cell recordings were prepared from thin-walled glass capillaries (1 mm outer diameter, 0.75 mm inner diameter) (World Precision Instruments, Inc., Hitchin, Herts., UK) using a two-stage pulling process on a Narishige PP-83 Puller (Narishige International Ltd, London, UK). Electrodes had a tip resistance of 4-8 MΩ when filled with intracellular solution (section 2.6.2.2).

2.6.4 Experimental protocol

A single 13 mm coverslip was placed in a perfusion bath mounted on the stage of an Olympus CKX41 inverted light microscope (Olympus UK, Southend-On-Sea, Essex, UK). The microscope was placed on an anti-vibration air table (Technical Manufacturing Corporation, Peabody, MA, USA) and the entire apparatus surrounded by a Faraday cage to reduce external electrical interference. Cells were viewed using a 40x objective lens with phase-contrast optics and were perfused continually at a rate of 2-5 ml/minute with ECS via a gravity-fed perfusion system from a 50 ml disposable syringe mounted on a clamp stand inside the Faraday cage. Perfusate was removed from the bath by suction (provided by an external Dynax 30 laboratory pump (Charles Austin Pumps Ltd, Byfleet, Surrey, UK) via a narrow glass tube pulled from thin-walled borosilicate glass (1 mm outer diameter, 0.75 mm inner diameter) (World Precision Instruments, Inc., Hitchin, Herts., UK) that in turn drained into a Büchner flask.

Agonists and antagonists were applied directly to cells *via* an RSC-160 Rapid Solution Changer (Bio-Logic SAS, Claix, France). This system allows rapid application (20-100 ms) of compound from a disposable 10 ml syringe connected to polyethylene tubing and glass tubes (1 mm outer diameter, 0.78 mm inner diameter) in near-vicinity of a cell of interest. Solutions could be applied manually, or via appropriate sets of commands provided by via a computer interface.

Intracellular solution was filtered through a 0.22 μm pore filter (Scientific Supplies Ltd, Hessle, Yorkshire, UK) and back-filled into recording microelectrodes using a MicroFil 34 gauge micropipette (World Precision Instruments, Inc.). The recording microelectrode was placed in an electrode holder that was in turn electrically coupled to an Axon CV-7A current- and voltage-clamp amplifier headstage (Molecular Devices (UK) Ltd, Wokingham, Berkshire, UK) and Multiclamp 700A Patch Clamp amplifier (Molecular Devices (UK) Ltd). A silver/silver chloride (Ag/AgCl) wire (0.25 mm diameter, Harvard Apparatus Ltd, Edenbridge, Kent, UK) in the bath connected to the earth of the amplifier completed the circuit.

2.6.4.1 Cell-attached configuration of the patch-clamp technique

Once mounted on the amplifier headstage, the recording microelectrode was lowered into the bath solution and positioned close to a chosen cell using a Scientifica PatchStar Micromanipultor (Scientifica Ltd, Uckfield, Sussex, UK). Once in solution, offset potentials were zeroed using automated pipette offset function of the MultiClamp 700A Commander amplifier control software (Molecular Devices (UK) Ltd). A Clampex-driven square wave pulse was applied to the cell, following which the microelectrode was advanced towards the cell. When the electrode came into contact with the cell membrane, a resultant increase in resistance (viewed as a decrease in the amplitude of the square wave current test pulse) was seen. A slight negative pressure was applied to the electrode, producing a further decrease in observed current until a high resistance (GΩ) seal was formed between the recording microelectrode glass and cell membrane. A holding potential of -60 mV was applied to the cell, which usually enhanced seal formation. Further suction was applied to the recording microelectrode until the resistance between the cell membrane and electrode exceeded 1 GΩ and the cell-attached configuration was achieved.

2.6.4.2 Whole-cell configuration of the patch-clamp technique

Following formation of the cell-attached configuration, whole-cell configuration was achieved with the application of a short burst of suction. The cell membrane was seen to have ruptured when a second set of transient current deflections, corresponding to the capacitive current of the cell membrane, appeared. Pipette capacitance was compensated for automatically prior to recording using the Multiclamp 700A Patch Clamp amplifier interface. Following compensation, cell membrane capacitance and pipette access resistance were noted. Memberane capacitance did not exceed 30 pF and did not vary greater than 10 pF in any one series of experiments presented herein. Series resistance (the sum of resistances between the amplifier input and pipette) was not compensated for either during recording or manually *post hoc*. In current-voltage experiments, only liquid junction potentials were adjusted for; series resistance compensation does not alter the reversal potential of currents when adjusted for with, or without liquid junction potential adjustment.

Currents were digitised using a Digidata 1322 A/D (analogue to digital) converter (Molecular Devices (UK) Ltd). Signals from voltage-clamp protocols were filtered at 1 kHz with an 8-pole low-pass Bessel filter and digitised at 2 kHz. Standard voltage-clamp protocol signals were sampled at a rate of 10 kHz, whilst ramp protocols were sampled at a rate of 20 kHz.

For standard recording of P2X receptors in the whole-cell configuration, cells were held at a membrane potential of -60 mV. Following confirmation of an ATP-sensitive current in aepP2X-$(His)_6$, current-voltage relationships for use in ionic permeability analysis were recorded. Cells were initially held at -60 mV and currents evoked by 100 μM ATP. At the apex of evoked current, voltage was stepped to +60 mV before ramping to -100 mV over 1 s during the course of ATP application (see Fig. 2.2). Cells were returned to -60 mV on completion of the ramp.

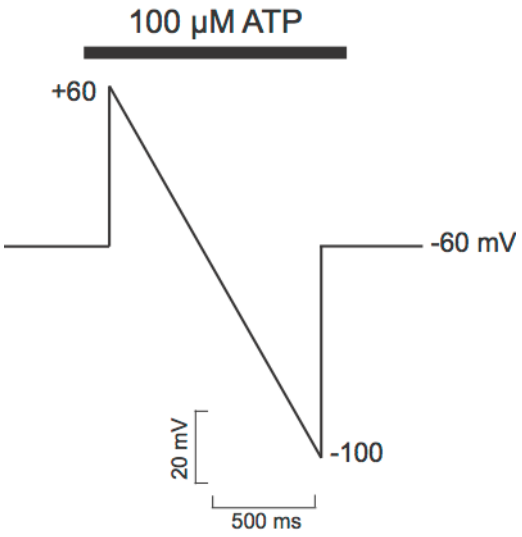

Fig. 2.2: voltage ramp and step protocol used in the recording of current-voltage relationships in aepP2X.

The period of extracellular 100 µM ATP is indicated above the ramp protocol. Cells were initially held at -60 mV holding potential before stepping to -60mV so as to coincide with maximal ATP-evoked current recorded at aepP2X.

2.6.5 Electrophysiology data analysis and presentation

Electrophysiology data were acquired using Clampex 9.0 (Axon Instruments), and analysed using Clampfit 9.0 (Axon Instruments). Statistics analyses were performed using GraphPad Prism 6.0 (GraphPad Software Inc., La Jolla, CA, USA). Data were plotted as peak current amplitudes or normalised current. Data were normalised to the maximum peak current in a dataset.

Data are presented as either grouped means (± standard error of the mean (SEM)), or as representative recordings, or both. Statistical comparisons were performed using repeated measures one-way ANOVA with Tukey's multiple comparison *post-hoc* test. The level of statistical significance was set at $p < 0.05$. The number of cells (n) tested in each experiment is shown in parentheses in text and figures.

2.6.5.1 ATP concentration-response curves

Data generated from concentration-dependent responses to extracellular ATP were fitted using the Hill equation:

$$Y = Maximum + \frac{Maximum - minimum}{1 + \left(\frac{X}{EC_{50}}\right)^{n_H}}$$

where Y is recorded current, Maximum is the largest peak current in a recording, Minimum is the smallest peak current, and EC_{50} is the ATP concentration that evokes 50% of maximum peak current, and n_H is the Hill coefficient.

2.6.5.2 aepP2X mono- and divalent cation permeability

Ionic permeabilities were calculated from shifts in recorded reveral potentials (E_{rev}) in solutions containing an ion of interest. Permeabilities are reported as relative to that of Na^+ ions (P_X/P_{Na}; where P_X is the ionic permeability of an ion *x* of interest, and P_{Na} is the permeability of Na^+ ions).

Reversal potential (E_{rev}), the voltage at which point the net ionic flux reverses direction, was calculated across a 1-2 mV portion of the current-voltage relationship, fitted with a linear function. Theoretical liquid junction potentials (LJP) arising from the differences in ionic compositions of extracellular solutions were calculated using JPCalcW (Barry, 1994) and subtracted from holding potential, accordingly. Resistance arising from the electrode and cell membrane (together representing the 'input resistance' observed by the amplifier) was not adjusted for in analyses of ionic permeability through aepP2X; 'compensation' for input resistance does not alter reversal potential between extracellular solutions of different ionic composition.

Monovalent ion permeabilities (P_X/P_{Na}) were calculated from:

$$P_X/P_{Na} = exp^{(\Delta E_{rev} F/RT)}$$

where ΔE_{rev} is the change in reversal potential between solutions of different ionic compositions, F is the Faraday constant (96485 C.mol^{-1}), R is the universal gas constant (8.31 J.mol^{-1}K^{-1}), *and* T is absolute temperature (298 K).

Relative permeability of Ca^{2+} to Na^{+} (P_{Na}/P_{Ca}) was calculated using a modified form of the Constant Field Equation according to Evans *et al.*, 1996, described by:

$$P_{Ca}/P_{Na} = \left([Na^{+}]_i \, exp^{E_{rev}F/RT}\right) - (P_{NMDG}/P_{Na})[NMDG^{+}]_o) \cdot \left[\frac{1 + exp^{E_{rev}F/RT}}{4[Ca^{2+}]_o}\right]$$

where P_{Ca}/P_{Na} is the relative permeability of Ca^{2+} ions to Na^{+} ions and E_{rev}, F, R, and T retain their definitions.

2.6.5.3 aepP2X chloride ion permeability

Relative chloride ion permeability was calculated according to

$$P_{Cl}/P_{Na} = \frac{\{1 - exp^{E_{rev}F/RT}([Na^{+}]_o - [Na^{+}]_i exp^{E_{rev}F)/RT})\}}{\{([Cl^{-}]_i exp^{-E_{rev}F/RT} - [Cl^{-}]_o)(1 - exp^{E_{rev}F)/RT})\}}$$

where P_{Cl}/P_{Na} is the relative permeability of Cl^{-} to Na^{+} ions. E_{rev}, F, R and T retain their meanings.

2.7 IMMUNOHISTOCHEMISTRY

To investigate the localisation of P2X receptor protein in *H. vulgaris* (AEP), immunohistochemistry (IHC) was performed on whole adult polyps. All polyps used in IHC were starved for 2 days prior to fixation.

2.7.1 Polyclonal antibody generation and choice of antigenic region

The current range of commercially available monoclonal and polyclonal antibodies against mammalian P2X receptors target epitopes in either the large extracellular domain region or intracellular N- or C-termini. Of the antibodies available against mammalian P2X homologues, primary amino acid sequence identities with aepP2X was low, making them unsuitable for use in determining protein localisation by IHC. As such, candidate antigenic regions were sought in the primary amino acid sequence of aepP2X based upon the topological position of homologous regions targeted by currently available commercial P2X receptor antibodies.

A polyclonal antibody using a rabbit host was developed in conjunction with Pierce Antibody (Thermo Fisher Scientific Inc., Rockford, IL, USA). An 18-mer peptide (H_2N-LLKKRFIYKEYKYQKIDD-COOH; molecular mass: 2393.88 Da), within an intracellular region of aepP2X was used for the generation of a synthetic peptide for rabbit immunisation. This decision was based on the Kyte-Doolittle hydrophilic profile (Kyte and Doolittle, 1982) of aepP2X (Fig. 2.3A1 and B1), which co-incided with transmembrane domain regions. The chosen antigenic region was predicted to lie below the predicted TM2 region of the aepP2X receptor (Fig. 2.2A2 and B2) within the receptor C-terminus. Furthermore, this region had an antigenic index of approximately 0.2 (Fig. 2.3A3 and B3) and surface probability of 0.7 (Fig. 2.3A4 and B4), suggesting it displayed immunogenicity and thus could induce the formation of antibodies against it.

Another hydrophilic and antigenic region was also predicted within the ECD of aepP2X (amino acid region 117 to 140). This region was not chosen due to the presence of a predicted *N*-linked glycosylation motif ('Nx(S/T)', where x is any amino acid except proline) that may reduce binding efficiency of IgG antibodies to aepP2X.

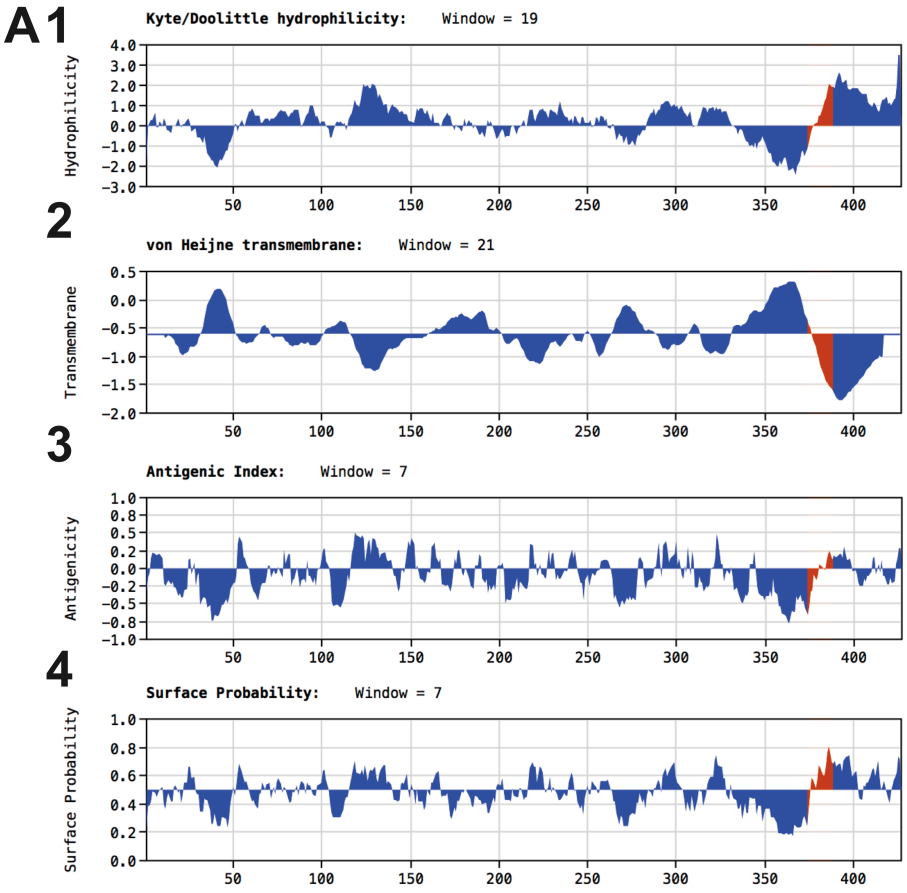
A1
Kyte/Doolittle hydrophilicity: Window = 19
Hydrophilicity
2
von Heijne transmembrane: Window = 21
Transmembrane
3
Antigenic Index: Window = 7
Antigenicity
4
Surface Probability: Window = 7
Surface Probability

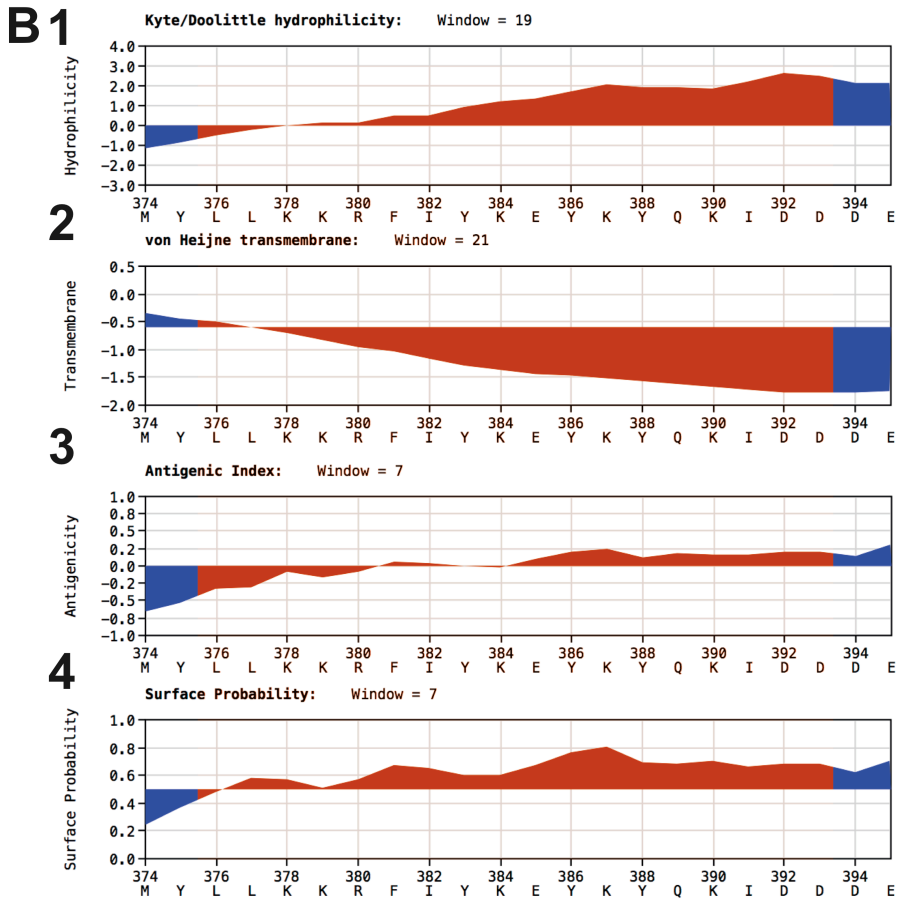
B1
Kyte/Doolittle hydrophilicity: Window = 19
Hydrophilicity
2
von Heijne transmembrane: Window = 21
Transmembrane
3
Antigenic Index: Window = 7
Antigenicity
4
Surface Probability: Window = 7
Surface Probability
M Y L L K K R F I Y K E Y K Y Q K I D D D E

Fig. 2.3: prediction of a suitable antigenic region for generation of a custom polyclonal antibody

In all plots (***A1*** to ***A4***), the region in which the antigenic peptide lies is highlighted in red. ***A1***, Kyte-Doolittle hydrophilicity profile of the full-length amino acid sequence of aepP2X. Regions predicted (with high probability) to be embedded within the membrane (notably transmembrane domains) lie had a hydrophilicity value of ≤ 1.0. ***A2***, von Heijne transmembrane domain (TMD) plot of aepP2X, where TMDs were predicted to be present if regions had a value greater than 1.0. At the C-terminus a short region predicted to display antigenicity (***A3***), and corresponding positive surface probability (***A4***). ***B1-B4***, expanded plots of the highlighted regions depicted in ***A1-A4***. The 18-mer amino acid sequence H_2N-LLKKRFIYKEYKYQKIDD-COOH (included below each plot) was chosen, and a peptide corresponding to this region synthesised for immunisation in rabbits.

'New Zealand that are Specific-Pathogen Free' strain white rabbits were used to generate the polyclonal antibody. To assess non-specific staining that may give spurious results in downstream applications, sera from five rabbits prior to immunisation (pre-immune sera) were used for IHC in whole fixed *Hydra* polyps *as per* the protocol detailed in section 2.7.2 at 1:2000 dilutions. From this, two rabbits from which sera gave the lowest level of background 'staining' were chosen for the immunisation protocol. These two rabbits (PA5618 and PA5619) were injected subcutaneously at day 0 with 0.25 mg of peptide antigen (in Complete Freund's Adjuvant) and 'boosted' with a further 0.1 mg at day 14. Blood serum (2 ml per rabbit) was sampled at days 0 (point of immunisation), 28, 56, 72 and 90, and used as described in section 2.7.2 at dilutions ranging from 1:500 to 1:5000. Rabbits were terminally bled at day 128.

2.7.1.1 Concentration of affinity-purified antibody solution

Following termination of the immunisation protocol, a 0.3 mg/ml solution of peptide affinity-purified anti-P2X polyclonal antibody (prepared from Day 72 serum; Thermo Fisher Scientific Inc.) was concentrated to approximately 20 mg/ml using a disposable protein concentrator (Pierce® Concentrator 9K molecular weight cut-off (MWCO) Thermo Scientific Inc.). An equal volume of 100% glycerol was added to the concentrate to reduce antibody denaturation due to repeated freeze-thaw cycles. NaN_3 (to a final concentration of 0.02% (w/v)) was also added to inhibit microbial growth. Aliquots of 10 µl were stored at -20 °C.

2.7.1.2 Preparation of Mowiol 4-88 mounting solution

For mounting of *Hydra* polyps on glass coverslips following whole-mount immunohistochemistry (IHC) (section 2.7.2), stocks of Mowiol 4-88 mounting solution were prepared as described previously (Harlow and Lane, 1998). Briefly, 4.8 g Mowiol 4-88 was mixed by hand with 12 g glyercol in a 100 ml glass beaker. Using a stir bar, 12 ml ddh_2O was added and stirred for approximately 3-5 hours at RT. Whilst continuing to stir the mixture, a further 24 ml of 0.2 M Tris-HCl (pH 8.5) was added, heating occasionally for 10 mins at 50 °C in a water bath until all Mowiol 4-88 had dissolved. Once dissolved, the mixture was centrifuged for 15 mins at 500 x *g* to clarify the solution. Aliquots of 5 ml were frozen at -20 °C where it remains stable for approximately 12 months. Once thawed, aliquots were kept at RT for a maximum of 1 month.

2.7.2 IHC protocol

IHC in whole fixed *Hydra* was performed using a protocol originally developed for use in *Drosophila* maxillary palps (Goldman *et al.*, 2005). 5 to 10 polyps were relaxed in 2% urethane (in S-medium) for 2 mins and fixed firstly in 4% methanol (MeOH)-free paraformaldehyde (PFA) (Thermo Fisher Scientific) in S-medium for 30 mins at RT, followed by 30 mins in 4% PFA in 1x PBS/0.2% (v/v) Triton X-100 (PTX). Fixative was removed and polyps rinsed 3x in PTX before washing 4 x 15 mins in PTX on a nutating rocker. Polyps were blocked in PTXb (1x PTX/3% (w/v) BSA) in a 1.5 ml microcentrifuge tube for 1 hour at RT, after which they were incubated with the primary antibody in PTXb at the appropriate concentration as detailed in Table 2.9 overnight at 4 °C. The following day, polyps were washed in 3 x 30 mins in PTX and then incubated in with an appropriate secondary antibody at 1:500 (typically 2 μg) for 2 hours at RT. A final series of washes (3 x 30 mins) in PTX were performed before mounting polyps in Mowiol 4-88 (Sigma-Aldrich) overlayed with a coverslip. Mounted slides were left to harden for 1 hour before visualisation using an Olympus BX60 epifluorescence microscope (Olympus, Southend-on-Sea, Essex, UK). For longer term storage (up to 3 days) of samples, coverslips were sealed with nail polish and stored in the dark at 4 °C.

Table 2.9: primary (1°) and secondary (2°) antibodies used in IHC and WB protocols

1°/2°	Host	Target	Conjugate	Supplier	Catalogue number	Use	Dilution
1°	Rabbit	Anti-GFP	Alexa Fluor® 488	Life Technologies	A-21311	IHC	1:5000
1°	Mouse	Anti-HHHH epitope	N/A	Qiagen	34670	WB	1:2000
1°	Mouse	Anti-β-actin	N/A	Abcam	ab8226	WB	1:5000
2°	Goat	Anti-rabbit	Alexa Fluor® 488	Life Technologies	A-11008	IHC	1:500
2°	Goat	Anti-rabbit	Alexa Fluor® 594	Life Technologies	A-11012	IHC	1:500
2°	Goat	Anti-rabbit	Alexa Fluor® 350	Life Technologies	A-11046		
2°	Horse	Anti-mouse	HRP	Cell Signalling Technologies	7076	WB	1:500

2.8 GENERATION OF TRANSGENIC *H. VULGARIS* (AEP) POLYPS

Transgenic *Hydra* in which an eGFP molecule was N-terminally fused to a P2X receptor under the control of the β-actin promoter (referred to herein as 'actin-P2X::eGFP') were developed in collaboration with Jörg Wittlieb and Dr Konstantin Khalturin (Prof. Dr Thomas Bosch research group) (Transgenic *Hydra* Facility, Christian-Albrechts Universität zu Kiel, Germany).

2.8.1.1 Construction of plasmids for microinjection

Constructs used to generate transgenic *H. vulgaris* (AEP) shared the common vector 'hotG' (Wittlieb *et al.*, 2006), a modified form of the pUC19 plasmid (Vieira and Messing, 1982) that consists of the β-actin promoter and terminator flanking an enhanced GFP (*egfp*) transcript region (Wittlieb *et al.*, 2006).

2.8.1.1.1 Actin promoter-driven expression of a P2X::eGFP fusion protein

For generation of transgenic *Hydra* overexpressing a *H. vulgaris* (AEP) P2X receptor::eGFP fusion protein driven by a *H. magnipapillata* β-actin promoter and terminator, the coding region of the *H. vulgaris* (AEP) P2X receptor (*aepp2x*) was amplified from adult polyp cDNA and inserted upstream of the eGFP cassette of the hotG vector. The coding region of *aepp2x* was amplified using PCR and the primers aepp2x_F_SbfI and aepp2x_R_PacI (Appendix, Table A12) resulting in an amplicon with 5' *Sbf*I and 3' *Pac*I restriction enzyme sites respectively. Both the gel-purified (section 2.4.3.1) *aepp2x* PCR amplicon and hotG vector were digested using *Sbf*I and *Pac*I restriction enzymes. Following ligation and transformation, constructs were sequenced using insert-specific primers (Appendix, Table A13) and the chosen colony used to generate a midiprep-scale stock of plasmid for embryo microinjection (section 2.8.1.2).

2.8.1.1.2 P2X promoter-driven expression of eGFP

For generation of transgenic *H. vulgaris* (AEP) polyps expressing eGFP under the control of a *H. magnipapillata* (105) P2X receptor and terminator (p2xprom-eGFP), a ca. 1.3 kb region predicted to constitute the *H. magnipapillata* P2X receptor promoter was amplified using the primers Hmp2xp_F_XbaI and Hmp2x_R_SbfI (Appendix, Table A112). These primers generate an amplicon with 5' *Xba*I and 3' *Sbf*I restriction sites, which was digested and ligated into the hotG vector thus replacing the original *H. magnipapillata* (105) actin promoter. The predicted terminator sequence of the *H. magnipapillata* P2X receptor gene was amplified using PCR and the primers Hmp2xt_F_AsiSI and Hmp2xt_R_Sbf1 (Appendix, Table A11) so as to introduce 5' AsiSI and 3' *Spe*I restriction sites into the terminator amplicon. Similarly, this amplicon was digested, and ligated into the hotG vector, replacing the original *H. magnipapillata* (105) β-actin terminator. PCR reactions were performed as described in section 2.4.5.2.2. The resultant plasmid construct (*Hmp2xp-egfp*) was prepared was sequenced using primers detailed in the Appendix (Table A11), and prepared for embryo microinjection (section 2.8.1.2).

2.8.1.2 Microinjection of *H. vulgaris* (AEP) embryos

Microinjection of *H. vulgaris* (AEP) embryos was performed in collaboration with Jörg Wittlieb (Prof. Thomas Bosch research group, Zoologisches Institüt, Christian-Albrechts Universität zu Kiel, Kiel, Germany).

Following purification (section 2.4.6.8), the plasmid construct was diluted to 1 µg/µl in a final volume of 15 µl nuclease-free water. Rhodamine B isothiocyanate–Dextran conjugate (Sigma-Aldrich) was added at 10% (v/v) final concentration for visualisation of construct solution following microinjection. The plasmid/rhodamine-dextran mixture was subsequently centrifuged for 2 hours at maximum speed at 4 °C to pellet any impurities present with aliquots of 3 µl removed from the final sample, being careful not to disturb any impurities that may have been collected during centrifugation.

Sexually reproducing polyps of *Hydra vulgaris* (AEP) readily develop viable embryos under laboratory conditions when fed intermittently. Embryos at the 2-8 cell-stage were manually separated from mature polyps of *Hydra* using a sterile scalpel blade and teasing needle under low magnification. Following separation from the main body of the polyp (using a sterile scalpel, cutting the adjoining 'egg cup' formation) embryos were maintained in a shallow Petri dish in S-medium prior until microinjection.

Embryos were injected according to Wittlieb *et al*. (2006) with minor modifications. Briefly, embryos were transferred to a shallow depression slide filled with S-medium (section 2.3.1) and mounted on a Zeiss Axiovert 100 inverted microscope (Carl Zeiss Microscopy GmBH, Munich, Germany) and correctly orientated and stabilised using gentle suction provided *via* a CellTram Vario pump (Eppendorf GmBH, Hamburg, Germany). Micropipettes for injection were pulled from borosilicate glass using a P-97 Flaming/Brown Micropipette Puller (Sutton Instruments Inc., CA, USA) and backfilled with 3 µl plasmid/10% (v/v) rhodamine-dextran solution (Sigma-Aldrich). Rhodamine-dextran was included in the plasmid mixture to confirm injection of plasmid in embryos by fluorescence microscopy. Embryos were injected at the apex of each cell with approximately 0.1 µ1 of construct (0.6 µg/µl) using a FemtoJet compressor module (Eppendorf). Following injection, embryos were maintained in

individual wells of a 12-well cell culture plate in S-medium at 18 °C and monitored regularly for expression of eGFP using a Leica Fluo MSV269 stereomicroscope (Leica Microsystems (UK) Ltd, Milton Keynes, Buckinghamshire, UK). Following hatching, transgenic *Hydra* expressed patches of eGFP-expressing cells ('chimeric polyps') in endodermal epithelial cells. Chimeric *Hydra* were maintained as described previously (sections 2.3.1 and 2.3.2) until polyps homogeneously expressed the P2X::eGFP fusion protein in all endodermal epithelial cells, with polyps propagating by asexual budding (section 1.7.5).

Chapter 3:

Cross-phylum analysis of predicted invertebrate P2X receptors

3 Cross-phylum analysis of predicted invertebrate P2X receptors

3.1 AIMS OF THE CURRENT CHAPTER

A comprehensive analysis of primary amino acid sequences identified through homology searching for P2X receptor homologues across a range of phyla is lacking in the literature. The current chapter aims to identify novel P2X receptor by homology searching of genomic and transcriptomic datasets of organisms from a range of phyla, with a major focus on the large Invertebrate group of organisms. Following retrieval, partial and full-length primary amino acid sequences corresponding to putative P2X receptor homologues were analysed, drawing upon our current understanding of the contribution of residues to the activation, modulation, and structural integrity of higher P2X receptors. In addition to the identification of novel P2X receptors in diverse range of phyla, special consideration is drawn to the evolution of this class of ligand-gated ion channel (LGICs), highlighting the extent to which this family is found within the evolutionary 'tree of life'. Furthermore, data are also presented that provide the first known illustration of P2X receptors from members of the large Insecta class of arthropods.

3.2 INTRODUCTION

Expansion of available genomic and transcriptomic sequence datasets of organisms from diverse phyla has enabled researchers to identify homologous sequences of biological and evolutionary interest. Indeed the development of high-throughput, 'next-generation' sequencing techniques has enabled the efficient assembly of sequence data from organisms that lack a reference genome (Metzker, 2010). RNA sequencing ('RNA-seq') tools are an especially low cost and rapid tool in determining the sequence of RNA transcripts that encode proteins (Marioni *et al.*, 2008). Furthermore, tissue- and developmental stage-specific transcriptomes can provide valuable information regarding transcript function and global expression levels within an organism (Metzker, 2010). In recent years, the expansion of both genomic and transcript sequence data has led to an increase in the identification of proteins with sequence identity to mammalian P2X receptors in a number of

invertebrate organisms. Furthermore, the cloning of P2X receptors from invertebrate organisms at key junctures in the evolutionary 'tree of life' has prompted the discussion of the evolutionary origins of this ligand-gated ion channel (LGIC) family.

A number of literature reviews, as well as original articles detailing the cloning, pharmacological and functional characterisation of P2X receptors from non-mammalian organisms have alluded to the presence of receptor homologues in invertebrate organisms. Furthermore, the apparent absence of a P2X receptor homologue has also been noted in some members of the Insecta class of the Arthropoda phylum (Harte and Ouzounis, 2002; Fountain and Burnstock, 2009; Fountain, 2013).

The increased availability of primary sequence data for a range of organisms has led to the identification of homologues of mammalian genes in diverse phyla more easily. As such, our understanding of the extent to which P2X receptors are found within the evolutionary 'tree of life' has expanded, leading to the identification of receptor homologues with novel pharmacological and functional characteristics. This was demonstrated by the identification, cloning and characterisation of a P2X receptor from the slime mould *Dictyostelium discoideum*, wherein the receptor was shown to play a novel intracellular role in osmoregulation (Fountain *et al.*, 2007). Furthermore, this receptor lacks many residues that have been shown previously to be required for correct P2X receptor function in human subunits, such as some involved in ATP binding (Fountain *et al.*, 2007). Despite this, many *D. discoideum* P2X isoforms are able to respond in a concentration-dependent manner to extracellular ATP in heterologous systems (Fountain *et al.*, 2007; Ludlow *et al.*, 2009; Baines *et al.*, 2013).

By identifying P2X receptors across a range of phyla, through the use of homology (BLAST) searching, potentially novel homologues may be uncovered. Furthermore, our knowledge of the organisms within which P2X receptor homologues are expressed will also be extended, allowing us to uncover the evolutionary history of this ligand-gated ion channel family.

3.2.1 P2X receptor motifs and key residues

The contribution of many amino acid residues and motifs to the function and expression of P2X receptors have been discussed previously within the current thesis (section 1.3). Whilst many residues have been the subject of site-directed mutagenesis studies of P2X receptor function, a core subset of residues are discussed in the current chapter; those involved in ATP binding, cysteine residues found in the large extracellular domain of P2X receptors, an N-terminal PKC phosphorylation motif, and a canonical C-terminal membrane localisation motif. Residues involved in conferring sensitivity to structurally related ATP agonists, and to the action of P2 receptor antagonists, although conserved amongst some P2X receptor subunits, are incompletely conserved across the P2X family as a whole. As such, these residues were not considered during the initial assessment of retrieved sequences following BLAST searches.

A retrieved sequence was considered a 'candidate' P2X receptor if it satisfied the following criteria, determined through multiple sequence alignments with previously characterised P2X receptor homologues and protein topology analysis:

1. A predicted protein topology of an extracellular domain (ECD) flanked by two extended regions of hydrophobicity (corresponding to transmembrane domains (TMDs) and intracellular termini
2. The presence of shared conserved cysteine residues within the predicted ECD
3. Shared ATP binding residues within the ECD
4. The presence of a membrane localisation motif (YxxxK, or variant thereof where x is any amino acid residue) (Chaumont *et al*., 2004) within the predicted C-terminal region of the retrieved receptor sequence
5. The presence of an N-terminal putative PKC phosphorylation motif (YxTx(K/R))

Further details regarding the assessment of retrieved sequences are provided in section 2.2.1.

3.3 RESULTS

Provided in the supplementary data accompanying this chapter is a spreadsheet detailing all hits retrieved following homology searching for candidate P2X receptors. These data are provided with details of *E*-values, scores, alignment lengths of the query sequence used and the protein region to which it aligns, and the associated accession number of retrieved hits.

3.3.1 P2X receptors in the Deuterostomia superphylum

The Deuterostomia superphylum is a major group of the Animalia kingdom, and a sister branch to the Bilateria, those organisms that display bilaterial symmetry along an axis (Blair and Hedges, 2005). Within the deuterostomes are the Chordata, Echinodermata, Hemichordata phyla and, debatably, the Xenoturbellida phylum.

3.3.2 P2X receptors in the Chordata

The Chordata phylum encompasses a large number of organisms that possess a notochord (although this may only be transiently present during embryogenesis), and a dorsal hollow nerve cord (Holland, 2005). They include the well-known vertebrates (fish, amphibians, birds, reptiles, and mammals), the urochordates (tunicates), and cephalochordates (amphioxus/lancelets). Together, these three phyla form the Deuterostomia superphylum. Much of our understanding of the molecular structure and function of P2X receptors has been derived from studies in vertebrate species, notably mice, rats, and humans. To assess the conservation of P2X receptors in Chordata, the genomes of members of the Urochordata and Cephalochordata subphyla were searched for receptor homologues.

The genomes of two tunicates are currently available: *Ciona intestinalis* (vase tunicate) (Dehal *et al.*, 2002), and *Ciona savignyi* (Vinson *et al.*, 2005; Small *et al.*, 2007), in addition to the genome of the cephalochordate *Branchiostoma floridae* (Florida lancelet) (Putnam *et al.*, 2008). No P2X receptor homologue was identified in either *C. intestinalis*, or *C. savignyi*, even in low stringency search conditions. Homology searching of these genomes identified a single coding sequence (CDS) of

1204 bp (XM_002605779.1; *Bflo*_p2x) encoding for a 401 amino acid protein with 24.2 to 45.2% sequence identity with hP2X1-7 subunits in *B. floridae*.

Multiple sequence alignment (MSA) with hP2X1-7 highlighted that *Bflo*_p2x is missing a 25 amino acid region in the predicted ECD of the protein. The analogous region in hP2X1-7 receptors contained two cysteine residues (hP2X1 numbering: C126 and C132) that are required in human isoforms to maintain structural integrity of the ECD (Ennion and Evans, 2002a; Clyne *et al.*, 2002b). However, many other regions characteristic of human and invertebrate P2X receptors are shared between *Bflo*_p2x and human homologues, and provided support for the presence of P2X receptors early in the chordate lineage.

3.3.3 P2X receptors in the Echinodermata and Hemichordata

Sharing a common Deuterostomia ancestor with Chordata, the Echinodermata (sea urchins, starfish, and sea cucumbers) and Hemichordata (acorn worms) phyla are composed of marine invertebrates.

The genomes of the echinoderm *Strongylocentrotus purpuratus* (purple sea urchin) (Sodergren *et al.*, 2006), and the hemichordate *Saccoglossus kowalevskii* (acorn worm) were searched for P2X receptor homologues. Previous studies have highlighted the presence of a P2X receptor homologue in the genome of *S. purpuratus* (Fountain and Burnstock, 2009; Cai, 2012). Homology searching of the *S. purpuratus* genome retrieved four sequences that met the criteria required for further consideration: XM_003727933.1 (*Spur*_p2xA); XM_791095.3 (*Spur*_p2xB); XM_787091.3 (*Spur*_p2xC); and XM_787766.3 (*Spur*_p2xD). Multiple sequence alignment of these retrieved sequences revealed a high percentage sequence residue identity between *Spur*_p2xA and *Spur*_p2xB (87.6%). However, a lower percentage identity was seen between both *Spur*_p2xA and *Spur*_p2xB, and *Spur*_p2xC and *Spur*_p2xD (10.1 to 28%). This is explained by the larger predicted length of this latter two retrieved hits of 702 and 716 amino acids, in comparison to 429 and 455 residues for *Spur*_p2xA and *Spur*_p2xB, respectively. Analysis of hydrophilicity of these sequences predicted two transmembrane domains (TMDs) in both *Spur*_p2xA and *Spur*_p2xB, flanking a large extracellular domain (ECD), whilst only one TMD

is predicted in the primary amino acid sequence of *Spur*_p2xC. No TMDs were predicted in *Spur*_p2xD. Although only one TMD was predicted in *Spur*_p2xC, an extracellular domain preceded this region. Multiple sequence alignment of *Spur*_p2xA-C with hP2X1-7 subunits predicted a region of 358 amino acids with a higher percentage sequence identity to *Spur*_p2xA and B, as well as hP2X1-7 subunits. This region corresponds to W47 to S400 in hP2X1 (P51575), which included residues all ATP binding sites and C-terminal 'YxxxK' motif. Of the ten ECD cysteine residues, nine were also conserved in *Spur*_p2xA-C. A tenth cysteine residue was present in *Spur*_p2xC, but appeared misaligned relative to the corresponding cysteine residue in *Spu*_p2xA and *Spu*_p2xB.

Analysis of the *S. kowalevskii* genome retrieved three predicted P2X receptor homologues: NM_001168169.1 (*Sko*_p2xA); XM_006821836.1 (*Sko*_p2xB); and XM_006821835.1 (*Sko*_p2xC). Translated products of these transcripts were 418, 419, and 290 amino acids in length, respectively, with multiple sequence alignment of these sequences revealing a shared residue identity amongst them of between 28.6 to 40.1%, and 16.2 to 51.2% with hP2X1-7 receptors. Key ATP binding residues are largely conserved in *Sko*_p2xA-C with the exception of equivalent N290 (hP2X1 numbering) residue, where a serine was found in its place. An F291>Y residue change is also seen in *Spur*_p2xC, in addition to 11 amino acids inserted within the conserved 'NFR' ATP binding motif found in many P2X receptor subunits (*Sko*_p2xC numbering: N194 to R207). A number of ECD cysteine residues are seemingly absent in the primary protein sequence of *Sko*_p2xC. Six cysteine residues, corresponding to conserved residues 1 to 6 (numbered in N-terminal to C-terminal order) in hP2X1-7 alignments, were seemingly absent. The C-terminal canonical membrane localisation motif ('YxxxK') was not conserved in *Sko*_p2xC, and appeared as 'FGGLC'. In *Sko*_p2xB, a similar motif is found at the equivalent position ('FDEIR'), and may suggest that there is not an absolute requirement for an aromatic tyrosine and basic lysine residue in the trafficking of P2X receptor to the cell membrane. Finally, The shorter sequences of both *Sko*_p2xB and *Sko*_p2xC suggested the absence of an N-terminal PKC phosphorylation motif in these proteins. This 'YxTx(K/R)' motif was identified in *Sko*_p2xA, but not in the sequence of *Sko*_p2xB or *Sko*_p2xC. Two transmembrane domains were predicted in *Sko*_p2xA, consistent with canonical P2X receptor topology. However, only one TMD was predicted in *Sko*_p2xB, and no TMD was predicted in *Sko*_p2xC.

3.3.4 P2X receptors in Arthropoda

The Arthropoda phylum is composed of five extant subphyla: Pycnogonida; Euchelicerata, Myriapoda, Crustacea and Hexapoda, (Edgecombe, 2010; Giribet and Edgecombe, 2012). To assess the extent to which P2X receptors are present in the Arthropoda, homology searching was performed within members of constituent subphyla. No genome is currently available for members of the Pycnogonida (marine sea spiders) subphylum, so could not be assessed for P2X receptor homologues.

3.3.4.1 P2X receptors in the Euchelicerata

The Euchelicerata includes a number of organism groups, including horseshoe crabs, scorpions, spiders and ticks (Arachnida), harvestmen, and Solifugae (Giribet and Edgecombe, 2012). To date, only one P2X receptor has been isolated from a member of the Euchelicerata (and indeed, the Arthropoda phylum as a whole): the cattle tick *Boophilus microplus* (Bavan *et al.*, 2011). Further analysis of available Euchelicerata transcriptomes from *Ixodes scapularis* (deer tick) identified three partial expressed sequence tags (ESTs) with homology to human P2X receptors. Following tBLASTn searching, three hits were retrieved that met inclusion criteria for further analysis: ISCW011650-RA (*Isc*_p2xA); ISCW019739-RA (*Isc*_p2xB); and ISCW019740-RA (*Isc*_p2xC). These partial ESTs encoded for partial protein sequences of 257, 318, and 81 amino acids, respectively. *Isc*_p2xA appeared to correspond to the homologous I144 to A371 region in hP2X1, with which *Isc*_p2xA shared a 37.7% sequence identity in pairwise alignment of the two homologous regions of these proteins. In contrast, pairwise alignment of *Isc*_p2xB and *Isc*_p2xC with hP2X1-7 suggested that these sequences share only a short sequence identity with human receptor subunits (homologous to regions G250 to R292 and L318 and V320, respectively). Consistent with the positions of these partial ESTs in multiple sequence alignment with hP2X1-7, *Isc*_p2xB was predicted to constitute a portion of the ECD of a P2X receptor, whilst *Isc*_p2xA and *Isc*_p2xC were predicted to include regions corresponding to the second transmembrane domain and partial ECD and C-terminal sequences.

Recently, draft genomes of two spider species have been made available; *Stegodyphus mimosarum* (African social velvet spider) and *Acanthoscurria geniculata* (Brazilian white-knee tarantula) (Sanggaard *et al.*, 2014). Homology searching of the genome of both *S. mimosarum* (BioProject ID: PRJNA222763) and *A. geniculata* (BioProject ID: PRJNA222762) returned high-scoring segment pair (HSP) alignments from both of these arachnids with sequence homology to hP2X1-7 receptors.

Retrieved hits from the transcriptome of *S. mimosarum* were of variable length, with no single hit appearing to represent a putative full-length sequence of a candidate P2X receptor. Multiple sequence alignment (MSA) of translated partial transcripts against hP2X1-7 receptors suggested that retrieved sequences represented portions of a predicted ECD and, in the case of the highest scoring hit (GAZR01003973.1), the second transmembrane domain and C-terminus. Pairwise alignment of this hit and the second and fourth highest scoring sequences (GAZR01004551.1 and GAZR01015239.1, respectively) revealed overlapping regions with 100% identity. GAZR01003973.1 and GAZR0100455.1, shared a 19 amino acid region, whilst GAZR0100455.1 and GAZR01015239.1 shared a 23 amino acid region (Fig. 3.1). This suggested that these three sequences may be derived from the same transcript. For further analysis, these sequences were merged and are referred to subsequently as *Smi*_p2x.

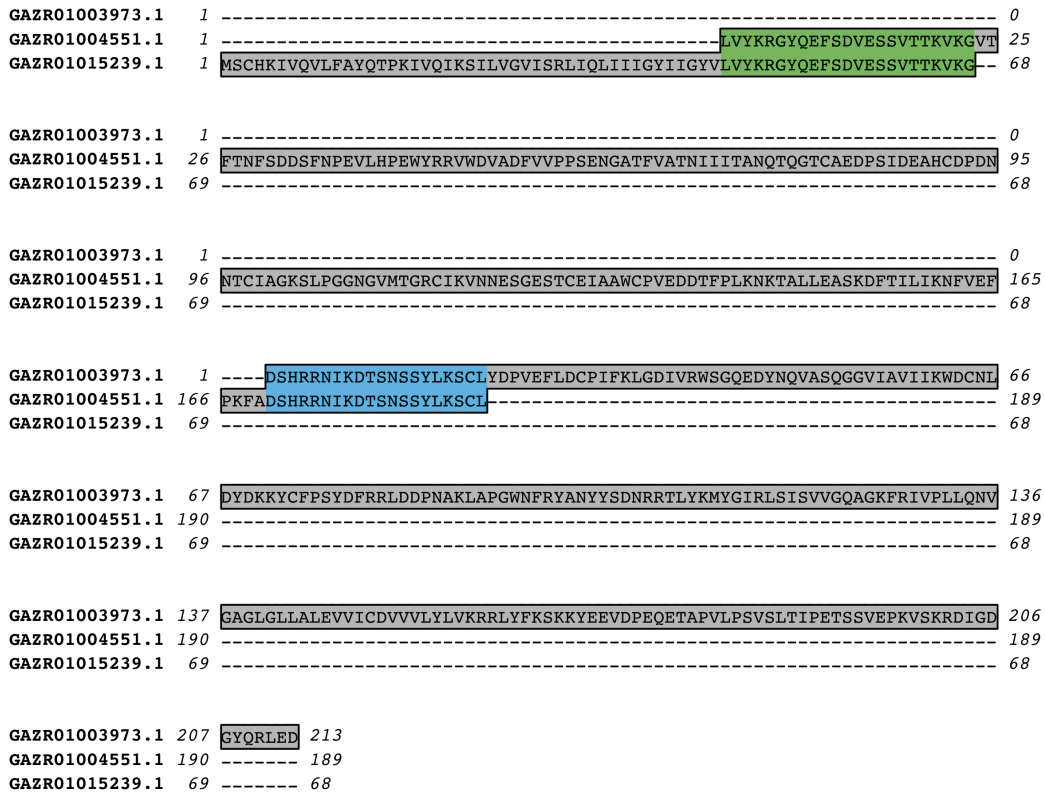

Fig. 3.1: multiple sequence alignment (MSA) of contiguous partial candidate *S. mimosarum* P2X receptor sequences

The protein products of three partial transcripts retrieved though homology searching of the transcriptome of the African social velvet spider (*S. mimorsarum*) was contiguous, suggesting that they represented a single transcript.

In MSA with hP2X1-7 subunits, *Smi*_p2x shared a 23.3 to 48% sequence identity with human receptor homologues, and shared all canonical ATP binding sites found in mammalian P2X receptor homologues. Topology analysis of *Smi*_p2x predicted two TMDs flanking a large ECD of 302 amino acids, as well intracellular N- and C-termini (Fig. 3.2). Furthermore, analysis of the primary sequence of these two termini identified an N-terminal PKC and a C-terminal membrane translocalisation motif, consistent with those found vertebrate and invertebrate P2X receptors (Fig. 3.2).

The remaining retrieved transcript sequence (GAZR01026140.1) encoded for a protein of 89 amino acids. MSA of this protein with *Smi*_p2x suggested that GAZR01026140.1 represented a portion of the first transmembrane domain (TM1) and a portion of the ECD of a candidate receptor (Fig. 3.2). Between the homologous

regions of *Smi*_p2x and GAZR01026140.1, the two sequences shared a 61.8% sequence identity. In light of differences in these protein sequences (which are also seen in the corresponding nucleotide sequences), these predicted transcripts might represent two distinct P2X receptors.

MSA of non-duplicated (non-redundant) translated protein products of retrieved transcripts from homology searching of *A. geniculata* suggested that at least two P2X-like genes are present in this tarantula. One of these non-redundant protein sequences (GAZS01036234.1) appeared to represent a truncated form of GAZS01036238.1 – these two sequences shared were identical except for a 25 residue region missing in the predicted ECD of GAZS01036234.1 (E105 to E123; GAZS01036238.1 numbering). Of the three retrieved sequences, only GAZS01073490.1 aappeared to represent a full-length sequence, and included a C-terminal membrane translocalisation motif (in contrast to the remaining two sequences, where this motif was seemingly absent) (Fig. 3.2). This sequence was subsequently renamed '*Age*_p2x'. Molecular cloning of these sequences would be required to determine whether this predicted absence is not due to sequencing error.

Further analysis of a tissue-specific transcriptome of the western black widow spider (*Latrodectus hesperus*) (Clarke *et al.*, 2014) identified a number of sequences with homology to human P2X receptors. Of the three retrieved transcripts, two appeared to represent a full length coding sequence (CDS): GBCS01010125.1 and GBCS01001793.1. These transcripts, and their respective translate products were subsequently termed *Lhe*_p2xA and *Lhe*_p2xB. *Lhe*_p2xA and *Lhe*_p2xB proteins shared a 52.9% primary sequence identity with each other, and a 22.9 to 44.5% identity with hP2X1-7 subunits. Consistent with P2X receptor topology both *Lhe*_p2xA and *Lhe*_p2xB possess two TMDs, a large ECD and two intracellular termini. All ten extracellular cysteine residues conserved amongst human P2X receptor subunits, as well as all ATP binding residues, were found in *Lhe*_p2xA and *Lhe*_p2xB (Fig. 3.2). N-terminal and C-terminal motifs were also conserved in these *L. hesperus* candidate P2X receptors (Fig. 3.2). Alignment of the *Lhe*_p2xA and *Lhe*_p2xB protein sequences with the translated products of the remaining two predicted transcripts (GBCS01015860.1) suggested that they represent C-terminal and regions of the ECD of putative P2X receptors. Unique assembled transcripts derived through *de novo* transcriptome assembly of cephalothorax, silk glands, or

venom glands tissue samples, suggested that P2X receptors may be expressed in the cephalothorax and venom glands of this spider, with no *p2x*-like transcripts in silk glands (Clarke *et al.*, 2014).

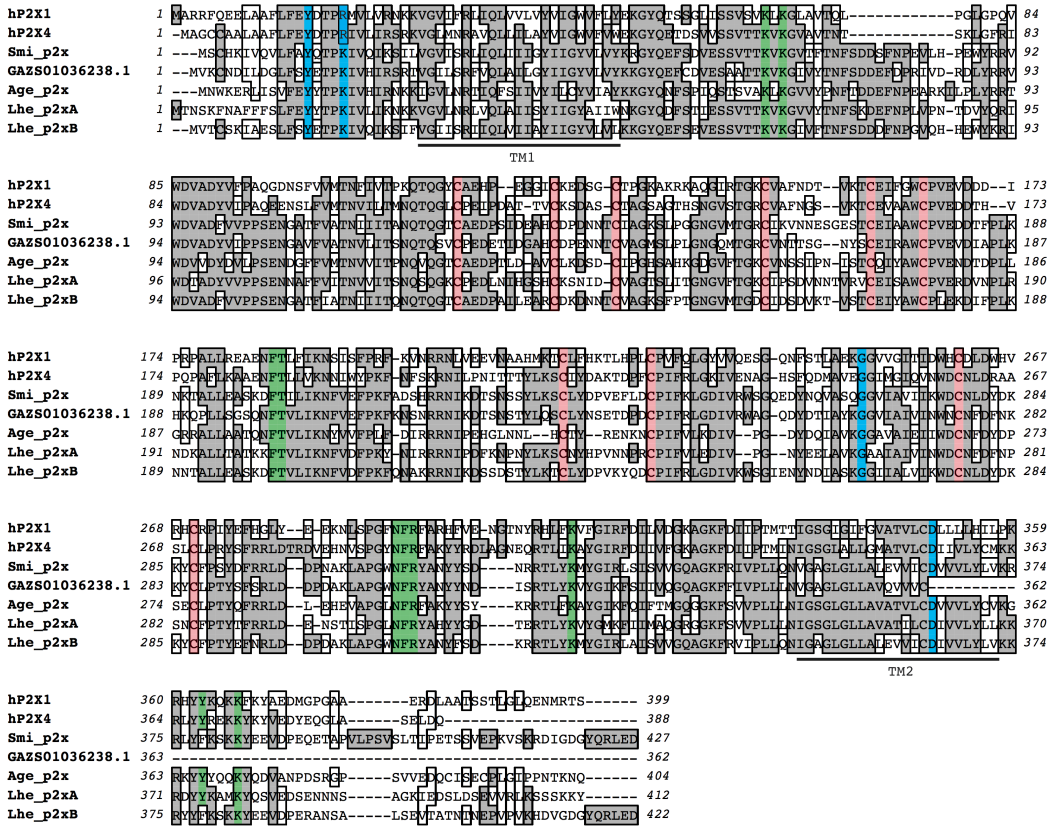

Fig. 3.2: MSA of candidate spider P2X receptors proteins

Protein sequences for predicted P2X receptor homologues from three spider species: *Stegodyphus mimorosum* (*Smi*_p2x); *Acanthascurria geniculata* (GAZS01036234.1 and *Age*_p2x); and *Latrodectus hesperus* (*Lhe*_p2xA and *Lhe*_p2xB) revealed a number of shared residues between these receptors and human P2X1 and P2X4 subunits. GAZS01036234.1 appeared to represent a truncated form of a full-length P2X receptor, due to the absence of a C-terminal 'YxxxK' translocalisation motif. Residues and motifs are highlighted accordingly: blue, N-terminal PKC phosphorylation motif and C-terminal membrane translocalisation motif, G250 and D250 (hP2X1 numbering) residues; green, ATP binding residues; red, extracellular domain cysteine residues. Transmembrane domains 1 and 2 (TM1 and TM2) are highlighted accordingly below the alignment, according to hP2X1 receptor sequence numbering. Sequences were aligned using the MUSCLE algorithm (Edgar, 2004) in MacVector.

3.3.4.2 P2X receptors in Myriapoda

The Myriapoda subphylum includes Chilopoda (centipedes), Diplopoda (millipedes), Pauropoda, and Symphyla (Miyazawa *et al.*, 2014). Transcriptomic data have recently been made available for a number of members of the Myriapoda phylum (Rehm *et al.*, 2014).

A single partial transcript sequence (GAKW01014925.1) was retrieved from the transcriptome of the pill millipede *Glomeris pustulata*. This returned HSPs of this partial sequence were non-overlapping, with the first encoding for a 279 amino acid protein, whilst the second encoded for a 51 amino acid protein. Hydrophilicity analysis suggested the first sequence represented a 6 residue intracellular N-terminus, TM1, and portions of a predicted ECD of a P2X receptor from *G. pustulata*. Conserved ATP binding residues (hP2X1 numbering) K68, K70, F185, and T186 were in the sequence of HSP1, whilst the remaining N290, N291, T292, and K309 were found within HSP2 (Fig. 3.3.). Furthermore, all ten ECD cysteine residues found in human P2X receptors were present within HSP1.

Furthermore, multiple partial transcript sequences were retrieved from the millipede *Strigamia maritima* following tBLASTn searching for a P2X receptor homologue in this species. Multiple sequence alignment of these retrieved sequences suggested that they were contiguous with each other (for example, AFFK01018242.1 and AFFK01017150.1), whilst others shared many residues. Furthermore, those regions that aligned with portions of hP2X1 and hP2X4 (Fig. 3.3) contained regions previously found to be important in P2X receptor function in mammals, such as the triplet 'NFR' ATP binding motif, and multiple ECD cysteine residues. Further molecular cloning is required in order to determine the full-length sequence of these sequences from both *G. pustulata* and *S. maritima*, although their high percentage sequence identity to human P2X receptor homologues, lent support to their being considered as candidate P2X receptors in this branch of the Arthropoda.

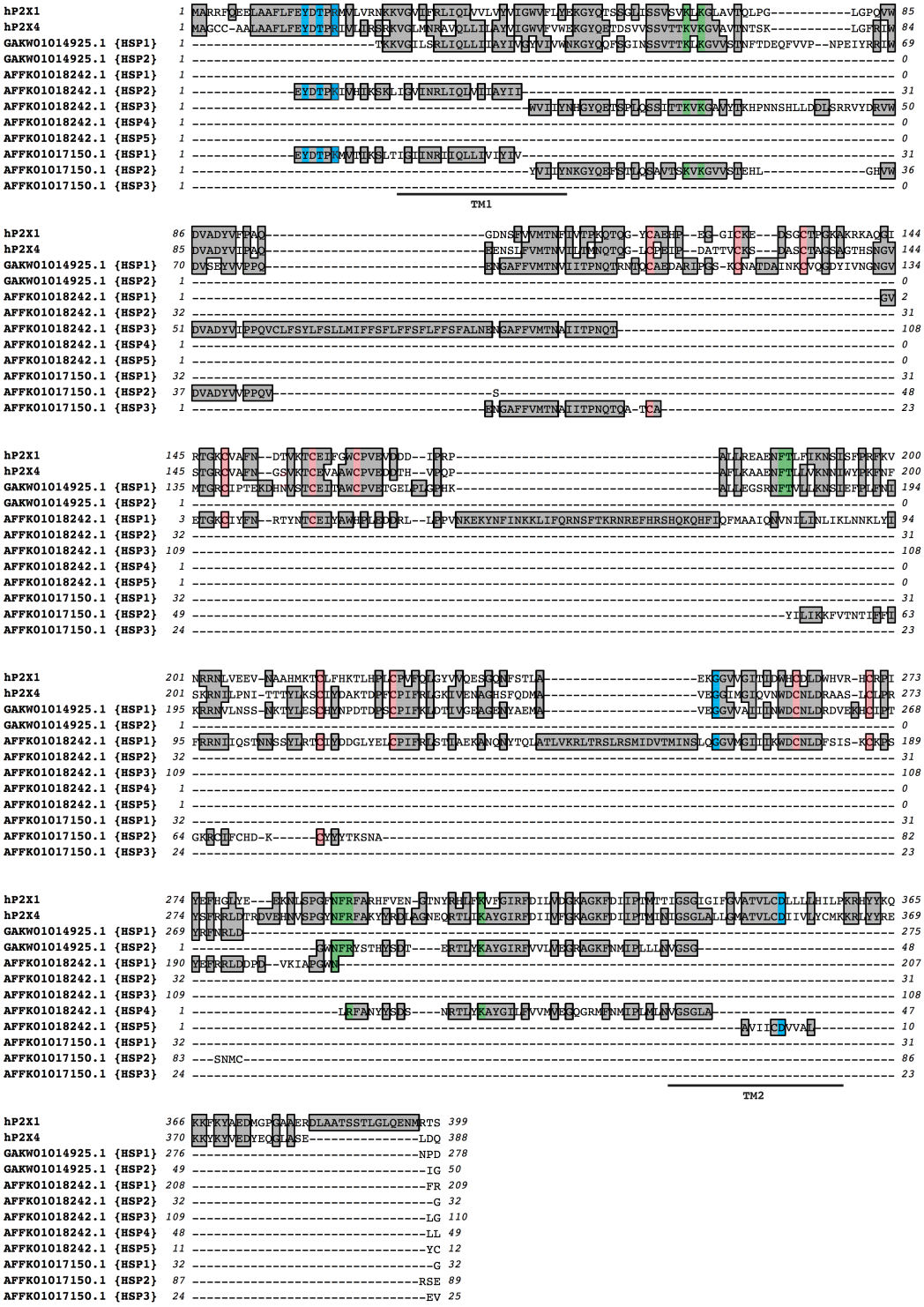
hP2X1
hP2X4
GAKW01014925.1 {HSP1}
GAKW01014925.1 {HSP2}
AFFK01018242.1 {HSP1}
AFFK01018242.1 {HSP2}
AFFK01018242.1 {HSP3}
AFFK01018242.1 {HSP4}
AFFK01018242.1 {HSP5}
AFFK01017150.1 {HSP1}
AFFK01017150.1 {HSP2}
AFFK01017150.1 {HSP3}
TM1
TM2

Fig. 3.3: MSA of candidate P2X receptors from the millipedes *G. pustulata* and *S. maritima*

Partial protein sequences corresponding to portions of a candidate P2X receptor homologues from two millipede species: *Glomeris pustulata* (GAKW01014925.1) and *Strigamia maritima* (AFFK0108242.1.1 and AFFK01017150.1) revealed a number of shared residues between these sequences and human P2X1 and P2X4 subunits. Many of the protein fragments retrieved from the transcriptome of *S. maritima* were almost contiguous, and may represent proteins derived from a full-length transcript. Residues and motifs shared between protein fragments and hP2X1 and hP2X4 are highlighted accordingly: blue, N-terminal PKC phosphorylation motif and C-terminal membrane translocalisation motif, G250 and D250 (hP2X1 numbering) residues; green, ATP binding residues; red, extracellular domain cysteine residues. Transmembrane domains 1 and 2 (TM1 and TM2) are highlighted accordingly below the alignment, according to hP2X1 receptor sequence numbering. Sequences were aligned using the T-Coffee algorithm (Notredame *et al.*, 2000) in MacVector.

3.3.4.3 P2X receptors in Crustacea

The large Crustacea subphylum includes crabs, lobsters, and shrimp amongst other organisms. Analysis of the only available crustacean genome – that of the branchipod *Daphnia pulex* (Colbourne *et al.*, 2011) – identified two candidate P2X receptors: hxNCBI_GNO_488034 (*Dpu*_p2xA), and hxNCBI_GNO_490034 (*Dpu*_p2xB). These candidate gene sequences are annotated on the reverse genome scaffold, separated by an intergenic region of approximately 5.2 kb. *Dpu*_p2xA and *Dpu*_p2xB genes are predicted to contain 7 and 8 exons, and are a total of 1648 and 1765 nucleotides in length, respectively. Predicted translated protein products of transcripts of these were 393 and 403 amino acids long, and shared an 86.9% primary sequence identity with each other. Between hP2X1-7 subunits, *Dpu*_p2xA and *Dpu*_p2xB shared a 23.9 to 44.4% primary sequence identity.

At the primary sequence level, *Dpu*_p2xA and *Dpu*_p2xB share a number of residues implicated in correct function of human P2X receptors. Consistent with human P2X receptor homologues, both *Dpu*_p2xB, possessed N- and C-terminal PKC and membrane translocalisation motifs. Furthermore, basic and aromatic amino acids conserved found in mammalian P2X receptors and many invertebrate homologues were also present in *D. pulex* homologues (Fig. 3.4).

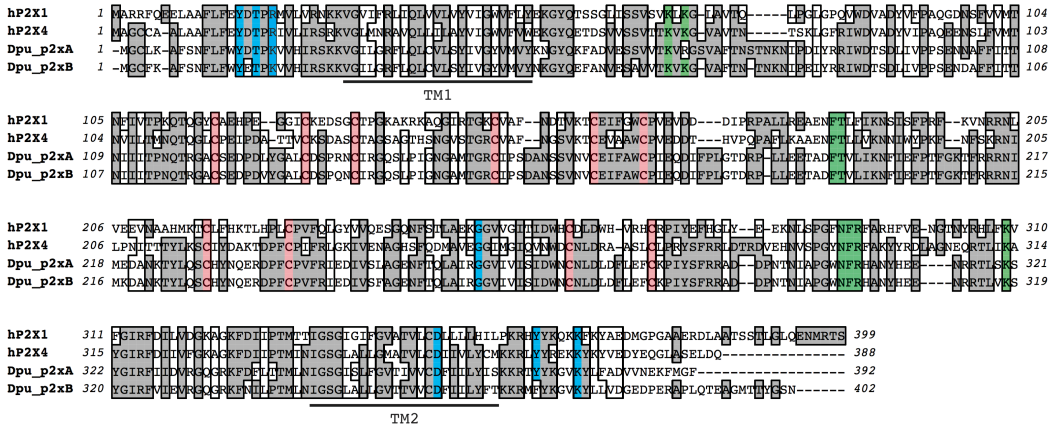

Fig. 3.4: MSA of predicted *Daphnia pulex* P2X receptor homologues

Protein sequences for predicted *D. pulex* P2X receptor homologues (*Dpu*_p2xA and *Dpu*_p2xB) revealed a number of shared residues between these receptors and human P2X1 and P2X4 subunits. Residues and motifs are highlighted accordingly: blue, N-terminal PKC phosphorylation motif and C-terminal membrane translocalisation motif, G250 and D250 (hP2X1 numbering) residues; green, ATP binding residues; red, extracellular domain cysteine residues. Transmembrane domains 1 and 2 (TM1 and TM2) are highlighted accordingly below the alignment, based on hP2X1 receptor sequence numbering. Sequences were aligned using the MUSCLE algorithm (Edgar, 2004) in MacVector.

3.3.4.4 P2X receptors in Hexapoda

The Hexapoda phylum is composed of two classes: the terrestrial Insecta class, as well as the wingless basal Entognatha class (Collembola + Protura + Diplura) (Gao *et al.*, 2008; Sasaki *et al.*, 2013) (Fig. 3.5).

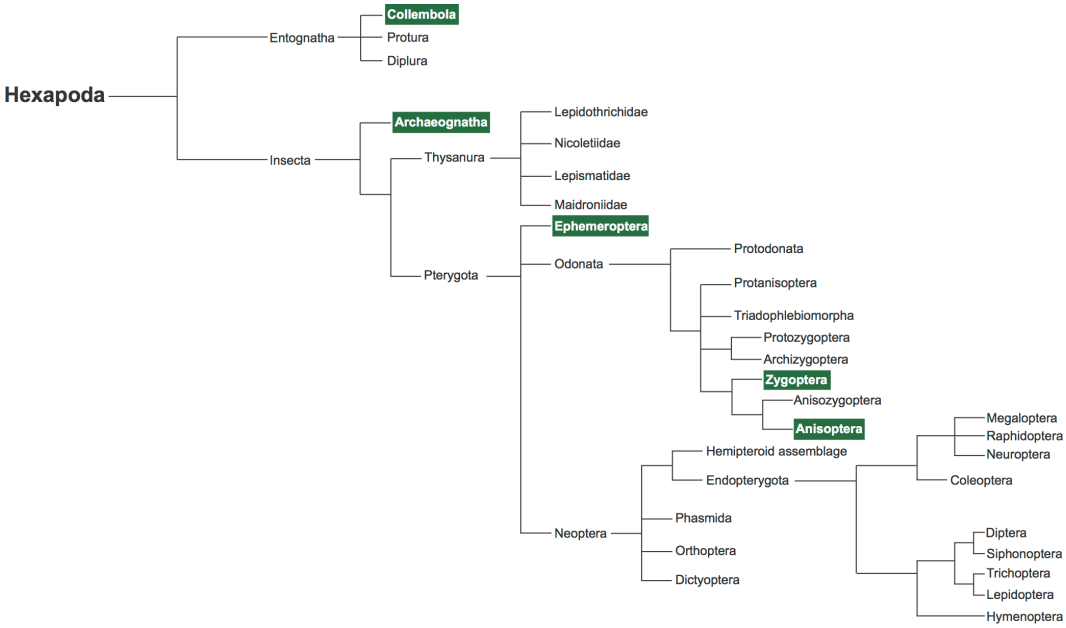

Fig. 3.5: Hexapoda phylogeny

The Hexapoda phylum is composed of two classes: Entognatha and Insecta (Ectognatha). Within the Entognatha are three orders, within which a candidate P2X receptor sequences were found in members of the Collembola (springtails). The Insecta includes bristletails, silvertails, and all winged insects. Candidate P2X receptor sequences were retrieved from members of the wingless Archaeognatha order (bristletails). Within the Pterygota subclass (winged insects), candidate P2X receptors were identified within the Ephemeroptera (mayfly). Within the carnivorous Odonata order (dragonflies and damselflies), candidate P2X sequences were found within the Zygoptera (damselflies) and Anisoptera (dragonflies). Within the Neoptera order are found the 'true insect' Diptera order, butterflies and moths (Lepidoptera) and Hymenoptera (wasps, bees, ants and sawflies). Although a P2X sequence was retrieved from EST data of the beetle *Diabtotica virgifera*, the high percentage sequence transcript nucleotide identity (ca. 99%) with a mammalian P2X4 receptor subtype (mouse P2X4) raises questions as to the origin of this sequence. As such, this sequence was not thought to have originated from *D. virgifera*. Constituent orders of the Hexapoda were retrieved from Sasaki *et al*. (2013). Orders in which candidate P2X receptor sequences were identified are highlighted in green.

Previous studies have failed to identify a P2X receptor homologue in the genomes of a number of members of the large Insecta class, including that of the fruitfly *Drosophila melanogaster* (Adams *et al.*, 2000). An early study made use of profile Hidden Markov Models (HMMs) derived from a sequence alignments of number of vertebrate P2X receptor sequences (Harte and Ouzounis, 2002). Profile HMMs are statistical probabilities of multiple sequence (MSA) alignments that provide information regarding to what extent of residue conservation within an MSA column (Krogh *et al.*, 1994). Furthermore, analysis using this method failed to identify

distant protein homologues of P2X receptors in the nematode *Caenorhabditis elegans* and the fungus *Saccharomyces cerevisae* (Harte and Ouzounis, 2002).

However, previous studies reporting the apparent absence of a P2X receptor homologue in insect species have focused on members of the Diptera and Hymenoptera orders which, amongst others, includes *D. melanogaster*, *Aedes aegypti,* and *Apis mellifera*. To assess whether P2X receptors are present in earlier diverging Hexapoda classes and early insects, and whether apparent loss of this LGIC family occurred only in Diptera, homology searching was performed across available hexapod genomes and transcriptomes via the NCBI BLAST server. This analysis was concluded on 9 September 2014, and does not include sequence information added to the database beyond this date.

A broad spectrum tBLASTn homology search (using human P2X4 as a query) against whole genome shotgun (WGS) contig sequences of available Hexapoda species (TaxID: 6960) retrieved hits with homology to hP2X4 in *Folsomia candida* (white springtail) (order: Collembola), *Orchesella cincta* (hairy-back girdled springtail) (order: Collembola), *Ladona fulva* (scarce chaser dragonfly) (order: Odonata), and *Ephemera danica* (green drake mayfly) (order: Ephemeroptera) (Fig. 3.10). Further analysis of expressed sequence tag (EST) data from hexapods revealed further homologous sequences to P2X receptors in *Ischnura elegans* (blue-tailed damselfly) (order: Odonata), *Anurida maritima* (seashore springtail) (order: Collembola), *Onychiurus arcticus* (Arctic springtail) (order: Collembola) (Clark *et al.*, 2007), and *Lepismachilis y-signata* (order: Archaeognatha) (Fig. 3.9). Finally, EST sequences were found in the coleopteran (beetle), *Diabrotica virgifera* (western corn rootworm beetle) (Flagel *et al.*, 2014) (Fig. 3.13), although it was unclear whether they represent a P2X receptor from this organism, or are due to some form of sequence contamination.

3.3.4.4.1 P2X receptors in Collembola

The Entognatha is of the two classes that forms the Hexapoda phylum (the other being the Ectognatha (class Insecta)) (Fig. 3.5). Within the Entognatha lie three orders: Diplura, Ellipura, and Protura. No genomic or transcriptomic data are

currently available for a member of the Diplura or Protura. However, candidate P2X receptors were identified in two members of the Collembola order; *Folsomia candida* and *Orchesella cincta*. Multiple sequence alignment with hP2X1-7 protein sequences of 7 hits retrieved following tBLASTn searching of an *F. candida* EST database suggested that only one sequence represented a full CDS of a candidate P2X receptor (GAMN01017925.1). Many of these retrieved sequences were contiguous with each other (Fig. 3.6). Analysis of GAMN01017925.1 identified that many residues implicated in vertebrate P2X receptor are not conserved within this sequence, including ATP binding residues, and a C-terminal membrane translocalisation motif (Fig. 3.6). Although none of the remaining partial transcript sequences included a full complement of residues implicated in human P2X receptor subunits, amongst these sequences many canonical motifs were found (Fig. 3.6). For instance, GAMN01013759.1 included an equivalent pair of lysines at the equivalent K68 and K70 position, as well as F185, T186, N290, F291, and R292 residues (Fig. 3.6). All ECD residues were found in retrieved sequences. As no partial transcript sequence was complete, it remains unclear how many unique candidate P2X receptor transcripts are present in *F. candida*, although the high sequence identity of retrieved sequences suggested that this receptor family is found in this member of the Collembola.

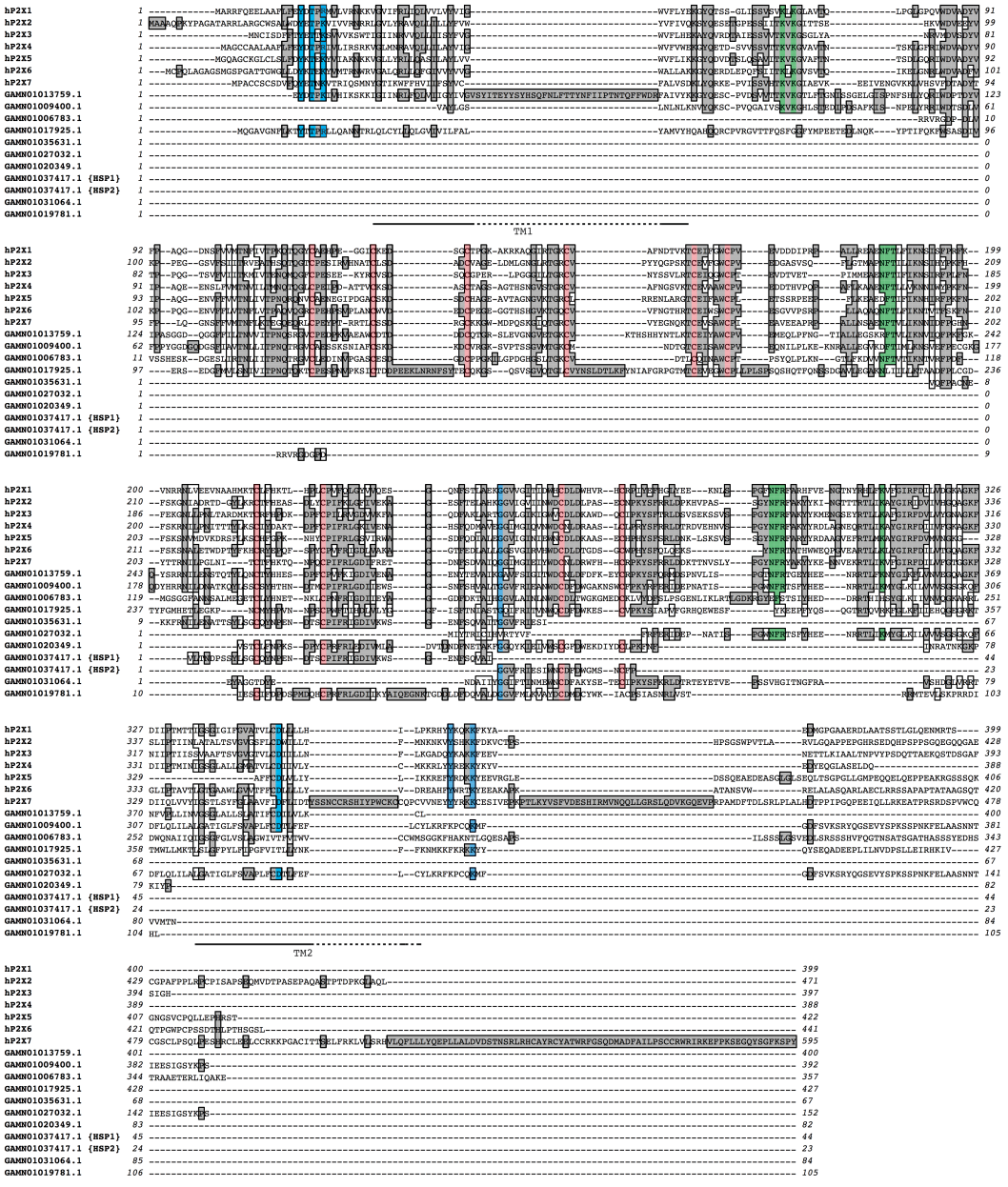

Fig. 3.6: MSA of partial *F. candida* candidate P2X receptor protein sequences

Alignment of translated partial EST sequences against human P2X receptor sequences suggested the presence of a candidate P2X receptor in the collembolean *F. candida*. Residues found to be important in human P2X receptors are highlighted (blue: extracellular cysteine residues; green: ATP binding residues; red: extracellular cysteine residues; blue: N-terminal PKC phosphorylation motif ('YxTx(K/R)'), and C-terminal membrane translocalisation motif ('YxxxK'). Additionally, G250 is also highlighted in blue. Alignments were performed using the MUSCLE algorithm (Edgar, 2004) in MacVector.

In contrast to candidate sequences found in *F. candida*, transcripts retrieved from the transcriptome of *O. cincta*, greater evidence existed for a full-length candidate P2X receptor CDS. Of seven retrieved hits, the translated protein of GAMM01009862.1 was the largest in length (437 amino acids), and shared a 23.5 to 38.1% primary sequence identity with hP2X1-7 receptor subunits. All ATP binding residues found in hP2X1-7 and ECD cysteine residues were conserved in GAMM01009862.1 (Fig. 3.7). An N-terminal PKC motif was also found in the protein sequence of this candidate P2X receptor, although the canonical C-terminal 'YxxxK' motif appeared as 'Y$(x)_4$K' (Fig. 3.7). The predicted protein topology of GAMM01009862.1 was also similar to that of P2X receptors.

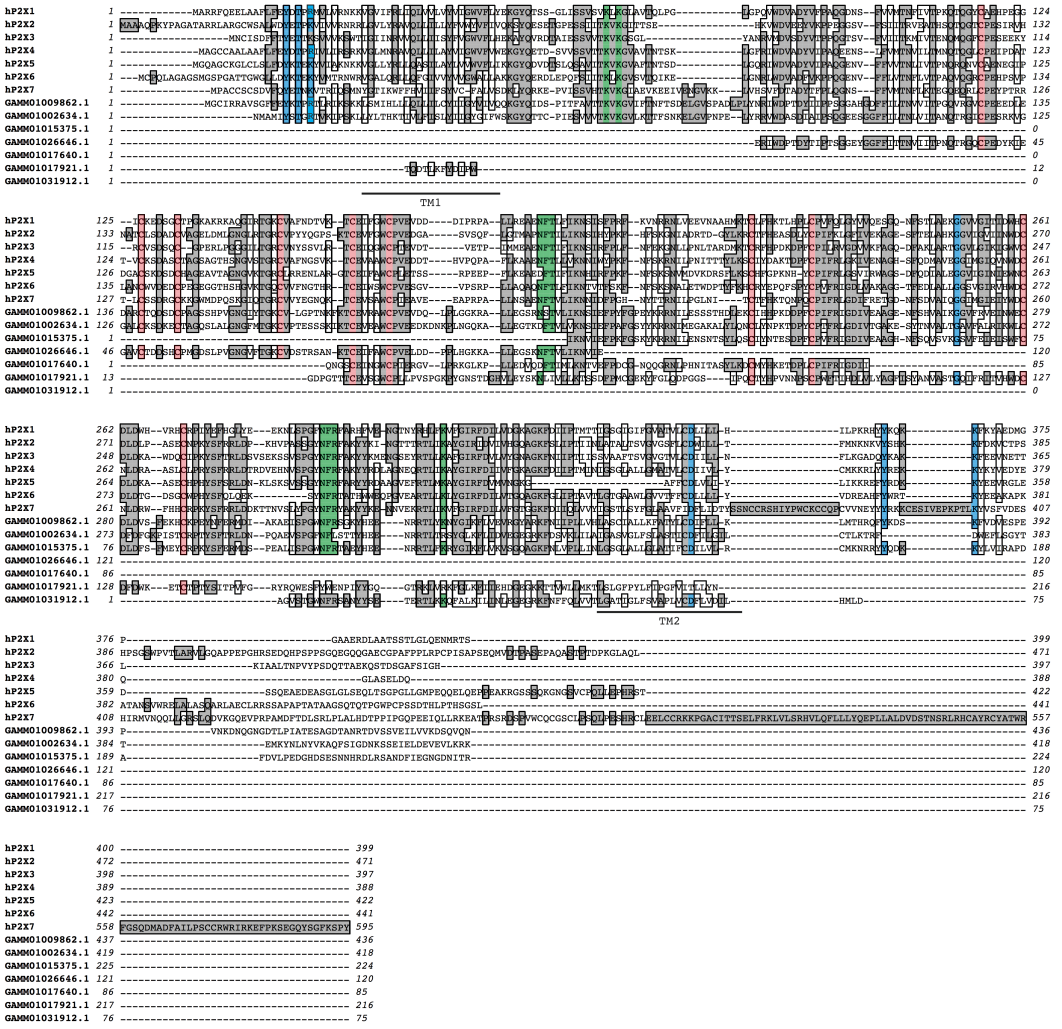

Fig. 3.7: MSA of a candidate *O. cincta* candidate P2X receptor protein sequence

Alignment of 73 amino acid residue translated from partial EST sequences against human P2X receptor sequences suggested the presence of a candidate P2X receptor in the collembolean *O. cincta*. Residues found to be important in human P2X receptors are highlighted (blue: extracellular cysteine residues; green: ATP binding residues; red: extracellular cysteine residues; blue: N-terminal PKC phosphorylation motif ('Yx(K/R)'), and C-terminal membrane translocalisation motif ('YxxxK'). Additionally, G250 is also highlighted in blue. Alignments were performed using the MUSCLE algorithm (Edgar, 2004) in MacVector.

An EST sequence (EW755769.1) of 231 bp encoding for a partial protein sequence of 78 amino acid residue was also identified in *O. arcticus*. Multiple sequence alignment of EW755769.1 against hP2X1-7 suggested that this sequence corresponded to a region of a putative ECD (Fig. 3.8). This was supported by the conservation of ATP binding residues (hP2X1 numbering N290, F291, R292, and

K309), extracellular cysteine residues (C217, C261, and C270), G250 (Digby *et al.*, 2005) (Fig. 3.8).

Similarly, a partial 327 bp EST sequence (FN193708.1) was retrieved following homology searching of the transcriptome of *A. maritima*. Across its 109 residue length, FN193708.1 shared a 41.7% primary sequence identity and 58.3% similarity with the homologous region in human P2X1 (E15 to K111) to which it aligned. This multiple sequence alignment suggested that the partial protein sequence of FN193708.1 is analogous to a region encompassing the N-terminus, TM1 and a portion of the ECD of a candidate P2X receptor (Fig. 3.8). Within this region, a canonical PKC phosphorylation site was found, as well as the equivalent ATP binding lysine residues, K68 and K70 (hP2X1 numbering; Ennion *et al.*, 2000) (Fig. 3.8).

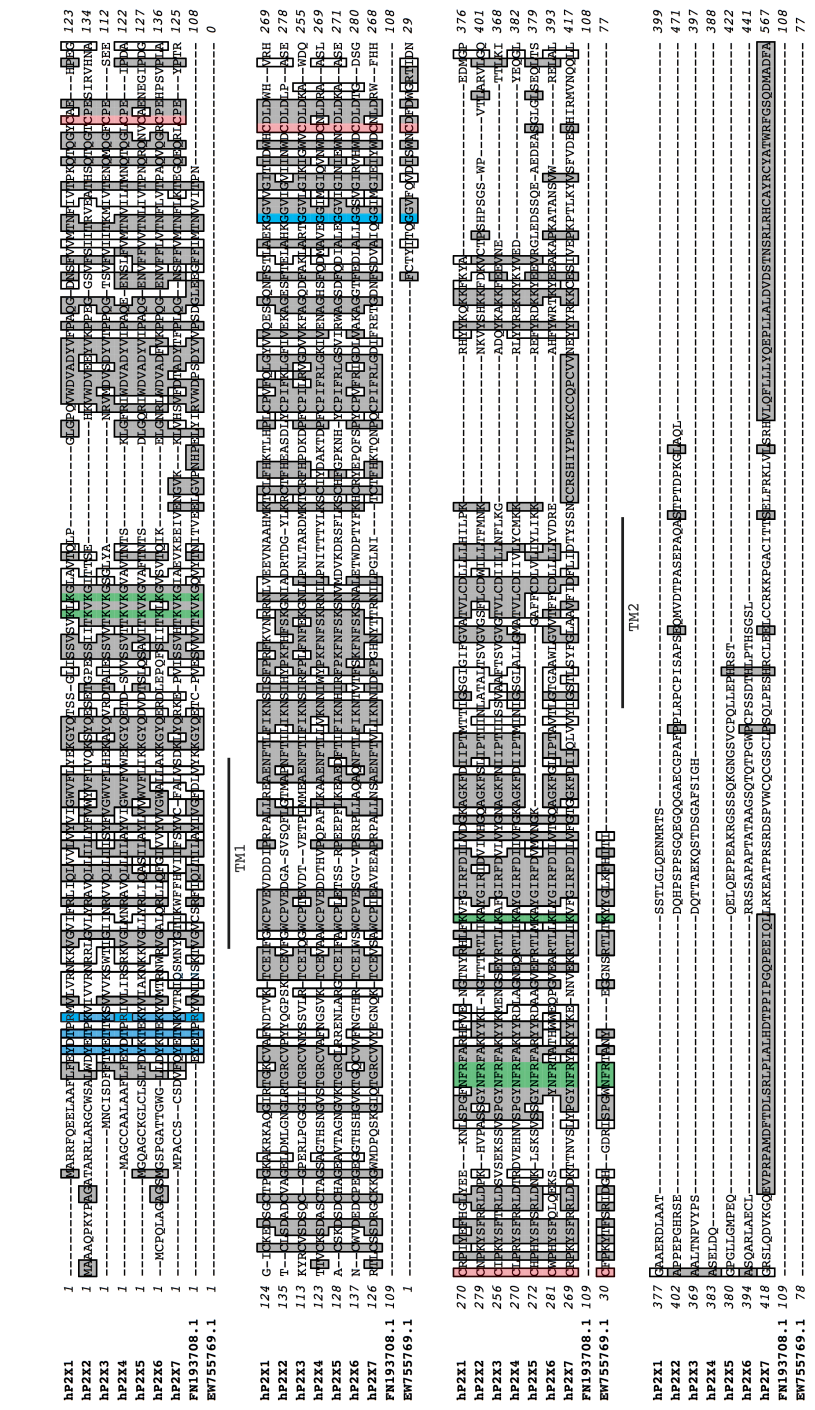
TM1
TM2

Fig. 3.8: MSA of a translated partial EST sequences from *A. maritima* and *O. arcticus*

Alignment of 73 residues translated partial EST sequences against human P2X receptor sequences suggested the presence of a candidate P2X receptor in the collembolean *O. arcticus*. Residues found to be important in human P2X receptors are highlighted (blue: extracellular cysteine residues; green: ATP binding residues; red: extracellular cysteine residues; blue: N-terminal PKC phosphorylation motif ('Yx(K/R)'), and C-terminal membrane translocalisation motif ('YxxxK'). Additionally, G250 (hP2X1 numbering) is also highlighted in blue. Alignments were performed generated using the MUSCLE algorithm (Edgar, 2004) in MacVector.

3.3.5 P2X receptors in the Insecta class

Previous studies have highlighted the apparent absence of P2X receptor homologues in members of the large Insecta class of organisms, including *D. melanogaster*, *Aedes. aegypti*, and *Bombyx. mori*. However, the Insecta is only one class of the larger Hexapoda phylum (Regier *et al.*, 2010) (Fig. 3.5). The search for a P2X receptor homologue in the Hexapoda phylum as a whole identified a number of sequence fragments in members of the Insecta class. These fragments shared significant primary sequence identity and similarity with members of the human P2X receptor family.

3.3.5.1 The Archaeognatha

Archaeognatha are a constituent order of the Insecta class and are commonly known as 'jumping bristletails' (Fig. 3.5). Members of this order are considered to be one of the most basal orders of insects, with fragmented fossil records from the mid-Devonian period (ca. 350 million years ago (MYA)) suggested to represent an ancestral bristletail (Labandeira *et al.*, 1988). However, the fragmented nature of these fossils has led some authors to suggest ancestry of this Insecta order cannot be postulated from these fossils alone, and may represent a more recent incest ancestor (Jeram *et al.*, 1990).

A partial EST with homology to mammalian P2X receptors was identified in a representative organism of the archaeognathan, *Lepismachilis y-signata* following tBLASTn search of EST data in this order (TaxID: 29994). The translated product of this partial EST (FN221719.1) was 114 amino acids long, and corresponded to the N-

terminal end, and a portion of the ECD of mammalian P2X receptors (Fig. 3.9) Within this homologous region, multiple sequence alignment with hP2X1-7 revealed a shared PKC phosphorylation motif, as well as shared K68 and K70 (hP2X1 numbering) that have previously been demonstrated to be required in ATP binding at P2X receptors (Ennion *et al.*, 2000) (Fig. 3.9). Across this homologous region, FN221719.1 shared a 39.5% sequence identity, and 57% similarity with hP2X1. Furthermore, hydrophilicity analysis of FN221719.1 also demonstrated that this partial protein sequence included a putative N-terminus, 22 amino acid transmembrane domain, and ECD segment. The shared motifs, and high percentage residue similarity with human P2X receptor subunits suggested that a hitherto unreported P2X receptor may be present in the Archaeognatha.

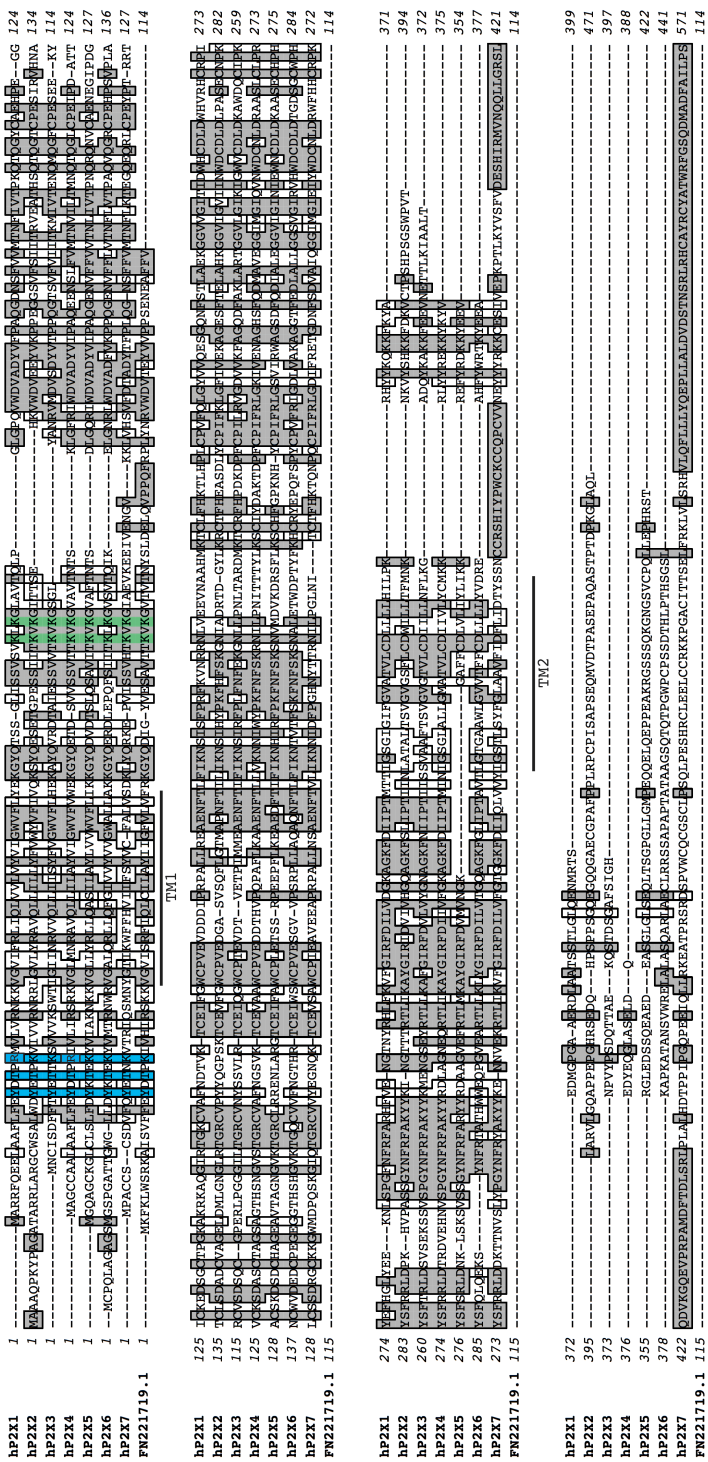
TM1
TM2

Fig. 3.9: MSA of the partial protein sequence of a candidate P2X receptor from an archaeognathan insect

Alignment of a partial protein sequence from the bristletail *L. y-signata* revealed that this organism appears to possess at least one candidate P2X receptor gene. Residues shared between hP2X1-7 receptor subunits and FN221719.1 retrieved protein fragments are highlighted: green, ATP binding residues and blue, PKC phosphorylation motif ('YxTx(K/R)'). Transmembrane domains 1 and 2 are depicted in horizontal lines below the alignment, based on hP2X1 numbering. Fragments were retrieved by tBLASTn searching of the NCBI expressed sequence tag (EST) database for the Archaeoptera order (TaxID: 29994). Sequences were aligned using the MUSCLE algorithm (Edgar, 2004) in MacVector.

3.3.5.2 Pterygota

The Pterygota subclass of winged insects encompasses the majority of insect species, including the Odonata (dragonflies and damselflies), Coleoptera (beetles), and Diptera (true flies) orders (Fig. 3.5). Homology searches performed against the Hexapoda phylum identified candidate P2X receptors in a number of constituent groups of organisms.

3.3.5.2.1 Ephemeroptera

Significant hits were retrieved from the ephemeropteran (mayfly) *Ephemera danica* following homology searching of whole genome shotgun sequence data of Pterygota (TaxID: 7946). Returned HSPs within two hits returned (AYNC01039758.1 and AYNC01027536.1) were of varying size and corresponded to portions of a putative receptor ECD, as suggested from multiple sequence alignment with human P2X receptor homologues (Fig. 3.10). HSPs within AYNC01039758.1 appeared contiguous, although it is unclear whether these sequences form part of the same transcript. Similar multiple sequence alignment of HSPs from AYNC01027536.1 again highlighted contiguity of sequences. Within HSPs of both AYNC01039758.1 and AYNC01027536.1, residues and motifs required for higher P2X receptor function and modulation were found, including ATP binding residues, PKC phosphorylation motifs, and ECD cysteine residues (Fig. 3.10). The high percentage sequence identity of many of these HSPs with human P2X receptor subunits lends further support to P2X receptors being present in this species of Ephermeroptera.

Furthermore, many of the fragments within these two hits shared a high percentage primary sequence identity, but others that aligned to the same homologous region of human P2X receptor subunits did not share 100% identity. As such, this suggested that at least two P2X receptor genes may be present in *E. danica.* Molecular cloning is required to determine this, however.

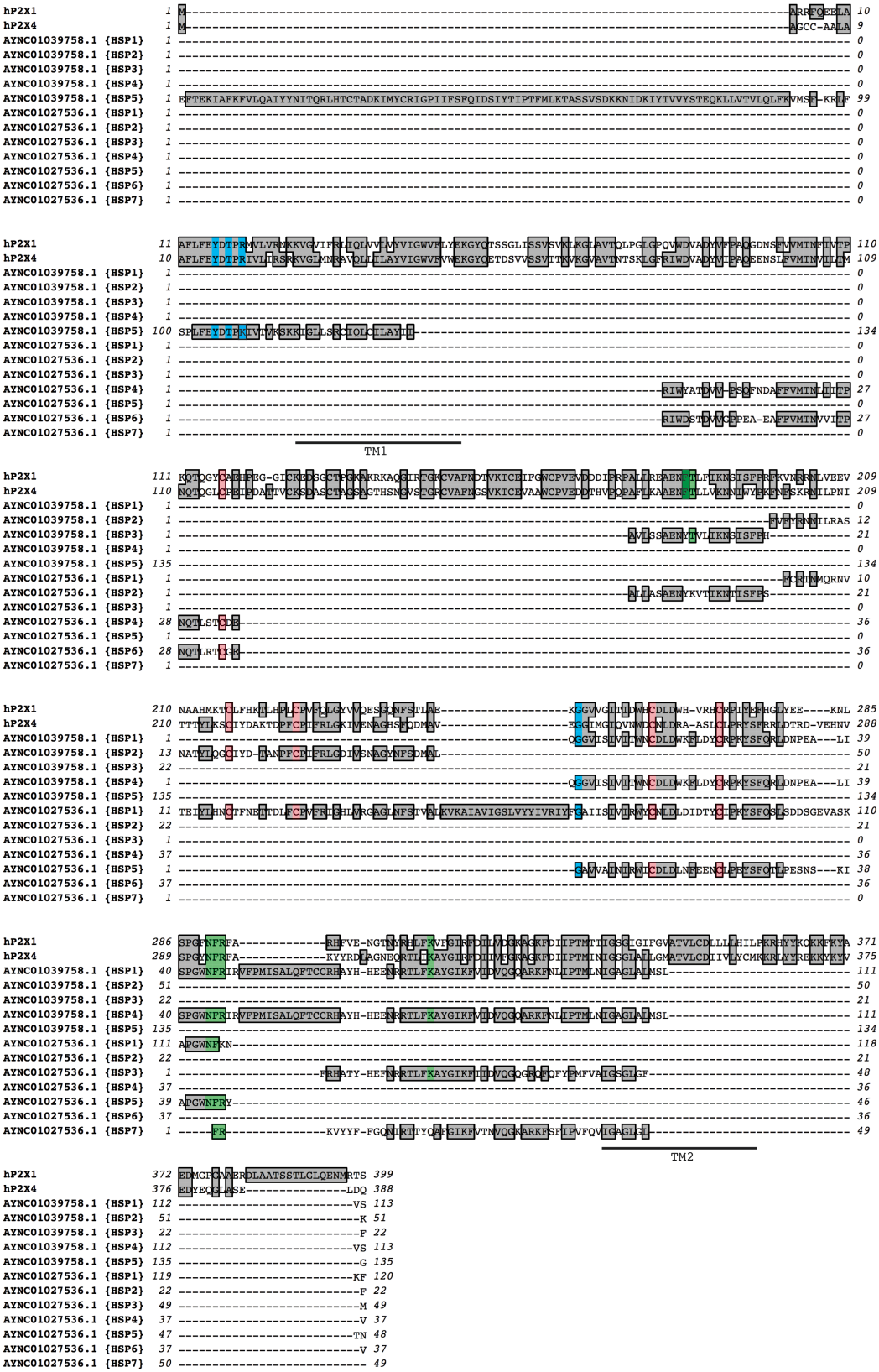
TM1
TM2

Fig. 3.10: MSA of candidate P2X receptor protein fragments from *E. danica*

Alignment of retrieved protein sequence fragments from the mayfly *E. danica* revealed that this organism appears to possess at least one candidate P2X receptor gene. Identical residues between aligned protein sequences are depicted in grey. Many of these fragments are contiguous, and may be derived from the same transcript. Residues shared between hP2X1, hP2X4 and *E. danica* retrieved protein fragments are highlighted: green, ATP binding residues; red, extracellular cysteine residues; and blue, PKC phosphorylation motif ('YxTx(K/R)') and G250 (hP2X1 numbering). Transmembrane domains 1 and 2 are depicted below the alignment, based on hP2X1 numbering. Fragments were retrieved by tBLASTn searching of the NCBI whole genome shotgun (WGS) sequencing database. Sequences were aligned by T-Coffee (Notredame *et al.*, 2000) using MacVector.

3.3.5.2.2 Odonata

The Odonata taxon is one of three constituent subphyla of the Pterygota subclass (winged insects) and includes the well-known carnivorous dragonflies (Anisoptera) and damselflies (Zygoptera) insects (Regier *et al.*, 2010) (Fig. 3.5). Partial nucleotide sequences were identified by homology searching of the genome of a member of both the Anisoptera (*Ladona fulva* (scarce chaser dragonfly)) and Zygoptera (*Ischnura elegans* (blue-tailed damselfly)).

Three hits were retrieved in *I. elegans* following homology searching of EST data available for this damselfly: FN217218.1; FN218973.1; and FN217821.1. These EST data are derived from a cDNA library of mRNA transcripts of *I. elegans* muscle tissue (Simon *et al.*, 2009). Multiple sequence alignment of the translated products of these three partial EST sequences against hP2X1-7 suggested that these sequences represent the putative N-terminal region and a partial ECD region of a candidate P2X receptor (Fig. 3.11). In support of retrieved sequences being candidate P2X receptors, the ATP binding residues K68 and K70 (hP2X1 numbering) were conserved in all sequences. The aromatic ATP binding residues F185 and T186 were incompletely conserved in two retrieved sequences (FN218218.1 and FN217821.1), whilst FN218973.1 was too short to align around this region. Across the regions in which partial *I. elegans* sequences align, all equivalent extracellular domain cysteine residues are present (hP2X1 numbering: C117; C126; C132; C149; C159; and C165) (Fig. 3.11).

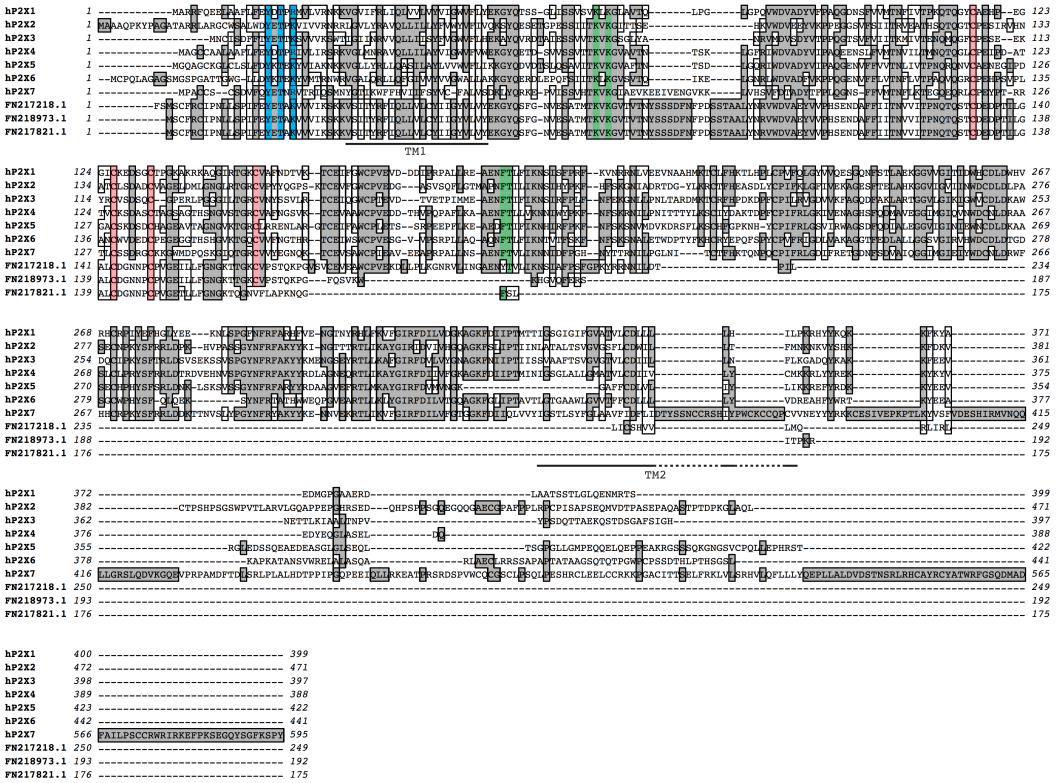

Fig. 3.11: MSA of candidate P2X receptor protein fragments from *I. elegans*

Alignment of retrieved protein sequence fragments from the damselfly *I. elegans* revealed that this organism appears to possess at least one candidate P2X receptor gene. Identical residues between aligned protein sequences are depicted in grey. Residues shared between hP2X1, hP2X4 and candidate *L. fulva* P2X receptor protein fragments are highlighted: green, ATP binding residues; red, extracellular cysteine residues; and blue, PKC phosphorylation motif ('YxTx(K/R)') and G250 (hP2X1 numbering). Transmembrane domains 1 and 2 are depicted by horizontal lines below the sequence alignment, based on hP2X1 numbering. Fragments were retrieved by tBLASTn searching of the NCBI whole genome shotgun (WGS) sequencing database. Sequences were aligned using the T-Coffee algorithm (Notredame *et al.*, 2000) in MacVector.

A number of partial protein sequences were retrieved following homology searching of WGS data of the dragonfly *L. fulva* which, when aligned with human P2X receptor homologues, appeared to represent portions of a receptor N-terminus and ECD (Fig. 3.12). Many of these partial protein sequences shared a high percentage sequence similarity and were partially identical with the largest of the partial protein sequences retrieved (APVN010152095.1). Conserved motifs and residues known to be involved in P2X receptor modulation in vertebrate and invertebrate homologues were also found in many of these aligned sequences (Fig. 3.12). These included many

extracellular domain cysteine residues, a number of ATP binding residues (such as the triplet 'NFR' ATP binding motif), and an N-terminal PKC phosphorylation motif (Fig. 3.12). The short length of partial protein sequences did not allow comparison of the C-terminal region of predicted *L. fulva* P2X receptors

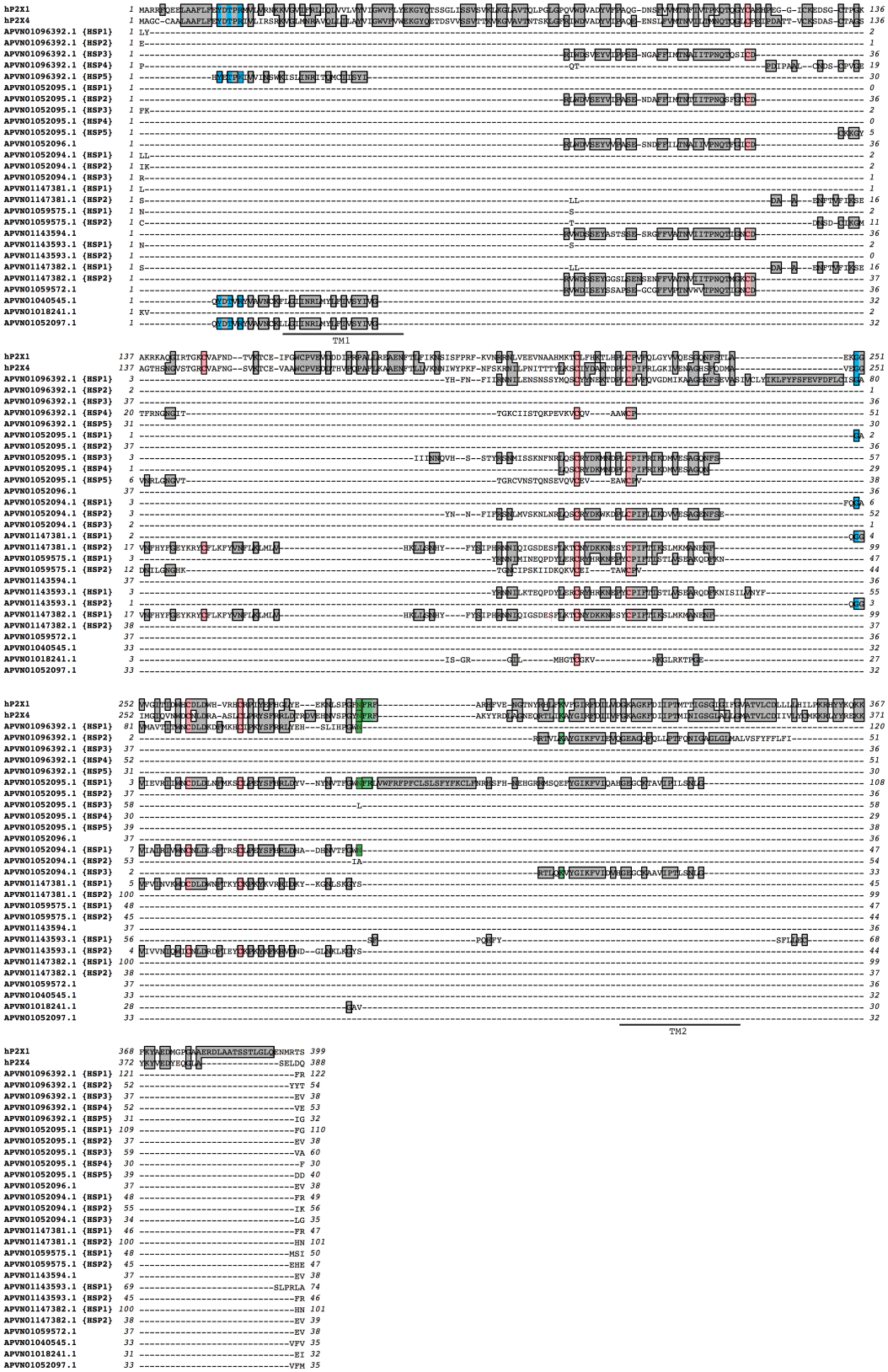
hP2X1
hP2X4
APVN01096392.1 {HSP1}
APVN01096392.1 {HSP2}
APVN01096392.1 {HSP3}
APVN01096392.1 {HSP4}
APVN01096392.1 {HSP5}
APVN01052095.1 {HSP1}
APVN01052095.1 {HSP2}
APVN01052095.1 {HSP3}
APVN01052095.1 {HSP4}
APVN01052095.1 {HSP5}
APVN01052096.1
APVN01052094.1 {HSP1}
APVN01052094.1 {HSP2}
APVN01052094.1 {HSP3}
APVN01147381.1 {HSP1}
APVN01147381.1 {HSP2}
APVN01059575.1 {HSP1}
APVN01059575.1 {HSP2}
APVN01143594.1
APVN01143593.1 {HSP1}
APVN01143593.1 {HSP2}
APVN01147382.1 {HSP1}
APVN01147382.1 {HSP2}
APVN01059572.1
APVN01040545.1
APVN01018241.1
APVN01052097.1
TM1
TM2

Fig. 3.12: MSA of candidate P2X receptor protein fragments from *L. fulva*

Alignment of retrieved protein sequence fragments from the dragonfly *L. fulva* revealed that this organism appears to possess at least one candidate P2X receptor gene. Some of the retrieved sequence fragments are identical or share a percentage sequence identity. A selected group of residues known to be important for the function of higher P2X receptors and shared between hP2X1, hP2X4 and *L. fulva* partial protein sequences are highlighted: green, ATP binding residues; red, extracellular cysteine residues; and blue, PKC phosphorylation motif ('YxTx(K/R)'), and G250 (hP2X1 numbering). Identical amino acids are shaded grey, regardless of their contribution to mammalian P2X receptor function. Fragments were retrieved by tBLASTn searching of the NCBI whole genome shotgun (WGS) sequencing database and aligned using the T-Coffee algorithm (Notredame *et al.*, 2000) in MacVector.

3.3.5.2.3 Neoptera

Neoptera encompasses winged insects, including 'true flies' (order Diptera), moths, and butterflies (order Lepidoptera), and bees, wasps, and ants (order Hymenoptera) (Trautwein *et al.*, 2012). No homologous P2X receptor protein sequence has been identified in available genomes of many neopterans (Harte and Ouzounis, 2002; Agboh *et al.*, 2004; Fountain *et al.*, 2007). However, the current study identified two EST sequences in the western corn rootworm beetle (*Diabrotica virgifera,* order: Coleoptera (TaxID: 1369033)) (EW761455.1 and EW764374.1), the translated products of which shared significant sequence identity with mammalian P2X receptors (Fig. 3.13).

Multiple sequence alignment demonstrated that these sequences are homologous to a region encompassing a portion of the ECD, TM2, and portion of the intracellular C-terminus of hP2X1-7 subunits. EW761455.1 is 66 amino acid residues longer than EW764374.1, but the two retrieved protein sequences shared a 100% primary sequence identity across a region of 90 residues (EWQ761455.1 numbering: K67 to Q157) (Fig. 3.13). This region is equivalent to the region V235 to N395 in hP2X1, within which can be found the ATP binding residues N290, F291, R292, and K309, and two ECD cysteine residues (C261 and C270; hP2X1 numbering) (Fig. 3.13). In the longer EW761455.1 sequence these residues are conserved. Indeed, across the equivalent region in hP2X1, EW761455.1 shares a 46.4% primary sequence identity. However, reciprocal BLAST (rBLAST) performed against nucleotide reference sequences (NCBI) using the full length retrieved EW761455.1 EST nucleotide

sequence retrieves a highly similar nucleotide sequence corresponding to the mouse (*M. musculus*) P2X4 receptor subtype. At the nucleotide level, these two sequences shared a 99% sequence identity. This high percentage sequence identity at the nucleotide level to a mammalian P2X receptor was concerning giving that it is estimated that mice and beetles diverged from a common ancestor around 780 million years ago (MYA) (Hedges *et al.*, 2006). In contrast, *M. musculus* is estimated to have diverged from a common ancestor to *B. taurus* relatively recently (ca. 94 MYA) (Hedges *et al.*, 2006), and alignment of regions corresponding to EW761455.1 in mouse P2X4 and *Bos Taurus* (cattle) (accession number: NM_001034049.1) P2X4 nucleotide sequences share an 84.3% identity.

Expansion of the search for a coleopteran P2X receptor in another beetle species (*Trilobium castaneum*, red flour beetle) (Richards *et al.*, 2008) using the BeetleBase website (available at: http://www.beetlebase.org (Wang *et al.*, 2007; Kim *et al.*, 2010) did not retrieve a significant hit with homology to mammalian receptor subunits.

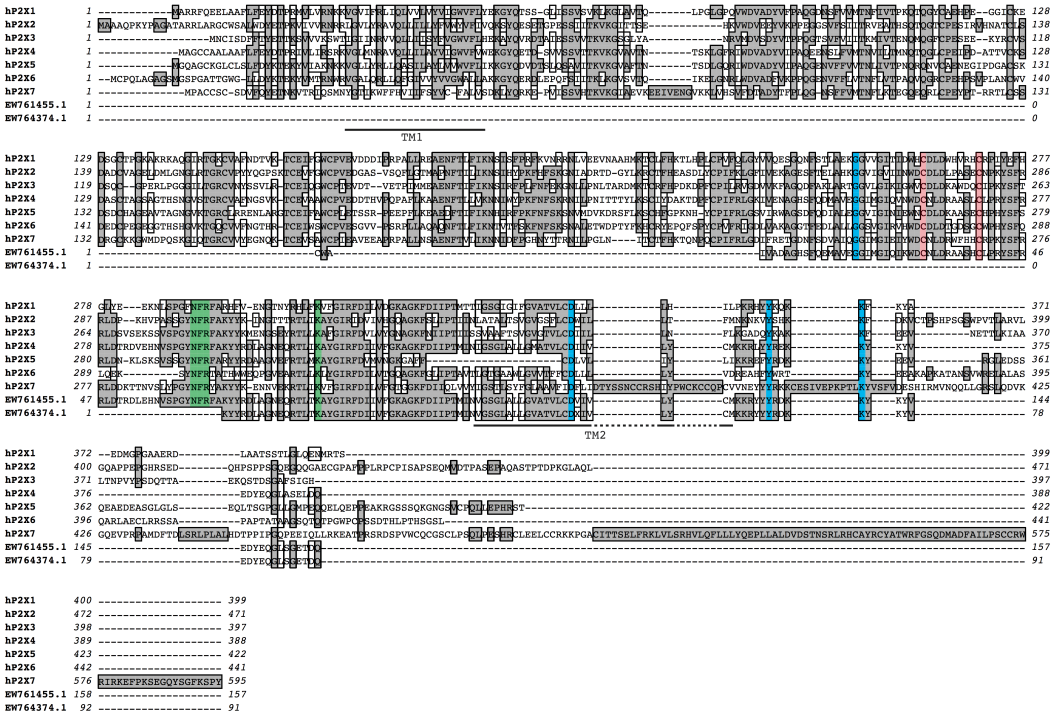

Fig. 3.13: MSA of candidate P2X receptor protein fragments from *D. virgifera*

Alignment of retrieved protein sequence fragments from the western corn rootworm beetle *D. virgifera* revealed that this beetle appears to possess at least one P2X receptor gene. Identical residues between aligned protein sequences are depicted in grey. Some residues implicated in mammalian P2X receptor function, and are shared between hP2X1, hP2X4 and *D. virgifera* retrieved protein fragments are highlighted: green, ATP binding residues; red, extracellular cysteine residues; and blue, C-terminal membrane translocalisation motif ('YxxxK'), D350, and G250 (hP2X1 numbering). Fragments were retrieved by tBLASTn searching of the NCBI whole genome shotgun (WGS) sequencing database. Sequences were using the MUSCLE algorithm (Edgar, 2004) in MacVector.

3.3.6 Predicted P2X receptors in Cnidaria and Ctenophora

The Cnidaria are a diverse phylum of corals, sea anemones, hydroids, and jellyfish, composed of five classes: Anthozoa; Cubozoa; Hydrozoa; Staurozoa; and Scyphozoa (Kayal *et al.*, 2013). At the time of writing, genomic or transcriptomic data for a member of the Staurozoa or Cubozoa classes are not available, and analyses were focussed on the remaining three classes. Genomic datasets for four cnidarian species were searched for P2X receptor homologues: *Acropora digitifera* (Shinzato *et al.*, 2011); *Aurelia aurita* (moon jellyfish) (Fuchs *et al.*, 2014); *Hydra magnipapillata* (Chapman *et al.*, 2010); and *Nematostella vectensis* (Putnam *et al.*, 2007). In addition,

the transcriptome of *Hydra vulgaris* (AEP) (Hemmrich and Bosch, 2008) was also assessed for P2X receptor homologues.

In the scphyozoan *Aurelia aurita*, homology searching using hP2X4 as a protein query retrieved two partial EST sequences: FTXYOTV01DGAOA and F2X1FZH02GP10X. The translated forms of these two sequences shared homology with portions of the ECD region of mammalian P2X receptors (Fig. 3.14). Whilst these sequences were not contiguous with each other, they were positioned at separate regions of the multiple sequence alignment. Further molecular cloning is required to determine whether these two partial sequences form part of a single P2X receptor gene in *A. aurita*, or form part of two separate genes. Analysis of predicted transcripts of the Anthozoan coral *A. digitfera* retrieved two transcript sequences: adi_v1.00700 and adi_v1.04925, the translated forms of which differed greatly in size from both vertebrate and invertebrate P2X receptors. At 990 amino acids in length, adi_v1.00700 was predicted to possess a protein folding topology unlike that seen for a P2X receptor, with multiple regions of hydrophobicity across its length. Multiple sequence alignment of this protein with human homologues identified regions within adi_v1.00700 that shared homology with human P2X receptors and that were considered important for receptor function, although these were confined to a region homologous to the ECD, TM2 and intracellular C-terminus of human receptors. Little homology was seen at the N-terminus of hP2X1-7 with adi_v1.00700.

In contrast, a second CDS retrieved from predicted transcripts of *A. digitifera* (adi_v1.04925) was considerably shorter than would be expected for a P2X receptor (245 amino acid residues). However, within this sequence a putative PKC phosphorylation motif, multiple shared ATP binding residues and a number of extracellular domain cysteine residues were found (Fig. 3.14). Whilst many of these regions were shared, multiple sequence analysis suggested that this *A. digitifera* protein sequence does share homology with mammalian P2X receptor homologues, the transcript from which it is derived may be incorrectly predicted. Molecular cloning of this sequence, in addition to adi_v1.00700, is required to determine whether a full-length CDS is available in this cnidarian that shares greater homology with human homologues.

Two predicted protein sequences were retrieved from the genome of sea anemone *N. vectensis* (Putnam *et al.*, 2007), referred to herein as *Nve*_p2xA and *Nve*_p2xB. Pairwise sequence alignment of these revealed that these receptors shared a 59.3% sequence identity with each other, and a 25 to 37.8% identity with hP2X1-7 subunits. Consistent with their inclusion as putative P2X receptors, both sequences shared ATP binding residues, extracellular domain cysteine residues, and two extended regions of hydrophobic amino acids consistent with the presence of TMDs (Fig 3.14).

Finally, candidate P2X receptors were identified in the genome and transcriptome of the hydrozoans *H. magnipapillata* and *H. vulgaris* (AEP), respectively. Two sequences were retrieved from *H, magnaipapillata*, one of which was of a length consistent with previously characterised P2X receptor ('CL1621Contig1; 1596 8 1307 minus strand', referred to herein as *Hma*_p2x). A second partial transcript sequence was also retrieved, the translated 290 amino acid protein of which aligned within the putative ECD of *Hma*_p2xA. At the protein level, these two homologous regions shared a primary sequence identity of 48.8% and similarity of 65.6%. One predicted transcript with homology to mammalian P2X receptors was identified in *H. vulgaris* (AEP) (referred to herein as aep_p2x). Multiple sequence alignment of protein sequences from the cnidarians *H. magnipapillata* (*Hma*_p2x), *H. vulgaris* (AEP) (aep_p2x), *N. vectensis* (*Nve*_p2x), and partial protein sequences from *A. digitifera* identified a number of shared amino acid residues between candidate receptors from this phylum, including ATP binding proteins and N- and C-terminal motifs (Fig. 3.14).

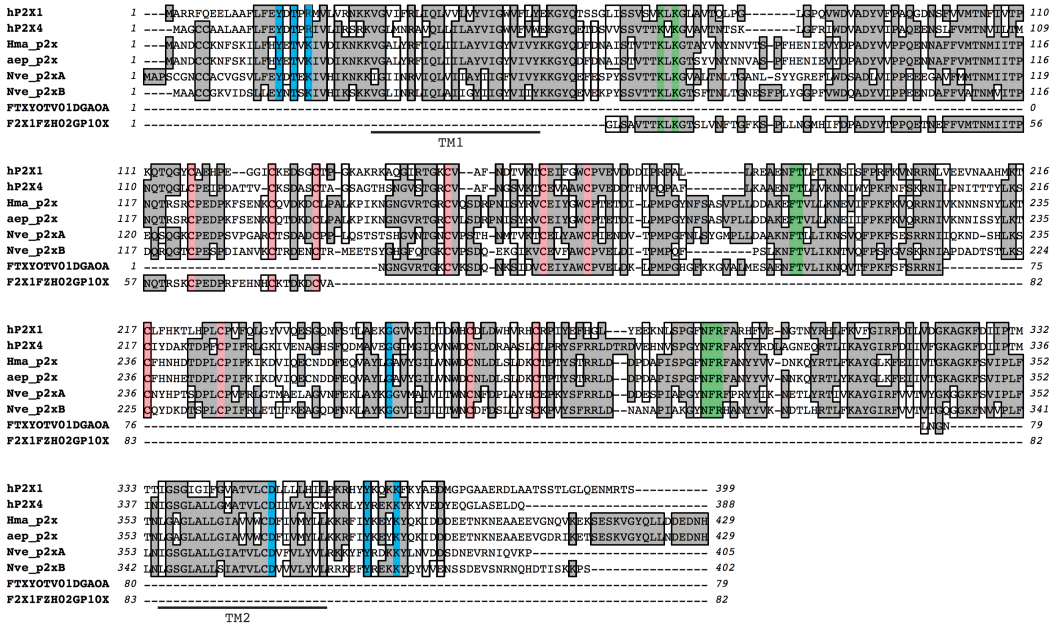

Fig. 3.14: MSA of predicted Cnidaria P2X receptor protein sequences with hP2X1 and hP2X4 receptors

Alignment of predicted full-length and partial protein sequence from various members of the Cnidaria phylum suggested that P2X receptors are present within this group of organisms. Identical residues between aligned protein sequences are depicted in grey, whilst chemically similar residues are only outlined. Many residues implicated in mammalian P2X receptor function are shared between hP2X1, hP2X4 and Cnidaria retrieved protein fragments and are highlighted accordingly: green, ATP binding residues; red, extracellular cysteine residues; and blue, C-terminal membrane translocalisation motif ('YxxxK'), D350, and G250 (hP2X1 numbering). *A. digitifera* sequences (FTXYOTV01DGAOA and F2X1FZH02GP10X) aligned to a homologous region in hP2X1 corresponding to portions of the ECD. Sequences were retrieved by tBLASTn searching of appropriate dataset as detailed in the Appendix, Table A1. Sequences were aligned by MUSCLE (Edgar, 2004) using MacVector. Species abbreviations: *Hma*_p2x (*Hydra magnipapillata*); aep_p2x (*Hydra vuglaris* (AEP)); and *Nve*_p2x (*Nematostella vectensis*). FTXYOT01DGAOA and F2X1FZH02GP10X refer to retrieved partial candidate *A. aurita* P2X receptor sequences. Sequences were aligned using the MUSCLE algorithm (Edgar, 2004) in MacVector.

Candidate P2X receptors were searched for in the Pacific sea gooseberry, *Pleurobachia brachei* (Moroz *et al.*, 2014). A partial mRNA sequence from *P. bachei*, encoding a protein 158 amino acid residues in length has been submitted directly to GenBank and has been suggested previously to constitute a Ctenophora P2X receptor homologue (Kohn and Moroz, 2010) (GenBank accession ID: GU395551.1). Using GU395551.1 as a query against transcriptome of *P. bachei*

(available at: http://rogaevlab.ru/pleurobrachia/blast) retrieves a putative full-length sequence (scaffold983.1_FGENESH_8; *Pba*_p2x) that shares a near 100% sequence identity with GU395551.1 (*E*-value = 3e-99) across its homologous region portion (Fig. 3.15B). Protein topology analysis, in addition to MSA with the putative full-length sequence of *Pba*_p2x suggested that the amino acid sequence of GU395551.1 encompasses a partial ECD, second TMD and a partial intracellular C-terminus. In contrast, *Pba*_p2x is 377 amino acids in length and was predicted to display a more complete P2X-like topology, with two TMDs predicted in the protein sequence (Fig. 3.15A). At the primary amino acid level, *Pba*_p2x shared a 7.9 to 48.0% sequence identity with hP2X1-7 and lacked a number of important regions shared amongst currently available P2X receptor sequences from a range of phyla. Although an N-terminal PKC motif was shared between *Pba*_p2x and hP2X1-7, the C-terminal 'YxxxK' membrane translocalisation motif was only partially conserved, lacking an equivalent lysine residue at position K366 (Fig. 3.15B). Surprisingly, only one of the ten ECD cysteine residues conserved amongst hP2X1-7 was found in *Pba*_p2x (equivalent to C132 in hP2X1) (Fig. 3.15B). In contrast, earlier diverging *Dictyostelium discoideum* P2X receptor subunits share two conserved cysteine residues with human homologues (Ludlow *et al.*, 2009). ATP binding residues and motifs are largely absent in *Pba*_p2x with only K309 shared with human homologues (Fig. 3.15B). Analysis of EST data for another ctenophore *Mnemiopsis leidyi* (Ryan *et al.*, 2013) retrieved partial nucleotide sequences, the translated forms of which also shared some primary sequence identity with human P2X receptor subunits.

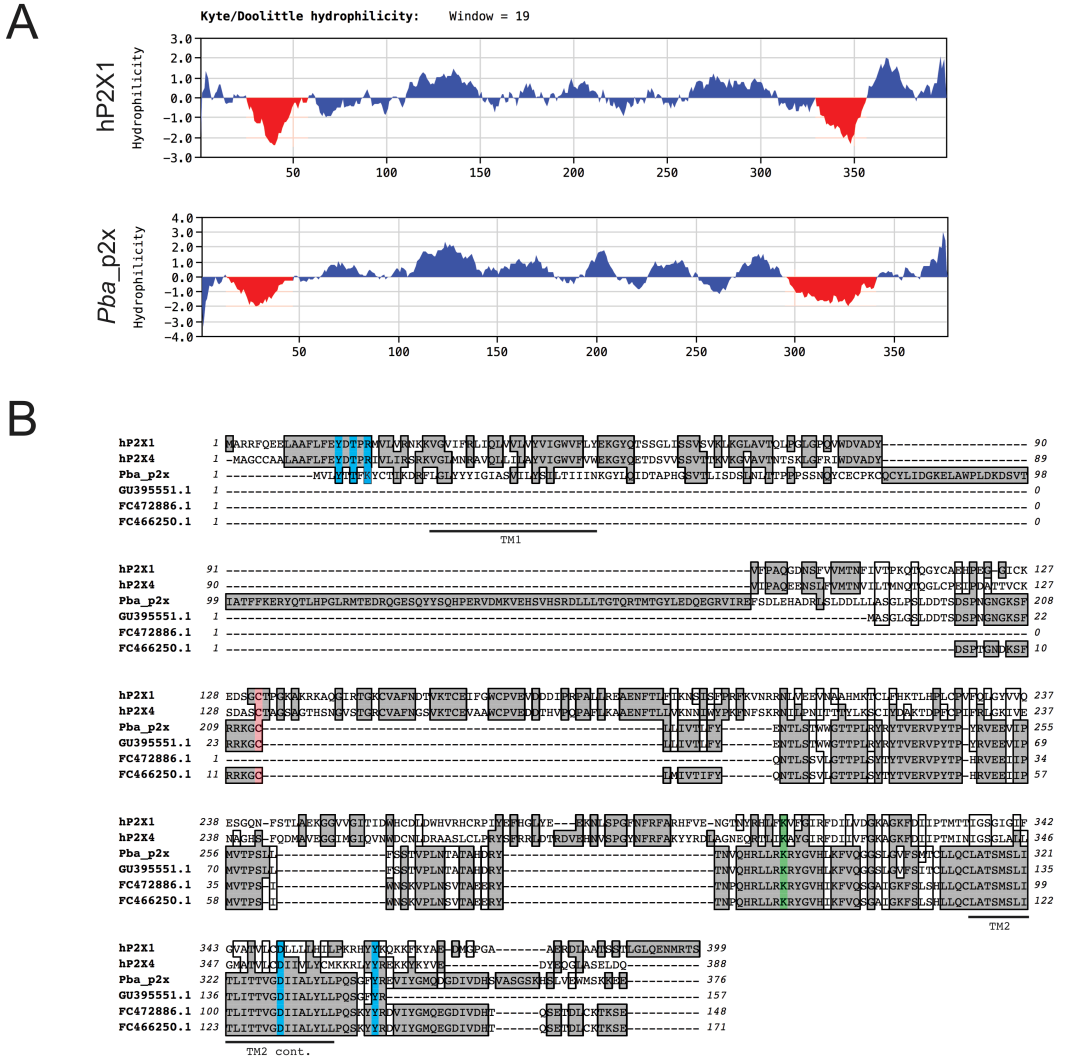

Fig. 3.15: topology and primary sequence analysis of candidate Ctenophora P2X receptors

Sequences with weak homology to human P2X receptor subunits were retrieved from the transcriptomes of two Ctenophora species; *Pleurobrachia bachei* and *Mnemiopsis bachei*. ***A***, a putative full-length sequence (*Pba*_p2x) was found following homology searching of the *P. bachei* transcriptome, topology analysis of which predicted the presence of two transmembrane domains (TMDs) (red), flanking a large extracellular domain, consistent with the topology of human P2X receptor subunits (hP2X1 is illustrated as an example). ***B***, multiple sequence alignment of hP2X1, hP2X4, a putative full-length *P. bachei* P2X receptor (scaffold983.1_FGENESH_8; *Pba*_p2x), a partial *P. bachei* P2X-like receptor sequence used as a query to identify *Pba*_p2x, and non-redundant P2X-like protein sequences identified in *M. leidyi*. Sequences were aligned using the MUSCLE algorithm (Edgar, 2004) in MacVector.

The low sequence identity and similarity of protein sequences to previously characterised P2X receptor sequences retrieved following homology searching genomic and transcriptomic Ctenophora datasets makes it unclear whether they

represent P2X receptors in this phylum. Although these sequences were predicted to possess a protein topology similar to that of P2X receptors in humans and other invertebrates, conservation of residues known to be critical to receptor function was poor. Further molecular cloning is required to determine a full-length transcript sequence of these receptors for further assessment of their primary sequence.

3.3.7 P2X receptors in the Platyhelminthes

The Platyhelminthes phylum is subdivided into four classes: the Turbellaria, and the parasitic Trematoda, Monogenea, and Cestoda (Riutort *et al.*, 2012). The cloning of a P2X receptor from the pathogenic trematode *Schistosoma mansoni* represented the first P2X receptor to be cloned in the Platyhelminthe phylum. Although a functional role for a P2X receptor in the trematode *S. mansoni* has not yet been determined, work by Sakurai *et al.* (2012) has highlighted expression of a P2X receptor in neoblasts in the turbellarian, *Dugesia japonica*. The medical and socioeconomic important of some organisms within this phylum, including *S. mansoni*, led to the extension of the search for candidate receptor homologues in Platyheminthes in a further four species: *Echinococcus granulosus* (Tsai *et al.*, 2013; Zheng *et al.*, 2013); *Echniococcus multilocularis*; *Hymenolepis microstoma*; and *Taenia solium* (Tsai *et al.*, 2013). These species are part of the Cestoda class of Platyhelminthes, more commonly referred to as parasitic flatworms (tapeworms) (Riutort *et al.*, 2012). Candidate P2X receptor sequences were identified in all four of these Cestoda species. Consistent with P2X receptor topology, extended regions of hydrophobicity consistent with the presence of transmembrane domains were predicted in a minimum of two sequences in each species (Fig. 3.16). In 'C' subunits of predicted receptors from *E. multilocularis* and *E. granulosus* (*Emult*_p2xC and *Egr*_p2xC, respectively), and the 'B' subtype P2X receptor predicted in *T. solium* (*Tso*_p2xB), the predicted intracellular N-terminus was shorter than that found in either mammalian, or other Cestoda P2X homologues (Fig. 3.16). Multiple sequence alignment supported this observation, which also included the apparent absence of much of the canonical PKC phosphorylation motif found in vertebrate and non-vertebrate P2X receptors. Whilst much of the intracellular N-terminus appeared to be absent in these receptor subunits, the predicted ECD region was longer than human P2X receptor subunits two regions

with high percentage sequence similarity to analogous regions in Cestoda P2X receptors were present.

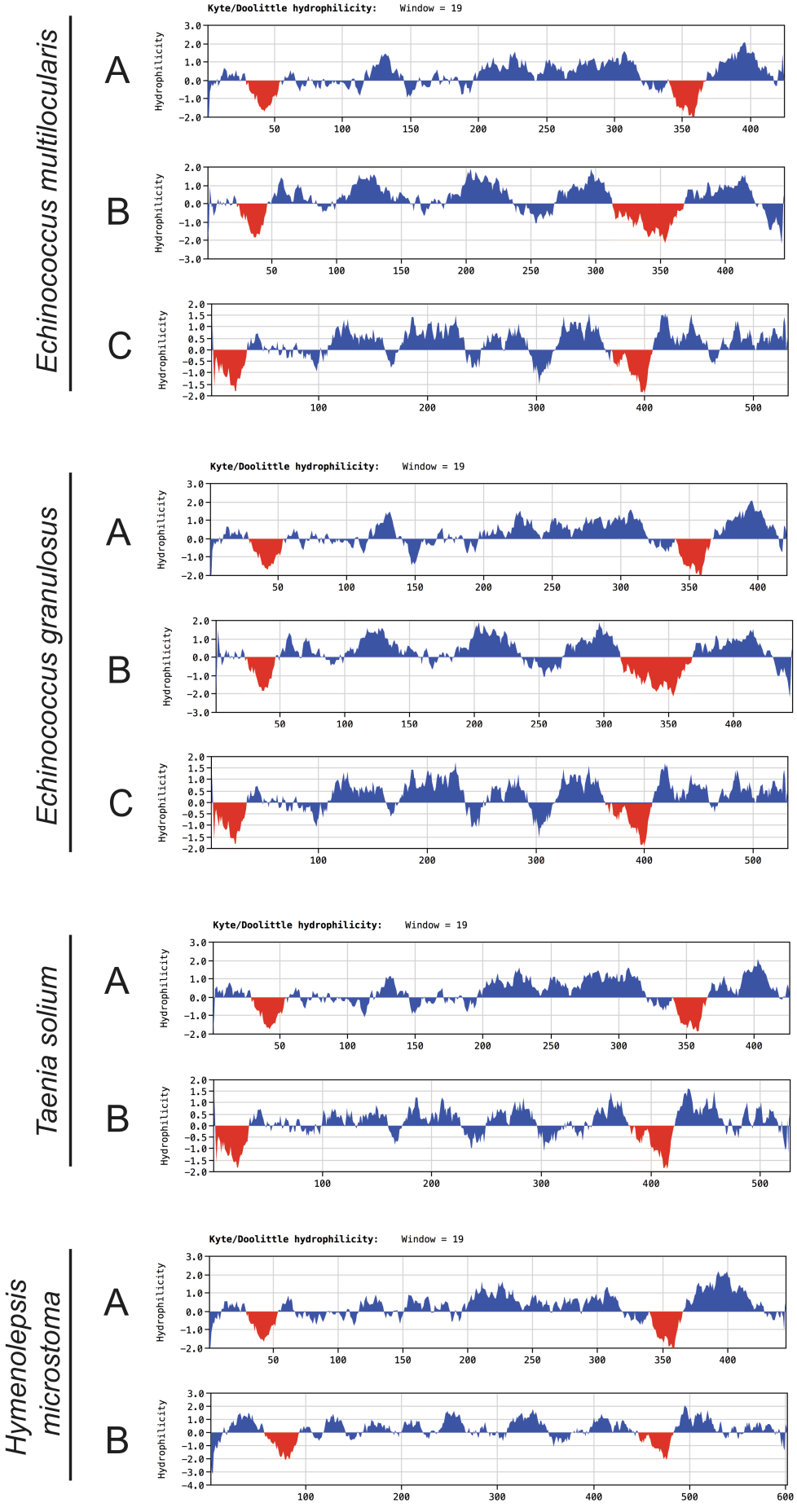
Echinococcus multilocularis
A
B
C
Kyte/Doolittle hydrophilicity: Window = 19
Hydrophilicity
Echinococcus granulosus
A
B
C
Kyte/Doolittle hydrophilicity: Window = 19
Hydrophilicity
Taenia solium
A
B
Kyte/Doolittle hydrophilicity: Window = 19
Hydrophilicity
Hymenolepsis microstoma
A
B
Kyte/Doolittle hydrophilicity: Window = 19
Hydrophilicity

Fig. 3.16: predicted protein topology of candidate full-length Cestoda P2X receptors

Protein sequences of candidate P2X receptors from members of the Cestoda class of the Platyhelminthes phylum: *Echinococcus multilocularis*; *Echinococcus granulosus*; *Taenia solium*; and *Hymenolepsis microstoma* are predicted to possess regions of hydrophobicity, consistent with the presence of transmembrane domains (coloured red). Multiple predicted receptor subunits are denoted as described previously (section 2.2.1).

Candidate P2X receptor sequences were identified in these further four species, and shared a 20.1 to 97.8% primary sequence identity between each other. Consistent with mammalian P2X receptor homologues, these Cestoda P2X receptors possessed basic and aromatic amino acids, previously identified as being important in the coordinated binding of ATP (Fig. 3.17). Furthermore, all ten ECD cysteine residues conserved in human P2X receptors were found shared in these the majority of these Cestoda P2X receptors, although C270 (hP2X1 numbering) is seemingly absent from the protein sequences of *Emult*_p2xC, *Egr*_p2xC, and *Tso*_p2xB (Fig. 3.17). Within these three sequences, as well as in *Hmi*_p2xB, the triplet 'NFR' motif and TM2 D350 residue is also seemingly absent (Fig. 3.17). The predicted N-termini of these sequences also appeared to be truncated, resulting in only a portion of the PKC phosphorylation motif being retained. Multiple sequence alignment identified regions within the predicted ECD of *Emult*_p2xC, *Egr*_p2xC, *Tso*_p2xB, and *Hmi*_p2xB that were largely conserved amongst these candidate Cestoda P2X receptors, that were not found in human P2X receptor subunits (Fig. 3.17). Molecular cloning is required to determine whether receptors are expressed in these Cestoda species.

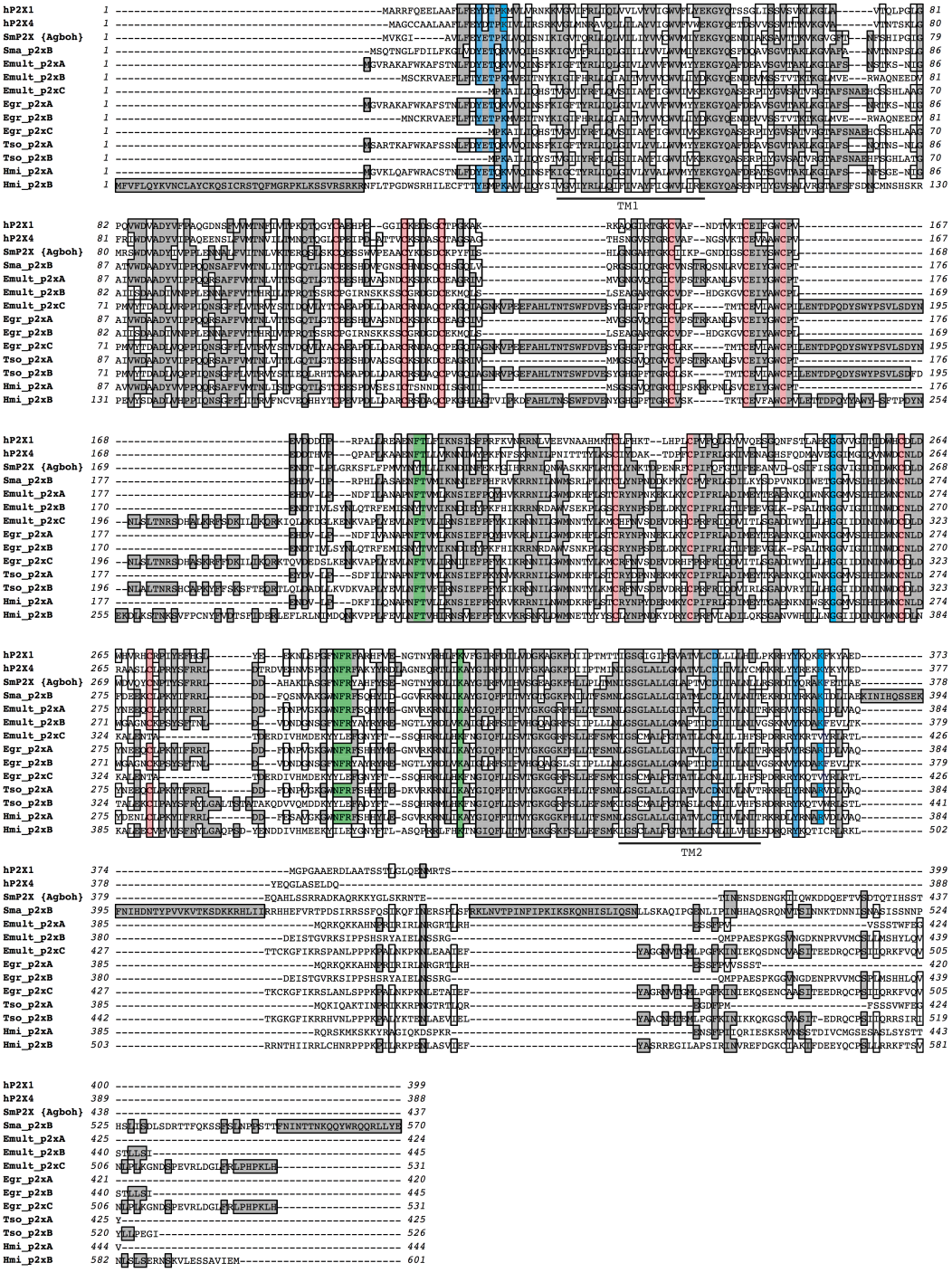
TM1
TM2

Fig. 3.17: MSA of candidate Platyhelminthes P2X receptor protein sequences with human P2X receptor subunits

Alignment of predicted full-length and partial protein sequence from various members of the Platyhelminthe phylum suggested that P2X receptors are present within this group of organisms. Identical residues between aligned protein sequences are depicted in grey, whilst chemically similar residues are only outlined. Many residues implicated in mammalian P2X receptor function are shared between hP2X1, hP2X4 and candidate Platyhelminthe P2X receptors, and are highlighted accordingly: green, ATP binding residues; red, extracellular cysteine residues; and blue, C-terminal membrane translocalisation motif ('YxxxK'), D350, and G250 (hP2X1 numbering). Sequences were retrieved by tBLASTn searching of appropriate datasets and aligned using the MUSCLE algorithm (Edgar, 2004) in MacVector. Species abbreviations: *Sm*_p2x (*Schistosoma mansoni*) (GenBank accession number: AJ783803; Agboh *et al.*, 2004); *Emult*_p2x (*Echinococcus multilocularis*); *Egr*_p2x (*Echinococcus granulosus*); *Tso*_p2x (*Taenia solium*); and *Hmi* (*Hymenolepis microstoma*).

3.3.8 Incomplete conservation of candidate P2X receptors in Nematoda

Partial ESTs with identity to mammalian P2X receptor homologues have been reported in the genomes of both *Xipenmia index* (California dagger nematode) and *Haemonchus contortus* (barbers' pole worm) (Fountain and Burnstock, 2009), whilst no P2X receptor homologue has been identified in the model nematode *C. elegans* (Harte and Ouzounis, 2002; Fountain and Burnstock, 2009). Extension of the search for nematode homologues of a mammalian P2X receptor in the genomes of specimens from the Bursaphelenchus, Dirofilaria, Loa, Meloidogyne, Onchocerca, Pristionchus, Panagrellus, Strongyloides, and Trichinella genera (Chen *et al.*, 2005) failed to identify further candidate nematode P2X receptors. Furthermore, homology searches of genomes of multiple species of the Caenorhabditis genus, beyond that of *C. elegans*, failed to identify a P2X receptor in this widely used model organism.

Partial ESTs from two nematode species - *Haemonchus contortus* (CB019691.1) and *Xiphinemia index* (XIC01614) – have been identified, and encode proteins with amino acid similarity to mammalian P2X receptor homologues having been identified previously (Fountain and Burnstock, 2009). Hydropathy plots of these predicted sequences from *H. contortus* and *X. index* correspond, in the former, to a portion of the P2X receptor extracellular domain and, in the latter, to a portion of the extracellular domain and entirety of the second transmembrane domain.

The 589 bp EST nucleotide sequence suggested to encode a P2X receptor from *H. contortus* was identified from a sequence deposited in GenBank (CB01961.1). To determine whether CB01961.1 is indeed a candidate P2X receptor, this partial EST sequence was used as a BLASTn query against the genome of *H. contortus* (via the Nematode.net portal: Martin *et al.*, 2012). One hit with 100% nucleotide sequence identity was retrieved; HC07532 and was predicted to encode for a protein 217 amino acid residues in length and displayed a low sequence identity with human P2X1-7 receptor subunits (6.8 to 9.0%). Protein topology analysis of HC07532 did not identify any extended regions of hydrophobic residues corresponding to membrane spanning domains. Based on this primary sequence, this may suggest that the previously suggested partial EST from *H. contortus* (Fountain and Burnstock, 2009) is not a P2X receptor homologue.

The nucleotide sequence of the predicted *X. index* P2X receptor XIC01614, retrieved through a tBLASTn search of EST sequences via the NEMBASE4 portal (Parkinson *et al.*, 2004; Elsworth *et al.*, 2011), encoded for a 247 amino acid protein. To assess database redundancy, a BLASTn search was also performed against the Nematode.net portal (Martin *et al.*, 2012) using the XIC0614 nucleotide sequence. A near-identical HSP was retrieved (X103839) but was 25 residues shorter than XIC0614. As such, pairwise alignment of X103839 and XIC01614 amino acid sequences revealed that the equivalent regions of the two translated sequences shared a 100% residue identity. XIC0614, the longer of the two partial EST sequences, was used for comparative primary protein sequence analysis.

Alignment with hP2X1 suggested that XIC01614 corresponded to a portion of the extracellular domain of the P2X receptor (residues 140 to 354). Across this region, the two amino acid sequences shared a 42.3% residue identity. In support of XIC01614 as a candidate nematode P2X receptor, all 7 ECD cysteine residues found in the corresponding regions of human P2X receptor subunits were conserved (hP2X1 numbering: C149, C159, C165, C217, C261, and C270) (Fig. 3.18). The remaining three cysteine residues (C117, C261, and C149) did not appear to be included in the partial XIC01614 EST translation. The C-terminal 'YxxxK' membrane stabilization motif (Chaumont *et al.*, 2004) is also conserved in XIC01614 (Fig. 3.18). With regards to residues implicated in the binding of ATP, F185 and T186 were conserved, as well as the NFR motif (N290-F291-R292). K309 was also conserved (Fig. 3.18).

Protein topology analysis of XIC01614 suggested that the sequence included a transmembrane domain (TM2; I203 to V225 (XIC01614 numbering)). Whilst no 'stop' codon was present in the XIC01614 EST sequence, 22 amino acid residues appear to constitute a portion of a C-terminal region following translation (Fig. 3.18).

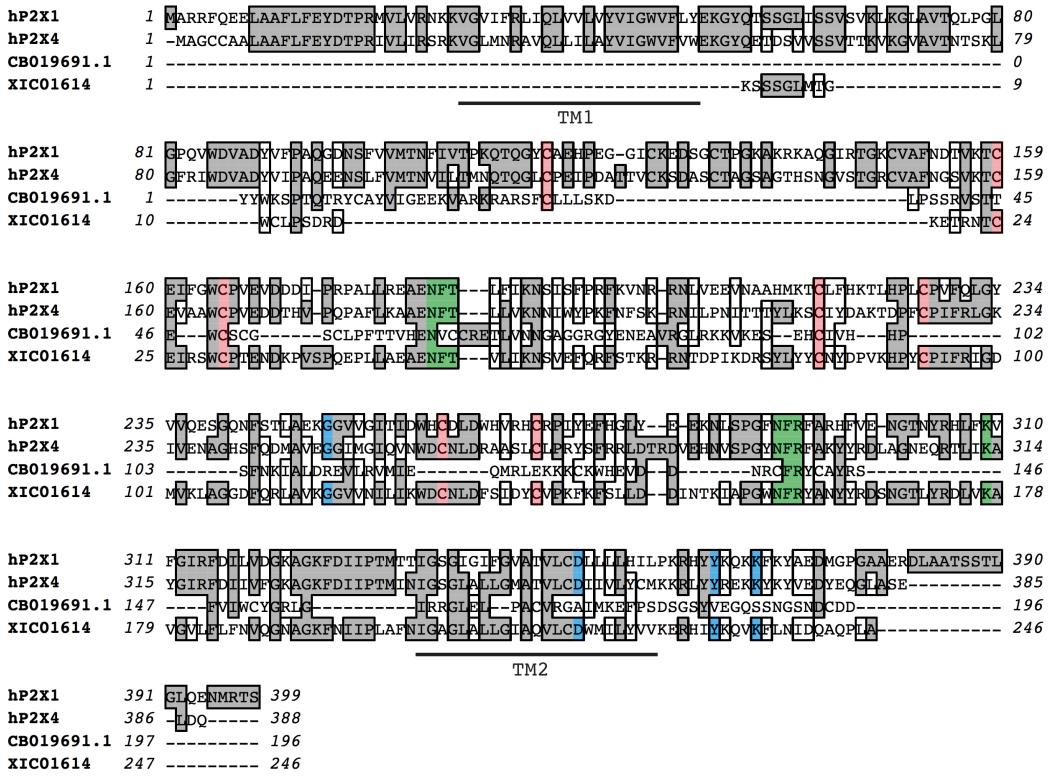

Fig. 3.18: MSA of protein sequences translated from partial ESTs from *H. contortus* and *X. index*

Partial EST sequences from two nematodes (*H. contortus* and *X. index*) thought to form part of a larger transcript encoding for a candidate P2X receptor protein were aligned with human P2X1 (hP2X1) and P2X4 (hP2X4) protein sequences by MUSCLE. The two nematode partial proteins shared sequence identity with human P2X receptor homologous, although that from *X. index* shares the greatest of the two. Horizontal lines below the alignment, based on hP2X1 topology, depict transmembrane domains 1 and 2. Accession numbers of candidate nematode P2X receptors CB019691.1 and XIC01614 correspond to *H. contortus* and *X. index*, respectively. Residues important in the function of mammalian P2X receptors and shared in the partial sequences of CB01969.1 and XIC01614 are depicted accordingly: green, ATP binding residues; red, ECD cysteine residues; blue, G250 and D350 (hP2X1 numbering), and YxxxK membrane translocalisation motif. Sequences were aligned using the MUSCLE algorithm (Edgar, 2004) in MacVector.

3.3.9 P2X receptors in Mollusca

The diverse Mollusca phylum includes the Gastropoda (snails, slugs and limpets), Bivalvia (clams and mussels), and Cephalopoda (squids and octopuses). Within the Mollusca, the Gastropoda subphylum is the most diverse, consisting of approximately 1000 extant species (Haszprunar and Wanninger, 2012).

Following the characterisation of a P2X receptor from the snail *Lymnaea stagnalis* (Bavan *et al.*, 2012), and the suggestion that the receptor may play a role in fictive feeding based on mRNA localization to neural circuits involved in this behaviour, publically available molluscan genome databases were analysed for further candidate receptors. No Cephalopoda genomic or transcriptomic data are currently available. However, these data are available for members of both the Gastropoda and Bivalvia orders (Table 3.1) and, were searched for candidate P2X receptor genes so as to expand our knowledge of this LGIC family in the Mollusca phylum.

Table 3.1: molluscan species in which searches for P2X receptor homologues were performed

Species	Common name	Class
Aplysia californica	California sea hare	Gastropoda
Biomphalaria glabrata	Bloodfluke planorb	Gastropoda
Lottia gigantea	Giant owl limpet	Gastropoda
Bithynia siamensis goniomphalos	*None*	Gastropoda
Pecten maximus	King scallop	Bivalvia
Mytilus galloprovincialis	Mediterranean mussel	Bivalvia
Placopecten magellanicus	Atlantic deep-sea scallop	Bivalvia
Elliptio complanata	Eastern elliptio	Bivalvia
Crassostrea gigas	Pacific oyster	Bivalvia

Nucleotide sequences that shared homology with mammalian P2X receptor proteins were identified in all molluscan species investigated as part of the current thesis. Many full-length CDS sequences were available from these species, but were shorter than predicted, such as a transcript retrieved from *B. glabrata* (Raghavan and Knight,

2006) (BGLTMP010712-RA; *Bgl*_p2x), that encoded for a protein 258 amino acids long. In contrast, nucleotide lengths of candidate P2X receptor sequences retrieved from WGS genomic data of *L. gigantea* (Simakov *et al.*, 2013) and *C. gigas* (Zhang *et al.*, 2012) were consistent with those of previously characterised vertebrate and invertebrate P2X receptors.

Two transcripts encoding candidate P2X receptors have been identified in the neuronal system of the gastropod *Aplysia californica* (California sea hare) and deposited into GenBank (AY389805 and AY389806) (Moroz *et al.*, 2006). These sequences shared a 67.3% primary sequence identity with each other, but AY389805 was shorter than its counterpart, with protein topology analysis predicting the presence of a portion of an ECD, one TMD and C-terminal intracellular domain. In contrast, the primary proteins sequence of AY389806 was predicted to include two intracellular domains, a large ECD and two TMDs, typical of P2X subunit topology. AY389806 (referred to subsequently as *Acal*_p2xA) shared all ten conserved cysteine residues found in mammalian P2X receptors, in addition to positively charged and aromatic ECD residues are involved in the coordinated binding of ATP in many P2X receptor subunits (Fig. 3.19). An N-terminal PKC motif and C-terminal membrane stabilisation motif was also conserved in *Acal*_p2xA. *Acal*_p2xA shared a 23.8 to 42.7% sequence identity with hP2X1-7 receptor subunits. Further analysis of NCBI WGS data for *A. califonica* (*via* the Mollusca TaxID 6447) retrieved a number of nucleotide sequences that, in their translated form, shared considerable sequence identity with both AY389805 and AY389806. In an attempt to retrieve the N-terminal portion of AY389805, a multiple sequence alignment of these hits was performed, and identified sequences with 100% identity across a homologous protein sequence of AY38905, but with a longer N-terminus that included a putative PKC phosphorylation motif. However, it was unclear where the true start codon lay for many of these sequences. As such, one sequence (GB01031437.1) was chosen to represent the N-terminus of AY38905. The original AY38905 sequence included a longer C-terminus than GB01031437.1, which was retained in the final merged, new *Acal*_p2xB sequence (Fig. 3.19). It is unclear whether the two putative *A. californica* P2X receptor sequence represented splice variants of one another, and further molecular cloning is required to confirm or deny this.

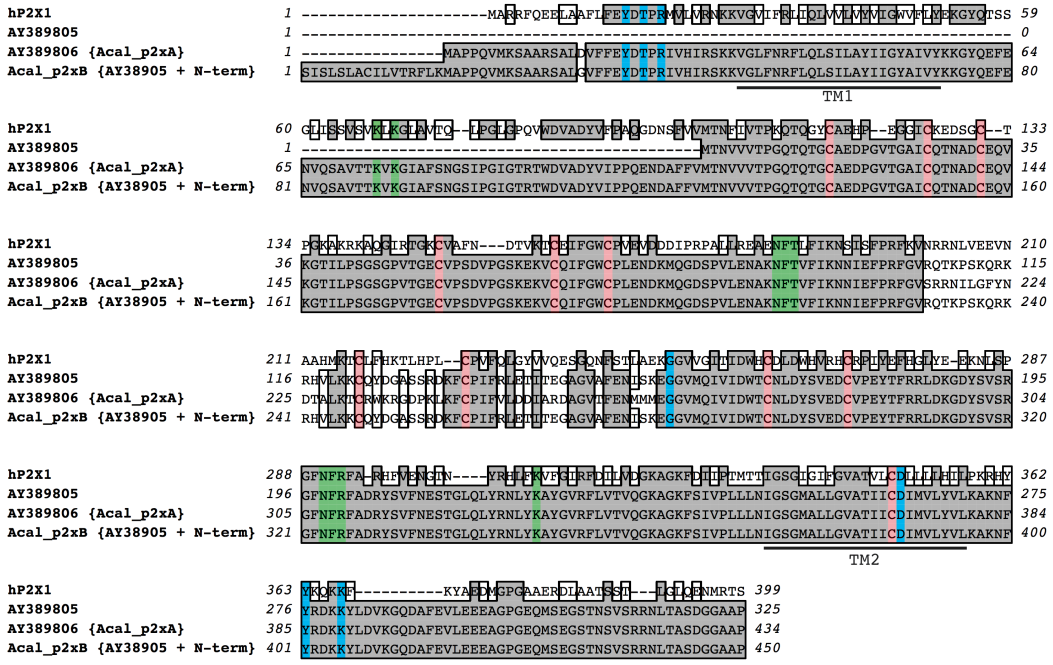

Fig. 3.19: MSA of putative full-length *A. californica* P2X receptors

Two putative full-length *A. californica* P2X receptors were retrieved through analysis of predicted transcripts from WGS sequence data (NCBI). Concatenation of a representative sequence retrieved from these data with one predicted sequence (based on shared residues in the ECD) resulted in a full-length sequence that included an N-terminal PKC phosphorylation motif and two ECD lysine residues known be involved in the co-ordinated binding of ATP (K68 and K70; hP2X1 numbering). Residues important in the function of mammalian P2X receptors and shared in the sequences of these two candidate *A. californica* P2X receptors and hP2X1 are depicted accordingly: green, ATP binding residues; red, ECD cysteine residues; blue, G250 and D350 (hP2X1 numbering), and YxxxK membrane translocalisation motif. Sequences were aligned using the MUSCLE algorithm (Edgar, 2004) in MacVector.

Furthermore, a full-length EST transcript sequence was identified from a haemocyte-specific cDNA library from *C. gigas* (Roberts *et al.*, 2009b). As with other Mollusca P2X receptors, this sequence shared all ATP binding residues, extracellular domain cysteine residues and N- and C-terminal motifs with mammalian P2X receptors (Fig. 3.20). Many of the other putative molluscan P2X receptors, retrieved through homology searching of genomic and transcriptomic sources, shared residues deemed important for mammalian P2X receptor function. As such, they were used for further phylogenetic analysis of invertebrate P2X receptors, where appropriate. A multiple sequence alignment of both full-length and partial, non-redundant candidate Mollusca

P2X receptors is illustrated in Fig. 3.20. These data suggested that, in addition to *L. stagnalis* (Bavan *et al.*, 2012), P2X receptors appear present in a number of gastropods, as well as in the Bilvalvia order of the Mollusca phylum.

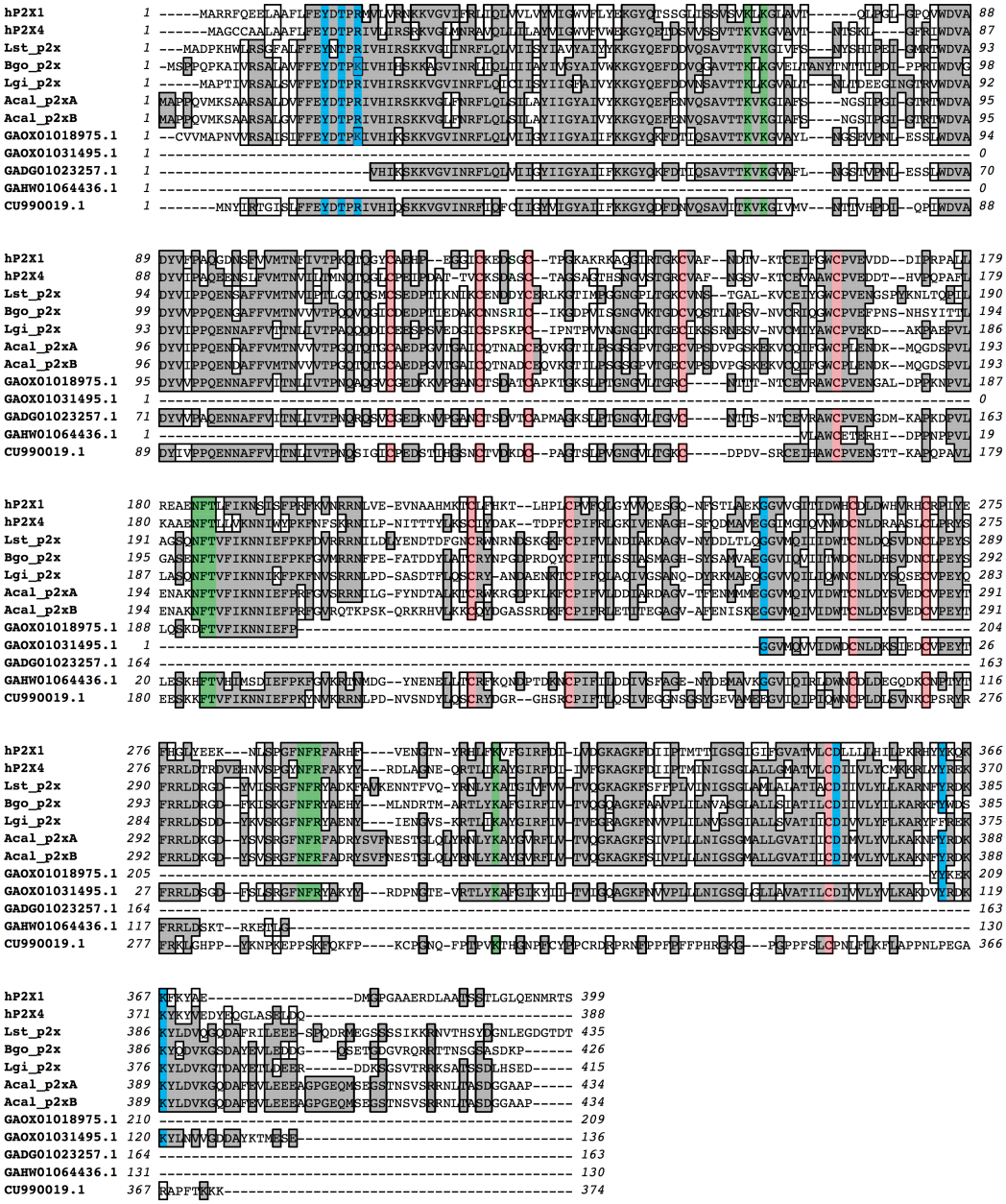

Fig. 3.20: MSA of non-redundant candidate P2X receptor protein sequences from a number of molluscs

A number of residues implicated in mammalian P2X receptor function are shared between candidate P2X receptors from molluscs and human P2X1 and P2X4 receptor subunits. These include ATP-binding residues (green), extracellular domain cysteine residues (red), and various motifs and residues involved in receptor modulation and expression (blue). Nomenclature of full-length sequences used are as follows: *Lst*_p2x, *Lymnaea stagnalis* (accession number: AV69113.1, Bavan *et al.*, 2012; *Bgo*_p2x*, Bithynia siamensis goniomophalos;* Lgi_p2x, *Lottia gigantea*; *Acal*_p2xA and *Acal*_p2xB, *Aplysia californica*. Partial sequence accession numbers used to refer to species as follows: GAOX01018975.1, *Mytilus galloprovincialis*; GAOX0131495.1, *Pectan maximus*; GADG01023257.1, *Placopectan magellanicus*; GAHW01064436.1, *Elliptio complanata*; and CU990019.1, *Crassostrea gigas.*

3.3.10 P2X receptors in Porifera and Placazoa

Porifera are believed to represent one of the oldest extant metazoan phyletic lineage, having emerged approximately 600 million years ago (MYA) (Srivastava *et al.*, 2010). To ascertain the extent to which P2X receptors appear to be present in this phylum, tBLASTn searches were performed against the genome of *Amphimedon queenslandica* (Srivastava *et al.*, 2010) and transcriptome datasets for both *Oscarella carmela* (slime sponge) and the freshwater sponge *Ephydatia muelleri* (Müller's freshwater sponge) (Hemmrich and Bosch, 2008). One candidate P2X receptor was identified in *A. queenslandica* (XM_003384088.1; *Aqu*_p2x), encoding a protein 422 residues in length. *Aqu*_p2x is predicted to possess a topology characteristic of P2X receptor subunits, consisting of two transmembrane domains spanned by a large ECD. 21.4 to 48.0% with hP2X1-7.

Four hits were retrieved following tBLASTn search of the *E. muelleri* transcriptome dataset: comp68168_c0_seq4; comp68168_c0_seq2; comp67432_c3_seq7; and comp84168_c0_seq2. Of these, comp84168_c0_seq possesses an open reading frame (ORF) encoding for a 108 amino acid protein, considerably shorter than one would expect, based on previously characterised P2X receptors. This sequence was excluded from further analysis. The remaining three, full-length predicted protein sequences are subsequently referred to as *Emu*_p2xA, *Emu*_p2xB, and *Emu*_p2xC, respectively.

Significant sequence identity existed between *Emu*_p2xA, *Emu*_p2xB, and *Emu*_p2xC (24.0 to 79.2%), and with hP2X1-7 homologues (17.0 to 38.2%), ranging between 411 and 609 residues in length. Both *Emu*_p2xA and *Emu*_p2xB possessed two regions predicted to be transmembrane domains. In contrast, *Emu*_p2xC was predicted to possess four extended regions of hydrophobic residues (ranging from 22 to 36 amino acids in length), suggesting the presence of approximately 4 TMDs, spanned by two ECDs between TM1-2 and TM3-4. At the primary sequence level, the consensus N-terminal PKC motif was absent in *Emu*_p2xC, but was conserved in *Emu*_p2xA and *Emu*_p2xB (Fig. 3.21). The C-terminal membrane stabilisation motif was only partially conserved in *Emu*_p2xC, appearing as '$Y(x)_5K$' (Fig. 3.21). All ten extracellular cysteine residues were found in the predicted ECDs of all *E. muelleri* P2X receptor subunits, as were the ATP binding residues K70, F185, T186, F291, and K309 (hP2X1 numbering) (Fig. 3.21). However, K68 was not found in *Emu*_p2xC where a serine residue (S107) was found in its place (Fig. 3.21). An aspartate residue found in TM2 (D350; hP2X1 numbering) is conserved between both *E. muelleri* and hP2X1-7 receptor subunits, as G250, previously identified to be important in the channel function of hP2X1 (Digby *et al.*, 2005) (Fig. 3.21).

A single hit was retrieved following BLAST search of the *Oscarella carmela* transcriptome (comp8618_c0_seq2; *Oca*_p2x), with a 1218 nucleotide CDS predicted to encode for a protein 406 residues in length. *Oca*_p2x shared a 35.1 to 68.5% sequence identity with *Aqu*_p2x and *E. muelleri* P2X receptor subunits, and 23.7 to 42.7% with hP2X1-7 subunits. Protein topology analysis suggested the existence of two TMDs and, in accordance with P2X receptor domain arrangement, a large ECD and intracellular N- and C-termini.

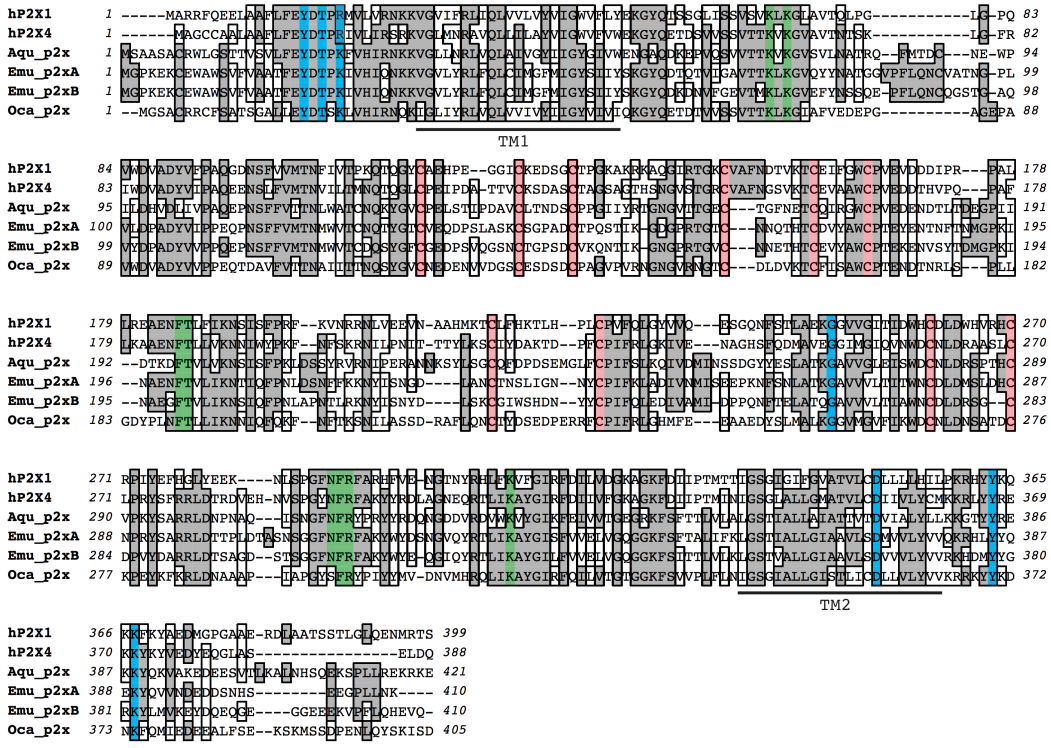

Fig. 3.21: MSA of candidate P2X receptors from Porifera

A number of residues implicated in mammalian P2X receptor function are shared between candidate P2X receptors from members of the Porifera phylum, and human P2X1 and P2X4 receptor subunits. These include ATP-binding residues (green), extracellular domain cysteine residues (red), and various motifs and residues involved in receptor modulation and expression (blue). Nomenclature of full-length sequences aligned are as follows: *Aqu*_p2x, *Amphimedon queenslandica*; *Emu*_p2xA and *Emu*_p2xB*, Ephydatia muelleri; and* Oca*_p2x, Oscarella carmela*. Sequences were aligned using the MUSCLE algorithm (Edgar, 2004) in MacVector.

Two predicted genes with significant sequence identity to hP2X1-7 appeared to be present in the genome of the only representative member of the Placozoa, *Trichoplax adhaerens* (Srivastava *et al.*, 2008). The predicted transcripts of these genes (XM_002115738.1; *Tad*_p2xA and XM_002113249.1; *Tad*_p2xB) encoded peptides 344 and 327 in length, respectively. Individual pairwise alignment of *Tad*_p2xA and *Tad*_p2xB sequences with hP2X1-7 suggested that these peptides lacked corresponding regions in human P2X receptor subunits crucial to receptor function, and the formation of a characteristic P2X protein topology. A portion of the ECD domain corresponding to E248-H296 in hP2X1 was absent in *Tad*_p2xA whilst two regions corresponding to a portion of the ECD (L72-A94) and ECD/TM2 junction (D320-I341) were absent in *Tad*_p2xB. Present at the N-terminus of both *T.*

adhaerens P2X receptor subunits is a conserved PKC phosphorylation site, as well as a C-terminal membrane stabilisation motif. ECD cysteine residues were largely conserved in both subunits, with the exception of C261 and C270 (hP2X1 numbering), which were absent from both sequences. With regards to residues involved in ATP binding in higher P2X receptor homologues, K68, K70 and K309 were conserved in both *Tad*_p2xA and *Tad*_p2xB. However, F185 and T186 were only present in *Tad*_p2xA and F291 was only present in *Tad*_p2xB.

3.3.11 P2X receptors in Choanoflagellata

The Choanoflagellata phylum encompasses a group of unicellular flagellate eukaryotes, with extant members representing the closest relative to the large metazoan phylum (King *et al.*, 2008). A P2X receptor has been cloned from *Monosiga brevicolis*, but a primary amino acid sequence is not currently publically available (Fountain *et al.*, 2008). To characterize conserved residues and motifs of this early P2X receptor, a tBLASTn search was performed to retrieve a full-length protein sequence of a receptor from *M. brevicollis*, from which two unique HSPs were identified (fgenesh2_pg.scaffold_3000573 and fgenesh1_pg.scaffold_3000578). These two predicted protein sequences shared a significant percentage sequence identity (72.5%) between each other and, between hP2X1-7 subunits, 20.7 to 34.7% and 15.6 to 26.5%, respectively. The comparatively low sequence identity of fgenesh1_pg.scaffold_3000578 to human P2X receptor subunits was due to an apparent truncation of the protein sequence within putative ECD of the receptor and, as such, was excluded from further analysis. Whilst the former predicted *M. brevicollis* P2X receptor appeared to possess two transmembrane domains, fgenesh1_pg.scaffold_3000578 appeared to represent a truncated form of fgenesh2_pg.scaffold_3000573 (referred to subsequently as '*Mbr*_p2x'). Multiple sequence alignment of fgenesh1_pg.scaffold_3000578 and *Mbr*_p2x suggested that the former sequence lacked significant portions of a predicted ECD, within which both the equivalent NFR triplet ATP binding motif and K309 (hP2X1 numbering) residue would be found in homologous mammalian receptor sequences.

At the primary sequence level, *Mbr*_p2x shared many residues and motifs deemed important in the function of mammalian P2X receptor. The N-terminal 'YxTx(K/R)'

PKC phosphorylation motif was conserved entirely (Fig. 3.22). Residues involved in the coordinated binding of ATP (K68, K70, F185, T186, F291 and K309) were all conserved, lying in the ECD flanked by two predicted TMDs (Fig. 3.22). A C-terminal membrane stabilisation motif was also conserved (Fig. 3.22).

A predicted P2X receptor from another choanoflagellate *Salpingoeca rosetta* (Fairclough *et al.*, 2013) has also been reported previously, although not confirmed through molecular cloning (Cai, 2012). This novel putative P2X receptor (accession number: PTSG_04102T0, referred to herein as *Sro*_p2x) shared a 54.3% sequence identity with *Mbr*_p2x and 20.6 to 43.7% identity with hP2X1-7 subunits. At the primary sequence *Sro*_p2x possessed many residues implicated in ATP binding in human receptor subunits, as well as many extracellular domain cysteine residues, although the equivalent hP2X1 C117 and C165 residues were seemingly absent in this candidate P2X receptor (Fig. 3.22). These same cysteine residues were also absent in the predicted amino acid sequence of sequence of *Mbr*_p2x.

The single-celled eukaryote *Capsaspora owczarzaki* (Suga *et al.*, 2013) is the only member of the Capsaspora genus, and forms the Filasterea clade in conjunction with *Ministerea vibrans* which, in turn, represents a sister group to Choanoflagellata and Metazoa (Shalchian-Tabrizi *et al.*, 2008). Extension of the search for further candidate P2X receptors in Choanoflagellata identified a single HSP with a 30.7% and 32.9% primary amino acid sequence identity with *Mbr*_p2xA and *Sro*_p2x, respectively, and between 21.7 to 47.8% across hP2X1-7 subunits. As in *Mbr*_p2x and *Sro*_p2x, mammalian ATP binding residues were conserved in the amino acid sequence of *Cow*_p2x but in contrast, all canonical human ECD cysteine residues were conserved in this putative choanoflagellate P2X receptor (Fig. 3.22).

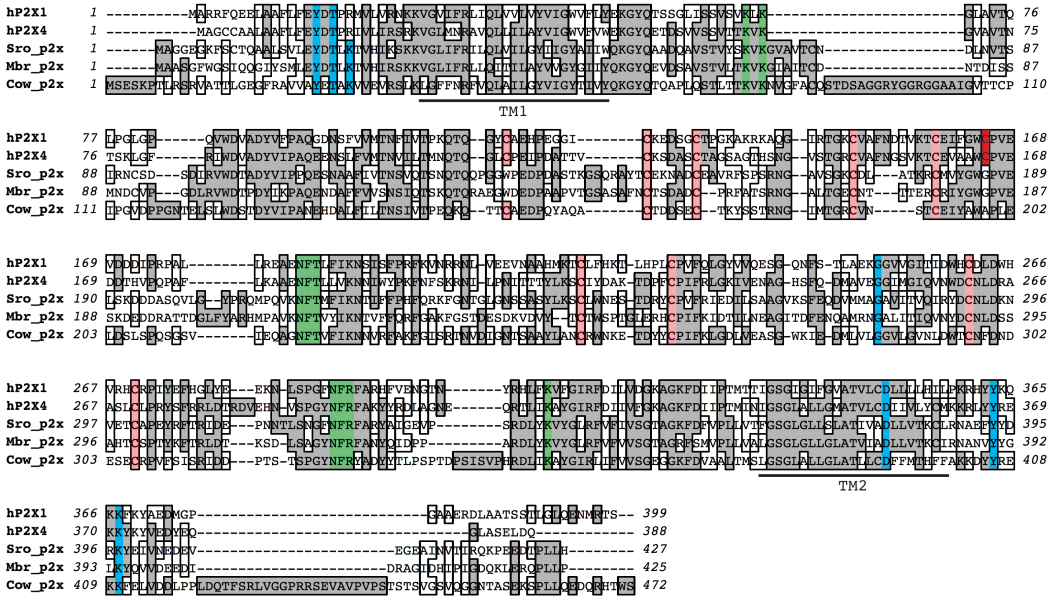

Fig. 3.22: MSA of Choanoflagellata and Filasterea P2X receptors

A number of residues implicated in mammalian P2X receptor function are shared between candidate P2X receptors from members of the Choanoflagellata (*M. brevicollis* and *Salpingoeca rosetta*) and Filasterea (*Capsaspora owczarzaki*) phyla, and human P2X1 and P2X4 receptor subunits. These include ATP-binding residues (green), extracellular domain cysteine residues (red), and various motifs and residues involved in receptor modulation and expression (blue). Transmembrane domains 1 and 2 (TM1 and TM2, respectively) are highlighted according to hP2X1 numbering. Nomenclature of full-length sequences aligned are as follows: *Sro*_p2x, *Salpingoeca rosetta*; *Mbr*_p2x, *Monosiga brevicollis*; and *Cow*_p2x, *Caspasora owczarzaki*. Sequences were aligned using the MUSCLE algorithm (Edgar, 2004) in MacVector.

3.3.12 P2X receptors in Amoebozoa

P2X receptors have been pharmacologically and functionally characterised from the social amoeba *D. discoideum* (Fountain *et al.*, 2007; Ludlow *et al.*, 2008; Ludlow *et al.*, 2009). To investigate the extent to which P2X receptors are present in amoeboid genomes, BLAST searches were performed against those of three further species: *Acanthamoeba castellanii* (Clarke *et al.*, 2013), *Entamoeba histolyica* (Loftus *et al.*, 2005), and *Polysphondylium pallidum*.

No hits were retrieved following BLAST search of *E. histolyica*, both when using hP2X1 receptor subtype and *Dd*P2XA receptor as a query. Three HSPs were

identified from *P. pallidum* (PPA1342200: *Ppa*_p2xA; PPA1415210: *Ppa*_p2xB; and PPA1315488: *Ppa*_p2xC) (see supplementary table). Consistent with the size of *Dictyostelium* P2X receptors, *P. pallidum p2x* genes were predicted to encode for proteins between 356 to 372 amino acids amino acids in length, with *Ppa*_p2xA and *Ppa*_p2xC predicted to possess two intracellular termini and two membrane-spanning domains spanned by a large extracellular domain (Fig. 3.28). However, topology analysis of the primary sequence of *Ppa*_p2xB only predicted an ECD, a second transmembrane domain and an intracellular C-terminus, and suggested that the sequence was devoid of the first transmembrane domain. Multiple sequence alignment of candidate *P. pallidum* P2X receptors with *Dd*P2XA-E and hP2X1.7 receptor subunits supported this finding (Fig. 3.23).

Significant sequence identity as found between the three predicted *P. pallidum* P2X receptor protein sequences (38.1 to 54.8%), and with the five *D. discoideum* P2XA-E subunits previously characterised (34.7 to 50.4%). Notably, *P. pallidum* P2X receptors displayed a similar low percentage sequence identity with hP2X1-7 receptors (9.1 to 17.2%) to that of *Dd*P2XA-E subunits (9.6 to 16.0%).

Multiple sequence alignment of candidate *P. pallidum* P2X receptors, including the seemingly TM1-less primary sequence of *Ppa*_p2xB, with *Dd*P2XA-E and hP2X1-7 revealed a number of shared features between subunits from both evolutionary distant P2X lineages. Two conserved cysteine residues were also shared between amoeboid *Ppa*_p2x1-3 subunits (C117 and C149; hP2X1 numbering), the same residues shared between *Dictyostelium* and human P2X receptors (Fig. 3.23). Conservation of ATP binding residues amongst candidate *Ppa*_p2x subunits varied with K68, K70, and F291 not conserved in *Ppa*_p2xA-C. As in *Dictyostelium* P2X subunits, the residues F185 and T186 were conserved in *P. pallidum*, although in *Ppa*_p2xA F185 is substituted for an also polar tryptophan residue (Fig. 3.23). Only in *Ppa*_p2xA was K309 conserved (Fig. 3.23).

In the infectious agent and amoeboid *A. castellanii*, four genes encoding protein products sharing significant sequence identity with *D. discoideum* P2X receptor subunits were retrieved (XM_004335559.1; XM_004337097.1; XM_004333964.1; and XM_004341457.1) with lengths ranging from 230 to 373 amino acids. Sequences are subsequently referred to as *Aca*_p2xA, *Aca*_p2xB, *Aca*_p2xC, and

*Aca*_p2xD, respectively. All proteins displayed a P2X-like protein topology, with the exception of XM_004333964.1, which was subsequently excluded from further sequence analysis due to its short length (230 amino acid residues), and truncated topology. The remaining three sequences shared a 17.2 to 39.5% residue identity with themselves and 17.3 to 39.6% identity with *D. discoideum* P2X receptors. Amongst the three sequences, XM_004341457.1 shared the lowest sequence identity between both remaining candidate *A. castellanii* P2X receptors and *Dictyostelium* P2X receptors. Interestingly, the range of sequence identity in *A. castellanii* candidate P2X receptors in comparison with hP2X1-7 (8.4 to 15.6%) was close to that for *D. discoideum* P2X receptors (9.6 to 15.9%).

In support of XM_004335559.1 (*Aca*_p2xA) and XM_004337097.1 (*Aca*_p2xB) being candidate P2X receptors, and XM_004341457.1 (*Aca*_p2xD) not being a member of this ion channel family, alignment of *Aca*_p2xA and *Aca*_p2xB illustrated that the two sequences shared a number of residues required for function in hP2X1-7 and *D. discoideum* (Fig. 3.28). These residues were largely absent in *Aca*_p2xD. Present at the N-terminus *Aca*_p2xB, but not that of *Aca*_p2xA was a conserved PKC phosphorylation motif (Boué-Grabot *et al.*, 2000; Ennion and Evans, 2002b), whilst a C-terminal 'YxxxK' membrane stabilisation motif (Chaumont *et al.*, 2004) was shared in both proteins (Fig. 3.23). An apparent absence of an N-terminal PKC motif in *Aca*_p2xA may be as a result of a truncated N-terminus of 12 amino acid residues, in comparison to a longer, 24 residue *Aca*_p2xB N-terminus. Consistent with both cloned *Dictyostelium* and predicted *Polysphondylium* P2X receptors, only two of the ten conserved ECD cysteine residues found in mammalian P2X receptor subunits were found in candidate *Aca*_p2xA and *Aca*_p2xB receptors (C117 and C149; hP2X1 numbering) (Fig. 3.23). Additionally, K68, K70, and K309 as well as the aromatic residue F291 were all seemingly absent from both *Aca*_p2xA and *Aca*_p2xB. F185 and T186 were both conserved in both subunits, consistent with other amoeboid P2X and P2X-like receptors (Fig. 3.23).

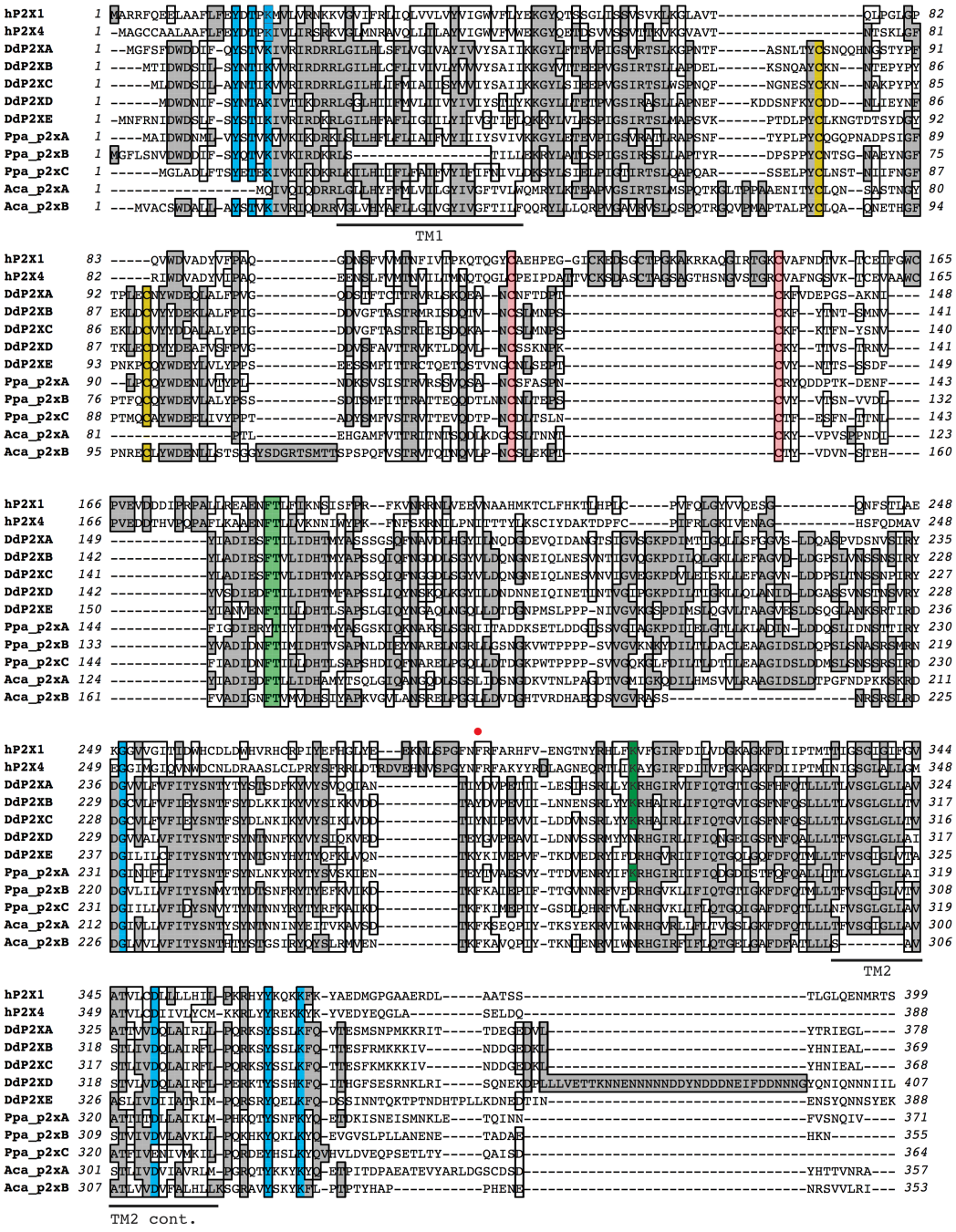
TM1
TM2
TM2 cont.

Fig. 3.23: MSA of retrieved candidate amoeboid P2X receptor protein sequences

A number of residues implicated in mammalian P2X receptor function are shared between candidate amoeboid P2X receptors and human P2X1 and P2X4 receptor subunits. These include ATP-binding residues (green), extracellular domain cysteine residues (red), and various motifs and residues involved in receptor modulation and expression (blue). The ATP binding 'NFR' motif is not found in its entirety in amoeboid P2X receptors, but an aromatic tyrosine or phenylalanine residue is found the equivalent position of F291 (hP2X1 numbering) (denoted by a red circle). Transmembrane domains (TM1 and TM2) are indicated according to the predicted position of these regions in the *Dd*P2XA receptor subtype. Two cysteine residues are shared amongst amoeboid P2X receptors that are not found in human P2X1 and P2X4 subunits, and may share a similar structural role to those found in human subunits. Species nomenclature is as follows: *Dd*, *Dictyostelium discoideum*; *Ppa*, *Polysphondylium pallidum*; and *Aca*, *Acanthamoeba castellanii*. Sequences were aligned using the MUSCLE algorithm (Edgar, 2004) in MacVector.

Retrieval of candidate P2X receptor sequences from other amoeboid species expands our knowledge of the extent to which P2X receptors are found in this group of unicellular eurkaryotes. Interestingly, the equivalent T186 residue (hP2X1 numbering) implicated in ATP binding in human receptors is shared both in amoeboid P2X receptors, as well as in candidate fungal receptors. This may suggest that the basic complement of amino acid residues required to confer ATP sensitivity in a P2X receptor is relatively small, or that homologues from basal eurkaryotes utilise currently uncharacterised residues in the coordinated binding of ATP.

3.3.13 Fungal P2X receptors

Recent BLAST analysis of early multicellular organisms has suggested the presence of putative P2X receptors in three basal species of: *Allomyces macrogynus* ATCC 38327 (division: Blastocladiomycota); *Batrachochytrium dendrobatidis*, and *Spizellomyces punctatus* DAOM BR117 (division: Chytridiomycota) (Cai and Clapham, 2011; Cai, 2012) (Fig. 3.24). Extension of this search into other members of the fungal kingdom using the JGI Fungal Genome Portal (Grigoriev *et al.*, 2011) identified further transcripts in another member of the Chytridiomyctota (*Catenaria anguillulae* PL171), as well as a member of the Entomophthoromycota (*Conidiobolus coronatus* NRLL29638), and Glomeromycota (*Rhizophagus irregularis* DAOM

181602) (Tisserant *et al.*, 2013) (Fig. 3.24).

No hits were retrieved from fungi using human P2X4 as a protein query, even under low stringency search conditions. However, putative P2X receptor-encoding transcripts were retrieved using the protein sequence of *D. discoideum* P2X receptor. Translated protein products of predicted transcripts from the genomes of these seven species ranged from 325 to 624 residues in length, with those from *R. irregularis* and *A. macrogynus* at the extremes of this range. Multiple sequence alignment of these sequences revealed a comparatively low shared sequence identity of these candidate fungal P2X receptors with the human P2X1 receptor subtype (9.0 to 14.7%), with the candidate P2X receptor form *R. irregularis* sharing the highest percentage sequence identity.

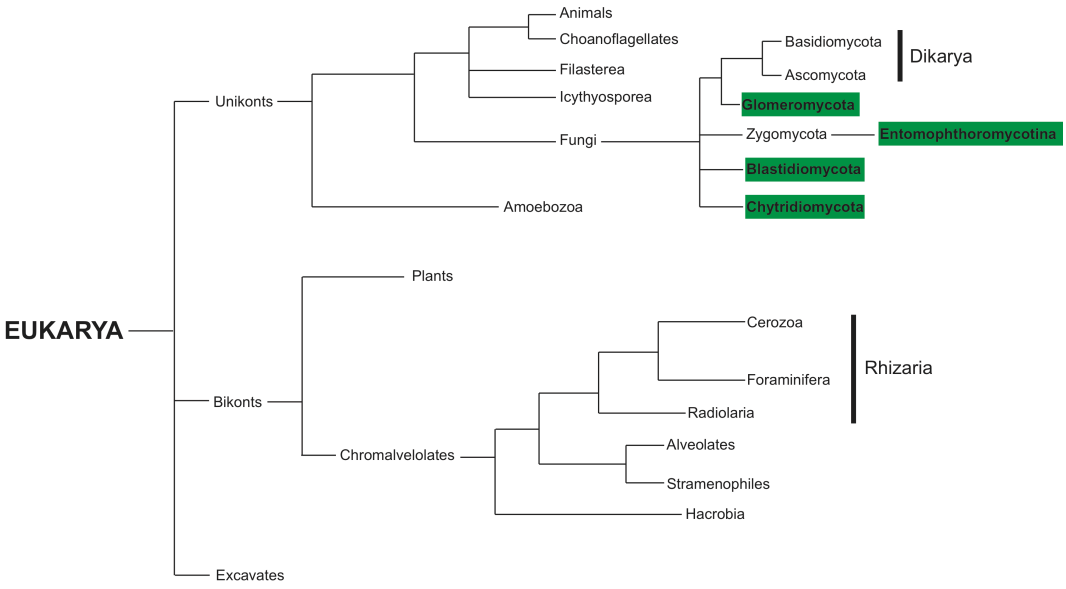

Fig. 3.24: fungal divisions in which transcripts encoding for candidate P2X receptor proteins were identified

The Fungi kingdom is considered part of the Unikonta group of organisms. Within the Fungi, candidate P2X receptors have been identified in Glomeromycota, Blastidiomycota, and Chytridiomycota divisions, as well as in the Entomophthoromycotina clade of the Zygomycota fungal division.

At the primary sequence level, many residues and motifs are shared amongst these candidate fungal P2X receptors. The N-terminal PKC phosphorylation motif ('YxTx(K/R)') was largely conserved amongst these sequences, with the exception of that retrieved from predicted transcripts of *C. coronatus*, where it was present as 'YNTFA' (Fig. 3.24). As reported previously (Cai, 2012), ECD cysteine residues are largely absent from candidate fungal P2X receptors, with only two conserved between those retrieved (equivalent to C117 and C132 in hP2X1) (Fig. 3.25). However, two further cysteine residues were conserved between all candidate fungal P2X receptors except that from *Piromyces* sp. E2 *(Pir*E2_p2x), positioned towards the putative N-terminus (Fig. 3.24). These may serve a similar structural function in fungal P2X receptors as those found in human P2X receptor subunits. K68 and K70 in hP2X1 are largely not conserved within fungal P2X receptors. Only in the protein sequence of *Spu*_p2x did it appear that an equivalent K70 residue was present (Fig. 3.25). In contrast, T186 was conserved amongst all fungal P2X receptors. F185 was only conserved in one *A. macrogynus* P2X receptor sybtype (*Ama*_p2xA), although the aromatic residue tyrosine was present at the equivalent position in *Ama*_p2xB, and candidate P2X receptors from *C. anguillae* and *C. coronatus* (Fig. 3.25). The triplet 'NFR' motif found in all mammalian P2X receptors is only conserved partially in P2X receptors from *B. dendrobatidis* and *S. punctatus*, where it was present as 'EFT' and 'EFK', respectively (Fig. 3.25). G250, a residue illustrated previously to be important for mammalian P2X receptor function (Digby *et al.*, 2005) was conserved throughout those fungal P2X receptors retrieved (Fig. 3.25). Interestingly, D350, a residue implicated in modulating the permeability of Ca^{2+} ions at mammalian P2X receptors (Samways and Egan, 2007) was only conserved in *B. dendrobatidis* (Fig. 3.25). However, a glutamate residue was found in the equivalent position in remaining fungal P2X receptors, and may suggest a conserved requirement of acidic residues at this position for mediating channel Ca^{2+} ion permeability, rather than an absolute requirement for an aspartate residue. Finally, the C-terminal 'YxxxK' motif was found in all candidate fungal P2X receptors with the exception of *Pir*E2_p2x (Fig. 3.25), although molecular cloning of this receptor is required to determine whether this absence is a true feature of the receptor, or whether it could be due to sequencing or transcript prediction error.

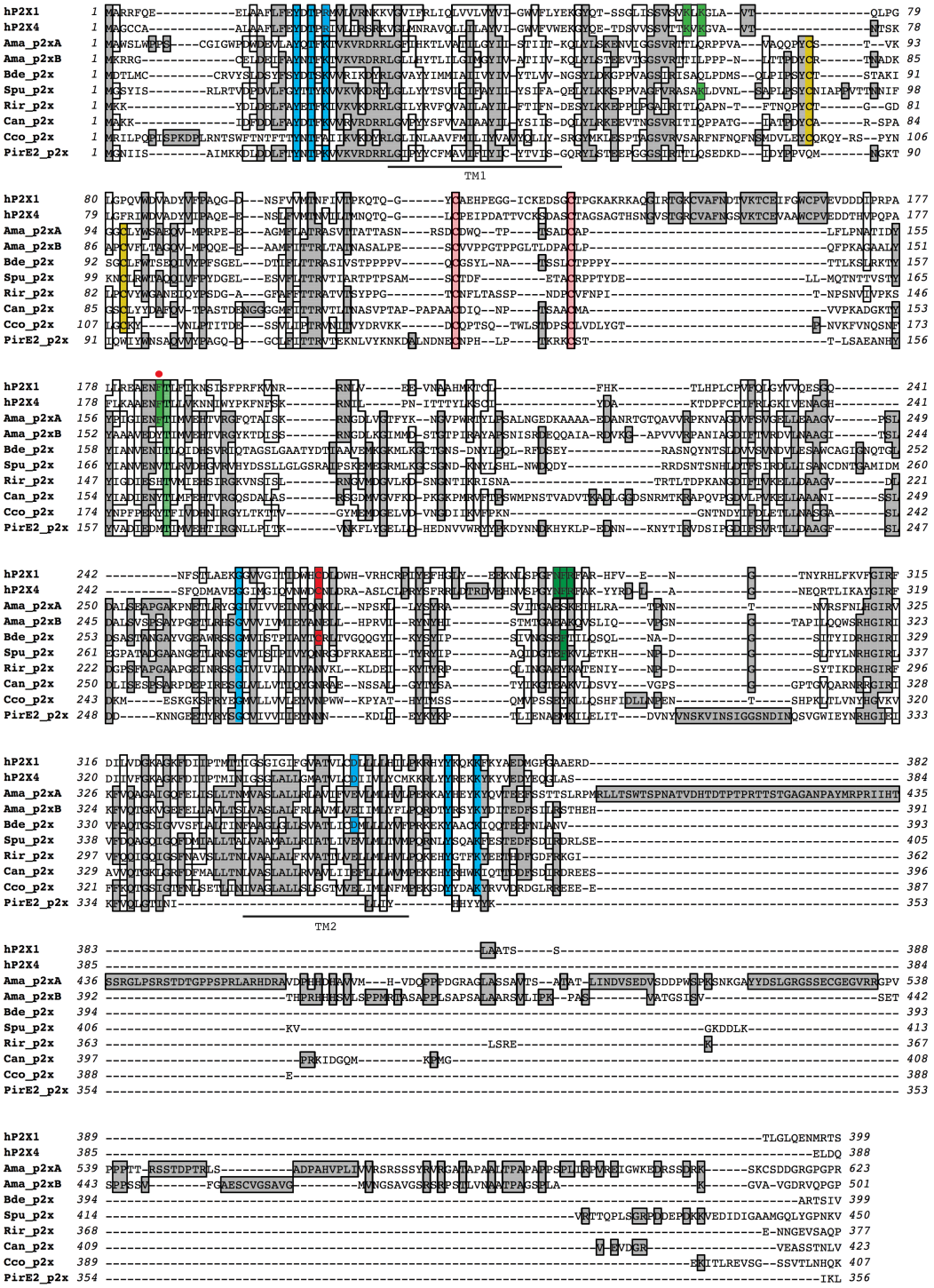
hP2X1
hP2X4
Ama_p2xA
Ama_p2xB
Bde_p2x
Spu_p2x
Rir_p2x
Can_p2x
Cco_p2x
PirE2_p2x
TM1
TM2

Fig. 3.25: MSA of putative fungal P2X receptor protein sequences with hP2X1 and hP2X4 subunits

Putative P2X receptors from a number of fungal species share low sequence identity with human P2X1 and hP2X4 subunits. A number of critical residues are conserved between these sequences, including an N-terminal PKC phosphorylation motif (YxTx(K/R)) and C-terminal membrane translocalisation motif (YxxxK) (blue), extracelllar domain cysteine residues (red), ATP binding residues (green), and G250 and D250 (hP2X1 numbering) (blue). *Ama*, *Allomyces macrogynus*; *Bde*, *Batrodochytrium dendrobatidis*; *Spu*, *Spizellomyces punctatus*, *Rir*, *Rhizophagus irregularis, Can*, *Catenaria anguillulae*, *Cco*, *Conidiobolus coronatus*; and *Pir*E2*, Piromyces* sp. E2. Sequences were aligned using the MUSCLE algorithm (Edgar, 2004) in MacVector.

Despite the low shared sequence identity in those P2X receptors suggested to be from fungi, primary sequence analysis following multiple alignment with human receptor subunits identified a number of shared residues between these phylogenetically distinct groups of organisms. Whilst it is unclear whether these candidate fungal P2X receptors function as ATP-gated ion channels, receptor homologues have been characterised in the amoeba *D. discoideum* P2X receptors from this amoeboid share a 13.3 to 15.0% sequence identity with human receptors, and lack many canonical ATP binding residues found in humans whilst still retaining sensitivity to this purine.

3.3.14 Candidate P2X receptors in the unicellular Bikonta

Whilst Fungi are considered a constituent kingdom of the Unikonta group of organisms, unicellular eukaryotes may also be found in the Bikonta (Burki and Pawlowski, 2006). Through homology searching of the Broad Institute 'Origins of Multicellularity' portal (Ruiz-Trillo *et al.*, 2007), transcripts encoding for proteins with weak homology to human P2X receptor subunits were retrieved from a number of unicellular eukaryotes. A single candidate P2X receptor-encoding transcript was identified from the Stramenopiles *Aplanochytrium kerguelense* and *Schizochytrium aggregatum*, and the rhizarian protist (phylum: Cerozoa) *Bigelowiella natans* (Curtis *et al.*, 2012).

In support of retrieved sequences from these organisms representing candidate P2X receptors, translated proteins of retrieved transcripts were predicted to include an N- and C-terminus, and an extended hydrophobic regions corresponding to two TMDs,

flanking a large ECD. Six sequences were retrieved from the predicted transcript database of *B. natans* (see supplementary data), with the three highest scoring protein derived from these transcripts of a length consistent with previously characterised P2X receptors. Furthermore, the three highest scoring protein sequences (referred to herein as *Bna*_p2xA, *Bna*_p2xB, and *Bna*_p2xC) were predicted to share a protein topology with previously characterised P2X receptors (Fig. 3.26). However, although *Bna*_p2xB and *Bna*_p2xC shared an 89% residue identity, predicted N-termini of these two proteins differed considerably, with that of *Bna*_p2xC consisting of an extended region within which the canonical N-terminal PKC motif was found (Fig. 3.25). In contrast, this motif was only conserved partially in *Bna*_p2xB. All but two ECD cysteine residues were identified in *Bna*_p2xA-C (equivalent to C217 and C227 in hP2X1) (Fig, 3.26). ATP binding residues were largely conserved amongst this predicted cerozoan P2X receptors, with the also aromatic tyrosine residue found in place of phenylalanine in the triplet 'NFR' motif in *Bna*_p2xB and *Bna*_p2xC (Fig. 3.25). Equally, tryptophan residues were found in place of phenylalanine in the doublet 'FT' ATP binding motif. Finally, the C-terminal membrane translocalisation motif was also largely conserved between human P2X subunits and candidate *B. natans* P2X receptors, although present as 'WxxxK' (Fig. 3.26).

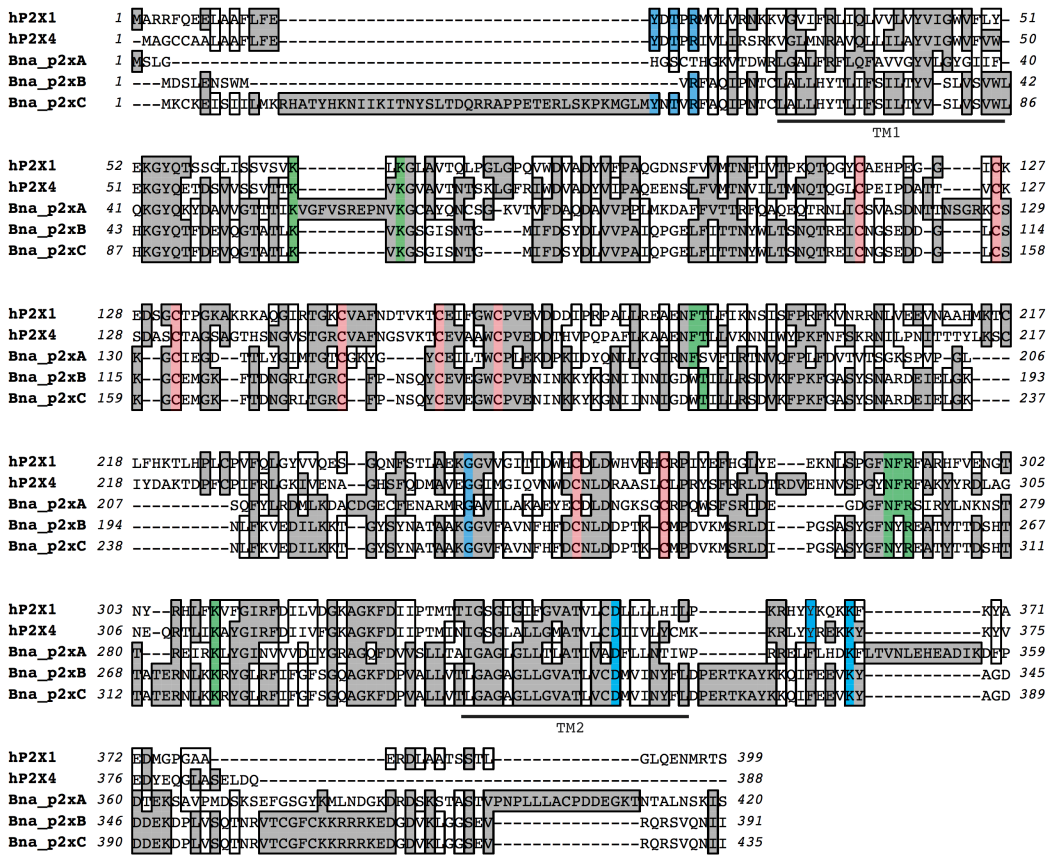

Fig. 3.26: MSA of three candidate *B. natans* P2X receptors

Putative P2X receptor subunits from the cerozoan *Bigelowiella natans* share sequence identity with human P2X1 and hP2X4 subunits. A number of critical residues are conserved between these sequences, including an N-terminal PKC phosphorylation motif (YxTx(K/R)) and C-terminal membrane translocalisation motif (YxxxK) (blue), extracellular domain cysteine residues (red), ATP binding residues (green), and G250 and D250 (hP2X1 numbering) (blue). Sequences were aligned using the MUSCLE algorithm (Edgar, 2004) in MacVector.

The remaining three translated protein sequences retrieved following homology searching of predicted *B. natans* transcripts were 1953, 278, and 1875 residues in length. Multiple sequence alignment of these proteins revealed identical shared residues both between each other, and with portions of *Bna*_p2xA-C. These redundant sequences were therefore excluded from further analyses.

In the Stramenopiles *Schizochytrium aggregatum* and *Aplanochytrium kerguelense*, two and four transcripts were identified following homology searching for candidate

P2X receptor sequences, respectively. The second of the two returned transcripts was identical to the highest scoring transcript (estExt_fgenesh1_pg.C_60087, referred to herein as *Sag*_p2x), but did not possess an extended predicted N-terminus of 17 amino acids. Within this extended region, a modified form of the PKC phosphorylation motif appeared as 'YMSVK' (Fig. 3.27). In support of the inclusion of *Sag*_p2x as a candidate P2X receptor, the majority of ATP binding residues were shared with human receptor subunits, although the triplet 'NFR' motif found in all known human P2X receptor sequences was present as 'NYR' in *Sag*_p2x (Fig. 3.27). Of the ten conserved cysteine residues found amongst human P2X receptor subunits, seven are conserved in *Sag*_p2x (Fig. 3.27).

Four transcripts were retrieved following homology searching for candidate P2X receptors in *Aplanochytrium kerguelense*. Multiple sequence alignment of protein products of these transcripts identified redundancy of two sequences. Accordingly, the two highest scoring protein sequences were used in further analyses: estExt_fgenesh1_pg.C_270194 and fgenesh1_kg.27_#_166_#_isotig02044. Whilst topology analysis of the former sequence (referred to subsequently as *Ake*_p2x) predicted the presence of two TMDs flanking an extracellular region, the latter sequence was predicted to possess seven regions of residue hydrophobicity (Fig. 3.26), reminiscent of that seen in G protein-coupled receptor (GPCRs).

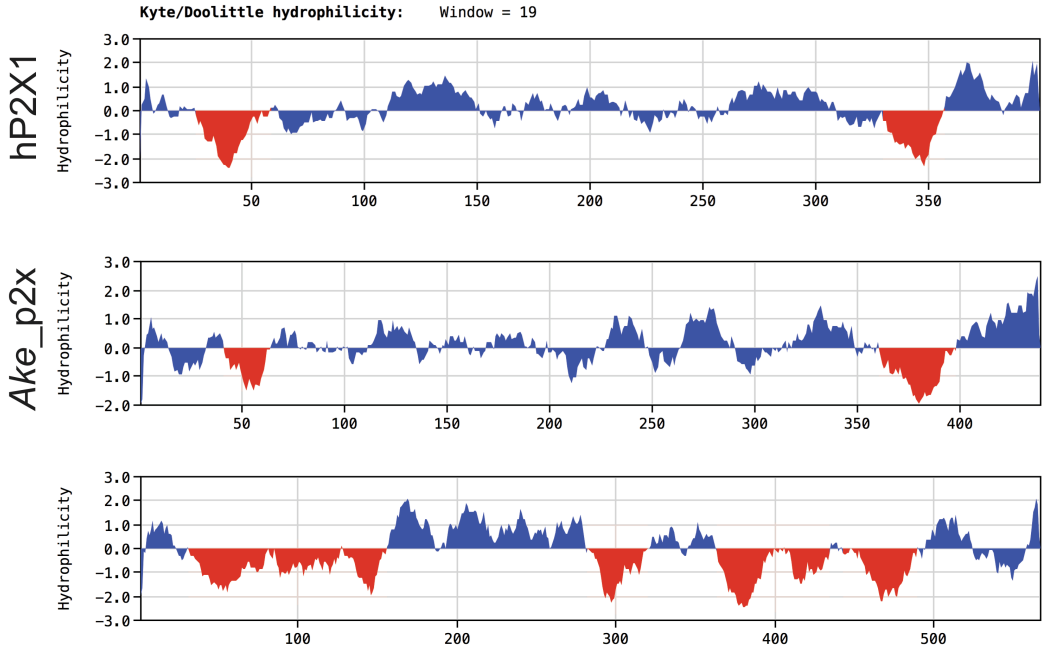

Fig. 3.27: topology analysis of non-redundant candidate P2X protein sequences of *Aplanochytrium kerguelense*

Consistent with human P2X receptors, the highest scoring retrieved hit following homology searching for candidate P2X receptors in *A. kerguelense* was predicted to possess two extended regions of hydrophobicity corresponding to transmembrane domains. A second returned hit that was not included in further analysis was predicted to possess a GPCR-like, seven TMD topology and, as such, was not considered to be a candidate P2X receptor.

At the primary sequence level, *Ake*_p2x displayed a 16 to 28.2% residue identity with human P2X receptor subunits, and a 43.1% identity with the fellow candidate Stramenopile *S. aggregatum* P2X receptor. Basic and aromatic ATP binding residues were shared in *Ake*_p2x, as was the canonical C-terminal membrane stabilisation motif and N-terminal PKC phosphorylation motif (Fig. 3.27). As in *Sag*_p2x, seven of ten conserved ECD cysteine residues were present in the protein sequence of *Ake*_p2x (Fig. 3.27). Despite a comparatively low primary sequence identity of candidate Stramenophile P2X receptors with human P2X subunits, these unicellular eukaryote proteins share a number of residues considered important for human P2X receptor function. Topological analysis also provided strong support in favour of their inclusion as early eukaryotic members of the P2X receptor family.

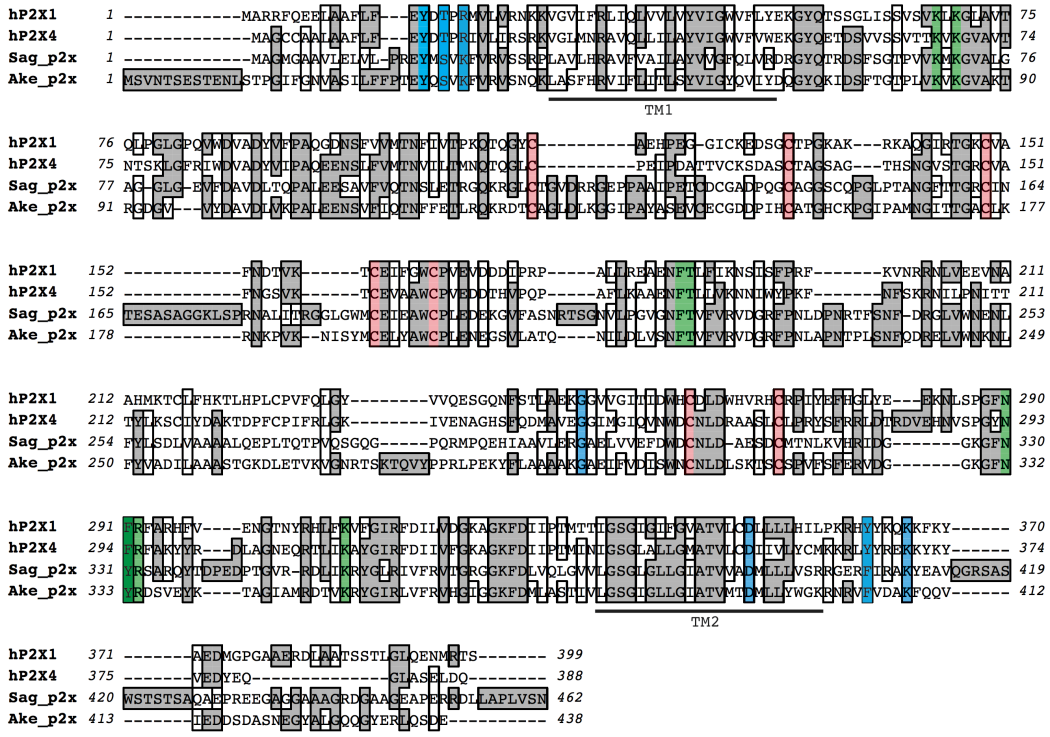

Fig. 3.28: MSA of candidate P2X receptors from two Stramenopiles

Putative P2X receptor subunits from the *Schizochytrium aggregatum* (*Sag*_p2x) and *Aplanochytrium kerguelense* (*Ake*_p2x) shared a number of critical residues are with human P2X receptor subunits (hP2X1 and hP2X4 are presented in this alignment), including an N-terminal PKC phosphorylation motif (YxTx(K/R)) and C-terminal membrane translocalisation motif (YxxxK) (blue), extracellular domain cysteine residues (red), ATP binding residues (green), and G250 and D250 (hP2X1 numbering) (blue). Sequences were aligned using the MUSCLE algorithm (Edgar, 2004) in MacVector.

No candidate P2X receptor was identified in the genome of the Ciliophora alveolate *Paramecium tetraurelia* (Aury *et al.*, 2006). However, sequences with protein homology to human P2X receptors were identified in the Dinoflagellata alveolates *Symbiodinium* sp., *Lingilodinium polyedrum*, *Pyrodinium bahamense* and *Alexandrium tamarense*. Through a broad homology search of WGS sequence data of the Alveolata superphylum (TaxID: 33630), full-length and non-redundant transcript sequences were retrieved from *Symbiodinium* sp. (GBGW01001110.1; *Sym*_p2x), *L. polyedrum* (GAPB01033764.1; *Lpo*_p2x), and *P. bahamense Pbah*_p2x (GAIO01008183.1), whilst a partial EST sequence was retrieved from *A. tamarense* (GAJB010022920.1; *Ata*_p2x).

Protein products of these novel candidate P2X receptors ranged from 348 to 309 amino acids in length, and were all predicted to possess two TMDs flanking a putative ECD. At the primary sequence level, these alveolate P2X receptors shared a 12.3 to 23.5% identity with human P2X1-7 subunits, with the highest identity for all receptors shared with human P2X4. In multiple sequence alignment with hP2X1 and hP2X4, candidate Alveolata P2X receptor sequences were shown to include a number of critical residues and motifs considered important in the function of previously characterised P2X receptor homologues. Of the ten conserved cysteine residues found in previously characterised mammalian P2X receptors, and many invertebrate homologues, seven were found in the primary amino acid alignment of candidate Alveolata (Fig. 3.29). The equivalent ECD C159 and C217 residues (hP2X1 numbering) were seemingly absent from these sequences and, although sequence identity of ATP binding residues and motifs was low in *Sym*_p2x and *Ata*_p2x, some residue substitutions retained chemical similarity (Fig. 3.29). For instance, the equivalent K68 and K70 residues in *Ata*_p2x were present as the equally positively charged histidine and arginine residues, respectively (Fig. 3.29). Similarly, the equivalent residue to K309 was present as an arginine in *Sym*_p2x, although absent in *Ata*_p2x. The 'NFR' ATP binding motif was only partially conserved in both candidate P2X receptors, as 'NIV' and 'AFN' in *Sym*_p2x and *Ata*_p2x, respectively (Fig. 3.29). Whilst the C-terminal 'YxxxK' was conserved in all candidate Alveolata receptors, a putative N-terminal PKC phosphorylation motif was conserved in its entirety only in *Sym*_p2x and *Pbah*_p2x, and present in a partial 'YYTRQ' and 'YNTRQ' in *Ata*_p2x and *Lpo*_p2x, respectively (Fig. 3.29).

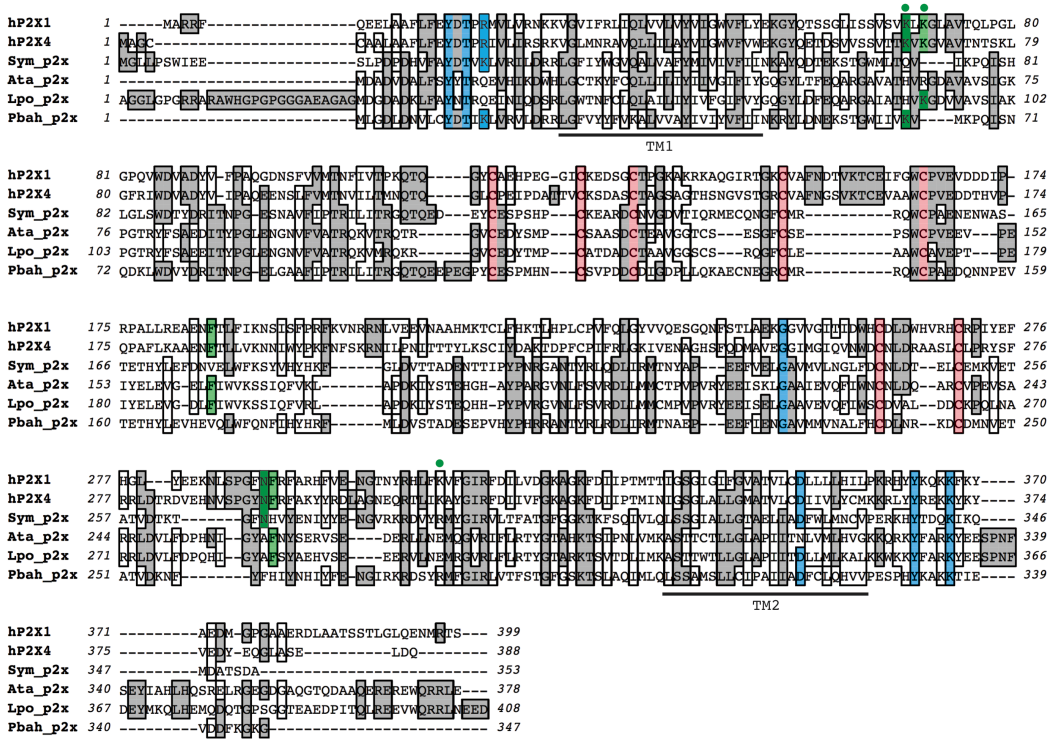

Fig. 3.29: MSA of candidate Alveolata P2X receptors

Putative P2X receptor subunits from the dinoflagellate alveolates *Symbiodinium* sp. (*Sym*_p2x), *Alexandrium tamarense* (*Ata*_p2x), *Lingilodinium polyedrum* (*Lpo*_p2x), and *Pyrodinium bahamense* (*Pbah*_p2x) shared a number of critical residues are with human P2X receptor subunits (hP2X1 and hP2X4 are presented in this alignment). These included a C-terminal PKC phosphorylation motif (YxTx(K/R)) and C-terminal membrane translocalisation motif (YxxxK) (blue), a number of ECD cysteine residues (red), some ATP binding residues (green), and G250 and D250 (hP2X1 numbering) (blue). A green circle above the alignment highlights residues that are chemically similar to conserved ATP binding residues in human P2X subunits. The N-terminal PKC phosphorylation motif was partially conserved in candidate P2X receptors from *L. polyedrum* and *P. bahamense*. TM1 and TM2 are placed below the alignment based on hP2X1 numbering. Sequences were aligned using the MUSCLE algorithm (Edgar, 2004) in MacVector.

3.3.15 Candidate P2X receptors in the Excavata kingdom

In addition to P2X receptors being identified in the unicellular bikonts and eukaryotic Alveolata, Stramenopile, and a member of the Rhizaria, candidate P2X receptors were also retrieved following homology searching of members of the Excavata kingdom of unicellular eukaryotes. Partial EST sequences were retrieved from two excavates; the euglenozoan *Euglena gracillis* (EC672030.1; *Egra*_p2x) and the malawimondozoan (TaxID: 136087) *Malawimonas jakobiformis* (EC723256.1;

*Mja*_p2x). Multiple sequence alignment of the predicted proteins with human P2X receptor subunits suggested that they are homologous to the N-terminus, TM1, and partial ECD of a candidate P2X receptor (Fig. 3.30). Although retrieved as partial sequences, submission of *Egra*_p2x and *Mja*_p2x to Pfam (Finn *et al.*, 2014) places these proteins within the P2X receptor family group (Pfam ID: PF00864).

At the primary sequence level, both partial protein sequences shared an N-terminal PKC phosphorylation motif with hP2X receptor subunits, and a number of ECD cysteine residues (Fig. 3.30). The equivalent K68 and K70 (hP2X1 numbering) were conserved in the partial sequence of *Mja*_p2x, but were not found in that of *Egra*_p2x (Fig. 3.30). Further molecular cloning is required to determine the full-length CDS of both these sequences, and assess their homology to previously characterised vertebrate and invertebrate P2X receptors.

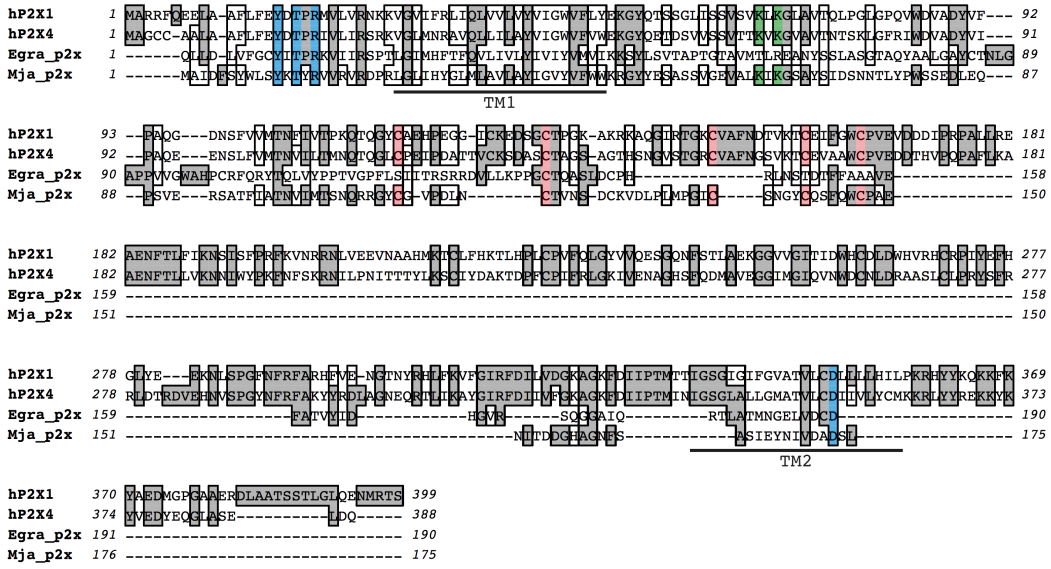

Fig. 3.30: MSA of candidate Excavata P2X receptors

Partial candidate P2X receptors were retrieved from the euglenozoan *Euglena gracillis* (*Egra*_p2x) and the malawimondozoan *Malawimonas jakobiformis* (*Mja*_p2x). These receptors appeared to represent the putative N-terminus, TM1 and portion of an ECD of a P2X receptor, based on alignment with homologous regions in the primary sequence of hP2X1 and hP2X4. Within this homologous region, the N-terminal PKC phosphorylation motif (YxTx(K/R)), and a number of ECD cysteine residues (red). Positively charged K68 and K70 residues were shared in *Egra*_p2x, but were seemingly absent in the primary amino acid sequence of *Mja*_p2x, although further molecular cloning is required to confirm this. TM1 and TM2 are placed below the alignment based on hP2X1 numbering. Sequences were aligned using the MUSCLE algorithm (Edgar, 2004) in MacVector.

3.3.16 A candidate P2X receptor in a member of the Streptophyta

It has been well documented that P2X receptors are seemingly absent from many higher plants, most notably the thale cress *Arabidopsis thaliana*. However, P2X receptors are not absent from the Plantae kingdom as a whole; homologues have been identified and cloned from the *Ostreococcus* species *O. tauri* and *O. lucimarinus* (Fountain *et al.*, 2008). A broad tBLASTn search was performed with EST databases available for members of the Plantae (TaxID: 3193). This retrieved two 5'-end nucleotide sequences encoding for non-redundant candidate P2X receptors in the green alga *Nitella hyalina*, a member of the Charophyta division of the larger

Archaeplastida group of plants. The dominant view is that the Charophyta represent the closest living ancestor to land plants (Karol *et al.*, 2001; Kranz *et al.*, 1995; Turmel *et al.*, 2006; Hori *et al.*, 2014). However, data are emerging that suggest that the Zygnematales ('pond scum') are the sister group to embryophytes – informally referred to as 'the land plants' (Wodniok *et al.*, 2011; Timme *et al.*, 2012; Zhong *et al.*, 2014).

In primary amino acid sequence alignment with human P2X receptor subunits, partial protein sequences retrieved from an *N. hyalina* EST dataset (HO528268.1 and HO495113.1) shared a 31.4 and 31.1% primary sequence identity with the homologous regions of human P2X receptor subunits, respectively. Multiple sequence alignment suggested that these regions encompassed a portion of the ECD, the entirety of a predicted second transmembrane domain, and a intracellular C-terminus of 23 to 33 amino acid, respectively (Fig. 3.31). Within both partial *N. hyalina* sequences, the triplet ATP binding motif, 'NFR' was conserved, as was the equivalent K309 residue (hP2X1 numbering) (Fig. 3.31). Two ECD cysteine residues were conserved with human P2X receptors (C261 and C270; hP2X1 numbering) (Fig. 3.31). Within these partial sequences, a C-terminal membrane translocalisation motif was also conserved with human P2X homologues and, interestingly, was present as 'YxxxK' in contrast to the modified form of the motif found in a P2X receptor from the chlorophyte algae *O. tauri* (Fountain *et al.*, 2008) (Fig. 3.31).

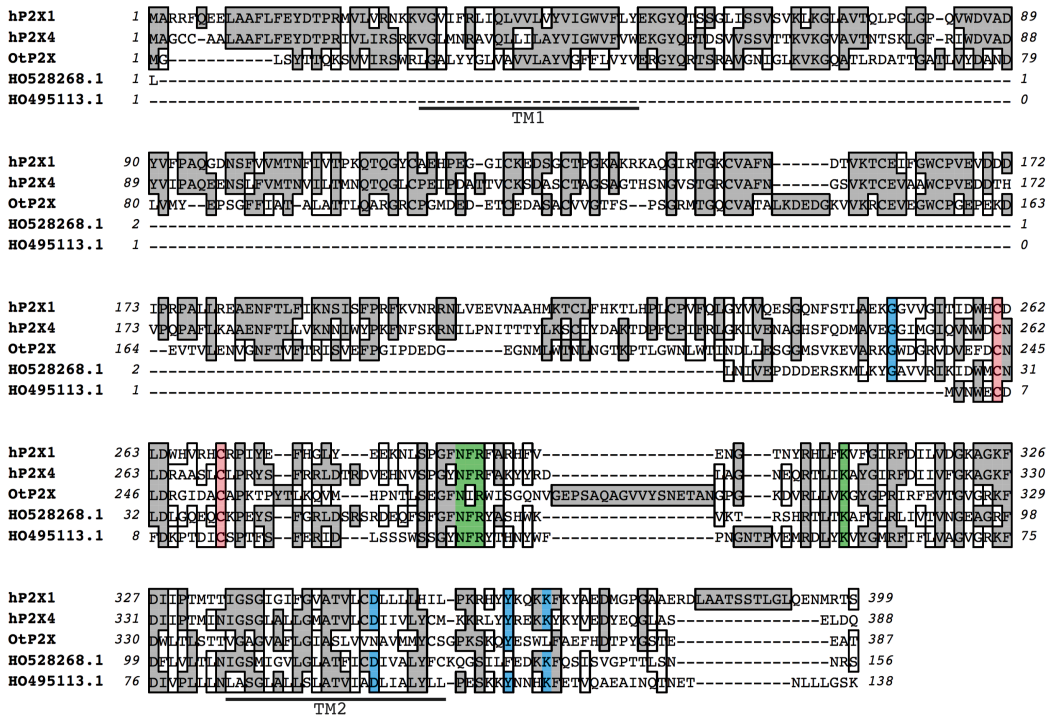

Fig. 3.31: MSA of putative partial candidate P2X receptors from *N. hyalina*

Partial candidate P2X receptors were retrieved from the charophyte *Nitella hyalina* (HO528268.1 and HO495113.1). These partial sequences appeared to represent the putative C-terminus, TM2 and portion of an ECD of a P2X receptor, based on alignment with homologous regions in the primary sequence of hP2X1, hP2X4 and *O. tauri* P2X. Within this homologous region, the C-terminal 'YxxxK' translocalisation motif, two ECD cysteine residues and some ATP binding residues were shared between these partial sequences and previously characterised sequences. TM1 and TM2 are placed below the alignment based on hP2X1 numbering. Sequences were aligned using the MUSCLE algorithm (Edgar, 2004) in MacVector.

A further candidate P2X receptor was identified in an EST dataset magnoliophyte *Erythranthe lewisii* ('great purple monkey flower') (previously *Mimulus lewisii*). Unusually, a candidate receptor sequence was not identified in another species of the same genus; *M. guttatus* (Hellsten *et al.*, 2013). Further characterisation of this sequence, and the conservation of P2X receptors in higher Streptophyta orders of the Embryophyta was beyond the scope of the current chapter.

It remains to be seen whether candidate P2X receptors identified in the current thesis in the early Fungi kingdom, and other early eukaryotes represent functional ATP-gated ion channels. Molecular cloning, followed by heterologous expression in an

appropriate system, and electrophysiological analysis of expressed proteins would help determine this.

A summary table of sequences presented in MSAs within the current chapter and their validity as a putative P2X receptors based on criteria outlined in section 3.2.1 is provided in table 3.2 below.

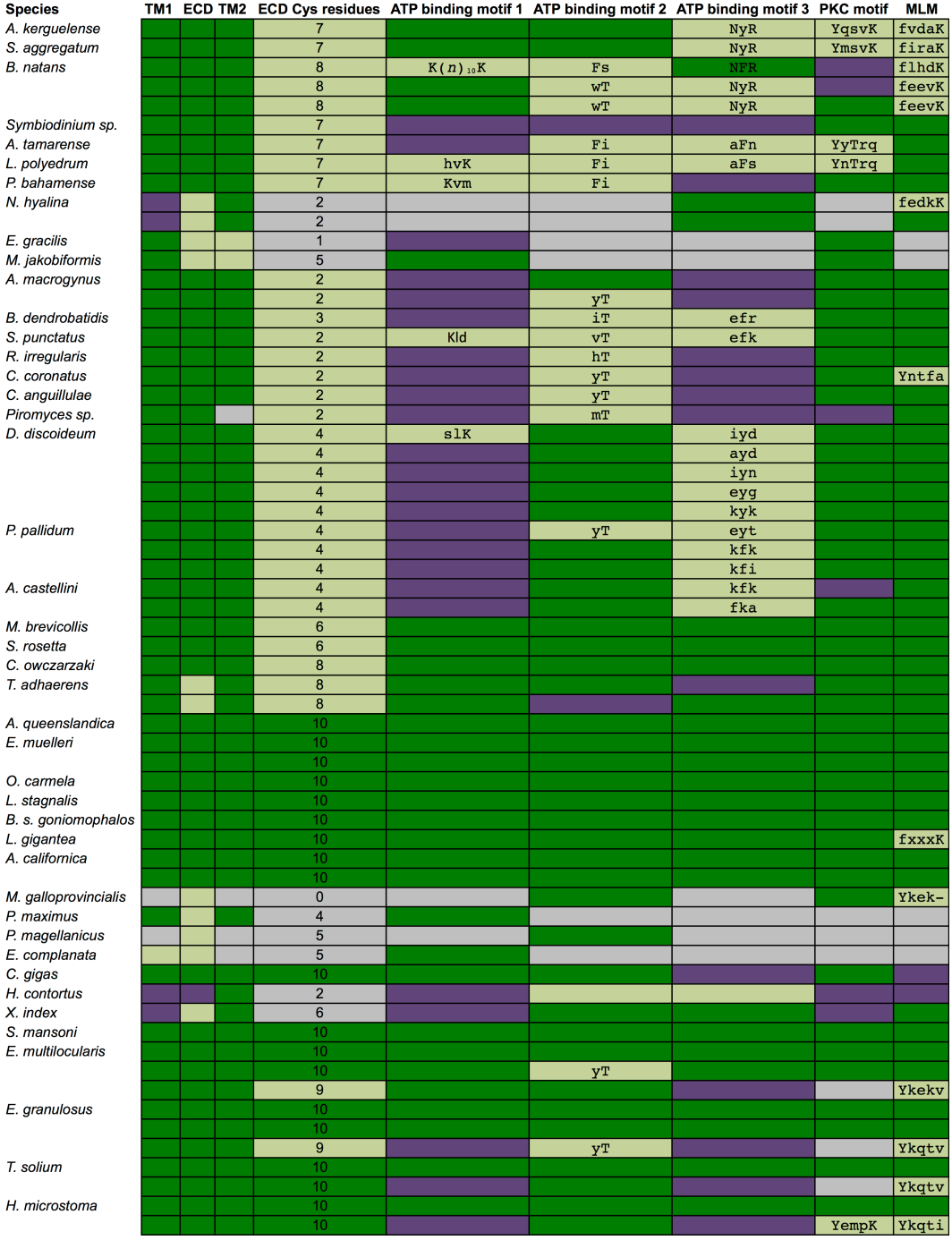

Species	TM1	ECD	TM2	ECD Cys residues	ATP binding motif 1	ATP binding motif 2	ATP binding motif 3	PKC motif	MLM
A. kerguelense				7			NyR	YqsvK	fvdaK
S. aggregatum				7			NyR	YmsvK	firaK
B. natans				8	K(*n*)$_{10}$K	Fs	NFR		flhdK
				8		wT	NyR		feevK
				8		wT	NyR		feevK
Symbiodinium sp.				7					
A. tamarense				7		Fi	aFn	YyTrq	
L. polyedrum				7	hvK	Fi	aFs	YnTrq	
P. bahamense				7	Kvm	Fi			
N. hyalina				2					fedkK
				2					
E. gracilis				1					
M. jakobiformis				5					
A. macrogynus				2					
				2		yT			
B. dendrobatidis				3		iT	efr		
S. punctatus				2	Kld	vT	efk		
R. irregularis				2		hT			
C. coronatus				2		yT			Yntfa
C. anguillulae				2		yT			
Piromyces sp.				2		mT			
D. discoideum				4	slK		iyd		
				4			ayd		
				4			iyn		
				4			eyg		
				4			kyk		
P. pallidum				4		yT	eyt		
				4			kfk		
				4			kfi		
A. castellini				4			kfk		
				4			fka		
M. brevicollis				6					
S. rosetta				6					
C. owczarzaki				8					
T. adhaerens				8					
				8					
A. queenslandica				10					
E. muelleri				10					
				10					
O. carmela				10					
L. stagnalis				10					
B. s. goniomophalos				10					
L. gigantea				10					fxxxK
A. californica				10					
				10					
M. galloprovincialis				0					Ykek-
P. maximus				4					
P. magellanicus				5					
E. complanata				5					
C. gigas				10					
H. contortus				2					
X. index				6					
S. mansoni				10					
E. multilocularis				10					
				10		yT			
				9					Ykekv
E. granulosus				10					
				10					
				9		yT			Ykqtv
T. solium				10					
				10					Ykqtv
H. microstoma				10					
				10				YempK	Ykqti

Species	TM1	ECD TM2	ECD Cys residues	ATP binding motif 1	ATP binding motif 2	ATP binding motif 3	PKC motif	MLM
P. bachei			1					Yrevi
M. leidyi			1					Yrdvi
H. magnipapillata			10					
H. vulgaris (AEP)			10					
N. vectensis			10					
			10					
A. aurita			3					
			3					
A. digitifera			8					
			5					
D. virgifera			2					
			0					
L. fulva			3			NpR		
			5					
			1					
			4			N--		
			5					
			1					
			4					
			5					
			1					
			1					
			0					
I. elegans			4		yT			
			4					
			3		Fs			
E. danica			4		yT			
			5					
L. y-signata			0					
O. cincta			10		sT			
			10			NFl		
			4					
			6					
			4					
			5					
			0					
A. maritima			1					
O. articus			2					
F. candida			10					
			10					kpcqK
			10			eFs		
			10					fkrkK
			2					
			0					kpcqK
			4					
			4					
			2					
			3					
D. pulex			10					
			10					fxxxK
G. pustulata			10					
S. maritima			9			N--		
			1			alR		
S. mimiorosum			10					fxxxK
A. geniculata			10					
L. hesperus			10					
			10					fxxxK
I. scapularis			6					
			1					
			1					
S. purpuratus			10					
			10					
			10					
S. kowalevskii			10					
			10					
			4		syT	NF(n)$_{11}$R		
B. floridae			10					

Table. 3.2: summary table of retrieved putative P2X receptor sequences identified in chapter 3

Putative P2X receptors presented in multiple sequence alignment in chapter 3 were identified according to criteria specified in section 3.2.1. Coloured cells indicate the following: *green*, a putative motif is present within a predicted receptor domain and is shared in its entirety with higher P2X receptor homologues; *light green*, a putative motif is partially shared with higher P2X receptor homologues within a predicted receptor domain; *purple*, a motif does not appear to be shared with a higher P2X receptor homologue, although hydropathy plots predicts the presence of a specific P2X receptor domain; *grey*, a partial retrieved sequence does not contain a specific P2X receptor domain and, as such, the presence of a given motif cannot be predicted. *Cys*, cysteine residue; *PKC*, protein kinase C motif ('YxTxK/R'); *MLM*, membrane localization motif ('YxxxK').

3.3.17 P2X receptors are seemingly absent from Bacteria and Archaea

It has been previously reported that P2X receptors are seemingly absent from the genome of *E. coli* (Blattner *et al.*, 1997). Extension of this search across 3595 representative bacterial species and strains via the RefSeq microbial genomes database (Tatusova *et al.*, 2014) confirmed these previous findings, even under low stringency homology search criteria.

Similarly, BLAT searching of available archaeal genomes via the UCSC Archaeal Genome Browser (Chan *et al.*, 2012) suggested that P2X receptors appear to be absent in a number of members of this domain, including *Thermosphaera aggregans*, *Acidilobus saccharovorans* 345 (Mardanov *et al.*, 2010), *Haloferax volcanii* DS2 (Hartman *et al.*, 2010), *Korarchaeum cryptofilum* OPF8 (Elkins *et al.*, 2008), *Nanoarchaeum equitans* (Waters *et al.*, 2003) and *Cenarchaeum symbosium* (Hallam *et al.*, 2006).

3.4 DISCUSSION

The current chapter has presented analyses of primary amino acid sequences of predicted P2X receptors in a range of eukaryotic phyla. I sought to expand our current understanding of the extent to which P2X receptors are expressed in the evolutionary tree of life, and assess the degree of conservation of amino acid in these predicted receptors with those of human P2X receptor subunits. A particular focus

was on a core subset of residues required for function of these receptors. Data are presented that extend our knowledge of P2X receptor expression into other metazoan organisms, in addition to extending our knowledge of putative fungal, plant, and amoeboid P2X receptors. Furthermore, candidate P2X receptors are described that expand our understanding of Arthropoda P2X receptors by providing the first description of this LGIC family in the Insecta class of organisms. The first candidate sequences are also described from early eukaryotic, non-plant species in the Bikonta eukaryotic ranking. A summary of P2X receptors identified previously, and those identified and described in the current thesis is provided in Fig. 3.32.

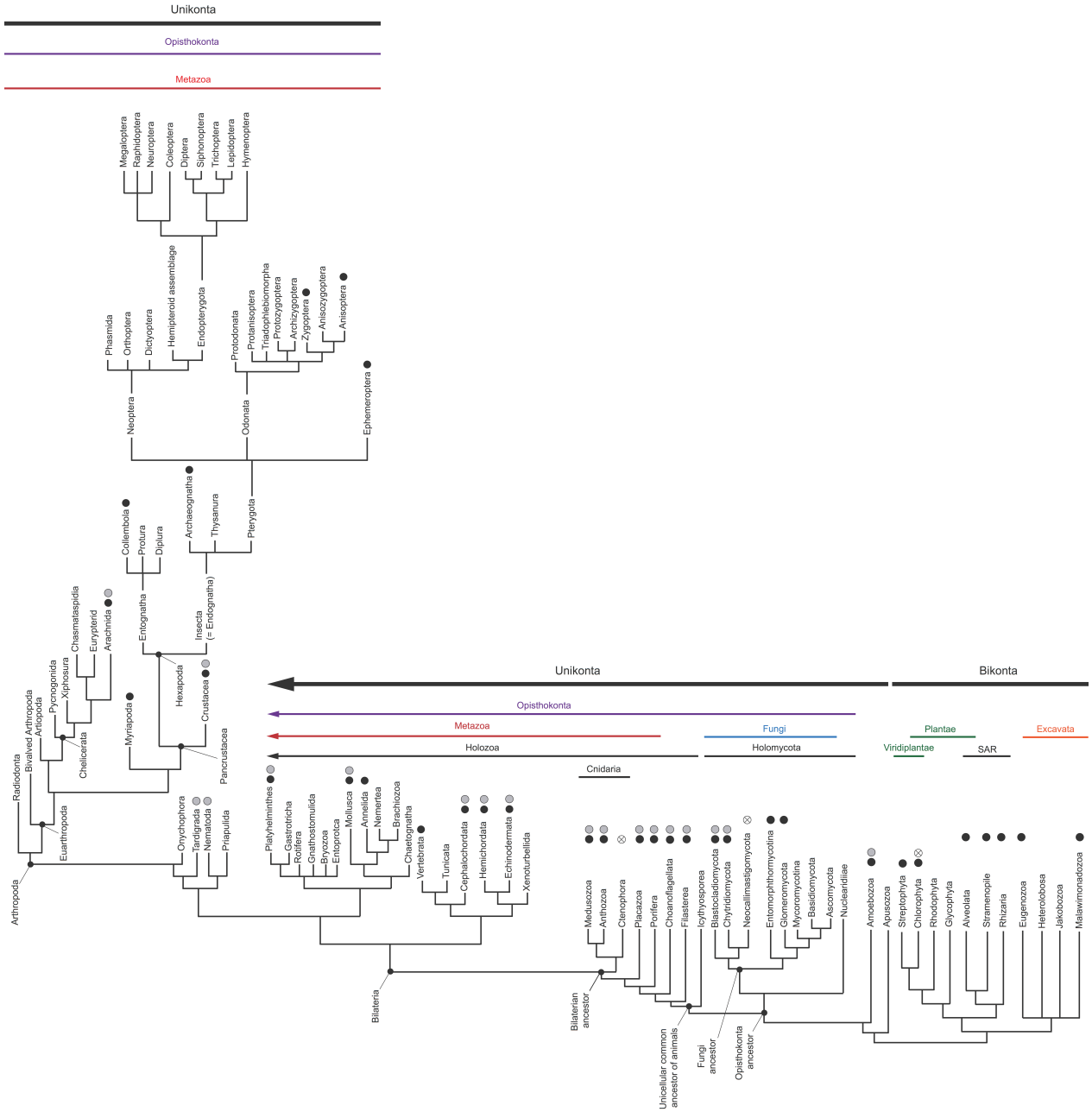
Unikonta
Opisthokonta
Metazoa
Megaloptera
Raphidoptera
Neuroptera
Coleoptera
Diptera
Siphonoptera
Trichoptera
Lepidoptera
Hymenoptera
Phasmida
Orthoptera
Dictyoptera
Hemipteroid assemblage
Endopterygota
Protodonata
Protaniscoptera
Triadophlebiomorpha
Protozygoptera
Archizygoptera
Zygoptera
Anisozygoptera
Anisoptera
Neoptera
Odonata
Ephemeroptera
Archaeognatha
Thysanura
Pterygota
Collembola
Protura
Dipura
Entognatha
Insecta
(= Endognatha)
Chasmataspidia
Eurypterid
Arachnida
Pycnogonida
Xiphosura
Chelicerata
Myriapoda
Hexapoda
Crustacea
Pancrustacea
Radiodonta
Bivalved Arthropoda
Artiopoda
Euarthropoda
Arthropoda
Onychophora
Tardigrada
Nematoda
Priapulida
Unikonta
Bikonta
Opisthokonta
Metazoa
Holozoa
Fungi
Holomycota
Plantae
Viridiplantae
SAR
Excavata
Cnidaria
Platyhelminthes
Gastrotricha
Rotifera
Gnathostomulida
Bryozoa
Entoprocta
Mollusca
Annelida
Nemertea
Brachiozoa
Chaetognatha
Vertebrata
Tunicata
Cephalochordata
Hemichordata
Echinodermata
Xenoturbellida
Bilateria
Medusozoa
Anthozoa
Ctenophora
Placazoa
Porifera
Choanoflagellata
Filasterea
Icythyosporea
Blastocladiomycota
Chytridiomycota
Neocallimastigomycota
Entomorphthoromycotina
Glomeromycota
Mycoromycotina
Basidiomycota
Ascomycota
Nucleariidae
Amoebozoa
Apusozoa
Streptophyta
Chlorophyta
Rhodophyta
Glycophyta
Alveolata
Stramenopile
Rhizaria
Eugenozoa
Heterolobosa
Jakobozoa
Malawimonadozoa
Bilaterian ancestor
Unicellular common ancestor of animals
Fungi ancestor
Opisthokonta ancestor

Fig. 3.33: expanded cladogram of illustrating P2X receptors identified in the Eukaryota domain
A number of candidate P2X receptors were identified in the current thesis through homology searching of a number of phyla throughout the eukaryotic lineage. To highlight the candidate P2X receptors identified in a number of members of the Hexapoda subphylum, the containing Arthropoda phylum is expanded. Grey circles highlight those P2X receptors cloned previously or alluded to in the literature, whilst a black circle highlights candidate P2X receptors identified in the current chapter. It is unclear whether sequences retrieved following homology searches of datasets available for members of the metazoan Ctenophora phylum and fungal Neocallimastigomycota division are candidate P2X receptors, due to low sequence homology and satisfaction of criteria detailed in section 3.2.1. The unrooted cladogram was drawn based on phylogenetic data combined from a number of sources, with a broad Bikonta-Unikonta division based on the guidelines posited by Adl *et al.* (2012). Metazoan phylogeny is adapted from Philippe *et al*. (2009) and Pick *et al.* (2010), with early metazoans taken from Ruiz-Trillo *et al.* (2007). Arthropoda (Legg *et al.*, 2013) and Hexapoda (Sasaki *et al.*, 2013) evolutionary relationships are expanded accordingly. Fungi phylogeny is adapted from Ebersberger *et al*. (2012) and Gryganskyi *et al.* (2013), and broad Plantae kingdom phylogeny is based on the description summarised in Leliaert *et al.* (2012).

3.4.1 Defining a P2X receptor: is there an early molecular component?

A P2X receptor, by definition, is an ion channel gated by the binding of ATP. Following binding, conformational changes in the extracellular domain and transmembrane domains (TMDs) result in the expansion of lateral fenestrations situated above the TMDs and the net flux of ions down their electrochemical gradient.

If one hypothetically regards a P2X receptor in isolation, without considering a physiological role for this LGIC family, could a receptor be synthesised with only basic molecular components? In the current chapter, a protein encoded from a retrieved transcript was considered to be a candidate P2X receptor if it was predicted to possess two transmembrane domains flanking a large ECD within which residues known to be required for ATP binding in human P2X receptors were present. A further stipulation was included that a minimum of two cysteine residues had to be present with this ECD for the sequence to be considered ‘candidate’. Furthermore, P2X receptors enable to the passage of ions from environmentally distinct cell compartments, and this requires them to be embedded in a plasma membrane. As such, for those sequences for which full-length transcripts were available, a further criterion that the translated protein product contained a C-terminal membrane translocalisation motif (Chaumont *et al.*, 2004) was also included. Although not

strictly necessary, it was clear that in those retrieved sequences that satisfied these criteria, an N-terminal PKC phosphorylation motif (YxTx(K/R)) was also present.

If one considers these factors, a 'blueprint' for a P2X receptor can be drawn, whereby the following characteristics for a receptor must be included:

1. The receptor must be membrane-bound
2. The receptor must include residues that are capable of binding ATP
3. A conduit for the passage of ions must be present
4. ATP binding should gate the passage of ions through a receptor conduit
5. The channel pore should be non-selectively permeable to cations

The presence of intracellular N- and C-termini also requires consideration when forming this 'minimal' P2X receptor. The elucidation of the first crystal structure for a P2X receptor (zfP2X4.1) required the expression of a truncated form of the full-length receptor, in which intracellular termini were largely absent (Kawate *et al.*, 2009). When expressed heterologously, this receptor (ΔzfP2X4-B) was only weakly activated by extracellular ATP, with inward current magnitudes generated by 1 mM approximately 200-times smaller than in the wild-type, non-truncated form of zfP2X4.1 (Kawate *et al.*, 2009). Within the remaining portion of the intracellular C-terminus, the membrane translocation motif remained (Kawate *et al.*, 2009). In the context of the five points posited as minimal requirements for a P2X receptor, and on the basis of the findings of Kawate *et al.* (2009), it can be suggested that a minimal requirement of the intracellular C-terminus should include this motif.

Previous findings by Fountain *et al.* (2007) and Ludlow *et al*. (2009) demonstrated that, although weakly homologous to human subunits, *Dictyotelium discoideum* P2X receptors do respond to extracellular ATP in a heterologous system. These amoeboid receptors are predicted to form a topology similar to that of mammalian P2X receptors, with two TMDs flanking an ECD. At the primary sequence level, all characterised sequences include a C-terminal membrane localisation motif, and only two out of ten ECD cysteine residues conserved in human P2X receptor homologues (Fountain *et al.*, 2007). Of those ATP binding residues and motifs found in human homologues, only F185, T186 and K309 are conserved in *D. discoideum* P2X receptors.

The evolutionary relationships and origins of early eukaryotes are unclear, but molecular clock estimates suggest that the major extant eukaryotes (Opisthokonta, SAR supergroup, Excavata and the Amoebozoa) are projected to have diverged from a common ancestor around 1600-1000 million years ago (Parfrey *et al.*, 2011). To date, the earliest P2X receptor that has been cloned is that from the unicellular eukaryotic algae *Ostreococcus tauri* (*Ot*P2X) (Fountain *et al.*, 2008). As a chlorophyte, *O. tauri* is grouped within the Bikonta group of eukaryotes, which includes the Excavata, Archaeplastida (Viridiplantae (Chlorophyta, Streptophyta, Rhodophyta) and Glycophyta), and the Stramenopiles, Alveolata, and Rhizaria (SAR) supergroup (Adl *et al.*, 2012). The current chapter has suggested the presence of P2X receptors within members of the SAR supergroup (section 3.3.14) and the Excavata (section 3.3.15). Cladograms illustrating intergroup relationships amongst extant eukaryotes and presented within the current thesis are displayed unrooted, as the root of the eukaryotic tree of life is unresolved. However, it is estimated that members of the Alveolata superphylum of the SAR supergroup emerged before the kingdom, diverging from a common ancestor ca. 1.1 million years ago (MYA) (Berney and Pawlowski, 2006; Hedges *et al.*, 2006). Whilst it remains to be seen whether those sequences recovered through homology searching of Alveolata superphylum members (section 3.3.14) function as ATP-gated ion channels, many residues are shared between candidate protein sequences and previously characterised P2X receptors. As such, these sequences could represent the earliest eukaryotic P2X receptors identified to date.

The low shared sequence identity of fungal P2X receptors with higher homologues raises important questions as to the conservation of residues within this LGIC family. In particular, questions arise as to the requirement of a core set residues required in order consider candidate sequences as 'P2X-like'. Protein sequences of retrieved hits identified through homology searching of various databases were predicted consistently to display a topology similar to that of characterised P2X receptors, whereby two TMDS and intracellular termini flank a large ECD. Many of these retrieved sequences also shared N-terminal or C-terminal PKC phosphorylation motif. However, within the predicted ECD of these sequences, residue conservation varied considerably within early eukaryotes. Although the root of the eukaryotic tree is unresolved, candidate P2X receptors from members of the Fungi kingdom (section 3.3.13) appeared to be the most divergent from metazoan forms of the receptor,

sharing the lowest primary sequence identity with human P2X receptors compared to other early eukaryotes, including those from the SAR and Excavata supergroups. These receptors all shared at minimum of one ATP binding residue or motif with human subunits, and may suggest a minimal requirement of these residues in the binding of ATP to initiate activation of the receptor. Whilst mutation of these residues in human P2X receptors often renders a receptor insensitive to extracellular ATP application, (Ennion *et al.*, 2000; Roberts and Evans, 2004; Wilkinson *et al.*, 2006) an absolute requirement for these receptors does not appear to exist in many invertebrate receptors. For instance, many ATP binding residues are absent in *Dictyostelium* P2X receptor subunits, yet they remain sensitive to this purine (Fountain *et al*., 2008; Ludlow *et al*., 2009). The incomplete conservation between fungal and human P2X receptors of many residues that are deemed important for human P2X receptor function may provide important information as to the basic complement of residues required to endow a protein with ionotropic, and ATP-sensitive characteristics, typical of a P2X receptor. Whilst ATP is the primary agonist of P2X receptors, other purine and pyrimidine compounds may prove efficacious at these evolutionary divergent candidate receptors. In future work, an understanding of the minimum molecular requirements of a protein to render it an ATP-gated ion channel may help identify functionally similar proteins to P2X receptors, in those organisms that do not appear to express this LGIC family.

3.4.2 Expansion of knowledge of P2X receptor within the Metazoa

Much of our knowledge regarding the pharmacological and *in vivo* function of P2X receptors has been derived from examination of chordate homologues of this LGIC family. Following the cloning of the first invertebrate P2X receptor (from the platyhelminthe *S. mansoni* (Agboh *et al.*, 2004), homologues have since been cloned from a number other invertebrates, including from a member of the Arthropoda (Bavan *et al.*, 2011) and Mollusca (Bavan *et al.*, 2012) phyla. In an attempt to expand our knowledge of metazoan P2X receptors, homology searches were performed, and candidate P2X receptor homologues identified, in a range of metazoan organisms.

Despite being morphologically derived, Ctenophora have been proposed to represent the earliest branching metazoan phylum (Dunn *et al.*, 2008; Ryan *et al.*, 2013; Moroz *et al.*, 2014). This stance is in disagreement with the hypothesis that Porifera represent the most basal metazoan phylum (Philippe *et al.*, 2009; Pick *et al.*, 2010), and that conclusions drawn by Dunn *et al*. (2008) are due to insufficient taxon sampling and long-branch attraction (LBA) between highly divergent outgroups and the Ctenophora (Pick *et al.*, 2010). Whilst sequences were retrieved from the ctenophore *Pleurobrachia bachei* (section 3.3.6), it was unclear whether they could be considered candidate P2X receptors. Although the retrieved protein sequence from *P. bachei* was predicted to possess two extended regions of hydrophobicity, the predicted ECD of this retrieved primary amino acid sequence shared a low sequence identity with human P2X receptor homologues. As a result, this made it difficult to ascertain whether this sequence could be characterised as a candidate P2X receptor, as many residues and motifs required for this characterisation were seemingly absent. Further molecular cloning is required to determine whether P2X receptors are present within this, and other Ctenophora, and therefore gain a greater understanding of coelenterate P2X receptors.

3.4.3 A coleopteran P2X receptor?

In the current thesis, a candidate P2X receptor sequence was identified in the coleopteran (beetle) *Diabrotica virgifera* (section 3.3.5.2.3) (Flagel *et al.*, 2014). The Coleoptera order diverged from a common ancestor to the Diptera approximately 300 MYA (Savard *et al.*, 2006), yet no dipteran P2X receptor homologue has been identified to date. At the primary amino acid level, these sequences shared an approximately 45% identity with the human P2X1 receptor, which was consistent with the shared sequence identity of many other candidate invertebrate P2X receptors identified in the current thesis. However, analysis of the nucleotide sequence identity of the retrieved transcripts for these putative P2X receptor homologues was higher between a representative chordate P2X4 receptor sequence (*Mus musculus* P2X4; mP2X4), than mP2X4 compared to another chordate (*Bos taurus* P2X4). The evolutionary distance *M. musculus* and the Coeloptera order is approximately 8 times that of *M. musculus* and *B. taurus* (Hedges *et al.*, 2006). The markedly similar sequence identity of nucleotides from distinct lineages casts some doubt as to whether

candidate partial P2X receptors identified in *D. virigifera* are indeed from this organism.

As a leaf beetle (Family Chrysomelidae), *D. virigifera* does not feed on livestock, which makes it unlikely that exogenous material from mammals would be responsible for the high similarity of *D. virgifera* P2X receptors to apparent homologues from this distant group. Interestingly, P2X receptors appeared to be seemingly absent in another coleopteran (*Tribolium castaneum*; Family Tenebrionidae), which is believed to have diverged prior to the Chrysomelidae (*D. virgifera*) (Hunt *et al.*, 2007; Marvaldi *et al.*, 2008). If a P2X receptor is indeed expressed in *D. virgifera*, the lineage-specific expression may provide valuable information regarding the apparent loss of P2X receptors in higher insects (Hymenoptera, Diptera, and Lepidoptera). The sequencing and assembly of genomes of other Chrysomelidae coelopterans would enable a broader understanding of the extent to which P2X receptors are present in this order, and whether sequences identified in *D. virgifera* are indeed true to the transcriptome of this organism. Interestingly, parasitism of *Diabrotica* species beetles by a wide range of organisms, including Nematoda and Fungi has been reported widely (Creighton and Fassuliotis, 1985; Naranjo and Steinkraus, 1988; Heineck-Leonal and Salles, 1997). In light of the apparent presence of P2X receptor homologues in some nematode (section 3.3.8) and fungal (section 3.3.13) species, a possible explanation for the apparently isolated expression of P2X receptors in the Coeloptera genus could be the inadvertent sequencing of a parasitic genome, leading to a 'false-positive' result following homology searching. Tissue-specific cDNA libraries or treatment with anti-parasitic compounds may reduce the likelihood of cloning of non-coleopteran P2X receptors, and therefore the information or rejection of P2X receptors being present in this Insecta lineage.

If molecular cloning confirmed the presence of a P2X receptor in *D. virgifera*, this would not only expand our understanding of Hexapoda P2X receptors, but potentially also provide important information regarding the retention of this LGIC family within higher Diptera. Expansion of the range of neopteran transcriptomic and genomic datasets would also help determine the lineage within which P2X receptors are retained.

3.4.4 P2X receptors are predicted to be expressed in non-neopteran insects

In this description, 'non-neopteran' insects refer to those from the Entognatha class (Collembola, Protura, and Diplura) and the Archaeognatha, Thysanura, and Pterygota orders of the Insecta (= Ectognatha). The data presented herein has identified candidate full-length or partial protein sequences with homology to human P2X receptors members of all but the Protura, Diplura and Thysanura groups, using a broader homology search of Hexapoda (TaxID: 6960) whole genome shotgun (WGS) sequence datasets. Using this approach, sequences with sequence identity to human P2X receptor subunits were identified in early basal Endognatha orders, as well as in later diverging orders of the Insecta class.

It had been demonstrated previously that P2X receptors, whilst retained in many taxonomic clades, were seemingly absent from the genomes of many 'higher' members of the Insecta class (Harte and Ouzounis, 2002; Agboh *et al.*, 2004;Fountain and Burnstock, 2009; Fountain, 2013). No previous study has identified candidate P2X receptors within the Hexapoda phylum, or constituent Insecta class. The current study has provided this first evidence by identifying putative P2X receptors in the Hexapoda, using a broader homology search of Hexapoda whole genome shotgun (WGS) sequence datasets, wherein sequences with sequence identity to human P2X receptor subunits were identified in early basal Endognatha orders, as well as in later diverging orders of the Insecta class.

In the current chapter, a number of candidate Arthropoda P2X receptors were identified, including within members of the Chelicerata (section 3.3.4.1) and Crustacea phyla (section 3.3.3.4.3). Much of our understanding of Arthropoda phylogeny has been derived from analysis of member morphology. Although the root of the Arthropoda tree of life is unresolved, the 'Myriochelata hypothesis', within which the Arthropoda are divided into the Chelicerata and Mandibulata (insects, crustaceans, and myriapods) (Hwang *et al.*, 2001) has gained the most support based on morphological (Popadic *et al.*, 1998), neural gene expression (Eriksson and Stollewerk, 2010) and gene sequence (Regier *et al.*, 2010; Meusemann *et al.*, 2010) data. Opponents of this root have stated that long-branch attraction falsely supports the Myriochelata hypothesis (Rota-Stabelli *et al.*, 2011). Candidate P2X receptors were identified in the Odonata and Ephemeroptera orders of Insecta, but were

seemingly absent in all but one of the available transcriptomic datasets available for the Neoptera (section 3.3.5.2.3). If one presumes that, perhaps, the high nucleotide sequence identity of the retrieved *D. virgifera* P2X receptor is due to some form of contamination during cDNA library assembly, this may suggest that this LGIC family has been secondarily lost in Neoptera. Receptors within the Insecta class may have been secondarily lost in this lineage, but retained within members of the Odonata and Ephemeroptera orders. Further sequencing of the genomes of other members of these orders would aid in confirming the widespread expression of P2X receptors in these lineages.

3.4.5 Tissue-specific transcriptomes: linking form and function?

In addition to transcriptomes being assembled from whole organisms, a wide-range of tissue- and cell-specific transcriptomes are available for a number of organisms, such as the olfactory antennae of *Drosophila* (Younus *et al.*, 2014), human brain tissue (Oldham *et al.*, 2008; Hawrylycz *et al.*, 2012; Miller *et al.*, 2014), and *Arabidopsis* (Fizames *et al.*, 2004; Müller *et al.*, 2007). Compartmentalisation of a transcript is functionally significant in many organisms, allowing cell-specific expression. The transcriptomes of many of the organisms investigated as part of the current thesis have been assembled on a tissue- and stage-specific basis.

Two candidate P2X receptors were identified in the western black widow spider (*Latrodectus hesperus*) transcriptome (Clarke *et al.*, 2014) (section 3.3.4.1). This transcriptome was assembled from the cephalothorax, venom glands, and silk glands of a female *L. hesperus* specimen (Clarke *et al.*, 2014). Analysis of annotated transcripts identifies a higher relative abundance of candidate *p2x* mRNA in the transcriptome of isolated venom glands and cephalothorax of *L. hesperus* (Clarke *et al.*, 2014). The cephalothorax (= prosoma) is the anteriormost portion of a spider's anatomy, and the point of attachment of the legs (Foelix, 2011). Broadly, the cephalothorax plays roles in locomotion and neural integration, but also houses a number of substructures, including the brain, anterior aorta, and anterior digestive tract (Foelix, 2011). The venom glands of female *Latrodectus* spiders are, in accordance with other members of the Araneomorphae spider suborder, quite large (Foelix, 2011). The cephalothorax transcriptome of *L. hesperus* presented in Clarke

et al. (2014) was prepared devoid of venom gland structures, and may suggest that P2X receptors play multiple roles in this species. The function of candidate P2X receptors from *L. hesperus* remains to be determined, but could identify homologous roles in other arachnids and the members of the Arthropoda phylum as a whole.

3.4.6 P2X receptors in socioeconomically important organisms: a clinical target?

A number of candidate P2X receptors have been identified in unicellular and multicellular eukaryotes which, either as disease vectors, or as infectious agents in themselves, are responsible for debilitating and life-threatening illnesses.

The cloning of the first invertebrate P2X receptor (that from the parasitic trematode *Schistosoma mansoni*) (Agboh *et al*., 2004) is yet to be investigated as a target for the chronic disease schistosomiasis. Schistosomiasis (also known as 'bilharzia') is thought to be prevalent in a 200 million people worldwide, although this is thought to be a dramatic underestimation (Fenwick, 2012; King and Bertino, 2008). Symptoms following schisotsome infection patients vary, but are typically intestinal or urinary in their presentation and can cause long-term complications such as diarrhoea and malnutrition (Fenwick, 2012). *S. mansoni* is transmitted to mammalian hosts through contaminated water supplies via the obligate intermediary host and freshwater snail *Biomphalaria glabrata* (Newton, 1953), which also appears to express a P2X receptor homologue (section 3.3 9). Further investigation of the role of P2X receptors in these organisms may identify a novel mechanism by which populations of both *S. mansoni* and *B. glabrata* may be controlled, or infection by *Schistosoma* may be treated. The identification of candidate P2X receptors in other paratistic tapeworms *Taenia* solium and *Echinococcus spp*. (section 3.3.7), causative zoonotic agents of taeniasis (Del Brutto, 2014) and hydatid disease in mammals (Thompson and Jenkins, 2014), may also represent useful clinical targets for these diseases.

Identification of P2X receptors in *Acanthamoeba* (section 3.3.12) may also represent a viable clinical target for the treatment of illnesses associated with members of this parasitic amoeba genus, most notably amoebic keratitis and encephalitis (Lorenzo-Morales *et al.,* 2013). Similarly, a candidate P2X receptor in the zygomycote *Conidiobolus coronatus*, a causative agent in Conidiobolomycosis (Renoirte *et al.*,

1965) (a fungal infection that presents with facial enlargement and deformity (Isa-Isa *et al.*, 2012; Fischer *et al.*, 2008)) has also been identified in the current thesis (section 3.3.13).

A caveat in the use of these potentially clinical P2X receptor targets is the specificity of available antagonists of this LGIC family. Whilst many antagonists are currently available that target specific P2X receptor subunits in humans, the widespread expression of many of these subunits makes the targeting of non-human P2X receptors uncertain. Pharmacological characterisation of these candidate P2X receptors is required in order to fully understand that efficacy of currently available antagonists, and develop species and subtype specific antagonists for use in the clinic.

It is clear that, in the advent of increasing numbers of transcriptomic and genomic data for a wide range of morphologically, and evolutionary distinct eukaryotic lineages, the number of candidate P2X receptors that will be identified will increase. Within the field, these resources are enormously valuable, potentially allowing novel P2X receptor function and pharmacology to be uncovered in highly divergent groups of organisms, evolutionary distant from humans and other higher metazoans. Of particular interest is the finding that P2X receptors appear to be present within members of the diverse Insecta class, which was previously believed to be devoid of P2X receptor homologues. This exciting finding is a major advance in the field, expanding the range of phyla in which it appears that P2X receptors are expressed, and increasing the possibility of identifying novel roles for ionotropic purinergic signalling in humans.

3.5 CONCLUSIONS

1. The current chapter has greatly expanded our understanding of the extent to which the P2X receptor family appears to be present within eukaryotic phylogeny, and has provided the first description of candidate P2X receptors in members of the diverse Insecta class of the Hexapoda.
2. Homology searching across multiple phyla supports the consensus that P2X receptors are widespread within eukaryotic phylogeny, but receptor

homologues do not appear to be expressed in representative species of the Bacteria or Archaea domains.

3. P2X receptors appear to be expressed in many clinically important organisms, and may represent useful targets for the treatment of diseases caused by exposure to these pathogens.
4. Contrary to previous suggestions, P2X receptors are present in early members of the large Insecta class of arthropods, and share many important residues and motifs required for the function of previously characterised eukaryotic P2X receptor homologues. This may suggest that P2X receptors were secondarily lost in higher insects, but retained in many early Insecta orders.
5. Although a P2X receptor homologue does not appear to be expressed in higher plants (e.g. *Arabidopsis thaliana*), partial nucleotide sequences with translated protein homology to human P2X receptors appear to be present in a member of the streptophyte algae, a sister group to extant land plants (Embryophyta).
6. A candidate P2X receptor was identified in a member of the sister group to Diptera (in which P2X receptors do not appear to be expressed), the Coeloptera. The higher percentage nucleotide sequence identity of this candidate P2X receptor (from the beetle *Diabrotica virgifera*) to a mammalian P2X receptor than P2X receptors within the mammalian clade
7. The availability of tissue- and stage-specific transcriptomic datasets may prove a valuable tool in suggesting putative roles for novel P2X receptors in a number of phyla.
8. Further molecular cloning is required in order to fully determine whether candidate P2X receptors identified in the current thesis are indeed ATP-gated ion channels. Expansion of genomic data may also clarify expression of P2X receptors within lineages that appear to have secondarily lost this gene family in related taxa.

Chapter 4:

Cloning, electrophysiological analysis and localisation of a novel P2X receptor from *Hydra*

4 Cloning, electrophysiological analysis and localisation of a novel P2X receptor from Hydra

4.1 AIMS OF THE CHAPTER

The current chapter describes the cloning and pharmacological analysis of a novel P2X receptor from the cnidarian *Hydra vulgaris* (AEP strain) (aepP2X) following its identification by homology searching of available transcriptomic data. In addition, results are presented that may provide initial evidence for the immunolocalisation of aepP2X using a custom polyclonal anti-serum raised against an antigenic peptide corresponding to portion of the aepP2X C-terminus. Data are subsequently discussed in relation to our current understanding of receptor pharmacology in those organisms from which P2X receptors have been cloned and pharmacologically analysed. Immunolocalisation data are placed within the greater context of cnidarian physiology, with the role of aepP2X as an ATP-gated ion channel discussed accordingly.

4.2 INTRODUCTION

Following the identification of putative P2X receptor homologues from species across a range of phyla, candidate receptors from three species were chosen for further analysis: *Hydra vulgaris* (AEP); *Daphnia pulex*; and *Trichoplax adhaerens*. These species, from the Cnidaria, Arthropoda, and Placazoa phyla, respectively, lie at phylogenetically informative positions in the evolutionary 'tree of life' or possess physiological or anatomical novelties that appear to have emerged in their phylum. Firstly, *Hydra* are widely believed to represent a modern day proxy for the first organisms to have developed a defined nervous system, in the form of a diffuse nerve net (Anderson and Spencer, 1989). Although the recent placement of Ctenophore as a basal group to Cnidaria through genomic (Ryan *et al.*, 2013; Moroz *et al.*, 2014) and phylogenetic (Dunn *et al.*, 2008; Hejnol *et al.*, 2009) analysis suggests that ctenophores may be the earliest organism to have developed a nerve net. However, it is unclear whether the Ctenophora lineage developed a nervous system independently to Cnidaria, or whether neurons emerged in a common ancestor of the two phyla

(Ryan, 2014), developing centralisation in bilaterian animals. Whilst both Ctenophora and Cnidaria are considered sister groups to the Bilateria (Collins, 1998; Medina *et al.*, 2001), the availability of tools that lend genetic tractability to *Hydra* led to the decision to investigate this cnidarian P2X receptor homologue rather than a Ctenophora P2X receptor.

4.2.1 Cloning of mammalian and non-mammalian P2X receptors

To date, seven P2X receptor subunits have been identified in vertebrates (Valera *et al.*, 1994; Brake *et al.*, 1994; Collo *et al.*, 1996; Chen *et al.*, 1995; Bo *et al.*, 1995; Buell *et al.*, 1996; Rassendren *et al.*, 1997), whilst, eight non-mammalian, invertebrate P2X receptors have been described (Agboh *et al*., 2004; Fountain *et al*., 2007; Ludlow *et al*., 2009; Bavan *et al*., 2009; Bavan *et al*., 2011; Bavan *et al*., 2012; Sakurai *et al*., 2012). Initial cloning of an ATP-gated ion channel (P2X1) was achieved in 1994 from rat vas deferens (Valera *et al.*, 1994). Injection of poly-$(A)^+$ RNA isolated from the tissue by oligo-d(T) cellulose chromatography into *Xenopus* oocytes resulted in functional ATP-evoked currents, as recorded by two-electrode voltage-clamp electrophysiology. The subsequent production of a unidirectional cDNA library allowed for the subdivision of the library and isolation of a clone of the rat P2X1 receptor cDNA encoding a protein of 399 amino acids (Valera *et al.*, 1994).

In light of the original finding that ATP could evoke inward currents in these cells (Nakazawa *et al.*, 1990a; Nakazawa *et al.*, 1990b; Nakazawa *et al.*, 1990c). The cloning of P2X2 from a cDNA expression library prepared from rat pheochromocytoma (PC12) cell mRNA (Brake *et al.*, 1994) followed the work of Valera *et al*. (1994) and encoded a protein 472 residues in length that, when expressed heterologously in *Xenopus* oocytes, produced functional ATP-gated currents (Brake *et al.*, 1994). The third P2X receptor subtype (P2X3) was cloned after identification of a ca. 3.8 kb mRNA transcript from rat dorsal root ganglion sensory neurons (Chen *et al.*, 1995). The availability of P2X1 and P2X2 receptor sequences resulted in the use of a low stringency screen for candidate P2X receptors in a rat hippocampal cDNA library and subsequent cloning of the P2X4 purinoceptor subtype that resulted in slow ATP-evoked inward currents in *Xenopus* oocytes (Bo *et al.*, 1995), P2X4 receptor cDNA was subsequently isolated from rat superior cervical

ganglion (Buell *et al.*, 1996) and rat brain (Soto *et al.*, 1996a), which produced functional ATP-evoked inward currents when expressed in HEK293 cells and *Xenopus* oocytes, respectively, where it also displayed a slow kinetic phenotype as originally described by Bo *et al.* (1995). Isolation of a P2X receptor cDNA from coeliac and cervical superior ganglia mRNA gave rise to the P2X5 and P2X6 receptor subunits (Collo *et al.*, 1996). P2X5 was subsequently also cloned from the rat heart (Garcia-Guzman *et al.*, 1996) and P2X6 from rat brain (Soto *et al.*, 1996b). Finally, cloning of the seventh (and largest at 595 residues) P2X receptor subtype (P2X7) was cloned from rat brain, revealing an interesting 'pore dilation' property that also permitted the passage of larger cations of up to ca. 900 Da upon continual activation by extracellular ATP (Surprenant *et al.*, 1996; Rassendren *et al.*, 1997). The cloning of these seven P2X receptor subunits represents the complement of ionotropic purinoceptors known to be present in mammals to date.

The availability of genomic and transcriptomic data has revolutionised the discovery process of potentially new homologues, which can then be cloned from both vertebrate and invertebrate species. Following the cloning of a P2X receptor from the trematode *S. mansoni* (Agboh *et al.*, 2004), multiple P2X receptors were subsequently cloned from the slime mould *D. discoideum* (Fountain *et al.*, 2007; Ludlow *et al.*, 2008; Ludlow *et al.*, 2009). A novel intracellular role for this receptor in responding to osmotic stress has been investigated, although it appears that the contribution that P2X receptors in *Dicytostelium* makes to regulatory volume decrease (RVD) is strain-dependent (Sivaramakrishnan and Fountain, 2013). P2XA-null transgenic AX2 strain *D. discoideum* cannot respond effectively to hypotonic stress through RVD (Fountain *et al.*, 2007), whilst the AX4 strain retains much of this ability (Ludlow *et al.*, 2009). P2X receptors have also been cloned from the green alga *O. tauri* and choanoflagellate *M. brevicollis* (Fountain *et al.*, 2008), the tardigrade *H. dujardini* (Bavan *et al.*, 2008), tick *B. microplus* (Bavan *et al.*, 2011), and snail *L. stagnalis* (Bavan *et al.*, 2012), and have been discussed previously (see Chapter 1.6).

4.2.2 Putative ion channels in *Hydra*

In light of the content of the current chapter, it is helpful to discuss our current understanding of ligand-gated ion channels (LGICs) in *Hydra*. Accounts of the

effects of neurotransmitters on *Hydra* previously known to modulate the activity of LGICs in higher organisms are numerous and wide-ranging. However, the majority of conclusions regarding neurotransmitter function *in vivo* originate from behavioural studies. Little pharmacological or sequence characterisation of putative receptors in *Hydra* is currently described in the literature, although radioligand binding studies do provide evidence in favour of membrane-bound neurotransmitter receptors in *Hydra* (Kass-Simon and Pierobon, 2007).

Reports of direct electrophysiological recording from isolated *Hydra* cells are limited, largely due to difficulties associated with GΩ membrane seal formation (Santillo *et al.*, 1997). However, membrane potential has been recorded from isolated epithelial cells of *H. vulgaris* (Santillo *et al.*, 1997), and from nematocytes of four marine hydrozoan species (*Stauridiosarsia producta*, *Coryne tubulosa, Sarsia tubulosa*d, and *Dipurena reesi*) (Oliver *et al.*, 2008) using whole-cell voltage-clamp electrophysiology.

4.2.2.1 GABAergic and glutamatergic transmission

Signalling by the typically inhibitory neurotransmitter γ-aminobutyric acid (GABA) *via* ionotropic GABA type A ($GABA_A$) and metabotropic type B ($GABA_B$) receptors is widespread in mammalian systems, where it exists as the primary inhibitory neurotransmitter in the adult central nervous system (CNS) (Bazemore *et al.*, 1957). Although our understanding of GABAergic signalling in mammals is extensive, its role in evolutionarily early organisms is unclear.

The first evidence for GABAergic signalling in *Hydra* came from Pierbon and colleagues who demonstrated that crude membrane preparations of *Hydra* could be labelled with radiolabelled GABA (^{3}H GABA) (Pierobon *et al.*, 1995). This specific labelling could be displaced completely by the GABA mimetic muscimol but not by the classic $GABA_A$ receptor competitive antagonist bicuculline, or GABA derivative (and $GABA_B$ receptor agonist) baclofen. Reduced glutathione (GSH) is known to stimulate mouth opening, and tentacle movement typical of behaviour seen during *Hydra* polyp feeding (Cliffe and Waley, 1958; Lenhoff and Bovaird, 1961). GABA prolongs the duration of this GSH-induced feeding response (Pierobon *et al.*, 1995);

this prolongation can be inhibited by the application of either bicuculline or baclofen (Pierobon *et al.*, 1995). Concas *et al.* (1998) later demonstrated that neurosteroids (tetrahydroprogesterone and tetrahydrodeoxycorticosterone), known to enhance inhibitory neurotransmission at mammalian synapses by $GABA_A$ receptors (Lambert *et al.*, 2003), prolonged the GSH-induced duration of mouth opening in a dose-dependent manner. In addition, GABA application also decreased the rate of spontaneous contractions, decreasing the number of electrical bursts associated with contractile events, a phenomenon that is also modulated by application of glutamate which causes an increase in burst frequency (Kass-Simon *et al.*, 2003). Application of low micromolar concentrations of the glutamate mimetics kainate and AMPA (2-amino-3-(5-methyl-3-oxo-1,2-oxazol-4-yl)propanoic acid) also caused an increase in burst frequency both in the polyp body column and tentacles (Kass-Simon *et al.*, 2003; Kass-Simon and Scappaticci Jr., 2004). This functional evidence for glutamatergic signaing in *Hydra* is corroborated by binding of radiolabelled glutamate (L-[^{3}H]glutamate) to membrane fractions. Interestingly, binding could be partially displaced by GSH, suggesting a potential receptor for this molecule (Bellis *et al.*, 1991).

4.2.2.2 Glycinergic transmission

The glycine receptor chloride channel is a member of the nicotinic acetylcholine receptor family of LGICs and, like $GABA_A$ receptors, is also implicated in inhibitory neurotransmission (Lynch, 2004). Although glycine is the primary ligand at these receptors, other amino acids can bind to the receptor (in order of potency: glycine > β-alanine > taurine > L-alanine) (Langosch *et al.*, 1990). Two lines of evidence exist for the presence of glycine receptors in *Hydra*. Firstly, the duration of GSH-induced mouth opening can be reduced by the addition of glycine in a concentration-dependent manner (Pierobon *et al.*, 2001). Furthermore, application of glycine and taurine (both agonists at glycine receptors) increases electrical rhythm and spontaneous contraction bursts in live polyps which can be inhibited by the receptor's antagonist strychnine (Ruggieri *et al.*, 2004).

4.2.2.3 NMDA receptors

N-methyl-D-glucamine (NMDG) signalling in *Hydra* has been well documented both at immunohistological and behavioural levels. Scappaticci and colleagues have illustrated in whole macerates of the tentacle and hypostome region, strong staining of nematocytes is evident, neurons and interstitial cells (both individual and in battery cells) using a monoclonal antibody raised against the NMDA1 receptor subunit (Scappaticci *et al.*, 2004). Interestingly, the NMDA1 receptor subunit appears to be expressed in the nucleolus of these cells suggesting a non-canonical expression pattern for this LGIC (Kass-Simon *et al.*, 2009). In support of a functional role for NMDA receptors in live polyps, application of nanomolar concentration NMDA to polyps dramatically reduced the duration of feeding-type behaviours induced by GSH application. Additionally, co-application of NMDA with kainate or AMPA increased the propensity of stenotele nematocysts to discharge following mechanical stimulation, illustrating a functional role for this LGIC in nematocyst discharge (Scappaticci and Kass-Simon, 2008). The NMDA receptor antagonist D-AP5 (D-2-amino-5-phosphonopentanoic acid) and AMPA/kainate receptor antagonist CNQX (6-cyano-7-nitroquinoxaline-2,3-dione) reduced the ability of NMDA agonists to increase the number of discharged stenotele cells (Scappaticci and Kass-Simon, 2008). Furthermore, there is some evidence for NMDA signalling in *Hydra*, with NMDA application causing rhythmic electrical potentials in both the body column and tentacles of whole polyps. To further support this observation, the application of D-AP5 abolishes rhythmic potentials (Kay and Kass-Simon, 2009). Thus, these pharmacological and whole polyp electrophysiological data provide strong evidence for functional roles for a number of LGICs in *Hydra* nematocysts, as well as in the inherent electrical activity of polyps.

4.2.2.4 Cloning of novel ion channels in *Hydra*

Although there is considerable functional evidence for physiological functions for ligand-gated ion channels in live *Hydra*, relatively few ion channels have been cloned from the Cnidaria phylum. There are no reports of a P2X receptor being cloned or functionally characterised in *Hydra*, or other members of the Cnidaria phylum, to

date, although homologues have been bioinformatically identified previously in members of this phylum (Fountain and Burnstock, 2009;

Four paralogues of a novel sodium channel closely related to the degenerin (DEG)/epithelial Na^+ channel (ENaC) family of ion channels, gated by the neuropeptides RFamide I and II (HyNaC), have been cloned and mRNA transcript localisation determined through whole-mount *in situ* hybridisation (Golubovic *et al.*, 2007). Transcripts were found to be present at the base of the tentacles of whole polyps and appear to be expressed on the basal surface of epithelial cells in close proximity to neurons, leading the authors to suggest that this channel could mediate fast contractile responses during feeding. In addition, heterologous expression of cDNA encoding each channel revealed a bisphasic current profile as well as concentration-dependent inward currents upon exposure to either RFamide I or II (Golubovic *et al.*, 2007). Further work has confirmed the work of Golubovic and colleagues that the channel is equally permeable to small cations such as K^+ and Li^+ (Golubovic *et al.*, 2007), adding that the channel forms a trimeric complex between the 2, 3 and 5 subunit paralogues in addition to the 2/3 channel described by Golubovic and colleagues (Dürrnagel *et al.*, 2010). The originally described biphasic kinetic profile of HyNaC channels when expressed heterologously in Xenopus oocytes, whereby a faster component gives rise to a slower transient component has since been found to be an artefact of secondary activation of Ca^{2+}-activated Cl^- channels in the oocyte, and the authors did find that the HyNaC channel is highly permeable to Ca^{2+} ions (P_{Ca}/P_{Na} = 3.8) (Dürrnagel *et al.*, 2012). Finally, expression cyclic nucleotide-gated ion channel homologues in Cnidaria has been highlighted (Plachetzki *et al.*, 2010), with a specific role for the channel in the modulation of nematocyst discharge whereby bright light reduces cnidocil discharge propensity (Plachetzki *et al.*, 2012). Functionally this mechanism is hypothesised to play a role in diurnal feeding patterns seen in *Hydra* in natural ecosystems (Plachetzki *et al.*, 2012).

Although a physiological function for these ion channels has not yet been fully determined, it is clear that investigation of this diverse group of transmembrane proteins in *Hydra* could provide a greater understanding of novel receptor pharmacology. Furthermore, characterisation of novel *Hydra* LGICS may highlight novel roles for homologous receptors in higher organisms.

4.3 RESULTS

4.3.1 Primary sequence analysis of aepP2X

The predicted cDNA of aepP2X encodes for a protein 432 amino acids in length. The cloned form of the receptor also encoded for a 432 amino acid protein, sharing a 100% sequence identity with its predicted sequence. 3' RACE was subsequently employed to identify the 3' poly-(A) mRNA sequence (section 2.4.5.2.3), which was present.

The primary amino acid sequence of aepP2X shares a 23.4 to 41.7% amino acid sequence identity with human P2X1-7 subunits, the greatest of which being with hP2X4. ATP binding motifs are also conserved in aepP2X, as are all ten ECD cysteine residues found in mammalian homologues. C-terminal residues required for membrane translocation (Chaumont *et al.*, 2004) and N-terminal PKC phosphorylation (Boué-Grabot *et al.*, 2000) are also conserved (Fig. 4.1).

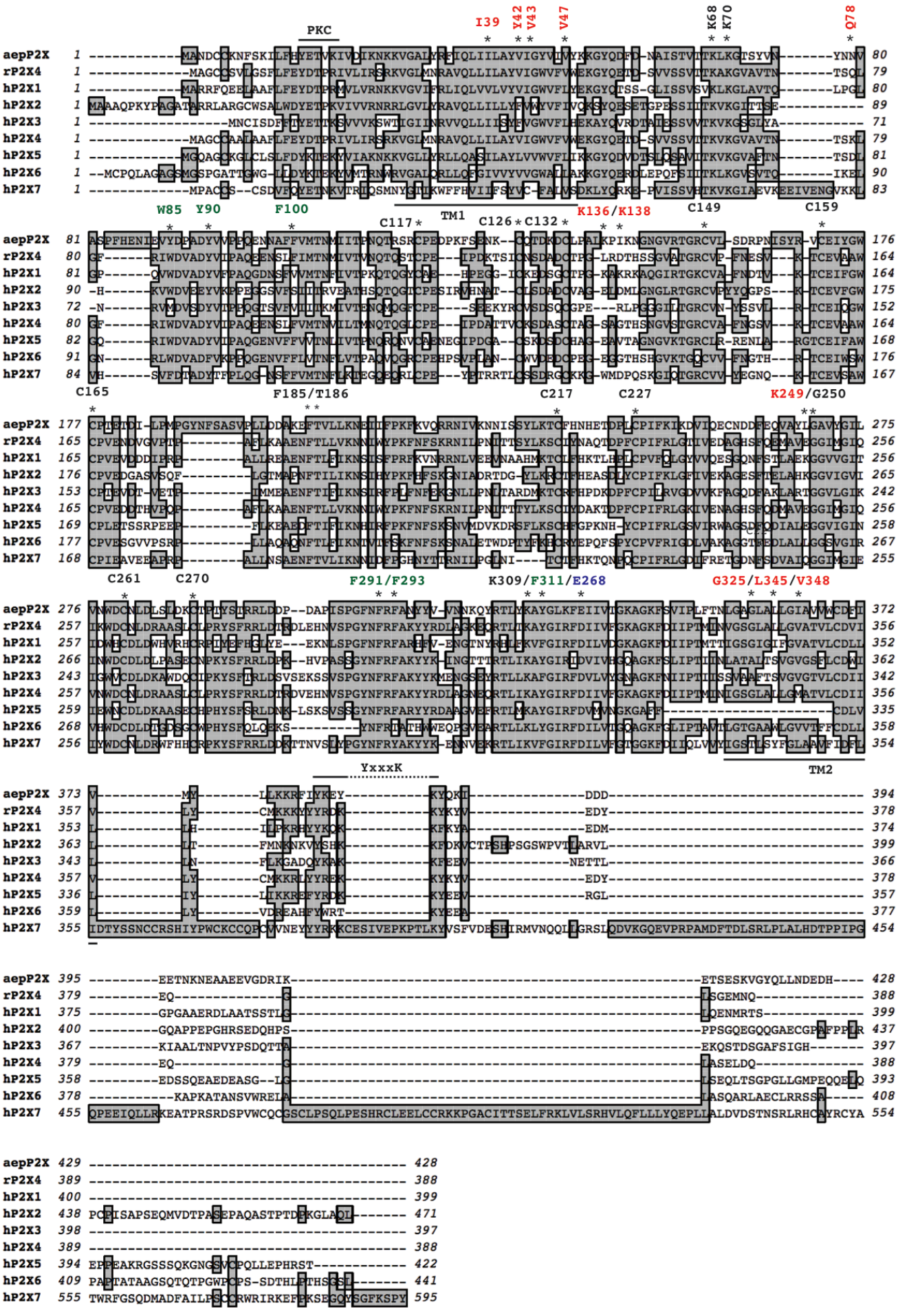
PKC
I39
Y42
V43
V47
K68
K70
Q78
W85
Y90
F100
TM1
K136/K138
C149
C159
C117
C126
C132
C165
F185/T186
C217
C227
K249/G250
C261
C270
F291/F293
K309/F311/E268
G325/L345/V348
YxxxK
TM2
aepP2X
rP2X4
hP2X1
hP2X2
hP2X3
hP2X4
hP2X5
hP2X6
hP2X7

Fig. 4.1: multiple sequence alignment (MSA) of cloned aepP2X, rP2X4 and hP2X1-7 subunits

aepP2X shares a 23.4 to 41.7% primary amino acid sequence identity with hP2X1-7 receptors. Residues that are identical between P2X receptors from all three species are shaded in grey. ATP binding residues, an N-terminal PKC phosphorylation motif, a C-terminal membrane localisation motif, and predicted TMDs are highlighted in black above the sequence. Residues that have been demonstrated to play a role in suramin, PPADS, or ivermectin sensitivity in previously characterised P2X receptors are highlighted in green, red, and blue, respectively. Sequences were aligned using the MUSCLE alignment algorithm (Edgar, 2004) (2.2.2). The rat P2X4 receptor primary amino acid sequence (accession number: U32497) was retrieved from UniProt (Bairoch *et al.*, 2005).

4.3.2 Pharmacological and biophysical characterisation of aepP2X

4.3.2.1 aepP2X functions as an ATP-gated ion channel in HEK293 cells

Functional responses of aepP2X to extracellular ATP when heterologously expressed in HEK93 cells were assessed using whole-cell patch-clamp in the voltage-clamp configuration. At a holding potential of -60 mV, concentration-dependent inward currents were evoked across a range of extracellular ATP concentrations (Fig. 4.2A-C), with an activation threshold concentration of approximately 30 μM (Fig. 4.2A) and an EC_{50} of 123.8 ± 21.8 μM (n = 8) Hill coefficient of 1.3 ± 0.1 (n = 8).

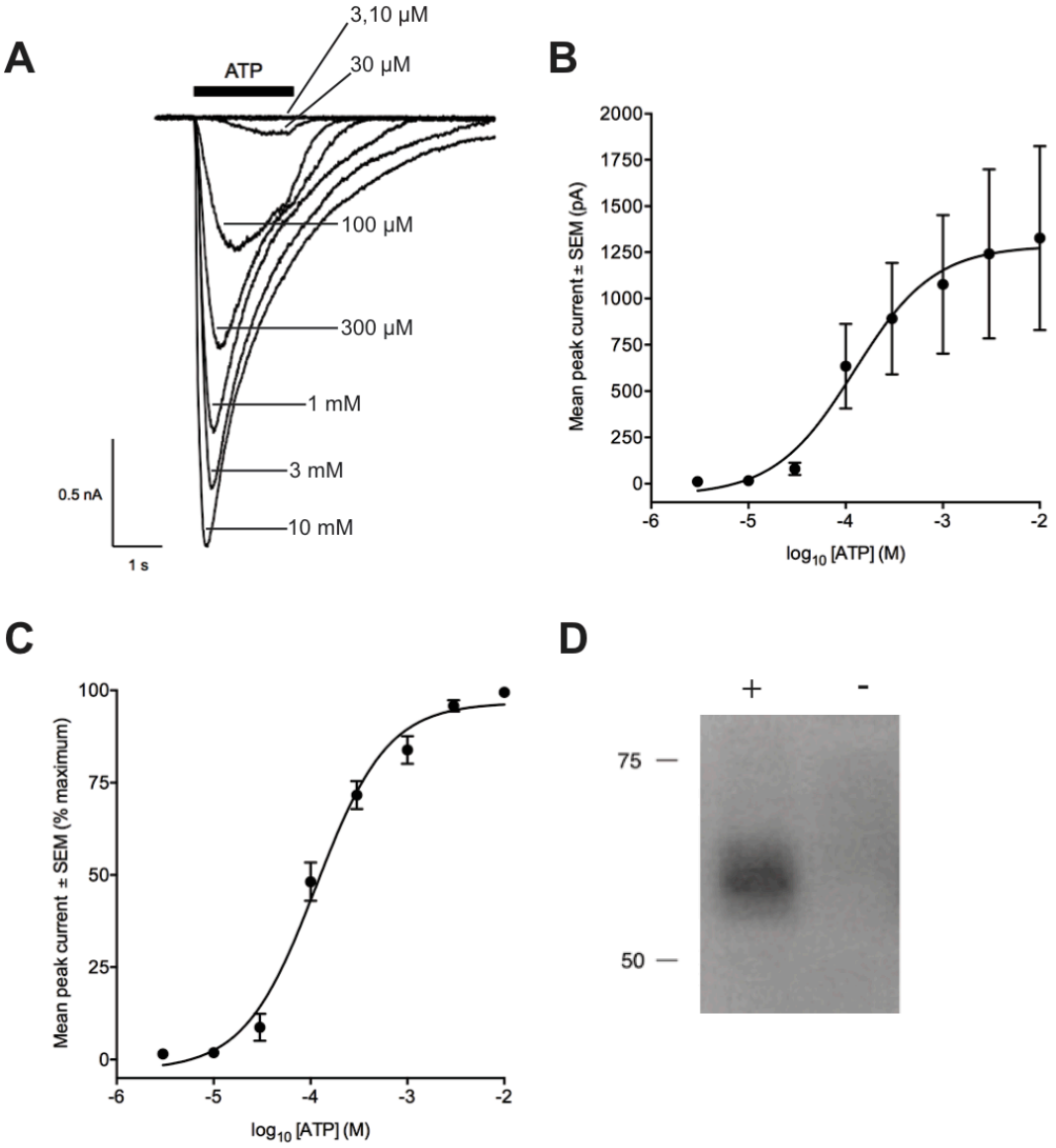

Fig. 4.2: extracellular ATP application evokes inward currents at aepP2X

Concentrations of ATP ranging from 3 µM to 10 mM were applied to HEK293 transiently transfected with aepP2X. ***A***, representative current recording traces of ATP-evoked inward currents, with duration of extracellular ATP application depicted by a black bar above the traces. Although no current was evoked at 3 and 10 µM ATP, inward currents were evoked at 30 µM. Currents were rapidly activating, but desensitised in the continued presence of extracellular ATP. ***B***, concentration-response curve of ATP-evoked currents in aepP2X (n = 8 cells). ***C***, normalised concentration-response curve of ATP-evoked currents in aepP2X-$(His)_6$. Currents ere normalised to the maximum current evoked in each cell (n = 8), due to either 3 or 10 mM ATP application. ***D***, Western blot of total protein lysate from HEK293 cells transiently expressing aepP2X-$(His)_6$ ('+') detected a single protein band at approximately 60 kDa. No bands were detected in 'mock' transfected control ('-') HEK293 cells.

4.3.2.2 Predicted N-linked glycosylation sites in aepP2X-$(His)_6$

Western blot analysis of HEK293 cells transiently transfected with aepP2X-$(His)_6$ detected a single band of approximately 60 kDa (Fig. 4.2D). The molecular weight of aepP2X-$(His)_6$ is predicted to be approximately 50 kDa, below that seen in Western blot analysis (Fig 4.2D). To assess this discrepancy, the primary amino acid sequence of aepP2X-$(His)_6$ was analysed for *N*-linked glycosylation motifs, a post-translational modification known to alter expression and function of higher P2X receptors (Roberts and Evans, 2006). Using the NetNGlyc 1.0 server (available at: http://www.cbs.dtu.dk/services/NetNGlyc/) to search for consensus 'Nx(S/T)' motifs identifies five predicted glycosylation motifs (Nx(S/T)), where 'x' is any amino acid except proline (Bause, 1983)) at N8, N117, N165, N190, and N228 (Fig. 4.3). *N*-linked glycan residues have a molecular weight of approximately 2 kDa suggesting that the discrepancy between observed and predicted weight may be due to post-translational *N*-linked glycosylation at these positions.

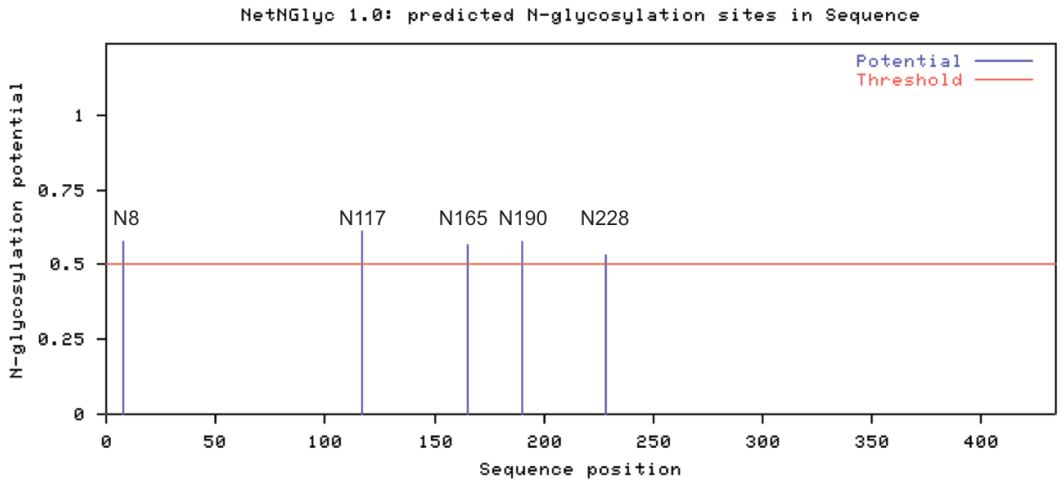

Fig. 4.3: predicted *N*-linked glycosylation sites in aepP2X-$(His)_6$

Predicted *N*-linked glycosylation sites ('Nx(S/T)') were identified using NetNGlyc. Five sites (N8, N117, N15, N190, and N228) within the primary amino aid sequence of aepP2X-$(His)_6$ are predicted exceed the cut off glycosylation potential of 0.5 (highlighted by a horizontal red line). Each *N*-glycan addition contributes approximately 2 kDa to the molecular weight of a protein, and may account for the discrepancy seen between the predicted and observed molecular weight of aepP2X-$(His)_6$ seen in Western blot analysis.

4.3.2.3 Activation and deactivation kinetics of aepP2X-$(His)_6$ to synthetic ATP analogues

At a holding potential of -60 mV, application of 100 μM ATP evoked robust and repeatable inward currents with rapid activation kinetics (Fig. 4.2A). Evoked currents were rapid, with the time taken for currents to increase from 10 to 90% of maximal current calculated to be 32.4 ± 2.8 ms at a rate of 14.2 ± 2.0 $pA.ms^{-1}$ (n = 41) with currents desensitising to 50% of maximum in 86.9 ± 65.0 ms at a rate of 0.3 ± 0.05 $pA.ms^{-1}$ (n = 41). Deactivation kinetics were considerably more variable. This variation appeared to arise from subtle changes in cell positioning relative to the direction of flow of agonist solutions.

4.3.2.4 Agonist insensitivity of aepP2X-$(His)_6$

Application of the synthetic ATP analogues α,β-meATP (n = 3) or β,γ-meATP (n = 1) at 1 mM failed to evoke inward currents at aepP2X-$(His)_6$, in contrast to many human P2X receptor homologues where they act as partial agonists (Fig. 4.4).

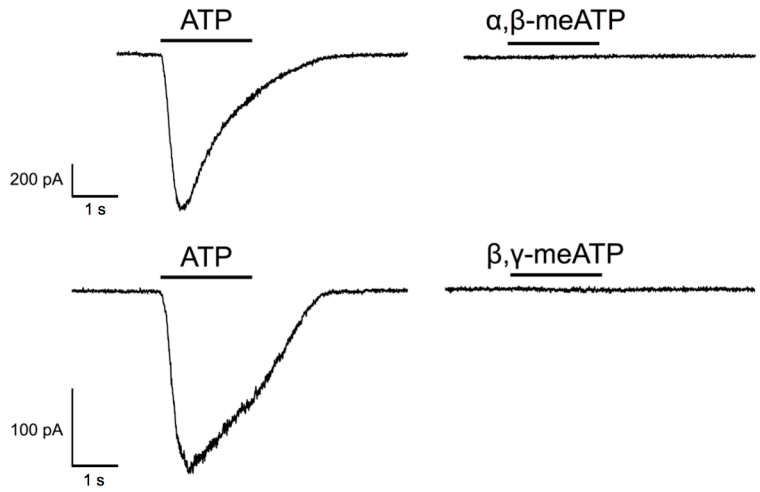

Fig. 4.4: aepP2X-(His)$_6$ does not respond to α,β-meATP or β,γ-meATP

Representative current traces from illustrating the ineffectiveness of the synthetic ATP analogues α,β-meATP and β,γ-meATP. Cells were held at a holding potential of -60 mV. *Upper traces*, extracellular application of 1 mM ATP evoked inward currents at aepP2X-(His)$_6$ when expressed heterologously in HEK293 cells whilst application of 1 mM α,β-meATP did not evoke currents. *Lower traces*, application of ATP evokes currents at aepP2X, whilst application of 1 mM β,γ-meATP does not evoke inward currents. Agonist applications are depicted by a black bar above each trace, with each applied for 2 seconds.

4.3.2.5 Co-application of the P2 antagonists suramin and PPADS are ineffective at aepP2X-(His)$_6$

Both vertebrate and invertebrate P2X receptor subunits are largely blocked by suramin and PPADS (pyridoxalphosphate-6-azophenyl-2',4'-disulfonic acid) (North and Suprenant, 2000; Fountain, 2013). At 100 μM, co-application of either suramin or PPADs failed to inhibit 100 μM ATP-evoked currents at aepP2X-(His)$_6$ (Figs. 4.5A, B, and C). Additionally, co-application of 100 μM brilliant blue G (BBG), 100 μM phenol red, or the P2X current modulating compound CORM-2 (30 μM) (Wilkinson *et al.*, 2009; Wilkinson and Kemp, 2011) all failed to inhibit 100 μM ATP-evoked currents at aepP2X-(His)$_6$ (Figs. 4.5A and B).

Whilst co-application of suramin or PPADS with ATP failed to inhibit aepP2X-(His)$_6$ currents, pre-application of either compound for 90 s followed by co-application with 100 μM ATP showed greater efficacy in inhibiting ATP-evoked currents compared to co-application with ATP alone (suramin: -36.7 ± 18.3%, p = 0.0178, n = 3 cells) and

PPADS: -58.7 ± 1.9%, $p = 0.029$, $n = 3$ cells) (Fig. 4.5D). Pre-application of suramin or PPADS for 3 s prior to co-application with 100 μM failed to significantly inhibit ATP-evoked currents (Fig. 4.5D).

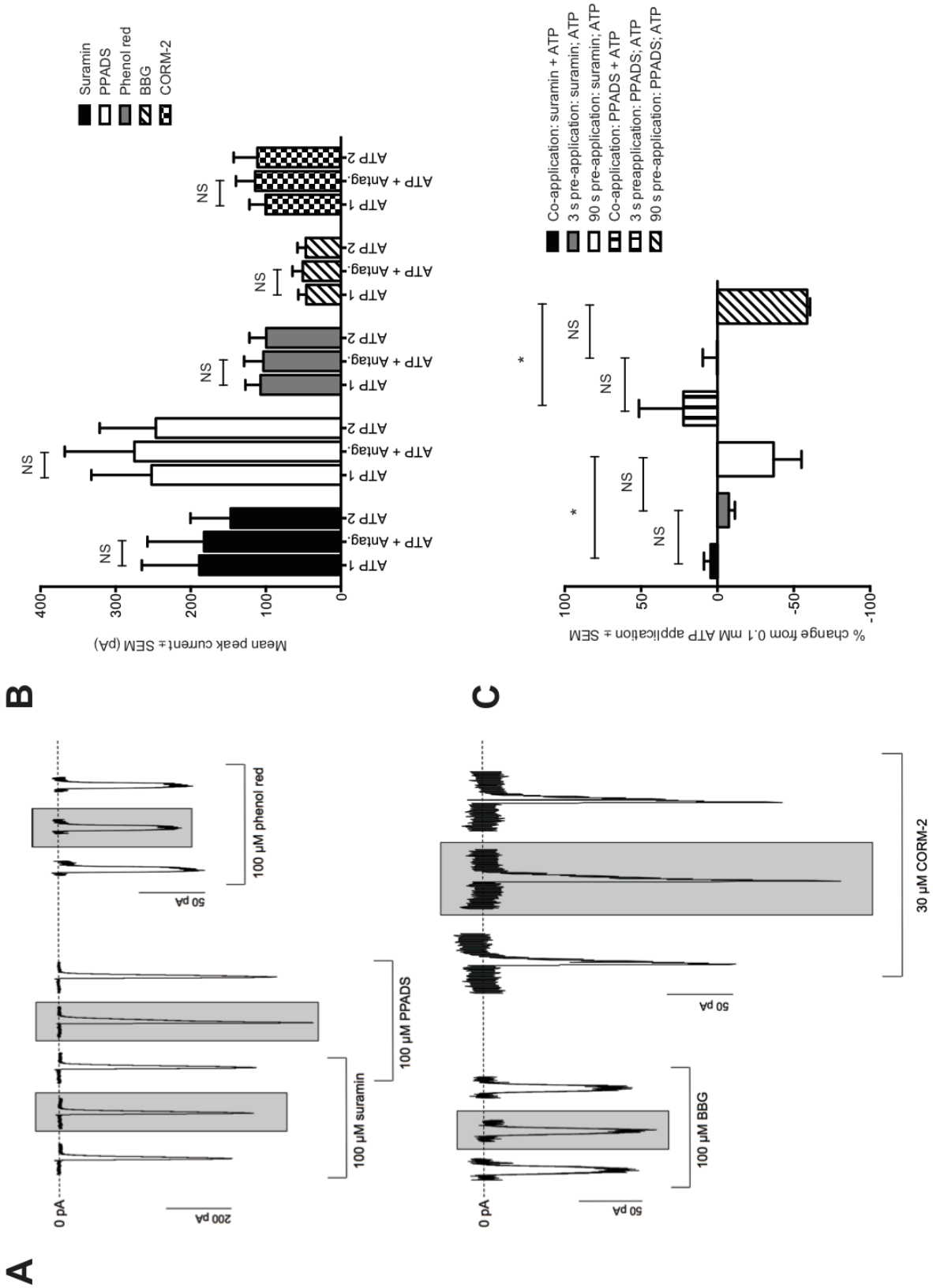
A
0 pA
200 pA
100 µM suramin
100 µM PPADS
100 µM phenol red
50 pA
B
Mean peak current ± SEM (pA)
Suramin
PPADS
Phenol red
BBG
CORM-2
ATP 1
ATP + Antag
ATP 2
NS
C
% change from 0.1 mM ATP application ± SEM
Co-application: suramin + ATP
3 s pre-application: suramin; ATP
90 s pre-application: suramin; ATP
Co-application: PPADS + ATP
3 s preapplication: PPADS; ATP
90 s pre-application: PPADS; ATP
*
NS
0 pA
50 pA
100 µM BBG
30 µM CORM-2

Fig. 4.5: effects of P2 receptor antagonists at aepP2X-(His)$_6$

The effects of the P2 receptor antagonists suramin, PPADS, phenol red, BBG and CORM-2 was tested at aepP2X-(His)$_6$ when expressed heterologously in HEK293 cells. Grey bars surrounding a raw trace highlight antagonist/100 μM ATP co-application. Traces flanking antagonist traces represent inward currents evoked by 100 μM applied alone. Between application of compounds, cells were washed for 90 s with ECS. ***A***, representative current recording traces of 100 μM ATP-evoked currents aepP2X-(His)$_6$ in the presence and absence of a co-applied P2 antagonist. *Top-left trace*, neither suramin nor PPADS (both at 100 μM) inhibit ATP-evoked inward currents at aepP2X-(His)$_6$ when co-applied. *Top-right trace*, 100 μM phenol red does not inhibit ATP-evoked aepP2X-(His)$_6$ currents. *Bottom-left*, 100 μM co-application of BBG does not inhibit aepP2X-(His)$_6$ ATP currents. *Bottom-right*, the CO-releasing compound (CORM-2) (30 μM) potentiates aepP2X-(His)$_6$ currents, but these currents are not statistically significant from control ATP currents. ***B****,* mean peak currents recorded in the presence of 100 μM ATP alone prior to ('ATP 1') co-application with an antagonist (concentrations detailed in ***A***) ('ATP + Antag.'), followed by a second 100 μM ATP application ('ATP 2'). No statistical significance (determined by repeated measures one-way ANOVA) is found between mean peak currents recorded in ATP alone versus those recorded in the presence of an antagonist (suramin; $F(1,5) = 1.20$, $p = 0.32$; PPADS: $F(1,3) = 1.67$, $p = 0.29$; phenol red: $F(1,3) = 0.70$, $p = 0.51$; BBG: $F(1,4) = 2.5$, $p = 0.18$); and CORM-2: $F(1,5) = 0.74$, $p = 0.51$). ***C***, graph illustrating percentage change in evoked current from a preceding 100 μM ATP application relative to currents evoked in the presence of suramin or PPADS alone, either compound co-applied after a 3 s pre-application, or either compound co-applied after a 90 s pre-application. A statistically significant difference between groups was found as determined by one-way ANOVA ($F(2,8) = 6.60$, $p = 0.020$). A Tukey *post-hoc* test reveals that the inhibition resulting from 90 s pre-application of 100 μM suramin was significantly greater than that of co-application of suramin of ATP alone (-36.7 ± 18.3%; $p = 0.018$). *Post-hoc* analysis of currents recorded following 90 s pre-application of 100 μM PPADS was also significantly greater that that of co-application of ATP and PPADS alone (-58.7 ± 3.4%, $p = 0.029$).

4.3.2.6 Ivermectin potentiates ATP-evoked currents through aepP2X-(His)$_6$

The broad spectrum antiparasitic, ivermectin (IVM), is known to potentiate hP2X4 receptor ATP-evoked currents (Khakh *et al.*, 1999b). Given the high percentage of residue sequence identity of aepP2X-(His)$_6$ to hP2X4 and conservation of residues implicated in the action of IVM at hP2X4, the effect of IVM at aepP2X-(His)$_6$ was assessed. Following a 3 s pre-incubation of 3 μM IVM alone, followed by its co-application with 100 μM ATP potentiated ATP-evoked currents through aepP2X-(His)$_6$ (41.5 ± 10%, $n = 5$ cells) that were recoverable after a 90 s wash with ECS (Figs 4.6A and B). Consistent with hP2X4 (Khakh *et al.*, 1999b), IVM-modulated currents through aepP2X-(His)$_6$ displayed significantly slowed, but recoverable,

deactivation kinetics (ATP control decay slope time = 348 ± 68 ms; IVM-potentiated decay slope time = 1614 ± 167 ms (p = 0.011; n = 5) (Figs. 4.6A and C).

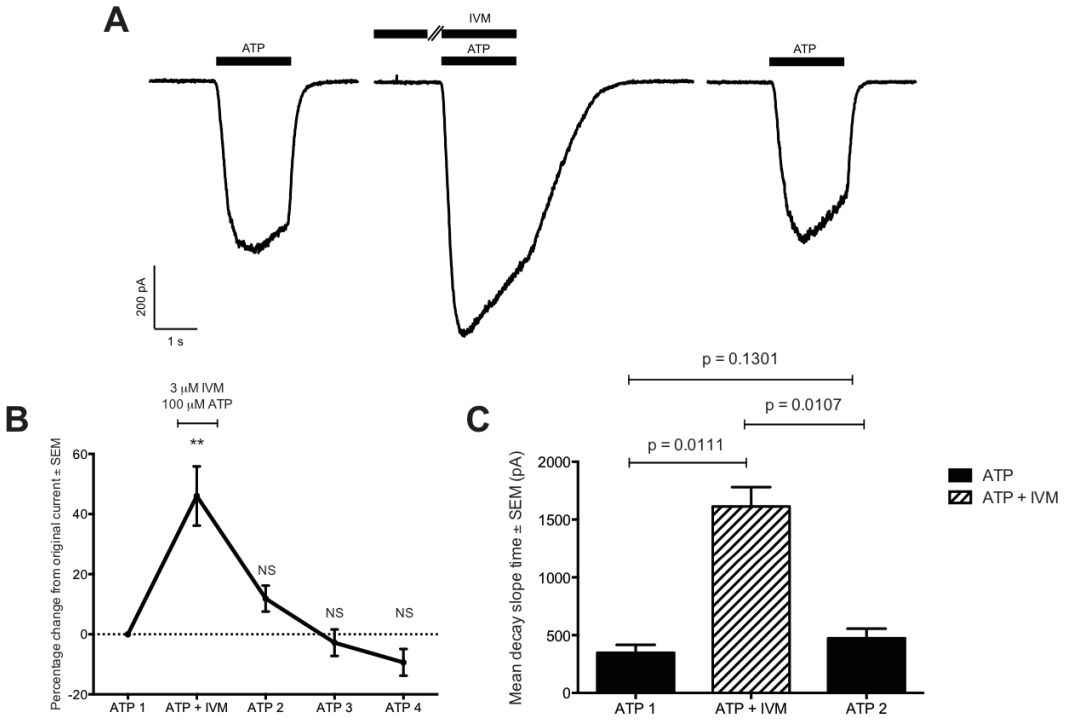

Fig. 4.6: ivermectin potentiates ATP-evoked currents at aepP2X-$(His)_6$

Ivermectin (IVM) (3 μM) was pre-applied to HEK293 cells expressing aepP2X-$(His)_6$ for 3 s prior to co-application with 100 μM ATP. ***A***, representative current recording traces of IVM-modulated ATP currents at aepP2X-$(His)_6$ expressed in HEK293 cells. Currents were recorded at a holding potential of -60 mV. *Left current trace* 100 uM ATP-evoked current before addition of IVM (3 μM); *middle trace*, IVM potentiates the amplitude as well as the duration of ATP-evoked currents; *right trace*, IVM-potentiated currents return to near pre-application levels. ***B,*** mean percentage change in peak current (from control 100 μM ATP application alone) data illustrating the recovery of ATP-evoked currents following co-application of IVM and ATP (n = 5 cells). Currents return to near pre-IVM levels within two 100 μM ATP applications following a significant percentage change in current relative to baseline ($F(1.461, 4.383) = 25.65$; p = 0.045 with repeated measures one-way ANOVA. A *post hoc* Fisher's least significant difference test was performed, and is illustrated on the graph where a highly statistically significant difference was found between the first ATP application (ATP 1) and ATP + IVM co-application (ATP+ IVM) (p = 0.0045). ***C***, summary of mean data from n = 5 cells illustrating a significant increased in the time of decay of ATP-evoked currents in the presence of IVM (3 μM) ($F(1.051, 4.208) = 36.59$; p = 0.0031 with repeated measures one-way ANOVA). P-values derived from Tukey's multiple comparison *post hoc* test are illustrated on the graph. * $p < 0.05$; ** $p < 0.005$; NS, non-statistically significant.

4.3.2.7 aepP2X is a cation permeable channel

P2X receptors display significant permeability to small monovalent cations (North, 2002). Some P2X receptors also display a significant permeability to Ca^{2+} (e.g. human P2X1 and rat P2X2 subunits (Evans *et al.*, 1996)) and Cl^- ions (e.g. hP2X5 (Bo *et al.*, 1995) and *Dictyostelium discoideum* P2XA (Fountain *et al.*, 2007)). To assess the ionic permeability of aepP2X-$(His)_6$ (relative to that of Na^+ ions), 100 μM ATP was applied to cells expressing the receptor in the presence of ECS containing different test cations. The relative permeability of chloride ions through aepP2X-$(His)_6$ was also determined through replacement of the major source of chloride ions (NaCl) with the larger anion, gluconate (sodium gluconate).

In symmetrical Na^+ concentration conditions, currents reversed at near 0 mV (-1.7 ± 1.4 mV; n = 24 cells). Replacement of extracellular Na^+ with the large cation, $NMDG^+$ (chloride salt), resulted in a leftward shift in reversal potential to close to -70 mV (-65.5 ± 3.0 mV, n = 10). Similarly, replacement of NaCl with Tris.Cl results in a leftward shift in reversal potential to near -50 mV (-48.3 ± 1.8 mV, n = 0.5). Accordingly, both $NMDG^+$ and $Tris^+$ ions are poorly permeable through relative to Na^+ ions (P_{NMDG}/P_{Na} = 0.1 ± 0.02; P_{Tris}/P_{Na} = 0.2 ± 0.009). aepP2X displayed considerable Ca^{2+} and K^+ ion permeability (P_{Ca}/P_{Na} = 1.8 ± 0.2, n = 5; P_K/P_{Na} = 1.7 ± 0.3, n = 7), but almost negligible Cl^- ion permeability (P_{Cl}/P_{Na} = 0.04 ± 0.02, n = 7) following equimolar substitution of NaCl with Na.gluconate. Calculated ionic permeabilities relative to that of Na^+ ions reveals a rank order of permeability of monovalent cations of: $Ca^{2+} \geq K^+ \geq Na^+ > Tris^+ > NMDG^+ > Cl^-$. Reversal potentials were determined according to section 2.6.5.2 and ionic permeabilities relative to that of Na^+ calculated according to sections 2.6.5.2 and 2.6.5.3. Reversal potential in each test condition, and calculated relative permeabilities to both organic and inorganic ions are summarised in Table 4.1.

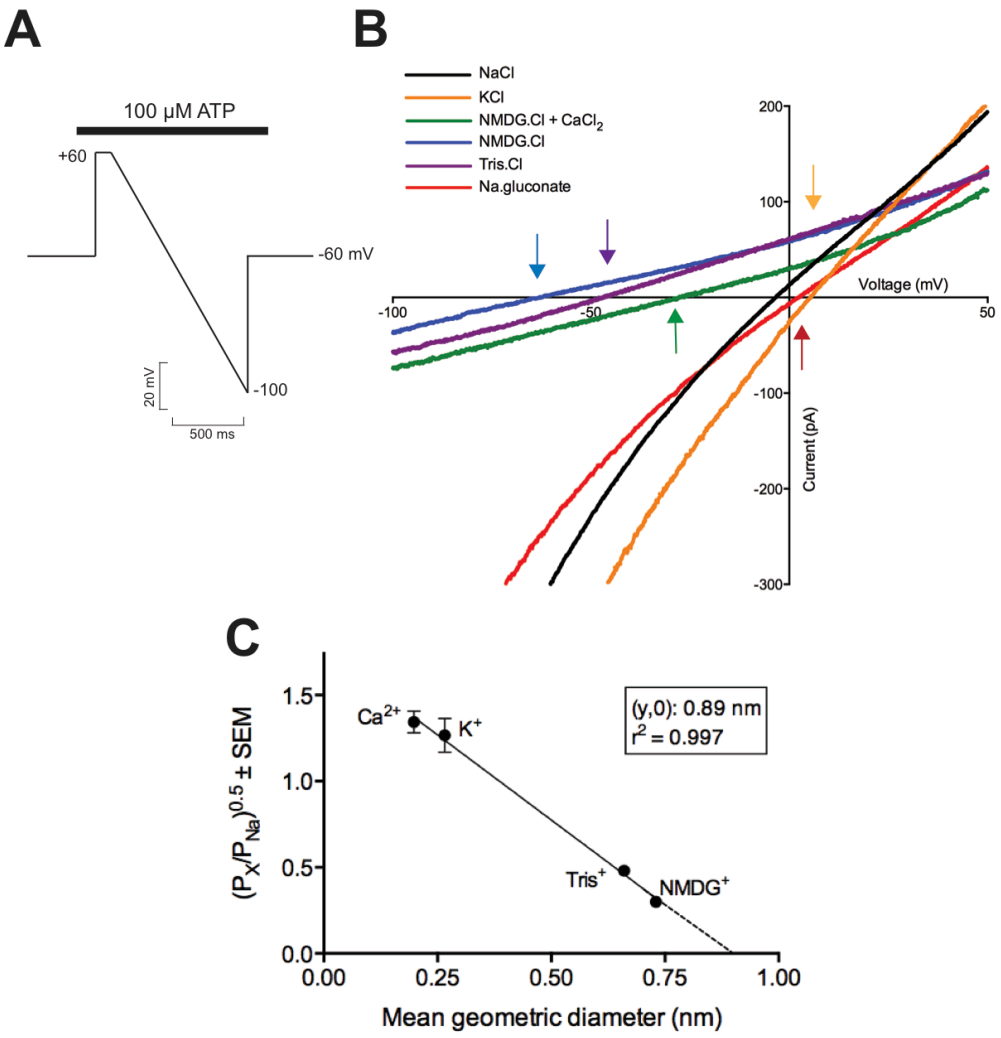

Fig. 4.7: ion permeation properties of aepP2X in HEK293 cells

A, voltage-ramp protocol used during ionic permeability studies in aepP2X Cells were held at -60 mV and 100 µM applied extracellularly (depicted by a black bar above the voltage-protocol). At peak currents, cells were stepped to +60 mV and held at this voltage for 100 ms to inactivate endogenous voltage-gated ion channel currents. Cells were subsequently ramped to -100 mV over 1 s in the continued presence of 100 µM ATP before returning to -60 mV. ***B***, current-voltage relationships of aepP2X-$(His)_6$ in various extracellular cation and anion solutions (labelled accordingly). Current-voltage relationships were adjusted for liquid junction potentials. The reversal potential for sodium (E_{Na}) was approximately 0 mV. Reversal potentials are highlighted by appropriately coloured arrows, corresponding to the major ion solution denoted in the panel key. Note the leftward shift in reversal potential seen in NMDG.Cl and Tris.Cl. solutions. Against a background of NMDG, reintroduction of 5 mM $CaCl_2$ into the recording ECS results in a rightward shift in the current-voltage relationship towards 0 mV. The *x*-axis of the graph depicting the current-voltage relationship is truncated to allow better resolution of reversal potentials for each condition. ***C***, permeability of four cations relative to that of sodium as a function of their mean ionic diameter (nm). Extrapolation of the line of best fit predicts a pore diameter of aepP2X close to 0.9 nm ($n \geq 5$ cells for each). Mean geometric ion diameters are taken from Hille, 1992.

Table 4.1: ionic permeability data for aepP2X in HEK293 cells

Ion of interest	*Erev (mV)*	P_x/P_{Na}	*n*
Na^+	-1.7 ± 1.4	-	24
Ca^{2+}	-25.5 ± 1.9	1.8 ± 0.2	5
K^+	+7.2 ± 2.1	1.7 ± 0.3	7
$Tris^+$	-48.3± 1.8	0.2 ± 0.009	5
$NMDG^+$	-65.5 ± 3.0	0.1 ± 0.02	10
Cl^-	1.9 ± 1.6	0.04 ± 0.02	7

Reversal potentials (E_{rev}) for aepP2X in various extracellular solutions, and corresponding calculated relative permeabilities for ions of interest. *n* = number of cells tested for each condition.

4.3.2.8 Estimation of aepP2X receptor channel pore diameter

Channel pore diameter (at its narrowest point) can be estimated using the principle of exclusion field theory (Dwyer *et al.*, 1980; Cohen *et al.*, 1992), whereby pore diameter limits the maximum diameter of an ion that can permeate through it (treating ions as spheres).

Plotting of the relative permeability of cations examined in section 4.3.2.7 (Ca^{2+}, K^+, $NMDG^+$, and $Tris^+$) to that of Na^+, as a function of their mean geometric diameter (Hille, 1992), estimates a pore diameter of 0.89 nm (Fig. 4.7C). This value agrees well with findings of previous studies of other P2X receptors in humans (Evans *et al.*, 1996; Eickhorst *et al.*, 2002a), and some invertebrate P2X receptors (Agboh *et al.*, 2004; Fountain *et al.*, 2008), where receptor pore diameter has been estimated to be between 0.8 to 1 nm.

4.3.3 Staining of nematocyst cells with anti-aepP2X antiserum

Staining of *H. vulgaris* (AEP) polyps with Day 0 PA5619 crude anti-P2X antiserum (taken from rabbit hosts immediately after immunisation with antigenic peptide)

(1:500 to 1:2000 dilution) did not reveal any staining of structures (Fig. 4.9A and B). In contrast, incubation of polyps with PA5619 Day 72 anti-P2X antiserum stained specific structures within the polyp with apparent regional variation. No staining was seen in the polyp foot and basal peduncle regions (Fig. 4.8E). However, a high density of distinct structures displayed immunoreactivity in the polyp body column (Fig. 4.8D and E), often organised in clusters of structures of the same size and morphology. Furthermore, these clusters were situated at, or near, the polyp ectodermal epithelial cell layer (Figs 4.8D and 4.9E-G). Immunoreactivity was also seen in the body column of developing buds emerging from the proximal mother polyp body column (Fig. 4.8C). Immunostaining of two morphologically distinct structures was evident in tentacles of both the mother polyp (4.8A and B) and emerging bud (Fig. 4.8C): larger stenotele nematocysts, and another distinct group of smaller structures. Both of these structures were also found in the body column, although fewer in number. No immunoreactivity was detected at the hypostome (Fig. 4.9B), or the tentacle zone (tz) of polyps (the region at which tentacles attach to the head region) (Fig. 4.9C).

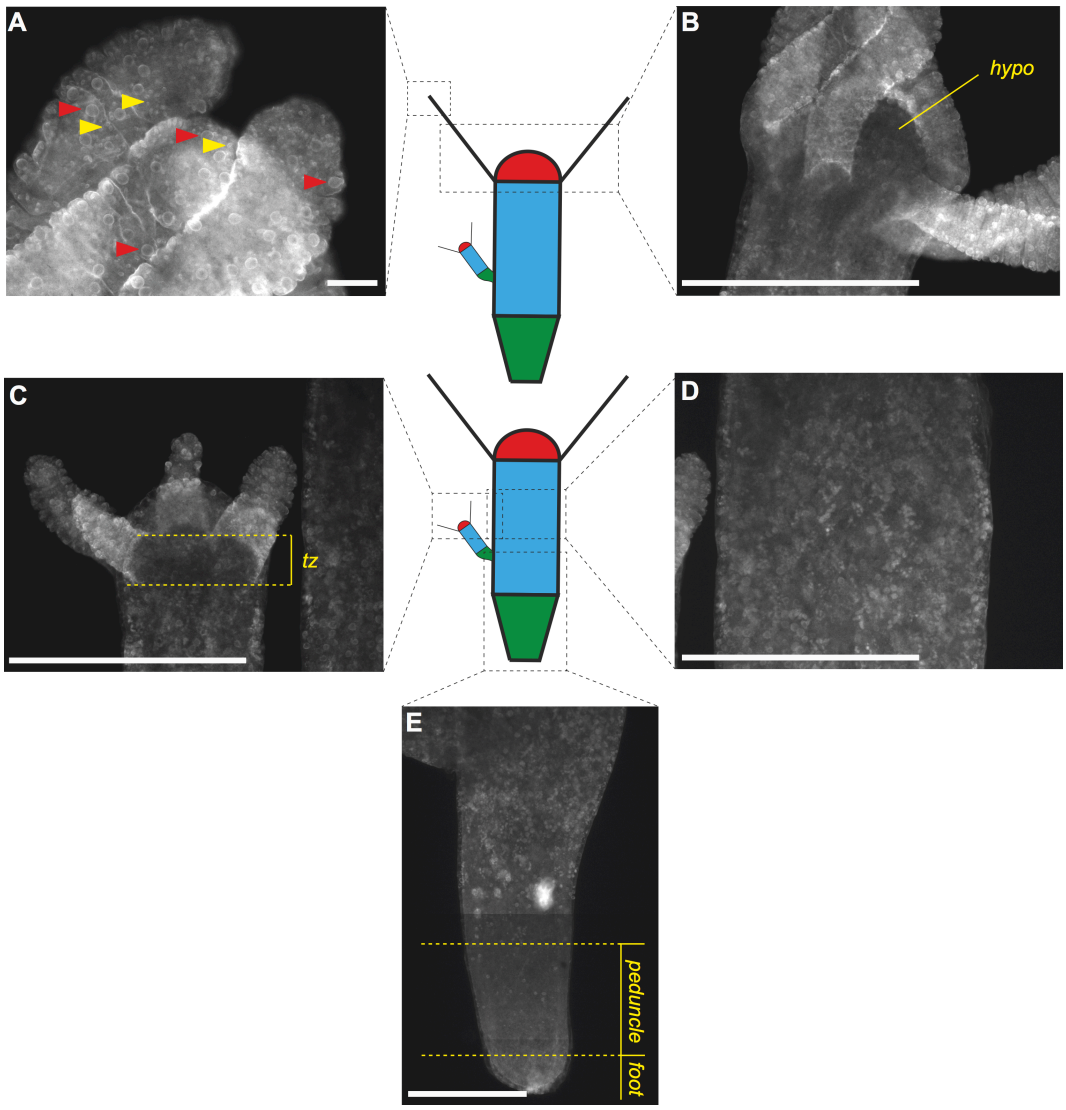

Fig. 4.8: immunostaining of whole *H. vulgaris* (AEP) polyps with Day 72 PA5619 anti-P2X antiserum

Incubation of polyps with antiserum at 1:2000 dilution revealed regional differences in staining in *H. vulgaris* (AEP) fixed polyps. Central cartoons illustrate major regions of a *Hydra* polyp: red = head region; blue = body column; green = peduncle and foot region. ***A***, immunostaining is evident in two morphologically distinct structures in tentacles: larger stenotele nematocysts (yellow triangles) and smaller (red triangles), presumably desmonemes with a role in prey capture in *Hydra* polyps. Both of these structures are also found in the body column of polyps. ***B, C***, at the apical body column and tentacle zone (*tz*) of polyps there was a marked reduction in immunofluorescence, with little staining in the hypostome region. ***D***, staining of was evident in the body column of polyps, with distinct clusters easy visible. ***B***, little immunostaining of structures was seen in the peduncle region of polyps, with no staining seen in the foot region. Some staining of structures was seen in the apical portion of the peduncle, increasing in density in the distal body column. Following incubation with anti-P2X antiserum, polyps were incubated in with 2 µg goat anti-rabbit 2° antibody coupled to an Alexa Fluor® 488 fluorophore. Scale bar = 100 µm (***A***), 500 µm for all other panels.

A number of morphologically distinct structures display immunostaining following IHC with day 72 PA5619 anti-P2X antiserum. Images taken of stained polyps such that a focus point is drawn to the edge of the body column highlights a number of clusters containing these structures, often in nests of 16 (Figs. 4.9E-D). The largest structures stained are approximately 20 μM in diameter and ovoid in shape (Figs. 4.9C and D). In addition, a reduced intensity of immunofluorescence was seen at the apex of these structures, suggestive of an operculum at this point. Taken together, this suggests that staining was seen in stenotele nematocysts. More specifically, the clustering of these structures suggests that the antiserum stained differentiating stenotele nematocysts within nematoblast clusters. Mature stenotele and desmoneme nematocysts embedded in the tentacles also show immunostaining (Fig. 4.9E and 4.9H).

Clusters of smaller, elongated immunofluorescent structures were also seen within the body column of *Hydra* polyps, often seemingly embedded within the ectodermal epithelial cell layer (Fig. 4.9F). The elongated morphology of these structures was indicative of desmoneme nematocysts (Hemmrich *et al.*, 2007). In addition to stenotele nematocysts, incubation of polyps with Day 72 PA5619 stained cylindrical structures within the body column of *Hydra* (Fig. 4.9E inset) and are also present in small clusters. The tapered morphology of these structures was different from that of desmoneme nematocysts, suggesting that they were from the isorhiza family of nematocysts (Hemmrich *et al.*, 2007).

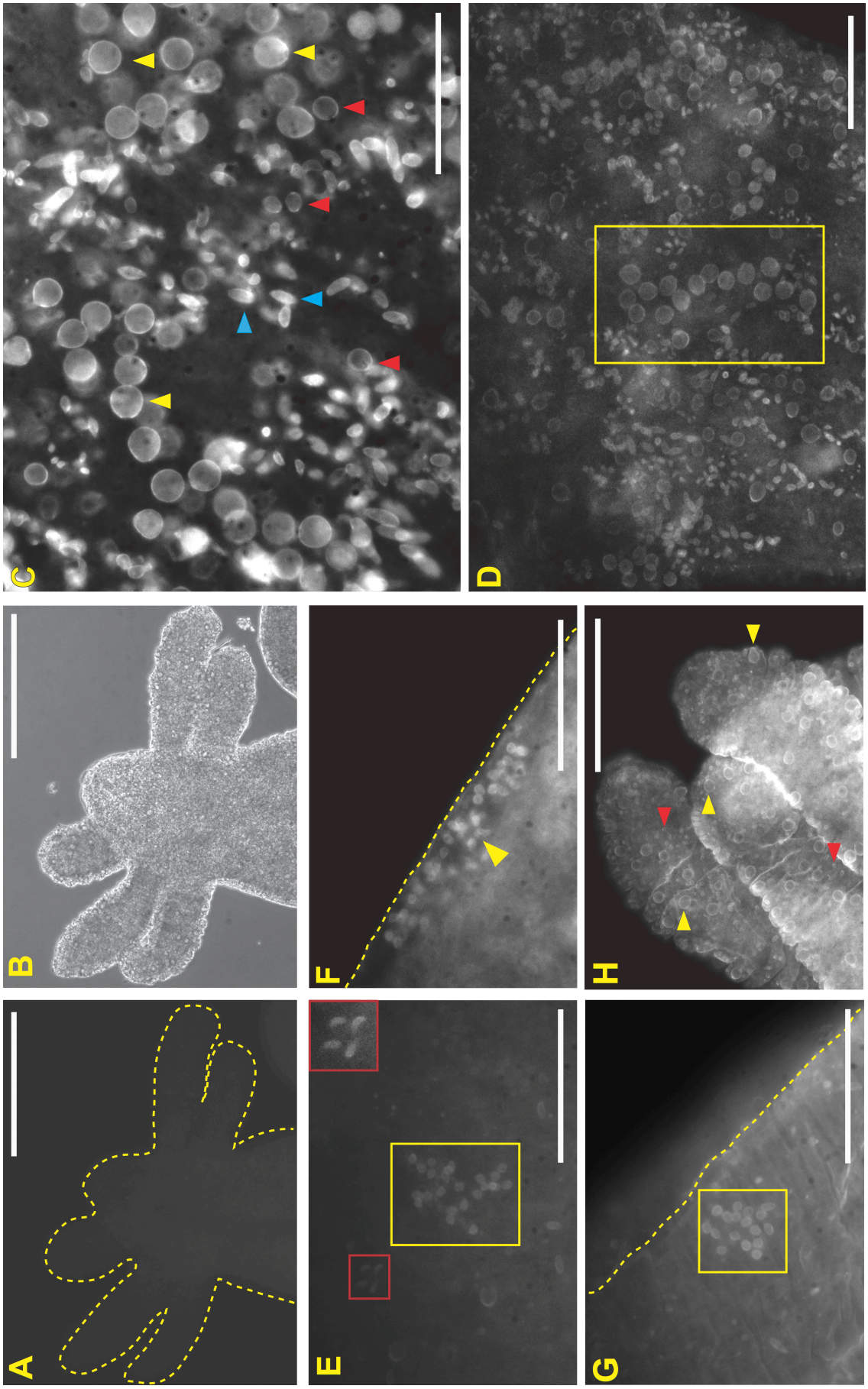
C
D
B
F
H
A
E
G

Fig. 4.9: immunostaining of nematocysts in whole *Hydra* polyps using anti-P2X antiserum

Fluorescence micrographs of whole *H. vulgaris* (AEP) polyps revealed staining of nematocyst structures following incubation with a 1:2000 dilution of anti-P2X polyclonal antiserum. ***A***, Representative immunofluorescence image illustrating lack of staining of polyps with Day 0 PA5619 antiserum (1:2000 dilution). Image is of head, tentacles, and apical body column of a *Hydra* polyp. A yellow line marks the boundary of the polyp. ***B***, light micrograph of polyp illustrated in image ***A***. ***C***, immunofluorescence image of body column of *Hydra* polyp illustrating staining of nematocysts with day 72 PA5619 anti-P2X antiserum. A number of nematocyst types displayed immunostaining. Yellow arrows indicate large stenotele nematocysts, red arrows indicate smaller stenotele nematocysts, and blue arrows indicate isorhiza-type nematocysts. ***D***, immunofluorescence image polyp body column highlighting region of cluster of 16 pre-mature stenotele nematocysts (yellow box). ***E***, immunofluorescence image of nematocyst clusters present in the body column of *Hydra*. A large cluster (yellow box) appeared to consist of desmoneme nematocysts, whilst a smaller cluster of 4 elongated nematocysts (expanded with greater contrast in the inset) appears to consist of an isorhiza-type nematocyst. ***F***, a nematocyst cluster present at the ectodermal epithelial cell layer of a polyp body column. A yellow dashed line demarcates the body column boundary. ***G***, a cluster of 16 desmoneme-type nematocysts situated close to the body column boundary of a polyp. ***H***, two nematocyst types were stained in tentacles of polyps following IHC using day 72 PA5619 anti-P2X antiserum. Stenotele nematocysts (yellow arrows) were stained at the tentacle edges, orientated with the apical pole towards the extracellular milieu, consistent with their role in prey capture. A smaller nematocyst type was also identified, likely to be desmoneme (red arrow). Scale bars: *A* and *B* = 500 μm; *E-H* = 100 μm.

4.3.4 Quinacrine staining of nematocysts in live *Hydra* polyps

The lipophilic acridine derivative, quinacrine, is known to bind to adenine-containing nucleotides (Irvin and Irvin, 1954), and has been used previously to identify ATP-containing vesicles in both cultured and native cells (Olson *et al.*, 1976; Crowe and Burnstock, 1982; De Proost *et al.*, 2009; Gonzales *et al.*, 2010). Subsequent excitation with UV light idenfies quinacrine-bound ATP by fluorescence.

To identify compartments in *Hydra* polyps in which ATP may be present and potentially released, whole live polyps were incubated in quinacrine (10 uM) and visualised under UV illumination. Fluorescence was seen in clusters of differentiating nematocysts (Figs. 4.10A, B and D) and stenotele nematocysts present at the ectodermal epithalial layer of the body column (Fig. 4.10B). An internal penetrating stylet within the stenotele nematocyst is clearly visible as a region of

more intense fluoresence, in addition to pairs of differentiating and migrating nemaocyts, likely to be desmoneme nematocysts due to their small size and morphology (Fig. 4.10B). Variable fluorescence intensity was also seen in structures throughout the polyp that were not identifiable by morphology alone (Figs 4.10C and D).

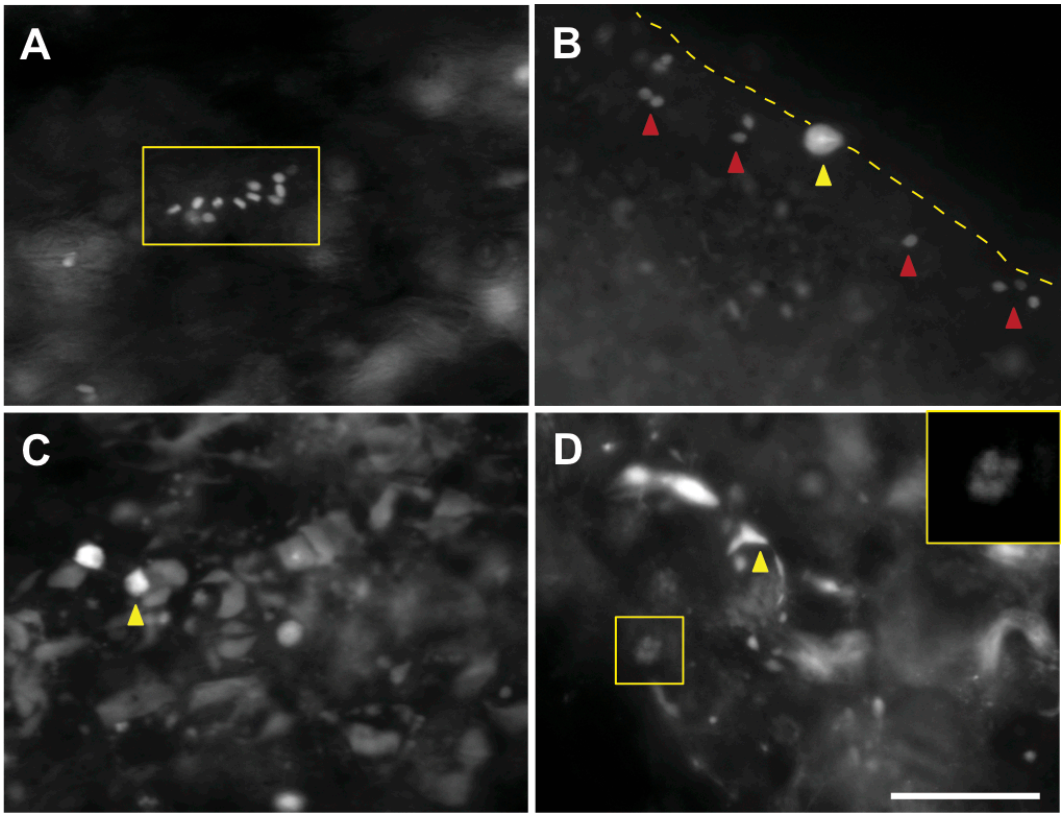

Fig. 4.10: staining of whole polyps using quinacrine

Fluorescence micrographs of whole, live *H. vulgaris* (AEP) polyps incubated in a solution of 10 µM quinacrine for 15 mins. Fluorescence was localised to a number of structures within the polyp. ***A***, cluster of differentiating nematocysts within the body column. ***B***, stenotele nematocys (yellow arrow) at the body column edge (demarcated by a dashed yellow line), within which was a structure of higher intensity fluorescence could be seen. Individual, or paired strucures were also paired within the ectodermal epithelial cell layer, and appeared to be demoneme nematocysts (red arrow). ***C***, structures of varying fluorescence were also stained in *Hydra*, although these did not display the distinctive morphology of nematocysts or other cell types. ***D***, further illustration of morphologically indistinct structures (yellow arrow) stained by quinacrine. A small cluster of 4 differentiating cells, presumably nematocysts, is highlighted in the yellow box (expanded in inset). Scale bar = 100 µm for all panels.

4.3.5 Mutually exclusive staining of non-nematocyst cells following antiserum polyclonal antibody staining

Staining of whole, fixed *Hydra* polyps with anti-serum suggests the presence of P2X receptor protein in a number of developing and pre-mature nematocyst complexes. To ascertain whether this staining pattern arose from binding of non-specific host antibodies, and was a true representation of the *in vivo* localisation of aepP2X, PA5619 was chosen for peptide-affinity purification.

In contrast to the pattern of expression described in section 4.3.3, purified anti-P2X antibody stained densely packed structures throughout the polyp, including in the peduncle and hypostome regions where no immunofluorescence signal was seen using antiserum from the same PA5619 rabbit. At dilutions of 1:500 (10 µg/ml), two structures appeared to be stained by purified anti-P2X polyclonal antibody. The predominant staining was of cells throughout the polyp (Fig. 4.11E), in which an unstained region was present within the centre of each structure. These cells were often seen in pairs in the body column of the polyp (Fig. 4.11F-G). Shifting the focal plane of imaging towards the user highlighted stained cells with 2 or 3 processes emanating from its soma (Fig. 4.11D) suggestive of staining of ganglionic neuron cells (Davies, 1971), as opposed to sensory neurons, the soma of which lie parallel to the polyp axis, at the endodermal/ectodermal epithelial boundary (Davies, 1969).

To assess whether the two cell types belong to the interstitial lineage of *Hydra*, from which specialized cells are derived, dual immunostaining was performed using a transgenic strain of *H. vulgaris* (AEP) expressing eGFP in neurons, interstitial stem cells, nematoblasts, gland cells, and spermatogonia (actin-eGFP^{icy}) (Wittlieb *et al.*, 2006).

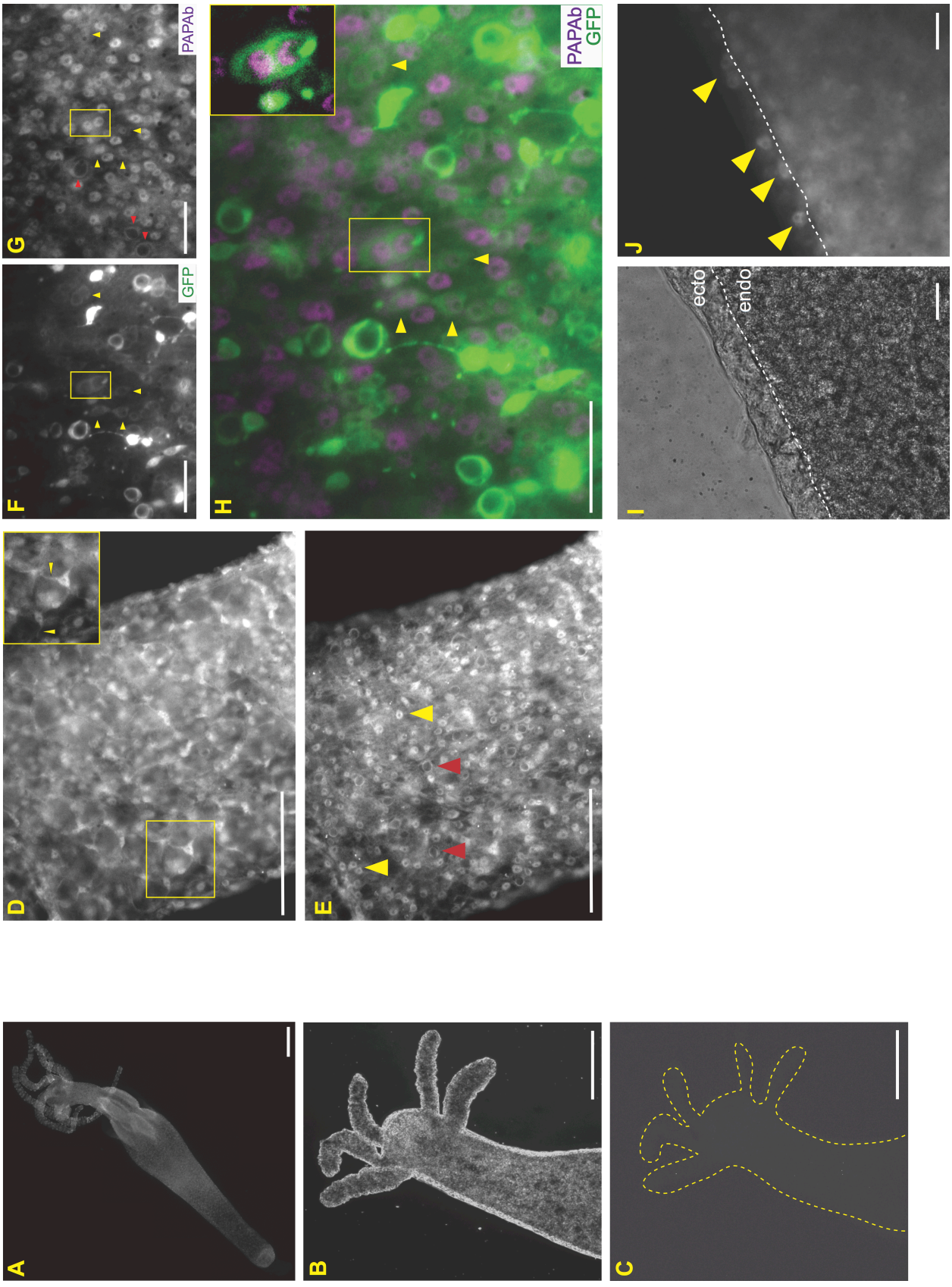
A
B
C
D
E
F
GFP
G
PAPAb
H
PAPAb
GFP
I
ecto
endo
J

Fig. 4.11: mutually exclusive staining of whole fixed *H. vulgaris* (AEP) polyps with affinity-purified Day 72 PA5619 anti-P2X antibody

Fluorescence micrographs of whole, fixed *H. vulgaris* (AEP) polyps using a peptide affinity-purified polyclonal antibody (PAPAb) derived from Day 72 PA5619 antiserum. ***A***, fluorescence micrograph of PAPAb immunostained polyp illustrating staining of structures throughout. No staining of structures was seen in the absence of PAPAb (***B***, representative brightfield image of polyp incubated with secondary antibody (2 ug) alone. ***C***, fluorescence micrograph of polyp ***B***, illustrating absence of staining in presence of secondary antibody alone. The polyp outline is highlighted by a dashed yellow line. ***D***, representative immunofluorescence image of the body column of a PAPAb-stained polyp (1:500; 10 µg/ml). PAPAb stained neuronal-type structures. Inset (yellow box) highlights a bi- and tripolar ganglionic neuron, with dendrites further highlighted by yellow arrows. Adjustment of focal plane upwards (towards viewer) revealed the staining of multiple structures. Structures highlighted by yellow arrows are present throughout a polyp, whilst single stenotele nematocysts are highlighted by red arrows. ***F***, anti-GFP fluorescence micrograph of transgenic actin-eGFP^{icy} illustrating GFP localisation GFP interstitial stem cells and derivatives of this lineage (red arrows = stenotele nematocysts; yellow arrows = interstitial stem cells). ***G***, immunofluorescence image of the same polyp using PAPAb revealed staining in nematocyst structure. ***H***, overlay image of ***F*** (green) and ***G*** (false coloured purple), revealed co-localisation of PAPAb staining in the nuclei, but not nucleoli, of interstitial stem cells. Inset highlights this co-localisation in a differentiating pair of interstitial stem cells. ***I, J***, consistent with the localisation of interstitial stem cells, PAPAb fluorescence signal was seen in cells located at the ectodermal (*ecto*)/endodermal (*endo*) epithelial cell boundary (dashed white line). Scale bars: A-C = 500 µm; D and E = 100 µm; F-J = 200 µm.

4.3.6 *H. magnipapillata* promoter-driven expression of eGFP in *H. vulgaris* (AEP) embryos

To investigate the *in vivo* localization of the *aepp2x* gene in live polyps, a plasmid construct was generated to drive expression of eGFP in cells utilizing a genus-specific promoter. In addition, transgenic *Hydra* polyps expressing an aepP2X::eGFP fusion potein could also be used to confirm the specific binding of custom anti-P2X antiserum and peptide antigen-purified antibody, whereby overlying fluorescence would be seen following IHC using an anti-GFP antibody and custom antibody. Although *Hydra* polyps from all known species are capable of reproducing sexually and, as such, are able to develop embryos (Martin *et al.*, 1997), only the 'AEP' strain of *H. vulgaris* can be cultured in laboratory settings to produce viable embryos.

Currently, transcriptomic data are available for *H. vulgaris* (AEP) (Hemmrich and Bosch, 2008). As such, non-transcriptomic sequence data for a gene of interest are

unavailable, making AEP-specific promoter-driven design and reporter expression difficult. However, genomic data are available from *H. magnipapillata* (105) (Chapman *et al.*, 2010). As such, 5' and 3' flanking sequences of a *H. magnipapillata* (105) *p2x* gene were cloned for the generation of a plasmid construct driving the expression of an enhanced GFP (eGFP) coding region cassette in *H. vulgaris* (AEP). The successful use of *H. magnipapillata* flanking sequences in the driven expression of AEP-derived genes has been described previously (Wittlieb *et al.*, 2006; Fraune *et al.*, 2010; Boehm *et al.*, 2012; Franzenburg *et al.*, 2013).

Of 47 embryos injected, 4 expressed eGFP approximately 10-12 months post-injection. eGFP expression did not appear to diminish, but polyps did not emerge from positive embryos and were deemed to be non-viable after a further 3 months of cultivation.

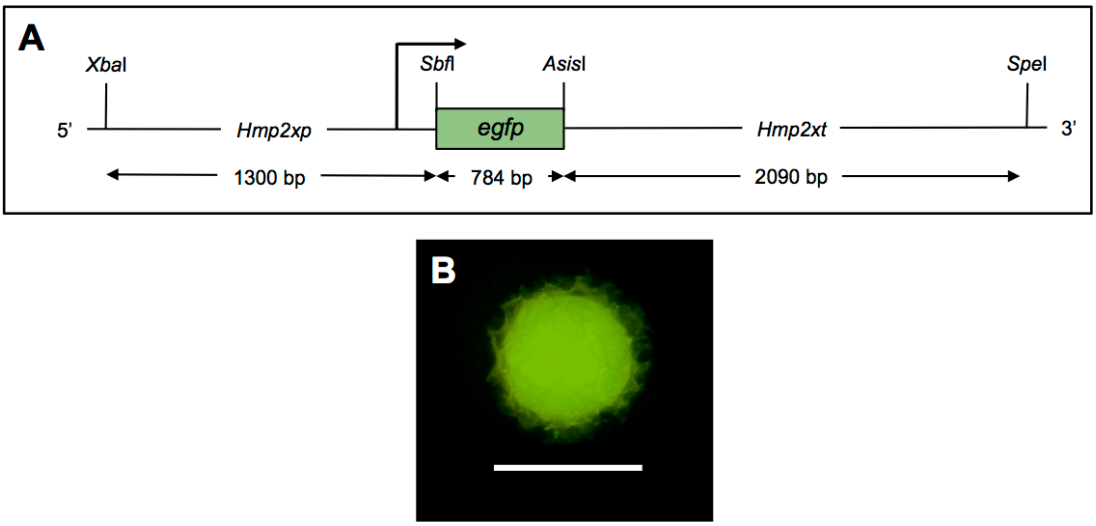

Fig. 4.12: expression of eGFP, driven by a *H. magnipapillata* P2X receptor promoter and terminator.

A, for generation of transgenic *H. vulgaris* (AEP) *Hmp2xp-egfp* transgenic polyps, an eGFP reporter construct was generated. A 1300 bp region amplified from *H. magnipapillata* gDNA corresponding to the 5' flanking region of the putative *H. magnipapillata* P2X receptor gene (*Hmp2xp*) was inserted upstream of an *egfp* cDNA cassette at *Xba*I and *Sbf*I restriction sites. A ca. 2.0 kb 3' flanking region from *H. magnipapillata* gDNA was also amplified and inserted downstream of the *egfp* cassette at *Asis*I and *Spe*I sites. ***B***, darkfield fluorescence image of a *H. vulgaris* (AEP) embryo approximately 12 months post-injection of the *Hmp2xp-efp* plasmid. *Hmp2xp*-efgp transgenic embryos expressed eGFP, but did not hatch. After a further 3 months post-induction of eGFP fluorescence, embryos were deemed non-viable. Scale bar = 1 mm.

4.3.7 Actin-driven expression of a P2X::eGFP fusion protein in endodermal epithelial cells of *Hydra*

Consistent with previous studies utilising actin promoter-driven constructs (Wittlieb *et al.*, 2006), *H. vulgaris* (AEP) embryos injected with *actin-aepp2x::egfp* expressed eGFP 36-48 hours post-injection, with fluorescence restricted to the site of injection. Of 30 embryos injected, 27 hatched within 2-3 months, with 6 of these polyps displaying varying levels of chimerism. eGFP fluorescence was seen at endodermal epithelial cell membranes, with these chimeric polyps expressing eGFP homogenously within 5-6 months post-hatching (4.13D). Polyps gradually decreased in size over a period of 8 months, with tentacles decreasing in length also. Polyps were not able to capture and retain *Artemia* for a sufficiently long period of time to feed effectively.

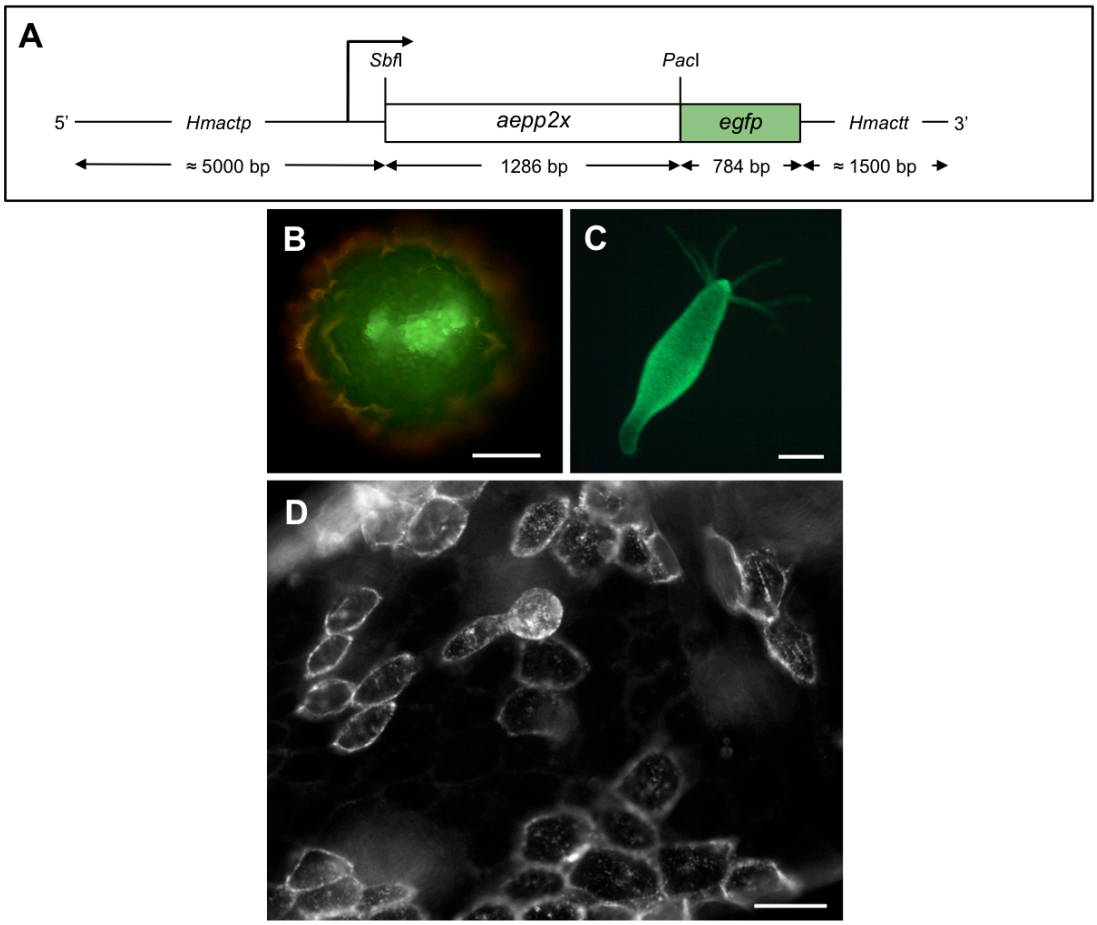

Fig. 4.13: expression of a P2X::eGFP fusion protein in *H. vulgaris* (AEP) polyps

To investigate the effect of overexpression of the coding region of aepp2x in *H. vulgaris* (AEP) polyps, a construct was designed so as to drive the expression of *aepp2x* in polyps under the control of the *H. magnipapillata* (105) actin promoter and terminator sequences. ***A***, *aepp2x* cDNA (1286 bp) was inserted in-frame and upstream of the *egfp* cassette at 5' *Pac*I and 3' *Sbf*I sites in the original 'hotG' plasmid construct (*actin-egfp*), resulting in a 2070 bp fusion cassette (*aepp2x::egfp*). ***B***, darkfield fluorescence micrograph of a *H. vulgaris* (AEP) embryo two days after injection with the *actin-aepp2x::egfp* construct. eGFP fluorescence is seen at focal regions within the embryo, corresponding to the sites of injection of the plasmid. ***C***, darkfield fluorescence image of a transgenic *H. vulgaris* (AEP) polyp homogenously expressing an aepP2X::eGFP fusion protein throughout the polyp (scale bar: 1mm). ***D***, fluorescence micrograph of eGFP-positive cells of a live chimeric transgenic polyp. Approximately 2-3 months post-injection, transgenic *Hydra* polyps hatched from embryos and displayed, corresponding to expression of the aepP2X::eGFP fusion protein in endodermal epithelial cells. Scale bar = 1 mm.

4.4 DISCUSSION

The current study has demonstrated that a member of the Cnidaria phylum expresses a P2X receptor homologue that, when expressed heterologously in HEK293 cells, forms an ATP-gated ion channel. I sought to characterise further this ATP sensitivity for comparative pharmacological analysis with P2X receptors. Although site-directed mutagenesis of conserved residues is beyond the scope of this thesis, the conservation of residues in light of our understanding of the molecular basis of P2X modulation is discussed.

4.4.1 Agonist sensitivity at aepP2X-$(His)_6$

When expressed heterologously, aepP2X revealed an EC_{50} of approximately 120 μM. This is within the range of EC_{50} values calculated from ATP concentration-response analyses of non-mammalian P2X receptor homologues (6 to 511 μM (Fountain, 2013)), but is greater than those recorded from many human subunits (1-10 μM; North and Suprenant, 2000), with the exception of hP2X7 (EC_{50} > 300 μM) (Suprenant *et al.*, 1996; Young *et al.*, 2007). Consistent with all known P2X receptors (North, 2002), the calculated Hill coefficient was found to be greater than 1. These data suggest that occupancy of one of three predicted ATP binding sites by

ATP causes a conformational change in receptor topology so as to increase the effectiveness of other ATP molecules to bind to remaining binding sites and open the channel (Browne and North, 2013).

Human P2X receptors display differential sensitivity to α,β-meATP, with hP2X1 responding to low concentrations (EC_{50} ca.1-3 μM; Valera *et al.*, 1994), whilst currents are not evoked at hP2X7 using concentrations of 1 mM α,β-meATP (Suprenant *et al*). The human P2X4 receptor is weakly activated by α,β-meATP (EC_{50} > 100 μM; Soto *et al.*, 1996a), but fails to elicit a response at the rat P2X4 receptor when expressed in HEK293 cells (Buell *et al.*, 1996; Collo *et al.*, 1996), where it also acts as a competitive antagonist with ATP (Jones *et al.*, 2000). At concentrations in excess of those tested at human P2X subunits (1 mM), the synthetic ATP analogue α,β-meATP fails to elicit a response at aepP2X in HEK293 cells (Fig. 4.4). Similarly, the ATP analogue β,γ-meATP (1 mM) also fails to elicit at a response at aepP2X when expressed in HEK293 cells (Fig. 4.4). β,γ-meATP is a partial agonist at human P2X1, P2X2, P2X3, and P2X7 receptors, but not P2X4 receptors (North and Suprenant, 2000). To date, no residues have been identified in human P2X receptors that may account for lower sensitivity of α,β-meATP compared to ATP. The two agonists share a common adenosine/ribose moiety, but differ in that a methyl group lies between the phosphate groups of the triphosphate moiety. The recent publication of the crystal structure of zfP2X4.1 has demonstrated that the adenine and ribose moiety of ATP lie within a binding site formed at the transmembrane cleft, whilst the triphosphate moiety is only partially exposed to the extracellular milieu (Hattori and Gouaux, 2012). Methyl groups positioned between phosphate moieties of either α,β-meATP or β,γ-meATP may be tolerated because they do no affect the mobility of the phosphates, thus allowing them to still interact with critical residues involved in their co-ordination within the inter-transmembrane binding cleft (L72, L316, N296, and R298; zfP2X4.1 numbering) (Hattori and Gouaux, 2012). The equivalent residues involved in coordination of ATP are conserved in aepP2X (Fig. 4.1).

In studies of the rat (but not human) P2X4 receptor, α,β-meATP also acts as a competitive antagonist to extracellular ATP (Jones *et al.*, 2000). However, firm evidence for the molecular basis of the weak agonist activity of α,β-meATP and β,γ-meATP (and antagonist activity of α,β-meATP at rat P2X4) is not available. As such,

the ineffectiveness of partial agonists at aepP2X may provide a valuable tool for uncovering the molecular basis underlying the pharmacology of partial agonists at P2X receptors.

4.4.2 Antagonist insensitivity at aepP2X-$(His)_6$

The broad-spectrum P2 receptor antagonists suramin and PPADS are largely ineffective at aepP2X in HEK293 cells, requiring pre-incubation to moderately block the receptor. Rat P2X4 displays low sensitivity to suramin and PPADS (Soto *et al.*, 1996b), as does hP2X4 (Garcia-Guzman *et al.*, 1997a). However, in contrast to mammalian P2X4 receptor subunits, prolonged pre-exposure to suramin does result in greater efficacy of the compound in inhibiting ATP-evoked currents (Fig. 4.5C).

At the primary sequence level, both basic and acidic amino acid residues in the extracellular domain (ECD) have been identified as being important in conferring suramin and PPADS sensitivity to P2X receptors. Human P2X1 and P2X2 receptors are blocked by suramin and PPADS (Valera *et al.*, 1994; King *et al.*, 1997), whilst these compounds only weakly block hP2X4 (Buell *et al.*, 1996; Garcia-Guzman *et al.*, 1997a). Multiple sequence alignment of aepP2X with human P2X receptors identified a lysine residue (K249; hP2X1 numbering) between conserved hP2X1 and hP2X2 that is believed to contribute to the selective action of suramin at these subunits. Site-directed mutagenesis of the equivalent glutamate residue in hP2X4 (E249) to lysine restores PPADS sensitivity in hP2X4 (Buell *et al.*, 1996). Alignment of aepP2X with hP2X1-7 reveals a leucine residue at this equivalent position (L268), which may account for the weak action of PPADS at this receptor. Similarly, rat P2X4 also displays low sensitivity to suramin and PPADS (Soto *et al.*, 1996a). Mutation of Q78 to lysine (Q78K) increases the efficacy of suramin at rP2X4 (Garcia-Guzman *et al.*, 1997a). This glutamate residue is not conserved in aepP2X, with an asparagine residue lying at the equivalent position (N79).

Recent mutational analysis of basic ECD residues has identified K138 as being involved in conferring suramin sensitivity to hP2X1 (Sim *et al.*, 2008). However, El-Ajouz *et al*. have not identified this residue as being important in hP2X1, although a K136D mutation does reduce the ability of suramin to antagonise ATP-evoked

currents (El-Ajouz *et al.*, 2012). Of these two residues, only K136 is conserved in aepP2X, whilst isoleucine is found in place of K138. A region of aromatic amino acids, close to the TMDs, has also been shown to increase the efficacy of suramin at hP2X1 (Roberts and Evans, 2004). Alanine substitutions at these positions (W85, Y90, F100, F291, F293, and F311) showed the greatest effect in reducing efficacy of suramin at hP2X1; aromatic residues are found at all equivalent positions in aepP2X (Roberts and Evans, 2004). Of these aromatic residues, tyrosine residues are found in place of equivalent W85 and F311 residues. The shared polar chemistry of these tryptophan and tyrosine residues means it is unlikely that these substitutions are responsible for the ineffectiveness of suramin in co-application with ATP at aepP2X.

Brilliant blue G (BBG) displays greatest efficacy as an antagonist at P2X7 subunits, and is largely ineffective at P2X4 subunits (Jiang *et al.*, 2000a). Consistent with the P2X4-type sequence identity of aepP2X, BBG is ineffective at the receptor when expressed in HEK293 cells (Fig. 4.5). Residues implicated in the action of BBG at P2X7 have not yet been identified, although it is possible that due to the shared polysulphonate structure of BBG with suramin, those residues implicated in suramin binding at P2X receptors are also responsible for the action of BBG at P2X4 and P2X7 (Jiang *et al.*, 2000a). Phenol red is ineffective at P2X4 receptor subunits (King *et al.*, 2005). Consistent with its inclusion with group II type P2X receptors (within which lies P2X4) (MacKenzie *et al.*, 1999), aepP2X is also not antagonised by phenol red. The carbon monoxide donor CORM-2 (tricarbonyldichlororuthenium(II) dimer) displays subtype-specific activity, potentiating ATP-evoked currents at P2X2 (Wilkinson *et al.*, 2009), but inhibiting currents at P2X4 (Wilkinson and Kemp, 2011). CORM-2 application does not significantly modify ATP-evoked currents at aepP2X-$(His)_6$ where, due to the high primary sequence identity of the receptor to hP2X4, it may be expected to inhibit currents in HEK293 cells. There are currently no reports of individual residues required for the action of CORM-2 at P2X2 and P2X4.

4.4.3 Ivermectin activity at aepP2X-$(His)_6$

As with hP2X4 receptors, ivermectin (IVM) potentiates ATP-evoked currents at aepP2X. Two mechanisms by which IVM may potentiate P2X4 currents have been proposed. P2X4 receptors have been shown to be cycled to and from the plasma

membrane (Bobanović *et al.*, 2002). In hP2X4 receptors, this cycling is dependent on the interaction of the AP2 adaptor complex with a C-terminal 'YGxxL' motif (Royle *et al.*, 2005). Mutation of this motif in P2X4 receptors results in the decreased internalisation, and increased surface membrane, expression of P2X4 (Royle *et al.*, 2005). In an AP2-null P2X4 receptor expressing cell line, (resulting in the disruption of an AP2/P2X4 interaction), it was demonstrated that IVM does not potentiate P2X4 currents (Toulmé *et al.*, 2006). In contrast, IVM potentiates P2X4 receptors in wild-type cells, and also increased the fraction of P2X4 receptors at the cell surface when expressed at a low channel density (Toulmé *et al.*, 2006). The C-terminal 'YGxxL' motif shown to be required for the increased membrane insertion following IVM application (Toulmé *et al.*, 2006) was not identified in aepP2X. This may suggest that IVM acts via another mechanism independent of potential modulation of aepP2X receptor membrane insertion and internalisation cycling.

IVM has also been shown to modulate P2X currents through the stabilisation of the receptor in its ATP-bound, open state (Priel and Silberberg, 2004). Further analysis in rat P2X4 has also demonstrated that IVM interacts allosterically with TMD residues positioned close to the protein-lipid bilayer surface (Silberberg *et al.*, 2007). Site-directed mutagenesis of TM1 and TM2 in rat P2X4 has identified residues that that lie in close proximity to each other at the TMD interface (Silberberg *et al.*, 2007). Point mutation of the TM1 residues (rat P2X4 numbering) I39, V42, V43, and V47, and the TM2 residues G342, L345, and V348 all resulted in a significant reduction in the efficacy of IVM at the receptor (Silberberg *et al.*, 2007). This suggested that IVM binds at the open-state cleft between TM1 and TM2 (Silberberg *et al.*, 2007). Furthermore, although a number of residues have been identified as being important in conferring the action of IVM at P2X4 receptors (Jelínkova *et al.*, 2008), a conserved binding motif has not been identified amongst receptors that are IVM-sensitive (Silberberg *et al.*, 2007; Jelínkova *et al.*, 2008), suggesting that a major determinant of IVM action is the shape of the hydrophobic crevice situated at the lipid-protein interface between transmembrane domains (Silberberg *et al*., 2007). With the exception of L345, all these residues are conserved in aepP2X, and may suggest that the common action of IVM between mammalian P2X receptors and aepP2X may be due to the shared hydrophobic environment crevice between TM1 and TM2, rather than an absolute requirement of a shared amino acid identity between P2X4 receptor subunits.

4.4.4 Ion permeability through aepP2X-$(His)_6$

When expressed heterologously in HEK293 cells, aepP2X-$(His)_6$ is permeable to Na^+, K^+ and Ca^{2+}, but is relatively impermeable to the larger inorganic cations $NMDG^+$, $Tris^+$, and to the large monovalent anion gluconate. This finding is in accordance with the ionic permeability of higher P2X receptors, as well as homologous characterised from lower organisms, such as *O. tauri* (Fountain *et al.*, 2008).

Whilst many P2X receptors display a significant permeability to Ca^{2+} ions (Evans *et al.*, 1996; Virginio *et al.*, 1998a; Agboh *et al.*, 2004), the algal P2X receptor from *O. tauri* is relatively impermeable to Ca^{2+} (Fountain *et al.*, 2008). This was found to be due to the presence of an asparagine residue (N353) lying in TM2, which is present as an aspartate residue across human P2X1-7 receptors. Subsequent substitution of N353 for aspartate (N354D) restores Ca^{2+} permeability in the *O. tauri* P2X receptor (Fountain *et al.*, 2008). In contrast, aepP2X displays Ca^{2+} ion permeability in experiments reintroducing 5 mM $CaCl_2$ in the presence of the non-permeant cation $NMDG^+$, resulting in a rightward shift in reversal potential. Analysis of the primary sequence of aepP2X reveals that, at the equivalent position to the *O. tauri* P2X receptor N353, residue is a glutamate residue (E268). This lends support to the consensus that a polar acidic residue present at this position endows Ca^{2+} ion permeability to P2X receptors (Samways and Egan, 2007).

Analysis of polar residues forming the channel pore of rat P2X2 has also highlighted the role of these residues in modulating cation permeability through the receptor (Migita *et al.*, 2001a). Mutagenesis of three polar residues (T336, T339, and S340; rP2X2 numbering) to tyrosine, thus reducing pore diameter through the introduction of a larger side chain, significantly reduced the channel's permeability to Ca^{2+} (Migita *et al.*, 2001a). These residues are present as either an alanine (T336A and T339A) or a leucine (S340L) residue in aepP2X, suggesting that hydrophobicity, but not polar nature of amino acids, is not an essential feature of residues in TM2 for conferring Ca^{2+} ion permeability in P2X receptors. Most of these residues are non-polar in other P2X receptors, supporting the view that hydrophobicity, rather than polarity of residues in TM2 at these positions are the primary determinants of Ca^{2+} permeability (Jiang *et al.*, 2013).

4.4.5 aepP2X immunohistochemistry: localisation of a P2X receptor in a phylum-specific structure?

Immunostaining of whole, fixed *H. vulgaris* (AEP) polyps using an antiserum raised against an antigenic region of the aepP2X C-terminus suggests expression of the receptor in differentiating and pre-mature nematocysts (Fig. 4.9C-G). Nematocysts develop within nematocytes, forming through the addition of protein-filled vesicles of the Golgi apparatus. Nematocytes arise from the interstitial stem cell lineage after having undergone five mitotic steps to form clusters of immature nematocytes termed nematoblasts (Bode and David, 1978). The differentiation of interstitial cells to nematoblasts, and subsequent development of nematocyst capsules within these cells occurs in the body column (Slautterback and Fawcett, 1959). Staining of clusters consisting of 4-16 structures of the same size and morphology using anti-aepP2X antiserum supports the finding that structures stained are differentiating nematocytes (nematoblasts) (Fig. 4.9). Furthermore, staining is also seen in mature stenotele and desmoneme nematocysts in polyp tentacles. In both staining patterns (mature and differentiating nematocysts), it is unclear whether the nematocyst proper is stained, or staining lies at the boundary between the nematocyst capsule and surrounding nematocyte. In support of staining of the nematocyst capsule, a decrease in fluorescence signal is seen at the apex of stained structures (Fig. 4.9C). This is consistent with the presence of an operculum through which a penetrating stylet evaginates following stimulation (Holstein and Tardent, 1984).

Staining using a peptide affinity-purified form of the same antiserum suggests staining in interstitial stem cell nuclei, with some single, mature stenotele nematocysts also displaying staining. No staining is seen in nematocyst clusters within the body column, as seen in antiserum staining (Fig. 4.11D and E). In support of the pattern of staining seen with antiserum, analysis of the primary aepP2X protein sequence using PSORT (Prediction of Protein Sorting Signals and Localization Sites in Amino Acid Sequences) II (Horton and Nakai, 1997) (available at: http://psort.hgc.jp/form2.html) does not identify with great probability the presence of nuclear sublocalisation sequences that may contribute to the transport of aepP2X to nuclei. P2X7 mRNA has been detected at the nuclear envelope of rat inhibitory hippocampal neurons (Atkinson *et al.*, 2002). However, some authors have disputed these findings (Sim *et al.*, 2004), highlighting that Atkinson and colleagues had not

performed appropriate negative controls using rodents deficient in P2X7. In their study, Sim *et al.* found nuclear staining in both wild-type mice, and the two currently available P2X7 knockout rats (Solle *et al.*, 2001; Ke *et al.*, 2003) using the same C-terminal P2X7 antibody used by Atkinson *et al*. (2002). As such, it was suggested by Sim *et al.* (2004) that apparent P2X7 nuclear staining in hippocampal neuron nuclei (Atkinson *et al.*, 2002) is a non-specific reaction with this antibody. No further nuclear localisation for other P2X receptor subunits has been reported in the literature. In *Hydra*, a non-canonical nucleolar localisation for a putative NMDA receptor has been described in large and small interstitial stem cells, neuroblasts, mature neurons, nematoblasts, and epithelial cells, using a monoclonal antibody against NMDA receptor subtype 1 (Scappaticci *et al.*, 2004; Kass-Simon *et al.*, 2009). However, the functional relevance of this localisation has not been determined.

The peptide affinity-purified antibody (PAPAb) also appears to stain ganglionic neuron cells in the body column of *Hydra* (Fig. 4.11D). This staining was not seen in immunostaining studies using the corresponding whole antiserum. Whilst P2X receptors are widely expressed in the nervous systems of higher organisms (Burnstock, 2014), and in the nervous system of the mollusc *L. stagnalis* (Bavan *et al.*, 2012), evidence for a role of ATP in neuronal transmission in Cnidaria is lacking. Quinacrine staining in the sea anemone *Actina equina* localises ATP to the apical cytoplasm of sensory neurons in hair bundles (Knight *et al.*, 1992), a structure analogous to the vertebrate acousticolateralis system. In the present study, incubation of whole polyps with quinacrine resulted in staining of nematocysts, including those in clusters and mature forms (Figs. 4.10A, B, and D), but not in neurons. Quinacrine has been used previously to identify adenine compound-contained vesicles in neurons (Bock, 1980; Knight *et al.*, 1992). Concurrently, staining in polyps seen following incubation with quinacrine (Figs. 4.10A, B, and D) may suggest the presence of ATP within nematocysts. However, quinacrine has also been used in the identification of cellular regions of low pH (Pierzyńska-Mach *et al.*, 2014) that may be independent of the presence of ATP. The accumulation of quinacrine in nematocysts may coincide with the final maturation steps of the organelle, which requires the establishment of a proton gradient across the capsule wall (Berking and Hermann, 2006). This requires the establishment of a proton gradient across the capsule wall that results in the formation of poly-γ-glutamate aggregates that store potential energy required for rapid nematocyst stylet firing (Berking and Hermann, 2006). Conversely, quinacrine

fluorescence could also represent a high ATP concentration component of toxin within the capsule, as has been demonstrated in tarantula spider toxins (Chan *et al.*, 1975). A viable culture of transgenic *H. vulgaris* (AEP) polyps, expressing either an eGFP reporter construct for visualisation of P2X receptor localisation *in vivo* (Fig. 4.12) would have been a valuable tool in the confirmation of binding of antiserum or purified antibody. Only one *p2x* gene appears to present in *H. vulgaris* (AEP) (section 3.3.6). Knockdown of this gene through RNA interference, or development of a *p2x*-null transgenic strain of *H. vulgaris* (AEP) would also aid in the validation of specificity of either the antiserum or purified antibody as binding to aepP2X in whole polyps.

A role for ATP in the maturation of nematocysts has been described in isolated nematocysts of the sea anemones (Cnidaria; class Anthozoa) *Diadumene lineata* (orange-striped green sea anemone) and *Metridium senile* (frilled anemone) (Greenwood *et al.*, 1989). Incubation of isolated nematocysts in a solution of 1.5 mM ATP solution for 3-5 days results in a lower percentage of late-stage immature nematocysts, suggesting that ATP may be involved in the maintenance and differentiation of nematocysts in these organisms (Greenwood *et al.*, 1989). In addition, it was found ATP was depleted more rapidly in isolations of undischarged nematocysts compared to those that were discharged (Greenwood *et al.*, 1989) although, in their study, it appears that Greenwood *et al.* (1989) did not replenish the ATP solution in which nematocysts were suspended, and may complicate findings through the presence of hydrolysation products of ATP (ADP, AMP, adenosine) acting at multiple effectors. The precise role of ATP in nematocyst development is unclear, although Greenwood *et al.* (1989) does suggest that ATP may act at soluble ATPase enzymes within the toxin of nematocysts, or at capsule wall-embedded ATPases. In addition, it has been suggested that ATP may be required in the final acidification step of the inner cyst that renders nematocysts functional (Berking and Hermann, 2006). In the scyphozoan *Pelagia noctiluca* (mauve stinger), an acute role for nucleotides in nematocyst function has been demonstrated. Incubation of dissected tentacles in solutions of 0.1 or 1 mM ATP causes an increase in the number of discharged nematocysts in response to mechanical stimulation (Morabito *et al.*, 2012). cAMP also elicited a similar response at the same concentrations and moreover, depletion of Ca^{2+} ions in the bathing solution (albeit in the absence of ATP or cAMP) reduced the number of discharge nematocysts upon mechanical stimulation

(Morabito *et al.*, 2012). Despite these findings, the site of action of ATP remains unclear, especially in light of the presence of other cell types of the tentacles used in the Morabito *et al.* (2012), including encapsulating nematocytes and neurons.

If the staining pattern seen when polyps incubated with antiserum is representative of the expression of the *H. vulgaris* (AEP) P2X receptor *in vivo*, this may suggest that the receptor plays a functional role in differentiating nematocysts. *Hydra* polyps display substantial tissue plasticity, in so much that interstitial stem cells are in a constant cycle of self-renewal, and differentiation into terminal products (David, 2012). These terminal products, which include nematocysts (and their Golgi apparatus-derived nematocyst organelle), are also in a state of flux, migrating to their final destination either during late differentiation, following maturation in the body column (as is the case with nematocytes). Beyond the scope of the current thesis is the determination of the orientation of the *H. vulgaris* (AEP) P2X receptor within nematocytes: is the receptor orientated with the ECD towards the nematocyst lumen, or towards the encapsulating nematocyte? Some P2X receptors are inhibited by H^+ ions (North, 2002), including the P2X4 receptor (Stoop *et al.*, 1997; Clarke *et al.*, 2000), with which aepP2X shares the greater sequence identity amongst human P2X subunits (section 4.3.1). The low pH within the nematocyst may inhibit aepP2X receptor orientated towards the nematocyst lumen. However, a histidine residue (H286; hP2X4 numbering) has been shown to confer P2X sensitivity in hP2X4 (Clarke *et al.*, 2000) is not shared in aepP2X, where an aspartate residue is found in its place (D302). Mutational analysis of the rat P2X7 ECD has identified a number of amino acid residues that, when mutagenised, reduce the potency of H^+ ions in the inhibition of ATP-evoked currents (Liu *et al.*, 2009a). Of the seven residues found to disrupt proton-mediated inhibition modulation of the receptor (H85, K110, K137, H219, and D197; rat P2X7 numbering) (Liu *et al.*, 2009a), only H219 is shared at the equivalent position (H237). The lack of conservation of residues implicated in inhibition by protons between higher P2X receptors and aepP2X may suggest that aepP2X is not modulated by pH. However, it is conceivable that other residues exist that may confer pH sensitivity to aepP2X, if it is modulated by pH.

In a situation where aepP2X is orientated with the ECD facing the nematocyst lumen, aepP2X may play a role as a sensor of intracellular ATP, as has been found in *Dictyostelium* P2X receptor subunits (Fountain *et al.*, 2007; Sivaramakrishnan and

Fountain, 2012b; Baines *et al.*, 2013) where *Dd*P2XA is orientated facing the acidic and calcium-enriched contractile vacuole (CV). Indeed, in *D. discoideum*, it has been proposed that ATP is translocated from outside of the CV *via* a vesicular adenine nucleotide transporter (VNUT), where it acts at *Dd*P2X receptors to activate receptor-mediate Ca^{2+} ion efflux from the CV (Sivaramakrishnan and Fountain, 2012b). The expression of a P2X receptor in an early metazoan organism would represent a major advance in the field as it could suggest a conserved intracellular function for a P2X through evolution.

However, aepP2X may also play a more acute role in nematocyst function. Incubation of isolated, whole tentacles from the cnidarian *P. noctiluca* (class: Scyphozoa) with ATP appears to sensitize nematocysts to mechanical stimulation (Morabito *et al.*, 2012), although it may be that ATP acts at a non-nematocytic effector within the tentacle. Indeed, modulation of mature stenotele and desmoneme nematocyst activity (via adjoining sensory neurons) by the neurotransmitters, GABA and glutamate has been reported in whole *H. vulgaris* tentacle preparations (Kass-Simon and Scappaticci Jr., 2004). This acute action of ATP in the modulation of nematocyst function may be supported if aepP2X is orientated with the extracellular, ATP-binding domain is exposed to an environment into which ATP is readily available from an external source. In the California spiny lobster, *Panulirus interruptus*, it has been hypothesised that ATP, acting through P2-like receptors acts as a signalling molecule in the detection of nucleotides that are released from cells of recently dead prey tissue (Carr *et al.*, 1986; Zimmer-Faust *et al.*, 1988). Incubation of fixed polyps with crude antiserum stains mature stenotele and desmoneme nematocysts in tentacles (section 4.3.3). It is known that both mechanical and chemical cues are involved in the discharge of mature nematocysts *Hydra*, and can stimulate discharge independent of sensory nerve activation (Aeme *et al.*, 1991). Mechanical stimulation of the apical cnidocil (see section 1.7.4.3) elicits an action potential in adjacent sensory neurons, and the Ca^{2+}-dependent discharge of the nematocyst inner stylet (Santoro and Salleo, 1991; Watson and Hessinger, 1994). Mechanical stimulation may arise from the contact of prey with tentacles, resulting in their penetration and capture (Özbek *et al.*, 2009b). Whilst *Hydra* polyps are not known to feed on decaying tissue, studies in other cnidarians have demonstrated that the application of aqueous extracts of prey results a burst of electrical activity in neurons associated with nematocysts (Purcell and Anderson, 1995; Price and

Anderson, 2006). ATP is present in cells of all animals; penetration of prey may result in the release of ATP, which could act at effectors in tentacles. If aepP2X is present in mature nematocysts in the tentacles, the receptor may be responsible transducing ATP release from prey into a functional role in feeding in *Hydra.*

Due to the mutually exclusive staining seen with antiserum raised against aepP2X, and the corresponding peptide-affinity purified antibody, it is as still unclear whether the staining pattern seen with anti-aepP2X antiserum is true to its expression pattern seen *in vivo*. If aepP2X is expressed in developing nematocysts, evidence from the literature for a role of ATP in the maturation of his organelle may hint at a role for the receptor in their development. However, considerable evidence exists for a functional role of neurotransmitters in *Hydra* and other members of the Cnidaria phylum. Whilst this evidence suggests the expression of neurotransmitter receptors for GABA and glutamate in neurons of Cnidaria, staining was only seen in PAPAb-treated polyps. The use of transgenic strains of *Hydra* that express eGFP in cells utilising the *aepp2x* receptor gene promoter may provide a novel and valuable tool for determining which staining pattern is representative of *in vivo* aepP2X localisation. In addition, viable polyps overexpressing aepP2X C-terminally fused to eGFP would also be valuable in confirming immunostaining patterns of either antiserum or peptide peptide affinity-purified anti-aepP2X antibody.

There appear to be no reports in the literature of mutually exclusive staining patterns between polyclonal antiserum and its corresponding purified antibody. As an external party performed the rabbit immunisations in the generation of a custom antibody, it is not possible to comment on the exact methodology by which custom antiserum and purified antibody were produced. It may be that an error occurred during this manufacturing process that resulted in the mishandling, or mislabeling of antiserum or purified antibody. Further work using the antiserum and purified antibody provided is required to ascertain whether staining patterns seen in polyps is true to the *in vivo* expression pattern of aepP2X. Due to time and funding constraints, it was not possible to repeat rabbit immunisations to ensure that downstream user error is not the underlying cause of the mutually exclusive staining patterns described in the current thesis.

4.5 CONCLUSIONS

1. *H. vulgaris* (AEP) expresses a P2X receptor homologue that responds in a concentration-dependent manner to extracellular ATP application when expressed heterologously in HEK293 cells. Calculation of the Hill coefficient of the concentration-response relationship to ATP suggests co-operative binding at aepP2X-$(His)_6$.
2. The insensitivity of aepP2X to the synthetic ATP analogues α,β-meATP and β,γ-meATP may prove the receptor a valuable tool in uncovering the molecular basis for partial agonist activity at P2X receptors.
3. ATP-evoked currents at aepP2X-$(His)_6$ are insensitive to modulation by classical P2 receptor antagonists. Only pre-application of suramin or PPADS for 90 s prior to co-application with a sub-EC_{50} concentration of ATP inhibits ATP-evoked currents through the receptor, albeit moderately. Similarly, aepP2X may prove a valuable tool in investigating antagonist insensitivity of specific P2X receptor subunits.
4. Relative cation permeabilities through aepP2X-$(His)_6$ are comparable to mammalian P2X receptors, and suggests a cation-selective ion channel. Consistent with the majority of P2X receptors currently known, aepP2X does not demonstrate a significant chloride ion or large cation permeability when expressed heterologously in HEK293 cells.
5. Incubation of polyps with a polyclonal antiserum raised against an antigenic region located in the C-terminus of aepP2X results in immunostaining of pre-mature/late-stage differentiating stenotele and nematocysts, often within characteristic clusters of proliferating nematoblasts. Staining is found in the body column of polyps, with a sharp border between the peduncle and head regions.
6. Unexpectedly, IHC in whole fixed polyps with a peptide affinity-purified form of the antiserum results in pattern of immunostaining that is mutually exclusive to that seen with the corresponding antiserum (in ganglionic nerve cell soma and dendrites and nucleoli of 1s and 2s interstitial stem cells). The reasoning for this difference in staining is not clear, although no nuclear localisation signals that may support the suggested expression of aepP2X in nuclear compartments are identified in the primary amino acid sequence of the receptor.

7. An aepP2X::eGFP fusion protein can be expressed, under the control of the β-actin promoter. Whilst eGFP can also be expressed in embryos of *H. vulgaris* (AEP), these embryos were not viable and did not hatch.

Chapter 5:

Cloning and electrophysiological analysis of novel P2X receptors from representative members of three invertebrate phyla

5 Cloning and electrophysiological analysis of novel P2X receptors from representative members of three invertebrate phyla

5.1 AIMS OF THE CHAPTER

In addition to the cloning of a novel P2X receptor from *H. vulgaris* (AEP), homology searching of genomic datasets identified candidate receptors in members of the Crustacea and Cephalochordata subphyla, as well as in a member of the Placazoa phylum. The current chapter describes the cloning and preliminary pharmacological analysis of novel P2X receptor homologues from a member of each group: *Daphnia pulex*; *Trichoplax adhaerens*; and *Branchiostoma floridae*, following their identification by homology searching of their respective genomes. These data are discussed in relation to our current understanding of receptor pharmacology in those organisms from which P2X receptors have been characterised. Furthermore, pharmacological data are placed in the wider context of organism biology and the placement of these novel P2X receptors through evolution.

5.2 INTRODUCTION

D. pulex, a microcrustacean and member of the large Arthropoda phylum (Colbourne *et al.*, 2011), is a representative species of the Crustacea subphylum. Bioinformatic analysis suggested that P2X receptors are seemingly absent from a number of dipteran insects, but are present in other Insecta orders. P2X receptor homologues have been identified in a member of the Arachnida class of arthropods, (Bavan *et al.*, 2011), but an understanding of P2X receptor function in the Arthropoda is unknown. Recent and comprehensive phylogenetic analysis of the Arthropoda places hexapods (and thus insects) as a paraphyletic group within Crustacea, whilst remaining a sister taxon to Hexapoda and sharing a common Pancrustacean ancestor (Legg *et al.*, 2013). Characterisation of *Daphnia* P2X receptors may provide a greater understanding of their function in the Arthropoda.

Finally, candidate P2X receptors from the representative, and only member species, of the Placazoa phylum *Trichoplax adhaerens* were chosen for further analysis due to the apparent absence of large protein regions containing residues thought to be important in the binding of ATP in higher P2X receptors (section 3.3.10). In addition, the phylogenetic position of *T. adhaerens* as a basal metazoan, emerging after the appearance of demosponges (Srivastava *et al.*, 2008), provides greater insight into the function and pharmacology of P2X receptors in multicellular organisms as well as expanding our knowledge of their evolutionary origin.

5.2.1 Ion channels in *Daphnia*

Our understanding of the complement of ion channels in *Daphnia* has been greatly enhanced following the availability of the genome sequence of one of these microcrustaceans (Colbourne *et al.*, 2011). Data are available from homology searching and phylogenomic analyses of genes predicted to encode for ion channels in this organism. Putative ion channel gene homologues encoding for the voltage-dependent ERG ('Ether-a-go-go') potassium channel (Martinson *et al.*, 2014) and a number of voltage-gated sodium (Na_v) channels (Li *et al.*, 2011) have ben described.

Effects of three commonly used benzodiazepines (positive allosteric modulators of the $GABA_A$ receptor), midazolam, pentobarbital, and ketamine, on expression levels of 108 mRNA transcripts predicted to encode for ion channels in *Daphnia* has been reported (Dong *et al.*, 2013). In that study, these compounds were all found to immobilise live daphnids, and incubation of daphnids in solutions of either one of these compounds altered mRNA transcript expression levels of a number of both VGICs, and LGICs (Dong *et al.*, 2013). For instance, incubation with 100 μM midazolam resulted in the upregulation of 19 ion channel genes, including those encoding for the cyclic nucleotide-gated (CNG) channel α1 (CNGA1), N-methyl D-aspartate 1 receptor (NMDAR1), and epithelial Na^+ channel (ENaC) (Dong *et al.*, 2013). Interestingly, the mRNA level of one of two predicted P2X receptor genes was also found to be upregulated (Dong *et al.*, 2013) following midazolam incubation. Co-incubation of midazolam with 10 μM flumazenil (a $GABA_A$ receptor antagonist (Fung and Fillenz, 1984)) prevented this increase, but did not downregulate P2X transcript levels below that seen in control, non-treated daphnids (Dong *et al.*, 2013).

Whilst no physiological role for P2X receptors in *Daphnia* has been suggested, the findings of Dong *et al*. (2013) may prompt an investigation into a potential functional interaction between P2X receptors and $GABA_A$ receptors proteins. Indeed, it has been reported that cross-talk exists between these two receptors in a number of native tissues, include neurons of the spinal dorsal horn (Hugel and Schlichter, 2000), dorsal root ganglion (Sokolova *et al.*, 2001), and myenteric plexus (Karanjia *et al.*, 2006), whereby co-application of GABA with ATP facilitates recorded current compared to either of these compounds alone. These findings may suggest that a similar interaction occurs between P2X and $GABA_A$ receptors in *Daphnia*. However, the concentration of midazolam used by Dong *et al.* (2013) is approximately 100 times that used in the clinic (Crevat-Pisano *et al.*, 1986). Whilst the pharmacology of the receptor at which midazolam appears to act in *Daphnia* is not known, it may be that the effects on ion channel mRNA levels in daphnids following their incubation in midazolam may be non-specific at the comparatively high concentration used relative to that in humans.

5.2.2 Ion channels in Trichoplax

Despite the absence of neuronal cells within *Trichoplax adhaerens* (Smith *et al.*, 2014), behavioural responses to external stimuli, and immunolocalisation of the neuropeptide RFamide to cells within the animal has been reported (Schuchert, 1993). The publication of the genome of *T. adhaerens* has identified putative genes encoding for ion channel homologues (Srivastava *et al.*, 2008). Amongst predicted genes identified include homologues of the voltage-gated L-type Ca^{2+} α1 and regulatory β-subunit, α- and β-subunits of the voltage-gated K^+ channel (K_v) family, Shaker and Shaw K^+ channel members, the voltage-insensitive K_v9 K^+ channel, and ionotropic glutamate receptors (iGluRs) (Srivastava *et al.*, 2008).

P2X receptors are predicted to be expressed in the genome of *T. adhaerens* (section 3.3.10), and have been alluded to in the literature (Fountain and Burnstock, 2009). However, no physiological role for this group of LGICs has been reported. Following a comprehensive analysis of the cellular anatomy of *T. adhaerens* (Smith *et al.*, 2014), a role for ATP as a putative signalling molecule, acting at P2X receptors, was hypothesised (Jorgensen, 2014). In their original analysis, Smith *et al.* (2014)

illustrated that antibodies against the secretory SNARE (SNAP (Soluble NSF Attachment Protein) REceptor) proteins, syntaxin1, synaptobrevin, and SNAP-25, and synapsin localises this group of proteins to gland cells of *Trichoplax* of the ventral epithelium. These cells are believed to be play a secretory role in *Trichoplax* (Grell and Benwitz, 1971). In the absence of a nervous system in *Trichoplax*, Jorgensen (2014) has suggested that ATP and glutamate may be released from vesicular stores, to act at P2X and ionotropic glutamate receptors, respectively (Jorgensen, 2014).

The functional role of P2X receptors in this organism remains unclear, but immunohistological staining using a custom antibody raised against the peptide sequence of the one predicted *T. adhaerens* P2X receptors (*Tad*P2XB) has suggested expression in fibre cells (Smith *et al.*, 2014). Fibre cells lie between the dorsal and ventral epithelia of *Trichoplax*, and have long processes that extend and make contact with most cells within the interior of the animal, including other fibre cells and lipophil cells (hypothesised to be involved in an, as yet unknown, secretory function) (Smith *et al.*, 2014). The function of fibre cells is not clear. Septal junctions identified at the end of fibre cell processes by transmission electron microscopy (TEM) have been suggested to be syncytial junctions (Grell, 1974). These junctions resemble those seen in excitable cells of syncytia of Hexactinellid sponges (Mackie and Singla, 1983). Neurons are not present in *Trichoplax*, and it is not certain whether junctions formed by fibre cells could support electrical conductivity, and whether this is physiological relevant.

It is unclear whether immunostaining for *Tad*P2XB is specific in the study of Smith *et al.* (2014), as no negative control were referred to. However, if the labelling reported by Smith *et al*. (2014) faithfully reflected the *in vivo* expression of the receptor it could, by its localisation, could indicate an early metazoan function for P2X receptors. Further work is required to determine whether fibre cells could support electrical activity but, if so, could provide evidence for the emergence of a neuronal role for P2X receptors in multicellular organisms.

5.2.3 Ion channels in *Branchisotoma*

In the cephalochordate and chordate proxy, *Branchiostoma floridae*, functional roles for a number of VGICs have been demonstrated. Voltage-gated Ca^{2+} currents have been recorded from muscle cells of *Branchiostoma lanceloteum* (Benterbusch and Melzer, 1992), and appear to resemble voltage-gated Ca^{2+} channel currents seen in human muscle cells (Smirnov and Aaronson, 1992). Furthermore, these Ca^{2+} channel currents recorded from striated and skeletal muscle of *B. floridae* have been characterised as L-type (Rogers and Brown, 2001), based on their inhibition by the L-type Ca^{2+} channel-specific antagonist, nifedipine (Striessnig *et al.*, 1998). In addition, stage-dependent expression of degenerin and amiloride-sensitive Na^{+} channels (DEG/NaC) has been demonstrated in *B. floridae* larvae primary sensory neurons by immunohistochemical methods (Candiani *et al.*, 2006). The expression of Na^{+} channels in *Branchiostoma* is supported by the identification of putative channel protein-encoding genes in the genome of *B. floridae* (Gur Barzilai *et al.*, 2012).

In addition to the characterisation of many VGICs, a number of neurotransmitter-gated GPCRs have also been described in *Branchiostoma* species. For instance, immunohistochemical data has highlighted staining in both the central and peripheral nervous system of *B. lanceolatum* (Anadón *et al.*, 1998), although it is unclear whether the antibodies used in this study are specific for ionotropic $GABA_A$, or metabotropic $GABA_B$ receptor subunits. Immunohistochemical data also exists for the expression of metabotropic serotonin (5-HT) receptors (Van Dongen *et al.*, 1985; Candiani *et al.*, 2005; Moret *et al.*, 2004) and dopamine receptors (Candiani *et al.*, 2005; Burman *et al.*, 2009; Burman and Evans, 2010) in *Branchiostoma* central and peripheral neurons.

The novel evolutionary position of *Daphnia*, *Trichoplax*, and *Branchiostoma* with respect to metazoan evolution could provide a greater understanding of the extent to which P2X receptor are present within the metazoan lineage. Although beyond the scope of the chapter, characterisation of the role of these invertebrate P2X receptors could also identify a new and non-canonical role for a P2X receptor, as well as provide a greater insight into the pharmacology of this unique group of LGICs.

5.3 RESULTS

5.3.1 Cloning of *Daphnia* P2X receptors

Two putative P2X receptors were predicted in the genome of *D. pulex* (section 3.3.4.3), spanning a genomic scaffold ca. 5.2 kbp in length, separated by a region of ca. 1.8 kb (Fig. 5.1).

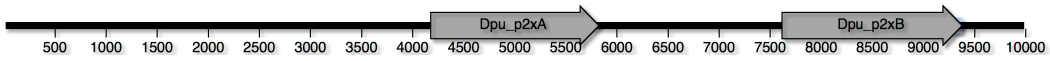

Fig. 5.1: illustration of position of *D. pulex* P2X receptors in the context of a genomic scaffold

The predicted gene sequences for two *D. pulex* P2X receptors (*Dpu*_p2xA and *Dpu*_p2xB) are annotated on the reverse genomic scaffold, but are reversed in the above figure for clarity. A non-coding region of approximately 1.8 kb is predicted to lie between *Dpu*_p2xA and *Dpu*_p2xB.

The two predicted genes are annotated on the reverse genomic scaffold and are referred to herein as *Dpu*_p2xA and *Dpu*_p2xB (in the 5' to 3' direction). *Dpu*_p2xA and *Dpu*_p2xB genes are predicted to contain 7 and 8 exons, and are a total of 1648 and 1765 nucleotides in length, respectively. Predicted translated protein products of these two genes are 393 and 403 amino acids long, and share an 86.9% primary sequence identity with each other. When aligned with hP2X1-7 subunits, *Dpu*_p2xA and *Dpu*_p2xB proteins share a 23.9 to 44.4% primary sequence identity (see section 3.3.4.3).

Prior to the commencement of this aspect of the current project, a full-length cDNA clone of predicted sequence of *Dpu_p2xb* had been synthesised, with the codon usage of the clone reflecting that of humans (section 2.4.5.2.4). Attempts to confirm the existence of *Dpu_p2xA* by PCR using either genomic DNA (gDNA) or cDNA template were unsuccessful, despite a number of primer pairs (detailed in Appendix Tables A8 and A9) being tested in combination with different temperature cycling conditions. A reduced extension temperature of 60 °C has been shown to aid in the amplification of A+T-rich nucleotide sequences by PCR (Su *et al.*, 1996). The predicted *Dpu*_p2xA gene sequence and flanking regions (ranging from primers

DaphA8F and DpuP2XA_R2) (2626 bp) (Fig. 5.2) was composed of approximately 66% adenine and thymine bases. In light of this, extension temperatures of 72 and 60 °C were tested for each primer pair detailed in table 5.1 at the range annealing temperatures tested, for reactions using both gDNA or cDNA as a template. Primer sequences are detailed in the supplementary data.

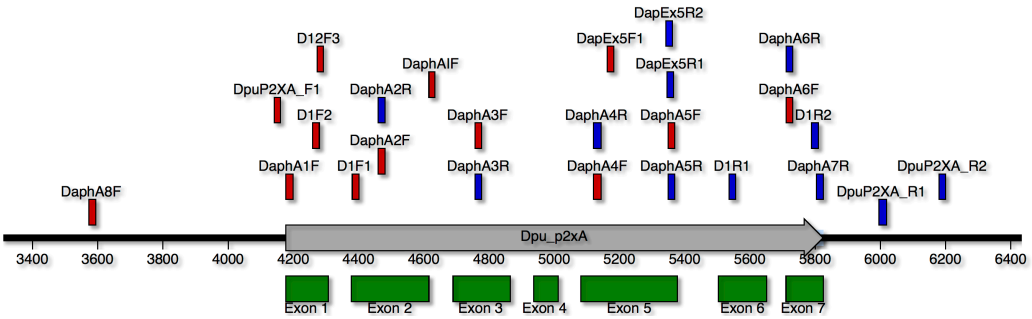

Fig 5.2: position of primers used used in the attempted amplification of the predicted *Dpu*_p2xA nucleotide sequence.

A number of primer pairs positioned within predicted exons (green) of the genomic sequence of *Dpu*_p2xA were tested at annealing temperatures of 45, 47, 50, 52, and 55 °C. Extension temperatures of 60 and 72 °C were tested at each annealing temperature. Primer sequences and combinations used with either genomic or complementary DNA templates are detailed in Appendix Tables 8 and 9, respectively. Predicted exon regions are indicated below *Dpu*_p2xA. Forward and reverse primers are highlighted in blue and red, respectively.

Following the synthesis of the predicted cDNA clone of *Dpu*_p2xB, the receptor was subsequently cloned from *D. pulex* cDNA, and the 3' cDNA end confirmed by 3' RACE (section 2.4.5.2.3.3). The translated product of *Dpu*P2XB was nearly identical to its predicted counterpart, sharing a 99.5% primary sequence identity, with only two amino acid changes present in the sequence encoded by the cloned allele of *Dpu*P2XB (hP2X1 numbering: K217>E and V325>I) (Fig. 5.3).

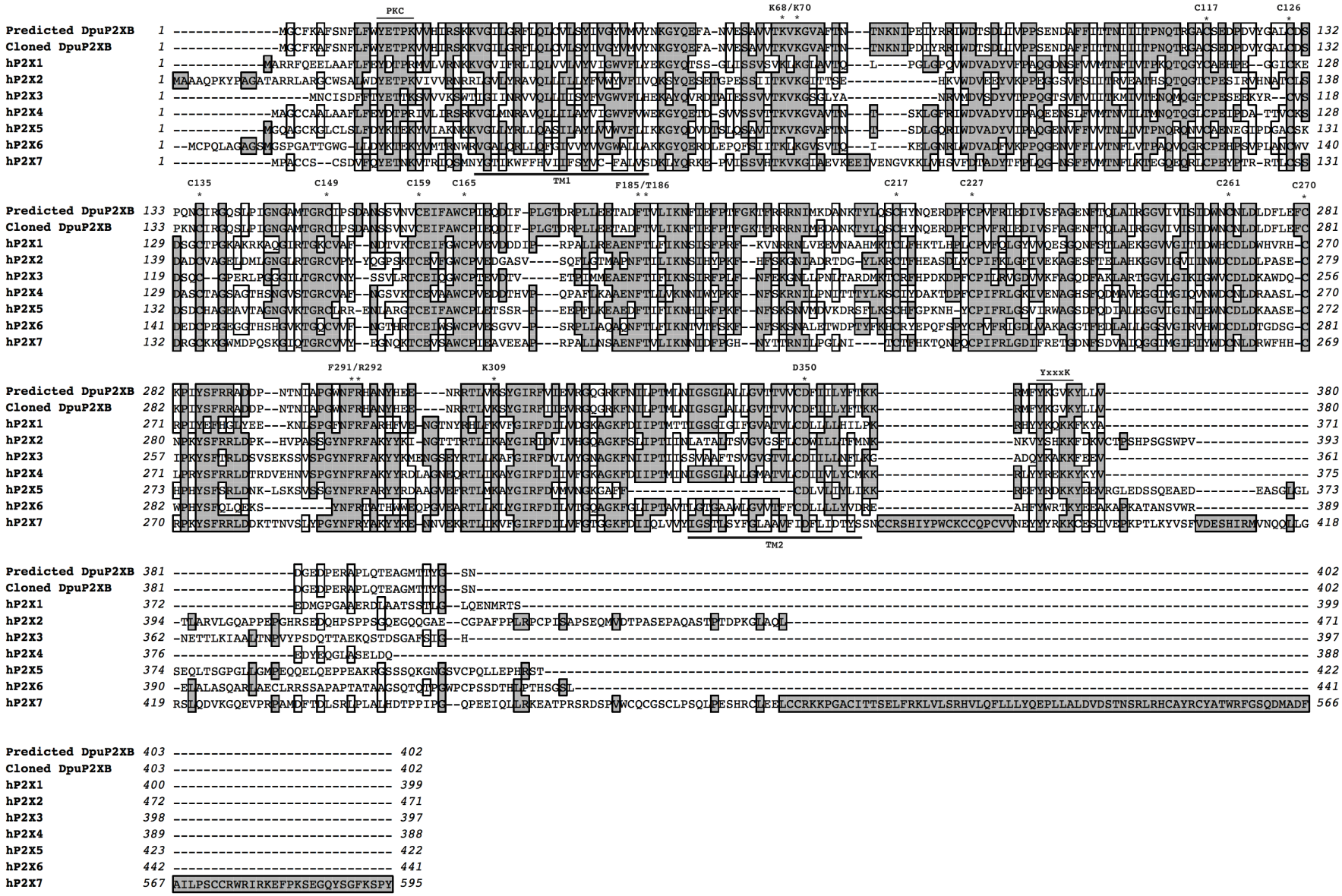
PKC
K68/K70
C117
C126
C135
C149
C159
C165
TM1
F185/T186
C217
C227
C261
C270
F291/R292
K309
D350
YxxxK
TM2
Predicted DpuP2XB
Cloned DpuP2XB
hP2X1
hP2X2
hP2X3
hP2X4
hP2X5
hP2X6
hP2X7

Fig. 5.3: multiple sequence alignment (MSA) of protein sequences predicted and cloned forms of DpuP2XB receptors with hP2X1-7 subunits

Predicted and cloned forms of the *Dpu*P2XB receptor share a 23.9 to 44.4% primary amino acid sequence identity with hP2X1-7 receptors. Residues that are identical between P2X receptors from all three species are outlined and shaded in grey, whilst residues with similar chemical identity are outlined only. Conserved ATP binding residues, an N-terminal PKC phosphorylation motif, and a C-terminal membrane localisation motif are highlighted above the sequences (hP2X1 numbering). Predicted TMDs (based on hP2X1) are highlighted below the alignment sequence. Sequences were aligned using the MUSCLE alignment algorithm (Edgar, 2004) (2.2.2).

5.3.2 Cloning of a *Branchiostoma* P2X receptor

One putative P2X receptor gene appeared to be present in the genome of *B. floridae* (*Bflo*_p2x), as identified by homology searching (section 3.3.2). The predicted translated product of the 1203 bp cDNA of *Bflo*_p2x was determined to be 401 amino acids. The consensus cDNA clone of *Bflo*_p2x receptor (amplified from adult *B. floridae* cDNA kindly provided by Dr Dave Ferrier (Scottish Oceans Institute, The University of St. Andrews, Scotland, UK)), the protein product of which is referred to subsequently as *Bflo*P2X, shared a 93.6% amino acid sequence identity with its predicted counterpart. The cloned form of the predicted *B. floridae* P2X receptor (*Bflo*P2X) was found to share a 24.8 to 46.4% primary sequence identity with hP2X1-7 subunits, and was found to be 425 amino acids in length. Furthermore, a 25 amino acid region within the predicted extracellular domain (ECD) of *Bflo*P2X was found to be included in the cloned sequence that was not present in the predicted *Bflo*_p2x sequence. Within this region was found to be two ECD cysteine residues that are conserved amongst hP2X1-7 receptor subunits C126 and C135 (Fig. 5.3).

PKC
K68/K70
C117
[C126]
C135
C149
C159
C165
TM1
F185/T186
C217
C227
C250
C261
C270
F291/R292
K309
D350
YxxxK
TM2
Bflo_p2x
BfloP2X
hP2X1
hP2X2
hP2X3
hP2X4
hP2X5
hP2X6
hP2X7

Fig. 5.4: MSAof predicted and cloned protein sequences of *Bflo*P2X with hP2X1-7 subunits

Predicted and cloned forms of the *Bflo*P2X receptor share a 24.8 to 46.4% primary amino acid sequence identity with hP2X1-7 receptors. Residues that are identical between P2X receptors from all three species are outlined and shaded in grey, whilst residues with similar chemical identity are outlined only. Conserved ATP binding residues, an N-terminal PKC phosphorylation motif, and a C-terminal membrane localisation motif are highlighted above the sequences (hP2X1 numbering). Predicted TMDs (based on hP2X1) are highlighted below the alignment sequence. Sequences were aligned using the MUSCLE alignment algorithm (Edgar, 2004) (section 2.2.2).

5.3.3 Cloning of *Trichoplax* P2X receptors

Homology searching identified two putative P2X receptors in the genome of *T. adhaerens*; *Tad*_p2xA and *Tad*_p2xB (section 3.3.10). Predicted *Tad*_p2xA and *Tad*_p2xB cDNA sequences are 1033 and 982 nucleotides long, the translated protein products of which are 343 and 326, respectively. In comparison to hP2X1-7, predicted *T. adhaerens* P2X subtype protein sequences are considerably shorter (detailed in section 3.3.10).

Subsequent cloning by RT-PCR, and sequencing of these two receptors using revealed that regions predicted to be absent in *Tad*_p2xA and *Tad*_p2xB are present. These cloned receptors (referred to subsequently as *Tad*P2XA and *Tad*P2XB) shared a 50.6% sequence identity between each other and were 393 and 304 residues long, respectively. Amongst hP2X1-7 receptor subunits, these two proteins shared a 23.3 to 43.7% and 24.1 to 44.8% primary sequence identity (*Tad*P2XA and *Tad*P2XB, respectively). As in their predicted counterparts (section 3.3.10), two extended regions of hydrophobic residues corresponding to TMDs were predicted to be present in both *Tad*P2XA and *Tad*P2XB.

In *Tad*_p2xA, a region of amino acids within the predicted ECD appeared to be absent (hP2X1 numbering: G250 to V298) (Fig. 5.5), and encompasses residues implicated in being important in the function of mammalian P2X receptors, including (hP2X1 numbering) G250, two ECD cysteine residues (C261 and C270), and residues that form an ATP binding motif (F291 and R292). Following cloning, this region (and encompassing residues conserved between hP2X1-7) was found to be present

(Fig. 5.5). In *Tad*_p2xB, three expanses of amino acids shared amongst hP2X1-7 receptors appeared to be absent (hP2X1 numbering: L72 to Q95; I173 to N201; and G324 to A345). These regions, predicted to lie within the predicted ECD of *Tad*_p2xA were present within the cloned form of *Tad*_p2xA (*Tad*P2XA). Resultantly, the ATP binding residues F185 and T186 were found to be present within this *Trichoplax* P2X receptor subtype (Fig. 5.5).

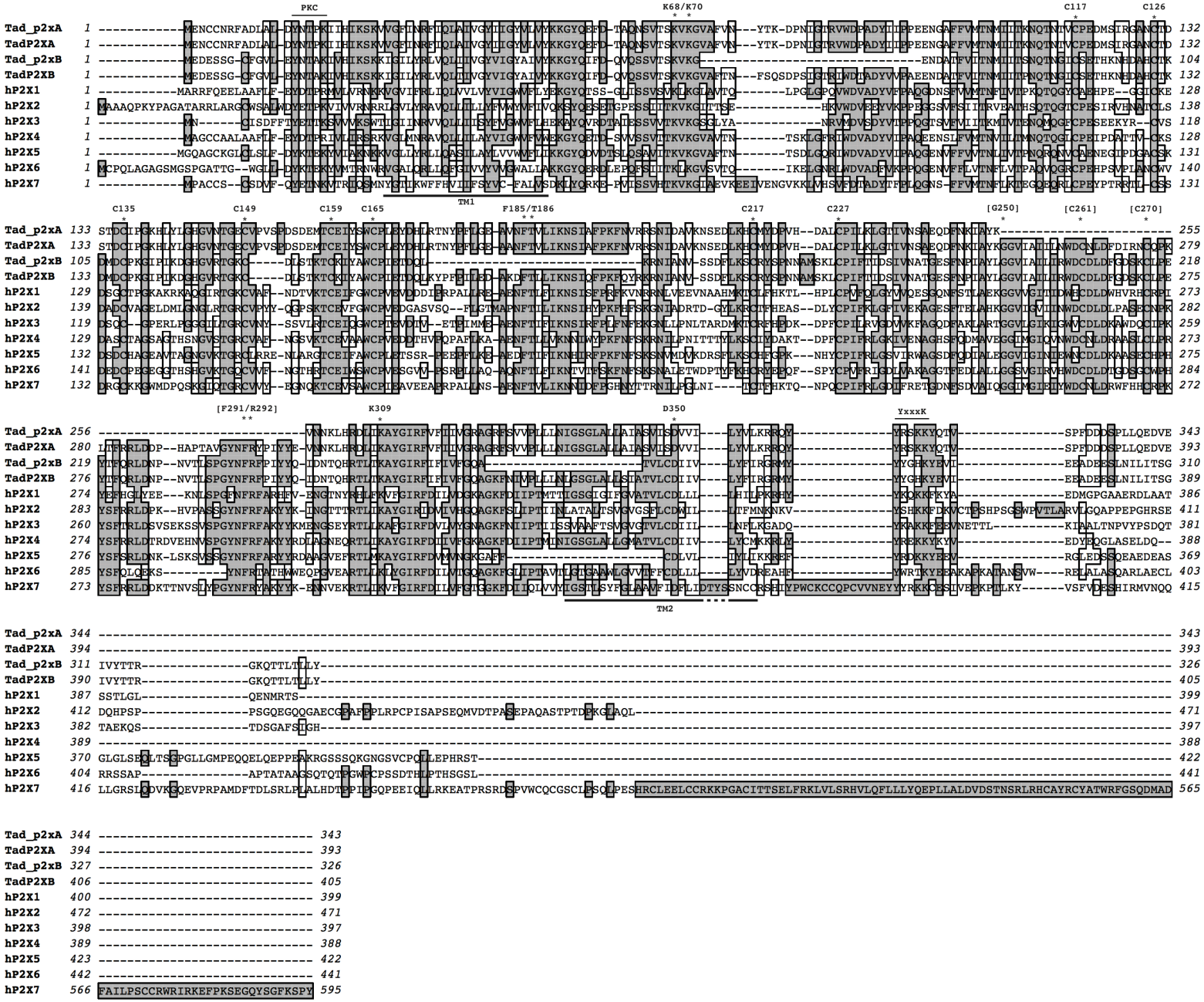
PKC
K68/K70
C117
C126
TM1
C135
C149
C159
C165
F185/T186
C217
C227
[G250]
[C261]
[C270]
[F291/R292]
K309
D350
YxxxK
TM2
Tad_p2xA
TadP2XA
Tad_p2xB
TadP2XB
hP2X1
hP2X2
hP2X3
hP2X4
hP2X5
hP2X6
hP2X7

Fig. 5.5: MSA of protein sequences predicted and cloned forms of *T. adhaerens* P2X receptors with hP2X1-7 subunits

Predicted and cloned forms of the *Tad*P2X receptor subunits share a 23.3 to 44.8% primary amino acid sequence identity with hP2X1-7 receptors. Residues that are identical between P2X receptors from all three species are outlined and shaded in grey, whilst residues with similar chemical identity are outlined only. Conserved ATP binding residues, an N-terminal PKC phosphorylation motif, and a C-terminal membrane localisation motif are highlighted above the sequences (hP2X1 numbering). Predicted TMDs (based on hP2X1) are highlighted below the alignment sequence. Sequences were aligned using the MUSCLE alignment algorithm (Edgar, 2004) (section 2.2.2).

5.3.4 Heterologous expression of cloned P2X receptors in HEK293 cells

When expressed heterologously in HEK293 cells, bands detected by Western blot analysis of transfected P2X receptors (all possessing a C-terminally fused to a hexahistidine motif) were found between ca. 60 to 80 kDa (Fig. 5.6). The predicted molecular masses of these proteins (45.7 to 50 kDa) following blotting of total protein lysate of P2X receptor-expressing HEK293 cells were larger than predicted. The largest of the differences between the predicted and empirically determined molecular masses was seen with total protein lysate of HEK293 cells transiently transfected with *Bflo*P2X, at approximately 80 kDa. This band also appeared to consist of higher and lower molecular weigh components. No band was detected in cells transiently transfected with pcDNA3.1$^{(+)}$ vector alone. Due to time constraints, expression of the two *T. adhaerens* P2X receptors was not tested by Western blot.

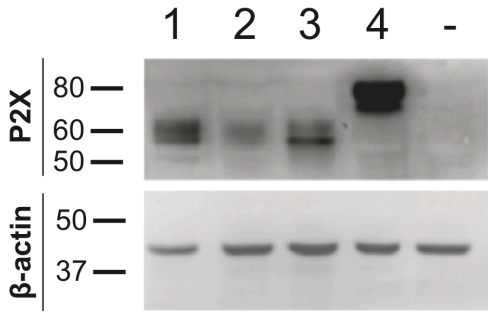

Fig. 5.6: total protein lysate isolated from P2X receptor-expressing HEK293 cells.

Western blots were performed against total protein lysate isolated from HEK293 cells transiently expressing P2X receptor/pcDNA3.1$^{(+)}$ constructs. Blots were prepared and analysed according to 2.4.9, with 10 µg loaded in each lane. Bands corresponding to transfected P2X receptors were detected for aepP2X, *Dpu*P2XB (both predicted and cloned forms), and *Bflo*P2XB at molecular weights range from ca.60 to 80 kDa. 1 = aepP2X; 2 = predicted/synthesised *Dpu*P2XB; 3 = cloned *Dpu*P2XB; 4 = *Bflo*P2XB; '-' = pcDNA3.1$^{(+)}$ vector. Each lane was loaded with 10 µg total protein lysate. β-actin was used as a loading control.

5.3.5 Pharmacological profile of *Dpu*P2X receptors

5.3.5.1 *Dpu*P2XB-$(His)_6$ is largely insensitive to extracellular ATP

Extracellular application of 100 µM ATP failed to evoke inward currents at either predicted/synthesised or cloned *Dpu*P2XB receptors in HEK293 cells. However, robust inward currents were evoked at ATP concentrations of 1-10 mM. Although HEK293 cells are known to express endogenously the P2X4 and P2X5 receptor subunits (Worthington *et al.*, 1999), HEK293 cells subjected to the same transfection protocol as *Dpu*P2XB-expressing cells, but using 'empty' pcDNA3.1$^{(+)}$ vector evoked either no or significantly smaller currents of between 5-100 pA (Fig. 5.5 and 5.7C). In contrast, mean peak currents evoked at *Dpu*P2XB receptors by 10 mM ATP were larger (ca. 100 to 1500 pA) (Fig. 5.7). At *Dpu*P2XB receptors, ATP threshold was approximated to be around 1 to 3 mM, based on the observation that currents were not evoked at lower ATP concentrations tested (0.1 and 0.3 mM) (Fig. 5.7A). Although larger, mean peak inward currents evoked at *Dpu*_p2xB (676.8 ± 116.2 pA (n = 12)) were not statistically significantly different from those evoked at *Dpu*P2XB (325.1 ± 34.9 pA (n = 11)), as determined by Student's unpaired two-tailed t-test (p = 0.013, n = 12 and 11).

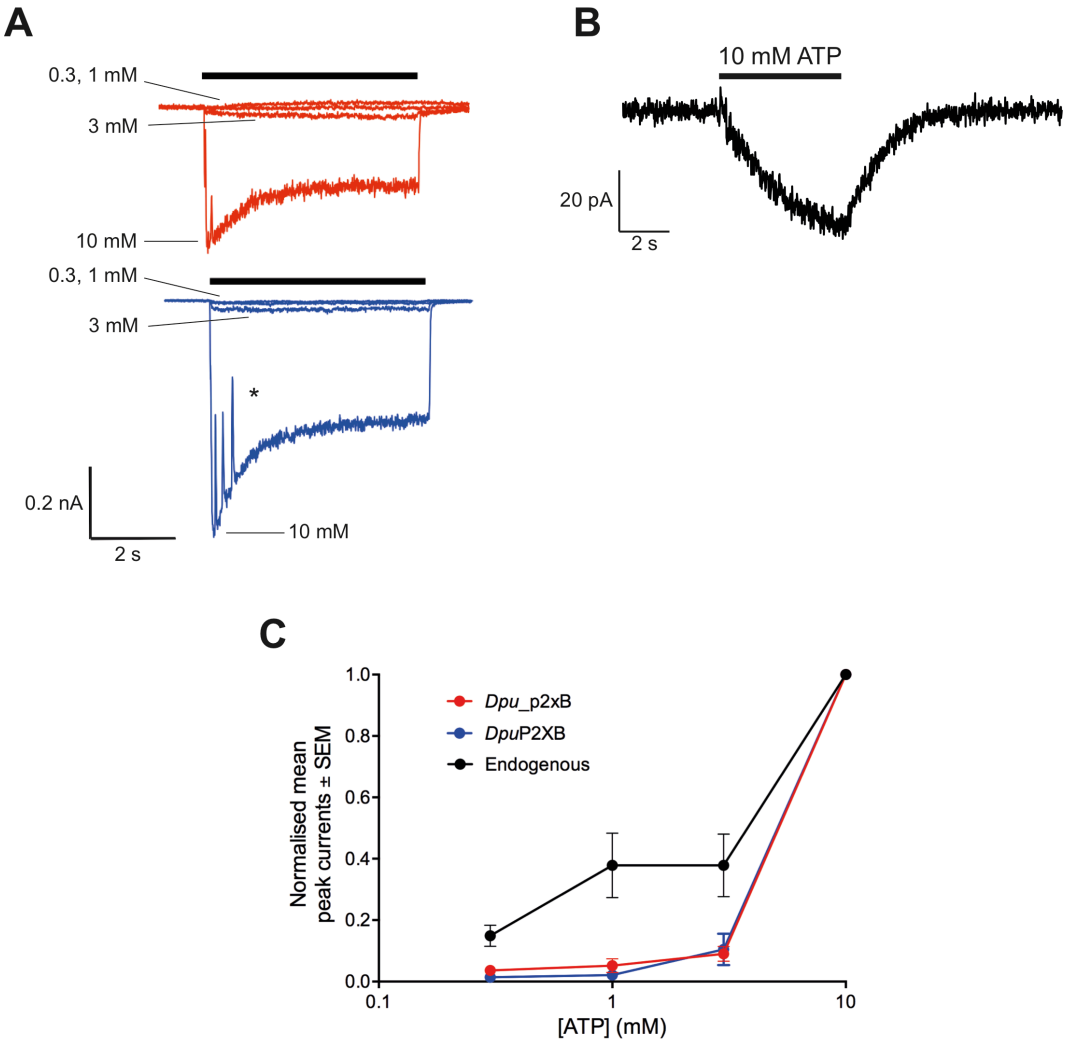

Fig. 5.7: ATP concentration-response data for *D. pulex* P2XB receptor forms

A, representative concentration-dependent inward current traces evoked by the extracellular application of 10 mM ATP to HEK293 cells transiently expressing either the predicted (*Dpu*_p2xB; red trace) or cloned (*Dpu*P2XB; blue trace) forms of the *D. pulex* P2XB. Cells were held at a holding potential of -60 mV. The duration of ATP application (5 s) is denoted by a black bar above the traces. ***B,*** Application of 10 mM evoked small, slow-activating currents in cells transiently transfected with pcDNA3.1$^{(+)}$ expression vector alone evoked either no inward current, or considerably smaller inward current that displayed slower activation kinetics than *D. pulex* P2XB receptors at an equimolar concentration of ATP. ***C***, concentration-response data for both *D. pulex* P2XB receptor forms and endogenous receptor current. Changes in current magnitude resulting from progressive increases in extracellular ATP concentration are similar for predicted/synthesised and cloned *Daphnia* P2XB receptors, but are less for the endogenous current seen in non-transfected cells (n = 4, 4, and 6 for *Dpu*_p2xB, *Dpu*P2XB and endogenous currents, respectively).

5.3.5.2 Activation and deactivation kinetics of *D. pulex* P2XB receptors

In HEK293 cells transfected with pcDNA3.1$^{(+)}$ vector alone, slowly-activating currents could be evoked with 10 mM extracellular ATP application (Figs. 5.7A and B). These currents were considerably smaller (Figs. 5.7B and 5.8) than those evoked by 10 mM in cells transiently transfected with either the predicted (*Dpu*_p2xB) or cloned (*Dpu*P2XB) form of *D. pulex* P2XB. *D. pulex* P2XB-expressing HEK293 cells also displayed faster activation kinetics than those recorded in HEK293 transfected with pcDNA3.1$^{(+)}$ vector alone (Figs. 5.7 and 5.8). In HEK293 cells co-transfected with *D. pulex* P2XB receptor and eGFP plasmids, 10 mM ATP-evoked currents from eGFP-positive (and therefore *D. pulex* P2XB transfected) cells could be distinguished from eGFP-negative, non-transfected cells based both on peak current magnitude and kinetic profile.

Application of 10 mM ATP to cells expressing either the predicted (*Dpu*_p2xB) or cloned (*Dpu*P2XB) forms of the *D. pulex* P2XB receptor resulted in rapidly activating inward currents (mean rise time: 303 ± 55 ms (n = 11), and 261 ± 90 ms (n = 12), respectively) (Fig. 5.8). In contrast, rise time at the currents recorded in empty vector-transfected HEK293 cells displayed a rise time of 3115.8 ± 321.2 ms (n = 96) (Fig. 5.8).

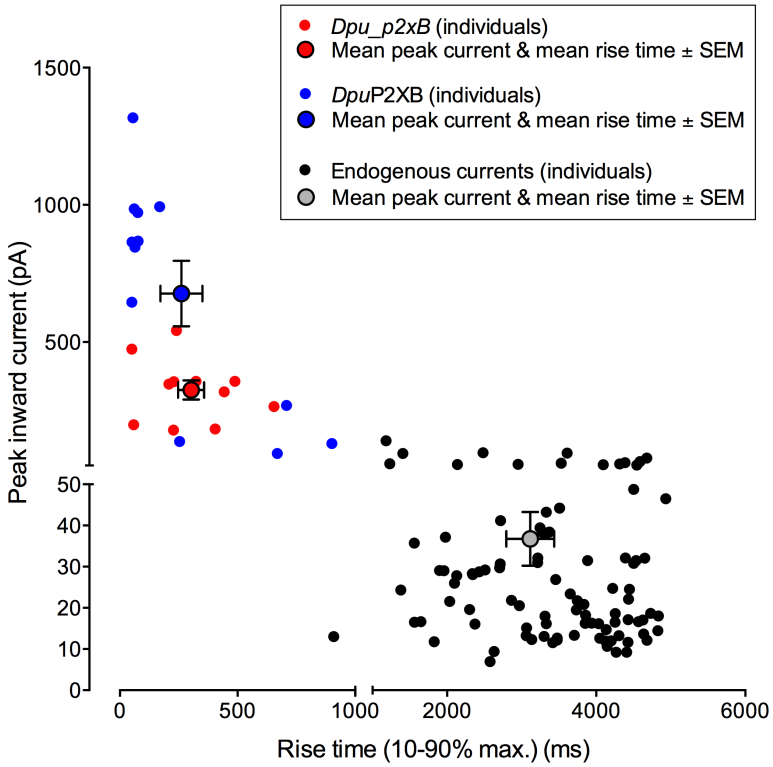

Fig. 5.8: scatterplot illustrating grouping of *D. pulex* P2XB receptor and endogenous receptor activity based on peak current and rise time

HEK293 cells transfected with pcDNA3.1$^{(+)}$ vector alone (black circles) could be distinguished from cells expressing either the predicted (*Dpu*_p2xB) (red circles) or cloned (*Dpu*P2XB) (blue circles) forms of the *D. pulex* P2XB receptor based on inward current magnitude and kinetic profile. Each individual data point represents a recording from a single cell. Mean peak inward current and rise time for predicted (*Dpu*_p2xB), cloned (*Dpu*P2XB), and endogenous currents are highlighted by black-outlined red, blue, or grey circles, respectively. No statistically significant difference was calculated between *Dpu*_p2xB and *Dpu*P2XB 10 mM ATP-evoked inward currents ($p = 0.013$; $n = 11$-12, two-tailed unpaired *t*-test). Inward currents evoked at both *D. pulex* P2XB receptor forms were very highly significantly different to those evoked in the slower-activating group of currents ($p < 0.001$; $n = 11$-96). Rise time was not found to be statistically significant between *Dpu*_p2xB and *Dpu*P2XB ($p = 0.71$; $n = 11$-12), but was found to be statistically different between these receptor forms and the slower-activating endogenous HEK293 current ($p < 0.001$; $n = 11$-96). Rise time was calculated as the time taken for current to increase between 10 and 90% of maximum current evoked by 10 mM ATP.

5.3.5.3 Recovery of *Dpu*P2XB ATP sensitivity in low divalent cation conditions

Daphnia species have been found in freshwater ecosystems around the world (Ebert, 2005) and are therefore subject to lower ion concentrations (Ebert, 2005; Weber and Pirow, 2009). To assess whether the high concentration of divalent cations (Mg^{2+} and

Ca^{2+}) was responsible for the insensitivity of *D. pulex* P2XB receptors to extracellular ATP when expressed heterologously in HEK293 cells, concentration-response curves were generated in nominally low-divalent cation concentration ECS (0 mM $MgCl_2$ and 0.2 mM $CaCl_2$) (ldECS).

In standard ECS (sECS) (containing 1 mM $MgCl^2$ and 2 mM $CaCl_2$). 10 mM ATP evoked robust inward currents in both predicted/synthesised and cloned forms of the *D. pulex* P2XB receptor (Figs. 5.9A and C). Replacement of perfusing ECS with one composed of a lower divalent cation concentration (ldECS; nominally free $MgCl_2$ and 0.2 mM $CaCl_2$) augmented the response of both *Dpu*_p2xB and *Dpu*P2XB to 10 mM ATP (Figs. 5.7A and C). In addition to augmenting the response of both receptors to 10 mM ATP the concentration-response curves for both receptors in ldECS were left-shifted.

At physiological pH (7.35-7.45), ATP is present in its ATP^{4-} ionic form. ATP^{4-} is chelated by Mg^{2+} and, to a lesser extent, Ca^{2+} ions (O'Sullivan and Perrin, 1964; Wilson and Chin, 1991a). To determine whether these augmented and left-shifted responses could be due to an increase in free ATP^{4-}, the free ATP^{4-} concentration in ldECS was estimated using Maxchelator (available at: http://maxchelator.stanford.edu/), and plotted against current responses recorded in sECS. Plotting these values revealed an overlap of concentration-response data recorded in ldECS with that predicted in a scenario where there is greater availability of $[ATP]^{4-}$ (Figs. 5.9B and D).

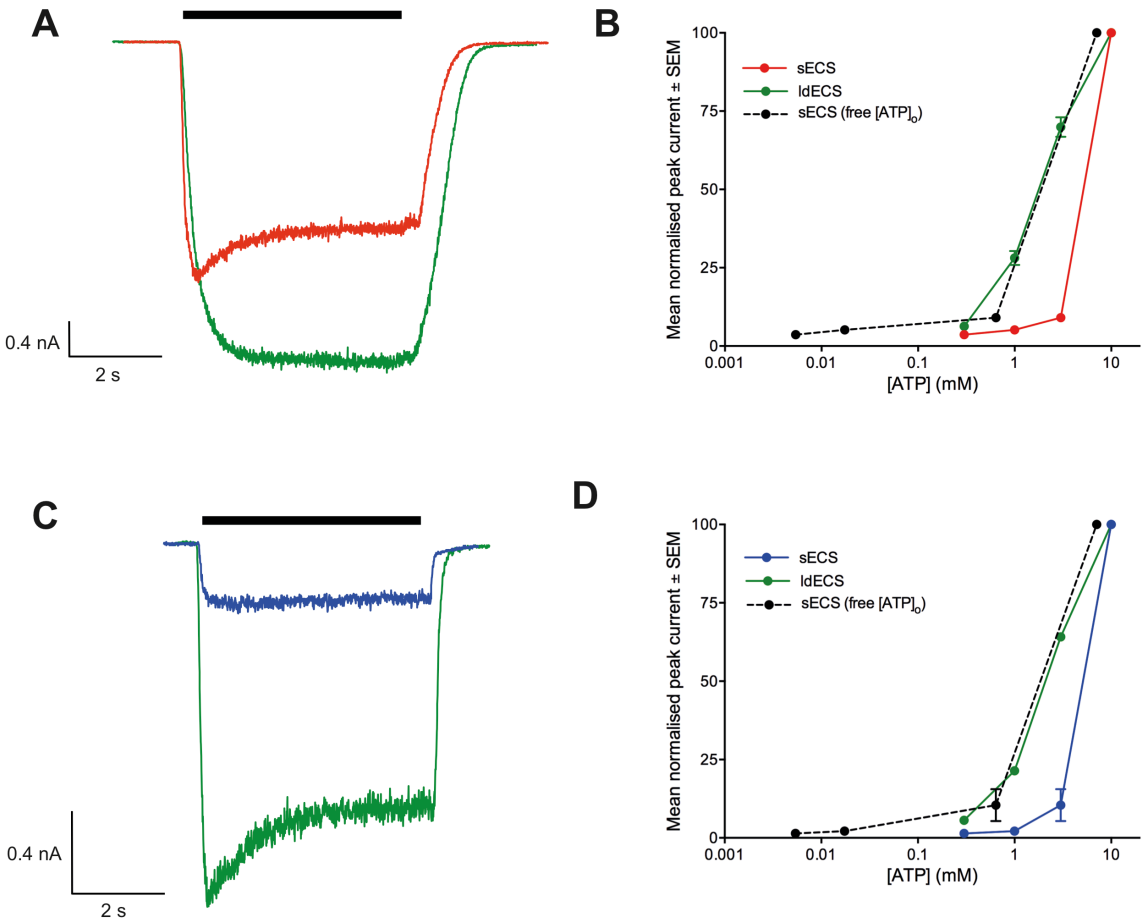
A
0.4 nA
2 s
B
Mean normalised peak current ± SEM
sECS
ldECS
sECS (free [ATP]o)
[ATP] (mM)
C
0.4 nA
2 s
D
Mean normalised peak current ± SEM
sECS
ldECS
sECS (free [ATP]o)
[ATP] (mM)

Fig. 5.9: improved ATP sensitivity of *Dpu*P2XB receptors in low divalent cation conditions

In standard ECS (sECS), predicted (*Dpu*_p2xB) and cloned (*Dpu*P2XB) receptor forms are largely insensitive to extracellular ATP application. ***A***, representative current traces recorded from HEK293 cells transiently expressing the predicted (*Dpu*_p2xB) *D. pulex* P2XB receptor form. In sECS (red trace), 10 mM ATP evokes robust inward currents that are augmented in low divalent cation concentration ECS (ldECS) (green trace). The black bar above the traces denotes the 5 s application of 10 mM extracellular ATP. ***B***, mean, normalised concentration-response data for *Dpu*_p2xB illustrated a concentration-dependent response of the receptor in sECS (red line) that was left-shifted in ldECS (green line). Plotting of currents recorded in sECS against estimated free (extracellular) ATP^{4-} concentration in ldECS estimates a leftward shift in these conditions that matches those responses seen in ldECS (dashed black line). ***C***, representative current traces recorded from HEK293 cells transiently expressing the cloned (*Dpu*P2XB) *D. pulex* receptor form. In sECS (blue trace), 10 mM ATP evokes robust inward currents that are augmented in low divalent cation concentration ECS (ldECS) (green trace). The black bar above the traces denotes the 5 s application of 10 mM extracellular ATP. ***D***, mean, normalised concentration-response data for *Dpu*P2XB illustrated a concentration-dependent response of the receptor in sECS (blue line) that was left-shifted in ldECS (green line). Plotting of currents recorded in sECS against estimated free (extracellular) ATP^{4-} concentration in ldECS estimates a leftward shift in these conditions that matches those responses seen in ldECS (dashed black line). Graphical data are normalised against the current evoked by 10 mM ATP. Free ATP^{4-} concentration in ldECS (nominally-free Mg^{2+} and 0.2 mM Ca^{2+}) was estimated using MaxChelator (available at: http://maxchelator.stanford.edu/).

5.3.6 *Bflo*P2X functions as an ATP-gated ion channel in HEK293 cells

Heterologous expression of *Bflo*P2X in HEK293 cells, and subsequent application of extracellular ATP evoked concentration-dependent inward currents (at a holding potential of -60 mV) (Fig. 5.10). At the concentrations of ATP tested (0.003 to 10 mM ATP), peak inward currents did not stabilise and plateau, resulting in an estimated EC_{50} for ATP of > 300 μM (n = 6) (Fig. 5.10B). Following whole-cell access, repeated extracellular applications of a test concentration of 1 mM ATP resulted in the desensitisation of *Bflo*P2X (Figs. 5.10C and D). Fitting of currents derived from fitted with a one-phase exponential decay function, and revealed a half-life of 1.4 ± 0.1 applications (n = 5) (Fig. 5.10B).

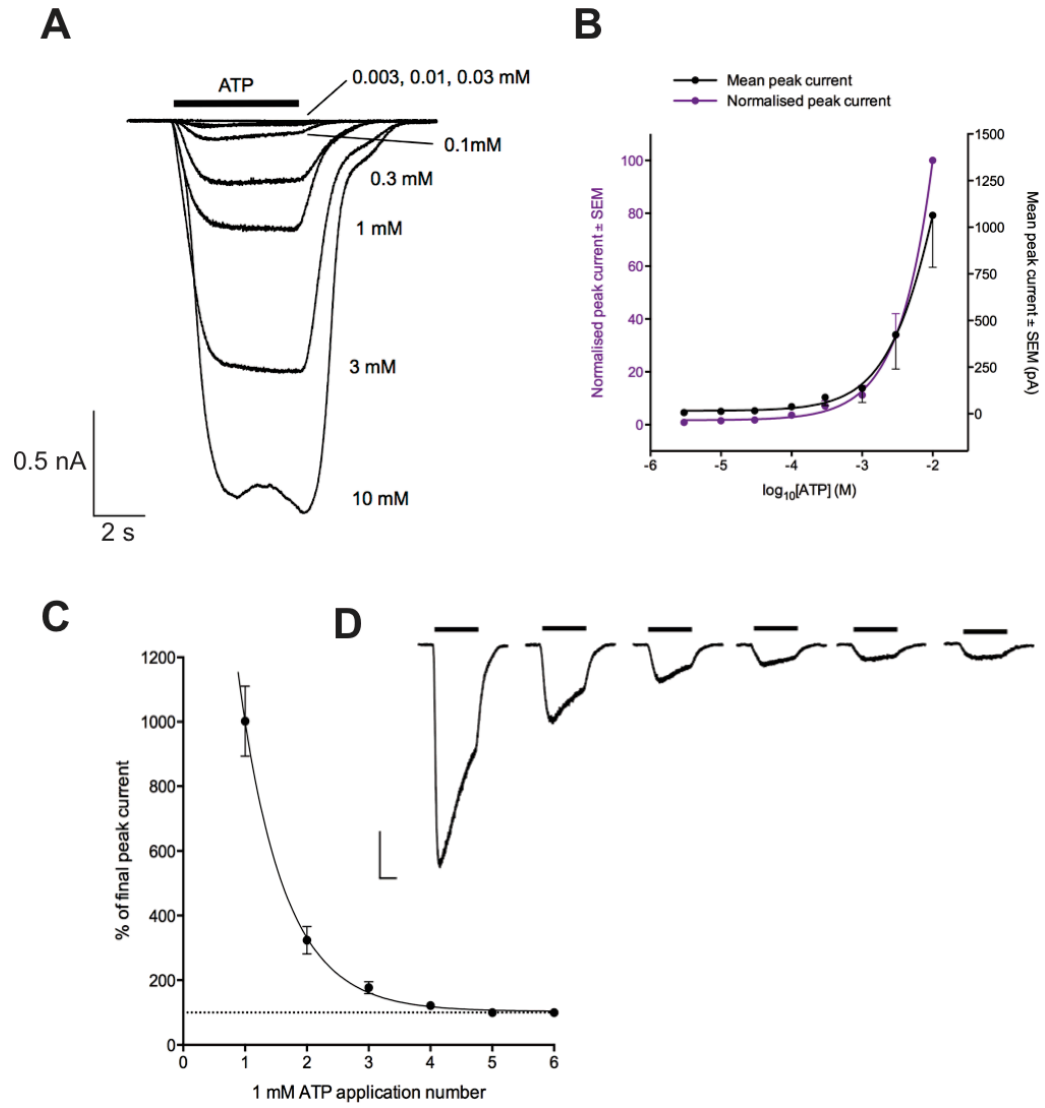

Fig. 5.10: concentration-dependent responses of *Bflo*P2X to ATP in HEK293 cells

Concentrations of ATP ranging from 3 μM to 10 mM were applied to HEK293 cells transiently transfected with *Bflo*P2X, at a holding potential of -60 mV. ***A***, representative current recording traces evoked inward currents, with duration of extracellular ATP application detonated by a black bar above the traces. Inward currents were evoked at a concentration threshold of approximately 30 to 100 μM. ***B***, mean peak (black line) and mean normalised peak currents evoked at a range of ATP concentrations. Evoked currents did not appear to reach a plateau and, as such, an ATP EC_{50} could not be calculated, but is estimated to be a minimum of 300 μM. ***C***, repeated application of 1 mM ATP resulted in the sequential reduction of evoked currents ('rundown') at *Bflo*P2X. Sequential currents could be fitted with a onephase exponential decay function, reaching half the maximal current recorded in the first 1 mM ATP applications by the second subsequent ATP application. ***D***, representative current traces of repeated applications of 1 mM ATP (denoted by black bars above each inward current) illustrating rundown of evoked current at *Bflo*P2X. Between each ATP application, cells were washed for 90 s with ECS. Scale bar = 0.2 nA and 1 s.

5.3.7 *Tad*P2XA is insensitive to extracellular ATP in HEK293 cells

Functional responses of the *T. adhaerens* P2XA receptor subtype to extracellular ATP were tested by whole-cell voltage-clamp electrophysiology in HEK293 cells, at a holding potential of -60 mV. No currents were detected to 1 mM ATP (n = 10). HEK293 cells were transiently co-transfected with 5 μg *Tad*P2XA (in pcDNA3.1$^{(+)}$ expression vector) and eGFP vector (0.1 μg), and only eGFP-expressing cells patched. It is possible that *Tad*P2XA-$(His)_6$ responds to an unknown agonist, but this was not tested in the current thesis due to time constraints.

5.4 DISCUSSION

The current chapter has demonstrated that members of the Crustacea, Cephalochordata, and Placazoa groups of organisms express at least one P2X receptor homologue. When expressed heterologously in the mammalian HEK293 cell line, these homologues form ATP-gated ion channels, with the exception of the one *Trichoplax adhaerens* receptor homologue tested (*Tad*P2XA). I sought to provide initial data investigating a novel feature of the pharmacology of P2X receptors from the microcrustacean *Daphnia pulex*, and the early chordate *Branchisotoma floridae*. Following this initial characterisation, I suggest mechanisms underlying findings, and attempt to relate these findings to organism biology where possible.

5.4.1 *Daphnia pulex* P2XA receptor

Attempts to confirm the expression of the *D. pulex* P2XA receptor (*Dpu*_p2xA) by PCR were unsuccessful, despite a number of different sequence-specific primer pairs being used in combination with different annealing and extension temperatures. In addition, both genomic DNA and complementary DNA (cDNA) templates were used with many of these primer pairs, where appropriate to the position of the primer within the predicted genomic sequence.

BLAST searching for the *D. pulex* P2X receptor homologues was performed using wFleaBase (Colbourne *et al.*, 2005), which, in addition to returning homologous sequences to a nucleotide or protein query, also provides information regarding the expression level of a retrieved sequence. Gene expression levels in *D. pulex* (TCO strain) in a variety of environmental conditions, including those exposed to heavy metals such as cadmium are available (Colbourne *et al.*, 2005). Expression levels of *Dpu*_p2xA (Fig. 5.11A) were found to be considerably lower than those predicted for the ('clonable') *Dpu*_p2xB gene (Fig. 5.11B) across a range of biological and environmental parameters, and may suggest a low copy number of *Dpu*_p2xA mRNA transcripts. *Dpu*_p2xA transcript expression levels were predicted to be reduced in a in both treated and non-treated (control) daphnids compared to expression levels of *Dpu*_p2xB. Although cadmium, heavy metal or Chaoborus (glassworm) predator exposure did not appear to alter transcript expression in either predicted *D. pulex* P2X receptor subtype, both subunits appeared reduced in male daphnids compared to females. (Fig. 5.11). Although attempts to maintain a parthenogenic (and therefore female) population of *D. pulex* were made, cDNA was generated from total RNA may have been isolated from male daphnids due to fluctuations in population sex ratios. Although care was taken to chose daphnids for total RNA isolation from 5 to 10 individual daphnids without apparent bias for size or activity (section 2.4.2), a larger number of male daphnids may have been chosen. As a result, the availability of *Dpu*_p2xA transcript for cDNA synthesis may have been reduced.

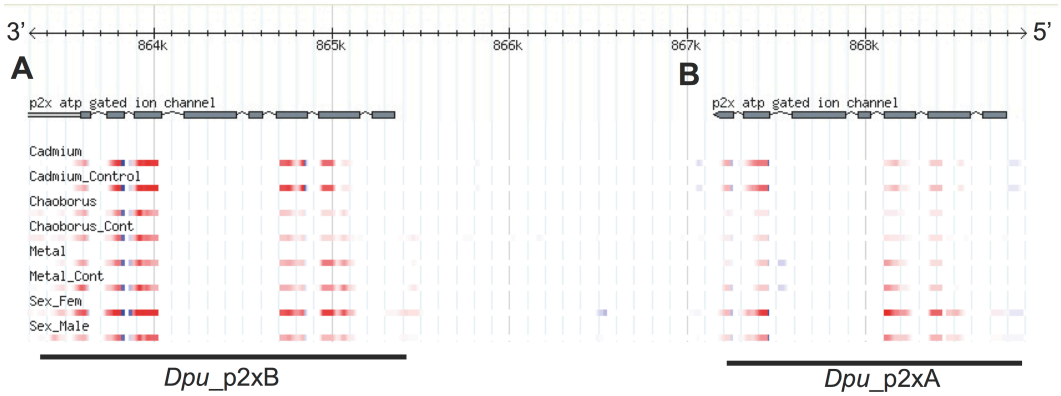

Fig. 5.11: wFleaBase screenshot illustrating expression levels of predicted *Dpu*_p2xA and *Dpu*_p2xB genes

Putative *D. pulex* P2X receptors were identified through homology searching of the *D. pulex* genome (section 3.3.4.3). P2X receptor genes were annotated on the reverse genomic scaffold, and were subsequently termed (in 5' to 3' direction) *Dpu*_p2xA (***A***) and *Dpu*_p2xB (***B***). Expression levels are displayed according to intensity of coloured bars, with low level gene expression represented by a lower intensity, and genes expressed at higher levels at a higher density. Expression levels of both predicted transcripts in a number of conditions are highlighted to the left of the panel. Coding regions as part of the gene structures of *Dpu*_p2xA and *Dpu*_p2xB are depicted in grey.

A low mRNA copy number may make attempts to amplify *Dpu*_p2xA by PCR from cDNA difficult. Attempts to amplify the receptor from a genomic DNA (gDNA) template using primers flanking the *Dpu*_p2xA, or both *Dpu*_p2xA and *Dpu*_p2xB genomic sequence also proved ineffective across a range of PCR conditions. This may suggest that primers used in PCR reactions did not bind effectively to target sequences. Conversely, sequencing errors may have occurred such that the *Dpu*_p2xA gene sequence is longer than predicted. As a result, extension temperatures used in the current study may not have been sufficient to enable amplification of a gene region of interest. Due to time constraints, further attempts to clone *Dpu*_p2xA were not made. Gene expression in *Daphnia* has been demonstrated to be modulated by changes in environment, leading to the description of its genome as being 'ecoresponsive' (Colbourne *et al.*, 2011). For instance, culturing *Daphnia* in low oxygen (hypoxia) environments leads to the upregulation of genes encoding for the oxygen-carrying metalloprotein haemoglobin, thus allowing individuals to adapt to this environmental stressor (Gorr *et al.*, 2004; Gerke *et al.*, 2011; Zeis *et al.*, 2013). Further work may involve assessment of changes in *D. pulex*

P2X receptor gene expression in stressor environments, such as hypoxia, using RT-qPCR (reverse-transcriptase-quantitative PCR), or gene microarrays

5.4.2 Low sensitivity of *D. pulex* P2XB to extracellular ATP

When expressed in HEK293 cells, both predicted/synthesised (*Dpu*_p2xB) and cloned (*Dpu*P2XB) forms of the *D. pulex* P2XB receptor, application of 100 μM ATP failed to evoked inward currents at a holding potential of -60 mV. However, application of 1 to 10 mM ATP concentrations evoked inward currents in both receptor forms (Fig. 5.7).

Although a slight reduction in peak inward current evoked at the cloned *Daphnia* P2XB receptor was seen upon application of 10 mM ATP, this was found to be not statistically significant (section 5.3.5.1). When recordings were made in an ECS containing a reduced Ca^{2+} ion concentration (0.2 mM) (relative to standard recording conditions) and nominally free Mg^{2+} ion concentration, currents evoked by 10 mM ATP were larger than those seen under standard recording conditions. This resulted in an apparent leftward shift in the concentration-response relationship to ATP, indicating that ATP was more effective at *D. pulex* P2XB receptors under low divalent cation conditions (Fig. 5.9).

In its ionised form (ATP^{4-}), ATP is known to be chelated by both Mg^{2+} and, to a lesser extent, Ca^{2+} ions (O'Sullivan and Perrin, 1964; Wilson and Chin, 1991a), through the binding of these cations to the β- and γ –phosphate moieties of ATP^{4-} (Jahngen and Rossomando, 1983). In the absence of chelating divalent cations, ATP^{4-} has been demonstrated to act as an agonist at all human P2X receptor subunits (Li *et al.*, 2013). To determine whether the leftward shift in the ATP concentration-dependent responses recorded at *D. pulex* P2XB receptor forms could be due to an increase in availability of free ATP^{4-}, currents recorded in standard ECS (sECS) (section 2.6.2.1) were plotted against estimated free ATP^{4-} concentrations in a low divalent cation solution (Fig. 5.9C). This resulted in a concentration-response relationship that matched that seen in ldECS. This suggests that the reduction of chelating divalent cations results in an increase in free ATP^{4-}, which in addition its chelated form, can act as an agonist at *D. pulex* P2XB receptors.

However, previous studies have demonstrated roles for divalent cations in the modulation of P2X receptor activity via mechanisms independent their ability chelate ATP^{4-} ions. At the rat P2X7 receptor, both Ca^{2+} and Mg^{2+} ions inhibit ATP-evoked currents (Suprenant *et al*., 1996; Rassendren *et al.*, 1997) (Ca^{2+} IC_{50} = ca. 3.2 mM; Mg^{2+} IC_{50} = ca. 0.5 mM (Virginio *et al.*, 1997)), acting as allosteric modulators (Virginio *et al.*, 1997), or by altering the ability of cations to permeate the channel pore (Khakh *et al.*, 1999a). Similar to data presented in the current chapter, reduction of extracellular (bath) Ca^{2+} ion concentration results in leftward shift in the concentration-response curve for ATP at P2X7 (Yan *et al.*, 2011). These concurrent findings are consistent may also suggest that free ATP^{4-} is a native agonist at *Dpu*P2XB, but does not exclude Ca^{2+} ions acting as an allosteric inhibitor of ATP-evoked currents. However, due to experimental design, it was not possible to differentiate between effects of Ca^{2+} in a fixed Mg^{2+} ion concentration in the current study.

The physiological relevance of these findings in *Daphnia* is unclear. *Daphnia* species are found in freshwater habitats around the world and, as such, are subjected to a low divalent cation environment (the Ca^{2+} ion concentration of freshwater environments has been found to be as low as 0.1 μM in some habitats (Weber and Pirow, 2009)). Although reports vary, it has been reported that in a freshwater environment containing between ca. 1 to 100 μM, total Ca^{2+} ion tissue concentration in the related *Daphnia magna* individuals can range between 0.005 to 20 μM (Alstad *et al.*, 1999). As such, ATP from its source is likely to be present largely in its acidic, ATP^{4-} form. This may result in ionic currents evoked at *Daphnia* P2X receptors by ATP^{4-} being of a magnitude sufficient to evoke downstream effects. Furthermore, the allosteric nature of Ca^{2+} ion inhibition of *Dpu*P2XB receptors may also be reduced, further increasing the potency of ATP^{4-} at the receptor.

Daphnia possess an open circulatory system that is required for oxygen transport throughout the organism via haemoglobin-rich haemolymph (Ebert, 2005). It has been demonstrated in *D. magna* that, when cultured in an environment of pH 7.8, haemolymph is alkaline at a pH of approximately 8.3 (Weber and Pirow, 2009). Recent work by Baines *et al*. (2013) demonstrated that current responses to ATP of *Dictyostelium* P2X receptors are influenced by changes in intracellular and extracellular cations. In that study, current recordings were made of *Dictyostelium*

discoideum P2X receptor-expressing HEK923 cells, adjusting the pH of extracellular and intracellular recording solutions to reflect conditions seen in the acidic contractile vacuole in which *Dictyostelium* P2X receptors are expressed (Baines *et al.*, 2013). Furthermore, ion concentrations in which recordings were made were also adjusted to reflect the major ion (K^+) in the contractile vacuole into which the ECD of the *Dictyostelium* P2XA (*Dd*P2XA) is exposed (Baines *et al.*, 2013). Whilst in symmetrical Na^+ ion conditions (pH 7.3 intra- and extracellular), ATP evoked inward currents at *Dd*P2XA (Fountain *et al.*, 2007; Baines *et al.*, 2013), and smaller currents at *Dd*P2XA (Baines *et al.*, 2013), currents were only evoked at *Dd*PXB when the intracellular solution was acidified (pH 6.2) (Baines *et al.*, 2013).

In the current thesis, extracellular and intracellular solutions used in whole-cell patch-clamp electrophysiology recordings had a pH of 7.3. In light of the previous findings of Baines *et al*. (2013), and the understanding that *Daphnia* haemolymph pH is alkaline relative to the external environment (Weber and Pirow, 2009), this may suggest that the recording environment used to gather whole-cell patch-clamp data presented in the current thesis may not have properly reflected the endogenous environment of *Daphnia* P2X receptors residues. Extracellular domain residues identified in rat P2X7 as being implicated in the inhibition of receptor current by H^+ (rP2X7 numbering: H185, K110, K137, H219, and D197) (Liu *et al.*, 2009a) were not conserved in *Dpu*P2XB receptor subunits (although chemically similar residues are found in place of K137 and D197 equivalent residues (*Dpu*P2XB numbering: R138 and E202, respectively). Whilst evidence at the primary sequence level for pH modulation of *Dpu*P2XB receptors is low, it is plausible that residues not previously implicated in pH modulation in higher organisms are required for potential pH modulation in *Daphnia* P2X receptors.

In addition, electrophysiological recordings of *Dpu*P2XB receptors are performed in a non-native human cell line (HEK293). For instance, post-translational modification processes of transiently transfected *Dpu*P2XB receptors that are inherent to mammalian cells, but not in native *Daphnia* cells may occur. Post-translational *N*-linked glycosylation modification of hP2X4 receptors has been demonstrated to vary according to the expression system used (Valente *et al.*, 2011). Furthermore, *N*-linked glycosylation has been demonstrated to be required for the efficient membrane expression and function of a number of P2X receptor subunits (Torres *et al.*, 1998;

Rettinger *et al.*, 2000; Vacca *et al.*, 2011). Whilst Western blot analysis of whole-cell lysate of HEK293 cells transiently expressing predicted and cloned forms of the *D. pulex* P2XB receptor forms demonstrates translation of single band corresponding to the receptor, this does not provide information as regarding the membrane expression of the receptor. Differences in post-translational modification of *Dpu*P2XB when expressed in HEK293 in comparison to its native environment may result in reduced membrane surface expression in HEK293 cells, and thus reduced membrane currents when subjected to extracellular ATP application, as seen in these previous studies. Immunohistochemical studies, and Western blot of membrane preparations of lysed HEK293 cells to determine the distribution of *Daphnia* P2XB receptors when expressed heterologously are necessary

Amino acid differences between both *Daphnia* P2XB receptor forms and hP2X1-7 subunits were identified in a multiple alignment of primary protein sequences (Fig. 5.2). Although many residues identified as being implicated in conferring ATP sensitivity in mammalian P2X receptors are shared in *Dpu*_p2xB and *Dpu*P2XB, a non-conserved candidate ECD residue was identified that may be responsible for the low potency of ATP at these receptors. In human P2X1, N184 to alanine does not result in any change in ATP potency at the receptor (Roberts and Evans, 2004). However, the equivalent asparagine residue has been shown to be glycosylated in rat P2X1 and P2X2 (Newbolt *et al.*, 1998; Rettinger *et al.*, 2000). This residue is present as an aspartate (D192) at the equivalent position in both *Dpu*_p2xB and *Dpu*P2XB receptor forms. This may suggest that this change could be, at least in part, responsible for the reduced potency of ATP at the receptor.

5.4.3 Putative roles for *Daphnia* P2X receptors

Evidence for a physiological, non-metabolic role for ATP or other nucleotides in *Daphnia* is not present in the literature. However, a role ATP in olfaction has been demonstrated in lobsters where it is hypothesized to be required in the detection of freshly dead prey organisms (Carr *et al.*, 1986; Carr *et al.*, 1987; Zimmer-Faust *et al.*, 1988). Unlike lobsters, *Daphnia* are filter feeders, generating water currents using caudal 'phylopods' that help direct food suspensions into the buccal cavity of the daphnid (Ebert, 2005). It is unclear whether a similar role may be seen in *Daphnia*

in order to identify areas of high densities of suspended algae. Additionally, purines applied to a cardioregulatory-denervated heart of the lobster *Homarus americanum* differentially modulate cardiac activity, with ATP, ADP and AMP increasing heart rate and cardiac contractile force (Maurer *et al.*, 2008). A number of P2 receptor subunits have been identified in mammalian ventricular (Shen *et al.*, 2006) and atrial (Musa *et al.*, 2009) cardiac myocytes, and may suggest a canonical role for P2 receptors in Crustacea, including in *D. pulex*.

Interestingly, a role for the GABAergic and cholinergic neurotransmitter systems was implicated in predator-specific response adaptations in *D. pulex* (Barry, 2002; Weiss *et al.*, 2012). In the presence of the natural predators the 'phantom midge larvae' (genus: Chaoborus) or the three-spined stickleback *Gasterosteus aculeatu*, *Daphnia* adapt to these cues. These cues can either be defensive, whereby daphnids develop small spikes on the dorsal carapace termed 'neckteeth' (Barry, 2002; Weiss *et al.*, 2012), or relate to the gross morphology, whereby daphnids shrink in size. Inhibition of the cholinergic neurotransmitter system by incubation of daphnids with atropine (a competitive agonist at muscarinic acetylcholine receptors (mAchRs) resulted in a decrease in neckteeth expression in Chaoborus-exposed *D. pulex*, whilst the inhibition of acetylcholinesterase (resulting in an increase in Ach levels) by physostigmine increases neckteeth in Chaoborus-exposed daphnids (Weiss *et al.*, 2012). Interestingly, incubation of daphnids with GABA, thus stimulating the GABAergic neurotransmitter pathway, had no effect on neckteeth development in daphnids concomitantly cultured with Chaoborus or *G. aculeatu*, but did reduce daphnid size relative to a non-treated daphnid population in *G. aculeatu* culture (Weiss *et al.*, 2012). The effects of atropine, physostigmine or GABA on morphological changes in *D. pulex* were not seen in isolation, requiring the presence of a chemical cue (a kairomone) from predators (Weiss *et al.*, 2012). It has been demonstrated that ATP is concomitantly released with a number of neurotransmitters, including GABA (Jo and Schlichter, 1999; Jo and Role, 2002) and Ach (Unsworth and Johnson, 1990; Duarte *et al.*, 1999). A similar role may be hypothesised in the nervous system of *D. pulex*, where ATP may be co-released with neurotransmitters to act at receptor effectors. With regards to a physiological role, the nervous system of *Daphnia* is centralised, and mediates many locomotory and sensory roles (Colbourne *et al.*, 2005). It may be hypothesised that, in the case of adaptation to the presence of predators, ATP could be co-released with neurotransmitters involved in mediating

this adaptation. However, the studies of Barry (2002) and Weiss *et al.* (2012) demonstrated that atropine was able to block the formation of neckteeth in *Daphnia* completely. If one were to hypothesis that P2X receptors are involved in the mediation of a predator adaptation response, it would be expected that a residual effect of this receptor would still be present following inhibition of cholinergic signalling.

Although evidence for the role of ATP in lobsters has been suggested, a role for ATP in *Daphnia* is still unclear. Studies investigating the role of purines in lobsters have suggested that ATP plays neuronal, and non-neuronal roles in this crustacean. Although beyond the scope of this thesis, identification of a role for a P2X receptor in *Daphnia*, especially in light of its insensitivity to extracellular ATP, would provide valuable insight into non-mammalian P2X receptor function and pharmacology, as well as the function of P2X receptors in the Pancrustacean lineage.

5.4.4 P2X receptor from an early chordate

Cloning, and subsequent heterologous expression of a predicted P2X receptor from the early chordate *Branchiostoma floridae*, confirmed the presence of an ATP-gated ion channel in this organism. Repeated application of extracellular ATP to *Bflo*P2X-expressing HEK293 cells results in the progressive rundown of evoked inward currents, reaching a steady state in around 5 to 6 applications (Fig. 5.10C). Cloning of a P2X receptor from *Branchiostoma*, as a modern day proxy for the first organisms to have developed a notochord (Wada and Satoh, 1994; Putnam *et al.*, 2008), provides a valuable insight into the chordate origins of P2X receptors. Indeed, use of *B. floridae* in the study of many developmental genes has provided information regarding the evolution of many vertebrate traits, including brain (Holland and Holland, 1999), kidney (Langeland *et al.*, 2006), and pituitary gland development (Candiani and Pestarino, 1998). An understanding of the ontogeny and phylogeny of P2X receptors in the chordate lineage, using *B. floridae* as a model organism, could provide researchers with an experimental system in which to investigate P2X receptor function in analogous organ systems in humans.

Whilst only a 'proof-of-principle' investigation into the expression and ATP sensitivity of *Bflo*P2X in HEK293 cells is presented currently, this chapter has demonstrated that *B. floridae* possesses a functional P2X receptor when expressed heterologously. In addition to possessing a hollow notochord, *Branchiostoma*, and other lancelets share many anatomical features with humans, including segmented musculature and a perforated pharyngeal region (Kowalevsky, 1866). Although beyond the scope of the chapter, a physiological role for *Bflo*P2X *in vivo* may be canonical, mediating the effects of extracellular ATP in similar structures in humans. Conversely, a novel role for P2X receptors in lancelets may be uncovered. Further work to determine this is required.

5.4.5 Expression of P2X receptors in HEK293 cells: Western blot analysis

When expressed heterologously in HEK293 cells, P2X receptors from mammalian and invertebrate species consistently appear as higher molecular weight bands than predicted from primary protein sequence analysis (Valente *et al.*, 2011). It has also been demonstrated that P2X receptors undergo post-translational modification, including phosphorylation and *N*-linked glycosylation that can modulate membrane surface expression and sensitivity to agonists.

Western blot analysis of total protein lysate from HEK293 cells transiently transfected with P2X receptors from *H. vulgaris* (AEP), *D. pulex*, and *B. floridae* all reveal bands of a molecular weight greater than predicted (Fig. 5.6). Whilst *N*-linked glycosylation may explain the increased size of protein bands for many of these receptors, this does not appear to explain the size of band seen in *Bflo*P2X, which appears as a band of approximately 80 kDa, near double its predicted molecular weight of ca. 48 kDa (Fig. 5.6).

In the primary protein sequence of *Bflo*P2X, five candidate *N*-linked glycosylation sites are predicted, based on the presence of the consensus motif 'Nx(S/T)'. However, if one presumes that all of the sites are used as targets for *N*-linked glycosylation in *Bflo*P2X when expressed in HEK293 cells, this does not fully account for the low mobility of the band seen in Western blot analysis. P2X receptors are also known to be phosphorylated; this modification has been demonstrated to accelerate the time

course of desensitisation of P2X1 and P2X2 receptors expressed in *Xenopus* oocytes, (Ennion and Evans, 2002b; Boué-Grabot *et al.*, 2000). In the primary amino acid sequence of *Bflo*P2X, 18 phosphorylation sites are predicted (table 5.1), using the NetPhos 2.0 server tool (Blom *et al.*, 1999) (available at: http://www.cbs.dtu.dk/services/NetPhos/).

Residue	Position	Threshold score
Serine	68	0.967
	132	0.770
	139	0.691
	295	0.786
	298	0.981
	322	0.970
Threonine	20	0.982
	113	0.840
	119	0.974
	120	0.941
Tyrosine	57	0.930
	222	0.958
	276	0.916
	285	0.504
	305	0.747
	380	0.954
	405	0.550
	422	0.896

Table 5.1: predicted phosphorylation sites in *Bflo*P2X

A total of 18 putative phosphorylation sites at serine, threonine, and tyrosine residues were identified in the primary amino acid sequence of *Bflo*P2X. The probability of phosphorylation at these residues was predicted based using a NetPhos 2.0, and a default threshold score of 0.5. Only scores above this threshold are displayed in the table.

An N-terminal PKC phosphorylation site is conserved in *Bflo*P2X (Tx(K/R)) (Boué-Grabot *et al.*, 2000) (Fig. 5.3). Consistent with a role for this motif in P2X receptors, the *Bflo*P2X receptor threonine residue (T20) within this motif is predicted to be phosphorylated (Table 5.1). Furthermore, although a C-terminal serine residue of rat P2X2 (S431) found to be involved in mediating protein kinase A (PKA)-dependent phosphorylation of the receptor (Chow and Wang, 1998) is not conserved in *Bflo*P2X, no C-terminal serine residue is predicted to be phosphorylated in *Bflo*P2X. Post-translational modification of proteins can alter their mobility in SDS-PAGE gels. Presuming that all predicted *N*-linked glycosylation sites of *Bflo*P2X are occupied when expressed heterologously in HEK293 cells, this only accounts for a 10 kDa shift in the expected protein band. It is unclear whether *Bflo*P2X is *N*-linked glycosylated and phosphorylated when expressed in HEK293 cells, and whether these post-translational modifications contribute to the slow mobility of *Bflo*P2X in SDS-PAGE/Western blot (Fig. 5.6). Further analysis through treatment of whole cell lysate expressing the receptor with de-phosphorylating and de-glycosylating enzymes would help to answer this question.

5.4.6 Metazoan P2X receptors in Placazoa

Phylogenetic analysis places Placazoa (and therefore *Trichoplax adhaerens*) as a basal metazoan, not *the* basal metazoan phylum; *T. adhaerens* appears to have diverged after Porifera, but before the divergence of Cnidaria and Bilateria (Dunn *et al.*, 2008; Srivastava *et al.*, 2008; Ryan *et al.*, 2013; Moroz *et al.*, 2014) (section 1.1.1). Analyses presented in the current thesis have identified putative P2X receptors in members of a number of metazoan phyla (Chapter 3). Based on the apparent absence of residues implicated in ATP binding, and formation of ECD topology in the predicted protein sequences of *T. adhaerens* P2XA and P2XB receptor, this organism was chosen for further analysis.

Identification and subsequent cloning of P2X receptors from *T. adhaerens* revealed that regions of both receptors were present (section 5.3.3). The draft assembly of the ca. 98 mega base pair (Mbp) genome of *T. adhaerens* has a sequence coverage of approximately 8-fold, and was derived using a whole-genome shotgun approach (Srivastava *et al.*, 2008). Errors in sequences using this method occur more regularly

than more advanced 'Next Generation Sequencing' (NGS) techniques, but whole-genome shotgun sequencing is faster and less expensive (Miller *et al.*, 2010; Desai *et al.*, 2013). Furthermore, NGS techniques also provide sequence data with a much higher fold sequence coverage (> 100-fold) (Miller *et al.*, 2010; Desai *et al.*, 2013). This may suggest that the apparent discrepancy in the predicted sequences of *T. adhaerens* P2X receptors arose from low sequence coverage in genome sequencing. Recent analyses have been performed in order to investigate the phylogenetic relationship of vertebrate and invertebrate P2X receptors throughout the evolutionary tree of life. Whilst many of the phylogenetic trees constructed have used sequences that have been cloned by PCR, many are also included that are predicted from genomic data alone, and whose expression has not been confirmed. These analyses have often included the predicted, and incomplete, protein sequences of both *T. adhaerens* P2X receptors (Fountain and Burnstock, 2009). As such, confirmation of expression and retrieval of complete cDNA sequences of both *Tad*P2XA and *Tad*P2XB (section 5.3.3), will prove valuable in the construction of more reliable phylogenetic trees, allowing researchers to derive evolutionary relationships between evolutionary distant organisms with greater confidence in the future.

Recent data provided by Smith *et al.* (2014) using a custom antibody against a peptide corresponding to the full length, predicted sequence of *Tad*P2XB suggested that the receptor is expressed in fibre cells that lie between dorsal and ventral epithelia of *T. adhaerens*. Although it is unclear whether the pattern of immunoreactivity seen in this study was specific, if true to the *in vivo* expression pattern of *Tad*P2XB, these findings could shed new light on the early evolutionary origins of neuronal P2X receptor function in multicellular organisms, given the function of fibre cell-like structures in some sponge classes (Mackie and Singla, 1983). Using a combinatorial localisation and pharmacological approach to determine the function of *T. adhaerens* P2X receptors would provide researchers with a greater insight to receptor function in Placazoa and a the evolutionary origins of P2X receptors.

5.5 CONCLUSIONS

1. At least one gene encoding a P2X receptor homologue is predicted to be encoded in the genomes of *Daphnia pulex*, *Trichoplax adhaerens*, and *Branchiostoma floridae*. Subsequent cloning and electrophysiological analysis of several of these predicted P2X receptors confirmed that they form an ATP-gated ion channel when expressed heterologously in HEK293 cells.
2. Attempts to amplify the predicted *D. pulex* P2XA receptor by PCR were unsuccessful, but predicted (*Dpu*_p2xB) and cloned (*Dpu*P2XB) forms of the *D. pulex* P2XB receptor are largely insensitive to extracellular ATP when expressed heterologously in HEK293 cells. The potency of ATP at these receptors can be increased in a low extracellular divalent cation environment, suggesting that ATP^{4-} is a ligand at *D. pulex* P2XB receptors and/or Ca^{2+} is an allosteric inhibitor of ATP-evoked inward currents.
3. *Branchiostoma floridae* expresses a P2X receptor homologue that, when expressed heterologously in HEK293 cells, responded in a concentration-dependent manner to extracellular ATP application. Furthermore, repeated application of extracellular ATP (1 mM) (with a 90 s ECS wash between applications) resulted in rundown of inward currents through the receptor
4. Contrary to predicted nucleotide and translated protein sequences for two *Trichoplax adhaerens* P2X receptor sequences, regions implicated in P2X receptor function in vertebrate and many invertebrate organisms are present in cloned forms of these receptors. This discrepancy may be due to sequencing errors arising from whole-genome shotgun sequencing methods used in the sequencing of *T. adhaerens*.
5. Application of 1 mM ATP to HEK293 cells heterologously expressing *T. adhaerens* P2XA (*Tad*P2XA) does not evoke inward currents at the receptor.

Chapter 6:

Conclusions and future directions

6 Conclusions and future directions

During the course of my thesis, I have investigated the putative expression of P2X receptors in a range of eukaryotic phyla. Based on these findings, the pharmacology of cloned P2X receptors from members of the Cnidaria, Arthropoda, Chordata, and Placazoa was assessed, with a major focus on a P2X receptor from the cnidarian *Hydra* (aepP2X). The localisation of aepP2X was also investigated using custom polyclonal antiserum and peptide affinity-purified antibody. In the following section, I should like to recapitulate the principle findings made during this study and methods required to advance the findings presented herein.

6.1 P2X RECEPTORS IN EUKARYOTIC PHYLOGENY

Previous studies have demonstrated or suggested the expression of P2X receptor homologues in a number of multicellular eukaryotes (Agboh *et al*., 2004; Bavan *et al*, 2008; Bavan *et al*., 2011; Sakurai *et al*., 2012; Bavan *et al*., 2012), amoeba (Fountain *et al*., 2007; Ludlow *et al*., 2009), unicellular algae and a chonaoflagellate (Fountain *et al*., 2008), and fungi (Cai and Clapham, 2011; Cai, 2012). Through homology searching of available transcriptomic and genomic datasets, I confirmed the findings of these studies and expanded on our understanding of these previously identified putative P2X receptors by analysing the primary amino acid sequences of these predicted proteins. Importantly, expansion of this homology search throughout a number of eukaryotic phyla identified, for the first time, partial and putatively full-length transcripts from a number of Insecta orders, the translated protein products of which shared considerable sequence homology to human P2X receptor subunits. Furthermore, candidate P2X receptors were identified in a multicellular alga (*Nitella hyalina*), widely considered a member of a sister taxon to land plants (Karol *et al.*, 2001; Kranz *et al.*, 1995; Turmel *et al.*, 2006; Hori *et al.*, 2014). To confirm function of candidate P2X receptors from insects and other eukaryotic organisms as ATP-gated ion channels, molecular cloning followed by heterologous expression in a mammalian system (such as HEK293 cells) should be performed. I anticipate that heterologous expression of these candidate receptors in a suitable expression system would result in the formation of an ATP-sensitive ion channel.

With the increasing availability of sequence data from organisms throughout the evolutionary 'tree of life', further in-depth analysis of the conservation of P2X receptors within phyla will be possible. As a result, an increasing number of roles for invertebrate P2X receptors may be uncovered, and may highlight previously unconsidered roles for this LGIC family in humans.

6.2 HYDRA EXPRESS A FUNCTIONAL ATP-GATED ION CHANNEL

I was able to demonstrate that, when expressed heterologously in HEK293 cells, a P2X receptor from the cnidarian *Hydra vulgaris* (AEP) ('aepP2X') responds in a concentration-dependent manner to extracellular ATP application, but is largely insensitive to several purinergic receptor antagonists. Residues implicated in antagonist efficacy at human P2X receptor subunits are incompletely conserved, suggesting a similar molecular basis of insensitivity of these antagonists at aepP2X. Future work may involve the site-directed mutagenesis of residues in aepP2X that may account for antagonist ineffectiveness, followed by re-assessment of the action of the antagonist in co- and pre-application with extracellular ATP. This includes L268, which lies at an equivalent position of a glutamate residue required for PPADS sensitivity in human P2X4 (section 4.4.2).

Mutually exclusive staining of distinct structures in whole *Hydra* polyps with polyclonal antiserum and peptide affinity-purified antibody does not provide a definitive answer as to the *in vivo* localisation of aepP2X. However, roles for aepP2X in the physiology and development of nematocysts have been described. Whilst a second inoculation programme may help to exclude the possibility of errors during antibody generation, further work is required to ascertain specific binding of polyclonal antibodies (in serum or purified form) to aepP2X. Western blot (WB) analysis against whole polyp and aepP2X-expressing HEK293 cell lysate using crude antiserum and purified polyclonal antibody should identify candidate protein bands of a size predicted for aepP2X. Pre-incubation of antiserum or peptide affinity-purified antibody with a ca. 200-fold excess of the peptide antigen used to evoke an antibody response in immunised rabbits (a so-called 'peptide competition assay' (PCA)) would help confirm specific band reactivity between aepP2X-specific crude serum or peptide purified antibodies in either Western blot or IHC protocols. Using this

method, if an antibody is specific to aepP2X, I would expect to see a loss of reactivity in either WB or IHC.

I have also demonstrated a 'proof of concept' transgenic *Hydra* line, whereby an aepP2X::eGFP fusion protein is overexpressed under the control of a *H. magnipapillata β-actin* promoter. Although slow to develop, this actin-aepP2X::eGFP transgenic line would prove useful in IHC using both forms of anti-aepP2X polyclonal antibody. Using these polyps, dual IHC performed using an anti-GFP antibody and either the crude antiserum or purified antibody should result in co-localisation of secondary antibody immunofluorescence if either of these custom antibodies targets aepP2X (and thus, the aepP2X::eGFP fusion protein).

Additionally, RNAi knockdown in *Hydra* polyps using *β-actin* promoter-driven 'hairpin' constructs to selectively reduce *aepp2x* mRNA transcript levels would provide a useful negative control in IHC experiments. Where specific binding of an antibody against aepP2X is seen in WT polyps, no staining of the same structures should be seen in the transgenic lines in which aepP2X transcript level is knocked down. Transgenic polyps stably expressing hairpin-type RNAi constructs have already developed, resulting in near complete reduction in either MyD88 (Franzenburg *et al.*, 2012) or FoxO (Boehm *et al.*, 2012) transcript levels, as demonstrated by RT-PCR and *in situ* hybridisation. Whole-mount *in situ* hybridisation of *Hydra* polyps may also corroborate findings from IHC, whereby *aepp2x* mRNA transcript may localise to the same structures identified in IHC with crude or purified antiserum.

Following confirmation of specific binding of either crude antiserum or PAPAb in either nematocysts (section 4.3.3) or interstitial cell nucleoli, respectively (section 4.3.5), functional assays are required to determine a role for aepP2X in *Hydra* physiology. Although the cell-type localisation of aepP2X is unclear, changes in cell morphology and number following RNAi knockdown of *aepp2x* transcript can be readily monitored following whole polyp maceration (David, 1973). Stable endodermal and ectodermal epithelial cell expression of the cytoplasmic Ca^{2+}-indicator GCaMP (Nakai *et al.*, 2001), under the control of a β-actin promoter, has been demonstrated in *H. vulgaris* (AEP) polyps (Weislogel, 2008). Similarly, using a *Hydra* sp. (or *H. vulgaris* (AEP)-specific) P2X receptor promoter to drive expression

of GCaMP in those cells expressing also aepP2X, an analysis of the *in vivo* ATP-evoked Ca^{2+} responses of this receptor can be performed. This transgenic line could be coupled with further pharmacological analysis of potential antagonists of aepP2X in heterologous systems to identify a suitable antagonist for blocking this receptor *in vivo*. Furthermore, high-speed microimaging of nematocyst discharge propensity in the presence of a specific antagonist (according to Holstein and Tardent (1984) and Nüchter *et al*., 2006), following their isolation in an undischarged form (as in Blanquet, 1983), may confirm the functional involvement of aepP2X in this cell type. If aepP2X is expressed in nematocysts, and is orientated such that its ECD is orientated towards the extracellular milieu, I would expect an antagonist of aepP2X to block the effect of ATP in discharge. Incubation of polyps with crude antiserum in IHC also appears to stain differentiating nematocyst. To confirm this, co-IHC using crude antiserum and an antibody specific to a protein present in differentiating nematocysts, such as cnidoin (Balasubramanian *et al.*, 2012) would be required.

6.3 FURTHER CHARACTERISATION OF NOVEL P2X RECEPTORS

In addition to cloning and functionally expressing a P2X receptor from *Hydra* in HEK293 cells, P2X receptor homologues were analysed from the microcrustacean *D. pulex*. One of two predicted receptors was amplified by PCR (*Dpu*P2XB), the other paralogue could not be amplified. Although ATP appears to be largely ineffective at this receptor, further work is required to determine whether another compound is this receptor's primary agonist. Recent work by Baines and colleagues has demonstrated that consideration of the ionic environment of the native system within which a P2X receptor is expressed is important, and can drastically alter the sensitivity of a receptor to ATP (Baines *et al*., 2013). Similar analyses should be performed with *Dpu*P2XB to assess whether simulation of *Daphnia* haemolymph pH and ionic composition in whole-cell electrophysiology recordings can also improve the ATP sensitivity of *Dpu*P2XB.

A single *p2x* receptor gene transcript from the amphioxus *Branchistoma floridae* was also identified, cloned and confirmed as an ATP-gated ion channel in HEK293 cells. In addition to further pharmacological characterisation of the sensitivity of *Bflo*P2X to purinergic agonists and antagonists, a functional role for this early chordate P2X

receptor must also be identified. In identifying a role for *Bflo*P2X, this may shed light on the origins of P2X receptor function in higher vertebrates, including humans. Morpholinos and antisense mRNA oligonucleotides have been used successfully to knockdown mRNA expression in *B. floridae* embryos (Holland and Onai, 2011), and may represent a valuable technique for analysing the role of this single amphioxus *p2x* receptor transcript. The well-defined anatomy of embryonic and mature forms of *B. floridae* (Jollie, 1962), in combination with the availability of established *in situ* hybridisation protocols for analysis of mRNA transcript expression in *B. floridae* (Holland *et al.*, 1992), would allow the cellular localisation of *p2x* mRNA to be determined with ease and a functional role hypothesised.

Further work is required to analyse the ineffectiveness of ATP at one of the two *T. adhaerens* P2X receptor paralogues, including the possibility of other purine compounds to activate *Tad*P2XA. In addition to pharmacological characterisation of *Tad*P2XB, co-expression of both paralogues may also provide important information regarding stoichiometry of *Trichoplax* P2X receptors in this system. Co-expression may be performed through heterologous expression of two plasmids encoding separately for *Tad*P2XA and *Tad*P2XB, or one plasmid containing three in-frame 'concatenated' transcripts. Expression of a concatenated transcript would allow control of the stoichiometry of a *T. adhaerens* P2X receptor protein, for instance a 2:1 ratio of *T. adhaerens p2xA* and *p2xB* transcript would result in a translated protein trimer containing two *Tad*P2XA subunits and one *Tad*P2XB subunit. The stoichiometry of a P2X receptor can alter its function, such as is seen in P2X2/3 heteromeric receptors. The trinitrophenol-substituted AMP compound, TNP-AMP antagonises P2X2 and P2X3 homomers with an IC_{50} of ca. 3 and 3500 nM, respectively, whilst a TNP-AMP antagonises currents through a heteromer of P2X2/3 at ca. 40 nM (Virginio *et al.*, 1998b). Construction of similar concatenated subunits, followed by analysis of expressed proteins in HEK293 cells by whole-cell voltage-clamp may reveal distinct pharmacological profiles of these two receptor subunits.

Finally, a recent comprehensive analysis of the cellular diversity of the placazoan *Trichoplax adhaerens* (Smith *et al.*, 2014) represents a significant advance in our understanding of the anatomy of this early metazoan. This study also suggested the expression of *Tad*P2XB in fibre cells of *Trichoplax* (Smith *et al*., 2014). Future work is required to confirm this finding in light of the current finding present herein that

the predicted transcript sequence is not the same as the predicted transcript (as confirmed by RT-PCR) (section 5.3.3). RNA interference (RNAi) has been used to investigate hypoxia-inducible transcription factor signalling pathway components in *T. adhaerens* (Loenarz *et al.*, 2011). To investigate the role of *Tad*P2X receptors in live animals, the use of small interfering RNAs (siRNAs) to selectively knockdown these transcripts could be used. Confirmation of *Tad*P2X receptor knockdown by a combinatorial approach of RT-PCR and *in situ* hybridisation would be required. Although the function of fibre cells is not clear, they may play a role in animal movement thorough contraction of surrounding epithelial cell. RNAi knockdown of *Tad*P2X receptor subunits by siRNAs and assessment of movement of treated animals may highlight a role for P2X receptors in these behaviours.

References

7 References

Abbracchio, M.P., Burnstock, G., Boeynaems, J.M. *et al.* (2006). International Union of Pharmacology LVIII: update on the P2Y G protein-coupled nucleotide receptors: from molecular mechanisms and pathophysiology to therapy. *Pharmacological Review*, **58** (3), pp. 281-341.

Abraham, E.H., Prat, A.G., Gerweck, L. *et al.* (1993). The multidrug resistance (*mdr1*) gene product functions as an ATP channel. . *Proceedings of the National Academy of Sciences*, **90** (1), pp. 312-316.

Acuna-Castillo, C., Coddou, C., Bull, P. & Huidobro-Toro, J.P. (2007). Differential role of extracellular hisitidines in copper, zinc, magnesium and proton modulation of the P2X7 purinergic receptor. . *Journal of Neurochemistry*, **101** (1), pp. 17-26.

Adams, M.D., Celniker, S.E., Holt, R.A. *et al.* (2000). The genome sequence of *Drosophila melanogaster*. *Science*, **287** (5461), pp. 2185-2195.

Adl, S.M., Simpson, A.G., Farmer, M.A. *et al.* (2005). The new higher level classification of eukaryotes with emphasis on the taxonomy of protists. *J Eukaryot Microbiol*, **52** (5), pp. 399-451.

Adl, S.M., Simpson, A.G., Lane, C.E. *et al.* (2012). The revised classification of eukaryotes. *Journal of Eukaryotic Microbiology*, **59** (5), pp. 429-493.

Aeme, B.L., Stidwill, R.P. & Tardent, P. (1991). Nematocysts discharge in *Hydra* does not require the presence of nerve cells. *Journal of Experimental Zoology*, **258** 137-141.

Afferent Pharmaceuticals. 2012. *A study to assess the efficacy of AF-219, a P2X3 receptor antagonist, in subjects with chronic cough* [Online]. Bethesda (MD): National Library of Medicine (US). Available: http://clinicaltrials.gov/show/NCT01432730 [Accessed 08 March 2013].

Afferent Pharmaceuticals. 2013a. *A four-week multicenter study evaluating the safety and efficacy of AF-219 in subjects with osteoarthritis of the knee* [Online]. Bethesda (MD): National Library of Medicine (US). Available: http://clinicaltrials.gov/show/NCT01554579 [Accessed 08 March 2013].

Afferent Pharmaceuticals. 2013b. *The safety and efficacy of AF-219 in female subjects with interstitial cystitis/bladder pain syndrome* [Online]. Bethesda (MD): National Library Of Medicine (US). Available: http://clinicaltrials.gov/show/NCT01569438 [Accessed 08 March 2013 2013].

Agboh, K.C., Webb, T.E., Evans, R.J. & Ennion, S.J. (2004). Functional characterization of a P2X receptor from *Schistosoma mansoni*. *Journal of Biological Chemistry*, **279** (40), pp. 41650-41657.

Aguinaldo, A.M., Turbeville, J.M., Linford, L.S. *et al.* (1997). Evidence for a clade of nematodes, arthropods and other moulting animals. *Nature*, **387** (6632), pp. 489-493.

Alföldi, J., Di Palma, F., Grabherr, M. *et al.* (2011). The genome of the green anole lizard and a comparative analysis with birds and mammals. *Nature*, **477** (7366), pp. 587-591.

Allsopp, R.C., Lalo, U. & Evans, R.J. (2010). Lipid raft association and cholesterol sensitivity of $P2X_{1-4}$ receptors for ATP: chimeras and point mutants identify intracellular amino-terminal residues involved in lipid regulation of $P2X_1$ receptors. *Journal of Biological Chemistry*, **285** (43), pp. 32770-32777.

Alstad, N.E., Skardal, W.L. & Hessen, D.O. (1999). The effect of calcium concentration on the calcification of *Daphnia magna*. *Limnology and Oceanography*, **44** (8), pp. 2011-2017.

Anadón, R., Adrio, F. & Rodríguez-Moldes, I. (1998). Distribution of GABA immunoreactivity in the central and peripheral nervous system of amphioxus (*Branchiostoma lanceolatum* Pallas). *Journal of Comparative Neurology*, **401** (3), pp. 293-307.

Anderson, P.A. & Spencer, A.N. (1989). The importance of cnidarian synapses for neurobiology. *Journal of Neurobiology*, **20** (5), pp. 435-457.

Aschrafi, A., Sadtler, S., Niculescu, C. *et al.* (2004). Trimeric architecture of homomeric $P2X_2$ and heteromeric $P2X_{1+2}$ receptor subtypes. *Journal of Molecular Biology*, **342** (1), pp. 333-343.

Ascoli-Christensen, A., Sutcliffe, J.F. & Albert, P.J. (1991). Purinoceptors in blood feeding behaviour in the stable fly, *Stomoxys calcitrans*. *Physiological Entomology*, **16** (2), pp. 145-152.

Atkinson, L., Milligan, C.J., Buckley, N.J. & Deuchars, J. (2002). An ATP-gated ion channel at the cell nucleus. *Nature*, **420** (6911), pp. 42.

Aury, J.M., Jaillon, O., Duret, L. *et al.* (2006). Global trends of whole-genome duplications revealed by the ciliate *Paramecium tetraurelia*. *Nature*, **444** (7116), pp. 171-178.

Baines, A., Parkinson, K., Sim, J.A. *et al.* (2013). Functional properties of five *Dictyostelium discoideum* P2X receptors. *Journal of Biological Chemistry*, **288** (28), pp. 20992-21000.

Bairoch, A., Apweiler, R., Wu, C.H. *et al.* (2005). The Universal Protein Resource (UniProt). *Nucleic Acids Research*, **33** (Database issue), pp. D154-159.

Balasubramanian, P.G., Beckmann, A., Warnken, U. *et al.* (2012). Proteome of *Hydra* nematocyst. *Journal of Biological Chemistry*, **287** (13), pp. 9672-9681.

Banta, A.M. (1919). Sex and sex intergrades in cladocera. *Proceedings of the National Academy of Sciences*, **4** (12), pp. 373-379.

Banta, A.M. & Brown, L.A. (1929). Control of sex in cladocera. III. Localization of the critical period for control of sex. *Proceedings of the National Academy of Sciences*, **15** (2), pp. 71-81.

Bao, L., Locovei, S. & Dahl, G. (2004). Pannexin membrane channels are mechanosensitive condiuts for ATP. *FEBS Letters*, **572** (1), pp. 65-68.

Barankiewicz, J. & Cohen, A. (1985). Purine nucleotide metabolism in resident and activated rat macrophages *in vitro*. *European Journal of Immunology*, **15** (6), pp. 627-631.

Barrera, N.P., Ormond, S.J., Henderson, R.M. *et al.* (2005). Atomic force microscopy imaging demonstrates that P2X2 receptors are trimers but that P2X6 receptor subunits do not oligomerize. *Journal of Biological Chemistry*, **280** (11), pp. 10759-10765.

Barry, M.J. (2002). Progress toward understanding the neurophysiological basis of predator-induced morphology in *Daphnia pulex*. *Physiological and Biochemical Zoology*, **75** (2), pp. 179-186.

Barry, P.H. (1994). JPCalc - a software package for calculating liquid junction potential corrections in patch-clamp, intracellular, epithelial and bilayer measurements and for correcting junction potential measurements. *Journal of Neuroscience Methods*, **51** 107-116.

Bause, E. (1983). Structural requirements of N-glycosylation of proteins. Studies with proline peptides as conformational probes. *Biochemical Journal*, **209** (2), pp. 331-336.

Bavan, S., Farmer, L., Singh, S.K. *et al.* (2011). The penultimate arginine of the carboxy terminus determines slow desensitization in a P2X receptor from the cattle tick *Boophilus microplus*. *Molecular Pharmacology*, **79** (4), pp. 776-785.

Bavan, S., Straub, V.A., Blaxter, M.L. & Ennion, S.J. (2008). A P2X receptor from the tardigrade species *Hypsibius dujardini* with fast kinetics and sensitivity to zinc and copper. *BMC Evolutionary Biology*, **9** (17), pp.

Bavan, S., Straub, V.A., Webb, T.E. & Ennion, S.J. (2012). Cloning and characterization of a P2X receptor expresed in the central nervous system of *Lymnaea stagnalis*. *PLoS One*, **7** (11), pp. e50487.

Baxter, A.W., Choi, S.J., Sim, J.A. & North, R.A. (2011). Role of P2X4 receptors in synaptic strengthening in mouse CA1 hippocampal neurons. . *European Journal of Neuroscience*, **34** (2), pp. 213-220.

Bazemore, A.W., Eilliot, K.a.C. & Florey, E. (1957). Isolation of factor I. *Journal of Neurochemistry*, **1** (4), pp. 334-339.

Bean, B.P. (1990). ATP-activated channels in rat and bullfrog sensory neurons: concentration dependence and kinetics. *Journal of Neuroscience*, **10** (1), pp. 1-10.

Beigi, R., Kobatake, E., Aizawa, M. & Dubyak, G.R. (1999). Detection of local ATP release from activated platelets using cell surface-attached firefly luciferase. *American Journal of Physiology*, **276** (1), pp. 267-278.

Bellis, S.L., Grosvenor, W., Kass-Simon, G. & Rhoads, D.E. (1991). Chemoreception in *Hydra vulgaris* (*attenuata*): initial characterization of two distinct binding sites for L-glutamic acid. *Biochimica et Biophysica Acta*, **1061** (1), pp. 89-94.

Benson, D.A., Clark, K., Karsch-Mizrachi, I. *et al.* (2014). GenBank. *Nucleic Acids Research*, **42** (Database issue), pp. D32-37.

Benterbusch, R. & Melzer, W. (1992). Ca^{2+} current in myotome cells of the lancelet (*Branchiostoma lanceolatum*). *Journal of Physiology*, **450** 437-453.

Berking, S. & Hermann, K. (2006). Formation and discharge of nematocysts is controlled by a proton gradient across the cyst membrane. *Helgoland Marine Research*, **60** (3), pp. 180-188.

Berney, C. & Pawlowski, J. (2006). A molecular time-scale for eukaryote evolution recalibrated with the continuous microfossil record. *Proceedings of the Royal Society of London B: Biological Sciences*, **273** (1596), pp. 1867-1872.

Bernier, L.P., Ase, A.R., Chevallier, S. *et al.* (2008a). Phosphoinositides regulate P2X4 ATP-gated ion channels through direct interactions. *Journal of Neuroscience*, **28** (48), pp. 12938-12945.

Bernier, L.P., Ase, A.R., Tong, X. *et al.* (2008b). Direct modulation of P2X1 receptor-channels by the lipid phosphatidylinositol 4,5-bisphosphate. *Molecular Pharmacology*, **74** (3), pp. 785-792.

Bernier, L.P., Blais, D., Boué- Grabot, É. & Séguéla, P. (2012). A dual polybasic motif determins phosphoinositide binding and regulation in the P2X channel family. *PLoS One*, **7** (7), pp. e40595.

Bian, X., Ren, J., Devries, M. *et al.* (2003). Peristalsis is impaired in the small intestine of mice lacking the $P2X_3$ subunit. *Journal of Physiology*, **551** (1), pp. 309-322.

Bianchi, B.R., Lynch, K.J., Touma, E. *et al.* (1999). Pharmacological characterization of recombinant human and rat P2X receptor subtypes. *European Journal of Pharmacology*, **376** (1-2), pp. 127-138.

Bianco, F., Ceruti, S., Colombo, A. *et al.* (2006). A role for $P2X_7$ in microglial proflieration. *Journal of Neurochemistry*, **99** (3), pp. 745-758.

Blair, J.E. & Hedges, S.B. (2005). Molecular phylogeny and divergence times of deuterostome animals. *Molecular Biology and Evolution*, **22** (11), pp. 2275-2284.

Blank, A., Gallant, J.A., Burgess, R.R. & Loeb, L.A. (1986). An RNA polymerase mutant with reduced accuracy of chain elongation. *Biochemistry*, **25** (20), pp. 5920-5928.

Blanquet, R.S. 1983. Isolating undischarged and discharged nematocysts from acontiate sea anemones. *In:* LENHOFF, H.M. (ed.) *Hydra: Research Methods.* Springer US.

Blattner, F.R., Plunkett, G.R., Bloch, C.A. *et al.* (1997). The complete genome sequence of *Escherichia coli* K-12. *Science*, **277** (5331), pp. 1453-1462.

Blom, N., Gammeltoft, S. & Brunak, S. (1999). Sequence and structure-based prediction of eukaryotic protein phosphorylation sites. *Journal of Molecular Biology*, **294** (5), pp. 1351-1362.

Bo, X., Schoepfer, R. & Burnstock, G. (2000). Molecular cloning and characterization of a novel ATP P2X receptor subtype from embryonic chick skeletal muscle. *Journal of Biological Chemistry*, **275** (19), pp. 14401-14407.

Bo, X., Zhang, Y., Nassar, M. *et al.* (1995). A P2X purinoceptor cDNA conferring a novel pharmacological profile. *FEBS Letters*, **375** (1-2), pp. 129-133.

Bobanović, L.K., Royle, S.J. & Murrell-Lagnado, R.D. (2002). P2X receptor trafficking in neurons is subunit specific. *Journal of Neuroscience*, **22** (12), pp. 4814-4824.

Bock, P. (1980). Identification of paraneurons by labelling with quinacrine (Atebrin). *Archivum Histologica Japonica*, **43** (1), pp. 35-44.

Bode, H.R. & David, C.N. (1978). Regulation of a multipotent stem cell, the interstitial cell of hydra. *Progress in Biophysics and Molecular Biology*, **33** (2), pp. 189-206.

Bode, H.R., Flick, K.M. & Smith, G.S. (1976). Regulation of interstitial cell differentiation in *Hydra attenuata*. I. Homeostatic control of interstitial cell population size. *Journal of Cell Science*, **20** (1), pp. 29-46.

Boehm, A.-M., Khalturin, K., Anton-Erxleben, F. *et al.* (2012). FoxO is a critical regulator of stem cell maintenance in immortal *Hydra*. *Proceedings of the National Academy of Sciences*.

Bosch, T.C. & David, C.N. (1986). Male and female stem cells and sex reversal in *Hydra* polyps. *Proceedings of the National Academy of Sciences*, **83** (24), pp. 9478-9482.

Bosch, T.C.G. & David, C.N. (1987). Stem cells of *Hydra magnipapillata* can differentiate into somatic cells and germ line cells. *Developmental Biology*, **121** (1), pp. 182-191.

Bosch, T.C.G. & David, C.N. (1990). Cloned interstitial stem cells grow as contiguous patches in hydra. *Developmental Biology*, **138** (2), pp. 513-515.

Boué-Grabot, E., Archambault, V. & Séguéla, P. (2000). A protein kinase C site highly conserved in P2X subunits controls the desensitization kinetics of $P2X_2$ ATP-gated channels. *Journal of Biological Chemistry*, **275** 10190-10195.

Bradford, M.M. (1976). A rapid and sensitive method for the quantitation of microgram quantities of protein utilizing the principle of protein-dye binding. *Annals of Biochemistry*, **72** 248-254.

Brake, A.J., Wagenbach, M.J. & Julius, D. (1994). New structural motif for ligand-gated ion channels defined by an ionotropic ATP receptor. *Nature*, **37** (6497), pp. 519-523.

Bridge, D., Cunningham, C.W., Schierwater, B. *et al.* (1992). Class-level relationships in the phylum Cnidaria: molecular and morphological evidence. *Proceedings of the National Academy of Sciences*, **89** (18), pp. 8750-8753.

Brien, P. (1953). La pérennité somatique. *Biological Reviews*, **28** (3), pp. 308-349.

Briggs, D.E.G. & Fortey, R.A. (1989). The early radiation and relationships of the major arthropod groups. *Science*, **246** (4927), pp. 241-243.

Brinkmann, M., Oliver, D. & Thurm, U. (1996). Mechanoelectric transduction in nematocytes of a hydropolyp (Corynidae). *Journal of Comparative Physiology A*, **178** 125-138.

Brown, S.G., Townsend-Nicholson, A., Jacobson, K.A. *et al.* (2002). Heteromultimeric $P2X_{1/2}$ receptors show a novel sensitivity to extracellular pH. *Journal of Pharmacology and Experimental Therapeutics*, **300** (2), pp. 673-680.

Browne, L.E., Compan, V., Bragg, L. & North, R.A. (2013). P2X7 receptor channels allow direct permeation of nanometer-sized dyes. *The Journal of Neuroscience*, **33** (8), pp. 3557-3566.

Browne, L.E. & North, R.A. (2013). P2X receptor intermediate activation states have altered nucleotide selectivity. *The Journal of Neuroscience*, **33** (37), pp. 14801-14808.

Buell, G., Lewis, C., Collo, G. *et al.* (1996). An antagonist-insensitive P2X receptor expressed in epithelia and brain. *EMBO Journal*, **15** (1), pp. 55-62.

Burki, F. & Pawlowski, J. (2006). Monophyly of Rhizaria and multigene phylogeny of unicellular bikonts. *Molecular Biology and Evolution*, **23** (10), pp. 1922-1930.

Burki, F., Shalchian-Tabrizi, K., Minge, M. *et al.* (2007). Phylogenomics reshuffles the eukaryotic supergroups. *PLoS One*, **2** (8), pp. e790.

Burman, C. & Evans, P.D. (2010). Amphioxus expresses both vertebrate-type and invertebrate-type dopamine D(1) receptors. *Invertebrate Neuroscience*, **10** (2), pp. 93-105.

Burman, C., Reale, V., Srivastava, D.P. & Evans, P.D. (2009). Identification and characterization of a novel amphioxus dopamine D-like receptor. *Journal of Neurochemistry*, **111** (1), pp. 26-36.

Burnstock, G. (1972). Purinergic nerves. *Pharmacological Review*, **24** (3), pp. 509-581.

Burnstock, G. (1996). Purinoceptors: onotogeny and phylogeny. *Drug Development Research*, **39** (3-4), pp. 204-242.

Burnstock, G. (2014). Physiopathological roles of P2X receptors in the central nervous system. *Curr Med Chem*.

Burnstock, G., Campbell, D., Stachell, D. & Symythe, A. (1970). Evidence that adenosine triphosphate or a related nucleotide is the transmitter substance released by non-adrenergic inhibitory nerves in the gut. *British Journal of Pharmacology*, **40** (4), pp. 668-688.

Burnstock, G., Campbell, G., Bennett, M. & Holman, M.E. (1963). Inhibition of the smooth muscle on the taenia coli. *Nature*, **200** 581-582.

Burnstock, G. & Verkhratsky, A. 2012. *Purinergic signalling and the nervous system,* Berlin, Springer Berlin Heidelberg.

Butler, K., English, A.R., Ray, V.A. & Timreck, A.E. (1970). Carbenicillin: chemistry and mode of action. *Journal of Infectious Diseases*, **122** S1-8.

Bzowska, A., Kulikowska, E. & Shugar, D. (2000). Purine nucleoside phosphorylases: properties, functions and clinical aspects. *Pharmacology and Therapeutics*, **88** 349-425.

Cai, X. (2012). P2X receptors homologs in basal fungi. *Purinergic Signaling*, **8** (1), pp. 11-13.

Cai, X. & Clapham, D.E. (2011). Ancestral Ca^{2+} signaling machinery in early animal and fungal evolution. *Molecular Biology and Evolution*, **29** (1), pp. 91-100.

Campbell, R.D. (1967). Tissue dynamics of steady state growth in *Hydra littoralis*. II. Patterns of tissue movement. *Journal of Morphology*, **121** (1), pp. 19-28.

Campbell, R.D. (1976). Elimination by *Hydra* interstitial and nerve cells by means of colchicine. *Journal of Cell Science*, **21** (1), pp. 1-13.

Campbell, R.D. (1987). Organization of the nematocyst battery in the tentacle of hydra: arrangement of the complex anchoring junctions between nematocytes, epithelial cells, and basement membrane. *Cell and Tissue Research*, **249** (3), pp. 647-655.

Campbell, R.D. (1989). Taxonomy of the European *Hydra* (Cnidaria: Hydrozoa): a re-examination of its history with emphasis on the species *H. vulgaris* Pallas, *H. attenuata* Pallas and *H. circumcincta* Schulze. *Zoological Journal of the Linnean Society*, **95** (3), pp. 219-244.

Campbell, R.D. & David, C.N. (1974). Cell cycle kinetics and development of *Hydra attenuata*. II. Interstitial cells. *Journal of Cell Science*, **16** (2), pp. 349-358.

Candiani, S., Oliveri, D., Parodi, M. *et al.* (2005). AmphiD1/beta, a dopamine D1/beta-adrenergic receptor from the amphioxus *Branchiostoma floridae*: evolutionary aspects of the catecholaminergic system during development. *Development, Genes and Evolution*, **215** (12), pp. 631-638.

Candiani, S., Oliveri, D., Parodi, M. & Pestarino, M. (2006). Expression of AmphiNaC, a new member of the amiloride-sensitive sodium channel related to degenerins and epithelial sodium channels in amphioxus. *Int J Biol Sci*, **2** (2), pp. 79-86.

Candiani, S. & Pestarino, M. (1998). Expression of the tissue-specific transcription factor Pit-1 in the lancelet, *Branchiostoma lanceolatum*. *Journal of Comparative Neurology*, **392** (3), pp. 343-351.

Cao, L., Broomhead, H.E., Young, M.T. & North, R.A. (2009). Polar residues in the second transmembrane domain of the rat P2X2 receptor that affect spontaneous gating, unitary conductance, and rectifcation. *Journal of Neuroscience*, **29** (45), pp. 14257-14264.

Carpenter, D., Meadows, H.J., Brough, S. *et al.* (1999). Site-specific splice varation of the human $P2X_4$ receptor. *Neuroscience Letters*, **273** (3), pp. 183-186.

Carr, W.E.S., Ache, B.W. & Gleeson, R.A. (1987). Chemoreceptors of crustaceans: similarities to receptors for neuroactive substances in internal tissues. *Environmental Health Perspectives*, **71** 31-46.

Carr, W.E.S., Gleeson, R.A., Ache, B.W. & Milstead, M.L. (1986). Olfactory receptors of the spiny lobster: ATPase-sensitive cells with similarites to P2-type purinoceptors of vertebrates. *Journal of Comparative Physiology A: Neuroethology, Sensory, Neural, and Behavioral Physiology*, **158** (3), pp. 331-338.

Cavalier-Smith, T. 1987. *The origin of fungi and pseudofungi,* Cambridge, Cambridge University Press.

Cavalier-Smith, T. (2002). The phagotrophic origin of eukaryotes and phylogenetic classification of Protozoa. *International Journal of Systematic and Evoutionaryl Microbiology*, **52** (2), pp. 297-354.

Cavalier-Smith, T. (2010). Kingdoms Protozoa and Chromista and the eozoan root of the eukaryotic tree. *Biol Lett*, **6** (3), pp. 342-345.

Cavalier-Smith, T., Chao, E.E., Snell, E.A. *et al.* (2014). Multigene eukaryote phylogeny reveals the likely protozoan ancestors of opisthokonts (animals, fungi, choanozoans) and Amoebozoa. *Molecular Phylogenetics and Evolution*.

Chan, P.P., Holmes, A.D., Smith, A.M. *et al.* (2012). The UCSC Archaeal Genome Browser: 2012 update. *Nucleic Acids Research*, **40** (Database issue), pp. D646-652.

Chan, T.K., Geren, C.R., Howell, D.E. & Odell, G.V. (1975). Adenosine triphosphate in tarantula spider venoms and its synergistic effect with the venom toxin. *Toxicon*, **13** (1), pp. 61-66.

Chapman, G.B. & Tilney, L.G. (1959a). Cytological studies of the nematocysts of Hydra. I. Desmonemes, isorihizas, cnidocils, and supporting structures. *The Journal of Biophysical and Biochemical Cytology*, **5** (1), pp. 69-78.

Chapman, G.B. & Tilney, L.G. (1959b). Cytological studies of the nematocysts of Hydra. II. The stenoteles. *The Journal of Biophysical and Biochemical Cytology*, **5** (1), pp. 79-84.

Chapman, J.A., Kirkness, E.F., Simakov, O. *et al.* (2010). The dynamic genome of *Hydra*. *Nature*, **464** (7288), pp. 592-596.

Chaumont, S., Jiang, L.-H., Penna, A. *et al.* (2004). Identification of a trafficking motif involved in the stabilization and polarization of P2X receptors. *Journal of Biological Chemistry*, **279** (28), pp. 29628-29638.

Cheeseman, M.T. (1998). Characterization of apyrase activity from the salivary glands of the cat flea *Ctenocephalides felis*. *Insect Biochemistry and Molecular Biology*, **28** (12), pp. 1025-1030.

Cheewatrakoolpong, B., Gilchrest, H., Anthes, J.C. & Greenfeder, S. (2005). Identification and characterization of splice variants of the human $P2X_7$ ATP channel. *Biochemical and Biophysical Research Communications*, **332** (1), pp. 17-27.

Chen, A.B., Arendall, W.B.R., Headd, J. *et al.* (2010). MolProbity: all-atom structure validation for macromolecular crystallography. *Acta Crystallographica Section D*, **66** (1), pp. 12-21.

Chen, C.C., Akopian, A.N., Sivilotti, L. *et al.* (1995). A P2X purinoceptor expressed by a subset of sensory neurons. *Nature*, **377** 428-431.

Chen, J.Y., Oliveri, P., Gao, F. *et al.* (2002). Precambrian animal life: probable developmental and adult cnidarian forms from Southwest China. *Developmental Biology*, **248** (1), pp. 182-196.

Chen, N., Harris, T.W., Antoshechkin, I. *et al.* (2005). WormBase: a comprehensive data resource for *Caenorhabditis* biology and genomics. *Nucleic Acids Research*, **33** (Database issue), pp. D383-389.

Chenna, R., Sugawara, H., Koike, T. *et al.* (2003). Multiple sequence alignment with the Clustal series of programs. *Nucleic Acids Research*, **31** (13), pp. 3497–3500.

Chessell, I.P., Hatcher, J.P., Bountra, C. *et al.* (2005). Disruption of the $P2X_7$ purinoceptor gene abolishes chronic inflammatory and neuropathic pain. *Pain*, **114** (3), pp. 386-396.

Chessell, I.P., Simon, J., Hibell, A.D. *et al.* (1998). Cloning and functional characterisation of the mouse $P2X_7$ receptor. *FEBS Letters*, **439** (1-2), pp. 26-30.

Choi, H.B., Ryu, J.K., Kim, S.U. & Mclarnon, J.G. (2007). Modulation of the purinergic P2X7 receptor attenuates lipopolysaccharide-mediated microglial activation and neuronal damage in inflamed brain. *The Journal of Neuroscience*, **27** (18), pp. 4957-4968.

Choi, J., Tanaka, K., Cao, Y. *et al.* (2014). Identification of a plant receptor for extracellular ATP. *Science*, **343** (6168), pp. 290-294.

Chomczynski, P. & Sacchi, N. (1987). Single-step method of RNA isolation by acid guanidinium thiocyanate-phenol-chloroform extraction. *Analytical Biochemistry*, **162** (1), pp. 156-159.

Chow, Y.W. & Wang, H.L. (1998). Functional modulation of $P2X_2$ receptors by cyclic AMP-dependent protein kinase. *Journal of Neurochemistry*, **70** (6), pp. 2606-2612.

Clark, A.A., Staniland, A.A., Marchand, F. *et al.* (2010). P2X7-dependent release of interleukin-1β and nociception in the spinal cord following liposaccharide. *Journal of Neuroscience*, **30** (2), pp. 573-582.

Clark, G., Fraley, D., Steinebrunner, I. *et al.* (2011). Extracellular nucleotides and apyrases regulate stomatal aperture in *Arabidopsis*. *Plant Physiology*, **156** (4), pp. 1740-1753.

Clark, M.S., Thorne, M.A., Purac, J. *et al.* (2007). Surviving extreme polar winters by desiccation: clues from Arctic springtail (*Onychiurus arcticus*) EST libraries. *BMC Genomics*, **8** 475.

Clarke, C.E., Benham, C.D., Bridges, A. *et al.* (2000). Mutation of histidine 286 of the human $P2X_4$ purinoceptor removes extracellular pH sensitivity. *Journal of Physiology*, **523** (3), pp. 697-703.

Clarke, M., Lohan, A.J., Liu, B. *et al.* (2013). Genome of *Acanthamoeba castellanii* highlights extensive lateral gene transfer and early evolution of tyrosine kinase signaling. *Genome Biology*, **14** (2), pp. R11.

Clarke, T.H., Garb, J.E., Hayashi, C.Y. *et al.* (2014). Multi-tissue transcriptomics of the black widow spider reveals expansions, co-options, and functional processes of the silk gland gene toolkit. *BMC Genomics*, **15** 365.

Cliffe, E.E. & Waley, S.G. (1958). Effect of analogues of glutathione on the feeding reaction of hydra. *Nature*, **182** (4638), pp. 804-805.

Clyne, J.D., Lapointe, L.D. & Hume, R.I. (2002a). The role of histidine residues in modulation of the rat $P2X_2$ purinoceptor by zinc and pH. *Journal of Physiology*, **539** (2), pp. 347-359.

Clyne, J.D., Wang, L.F. & Hume, R.I. (2002b). Mutational analysis of the conserved cysteines of the rat $P2X_2$ purinoceptor. *Journal of Neuroscience*, **22** (10), pp. 3873-38780.

Cockayne, D.A., Dunn, P.M., Zhong, Y. *et al.* (2005). $P2X_2$ knockout mice and $P2X_2/P2X_3$ double knockout mice reveal a role for the $P2X_2$ receptor subunit in mediating multiple sensory effects of ATP. *Journal of Physiology*, **567** (2), pp. 621-639.

Coddou, C., Lorca, R.A., Acuña-Castillo, C. *et al.* (2005). Heavy metals modulate the activity of the purinergic $P2X_4$ receptor. *Toxicology and Applied Pharmacology*, **202** (2), pp. 121-131.

Cohen, B.N., Labarca, C., Davidson, N. & Lester, H.A. (1992). Mutations in M2 alter the selectivity of the mouse nicotinic acetylcholine receptor for organic and alkali metal cations. *Journal of General Physiology*, **100** 373-400.

Colbourne, J.K., Pfrender, M.E., Gilbert, D. *et al.* (2011). The Ecoresponsive Genome of *Daphnia pulex*. *Science*, **331** (6017), pp. 555-561.

Colbourne, J.K., Singan, V.R. & Gilbert, D.G. (2005). wFleaBase: the *Daphnia* genome database. *BMC Bioinformatics*, **6** (45), pp.

Colgan, S.P., Eltzschig, H.K., Eckle, T. & Thompson, L.F. (2006). Physiological roles for ecto-5'-nucleotidase (CD73). *Purinergic Signaling*, **2** 351-360.

Collins, A.G. (1998). Evaluating multiple alternative hypotheses for the origin of Bilateria: an analysis of 18S rRNA molecular evidence. *Proceedings of the National Academy of Sciences USA*, **95** (26), pp. 15458-15463.

Collo, G., North, R.A., Kawashima, E. *et al.* (1996). Cloning of $P2X_5$ and $P2X_6$ receptors and the distribution and properties of an extended family of ATP-gated ion channels. *Journal of Neuroscience*, **16** (8), pp. 2495-2507.

Cook, C.E., Smith, M.L., Telford, M.J. *et al.* (2001). Hox genes and the phylogeny of the arthropods. *Current Biology*, **11** (10), pp. 759-763.

Creighton, C.S. & Fassuliotis, G. (1985). *Heterorhabditis* sp. (Nematoda: Heterorhabditidae): A Nematode Parasite Isolated from the Banded Cucumber Beetle *Diabrotica balteata*. *J Nematol*, **17** (2), pp. 150-152.

Crevat-Pisano, P., Dragna, S., Granthil, C. *et al.* (1986). Plasma concentrations and pharmacokinetics of midazolam during anaesthesia. *Journal of Pharmacy and Pharmacology*, **38** (8), pp. 578-582.

Crowe, R. & Burnstock, G. (1982). Fluorescent histochemical localisation of quinacrine-positive neurones in the guinea-pig and rabbit atrium. *Cardiovasc Research*, **16** (7), pp. 384-390.

Curtis, B.A., Tanifuji, G., Burki, F. *et al.* (2012). Algal genomes reveal evolutionary mosaicism and the fate of nucleomorphs. *Nature*, **492** (7427), pp. 59-65.

Da Silva, F.B., Muschner, V.C. & Bonatto, S.L. (2006). Phylogenetic position of Placozoa based on large subunit (LSU) and small subunit (SSU) rRNA genes. *Genetics and Molecular Biology*, **30** (1), pp. 127-132.

Dale, H.H. (1934). Pharmacology and nerve endings. *Proceedings of the Royal Society of Medicine*, **28** 319-330.

David, C.N. (1973). A quantitiate method for maceration of Hydra tissue. *Wilhelm Roux's Archives of Developmental Biology*, **171** 259-268.

David, C.N. (2012). Interstitial stem cells in *Hydra*: multipotency and decision-making. *International Journal of Developmental Biology*, **56** (6-8), pp. 489-497.

David, C.N. & Campbell, R.D. (1972). Cell cycle kinetics and development of *Hydra attenuata*. I. Epithelial cells. *Journal of Cell Science*, **11** (2), pp. 557-568.

David, C.N. & Gierer, A. (1974). Cell cycle kinetics and development of *Hydra attenuata*. II. Nerve and nematocyte differentiation. *Journal of Cell Science*, **16** (2), pp. 359-375.

David, C.N. & Plotnick, I. (1980). Distribution of interstitial stem cells in *Hydra*. *Developmental Biology*, **76** (1), pp. 175-184.

Davidson, W.S., Koop, B.F., Jones, S.J. *et al.* (2010). Sequencing the genome of the Atlantic salmon (*Salmo salar*). *Genome Biology*, **11** (9), pp. 403.

Davies, L.E. (1969). Differentiation of neurosensory cells in Hydra. *Journal of Cell Science*, **5** (3), pp. 699-726.

Davies, L.E. (1971). Differentiation of ganglionic cells in Hydra. *Journal of Experimental Zoology*, **176** (1), pp. 107-128.

De Proost, I., Pintelon, I., Wilkinson, W.J. *et al.* (2009). Purinergic signaling in the pulmonary neuroepithelial body microenvironment unraveled by live cell imaging. *Faseb Journal*, **23** (4), pp. 1153-1160.

Dehal, P., Satou, Y., Campbell, R.K. *et al.* (2002). The draft genome of *Ciona intestinalis:* insights into chordate and vertebrate origins. *Science*, **298** (5601), pp. 2157-2167.

Del Brutto, O.H. (2014). Neurocysticercosis. *Handb Clin Neurol*, **121** 1445-1459.

Denlinger, L.C., Fisette, P.L., Sommer, J.A. *et al.* (2001). Cutting edge: the nucleotide receptor $P2X_7$ contains multiple protein- and lipid-interaction motifs including a potential binding site for bacterial lipopolysaccharide. *Journal of Immunology*, **167** (4), pp. 1871-1876.

Derelle, R. & Lang, B.F. (2012). Rooting the eukaryotic tree with mitochondrial and bacterial proteins. *Molecular Biolpgy and Evolution*, **29** (4), pp. 1277-1289.

Desai, A., Marwah, V.S., Yadav, A. *et al.* (2013). Identification of optimum sequencing depth especially for de novo genome assembly of small genomes using next generation sequencing data. *PLoS One*, **8** (4), pp. e60204.

Dhulipala, P.D., Wang, Y.X. & Kotlikoff, M.I. (1998). The human $P2X_4$ receptor gene is altenatively spliced. *Gene*, **207** (2), pp. 259-266.

Diaz-Hernandez, M., Cox, J.A., Migita, K. *et al.* (2002). Cloning and characterization of two novel zebrafish P2X receptor subunits. *Biochemical and Biophysical Research Communications*, **295** (4), pp. 849-853.

Digby, H.R., Roberts, J.A., Sutcliffe, M.J. & Evans, R.J. (2005). Contribution of conserved glycine residues to ATP action at human $P2X_1$ receptors: mutagenesis indicates that the glycine at position 250 is important for channel function. *Journal of Neurochemistry*, **95** (6), pp. 1746-1754.

Dolezelova, E., Nothacker, H.P., Civelli, O. *et al.* (2007). A Drosophila adenosine receptor activates cAMP and calcium signaling. *Insect Biochemistry and Molecular Biology*, **37** (4), pp. 318-329.

Dong, C., Hu, A., Ni, Y. *et al.* (2013). Effects of midazolam, pentobarbital and ketamine on the mRNA expression of ion channels in a model organism *Daphnia pulex*. *BMC Anesthesiol*, **13** (1), pp. 32.

Drew, D., Newstead, S., Sonoda, Y. *et al.* (2008). GFP-based optimization scheme for the overexpression and purification of eukaryotic membrane proteins in *Saccharomyces cerevisiae*. *Nature Protocols*, **3** (5), pp. 784-798.

Drury, A.N. & Szent-Györgyi, A. (1929). The physiological activity of adenine compounds with special reference to their action upon the mammalian heart. *Journal of Physiology*, **68** (3), pp. 182-188.

Duarte, C.B., Santos, P.F. & Carvalho, A.P. (1999). Corelease of two functionally opposite neurotransmitters by retinal amacrine cells: experimental evidence and functional significance. *Journal of Neuroscience Research*, **58** (4), pp. 475-479.

Dübel, S., Hoffmeister, S.A. & Schaller, H.C. (1987). Differentiation pathways of ectodermal epithelial cells in hydra. *Differentiation*, **35** (3), pp. 181-189.

Duman-Scheel, M. & Patel, N.H. (1999). Analysis of molecular marker expression reveals neuronal homology in distantly related arthropods. *Development*, **126** (11), pp. 2327-2334.

Dunn, C.W., Hejnol, A., Matus, D.Q. *et al.* (2008). Broad phylogenomic sampling improves resolution of the animal tree of life. *Nature*, **452** (7188), pp. 745-749.

Dürrnagel, S., Falkenburger, B.H. & Gründer, S. (2012). High Ca^{2+} permeability of a peptide-gated DEG/ENaC from *Hydra*. *The Journal of General Physiology*, **140** (4), pp. 391-402.

Dürrnagel, S., Kuhn, A., Tsiairis, C.D. *et al.* (2010). Three homologous subunits form a high-affinity peptide-gated ion channel in *Hydra*. *Journal of Biological Chemistry*, **285** (16), pp. 11958-11965.

Dutton, J.L., Poronnik, P., Li, G.H. *et al.* (2000). P2X1 receptor membrane redistribution and down-regulation visualized by using receptor-coupled fluorescent protein chimeras. *Neuropharmacology*, **39** (11), pp. 2054-2066.

Dwyer, T.M., Adams, D.J. & Hille, B. (1980). The permeability of the endplate channel to organic cations in frog muscle. *Journal of General Physiology*, **75** (5), pp. 469-492.

Ebert, D. 2005. *Ecology, Epidemiology, and Evolution of Parasitism in Daphnia,* Bethesda (MD), USA, National Center for Biotechnology Information.

Edgar, R.C. (2004). MUSCLE: a multiple sequence alignment method with reduced time and space complexity. *BMC Bioinformatics*, **5** 113.

Edgecombe, G.D. (2010). Arthropod phylogeny: an overview from the perspectives of morphology, molecular data and the fossil record. *Arthropod Structure and Development*, **39** (2-3), pp. 74-87.

Egan, T.M., Cox, J.A. & Voigt, M.M. (2000). Molecular cloning and functional characterization of the zebrafish ATP-gated ionotropic receptor P2X(3) subunit. *FEBS Letters*, **475** (3), pp. 287-290.

Egan, T.M., Haines, W.R. & Voigt, M.M. (1998). A domain contributing to the ion channel of ATP-gated $P2X_2$ receptors identified by the substituted cysteine accessibility method. *Journal of Neuroscience*, **18** (7), pp. 2350-2359.

Eickhorst, A.N., Berson, A., Cockayne, D. *et al.* (2002a). Control of $P2X_2$ channel permeability by the cytosolic domain. *Journal of General Physiology*, **120** 119-131.

Eickhorst, A.N., Berson, A., Cockayne, D. *et al.* (2002b). Control of $P2X_2$ channel permeability by the cytosolic domain. *Journal of General Physiology*, **120** (2), pp. 119-131.

El-Ajouz, S., Ray, D., Allsopp, R.C. & Evans, R.J. (2012). Molecular basis of selective antagonism of the P2X1 receptor for ATP by NF449 and suramin: contribution of basic amino acids in the cysteine-rich loop. *British Journal of Pharmacology*, **165** (2), pp. 390-400.

Elkins, J.G., Podar, M., Graham, D.E. *et al.* (2008). A korarchaeal genome reveals insights into the evolution of the Archaea. *Proceedings of the National Academy of Sciences USA*, **105** (23), pp. 8102-8107.

Elsworth, B., Wasmuth, J. & Blaxter, M. (2011). NEMBASE4: the nematode transcriptome resource. *International Journal for Parasitology*, **41** (8), pp. 881-894.

Emerson, M.J. & Schram, F.R. 1997. *In:* FORTEY, R.A. & THOMAS, R.H. (eds.) *Arthropod Relationships.* London: Chapman & Hall.

Engel, U., Ozbek, S., Streitwolf-Engel, R. *et al.* (2002). Nowa, a novel protein with minicollagen Cys-rich domains, is involved in nematocyst formation in *Hydra*. *Journal of Cell Science*, **115** (20), pp. 3923-3934.

Engel, U., Pertz, O., Fauser, C. *et al.* (2001). A switch in disulfide linkage during minicollagen assembly in *Hydra* nematocysts. *EMBO Journal*, **20** (12), pp. 3063-3073.

Ennion, S., Hagan, S. & Evans, R.J. (2000). The role of positively charged amino acids in ATP recognition by human $P2X_1$ receptors. *Journal of Biological Chemistry*, **275** (38), pp. 29361-29367.

Ennion, S.J. & Evans, R.J. (2000). Agonist-stimulated internalisation of the ligand-gated ion channel $P2X_1$ in rat vas deferens. *FEBS Letters*, **489** (2-3), pp. 154-158.

Ennion, S.J. & Evans, R.J. (2002a). Conserved cysteine residues in the extracellular loop of the human $P2X_1$ receptor form disulfide bonds and are involved in receptor trafficking to the cell surface. *Molecular Pharmacology*, **61** (2), pp. 303-311.

Ennion, S.J. & Evans, R.J. (2002b). $P2X_1$ receptor subunit contribution to gating revealed by a dominant negative PKC mutant. *Biochemical and Biophysical Research Communications*, **291** (3), pp. 611-616.

Eriksson, B.J. & Stollewerk, A. (2010). Expression patterns of neural genes in *Euperipatoides kanangrensis* suggest divergent evolution of onychophoran and euarthropod neurogenesis. *Proceedings of the National Academy of Sciences USA*, **107** (52), pp. 22576-22581.

Estep, P.W. (2010). Declining asexual reproduction is suggestive of senescence in hydra: comment on Martinez, D., "Mortality patterns suggest lack of senescence in hydra." Exp Gerontol 33, 217-25. *Experimental Gerontology*, **45** (9), pp. 645-646.

Evans, R.J., Lewis, C., Buell, G. *et al.* (1995). Pharmacological characterization of heterologously expressed ATP-gated cation channels (P2x purinoceptors). *Molecular Pharmacology*, **48** (2), pp. 178-183.

Evans, R.J., Lewis, C., Virginio, C. *et al.* (1996). Ionic permeability of, and divalent cation effects on, two ATP-gated cation channels (P2X receptors) expressed in mammalian cells. *Journal of Physiology*, **497** (2), pp. 413-422.

Evenson, W.E., Boden, L.M., Muzikar, K.A. & O'leary, D.J. (2012). ^{1}H and ^{13}C NMR assignments for the cyanine dyes SYBR Safe and thiazole orange. *Journal of Organic Chemistry*, **77** (23), pp. 10967-10971.

Fairclough, S.R., Chen, Z., Kramer, E. *et al.* (2013). Premetazoan genome evolution and the regulation of cell differentiation in the choanoflagellate *Salpingoeca rosetta*. *Genome Biology*, **14** (2), pp. R15.

Falzoni, S., Munerati, M., Ferrari, D. *et al.* (1995). The purinergic P2Z receptor of human macrophage cells. Characterization and possible physiological role. *Journal of Clinical Investigation*, **95** (3), pp. 1207-1216.

Fedan, J.S., Hogabook, Westfall, D.P. & O'donnell, J.P. (1982). Comparison of the effects of arylazido aminopropionyl ATP ($ANAPP_3$), an ATP antagonist, on responses of the smooth muscle of the guinea-pig vas deferens to ATP and related nucleotides. *European Journal of Pharmacology*, **85** (3-4), pp. 277-290.

Fenwick, A. (2012). The global burden of neglected tropical diseases. *Public Health*, **126** (3), pp. 233-236.

Feranchak, A.P., Fitz, J.G. & Roman, R.M. (2000). Volume-sensitive purinergic signaling in human hepatocytes. *Journal of Hepatology*, **33** (2), pp. 174-182.

Finn, R.D., Bateman, A., Clements, J. *et al.* (2014). Pfam: the protein families database. *Nucleic Acids Research*, **42** (Database issue), pp. D222-230.

Fischer, N., Ruef, C., Ebnother, C. & Bachli, E.B. (2008). Rhinofacial *Conidiobolus coronatus* infection presenting with nasal enlargement. *Infection*, **36** (6), pp. 594-596.

Fizames, C., Munos, S., Cazettes, C. *et al.* (2004). The Arabidopsis root transcriptome by serial analysis of gene expression. Gene identification using the genome sequence. *Plant Physiology*, **134** (1), pp. 67-80.

Flagel, L.E., Bansal, R., Kerstetter, R.A. *et al.* (2014). Western corn rootworm (*Diabrotica virgifera virgifera*) transcriptome assembly and genomic analysis of population structure. *BMC Genomics*, **15** 195.

Fodor, J., Matta, C., Juhasz, T. *et al.* (2009). Ionotropic purinergic receptor P2X4 is involved in the regulation of chondrogenesis in chicken micromass cell cultures. *Cell Calcium*, **45** (5), pp. 421-430.

Foelix, R.F. 2011. *Biology of Spiders,* New York, Oxford University Press USA.

Fountain, S.J. (2013). Primitive ATP-activated P2X receptors: discovery, function and pharmacology. *Front Cell Neurosci*, **7** 247.

Fountain, S.J. & Burnstock, G. (2009). An evolutionary history of P2X receptors. *Purinergic Signaling*, **5** (3), pp. 269-272.

Fountain, S.J., Cao, L., Young, M.T. & North, R.A. (2008). Permeation properties of a P2X receptor in the green algae *Ostreococcus tauri*. *Journal of Biological Chemistry*, **283** (22), pp. 15122-15126.

Fountain, S.J., Parkinson, K., Young, M.T. *et al.* (2007). An intracellular P2X receptor required for osmoregulation in *Dictyostelium discoideum*. *Nature*, **448** (7150), pp. 200-203.

Franzenburg, S., Fraune, S., Künzel, S. *et al.* (2012). MyD88-deficient *Hydra* reveal an ancient function of TLR signaling in sensing bacterial colonizers. *Proceedings of the National Academy of Sciences*, **109** (47), pp. 19374-19379.

Franzenburg, S., Walter, J., Kunzel, S. *et al.* (2013). Distinct antimicrobial peptide expression determines host species-specific bacterial associations. *Proceedings of the National Academy of Sciences USA*, **110** (39), pp. E3730-3738.

Fraune, S. & Bosch, T.C. (2007). Long-term maintenance of species-specific bacterial microbiota in the basal metazoan *Hydra*. *Proceedings of the National Academy of Sciences*, **104** (32), pp. 13146-13151.

Fu, W., Mccormick, T., Qi, X. *et al.* (2009). Activation of P2X7-mediated apoptosis inhibits DMBA/TPA-induced formation of skin papillomas and cancer in mice. *BMC Cancer*, **9** 114.

Fuchs, B., Wang, W., Graspeuntner, S. *et al.* (2014). Regulation of polyp-to-jellyfish transition in *Aurelia aurita*. *Current Biology*, **24** (3), pp. 263-273.

Fung, S.C. & Fillenz, M. (1984). Multiple effects of drugs acting on benzodiazepine receptors. *Neuroscience Letters*, **50** (1-3), pp. 203-207.

Galliot, B. (2012). Hydra, a fruitful model system for 270 years. *International Journal of Developmental Biology*, **56** (6-8), pp. 411-423.

Galliot, B. & Quiquand, M. (2011). A two-step process in the emergence of neurogenesis. *European Journal of Neuroscience*, **34** (6), pp. 874-862.

Galun, R., Friend, W.G. & Nudelman, S. (1988). Purinergic reception by culicine mosquitoes. *Journal of Comparative Physiology A*, **163** (5), pp. 665-670.

Galun, R. & Kabayo, J.P. (1988). Gorging response of *Glossina palpalis palpalis* to ATP analogues. *Physiological Entomology*, **13** (4), pp. 419-423.

Galun, R., Koontz, L.C., Gwadz, R.W. & Ribeiro, J.M.C. (1985). Effect of ATP analogues on the gorging response of *Aedes aegypti*. *Physiological Entomology*, **10** (3), pp. 275-281.

Gao, Y., Bu, Y. & Luan, Y.X. (2008). Phylogenetic relationships of basal hexapods reconstructed from nearly complete 18S and 28S rRNA gene sequences. *Zoolog Sci*, **25** (11), pp. 1139-1145.

Garcia-Fernàndez, J. & Holland, P.W. (1994). Archetypal organization of the amphioxus *Hox* gene cluster. *Nature*, **370** (6490), pp. 563-569.

Garcia-Guzman, M., Soto, F., Gomez-Hernandez, J.M. *et al.* (1997a). Characterization of recombinant human $P2X_4$ receptor reveals pharmacological differences with the rat homologue. *Molecular Pharmacology*, **51** (1), pp. 109-118.

Garcia-Guzman, M., Soto, F., Laube, B. & Stühmer, W. (1996). Molecular cloning and functional expression of a novel rat heart P2X purinoceptor. *FEBS Letters*, **388** (2-3), pp. 123-127.

Garcia-Guzman, M., Stuhmer, W. & Soto, F. (1997b). Molecular characterization and pharmacological properties of the human $P2X_3$ purinoceptor. *Brain Research - Molecular Brain Research*, **47** (1-2), pp. 59-66.

Gerke, P., Bording, C., Zeis, B. & Paul, R.J. (2011). Adaptive haemoglobin gene control in *Daphnia pulex* at different oxygen and temperature conditions. *Comparative Biochemistry and Physiology. Part A, Molecular and Integrative Physiology*, **159** (1), pp. 56-65.

Giribet, G. & Edgecombe, G.D. (2012). Reevaluating the arthropod tree of life. *Annual Review of Entomology*, **57** 167-186.

Gitter, A.H., Oliver, D. & Thurm, U. (1994). Calcium- and voltage-dependence of nematocyst discharge in *Hydra vulgaris*. *Journal of Comparative Physiology A*, **175** (1), pp. 115-122.

Gleeson, R.A., Carr, W.E. & Trapido-Rosenthal, H.G. (1989). ATP-sensitive chemoreceptors: antagonism by other nucleotides and the potential implications of ectonucleotidase activity. *Brain Research*, **497** (1), pp. 12-20.

Goding, J.W., Grobben, B. & Slegers, G.H. (2003). Physiological and pathophysiological functions of the ecto-nucleotide pyrophosphatase/phosphodiesterase family. *Biochimica et Biophysica Acta*, **1638** (1), pp. 1-19.

Goldman, A.L., Van Der Goes Van Naters, W., Lessing, D. *et al.* (2005). Coexpression of two functional odor receptors in one neuron. *Neuron*, **45** (5), pp. 661-666.

Golubovic, A., Kuhn, A., Williamson, M. *et al.* (2007). A peptide-gated ion channel from the freshwater polyp *Hydra*. *Journal of Biological Chemistry*, **282** (48), pp. 35098-35103.

Gomez, G. & Sitkovsky, M.V. (2003). Differential requirement for A_{2a} and A_3 adenosine receptors for the protective effect of inosine *in vivo*. *Blood*, **102** (13), pp. 4472-4478.

Gonzales, E., Julien, B., Serriere-Lanneau, V. *et al.* (2010). ATP release after partial hepatectomy regulates liver regeneration in the rat. *Journal of Hepatology*, **52** (1), pp. 54-62.

Gonzales, E.B., Kawate, T. & Gouaux, E. (2009). Pore architecture and ion sites in acid-sensing ion channels and P2X receptors. *Nature*, **460** (7255), pp. 599-604.

Gorr, T.A., Cahn, J.D., Yamagata, H. & Bunn, H.F. (2004). Hypoxia-induced synthesis of hemoglobin in the crustacean *Daphnia magna* is hypoxia-inducible factor-dependent. *Journal of Biological Chemistry*, **279** (34), pp. 36038-36047.

Greco, N.J., Tonon, G., Chen, W. *et al.* (2001). Novel structurally altered $P2X_1$ receptor is preferentially activated by adenosine diphosphate in platelets and megakaryocytic cells. *Blood*, **98** (1), pp. 100-107.

Greenwood, P.G., Johnson, L.A. & Mariscal, R. (1989). Depletion of ATP in suspensions of isolated cnidae: A possible role of ATP in the maturation and maintainance of anthozoan cnidae. *Comparative Biochemistry and Physiology: Part A Physiology*, **93** (4), pp. 761-765.

Grell, K.G. (1974). Spezifische Verbindungsstrukturen der Faserzellen von *Trichoplax adhaerens.* F.E. Schulze. . *Zeitschrift für Naturforschung*, **29** 790.

Grell, K.G. & Benwitz, G. (1971). Die Ultrastruktur von *Trichoplax adhaerens*. *Cytobiologie*, **4** 216-240.

Grigoriev, I.V., Cullen, D., Goodwin, S.B. *et al.* (2011). Fueling the future with fungal genomics. *Mycology*, **2** (3), pp. 192-209.

Gu, J.G. & Macdermott, A.B. (1997). Activation of ATP P2X receptors elicits glutamate release from sensory neuron synapses. *Nature*, **389** (6652), pp. 749-753.

Guillard, R.R.L. 1975. *Culture of phytoplankton for feeding marine invertebrates.,* New York, Plenum Press

Guillen, E. & Hirschberg, C.B. (1995). Transport of adenosine triphosphate into endoplasmic reticulum proteoliposomes. *Biochemistry*, **34** (16), pp. 5472-5476.

Gur Barzilai, M., Reitzel, A.M., Kraus, J.E. *et al.* (2012). Convergent evolution of sodium ion selectivity in metazoan neuronal signaling. *Cell Rep*, **2** (2), pp. 242-248.

Gustafsson, C., Govindarajan, S. & Minshull, J. (2004). Codon bias and heterologous protein expression. *Trends Biotechnol*, **22** (7), pp. 346-353.

Haines, W.R., Torres, G.E., Voigt, M.M. & Egan, T.M. (1999). Properties of the novel ATP-gated ionotropic receptor composed of the $P2X_1$ and $P2X_5$ isoforms. *Molecular Pharmacology*, **56** (4), pp. 720-727.

Haines, W.R., Voigt, M.M., Migita, K. *et al.* (2001). On the contribution of the first transmembrane domain to whole-cell current through an ATP-gated ionotropic P2X receptor. *Journal of Neuroscience*, **21** (16), pp. 5885-5892.

Hakansson, K.O. (2009). The structure of Mg-ATPase nucleotide-binding domain at 1.6 Å reveals a unique ATP-binding motif. *Acta Crystallographica Section D: Biological Crystallography*, **65** (11), pp. 1181-1186.

Hallam, S.J., Konstantinidis, K.T., Putnam, N. *et al.* (2006). Genomic analysis of the uncultivated marine crenarchaeote *Cenarchaeum symbiosum*. *Proceedings of the National Academy of Sciences USA*, **103** (48), pp. 18296-18301.

Hamagishi, Y., Tone, H., Oki, T. & Inui, T. (1980). Effect of adenosine-5'-triphosphate-3'-diphosphate and related nucleoside polyphosphates on the spore gemination of *Streptomyces galilaeus*. *Annals of Microbiology*, **125** (3), pp. 285-289.

Hamdan, F.F., Mousa, A. & Ribeiro, P. (2002). Codon optimization improves heterologous expression of a *Schistosoma mansoni* cDNA in HEK293 cells. *Parasitology Research*, **88** (6), pp. 583-586.

Hamill, O.P., Marty, A., Neher, E. *et al.* (1981). Improved patch-clamp techniques for high-resolution current recording from cells and cell-free membrane patches. *Pflügers Archiv: European Journal of Physiology*, **391** (2), pp. 85-100.

Hardy, L.A., Harvey, I.J., Chambers, P. & Gillespie, J.I. (2000). A putatively alternatively spliced variant of the $P2X_1$ purinoreceptor in human bladder. *Experimental Physiology*, **85** (4), pp. 461-463.

Harlow, E. & Lane, D. 1998. *Using antibodies: a laboratory manual,* Woodbury, New York, Cold Spring Harbor Press.

Harte, R. & Ouzounis, C.A. (2002). Genome-wide detection and family clustering of ion channels. *FEBS Letters*, **514** (2-3), pp. 129-134.

Hartman, A.L., Norais, C., Badger, J.H. *et al.* (2010). The complete genome sequence of *Haloferax volcanii* DS2, a model archaeon. *PLoS One*, **5** (3), pp. e9605.

Haszprunar, G. & Wanninger, A. (2012). Molluscs. *Current Biology*, **22** (13), pp. R510-514.

Hattori, M. & Gouaux, E. (2012). Molecular mechanism of ATP binding and ion channel activation in P2X receptors. *Nature*, **485** (7397), pp. 207-212.

Hausmann, K. & Holstein, T. (1985). Bilateral symmetry in the cnidocil-nematocyst complex of the freshwater medusa *Craspedacusta sowerbii* Lankester (Hydrozoa, Limnomedusae). *Journal of Ultrastructure Research*, **90** (1), pp. 89-104.

Hawrylycz, M.J., Lein, E.S., Guillozet-Bongaarts, A.L. *et al.* (2012). An anatomically comprehensive atlas of the adult human brain transcriptome. *Nature*, **489** (7416), pp. 391-399.

Hayakawa, E., Takahashi, T., Nishimiya-Fujisawa, C. & Fujisawa, T. (2007). A novel neuropeptide (FRamide) family identified by a peptidomic approach in *Hydra magnipapillata*. *The FEBS Journal*, **274** (20), pp. 5438-5448.

Haynes, J. & Burnett, A.L. (1963). Dedifferentiation and redifferentiation of cells in *Hydra viridis*. *Science*, **142** (3598), pp. 1481-1483.

He, M.-L., Koshimizu, T.-A., Tomić, M. & Stojilkovic, S.S. (2002). Purinergic $P2X_2$ receptor desensitization depends on coupling between ectodomain and C-terminal domain. *Molecular Pharmacology*, **62** (5), pp. 1187-1197.

Hebert, P.D.N., Remigio, E.A., Colbourne, J.K. *et al.* (2002). Accelerated molecular evolution in halophilic crustaceans. *Evolution*, **56** (5), pp. 909-926.

Hechler, B., Lenain, N., Marchese, P. *et al.* (2003). A role of the fast ATP-gated $P2X_1$ cation channel in thrombosis of small arteries *in vivo*. *Journal of Experimental Medicine*, **198** (4), pp. 661-667.

Hedges, S.B., Dudley, J. & Kumar, S. (2006). TimeTree: a public knowledge-base of divergence times among organisms. *Bioinformatics*, **22** (23), pp. 2971-2972.

Heimfeld, S. & Bode, H.R. (1985). Growth regulation of the interstitial cell population in hydra. I. Evidence for global control by nerve cells in the head. *Developmental Biology*, **110** (2), pp. 297-307.

Heineck-Leonal, M.A. & Salles, L.a.B.I. (1997). Incidence of parasitoids and pathogens in adults of *Diabrotica* speciosa (Germ.) (Coleoptera: Chrysomelidae) in Pelotas, RS. *Anais da Sociedade Entomológica do Brasil*, **26** (1), pp. 81-85.

Hejl, J.L., Skals, M., Leipziger, J. & Praetorius, H.A. (2013). P2X receptor stimulation amplifies complement-induced haemolysis. *Pflügers Archiv: European Journal of Physiology*, **465** (4), pp. 529-541.

Hejnol, A., Obst, M., Stamatakis, A. *et al.* (2009). Assessing the root of bilaterian animals with scalable phylogenomic methods. *Proceedings of the Royal Society B: Biological Sciences*, **276** (1677), pp. 4261-4270.

Hellsten, U., Wright, K.M., Jenkins, J. *et al.* (2013). Fine-scale variation in meiotic recombination in *Mimulus* inferred from population shotgun sequencing. *Proceedings of the National Academy of Sciences USA*, **110** (48), pp. 19478-19482.

Hemmrich, G., Anokhin, B., Zacharias, H. & Bosch, T.C. (2007). Molecular phylogenetics in *Hydra*, a classical model in evolutionary development. *Molecular Phylogenetics and Evolution*, **44** (1), pp. 281-290.

Hemmrich, G. & Bosch, T.C.G. (2008). Compagen, a comparative genomics platform for early branching metazoan animals reveals early origins of of genes regulating stem cell differentiation. *Bioessays*, **30** (10), pp. 1010-1018.

Hickman, S.E., El Khoury, J., Greenberg, S. *et al.* (1994). P2Z adenosine triphosphate receptor activity in cultured human monocyte-derived macrophages. *Blood*, **84** (8), pp. 2452-2456.

Hille, B. 1992. *Ionic Channels of Excitable Membranes,* Sunderland, MA, USA, Sinauer Associates.

Hogaboom, G.K., O'donnell, J.P. & Fedan, J.S. (1980). Purinergic receptors: photoaffinity analog of adenosine triphosphate is a specific adenosine triphosphate antagonist. *Science*, **208** (4449), pp. 1273-1276.

Holland, L.Z. & Holland, N.D. (1999). Chordate origins of the vertebrate central nervous system. *Current Opinions in Neurobiology*, **9** (5), pp. 596-602.

Holland, L.Z. & Onai, T. (2011). Analyses of gene function in amphioxus embryos by microinjection of mRNAs and morpholino oligonucleotides. *Methods in Molecular Biology*, **770** 423-438.

Holland, P.W., Holland, L.Z., Williams, N.A. & Holland, N.D. (1992). An amphioxus homeobox gene: sequence conservation, spatial expression during development and insights into vertebrate evolution. *Development*, **116** (3), pp. 653-661.

Hollopeter, G., Jantzen, H.M., Vincent, D. *et al.* (2001). Identification of the platelet ADP receptor targeted by antithrombotic drugs. *Nature*, **409** (6817), pp. 202-207.

Holstein, T. (1981). The morphogenesis of nematocytes in Hydra and Forskålia: an ultrastructural study. *Journal of Ultrastructure Research*, **75** (3), pp. 276-290.

Holstein, T. & Tardent, P. (1984). An ultrahigh-speed analysis of exocytosis: nematocyst discharge. *Science*, **223** (4638), pp. 830-833.

Holstein, T.W., Hobmayer, E. & David, C.N. (1991). Pattern of epithelial cell cycling in hydra. *Developmental Biology*, **148** (2), pp. 602-611.

Holton, F.A. & Holton, P. (1954). The capillary dilator substances in dry powders of spinal roots; a possible role of adenosine triphosphate in chemical transmission from nerve endings. *Journal of Physiology*, **126** (1), pp. 124-140.

Holton, P. (1959). The liberation of adenosine triphosphate on antidromic stimulation of sensory nerves. *Journal of Physiology*, **143** (3), pp. 494-504.

Hori, K., Maruyama, F., Fujisawa, T. *et al.* (2014). *Klebsormidium flaccidum* genome reveals primary factors for plant terrestrial adaptation. *Nature Communications*, **5** 3978.

Horton, P. & Nakai, K. (1997). Better prediction of protein cellular localization sites with the *k* nearest neighbors classifier. *Proceedings of the 5th International Conference on Intelligent Systems for Molecular Biology*, **5** 147-152.

Hosoi, T. (1958). Adenosine-5' phosphates as the stimulating agents in blood for inducing gorging of the mosquito. *Nature*, **181** 1664-1665.

Hoyle, C.H.V., Knight, G.E. & Burnstock, G. (1989). Actions of adenylyl compounds in the pedal disc of the cnidarian *Actina equina*. *Comparative Biochemistry and Physiology*, **94** (1), pp. 111-114.

Hugel, S. & Schlichter, R. (2000). Presynaptic P2X receptors facilitate inhibitory GABAergic transmission between cultured rat spinal cord dorsal horn neurons. *Journal of Neuroscience*, **20** (6), pp. 2121-2130.

Hunt, T., Bergsten, J., Levkanicova, Z. *et al.* (2007). A comprehensive phylogeny of beetles reveals the evolutionary origins of a superradiation. *Science*, **318** (5858), pp. 1913-1916.

Hwang, U.W., Friedrich, M., Tautz, D. *et al.* (2001). Mitochondrial protein phylogeny joins myriapods with chelicerates. *Nature*, **413** (6852), pp. 154-157.

Imamura, H., Nhat, K.P.H., H., T. *et al.* (2009). Visualization of ATP levels inside living cells with fluorescence resonance energy transfer-based genetically encoded indicators. *Proceedings of the National Academy of Sciences*, **106** (37), pp. 15651-15656.

Inoue, H., Nojima, H. & Okayama, H. (1990). High efficiency transformation of *Escherichia coli* with plasmids. *Gene*, **96** (1), pp. 23-28.

Inscho, E.W., Cook, A.K., Imig, J.D. *et al.* (2003). Physiological role for $P2X_1$ receptors in renal microvascular autoregulatory behavior. *Journal of Clinical Investigation*, **112** (12), pp. 1895-1905.

Irvin, J.L. & Irvin, E.M. (1954). The interaction of quinacrine with adenine nucleotides. *Journal of Biological Chemistry*, **210** (1), pp. 45-56.

Isa-Isa, R., Arenas, R., Fernandez, R.F. & Isa, M. (2012). Rhinofacial conidiobolomycosis (entomophthoramycosis). *Clincial Dermatology*, **30** (4), pp. 409-412.

Jahngen, J.H. & Rossomando, E.F. (1983). Resolution of an ATP-metal chelate from metal-free ATP by reverse-phase high-performance liquid chromatography. *Analytical Biochemistry*, **130** (2), pp. 406-415.

Jarvis, M.F. (2003). Contributions of $P2X_3$ homomeric and heteromeric channels to acute and chronic pain. *Expert Opinion on Therapeutic Targets*, **7** (4), pp. 513-522.

Jasti, J., Furukawa, H., Gonzales, E.B. & Gouaux, E. (2007). Structure of acid-sensing ion channel 1 at 1.9Å resolution and low pH. *Nature*, **449** (7160), pp. 316-323.

Jelínkova, I., Vavra, V., Jindrichova, M. *et al.* (2008). Identification of $P2X_4$ receptor transmembrane residues contributing to channel gating and interaction with ivermectin. *Pflüfgers Archiv - European Journal of Physiology*, **456** (5), pp. 939-950.

Jensik, P.J., Holbird, D., Collard, M.W. & Cox, T.C. (2001). Cloning and characterization of a functional P2X receptor from larval bullfrog skin. *American Journal of Physiology - Cell Physiology*, **281** (3), pp. C954-962.

Jeram, A.J., Selden, P.A. & Edwards, D. (1990). Land animals in the silurian: arachnids and myriapods from shropshire, England. *Science*, **250** (4981), pp. 658-661.

Jiang, L.-H., Mackenzie, A.B., North, R.A. & Suprenant, A. (2000a). Brilliant blue G selectively blocks ATP-gated rat $P2X_7$ receptors. *Molecular Pharmacology*, **58** (1), pp. 82-88.

Jiang, L.-H., Rassendren, F., Suprenant, A. & North, R.A. (2000b). Identification of amino acid residues contributing to the ATP-binding site of a purinergic P2X receptor. *Journal of Biological Chemistry*, **275** (44), pp. 190-196.

Jiang, L.H., Kim, M., Spelta, V. *et al.* (2003). Subunit arrangement in P2X receptors. *Journal of Neuroscience*, **23** (26), pp. 8903-8910.

Jiang, R., Lemoine, D., Martz, A. *et al.* (2011). Agonist trapped in ATP-binding sites of the $P2X_2$ receptor. *Proceedings of the National Academy of Sciences USA*, **108** (22), pp. 9066-9071.

Jiang, R., Taly, A. & Grutter, T. (2013). Moving through the gate in ATP-activated P2X receptors. *Trends in Biochemical Sciences*, **38** (1), pp. 20-29.

Jo, Y.H. & Role, L.W. (2002). Coordinate release of ATP and GABA at in vitro synapses of lateral hypothalamic neurons. *The Journal of Neuroscience*, **22** (12), pp. 4794-4804.

Jo, Y.H. & Schlichter, R. (1999). Synaptic corelease of ATP and GABA in cultured spinal neurons. *Nature Neuroscience*, **2** (3), pp. 241-245.

Jollie, M. 1962. *Chordate Morphology,* New York, Reinhold.

Jones, C.A., Chessell, I.P., Simon, J. *et al.* (2000). Functional characterization of the $P2X_4$ receptor orthologues. *British Journal of Pharmacology*, **129** (2), pp. 388-394.

Jones, C.A., Vial, C., Sellers, L.A. *et al.* (2004). Functional regulation of $P2X_6$ receptors by N-linked glycosylation: identification of a novel αβ-methylene ATP-sensitive phenotype. *Molecular Pharmacology*, **65** (4), pp. 979-985.

Jorgensen, E.M. (2014). Animal evolution: looking for the first nervous system. *Current Biology*, **24** (14), pp. R655-658.

Jung, S., Dingley, A.J., Augustin, R. *et al.* (2009). Hydramacin-1, structure and antibacterial activity of a protein from the basal metazoan *Hydra*. *Journal of Biological Chemistry*, **284** (3), pp. 1896-1905.

Kahlenberg, J.M. & Dubyak, G.R. (2004). Mechanisms of caspase-1 activation by $P2X_7$ receptor-mediated K^+ release. *American Journal of Physiology: Cell Physiology*, **286** (5), pp. 1100-1108.

Karanjia, R., Garcia-Hernandez, L.M., Miranda-Morales, M. *et al.* (2006). Cross-inhibitory interactions between $GABA_A$ and P2X channels in myenteric neurones. *European Journal of Neuroscience*, **23** (12), pp. 3259-3268.

Karol, K.G., Mccourt, R.M., Cimino, M.T. & Delwiche, C.F. (2001). The closest living relatives of land plants. *Science*, **294** (5550), pp. 2351-2353.

Kass-Simon, G., Pannaccione, A. & Pierobon, P. (2003). GABA and glutamate receptors are involved in modulating pacemaker activity in hydra. *Comparative Biochemistry and Physiology - Part A: Molecular & Integrative Physiology*, **136** (2), pp. 329-342

Kass-Simon, G. & Pierobon, P. (2007). Cnidarian chemical neurotransmission, an updated overview. *Comparative Biochemistry and Physiology, Part A*, **146** 9-25.

Kass-Simon, G. & Scappaticci Jr., A.A. (2004). Glutamatergic and GABAnergic control in the tentacle effector systems of *Hydra vulgaris*. *Hydrobiologia*, **530/531** 67-71.

Kass-Simon, G., Zompa, M.A., Scappaticci, A.A. *et al.* (2009). Nucleolar binding of an anti-NMDA receptor antibody in hydra: a non-canonical role for an NMDA receptor protein? *Journal of Experimental Zoology A: Ecological Genetics and Physiology*, **311** (10), pp. 763-775.

Kato, S., Yoshida, M. & Kato-Yamada, Y. (2007). Role of the epsillon subunit of thermophilic F1-ATPase as a sensor for ATP. *Journal of Biological Chemistry*, **282** (52), pp. 37618-37623.

Katz, L.A., Grant, J.R., Parfrey, L.W. & Burleigh, J.G. (2012). Turning the crown upside down: gene tree parsimony roots the eukaryotic tree of life. *Syst Biol*, **61** (4), pp. 653-660.

Kawaida, H., Shimizu, H., Fukjisawa, T. *et al.* (2010). Molecular phylogenetic study in genus *Hydra*. *Gene*, **468** (1-2), pp. 30-40.

Kawate, T., Michel, J.C., Birdsong, W.T. & Gouaux, E. (2009). Crystal structure of the ATP-gated $P2X_4$ ion channel in the closed state. *Nature*, **460** (7255), pp. 592-598.

Kay, J.C. & Kass-Simon, G. (2009). Glutamatergic transmission in hydra: NMDA/D-serine affects the electrical activity of the body and tentacles of *Hydra vulgaris* (Cnidaria, Hydrozoa). *Biol Bull*, **216** (2), pp. 113-125.

Kayal, E., Roure, B., Philippe, H. *et al.* (2013). Cnidarian phylogenetic relationships as revealed by mitogenomics. *BMC Evolutionary Biology*, **13** (5), pp.

Ke, H.Z., Qi, H., Weidema, A.F. *et al.* (2003). Deletion of the $P2X_7$ nucleotide receptor reveals its regulatory roles in bone formation and resorption. *Molecular Endocrinology*, **17** (7), pp. 1356-1367.

Kent, W.J. (2002). BLAT-the BLAST-like alignment tool. *Genome Research*, **12** (4), pp. 656-664.

Keystone, E.C., Wang, M.M., Layton, M. *et al.* (2012). Clinical evaluation of the efficacy of the P2X7 purinergic receptor antagonist AZD9056 on the signs and symptoms of rheumatoid arthritis in patients with active disease despite treatment with methotrexate or sulphasalazine. *Annals of the Rheumatic Diseases*, **71** (10), pp. 1630-1635.

Khakh, B.S. (2001). Molecular physiology of P2X receptors and ATP signalling at synapses. *Nature Reviews Neuroscience*, **2** (3), pp. 165-174.

Khakh, B.S., Bao, X.R., Labarca, C. & Lester, H.A. (1999a). Neuronal P2X transmitter-gated cation channels change their ion selectivity in seconds. *Nature Neuroscience*, **2** (4), pp. 322-330.

Khakh, B.S. & North, R.A. (2012). Neuromodulation by extracellular ATP and P2X receptors in the CNS. *Neuron*, **76** (1), pp. 51-69.

Khakh, B.S., Proctor, W.R., Dunwiddie, T.V. *et al.* (1999b). Allosteric control of gating and kinetics at $P2X_4$ receptor channels. *Journal of Neuroscience*, **19** (17), pp. 7289-7299.

Khalturin, K., Anton-Erxleben, F., Milde, S. *et al.* (2007). Transgenic stem cells in *Hydra* reveal an early evolutionary origin for key elements controlling self-renewal and differentiation. *Developmental Biology*, **309** (1), pp. 32-44.

Kim, H.S., Murphy, T., Xia, J. *et al.* (2010). BeetleBase in 2010: revisions to provide comprehensive genomic information for Tribolium castaneum. *Nucleic Acids Research*, **38** (Database issue), pp. D437-442.

Kim, J., Kim, W. & Cunningham, C.W. (1999). A new perspective on lower metazoan relationships from 18S rDNA sequences. *Molecular Biology and Evolution*, **16** (3), pp. 423-427.

Kim, S.-Y., Sivaguru, M. & Stacey, G. (2006). Extracellular ATP in plants. Visualization, localization, and analysis of physiological signficance in growth and signaling. *Plant Physiology*, **142** (3), pp. 984-992.

Kimura, S., Tokishita, S., Ohta, T. *et al.* (1999). Heterogeneity and differential expression under hypoxia of two-domain hemoglobin chains in the water flea, *Daphnia magna*. *Journal of Biological Chemistry*, **274** (15), pp. 10649-10653.

King, B.F., Knowles, I.D., Burnstock, G. & Ramage, A.G. (2004). Investigation of the effects of P2 purinoceptor ligands on the micturition reflex in female urethane-anaesthetized rats. *British Journal of Pharmacology*, **142** (3), pp. 519-530.

King, B.F., Liu, M., Townsend-Nicholson, A. *et al.* (2005). Antagonism of ATP responses at P2X receptor subtypes by the pH indicator due, Phenol red. *British Journal of Pharmacology*, **145** (3), pp. 313-322.

King, B.F., Townsend-Nicholson, A., Wildman, S.S. *et al.* (2000). Coexpression of rat $P2X_2$ and $P2X_6$ subunits in *Xenopus* oocytes. *Journal of Neuroscience*, **20** (13), pp. 4871-4877.

King, B.F., Wildman, S.S., Ziganshina, L.E. *et al.* (1997). Effects of extracellular pH on agonism and antagonism at a recombinant $P2X_2$ receptor. *British Journal of Pharmacology*, **121** (7), pp. 1445-1453.

King, C.H. & Bertino, A.M. (2008). Asymmetries of poverty: why global burden of disease valuations underestimate the burden of neglected tropical diseases. *PLoS Negl Trop Dis*, **2** (3), pp. e209.

King, N., Westbrook, M.J., Young, S.L. *et al.* (2008). The genome of the choanoflagellate *Monosiga brevicollis* and the origin of metazoans. *Nature*, **451** (7180), pp. 783-788.

Klüttgen, B., Dülmera, U., Engelsa, M. & Rattea, H.T. (1994). ADaM, an artificial freshwater for the culture of zooplankton. *Water Research*, **28** (3), pp. 743-746.

Knight, G.E., Hoyle, C.H. & Burnstock, G. (1992). Quinacrine-staining of neurones, and activity of purine nucleosides and nucleotides in marine and terrestrial invertebrates from several phyla. *Comparative Biochemistry and Physiology, Part C*, **102** (2), pp. 305-314.

Knowles, A.F. (2009). The single *NTPase* gene of *Drosophila melanogaster* encodes an intracellular nucleoside triphosphate diphosphohydrolase 6 (NTPDase6). *Archives of Biochemistry and Biophysics*, **484** (1), pp. 70-79.

Koch, A.W., Holstein, T.W., Mala, C. *et al.* (1998). Spinalin, a new glycine- and histidine-rich protein in spines of *Hydra* nematocysts. *Journal of Cell Science*, **111** (11), pp. 1545-1554.

Koizumi, O. & Bode, H.R. (1986). Plasticity in the nervous system of adult hydra. I. The position-dependent expression of FMRFamide-like immunoreactivity. *Developmental Biology*, **116** (2), pp. 407-421.

Koizumi, O., Heimfeld, S. & Bode, H.R. (1988). Plasticity in the nervous system of adult hydra. II. Conversion of ganglion cells of the body column into epidermal sensory cells of the hypostome. *Developmental Biology*, **129** (2), pp. 358-371.

Koizumi, O., Wilson, J.D., Grimmelikhuijzen, C.J.P. & Westfall, J.A. (1989). Ultrastructural localizationof RFamide-like peptides in neuronal dense-cored vesicles in the peduncle of *Hydra*. *Journal of Experimental Zoology*, **249** (1), pp. 17-22.

Korcok, J., Raimundo, L.N., Ke, H.Z. *et al.* (2004). Extracellular nucleotides act through P2X7 receptors to activate NF-κB in osteoclasts. *Journal of Bone and Mineral Research*, **19** (4), pp. 642-651.

Koshimizu, T., Tomić, M., Koshimizu, M. & Stojilkovic, S.S. (1998). Identification of amino acid residues contributing to desensitization of the $P2X_2$ receptor channel. *Journal of Biological Chemistry*, **273** (21), pp. 12853-12857.

Koshimizu, T.-A., Koshimizu, M. & Stojilkovic, S.S. (1999). Contributions of the C-terminal domain to the control of P2X receptor desensitization. *Journal of Biological Chemistry*, **274** (53), pp. 37651-37657.

Kotnis, S., Bingham, B., Vasilyev, D.V. *et al.* (2010). Genetic and functional analysis of human P2X5 reveals a distinct pattern of exon 10 polymorphism with predominant expression of the nonfunctional receptor isoform. *Molecular Pharmacology*, **77** (6), pp. 953-960.

Kowalevsky, A.O. (1866). Entwicklungsgeschichte des Amphioxus lanceolatus. *Mémoires de l'Académie Impériale des Sciences de St. Pétersbourg,*, **11** (1), pp. 1-17.

Kranz, H.D., Miks, D., Siegler, M.L. *et al.* (1995). The origin of land plants: phylogenetic relationships among charophytes, bryophytes, and vascular plants inferred from complete small-subunit ribosomal RNA gene sequences. *J Mol Evol*, **41** (1), pp. 74-84.

Kreda, S.M., Seminario-Vidal, L., Van Heusden, C.A. *et al.* (2010). Receptor-promoted exocytosis of airway epithelial mucin granules containing a spectrum of adenine nucleotides. *Journal of Physiology*, **588** (12), pp. 2255-2267.

Krogh, A., Brown, M., Mian, I.S. *et al.* (1994). Hidden Markov models in computational biology. Applications to protein modeling. *Journal of Molecular Biology*, **235** (5), pp. 1501-1531.

Krogh, A., Larsson, B., Von Heijne, G. & Sonnhammer, E.L. (2001). Predicting transmembrane protein topology with a hidden Markov model: application to complete genomes. *Journal of Molecular Biology*, **305** (3), pp. 567-580.

Krueger, J.M., Taishi, P., De, A. *et al.* (2010). ATP and the purine type 2 X7 receptor affect sleep. *Journal of Applied Physiology*, **109** (5), pp. 1318-1327.

Kucenas, S., Li, Z., Cox, J.A. *et al.* (2003). Molecular characterization of the zebrafish P2X receptor subunit gene family. *Neuroscience*, **121** (4), pp. 935-945.

Kurz, E.M., Holstein, T.W., Petri, B.M. *et al.* (1991). Mini-collagens in hydra nematocytes. *Journal of Cell Biology*, **115** (4), pp. 1159-1169.

Kyte, J. & Doolittle, R.F. (1982). A simple method for displaying the hydropathic character of a protein. *Journal of Molecular Biology*, **157** (1), pp. 105-132.

Labandeira, C.C., Beall, B.S. & Hueber, F.M. (1988). Early insect diversification; evidence from a Lower Devonian bristletail from Québec. *Science*, **242** (4880), pp. 913-916.

Labasi, J.M., Petrushova, N., Donovan, C. *et al.* (2002). Absence of the $P2X_7$ receptor alters leukocyte function and attenuates an inflammatory response. *Journal of Immunology*, **168** (12), pp. 6436-6445.

Lambert, J.J., Belelli, D., Peden, D.R. *et al.* (2003). Neurosteroid modulation of $GABA_A$ receptors. *Prog Neurobiol*, **71** (1), pp. 67-80.

Lang, B.F., O'kelly, C., Nerad, T. *et al.* (2002). The closest unicellular relatives of animals. *Current Biology*, **12** (20), pp. 1773-1778.

Langeland, J.A., Holland, L.Z., Chastain, R.A. & Holland, N.D. (2006). An amphioxus LIM-homeobox gene, AmphiLim1/5, expressed early in the invaginating organizer region and later in differentiating cells of the kidney and central nervous system. *Int J Biol Sci*, **2** (3), pp. 110-116.

Langosch, D., Becker, C.M. & Betz, H. (1990). The inhibitory glycine receptor: a ligand-gated chloride channel of the central nervous system. *European Journal of Biochemistry*, **194** (1), pp. 1-8.

Lazarowski, E.R. (2012). Vesicular and conductive mechanisms of nucleotide release. *Purinergic Signaling*, **8** (3), pp. 359-373.

Lê, K.T., Babinski, K. & Séguéla, P. (1998). Central $P2X_4$ and $P2X_6$ channel subunits coassemble into a novel heteromeric ATP receptor. *Journal of Neuroscience*, **18** (18), pp. 7152-7159.

Lê, K.T., Paquet, M., Nouel, D. *et al.* (1997). Primary structure and expression of a naturally truncated human P2X ATP receptor subunit from brain and immune system. *FEBS Letters*, **418** 195-199.

Lee, M.S., Park, W.S., Kim, Y.H. *et al.* (2012). Intracellular ATP assay of live cells using PTD-conjugated luciferase. *Sensors (Basel)*, **12** (11), pp. 15628-15637.

Legg, D.A., Sutton, M.D. & Edgecombe, G.D. (2013). Arthropod fossil data increase congruence of morphological and molecular phylogenies. *Nature Communications*, **4** (2485), pp.

Lenhoff, H. & Bovaird, J. (1961). Action of glutamic acid and glutathione analogues on the *Hydra* glutathione-receptor. *Nature*, **189** 486-487.

Lewis, C., Neidhart, S., Holy, C. *et al.* (1995). Coexpression of $P2X_2$ and $P2X_3$ receptor subunits can account for ATP-gated currents in sensory neurons. *Nature*, **377** (6548), pp. 432-435.

Li, J., Waterhouse, R.M. & Zdobnov, E.M. (2011). A remarkably stable TipE gene cluster: evolution of insect Para sodium channel auxiliary subunits. *BMC Evolutionary Biology*, **11** 337.

Li, M., Kim, T.J., Kwon, H.J. & Suh, J.W. (2008). Effects of extracellular ATP on the physiology of *Streptomyces coelicolor* A3(2). *FEMS Microbiology Letters*, **286** (1), pp. 24-31.

Li, M., Silberberg, S.D. & Swartz, K.J. (2013). Subtype-specific control of P2X receptor channel signaling by ATP and Mg^{2+}. *Proceedings of the National Academy of Sciences USA*, **110** (36), pp. E3455-3463.

Li, Z., Migita, K., Samways, D.S. *et al.* (2004). Gain and loss of channel function by alanine substitutions in the transmembrane segments of the rat ATP-gated $P2X_2$ receptor. *Journal of Neuroscience*, **24** (33), pp. 7378-7386.

Liscia, A. (1985). ATP influences the elctrophysiological responses of labellar chemosensilla of *Phormia regina* meigen (diptera calliphoridae to salt and sugar stimulation. *Monitore Zoologico Italiano*, **19** 261-265.

Littlefield, C.L. (1985). Germ cells in *Hydra oligactis* males. I. Isolation of a subpopulation of interstitial cells that is developmentally restricted to sperm production. *Developmental Biology*, **112** (1), pp. 185-193.

Littlefield, C.L. (1991). Cell lineages in *Hydra*: isolation and characterization of an interstitial stem cell restricted to egg production in *Hydra oligactis*. *Developmental Biology*, **143** (2), pp. 378-388.

Littleton, J.T. & Ganetzky, B. (2000). Ion channels and synaptic organization: analysis of the *Drosophila* genome. *Neuron*, **36** (1), pp. 35-43.

Liu, X., Ma, W., Surprenant, A. & Jiang, L.H. (2009a). Identification of the amino acid residues in the extracellular domain of rat $P2X_7$ receptor involved in functional inhibition by acidic pH. *British Journal of Pharmacology*, **156** (1), pp. 135-142.

Liu, Y., Steenkamp, E.T., Brinkmann, H. *et al.* (2009b). Phylogenomic analyses predict sistergroup relationship of nucleariids and fungi and paraphyly of zygomycetes with significant support. *BMC Evolutionary Biology*, **9** 272.

Loenarz, C., Coleman, M.L., Boleininger, A. *et al.* (2011). The hypoxia-inducible transcription factor pathway regulates oxygen sensing in the simplest animal, *Trichoplax adhaerens*. *EMBO Rep*, **12** (1), pp. 63-70.

Loftus, B., Anderson, I., Davies, R. *et al.* (2005). The genome of the protist parasite *Entamoeba histolytica*. *Nature*, **433** (7028), pp. 865-868.

Loh, E.Y., Elliot, J.F., Cwirla, S. *et al.* (1989). Polymerase chain reaction with single-sided specificity: analysis of T cell receptor delta chain. *Science*, **243** (4888), pp. 217-220.

Łomnicki, A. & Slobodkin, L.B. (1966). Floating in *Hydra littoralis*. *Ecology*, **47** (6), pp. 881-889.

Lorca, R.A., Coddou, C., Gazitúa, M.C. *et al.* (2005). Extracellular histidine residues identify common structural determinants in the copper/zinc $P2X_2$ receptor modulation. *Journal of Neurochemistry*, **95** (2), pp. 499-512.

Lotan, A., Fishman, L., Loya, Y. & Zlotkin, E. (1995). Delivery of a nematocyst toxin. *Nature*, **375** (6531), pp. 456.

Ludlow, M.J., Durai, L. & Ennion, S.J. (2009). Functional characterization of intracellular *Dictyostelium discoideum* P2X receptors. *Journal of Biological Chemistry*, **284** (50), pp. 35227-35239.

Ludlow, M.J., Traynor, D., Fisher, P.R. & Ennion, S.J. (2008). Purinergic-mediated Ca^{2+} influx in *Dictyostelium discoideum*. *Cell Calcium*, **44** (6), pp. 567-579.

Luthardt, J., Borvendeg, S.J., Sperlagh, B. *et al.* (2003). $P2Y_1$ receptor activation inhibits NMDA receptor-channels in layer V pyramidal neurons of the rat prefrontal and parietal cortex. *Neurochemistry International*, **42** (2), pp. 161-172.

Lynch, J.W. (2004). Molecular structure and function of the glycine receptor chloride channel. *Physiological Reviews*, **84** (4), pp. 1051-1095.

Lynch, K.J., Touma, E., Niforatos, W. *et al.* (1999). Molecular and functional characterization of human $P2X_2$ receptors. *Molecular Pharmacology*, **56** (6), pp. 1171-1181.

Mackenzie, A.B., Surprenant, A. & North, R.A. (1999). Functional and molecular diversity of purinergic ion channel receptors. *Annals of the New York Academy of Science*, **868** 716-729.

Mackie, G.O. & Singla, C.L. (1983). Studies on Hexactinellid Sponges. I. Histology of *Rhabdocalyptus dawsoni* (Lambe, 1973). *Philosophical Transactions of the Royal Society B. Biological Sciences*, **301** 365-400.

Mantiatis, T., Fritsch, E.F. & Sambrook, J. 1982. *Molecular Cloning: A Laboratory Manual,* Cold Spring Habor, New York, Cold Spring Habor Laboratory.

Mardanov, A.V., Svetlitchnyi, V.A., Beletsky, A.V. *et al.* (2010). The genome sequence of the crenarchaeon *Acidilobus saccharovorans* supports a new order, Acidilobales, and suggests an important ecological role in terrestrial acidic hot springs. *Applied Environmental Microbiology*, **76** (16), pp. 5652-5657.

Marioni, J.C., Mason, C.E., Mane, S.M. *et al.* (2008). RNA-seq: an assessment of technical reproducibility and comparison with gene expression arrays. *Genome Research*, **18** (9), pp. 1509-1517.

Martin, J., Abubucker, S., Heizer, E. *et al.* (2012). Nematode.net update 2011: addition of data sets and tools featuring next-generation sequencing data. *Nucleic Acids Research*, **40** (Database issue), pp. D720-728.

Martin, V.J., Littlefield, C.L., Archer, W.E. & Bode, H.R. (1997). Embryogenesis in *Hydra*. *Biological Bulletins*, **192** 345-363.

Martinez, D.E. (1998). Mortality patterns suggest lack of senescence in *Hydra*. *Experimental Gerontology*, **33** (3), pp. 217-225.

Martinson, A.S., Van Rossum, D.B., Diatta, F.H. *et al.* (2014). Functional evolution of Erg potassium channel gating reveals an ancient origin for I_{Kr}. *Proceedings of the National Academy of Sciences USA*, **111** (15), pp. 5712-5717.

Marvaldi, A.E., Duckett, C.N., Kjer, K.M. & Gillespie, J.J. (2008). Structural alignment of 18S and 28S rDNA sequences provides insights into phylogeny of Phytophaga (Coleoptera: Curculionoidea and Chrysomeloidea). *Zoologica Scripta*, **38** (1), pp. 63-77.

Maurer, G., Wilkens, J.L. & Grieshaber, M.K. (2008). Modulatory effects of adenosine and adenine nucleotides on different heart preparations of the American lobster, *Homarus americanus*. *Journal of Experimental Biology*, **211** (Pt 5), pp. 661-670.

Medina, M., Collins, A.G., Silberman, J.D. & Sogin, M.L. (2001). Evaluating hypotheses of basal animal phylogeny using complete sequences of large and small subunit rRNA. *Proceedings of the National Academy of Sciences*, **98** (17), pp. 9707-9712.

Melchoir, N.C. (1954). Sodium and potassium complexes of adenosinetriphosphate: equilibrium studies. *Journal of Biological Chemistry*, **208** (2), pp. 615-627.

Metzker, M.L. (2010). Sequencing technologies - the next generation. *Nature Reviews Genetics*, **11** (1), pp. 31-46.

Meusemann, K., Von Reumont, B.M., Simon, S. *et al.* (2010). A phylogenomic approach to the Arthropod tree of life. *Molecular Biology and Evolution*, **27** (11), pp. 2451-2464.

Mezei, L.M. & Storts, D.R. 1994. *Purification of PCR products,* Boca Raton, FL, 21, CRC Press.

Migita, K., Haines, W.R., Voigt, M.M. & Egan, T.M. (2001a). Polar residues of the second transmembrane domain influence cation permeability of the ATP-gated $P2X_2$ receptor. *Journal of Biological Chemistry*, **276** (33), pp. 30934-30941.

Migita, K., Haines, W.R., Voigt, M.M. & Egan, T.M. (2001b). Polar residues of the second transmembrane domain influence cation permeability of the ATP-gated P2X(2) receptor. *Journal of Biological Chemistry*, **276** (33), pp. 30934-30941.

Miller, J.A., Ding, S.L., Sunkin, S.M. *et al.* (2014). Transcriptional landscape of the prenatal human brain. *Nature*, **508** (7495), pp. 199-206.

Miller, J.R., Koren, S. & Sutton, G. (2010). Assembly algorithms for next-generation sequencing data. *Genomics*, **95** (6), pp. 315-327.

Mio, K., Ogura, T., Yamamoto, T. *et al.* (2009). Reconstruction of the $P2X_2$ receptor reveals a vase-shaped structure with lateral tunnels above the membrane. *Structure*, **17** (2), pp. 266-275.

Mitchell, B.K. (1976). ATP reception by the tsetse, *Glossina morsitans West*. *Experientia*, **32** (2), pp. 192-194.

Miyazawa, H., Ueda, C., Yahata, K. & Su, Z.H. (2014). Molecular phylogeny of Myriapoda provides insights into evolutionary patterns of the mode in post-embryonic development. *Sci Rep*, **4** (4127), pp.

Morabito, R., Marino, A. & La Spada, G. (2012). Nematocytes' activation in Pelagia noctiluca (Cnidaria, Scyphozoa) oral arms. *Journal of Comparative Physiology, A. Neuroethology, Sensory, Neural and Behavioral Physiology*, **198** (6), pp. 419-426.

Moreno-Hagelsieb, G. & Latimer, K. (2008). Choosing BLAST options for better detection of orthologs as reciprocal best hits. *Bioinformatics*, **24** (3), pp. 319-324.

Moret, F., Guilland, J.C., Coudouel, S. *et al.* (2004). Distribution of tyrosine hydroxylase, dopamine, and serotonin in the central nervous system of amphioxus (*Branchiostoma lanceolatum*): implications for the evolution of catecholamine systems in vertebrates. *Journal of Comparative Neurology*, **468** (1), pp. 135-150.

Moroz, L.L., Edwards, J.R., Puthanveettil, S.V. *et al.* (2006). Neuronal transcriptome of Aplysia: neuronal compartments and circuitry. *Cell*, **127** (7), pp. 1453-1467.

Moroz, L.L., Kocot, K.M., Citarella, M.R. *et al.* (2014). The ctenophore genome and the evolutionary origins of neural systems. *Nature*.

Müller, J.F. (1950). Some observations on the structure of hydra, with particular reference to the muscular system. *Transactions of the American Microscopal Society*, **69** 133-147.

Müller, R., Morant, M., Jarmer, H. *et al.* (2007). Genome-wide analysis of the Arabidopsis leaf transcriptome reveals interaction of phosphate and sugar metabolism. *Plant Physiology*, **143** (1), pp. 156-171.

Mulyran, K., Gitterman, D.P., Lewis, C.J. *et al.* (2000). Reduced vas deferences contracility and male infertility in mice lacking $P2X_1$ receptors. *Nature*, **403** (6765), pp. 86-89.

Musa, H., Tellez, J.O., Chandler, N.J. *et al.* (2009). P2 purinergic receptor mRNA in rat and human sinoatrial node and other heart regions. *Naunyn Schmiedeberg's Archives of Pharmacology*, **379** (6), pp. 541-549.

Nakai, J., Ohkura, M. & Imoto, K. (2001). A high signal-to-noise Ca^{2+} probe composed of a single green fluorescent protein. *Nat Biotechnol*, **19** (2), pp. 137-141.

Nakamura, S. & Tamm, S.L. (1985). Calcium control of ciliary reversal in ionophore-treated and ATP-reactivated comb plates of ctenophores. *Journal of Cell Biology*, **100** (5), pp. 1447-1454.

Nakazawa, K., Fujimori, K., Takanaka, A. & Inoue, K. (1990a). An ATP-activated conductance in pheochromocytoma cells and its suppression by extracellular calcium. *Journal of Physiology*, **428** 257-272.

Nakazawa, K., Fujimori, K., Takanaka, A. & Inoue, K. (1990b). Reversible and selective antagonism by suramin of ATP-activated inward current in PC12 phaeochromocytoma cells. *British Journal of Pharmacology*, **101** (1), pp. 224-226.

Nakazawa, K., Inoue, K., Fujimori, K. & Takanaka, A. (1990c). ATP-activated single-channel currents recorded from cell-free patches of pheochromocytoma PC12 cells. *Neuroscience Letters*, **119** (1), pp. 5-8.

Naranjo, S.E. & Steinkraus, D.C. (1988). Discovery of an entomophthoralean fungus (Zygomycetes: Entomophthorales) infecting adult northern corn rootworm, *Diabrotica barberi* (Coleoptera: Chrysomelidae). *Journal of Invertebrate Pathology*, **51** (3), pp. 298-300.

Nardi, F., Spinsanti, G., Boore, J.L. *et al.* (2003). Hexapod origins: monophyletic or paraphyletic? *299*, **5614** (1887-1889), pp.

Neher, E. & Sakmann, B. (1976). Single-channel currents recorded from membrane of denervated frog muscle fibres. *Nature*, **260** 299-802.

Newbolt, A., Stoop, R., Virginio, C. *et al.* (1998). Membrane topology of an ATP-gated ion channel (P2X receptor). *Journal of Biological Chemistry*, **273** (24), pp. 15177-15182.

Newton, W.L. (1953). The inheritance of susceptibility to infection with *Schistosoma mansoni* in *Australorbis glabratus*. *Experimental Parasitology*, **2** (3), pp. 242-257.

Nicke, A., Baumert, H.G., Rettinger, J. *et al.* (1998). $P2X_1$ and $P2X_3$ receptors form stable trimers: a novel structural motif of ligand-gated ion channels. *EMBO Journal*, **17** (11), pp. 3016-3028.

North, R.A. (2002). Molecular physiology of P2X receptors. *Physiological Reviews*, **82** (4), pp. 1013-1064.

North, R.A. & Suprenant, A. (2000). Pharmacology of cloned P2X receptors. *Annual Review of Pharmacology and Toxicology*, **40** (563-580), pp.

Notredame, C., Higgins, D.G. & Heringa, J. (2000). T-Coffee: A novel method for fast and accurate multiple sequence alignment. *Journal of Molecular Biology*, **302** (1), pp. 205-217.

Nüchter, T., Benoit, M., Engel, U. *et al.* (2006). Nanosecond-scale kinetics of nematocyst discharge. *Current Biology*, **16** (9), pp. R316-318.

O'sullivan, W.J. & Perrin, D.D. (1964). The stability constants of metal-adenine nucleotide complexes. *Biochemistry*, **3** 18-26.

Ohara, O., Dorit, R.L. & Gilbert, W. (1989). One-sided polymerase chain reaction: the amplification of cDNA. *Proceedings of the National Academy of Sciences*, **86** (15), pp. 5673-5677.

Oldham, M.C., Konopka, G., Iwamoto, K. *et al.* (2008). Functional organization of the transcriptome in human brain. *Nature Neuroscience*, **11** (11), pp. 1271-1282.

Oliver, D., Brinkmann, M., Sieger, T. & Thurm, U. (2008). Hydrozoan nematocytes send and receive synaptic signals induced by mechano-chemical stimuli. *Journal of Experimental Biology*, **211** (17), pp. 2876-2888.

Olson, L., Alund, M. & Norberg, K.A. (1976). Fluorescence-microscopical demonstration of a population of gastro-intestinal nerve fibres with a selective affinity for quinacrine. *Cell and Tissue Research*, **171** (4), pp. 407-423.

Ostrom, R.S., Gregorian, C. & Insel, P.A. (2000). Cellular release of and response to ATP as key determinants of the set-point of signal transduction pathways. *Journal of Biological Chemistry*, **275** (16), pp. 11735-11739.

Otto, J.J. & Campbell, R.D. (1977). Tissue economics of hydra: regulation of cell cycle, animal size and development by controlled feeding rates. *Journal of Cell Science*, **28** 117-132.

Özbek, S., Balasubramanian, P.G. & Holstein, T.W. (2009a). Cnidocyst structure and biomechanics of discharge. *Toxicon*, **54** (8), pp. 1038-1045.

Özbek, S., Balasubramaniana, P.G. & Holstein, T.W. (2009b). Cnidocyst structure and the biomechanics of discharge. *Toxicon*, **54** (8), pp. 1038-1045.

Pankratov, Y., Lalo, U., Verkhratsky, A. & North, R.A. (2006). Vesicular release of ATP at central synapses. *Pflüfgers Archiv - European Journal of Physiology*, **452** (2), pp. 589-597.

Parfrey, L.W., Lahr, D.J., Knoll, A.H. & Katz, L.A. (2011). Estimating the timing of early eukaryotic diversification with multigene molecular clocks. *Proceedings of the National Academy of Sciences USA*, **108** (33), pp. 13624-13629.

Parish, R.W. & Weibel, M. (1980). Extracellular ATP, ecto-ATPase and calcium influx in *Dictyostelium discoideum* cells. *FEBS Letters*, **118** (2), pp. 263-266.

Parkinson, J., Whitton, C., Schmid, R. *et al.* (2004). NEMBASE: a resource for parasitic nematode ESTs. *Nucleic Acids Research*, **32** (Database issue), pp. D427-430.

Parvathenani, L.K., Tertyshnikova, S., Greco, C.R. *et al.* (2003). P2X7 mediates superoxide production in primary microglia and is up-regulated in a transgenic mouse model of Alzheimer's disease. *Journal of Biological Chemistry*, **278** (15), pp. 13309-13317.

Pelegrin, P. & Suprenant, A. (2006). Pannexin-1 mediates large pore formation and interleukin-1β release by the ATP-gated $P2X_7$ receptor. *EMBO Journal*, **25** (21), pp. 5071-5082.

Philippe, H., Derelle, R., Lopez, P. *et al.* (2009). Phylogenomics revives traditional views on deep animal relationships. *Current Biology*, **19** (8), pp. 706-712.

Pick, K.S., Philippe, H., Schreiber, F. *et al.* (2010). Improved phylogenomic taxon sampling noticeably affects nonbilaterian relationships. *Molecular Biology and Evolution*, **27** (9), pp. 1983-1987.

Pierobon, P., Concas, A., Santoro, G. *et al.* (1995). Biochemical and functional identification of GABA receptors in *Hydra vulgaris*. *Life Sciences*, **56** (18), pp. 1485-1497.

Pierobon, P., Minei, R., Porcu, P. *et al.* (2001). Putative glycine receptors in *Hydra*: a biochemical and behavioural study. *European Journal of Neuroscience*, **14** (10), pp. 1659-1666.

Pierzyńska-Mach, A., Janowski, P.A. & Dobrucki, J.W. (2014). Evaluation of acridine orange, LysoTracker Red, and quinacrine as fluorescent probes for long-term tracking of acidic vesicles. *Cytometry A*, **85** (8), pp. 729-737.

Pizzo, P., Murgia, M., Zambon, A. *et al.* (1992). Role of P2z purinergic receptors in ATP-mediated killing of tumor necrosis factor (TNF)-sensitive and TNF-resistant L929 fibroblasts. *Journal of Immunology*, **149** (10), pp. 3372-3379.

Plachetzki, D.C., Fong, C.R. & Oakley, T.H. (2010). The evolution of phototransduction from an ancestral cyclic nucleotide gated pathway. *Proceedings of the Royal Society B: Biological Sciences*, **277** (1690), pp. 1963-1969.

Plachetzki, D.C., Fong, C.R. & Oakley, T.H. (2012). Cnidocyte discharge is regulatored by light and opsin-mediated phototransduction. *BMC Biology*, **10** 17.

Popadic, A., Panganiban, G., Rusch, D. *et al.* (1998). Molecular evidence for the gnathobasic derivation of arthropod mandibles and for the appendicular origin of the labrum and other structures. *Development, Genes and Evolution*, **208** (3), pp. 142-150.

Pothier, F., Forget, J., Sullivan, R. & Couillard, P. (1987). ATP and the contractile vacuole in *Amoeba proteus*: Mechanism of action of exogenous ATP and related nucleotides. *Journal of Experimental Zoology*, **243** (3), pp. 379-287.

Praetorius, H.A. & Leipziger, J. (2009). ATP release from non-excitable cells. *Purinergic Signaling*, **5** (4), pp. 433-446.

Price, R.B. & Anderson, P.A. (2006). Chemosensory pathways in the capitate tentacles of the hydroid *Cladonema*. *Invertebrate Neuroscience*, **6** (1), pp. 23-32.

Priel, A. & Silberberg, S.D. (2004). Mechanism of ivermectin facilitation of human $P2X_4$ receptor channels. *Journal of General Physiology*, **123** (3), pp. 281-293.

Prusch, R.D., Benos, D.J. & Ritter, M. (1976). Osmoregulatory control mechanisms in freshwater coelenterates. *Comparative Biochemistry and Physiology A: Comparative Physiology*, **53** (2), pp. 161-164.

Purcell, J.E. & Anderson, P.a.V. (1995). Electrical responses to water-soluble components of fish mucus recorded from the cnidocytes of a fish predatory, *Physalia physalis*. *Marine and Freshwater Behaviour and Physiology*, **26** 149-162.

Putnam, N.H., Butts, T., Ferrier, D.E. *et al.* (2008). The amphioxus genome and the evolution of the chordate karyotype. *Nature*, **453** (7198), pp. 1064-1071.

Putnam, N.H., Srivastava, M., Hellsten, U. *et al.* (2007). Sea anemone genome reveals ancestral eumetazoan gene repertoire and genomic organization. *Science*, **317** (5834), pp. 86-94.

Qureshi, O.S., Paramasivam, A., Yu, J.C. & Murrell-Lagnado, R.D. (2007). Regulation of $P2X_4$ receptors by lysosomal targeting, glycan protection and exocytosis. *Journal of Cell Science*, **120** (21), pp. 3838-3849.

Raghavan, N. & Knight, M. (2006). The snail (*Biomphalaria glabrata*) genome project. *Trends in Parasitology*, **22** (4), pp. 148-151.

Rassendren, F., Buell, G., Newbolt, A. *et al.* (1997). Identification of amino acid residues contributing to the pore of a P2X receptor. *EMBO Journal*, **16** (12), pp. 3446-3454.

Regier, J.C., Shultz, J.W., Zwick, A. *et al.* (2010). Arthropod relationships revealed by phylogenomic analysis of nuclear protein-coding sequences. *Nature*, **463** (7284), pp. 1079-1083.

Rehm, P., Meusemann, K., Borner, J. *et al.* (2014). Phylogenetic position of Myriapoda revealed by 454 transcriptome sequencing. *Molecular Phylogenetics and Evolution*, **77** 25-33.

Ren, J., Bian, X., Devries, M. *et al.* (2003). $P2X_2$ subunits contribute to fast synaptic excitation in myenteric neurons of the mouse small intestine. *Journal of Physiology*, **552** (3), pp. 809-821.

Renoirte, R., Vandepitte, J., Gatti, F. & Werth, R. (1965). Nasofacial phycomycosis (rhinophycomycosis) due to *Entomophtora coronata*. *Bull Soc Pathol Exot Filiales*, **58** (5), pp. 847-862.

Rettinger, J., Aschrafi, A. & Schmalzing, G. (2000). Roles of individual *N*-glycans for ATP potency and expression of the rat $P2X_1$ receptor. *Journal of Biological Chemistry*, **275** (43), pp. 33542-33547.

Richards, S., Gibbs, R.A., Weinstock, G.M. *et al.* (2008). The genome of the model beetle and pest *Tribolium castaneum*. *Nature*, **452** (7190), pp. 949-955.

Riutort, M., Álvarez-Presas, M., Lázaro, E. *et al.* (2012). Evolutionary history of the Tricladida and the Platyhelminthes: an up-to-date phylogenetic and systematic account. *International Journal of Developmental Biology*, **56** (1-3), pp. 5-17.

Roberts, J.A. & Evans, R.J. (2004). ATP binding at human $P2X_1$ receptors. Contribution of aromatic and basic amino acids revealed using mutagenesis and partial agonists. *Journal of Biological Chemistry*, **279** (10), pp. 9043-9055.

Roberts, J.A. & Evans, R.J. (2006). Contribution of conserved polar glutamine, asparagine and threonine residues and glycosylation to agonist action at human $P2X_1$ receptors for ATP. *Journal of Neurochemistry*, **96** (3), pp. 843-852.

Roberts, J.A., Valente, M., Allsopp, R.C. *et al.* (2009a). Contribution of the region Glu181 to Val200 of the extracellular loop of the human $P2X_1$ receptor to agonist binding and gating revealed using cysteine scanning mutagenesis. *Journal of Neurochemistry*, **109** (4), pp. 1042-1052.

Roberts, S., Goetz, G., White, S. & Goetz, F. (2009b). Analysis of genes isolated from plated hemocytes of the Pacific oyster, *Crassostreas gigas*. *Marine Biotechnology (NY)*, **11** (1), pp. 24-44.

Robson, E.A. (1973). The discharge of nematocysts in relation to properties of the capsule. **20** (Publications of the Seto Marine Laboratory), pp. 653-665.

Robson, S.C., Sevigny, J. & Zimmermann, H. (2006). The E-NTPDase family of ectonucleotidases: structure function relationship and pathophysiological significance. *Purinergic Signaling*, **2** 409-430.

Rogers, C.M. & Brown, E.R. (2001). Differential sensitivity to calciseptine of L-type Ca^{2+} currents in a 'lower' vertebrate (*Scyliorhinus canicula*), a protochordate (*Branchiostoma lanceolatum*) and an invertebrate (*Alloteuthis subulata*). *Experimental Physiology*, **86** (6), pp. 689-694.

Rogozin, I.B., Basu, M.K., Csuros, M. & Koonin, E.V. (2009). Analysis of rare genomic changes does not support the unikont-bikont phylogeny and suggests cyanobacterial symbiosis as the point of primary radiation of eukaryotes. *Genome Biology and Evolution*, **1** 99-113.

Rong, W., Gourine, A.V., Cockayne, D.A. *et al.* (2003). Pivotal role of nucleotide $P2X_2$ receptor subunit of the ATP-gated ion channel mediating ventilatory responses in hypoxia. *Journal of Neuroscience*, **23** (36), pp. 11315-11321.

Rosenberger, R.F. & Hilton, J. (1983). The frequency of transcriptional and translational errors at nonsense codons in the *lacZ* gene of E*scherichia coli*. *Molecular and General Microbiol*, **191** (2), pp. 207-212.

Rota-Stabelli, O., Campbell, L., Brinkmann, H. *et al.* (2011). A congruent solution to arthropod phylogeny: phylogenomics, microRNAs and morphology support monophyletic Mandibulata. *Proceedings of the Royal Society B: Biological Sciences*, **278** (1703), pp. 298-306.

Royle, S.J., Bobanović, L.K. & Murrell-Lagnado, R.D. (2002). Identification of a non-canonical tyrosine-based endocytic motif in an ionotropic receptor. *Journal of Biological Chemistry*, **277** (38), pp. 35378-35385.

Royle, S.J., Qureshi, O.S., Bobanović, L.K. *et al.* (2005). Non-canonical YXXGPhi motifs: recognition by AP2 and preferential utilization in $P2X_4$ receptors. *Journal of Cell Science*, **118** (14), pp. 3073-3080.

Ruggieri, R.D., Pierobon, P. & Kass-Simon, G. (2004). Pacemaker activity in hydra is modulated by glycine receptor ligands. *Comparative Biochemistry and Physiology. Part A , Molecular and Integrative Physiology*, **138** (2), pp. 193-202.

Ruiz-Trillo, I., Burger, C., Holland, P.W. *et al.* (2007). The origins of multicellularity: a multi-taxon genome initiative. *Trends in Genetics*, **23** (3), pp. 113-118.

Ruppelt, A., Ma, W., Borchardt, K. *et al.* (2001). Genomic structure, developmental distribution and functional properties of the chicken $P2X_5$ receptor. *Journal of Neurochemistry*, **77** (5), pp. 1256-1265.

Ryan, J.F. (2014). Did the ctenophore nervous system evolve independently? *Zoology (Jena)*.

Ryan, J.F., Pang, K., Schnitzler, C.E. *et al.* (2013). The genome of the ctenophore *Mnemiopsis leidyi* and its implications for cell type evolution. *Science*, **342** (6164), pp. 1336-1350.

Sabirov, R. & Okada, Y. (2005). ATP release *via* anion channels. *Purinergic Signaling*, **1** (14), pp. 311-328.

Sakurai, T., Lee, H., Kashima, M. *et al.* (2012). The planarian P2X homolog in the regulation of asexual reproduction. *International Journal of Developmental Biology*, **56** (1-3), pp. 173-182.

Salleo, A., La Spada, G., Denaro, M.G. & Falzea, G. (1986). Effects produced by SCN^- and thioglycolate on isolated nematocysts of *Pelagia noctiluca*. *Cell and Molecular Biology*, **32** (6), pp. 661-666.

Samways, D.S.K. & Egan, T.M. (2007). Acidic amino acids impart enhanced Ca^{2+} permeability and flux in two members of the ATP-gated P2X receptor family. *Journal of General Physiology*, **129** (3), pp. 245-256.

Samways, D.S.K., Khakh, B.S., Dutertre, S. & Egan, T.M. (2011). Preferential use of unobstructed lateral portals as the access route to the pore of human ATP-

gated ion channels (P2X receptors). *Proceedings of the National Academy of Sciences*, **108** (33), pp. 13800-13805.

Sanggaard, K.W., Bechsgaard, J.S., Fang, X. *et al.* (2014). Spider genomes provide insight into composition and evolution of venom and silk. *Nature Communications*, **5** (3765), pp.

Santillo, S., Taddei-Ferretti, C. & Nobile, M. (1997). Resting potentials recorded in the whole-cell configuration from epithelial cells of *Hydra vulgaris*. *Italian Journal of Zoology*, **64** 7-11.

Santoro, G. & Salleo, A. (1991). The discharge of *in situ* nematocysts of the Acontia of *Aiptasia Mutabilis* is a Ca^{2+}-induced response. *The Journal of Experimental Biology*, **156** 173-185.

Sanz, J.M., Chiozzi, P., Ferrari, D. *et al.* (2009). Activation of microglia by amyloid β requires $P2X_7$ receptor expression. *Journal of Immunology*, **182** (7), pp. 4378-4385.

Sarras, M.P. (2012). Components, structure, biogenesis and function of the *Hydra* extracellular matrix in regeneration, pattern formation and cell differentiation. *International Journal of Developmental Biology*, **56** 567-576.

Sasaki, G., Ishiwata, K., Machida, R. *et al.* (2013). Molecular phylogenetic analyses support the monophyly of Hexapoda and suggest the paraphyly of Entognatha. *BMC Evolutionary Biolology*, **13** 236.

Savard, J., Tautz, D. & Lercher, M.J. (2006). Genome-wide acceleration of protein evolution in flies (Diptera). *BMC Evolutionary Biology*, **6** 7.

Savi, P., Labouret, C., Deleseque, N. *et al.* (2001). P2y(12), a new platelet ADP receptor, target of clopidogrel. *Biochemical and Biophysical Research Communications*, **283** (2), pp. 379-383.

Scappaticci, A., A, & Kass-Simon, G. (2008). NMDA and $GABA_B$ receptors are involved in controlling nematocyst discharge in hydra. *Comparative Biochemistry and Physiology, Part A: Molecular and Integrate Physiology*, **150** (4), pp. 415-422.

Scappaticci, A.A., Jacques, R., Carroll, J.E. *et al.* (2004). Immunocytochemical evidence for an NMDA1 receptor subunit in dissociated cells of *Hydra vulgaris*. *Cell and Tissue Research*, **316** (2), pp. 263-270.

Schmid, T. & David, C.N. (1986). Gland cells in *Hydra*: cell kinetics and development. *Journal of Cell Science*, **85** (197-215), pp.

Schmutz, J., Cannon, S.B., Schlueter, J. *et al.* (2010). Genome sequence of the palaeopolyploid soybean. *Nature*, **463** (7278), pp. 178-183.

Schuchert, P. (1993). *Trichoplax adhaerens* (Phylum Placozoa) has cells that react with antibodies against the neuropeptide RFamide. *Acta Zoologica*, **74** (2), pp. 115-117.

Schulze, F.E. (1883). *Trichoplax adhaerens*, nov. gen., nov. spec. . *Zoologisches Anzeiger*, **6** 92-97.

Scotto-Lavino, E., Du, G. & Frohman, M.A. (2006). 3' end cDNA amplification using classic RACE. *Nature Protocols*, **1** (6), pp. 2742-2745.

Shalchian-Tabrizi, K., Minge, M.A., Espelund, M. *et al.* (2008). Multigene phylogeny of choanozoa and the origin of animals. *PLoS One*, **3** (5), pp. e2098.

Sharkey, D.J., Scalice, E.R., Christy Jr., K.G. *et al.* (1994). Antibodies as thermolabile switches: high temperature triggering for the polymerase chain reaction. *Biotechnology (NY)*, **12** (5), pp. 506-509.

Shen, J.B., Pappano, A.J. & Liang, B.T. (2006). Extracellular ATP-stimulated current in wild-type and $P2X_4$ receptor transgenic mouse ventricular myocytes: implications for a cardiac physiologic role of $P2X_4$ receptors. *Faseb Journal*, **20** (2), pp. 277-284.

Shinzato, C., Shoguchi, E., Kawashima, T. *et al.* (2011). Using the *Acropora digitifera* genome to understand coral responses to environmental change. *Nature*, **476** (7360), pp. 320-323.

Silberberg, S.D., Li, M. & Swartz, K.J. (2007). Ivermectin Interaction with transmembrane helices reveals widespread rearrangements during opening of P2X receptor channels. *Neuron*, **54** (2), pp. 263-274.

Sim, J.A., Broomhead, H.E. & North, R.A. (2008). Ectodomain lysines and suramin block of $P2X_1$ receptors. *Journal of Biological Chemistry*, **283** (44), pp. 29841-29846.

Sim, J.A., Chaumont, S., Jo, J. *et al.* (2006). Altered hippocampal synaptic potentiation in $P2X_4$ knock-out mice. *Journal of Neuroscience*, **26** (35), pp. 9006-9009.

Sim, J.A., Young, M.T., Sung, H.Y. *et al.* (2004). Reanalysis of $P2X_7$ receptor expression in rodent brain. *The Journal of Neuroscience*, **24** (28), pp. 6307-6314.

Simakov, O., Marletaz, F., Cho, S.J. *et al.* (2013). Insights into bilaterian evolution from three spiralian genomes. *Nature*, **493** (7433), pp. 526-531.

Simon, S., Strauss, S., Von Haeseler, A. & Hadrys, H. (2009). A phylogenomic approach to resolve the basal pterygote divergence. *Molecular Biology and Evolution*, **26** (12), pp. 2719-2730.

Sivaramakrishnan, V. & Fountain, S.J. (2012a). Intracellular P2X receptors as novel calcium release channels and modulators of osmoregulation in *Dictyostelium*: A comparison of two laboratory strains. *Channels (Austin)*, **7** (1), pp. 1-4.

Sivaramakrishnan, V. & Fountain, S.J. (2012b). A mechanism of intracellular P2X receptor activation. *Journal of Biological Chemistry*, **287** (34), pp. 28315-28326.

Sivaramakrishnan, V. & Fountain, S.J. (2013). Intracellular P2X receptors as novel calcium release channels and modulators of osmoregulation in *Dictyostelium*: a comparison of two common laboratory strains. *Channels (Austin)*, **7** (1), pp. 43-46.

Slautterback, D.B. & Fawcett, D.W. (1959). The development of the cnidoblasts of *Hydra*; an electron microscope study of cell differentiation. *Journal of Biophysical and Biochemical Cytology*, **5** (3), pp. 441-452.

Small, K.S., Brudno, M., Hill, M.M. & Sidow, A. (2007). A haplome alignment and reference sequence of the highly polymorphic *Ciona savignyi* genome. *Genome Biology*, **8** (3), pp. R41.

Smirnov, S.V. & Aaronson, P.I. (1992). Ca^{2+} currents in single myocytes from human mesenteric arteries: evidence for a physiological role of L-type channels. *Journal of Physiology*, **457** 455-475.

Smith, C.L., Varoqueaux, F., Kittelmann, M. *et al.* (2014). Novel Cell Types, Neurosecretory Cells, and Body Plan of the Early-Diverging Metazoan *Trichoplax adhaerens*. *Current Biology*, **24** (14), pp. 1565-1572.

Sodergren, E., Weinstock, G.M., Davidson, E.H. *et al.* (2006). The genome of the sea urchin *Strongylocentrotus purpuratus*. *Science*, **314** (5801), pp. 941-952.

Sokolova, E., Nistri, A. & Giniatullin, R. (2001). Negative cross talk between anionic $GABA_A$ and cationic P2X ionotropic receptors of rat dorsal root ganglion neurons. *Journal of Neuroscience*, **21** (14), pp. 4958-4968.

Solle, M., Labasi, J., Perregaux, D.G. *et al.* (2001). Altered cytokine production in mice lacking $P2X_7$ receptors. *Journal of Biological Chemistry*, **276** (1), pp. 125-132.

Song, C.J., Steinebrunner, I., Wang, X. *et al.* (2006). Extracellular ATP induces the accumulation of superoxide via NADPH oxidase in Arabidopsis. *Plant Physiology*, **140** (14), pp. 1222-1232.

Soto, F., Garcia-Guzman, M., Gomez-Hernandez, J.M. *et al.* (1996a). $P2X_4$: an ATP-activated ionotropic receptor cloned from rat brain. *Proceedings of the National Academy of Sciences USA*, **93** (8), pp. 3684-3668.

Soto, F., Garcia-Guzman, M., Karschin, C. & Stühmer, W. (1996b). Cloning and tissue distribution of a novel P2X receptor from rat brain. *Biochemical and Biophysical Research Communications*, **223** (2), pp. 456-460.

Soto, F., Krause, U., Borchardt, K. & Ruppelt, A. (2003). Cloning, tissue distribution and functional characterization of the chicken $P2X_1$ receptor. *FEBS Letters*, **533** (1-3), pp. 54-58.

Srivastava, M., Begovic, E., Chapman, J. *et al.* (2008). The *Trichoplax* genome and the nature of placozoans. *Nature*, **454** (7207), pp. 955-961.

Srivastava, M., Simakov, O., Chapman, J. *et al.* (2010). The *Amphimedon queenslandica* genome and the evolution of animal complexity. *Nature*, **466** 720–726.

Steinebrunner, I., Wu, J., Sun, Y. *et al.* (2003). Disruption of apyrases inhibits pollen germination in Arabidopsis. *Plant Physiology*, **131** (4), pp. 1638-1647.

Stewart, A.P., Haerteis, S., Diakov, A. *et al.* (2011). Atomic force microscopy reveals the architecture of the epithelial sodium channel (ENaC). *Journal of Biological Chemistry*, **286** (37), pp. 31944-31952.

Stock, T.C., Bloom, B.J., Wei, N. *et al.* (2012). Efficacy and safety of CE-224,535, an antagonist of P2X7 receptor, in patients with rheumatoid arthritis inadequately controlled by methotrexate. *Journal of Rheumatology*, **39** (4), pp. 720-727.

Stokes, L. (2013). Rab5 regulates internalisation of P2X4 receptors and potentiation by ivermectin. *Purinergic Signaling*, **9** (1), pp. 113-121.

Stoop, R., Surprenant, A. & North, R.A. (1997). Different sensitivities to pH of ATP-induced currents at four cloned P2X receptors. *Journal of Neurophysiology*, **78** (4), pp. 1837-1840.

Stoop, R., Thomas, S., Rassendren, F. *et al.* (1999). Contribution of individual subunits to the multimeric $P2X_2$ receptor: estimates based on methanethiosulfonate block at T336C. *Molecular Pharmacology*, **56** (5), pp. 973-981.

Stout, C.E., Constantin, J.L., Naus, C.C. & Charles, A.C. (2002). Intracellular calcium signaling in astrocytes *via* ATP release through connexin hemichannels. *Journal of Biological Chemistry*, **277** (12), pp. 10482.

Striessnig, J., Grabner, M., Mitterdorfer, J. *et al.* (1998). Structural basis of drug binding to L Ca^{2+} channels. *Trends in Pharmacological Sciences*, **19** (3), pp. 108-115.

Su, X.-Z., Wu, Y., Sifri, C.D. & Wellems, T.E. (1996). Reduced extension temperatures required for PCR amplificiation of extremely A+T-rich DNA. *Nucleic Acids Research*, **24** (8), pp. 1574-1575.

Suga, H., Chen, Z., De Mendoza, A. *et al.* (2013). The Capsaspora genome reveals a complex unicellular prehistory of animals. *Nature Communications*, **4** 2325.

Sugiyama, T. & Fujisawa, T. (1978). Genetic analysis of developmentla mechanisms in *Hydra*. II. Isolation and chatacterization of an interstitial cell-deficient strain. *Journal of Cell Science*, **29** (35-52), pp.

Suprenant, A., Rassendren, F., Kawashima, E. *et al.* (1996). The cytolytic P_{2Z} receptor for extracellular ATP identified as a P2X receptor ($P2X_7$). *Science*, **272** (5262), pp. 735-738.

Surprenant, A., Rassendren, F., Kawashima, E. *et al.* (1996). The cytolytic P_{2Z} receptor for extracellular ATP identified as a P2X receptor ($P2X_7$). *Science*, **272** (5262), pp. 735-738.

Szczepanek, S., Cikala, M. & David, C.N. (2001). Poly-γ-glutamate synthesis during formation of nematocyst capsules in *Hydra*. *Journal of Cell Science*, **115** (4), pp. 745-751.

Takahashi, T., Koizumi, O., Ariura, Y. *et al.* (2000). A novel neuropeptide, Hym-355, positively regulates neuron differentiation in Hydra. *Development*, **127** (5), pp. 997-1005.

Takahashi, T., Koizumi, O., Hayakawa, E. *et al.* (2009). Further characterization of the PW peptide family that inhibits neuron differentiation in *Hydra*. *Development, Genes and Evolution*, **219** (3), pp. 119-129.

Tamm, S.L. & Tamm, S. (1989). Calcium sensitivity extends the length of ATP-reactivated ciliary axonemes. *Proceedings of the National Academy of Sciences*, **86** (18), pp. 6987-6991.

Tang, Y., Matsuoka, I., Ono, T. *et al.* (2008). Selective up-regulation of $P2X_4$-receptor gene expression by interferon-γ in vascular endothelial cells. *Journal of Pharmacological Science*, **107** (4), pp. 419-427.

Tardent, P. (1995). The cnidarian cnidocyte, a high-tech cellular weaponry. *Bioessays*, **17** (4), pp. 351-362.

Tardent, P. & Holstein, T. (1982). Morphology and morphodynamics of the stenotele nematocyst of *Hydra attenuata* Pall. (Hydrozoa, Cnidaria). *Cell and Tissue Research*, **224** (2), pp. 269-290.

Tatusova, T., Ciufo, S., Fedorov, B. *et al.* (2014). RefSeq microbial genomes database: new representation and annotation strategy. *Nucleic Acids Research*, **42** (Database issue), pp. D553-559.

Telford, M.J. (2006). Animal phylogeny. *Current Biology*, **16** (23), pp. R981-R985.

Thompson, R.C. & Jenkins, D.J. (2014). Echinococcus as a model system: biology and epidemiology. *International of Journal for Parasitology*.

Timme, R.E., Bachvaroff, T.R. & Delwiche, C.F. (2012). Broad phylogenomic sampling and the sister lineage of land plants. *PLoS One*, **7** (1), pp. e29696.

Tindell, K.R. & Kunkel, T.A. (1988). Fidelity of DNA synthesis by the *Thermus aquaticus* DNA polymerase. *Biochemistry*, **27** (16), pp. 6008-6013.

Tisserant, E., Malbreil, M., Kuo, A. *et al.* (2013). Genome of an arbuscular mycorrhizal fungus provides insight into the oldest plant symbiosis. *Proceedings of the National Academy of Sciences USA*, **110** (50), pp. 20117-20122.

Torres, G.E., Egan, T.M. & Voigt, M.M. (1998). *N*-linked glycosylation is essential for the functional expression of the recombinant $P2X_2$ receptor. *Biochemistry*, **37** (42), pp. 14845-14851.

Torres, J., Rivera, A., Clark, G. & Roux, S.J. (2008). Participation of extracellular nucleotides in the wound response of *Dasycladus vermicularis* and *Acetabularia acetabulum* (dasycladales, chlorophyta). *Journal of Phycology*, **44** (6), pp. 1504-1511.

Toulmé, E., Soto, F., Garret, M. & Boué-Grabot, E. (2006). Functional properties of internalization-deficient $P2X_4$ receptors reveal a novel mechanism of ligand-gated channel facilitation by ivermectin. *Molecular Pharmacology*, **69** (2), pp. 576-587.

Trautwein, M.D., Wiegmann, B.M., Beutel, R. *et al.* (2012). Advances in insect phylogeny at the dawn of the postgenomic era. *Annual Reviews in Entomology*, **57** 449-468.

Trembley, A. 1744. *Memoires, pour servir à l'historie d'un genre de polypes d'eau douce, à bras en forme de cornes*, Jean and Herman Verbeek.

Tsai, I.J., Zarowiecki, M., Holroyd, N. *et al.* (2013). The genomes of four tapeworm species reveal adaptations to parasitism. *Nature*, **496** (7443), pp. 57-63.

Tsuda, M., Kuboyama, K., Inoue, T. *et al.* (2009). Behavioural phenotypes of mice lacking purinergic P2X4 receptors in acute and chronic pain assays. *Molecular Pain*, **5** 28.

Tsuda, M., Shigemoto-Mogami, Y., Koizumi, S. *et al.* (2003). P2X4 receptors induced in spinal microglia gate tactile allodynia after nerve injury. *Nature*, **424** (6950), pp. 778-783.

Turmel, M., Otis, C. & Lemieux, C. (2006). The chloroplast genome sequence of *Chara vulgaris* sheds new light into the closest green algal relatives of land plants. *Molecualar Biology and Evolution*, **23** (6), pp. 1324-1338.

Ulmann, L., Hatcher, J.P., Hughes, J.P. *et al.* (2008). Up-regulation of P2X4 receptors in spinal microglia after peripheral nerve injury mediates BDNF release and neuropathic pain. *Journal of Neuroscience*, **28** (44), pp. 11263-11268.

Ulmann, L., Hirbec, H. & Rassendren, F. (2010). $P2X_4$ receptors mediate PGE2 release by tissue-resident macrophages and initiate inflammatory pain. *EMBO Journal*, **29** (14), pp. 2290-2300.

Unsworth, C.D. & Johnson, R.G. (1990). Acetylcholine and ATP are coreleased from the electromotor nerve terminals of *Narcine brasiliensis* by an exocytotic mechanism. *Proceedings of the National Academy of Sciences USA*, **87** (2), pp. 553-557.

Urano, T., Nishimori, H., Han, H. *et al.* (1997). Cloning of P2XM, a novel human P2X receptor gene regulated by p53. *Cancer Research*, **57** (15), pp. 3281-3287.

Uysal, S., Vasquez, V., Tereshko, V. *et al.* (2009). Crystal structure of full-length KcsA in its closed conformation. *Proceedings of the National Academy of Sciences USA*, **106** (16), pp. 6644-6649.

Vacca, F., D'ambrosi, N., Nestola, V. *et al.* (2011). N-Glycans mutations rule oligomeric assembly and functional expression of $P2X_3$ receptor for extracellular ATP. *Glycobiology*, **21** (5), pp. 634-643.

Valente, M., Watterson, S.J., Parker, M.D. *et al.* (2011). Expression, purification, electron microscopy, N-glycosylation mutagenesis and molecular modeling of human P2X4 and Dictyostelium discoideum P2XA. *Biochimica et Biophysica Acta*, **1808** (12), pp. 2859-2866.

Valenzuela, J.G., Charlab, R., Galperin, M.Y. & Ribeiro, J.M. (1998). Purification, cloning, and expression of an apyrase from the bed bug *Cimex lectularius*. A new type of nucleotide-binding enzyme. *Journal of Biological Chemistry*, **273** (46), pp. 30583-30590.

Valera, S., Hussy, N., Evans, R.J. *et al.* (1994). A new class of ligand-gated ion channel defined by P2x receptor for extracellular ATP. *Nature*, **371** (6497), pp. 516-519.

Van Dongen, P.A., Hökfelt, T., Grillner, S. *et al.* (1985). Immunohistochemical demonstration of some putative neurotransmitters in the lamprey spinal cord and spinal ganglia: 5-hydroxytryptamine-, tachykinin-, and neuropeptide-Y-immunoreactive neurons and fibers. *Journal of Comparative Neurology*, **234** (4), pp. 501-522.

Van Leeuwenhoek, A. (1702). Part of a letter from Mr Antony van Leeuwenhoek, FRS concerning green weeds growing in water, and some animalcula found about them. *Philosophical Transactions of the Royal Society*, **23** 1304-1311.

Vartian, N. & Boehm, S. (2001). P2Y receptor-mediated inhibition of voltage-activated Ca^{2+} currents in PC12 cells. *European Journal of Neuroscience*, **13** (5), pp. 899-908.

Vial, C. & Evans, R.J. (2005). Disruption of lipid rafts inhibits $P2X_1$ receptor-mediated currents and arterial vasoconstriction. *Journal of Biological Chemistry*, **280** (35), pp. 30705-30711.

Vial, C., Tobin, A.B. & Evans, R.J. (2004). G-protein-coupled receptor regulation of P2X1 receptors does not involve direct channel phosphorylation. *Biochemical Journal*, **382** (1), pp. 101-110.

Vieira, J. & Messing, J. (1982). The pUC plasmids, an M13mp7-derived system for insertion mutagenesis and sequencing with synthetic universal primers. *Gene*, **19** (3), pp. 259-268.

Vinson, J.P., Jaffe, D.B., O'neill, K. *et al.* (2005). Assembly of polymorphic genomes: algorithms and application to *Ciona savignyi*. *Genome Research*, **15** (8), pp. 1127-1135.

Virginio, C., Church, D., North, R.A. & Suprenant, A. (1997). Effects of divalent cations, protons and calmidazolium at the rat $P2X_7$ receptor. *Neuropharmacology*, **36** (9), pp. 1285-1294.

Virginio, C., North, R.A. & Suprenant, A. (1998a). Calcium permeability and block at homomeric and heteromeric $P2X_2$ and $P2X_3$ receptors, and P2X receptors in rat nodose neurones. *Journal of Physiology*, **510** (1), pp. 27-35.

Virginio, C., Robertson, G., Suprenant, A. & North, R.A. (1998b). Trinitrophenyl-substituted nucleotides are potent antagonists selective for $P2X_1$, $P2X_3$, and heteromeric $P2X_{2/3}$. *Molecular Pharmacology*, **53** (6), pp. 969-973.

Vlaskovska, M., Kasakov, L., Rong, W. *et al.* (2001). $P2X_3$ knock-out mice reveal a major sensory role for urothelially release ATP. *Journal of Neuroscience*, **21** (15), pp. 5670-5677.

Von Heijne, G. (1986). The distribution of positively charged residues in bacterial inner membrane proteins correlates with the trans-membrane topology. *EMBO Journal*, **5** (11), pp. 3021-3027.

Von Kügelgen, I., Allgaier, C., Schobert, A. & Starke, K. (1994). Co-release of noradrenaline and ATP from cultured sympathetic neurons. *Neuroscience*, **61** (2), pp. 199-202.

Wada, H. & Satoh, N. (1994). Details of the evolutionary history from invertebrates to vertebrates, as deduced from the sequences of 18S rDNA. *Proceedings of the National Academy of Sciences USA*, **91** (5), pp. 1801-1804.

Wainright, P.O., Hinkle, G., Sogin, M.L. & Stickel, S.K. (1993). Monophyletic origins of the metazoa: an evolutionary link with fungi. *Science*, **260** (5106), pp. 340-342.

Walker, J.E., Saraste, E., Runswork, M.J. & Gay, N.J. (1982). Distantly related sequences in the alpha- and beta-subunits of ATP synthase, myosin, kinases and other ATP requiring enzymes. *The EMBO Journal*, **1** (8), pp. 945-951.

Wang, L., Wang, S., Li, Y. *et al.* (2007). BeetleBase: the model organism database for *Tribolium castaneum*. *Nucleic Acids Research*, **35** (Database issue), pp. D476-479.

Waters, E., Hohn, M.J., Ahel, I. *et al.* (2003). The genome of *Nanoarchaeum equitans*: insights into early archaeal evolution and derived parasitism. *Proceedings of the National Academy of Sciences USA*, **100** (22), pp. 12984-12988.

Watson, G.M. & Hessinger, D.A. (1994). Evidence for calcium channels involved in regulating nematocyst discharge. *Comparative Biochemistry and Physiology: Comparative Physiology*, **107** (3), pp. 473-481.

Watson, G.M., Venable, S., Hudson, R.R. & Repass, J.J. (1999). ATP enhances repair of hair bundles in sea anemones. *Hearing Research*, **136** (1-2), pp. 1-12.

Webb, T.E., Simon, J., Krishek, B.J. *et al.* (1993). Cloning and functional expression of a brain G-protein-coupled ATP receptor. *FEBS Letters*, **324** (2), pp. 219-225.

Weber, A.K. & Pirow, R. (2009). Physiological responses of *Daphnia pulex* to acid stress. *BMC Physiology*, **9** 9.

Weber, J. (1989). Nematocysts (stinging capsules of Cnidaria) as Donnan-potential-dominated osmotic systems. *European Journal of Biochemistry*, **184** (2), pp. 465-476.

Weber, J. (1990). Poly(ϒ-glutamic acid)s are the major constituents of nematocysts in *Hydra* (*Hydroxoa*, *Cnidaria*). *Journal of Biological Chemistry*, **265** (17), pp. 9664-9669.

Weber, J. (1995). Novel tools for the study of development, migration and turnover of nematocytes (cnidarian stinging cells). *Journal of Cell Science*, **108** (1), pp. 403-412.

Weislogel, J.-M. 2008. *Visualisation of nuclear calcium signals using rekombinant calcium indicators in in vivo systems.* Dr. rer. nat, Universität Heidelberg, Germany.

Weiss, L.C., Kruppert, S., Laforsch, C. & Tollrian, R. (2012). Chaoborus and gasterosteus anti-predator responses in *Daphnia pulex* are mediated by independent cholinergic and gabaergic neuronal signals. *PLoS One*, **7** (5), pp. e36879.

Whittaker, V.P., Dowdall, M.J. & Boyne, A.F. (1972). The storage and release of acetylcholine by cholinergic nerve terminals: recent results with non-mammalian preparations. *Biochem Soc Symp*, (36), pp. 49-68.

Wildman, S.S., Brown, S.G., Rahman, M. *et al.* (2002). Sensitization by extracellular Ca^{2+} of rat $P2X_5$ receptor and its pharmacological properties compared with rat $P2X_1$. *Molecular Pharmacology*, **62** (4), pp. 957-966.

Wildman, S.S., King, B.F. & Burnstock, G. (1999a). Modulation of ATP-responses at recombinant $rP2X_4$ receptors by extracellular pH and zinc. *British Journal of Pharmacology*, **126** (3), pp. 762-768.

Wildman, S.S., King, B.F. & Burnstock, G. (1999b). Modulatory activity of extracellular H^+ and Zn^{2+} on ATP-responses at $rP2X_1$ and $rP2X_3$ receptors. *British Journal of Pharmacology*, **128** (2), pp. 486-492.

Wilkinson, W.J., Gadeberg, H.C., Harrison, A.W. *et al.* (2009). Carbon monoxide is a rapid modulator of recombinant and native $P2X_2$ ligand-gated ion channels. *British Journal of Pharmacology*, **158** (3), pp. 862-871.

Wilkinson, W.J., Jiang, L.H., Suprenant, A. & North, R.A. (2006). Role of ectodomain lysines in the subunits of the heteromeric $P2X_{2/3}$ receptor. *Molecular Pharmacology*, **70** (4), pp. 1159-1163.

Wilkinson, W.J. & Kemp, P.J. (2011). The carbon monoxide donor, CORM-2, is an antagonist of ATP-gated, human P2X4 receptors. *Purinergic Signaling*, **7** (1), pp. 57-64.

Wilson, H.L., Wilson, S.A., Suprenant, A. & North, R.A. (2002). Epithelial membrane proteins induce membrane blebbing and interact with the $P2X_7$ receptor C terminus. *Journal of Biological Chemistry*, **277** (37), pp. 34017-34023.

Wilson, J.E. & Chin, A. (1991a). Chelation of divalent cations by ATP, studied by titration calorimetry. *Analytical Biochemistry*, **193** (1), pp. 16-19.

Wilson, J.E. & Chin, A. (1991b). Chelation of divalent cations by ATP, studied by titration calorimetry. *Analytical Biochemistry*, **193** (1), pp. 16-19.

Wirkner, K., Köles, L., Thümmler, S. *et al.* (2002). Interaction between P2Y and NMDA receptors in layer V pyramidal neurons of the rat prefrontal cortex. *Neuropharmacology*, **42** (4), pp. 476-488.

Wirkner, K., Stanchev, D., Milius, D. *et al.* (2008). Regulation of the pH sensitivity of human $P2X_3$ receptors N-linked glycosylation. *Journal of Neurochemistry*, **107** (5), pp. 1216-1224.

Wittlieb, J., Khalturin, K., Lohmann, J.U. *et al.* (2006). Transgenic Hydra allow *in vivo* tracking of individual stem cells during morphogenesis. *Proceedings of the National Academy of Sciences USA*, **103** (16), pp. 6208–6211.

Wodniok, S., Brinkmann, H., Glockner, G. *et al.* (2011). Origin of land plants: do conjugating green algae hold the key? *BMC Evolutionary Biology*, **11** 104.

Worthington, R.A., Dutton, J.L., Poronnik, P. *et al.* (1999). Localisation of P_{2X} receptors in human salivary gland epithelial cells and human embryonic kidney cells by sodium dodecyl sulfate-polyacrylamide gel electrophoresis/Western blotting and immunofluorescence. *Electrophoresis*, **20** (10), pp. 2065-2070.

Wu, J., Steinebrunner, I., Sun, Y. *et al.* (2007). Apyrases (nucleoside triphosphate-diphosphohydrolases) play a key role in growth control in Arabidopsis. *Plant Physiology*, **144** (2), pp. 961-975.

Yamamoto, K., Sokabe, T., Matsumoto, T. *et al.* (2006). Impaired flow-dependent control of vascular tone and remodeling in $P2X_4$-deficient mice. *Nature Medicine*, **12** (1), pp. 133-137.

Yan, Z., Khadra, A., Sherman, A. & Stojilkovic, S.S. (2011). Calcium-dependent block of $P2X_7$ receptor channel function is allosteric. *Journal of General Physiology*, **138** (4), pp. 437-452.

Yegutkin, G., Bodin, P. & Burnstock, G. (2000). Effect of shear stress on the release of soluble ecto-enzymes ATPase and 5'-nucleotidase along with endogenous ATP from vascular endothelial cells. *British Journal of Pharmacology*, **129** (5), pp. 921-926.

Yegutkin, G.G. (2008). Nucleotide- and nucleoside-converting ectoenzymes: Important modulators of purinergic signalling cascade. *Biochimica et Biophysica Acta*, **1783** (5), pp. 673-694.

Yoshida, K., Fujisawa, T., Hwang, J.S. *et al.* (2006). Degeneration after sexual differentiation in hydra and its relevance to the evolution of aging. *Gene*, **385** 64-70.

Young, M.T. (2010). P2X receptors: dawn of the post-structure era. *Trends in Biochemical Science*, **35** (2), pp. 83-90.

Young, M.T., Pelegrin, P. & Surprenant, A. (2007). Amino acid residues in the $P2X_7$ receptor that mediate differential sensitivity to ATP and BzATP. *Molecular Pharmacology*, **71** (1), pp. 92-100.

Younus, F., Chertemps, T., Pearce, S.L. *et al.* (2014). Identification of candidate odorant degrading gene/enzyme systems in the antennal transcriptome of *Drosophila melanogaster*. *Insect Biochemistry and Molecular Biology*, **53c** 30-43.

Yu, J.K., Satou, Y., Holland, N.D. *et al.* (2007). Axial patterning in cephalochordates and the evolution of the organizer. *Nature*, **445** (7128), pp. 613-617.

Zeis, B., Becher, B., Goldmann, T. *et al.* (2003). Differential haemoglobin gene expression in the crustacean *Daphnia magna* exposed to differential oxygen patrial pressures. *Biological Chemistry*, **384** (8), pp. 1133-1145.

Zeis, B., Becker, D., Gerke, P. *et al.* (2013). Hypoxia-inducible haemoglobins of *Daphnia pulex* and their role in the response to acute and chronic temperature increase. *Biochimica et Biophysica Acta*, **1834** (9), pp. 1704-1710.

Zeis, B., Lamkemeyer, T., Paul, R.J. *et al.* (2009). Acclimatory response of the *Daphnia pulex* proteome to environmental changes. I. Chronic exposure to hypoxia affects the oxygen transport system and carbohydrate metabolism. *BMC Physiology*, **9** 7.

Zemkova, H., He, M.L., Koshimizu, T.A. & Stojilkovic, S.S. (2004). Identification of ectodomain regions contributing to gating, deactivation, and resensitization of purinergic P2X receptors. *Journal of Neuroscience*, **24** (31), pp. 6968-6978.

Zhang, G., Fang, X., Guo, X. *et al.* (2012). The oyster genome reveals stress adaptation and complexity of shell formaiton. *Nature*, **490** (7418), pp. 49-54.

Zheng, H., Zhang, W., Zhang, L. *et al.* (2013). The genome of the hydatid tapeworm *Echinococcus granulosus*. *Nature Genetics*, **45** (10), pp. 1168-1175.

Zhong, B., Xi, Z., Goremykin, V.V. *et al.* (2014). Streptophyte algae and the origin of land plants revisited using heterogeneous models with three new algal chloroplast genomes. *Molecular Biology and Evolution*, **31** (1), pp. 177-183.

Zhong, Y., Dunn, P.M., Bardini, M. *et al.* (2001). Changes in P2X receptor responses of sensory neurons from $P2X_3$-deficient mice. . *European Journal of Neuroscience*, **14** (11), pp. 1784-1792.

Zhou, Z., Monsma, L.R. & Hume, R.I. (1998). Identifcation of a site that modifies desensitization of $P2X_2$ receptors. *Biochemical and Biophysical Research Communications*, **252** (3), pp. 541-545.

Zimmer-Faust, R.K., Gleeson, R.A. & Carr, W.E.S. (1988). The behavioral response of spiny lobsters to ATP: Evidence for mediation by P_2-like chemosensory receptors. *Biological Bulletins*, **175** (1), pp. 167-174.

Zimmerman, A.M., Landau, J.V. & Marsland, D. (1958). The effects of adenosine triphosphate and dinitro-o-cresol upon the form and movement of amoeba proteus: a pressure-temperature study. *Experimental Cell Research*, **15** (3), pp. 484-495.

8 Appendix

In this Appendix, primer sequences and combinations used to amplify P2X receptor gene or transcript sequences are provided.

Table A1: list of species and associated genomic or transcriptomic database within which homology searches were performed

Species	Phylum/Class*/Division †	Database/sequence origin	Site
Branchiostoma floridae	Chordata	NCBI	http://blast.ncbi.nlm.nih.gov/Blast.cgi
Ciona intestinalis	Chordata	NCBI	
Saccoglossus kowalevskii	Hemichordata	NCBI	
Strongylocentrotus purpuratus	Echniodermata	NCBI	http://blast.ncbi.nlm.nih.gov/Blast.cgi
Hypsibius dujardini	Tardigrada	Prof. Mark Blaxter Research Group	http://badger.bio.ed.ac.uk/H_dujardini/
Daphnia pulex	Crustacea	wFleaBase	http://wfleabase.org/blast/
Drosophila melanogaster	Arthropoda	FlyBase	http://flybase.org/blast/
Ixodes scapularis	Arthropoda	VectorBase	https://www.vectorbase.org/blast
Diabrotica virgifera	Insecta*	NCBI	http://blast.ncbi.nlm.nih.gov/Blast.cgi
Folsomia candida	Insecta*	NCBI	
Orchesella cincta	Insecta*	NCBI	
Acanthascurria geniculata	Insecta*	NCBI	
Steodyphus mimosrosum	Insecta*	NCBI	
Lactrodectrus hesperus	Insecta*	NCBI	
Glomeris pustulata	Insecta*	NCBI	
Strigamia maritima	Insecta*	NCBI	
Caenorhabditis elegans	Nematoda*	WormBase	http://www.wormbase.org/tools/blast_blat
Xiphinema index	Nematoda*	Nematode.net NEMBASE4	http://nematode.net/NN3_frontpage.cgi http://xyala.cap.ed.ac.uk/services/blastserver/

Schistosoma mansoni	Trematoda*	Wellcome Trust Sanger Institute	http://www.sanger.ac.uk/cgi-bin/blast/submitblast/s_mansoni
Echinococcus multilocularis	Cestoda*	Wellcome Trust Sanger Institute	http://www.sanger.ac.uk/cgi-bin/blast/submitblast/Echinococcus
Echinococcus granulosus	Cestoda*	Wellcome Trust Sanger Institute	http://www.sanger.ac.uk/cgi-bin/blast/submitblast/Echinococcus
Taenia solium	Cestoda*	GeneDB	http://www.genedb.org/blast/submitblast/GeneDB_Tsolium
Capitella teleta	Annelida	JGI	http://genome.jgi-psf.org/pages/blast.jsf?db=Capca1
Helobdella robusta	Annelida	JGI	http://genome.jgi.doe.gov/pages/blast.jsf?db=Helro1
Biomphalaria glabrata	Mollusca	VectorBase	https://www.vectorbase.org/blastd
Crassostrea gigas	Mollusca	OysterDB	http://oysterdb.cn/blast.html
Lottia gigantea	Mollusca	JGI	http://genome.jgi.doe.gov/pages/blast.jsf?db=Lotgi1
Acropora digitifera	Cnidaria	Compagen	http://www.compagen.org/blast.html
Hydra magnipapillata (105)	Cnidaria	NCBI	http://blast.ncbi.nlm.nih.gov/Blast.cgi
Hydra vulgaris (AEP)	Cnidaria	Compagen	http://www.compagen.org/blast.html
Nematostella vectensis	Cnidaria	Compagen	
Mnemiopsis leidyi	Ctenophora	NCBI *M. leidyi* portal	http://research.nhgri.nih.gov/mnemiopsis/blast/
Pleurobachia bachei	Ctenophora	NeuroBase	http://moroz.hpc.ufl.edu/slimebase2/blast.php?view=blast
Ephydatia muelleri	Porifera	Compagen	http://www.compagen.org/blast.html
Oscarella carmela	Porifera	Compagen	
Amphimedon queenslandica	Porifera	NCBI	http://blast.ncbi.nlm.nih.gov/Blast.cgi
Trichoplax adhaerens (Grell)	Placazoa	NCBI	
Monosiga brevicollis	Choanoflagellatea*	JGI	http://genome.jgi-psf.org/pages/blast.jsf?db=Monbr1
Salpingoeca rosetta	Choanoflagellatea*	Broad Institute	http://www.broadinstitute.org/annotation/genome/multicellularity_project/Blast.html?sp=Stblastn

Capsaspora owczarzaki ATCC 30864	Filasterea*	NCBI Broad Institute	http://blast.ncbi.nlm.nih.gov/Blast.cgi http://www.broadinstitute.org/annotation/genome/multicellularity_project/Blast.html?sp=Stblastn
Sphaeroforma artica JP617	Mesomycetozoea†	Broad Institute	http://www.broadinstitute.org/annotation/genome/multicellularity_project/Blast.html?sp=Stblastn
Schizosacchaeomyces pombe	Ascomycota†	PomBase	http://genomebrowser.pombase.org/Multi/blastview
Neurospora crassa	Ascomycota†	Broad Institute	http://www.broadinstitute.org/annotation/genome/neurospora/Blast.html
Saccharomyces cerevisae	Ascomycota†	Saccharomyces Genome Database	http://www.yeastgenome.org/cgi-bin/blast-sgd.pl
Allomyces macrogynus ATCC 38327	Blastocladiomycota†	Broad Institute	http://www.broadinstitute.org/annotation/genome/multicellularity_project/Blast.html?sp=Stblastn
Batrachochytrium dendrobatidis	Chytridiomiomycota†	JGI	http://genome.jgi.doe.gov/pages/blast.jsf?db=Batde5
Spizellomyces punctatus DAOM BR117	Chytridiomiomycota†	Broad Institute	http://www.broadinstitute.org/annotation/genome/multicellularity_project/Blast.html?sp=Stblastn
Rhizophagus irregularis	Glomeromycota†	JGI	http://genome.jgi.doe.gov/pages/blast.jsf?db=Gloin1
Conidiobolus coronatus NRRL28638	Entomophthoromycota†	JGI	http://genome.jgi.doe.gov/Conco1/Conco1.home.html
Schizochytium aggregatum	Myxomyctota†	JGI	http://genome.jgi.doe.gov/pages/blast.jsf?db=Schag1
Thecamonas trahans ATCC 50062	Protozoa	Broad Institute	http://www.broadinstitute.org/annotation/genome/multicellularity_project/Blast.html?sp=Stblastn
Dictyostelium discoideum	(Amoeba)	dictyBase	http://dictybase.org/tools/blast
Polysphondylium pallidum	(Amoeba)	dictyBase	
Entamoeba histolytica	(Amoeba)	JCVI	http://blast.jcvi.org/er-blast/index.cgi?project=eha1

Acanthamoeba castellanii	(Amoeba)	NCBI	http://blast.ncbi.nlm.nih.gov/Blast.cgi
Physcomitrella patens	Bryophyta†	Phytozome 9.1	http://www.phytozome.net/search.php?show=blast
Arabidopsis thaliana	Magnoliophyta†	Phytozome 9.1	
Sorghum bicolor	Magnoliophyta†	Phytozome 9.1	
Solanum lycopersicum	Magnoliophyta†	Phytozome 9.1	
Glycine max	Magnoliophyta†	Phytozome 9.1	
Oryza sativa	Magnoliophyta†	Phytozome 9.1	
Chlamydomonas reinhardtii	Chlorophyta†	Phytozome 9.1	
Volox carteri	Chlorophyta†	Phytozome 9.1	
Ostreococcus tauri	Chlorophyta†	Phytozome 9.1	
Micromonas pusilla RCC299	Chlorophyta†	Phytozome 9.1	
Nitella hyalina	Charophyta	NCBI	http://blast.ncbi.nlm.nih.gov/Blast.cgi
Aplanochytrium kerguelense PBS07	Heterokonta	JGI	http://genome.jgi.doe.gov/pages/blast.jsf?db=Aplke1
Toxoplasma gondii	Apicomplexa	ToxoDB	http://toxodb.org/toxo/
Plasmodium falciparum	Apicomplexa	GeneDB	http://www.genedb.org/blast/submitblast/GeneDB_Pfalciparum
Paramecium tetraurelia	Ciliophora	ParameciumDB	http://paramecium.cgm.cnrs-gif.fr/cgi/tool/blast
Bigelowiella natans	Cercozoa	JGI	http://genome.jgi.doe.gov/pages/blast.jsf?db=Bigna1
Emiliania huxleyi	Haptophyta†	JGI	http://genome.jgi.doe.gov/pages/blast.jsf?db=Emihu1
Guillardia theta	Cryptophyta†	JGI	http://genome.jgi.doe.gov/pages/blast.jsf?db=Guith1
Mycobacterium tuberculosis	Actinobacteria	TB Genome Database	http://genome.tbdb.org/annotation/genome/tbdb/Blast.html
Chlamydia trachomatis	Chlamydiae	Wellcome Trust Sanger Institute	http://www.sanger.ac.uk/cgi-bin/blast/submitblast/c_trachomatis
Cyanobacteria bacterium	Cyanobacteria	NCBI Microbial BLAST	http://blast.ncbi.nlm.nih.gov/Blast.cgi?PAGE_TYPE=BlastSearch&BLAST_SPEC=MicrobialGenomes

Clostridium difficile	Firmicutes	Wellcome Trust Sanger Institute	http://www.sanger.ac.uk/cgi-bin/blast/submitblast/c_difficile
Staphylococcus aureus	Firmicutes	Wellcome Trust Sanger Institute	http://www.sanger.ac.uk/cgi-bin/blast/submitblast/s_aureus
Agrobacterium tumefaciens	Proteobacteria	NCBI Microbial BLAST	http://blast.ncbi.nlm.nih.gov/Blast.cgi?PAGE_TYPE=BlastSearch&BLAST_SPEC=MicrobialGenomes
Escherichia coli	Proteobacteria	NCBI Microbial BLAST	
Vibrio cholerae	Proteobacteria	NCBI Microbial BLAST	
Borrelia burgdorferi	Spirochaetes	NCBI Microbial BLAST	
Thermosphaera aggregans	Crenarchaeota	UCSC Archaeal BLAST	http://archaea.ucsc.edu/cgi-bin/hgBlat
Acidilobus saccharovorans	Crenarchaeota	UCSC Archaeal BLAST	
Haloferax volcanii	Euryarchaeota	UCSC Archaeal BLAST	
Korarchaeum cryptofilum	Korarchaeota	UCSC Archaeal BLAST	
Nanoarchaeum equitans	Nanoarchaeota	UCSC Archaeal BLAST	
Cenarchaeum symbosium	Crenarchaeota	UCSC Archaeal BLAST	

Table of species analysed, their respective phylum, Class or order, and the database within which BLAST searches were performed. BLAST searchers were performed as detailed in section 2.2.1.

Table A2: list of retrieved hits identified through homology searching of eukaryotic species

Species	Dataset	Database	Homology search	Score (bits)	Score (raw)	*E*-value	Aln. Length	% identity	Accession/file number
Branchiostoma floridae	Genomic	NCBI	tBLASTn	339	870	9.00E-113	986	51	XM_002605779.1
Ciona intestinalis	Genomic	NCBI	tBLASTn	No significant hits found					
Saccoglossus kowalevskii	Genomic	NCBI	tBLASTn	357	915	4.00E-118	1115	53	NM_001168169.1
				241	614	2.00E-74	824	45	XM_006821836.1
				127	319	4.00E-33	623	33	XM_006821835.1
Strongylocentrotus purpuratus	Genomic	NCBI	tBLASTn	337	863	2.00E-102	1085	49	XM_003727933.1
				324	831	3.00E-98	1067	48	XM_791095.3
				288	736	1.00E-85	986	49	XM_787091.3
Hypsibius dujardini	Transcripts	http://badger.bio.ed.ac.uk/H_dujardini/	tBLASTn	315		3.00E-86			nHd.2.3.1.t18877-RA
				274		7.00E-74			nHd.2.3.1.t02485-RA
				262		2.00E-70			nHd.2.3.1.t08016-RA
				259		2.00E-69			nHd.2.3.1.t06477-RA
				252		2.00E-67			nHd.2.3.1.t19135-RA
				208		4.00E-54			nHd.2.3.1.t16209-RA
				150		8.00E-			nHd.2.3.1.t19881-RA

				150		37 1.00E-36			nHd.2.3.1.t16757-RA
				120		1.00E-27			nHd.2.3.1.t09286-RA
				105		5.00E-23			nHd.2.3.1.t14869-RA
				99		4.00E-21			nHd.2.3.1.t20603-RA
				96.3		2.00E-20			nHd.2.3.1.t20213-RA
				73.9		1.00E-13			nHd.2.3.1.t20759-RA
Daphnia pulex	Genomic	Wfleabase	tBLASTn	311	797	9.00E-85	1052	44	hxNCBI_GNO_488034
				297	761	1.00E-80	1058	42	hxNCBI_GNO_490034
Drosophila melanogaster	Genomic	FlyBase	tBLASTn	No hits found					
Diabrotica virgifera	EST (*Diabrotica virgifera* TaxID: 50389)	NCBI	tBLASTn	254	650	5.00E-83	461	90	EW761455.1
				135	339	1.00E-38	272	90	EW764374.1
Folsomia candida	Genomic (WGS)	NCBI	tBLASTn	301	771	8.00E-96	1220	40	GAMN01013759.1
				209	531	2.00E+61	848	37	GAMN01009400.1
				137	344	1.00E+35	839	30	GAMN01006783.1
				92.4	228	6.00E-20	857	28	GAMN01017925.1
				61.6	148	1.00E-11	194	45	GAMN01035631.1

				55.8	133	2.00E-08	230	31	GAMN01027032.1
				51.2	121	3.00E-07	245	30	GAMN01020349.1
				44.3	103	2.00E-06	131	41	GAMN01037417.1
				25.4	54	2.00E-06	68	39	
				46.2	108	3.00E-06	140	40	GAMN01031064.1
				42.7	99	3.00E-04	230	31	GAMN01019781.1
Orchesella cincta	Genomic (WGS)	NCBI	tBLASTn	260	664	1.00E-80	1085	44	GAMM01009862.1
				259	663	4.00E-80	1076	41	GAMM01002634.1
				169	427	1.00E-48	509	51	GAMM01015375.1
				932	230	1.00E-22	353	47	GAMM01026646.1
				77.4	189	4.00E-17	251	42	GAMM01017640.1
				60.1	144	3.00E-10	557	27	GAMM01017921.1
				46.6	109	2.00E-06	197	33	GAMM01031912.1
Acanthoscurria geniculata	WGS (BioProject ID: PRJNA222762)	NCBI	tBLASTn	309	792	3.00E-99	1049	48	GAZS01036238.1
				291	744	1.00E-92	1046	44	GAZS01073490.1
				273	697	2.00E-85	977	45	GAZS01036234.1
				241	616	5.00E-74	809	45	GAZS01036235.1

				44.7	104	2.00E-04	95	63	
				151	382	6.00E-43	500	48	GAZS01011145.1
				106	265	2.00E-25	353	55	GAZS01036236.1
				103	257	2.00E-24	344	55	GAZS01036237.1
				96.7	239	8.00E-24	323	44	GAZS01005499.1
				80.5	197	9.00E-18	146	63	GAZS01058080.1
				67.4	163	6.00E-13	365	32	GAZS01084718.1
				63.5	153	6.00E-12	125	64	GAZS01021491.1
Stegodyphus mimorosum	WGS (BioProject ID: PRJNA222763)	NCBI	tBLASTn	155	391	3.00E-44	464	47	GAZR01003973.1
				130	326	1.00E-35	566	47	GAZR01001455.1
				68.2	165	2.00E-14	256	54	GAZR01026140.1
				34.7	78	5.00E-03	125	52	GAZR01015239.1
				30.8	68	2.00E-01	80	44	GAZR01013643.1
				26.2	56	7.50E+00	62	43	GAZR01006843.1
Lactrodectrus hesperus	Transcriptome Shotgun Assembly (TaxID: 256737)	NCBI	tBLASTn	319	817	2.00E-99	1061	48	GBCS01010125.1
				297	761	5.00E-93	1076	47	GBCS01001793.1
				138	34	1.00E-	420	46	GBCS01015860.1

					8	35			
Ixodes scapularis	Transcripts	VectorBase	tBLASTn	514		5.00E-62	641	46	ISCW011650-RA
				127		4.00E-08	137	48	ISCW019739-RA
				115		2.00E-07	122	115	ISCW019740-RA
Glomeris pustulata	WGS (Myriapoda TaxID 61985)	NCBI (Myriapoda)	tBLASTn	228	582	8.00E-72	833	48	GAKW01014925.1
				63.5	153	8.00E-72	149	52	
Strigamia maritima	WGS (Myriapoda TaxID 61985)	NCBI (Myriapoda)	tBLASTn	97.8	242	4.00E-28	368	42	AFFK01017152.1
				48.1	113	4.00E-28	152	46	
				112	279	3.00E-25	650	31	AFFK0108242.1
				47.8	112	4.00E-11	95	59	
				40.8	94	4.00E-11	504	35	
				57,4	137	2.00E-08	332	55	
				21.9	45	2.00E-08	146	50	
				44.7	104	7.00E-04	95	53	AFFK01017150.1
				35.4	80	4.30E-01	272	30	
				33.5	75	1.90E+00	74	56	
				35	79	6.10E-01	335	29	AFFK01017151.1
				34.7	78	6.10E-	350	27	AFFK01003302.1

						01			
				31.6	70	7.00E+00	101	35	AFFK01017116.1
				31.6	70	7.30E+00	122	36	AFFK01017135.1
				31.6	70	7.50E+00	122	36	AFFK01019140.1
				31.6	70	7.50E+00	155	27	AFFK01022209.1
Caenorhabditis elegans	Genomic	WormBase	tBLASTn	No hits found					
Xiphinema index	Genomic	Nematode.net	tBLASTn	197.3	546	6.60E-54	662	47	X103839
		NEMBASE4	tBLASTn	213	542	2.00E-68	662	47	XC01614
Schistosoma mansoni	Genome assembly (v3.0)	Wellcome Trust Sanger Institute	tBLASTn	286.7	800	2.00E-79	1046	44	contig_0032200
				240.2	668	5.00E-64	926	41	contig_0032232
				131.8	360	3.00E-32	389	52	contig_0045550
				62.4	163	2.00E-19	230	40	contig_0034163
Echinococcus multilocularis	Genes	Wellcome Trust Sanger Institute	tBLASTn	264.8	738	9.70E-74	1043	43	EmuJ_000839300.1
				243.4	677	2.70E-67	1053	41	EmuJ_000977600.1
				105.4	285	6.10E-41	503	35	EmuJ_000815100.1
Echninococcus granulosus	Genome assembly (version 4)	Wellcome Trust Sanger Institute	tBLASTn	259.6	723	3.6E-72	1043	42	EgrG_000839300.1
				239.9	667	2.9E-66	1053	40	EgrG_000977600.1
				100.8	27	1.7E-36	551	34	EgrG_000815100.1

					2				
Taenia solium	Taenia solium Genes	GeneDB	tBLASTn	266.3	742	3.00E-74	1043	43	TsM_000577800.1
				113.5	308	5.00E-53	548	35	TsM_001187100.1
				157.5	433	3.00E-41	839	35	TsM_000842900.1
				56.1	145	1.00E-09	155	56	TsM_000842800.1
Hymenolepsis microstoma	Genome assembly	Wellcome Trust Sanger Institute	tBLASTn	270	753	2E-74	1043	43	5623
				109.6	297	3E-40	590	33	1610
				67.9	150	2E-22	173	49	9345
				54.7	141	5E-20	176	48	607
Capitella teleta	FilteredModelsv1 (transcripts)	JGI	tBLASTn		951	7.68E-101			jgi|Capca1|169132|estExt_Genewise1Plus.C_150044
Helobdella robusta	FilteredModelsv1 (transcripts)	JGI	tBLASTn	No hits found					
Biomphalaria glabrata	Predicted transcripts (BglaB1.1 geneset)	VectorBase	tBLASTn		306	4.00E-32	470	42	BGLTMP010712-RA
Lymnaea stagnalis									K7QP77
Lottia gigantea	Lotgi1_GeneModels_FilteredModels1_nt (predicted transcripts)	JGI	tBLASTn		949	6.00E-92	7993		jgi|Lotgi1|207736|estExt_fgenesh2_pm.C_sca_1440001
Aplysia californica	WGS	NCBI	tBLASTn	331	849	3.00E-107	1079	48	GBBG010314371.1
				301	770	7.00E-93	1028	46	GBBE01034858.1
				269	688	4.00E-83	1640	46	GBDA01144355.1
				259	66	2.00E-	947	46	GBBV01026431.1

					3	80			
				259	66	2.00E-80	947	45	GBDA01144354.1
				260	66	1.00E-78	851	45	GBAV01062255.1
				251	64	2.00E-77	839	47	GBBV01026432.1
				241	61	1.00E-73	818	46	GBCZ01039000.1
				231	58	6.00E-70	818	445	GBCZ01039002.1
				199	50	2.00E-57	737	45	GBCZ01038999.1
				194	49	8.00E-57	683	45	GBBW01055433.1
				177	45	2.00E-50	666	45	GBBW01055434.1
				151	38	1.00E-38	413	53	GBBW01054297.1
				99.4	24	3.00E-33	278	54	GBAQ01007159.1
				68.2	16	3.00E-33	227	44	
				122	30	2.00E-30	497	41	GBAV01062256.1
				124	31	6.00E-28	338	53	GBCZ01038996.1
				124	31	2.00E-28	338	53	GBCZ01038994.1
				106	26	2.00E-25	305	53	GBAQ01008309.1
				85.9	21	7.00E-18	242	54	GBAV01103187.1
				87.8	21	8.00E-	233	56	GBBV01026430.1

					6	17			
				87.8	216	2.00E-16	233	56	GBDA01144353.1
				76.6	187	6.00E-15	146	65	GBBG01031439.1
				74.3	181	9.00E-14	344	37	GBAQ01079740.1
				61.6	148	3.00E-08	122	10	GBBG01031438.1
				61.2	147	1.00E-07	194	46	AASC03103758.1
				55.8	133	4.00E-06	152	45	
				48.9	115	7.00E-06	152	47	
				39.7	91	6.00E-01	209	43	
				55.5	132	7.00E-06	104	74	AASC03103759.1
				37.4	85	2.50E+00	161	57	
				36.2	82	5.90E+00	89	50	
Bithynia siamensis goniomophalos	WGS	NCBI	tBLASTn	315	806	4.00E-100	1073	46	GAGS01034857.1
				303	777	1.00E-95	1276	46	GAGS01034858.1
				258	659	9.00E-79	980	46	GAGS01035856.1
				156	395	4.00E-41	878	38	GAGS01035853.1
				55.5	132	3.00E-06	392	29	
				152	38	7.00E-	539	45	GAGS01034854.1

					5	41			
				121	304	3.00E-37	476	44	GAGS01034852.1
				58.9	141	3.00E-37	401	34	
				55.5	132	3.00E-06	392	29	
				130	326	3.00E-32	479	44	GAGS01034855.1
				69.3	168	2.00E-11	134	60	GAGS01034859.1
				44.3	103	5.00E-03	86	55	
Pecten maximus	WGS	NCBI	tBLASTn	143	360	1.00E-37	566	49	GAOX01018975.1
				142	359	2.00E-37	329	56	GAOX01031495.1
Mytilus galloprovincialis	WGS	NCBI	tBLASTn	115	287	6.00E-27	485	43	GAEN01003082.1
				70.1	170	1.00E-10	185	52	ABJB012282896.1
				67.8	164	6.00E-10	185	56	ABJB011459086.1
				62	149	4.00E-08	134	53	ABJB011722331.1
				61.2	147	6.00E-08	134	53	ABJB011064243.1
				53.5	127	2.00E-05	95	72	ABJB010907617.1
				52.8	125	4.00E-05	167	72	ABJB011560648.1
Placopectan magellanicus	WGS	NCBI	tBLASTn	109	272	8.00E-26	488	49	GADG01023257.1
Elliptio complanata	WGS	NCBI	tBLASTn	94.4	23	7.00E-	368	38	GAHW01064436.1

					3	21			
Cassostrea gigas	EST	NCBI	tBLASTn	243	619	4.00E-74	914	44	CU990019.1
				229	584	2.00E-70	969	47	EW777773.1
				227	578	2.00E-68	980	42	CU991137.1
				48.9	115	6.00E-05	961	33	
				172	437	2.00E-49	578	49	HS125933.1
				173	438	2.00E-49	578	49	HS136997.1
				172	437	2.00E-49	578	49	HS138412.1
				156	394	5.00E-43	623	46	HS161381.1
				152	385	3.00E-42	530	49	HS131447.1
				125	313	9.00E-33	392	43	CB617507.1
				108	271	2.00E-30	365	52	HS143797.1
				45.8	107	2.00E-30	164	43	
				87.8	216	1.00E-18	218	56	HS138413.1
				75.5	184	3.00E-14	191	56	HS125934.1
				63.9	154	2.00E-10	155	60	HS131448.1
				48.9	115	3.00E-08	122	56	HS161382.1
				30.8	68	3.00E-	125	38	

						08			
				52.8	125	1.00E-06	134	56	HS136998.1
Acropora digitifera	ADIG_T-CDS_111201	Compagen	tBLASTn	193	491	2.00E-49	1079	40	adi_v1.00700
				134	336	2.00E-31	833	30	adi_v1.04925
Hydra magnipapillata	HMAG_T-CDS_051019 (transcriptomic)	Compagen	tBLASTn	312	800	5.00E-86	1085	44	CL1621Contig1; 1596 8 1307 minus strand
				179	453	8.00E-46	857	35	CL5264Contig1 983 168 1032
Hydra vulgaris (AEP)		Compagen	tBLASTn	315	806	2.00E-86	1085	45	HAEP_xT-CDS_v02_9144
Aurelia aurita		Compagen (Aurelia aurita sub-site)	tBLASTn	75.1	183	1.00E-14	227	49	FTZYOTV01DGAOA
				60.5	145	2.00E-10	167	53	F2X1FZH02GP10X
Nematostella vectensis	NVEC_G-PEP_111130	Compagen	BLASTp	337	864	5.00E-93	360	48	jgi|Nemve1|102596|e_gw.65.61.1
				321	822	4.00E-88	352	46	jgi|Nemve1|104653|e_gw.73.177.1
Mnemiopsis leidyi	Genomic	NCBI M. leidyi portal	tBLASTn	36.2	82	0.028	164	29	FC42886.1
				35.8	81	0.034	164	29	FC476889.1
				35.8	81	0.035	164	29	CF931441.1
				35.8	81	0.035	164	29	FC466250.1
				35.8	81	0.04	164	29	FC463003.1
Ephydatia muelleri	EMUE_T-CDS_130911	Compagen	tBLASTn	244	623	1.00E-64	1073	39	comp68168_c0_seq4
				229	585	3.00E-60	1052	38	comp68168_c0_seq2
				166	419	5.00E-41	1064	29	comp67432_c1_seq1

				44.7	104	2.00E-04	233	35	comp67794_c3_seq7
Oscarella carmela	OCAR_T-CDS_130911	Compagen	tBLASTn	315	807	5.00E-86	1034	45	comp8618_c0_seq2
Amphimedon queenslandica	Genomic	NCBI	tBLASTn	272	696	4.00E-86	1076	44	XM_003384088.1
Trichoplax adhaerens	Genomic	NCBI	tBLASTn	232 208	591 529	2.00E-72 2.00E-63	902 800	40 39	XM_002115738.1 XM_002113249.1
Monosiga brevicollis	Monbr1_all_transcripts	JGI	tBLASTn		603 603 603 342	6.50E-50 1.00E-49 1.00E-49 3.10E-28			jgi|Monbr1|23217|fgenesh2_pg.scaffold_3000573 jgi|Monbr1|31366|estExt_fgenesh2_pg.C_30571 jgi|Monbr1|36044|estExt_fgenesh1_pg.C_30574 jgi|Monbr1|6080|fgenesh1_pg.scaffold_3000578
Salpingoeca rosetta	Genomic Transcripts	NCBI Broad Institute	tBLASTn	267 267 44.7	683 683 104	1.00E-82 4.00E-71 6.00E-04	1106 1106 548	41 39 21	XM_004994942.1 PTSG_04102T0 PTSG_08528.1
Capsaspora owczarzaki	Genomic Transcripts	NCBI Broad Institute	tBLASTn tBLASTn	241 241	616 615	1.00E-74 3.00E-63	1118 1124	39 38	XM_004365091.1 CAOG_00277
Sphaeroforma artica	Transcripts	Broad Institute	tBLASTn	No hits found					
Schizosacchaeomyces pombe	Genomic	PomBase	tBLASTn	No hits found					
Neurospora crassa	Transcripts	Broad Institute	tBLASTn	No hits found					
Saccharomyces cerevisae	Genomic	Saccharomyces Genome Database	tBLASTn	No hits found					

Allomyces macrogynus	Transcripts	Broad Institute	tBLASTn	57.4 47.8	137 112	8.00E-08 6.00E-05	449 458	26 21	AMAG_19722.2 AMAG_07407.2
Batrachochytrium dendrobatidis	JAM81 v1.0 Batde5_best_transcripts	JGI	tBLASTn		147	4.70E-07	1577		jgi|Batde5|33275|estExt_fgenesh1_pm.C_70013
Spizellomyces punctatus	Transcripts	Broad Institute	tBLASTn	134	336	7.80E-31	1166	28	SPPG_00335T0
Rhizophagus irregularis	Gloin1_all_transcripts_20120510.nt	JGI	tBLASTn	156		5.20E-08	346		jgi|Gloin1|339541|fgenesh1_kg.6983_#_2_#_ACTTGA_L001_R1_(paired)_contig_1673
Thecamonas trahans	Transcripts	Broad Institute	tBLASTn	No hits found					
Polysphondylium pallidum	Coding sequences - DNA	DictyBase	tBLASTn	298 233 217	763 593 552	2.00E-81 1.00E-61 6.00E-57	869 998 1022	42 38 32	PPA1324200 PPA1415210 PPA1315488
Entamoeba histolytica	CDS (all contigs)	JCVI	tBLASTn	No significant hits					
Acanthamoeba castellanii	Genomic	GenBank	tBLASTn	193 178 54.7 53.1	491 452 130 126	1.00E-57 7.00E-52 2.00E-08 7.00E-08	1031 1004 812 903	41 38 23 24	XM_004335559.1 (ACA1_024220) XM_004337097.1 (ACA1_216340) XM_004333964.1 (ACA1_344690) XM_004341457.1 (ACA1_266760)
Nitella hyalina	EST (Plants TaxID: 3193)	NCBI	tBLASTn	108 89.7	269 221	4.00E-25 2.00E-18	371 353	42 43	HO528268.1 HO495113.1
Physcomitrella	Genomic	Phytozome	tBLASTn	No hits found					

patens									
Arabidopsis thaliana	Genomic	Phytozome	tBLASTn	No hits found					
Sorghum bicolor	Genomic	Phytozome	tBLASTn	No hits found					
Solanum lycopersicum	Genomic	Phytozome	tBLASTn	No hits found					
Glycine max	Genomic	Phytozome	tBLASTn	No hits found					
Oryza sativa	Genomic	Phytozome	tBLASTn	No hits found					
Chlamydomonas reinhardtii	Genomic	Phytozome	tBLASTn	No hits found					
Volox carteri	Genomic	Phytozome	tBLASTn	No hits found					
Ostreococcus tauri	BestModelsv2_trans	JGI	tBLASTn	 315 243	 	 5.70E-20 9.60E-15	 1163 1364	 	jgi|Ostta4|23918|estExt_fgenesh1_pg.C_Chr_07.00010144 jgi|Ostta4|33863|0700010216
Micromonas pusilla	Phytozome	Phytozome	tBLASTn	No hits found					
Nitella hyalina									
Aplanochytrium kerguelense	Aplke1_all_transcripts_20121220.nt	JGI	tBLASTn	399 399 399 365	 	8.00E-25 2.00E-24 2.00E-24 9.00E-22	 	 	jgi|Aplke1|100778|estExt_fgenesh1_pg.C_270194 jgi|Aplke1|49306|fgenesh1_kg.27_#_166_#_isotig02044 jgi|Aplke1|49305|fgenesh1_kg.27_#_165_#_isotig02043 jgi|Aplke1|59972|fgenesh1_pg.27_#_194
Toxoplasma gondii	Transcripts	ToxoDB	tBLASTn	No hits found					
Plasmodium falciparum	Plasmodium falciparum 3D7 genes	GeneDB	tBLASTn	46 45 42.2 41.9	126 123 115 114	1.70E-04 3.90E-04 2.00E-03 3.10E-03	626 800 221 686	21 21 32 20	PF3D7_0806500.1 PF3D7_1444100.1 PF3D7_0114300.1 PF3D7_0709400.1

Paramecium tetraurelia	Genomic (MAC assembly strain d4-2)	ParameciumDB	tBLASTn	No significant hits					
Bigelowiella natans	Bigna1_all_transcripts	JGI	tBLASTn	359 347 347 359 288 321		2.00E-25 7.00E-24 9.00E-24 2.00E-23 3.00E-22 2.00E-18			jgi|Bigna1|146037|aug1.107_g20745 jgi|Bigna1|74301|fgenesh1_pg.28_#_137 jgi|Bigna1|135214|aug1.28_g9922 jgi|Bigna1|91581|estExt_fgenesh1_pg.C_1070048 jgi|Bigna1|65381|fgenesh1_kg.107_#_30_#_5887_1_CFAO_EXTA jgi|Bigna1|83406|fgenesh1_pg.107_#_48
Symbiodinium sp.	WGS (Alveolata: 33630)	NCBI	tBLASTn	104	259	2.00E-22	938	26	GBGW01001110.1
Alexandrium tamarense	WGS (Alveolata: 33630)	NCBI	tBLASTn	104	259	2.00E-22	938	26	GAJB010022920.1
Lingilodinium polyedrum	WGS (Alveolata: 33630)	NCBI	tBLASTn	90.1	222	1.00E-17	935	25	GABP01033764.1
Pyrodinium bahamense	WGS (Alveolata: 33630)	NCBI	tBLASTn	78.6	192	1.00E-13	926	23	GAIO01008183.1
Euglena gracillis	EST (Euglenozoa: 33682)	NCBI	tBLASTn	40.4	93	1.00E-03	119	45	EC672030.1
Malawimonas jakobiformis	EST (Malawimonadozoa: 136087)	NCBI	tBLASTn	72	175	4.00E-15	479	33	EC723256.1
Schizochytrium aggregatum	Schag1_all_transcripts_20121220.nt	JGI JGI	tBLASTn tBLASTn	376 368		1.00E-22 4.00E-22			jgi|Schag1|101892|estExt_fgenesh1_pg.C_60087 jgi|Schag1|89608|fgenesh1_pg.6_#_87
Emiliania huxleyi	Best transcripts	JGI	tBLASTn	No hits found					
Guillardia theta	Filtered model	JGI	tBLASTn	No hits found					

	transcripts			
Mycobacterium tuberculosis	Transcripts	TB Genome Database	tBLASTn	No hits found
Chlamydia trachomatis	Jali assembled reads	Wellcome Trust Sanger Institute	tBLASTn	No hits found
Cyanobacteria bacterium	Genomic	NCBI Microbial BLAST	tBLASTn	No hits found
Clostridium difficile	Genomic assembly	Wellcome Trust Sanger Institute	tBLASTn	No hits found
Staphylococcus aureus	Genomic assembly	Wellcome Trust Sanger Institute	tBLASTn	No hits found
Agrobacterium tumefaciens	Genome	NCBI Microbial BLAST	tBLASTn	No hits found
Escherichia coli	Genome	NCBI Microbial BLAST	tBLASTn	No hits found
Vibrio cholerae	Genome	NCBI Microbial BLAST	tBLASTn	No hits found
Borrelia burgdorferi	Genome	NCBI Microbial BLAST	tBLASTn	No hits found
Thermosphaera aggregans	Genome	UCSC Archaeal BLAST	BLAT	No hits found
Acidilobus saccharovorans	Genome	UCSC Archaeal BLAST	BLAT	No hits found
Haloferax volcanii	Genome	UCSC Archaeal BLAST	BLAT	No hits found
Korarchaeum cryptofilum	Genome	UCSC Archaeal BLAST	BLAT	No hits found
Nanoarchaeum equitains	Genome	UCSC Archaeal BLAST	BLAT	No hits found
Cenarchaeum symbosium	Genome	UCSC Archaeal BLAST	BLAT	No hits found

Table of species searched for candidate P2X receptors, the database type within which searches were performed and the BLAST algorithm used *Expect* (*E*)-value, score, normalised bit score, length of alignment of high scoring segment pair (HSP), and accession number of retrieved hit. Multiple hits retrieved from one species database are also detailed accordingly.

Table A3: pGEM-T® Easy and pcDNA3.1$^{(+)}$ plasmid construct MCS (multiple cloning site) sequencing primers

Name	Sequence (5'-3')	For/rev	Length (nt)	Tm (°C)	Use
T7	TAA TAC GAC TCA CTA TAG GG	For	20	56	Sequencing of pGEM-T® Easy vector MCS
SP6	CAT TTA GGT GAC ACT ATA G	Rev	19	52	
T7pcDNA	TAA TAC GAC TCA CTA TAG GG	For	20	56	Sequencing of pcDNA3.1$^{(+)}$ vector MCS
BGHpcDNA	TAG AAG GCA CAG TCG AGG	Rev	18	56	

Constructs were sequenced according to section 2.4.6.2. 'For' and 'Rev' designations refer to forward and reverse primer sequences, repectively.

Table A4: invertebrate P2X receptor amplification primers

Name	Sequence (5'-3')	For/rev	Length (nt)	Tm (°C)	Use
aepP2X_F	GAT GGC CAA CGA CTG TTG CAA G	For	22	57	Amplification of *H. vulgaris* (AEP) P2X receptor
aepP2X_R	CGT GGA TGA AGT TGT TAA TGA TTG	Rev	24	52	
DpuP2XB_F	ATG GGT TGT TTC AAA GCA TTT T	For	22	47	Amplification of *D. pulex* (TCO strain) P2XB receptor
DpuP2XB_R	TCA ATT GCT CCC ATA AGT TGT CA	Rev	23	55	
BfloP2X_F	ATG GCG GAA GGT CCG AGT	For	18	53	Amplification of *B. floridae* P2X receptor
BfloP2X_R	TTA CGA GCC ATA GCT TCC ATT G	Rev	22	53	
TadP2XA_F	ATG GAA AAC TGT TGC AAT AGA TTC	For	24	51	Amplification of *T. adhaerens* (Grell strain) P2XA receptor
TadP2XA_R	TTA TTC CAC GTC CTC TTG TAA TAA CG	Rev	26	55	
TadP2XB_F	ATG GAG GAC GAA TCG AGT G	For	19	51	Amplification of *T. adhaerens* (Grell strain) P2XB receptor
TadP2XB_R	TTA GTA GAG TAA AGT CAA AGT CG	Rev	23	50	

Invertebrate P2X receptors were amplified using the Platinum® *Taq* DNA Polymerase High Fidelity (Life Technologies) enzyme mixture, according to section 2.4.5.2.2. 'For' and 'Rev' designations refer to forward and reverse primer sequences, repectively.

Table A5: primers used for the addition of C-terminal hexahistidine tag to cloned invertebrate P2X receptors, and subsequent subcloning into pcDNA3.1$^{(+)}$ expression vector

Name	Sequence (5'-3')	For/ rev	Length (nt)	Tm (°C)	Use
DaphP2XB_F _KpnI	ATA **GGT ACC** ATG GGC TGT TTA AGG CAT TC	For	26	47	Amplification of *D. pulex* (TCO strain) P2XB receptor with an in-frame C-terminal hexahistidine tag, and 5' and 3'***Kpn*I** and ***Not*I** restriction sites
DaphP2XB_ R_ His_NotI	ATA **GCG GCC GC**T CAA TGA TGA TGA TGG TGG TGA TTG CTC CCA TAA GTT GTC A	Rev	53	55	
TadP2XA_F_ KpnI	ATA **GGT ACC** ATG GAA AAC TGT TGC AAT AGA TTC G	For	34	51	Amplification of *T. adhaerens* (Grell strain) P2XB receptor with an in-frame C-terminal hexahistidine tag, and 5' and 3'***Kpn*I** and ***Not*I** restriction sites
TadP2XA_R_ His_NotI	TAT **GCG GCC GC**T TAA TGA TGG TGA TGG TGG TGT TCC ACG TCC TCT TGT AAT AAC G	Rev	56	55	
BfloP2X_F_ KpnI	ATA **GGT ACC** ATG GCG GAA GGT CCG AGT	For	52	53	Amplification of *B. floridae* (TCO strain) P2XB receptor with an in-frame C-terminal hexahistidine tag, and 5' and 3'***Kpn*I** and ***Not*I** restriction sites
BfloP2X_R_ His_NotI	TAT **GCG GCC GC**T TAA TGA TGG TGA TGG TGG TGC GAG CCA TAG CTT CCA TT	Rev	51	53	

C-terminal hexahistidine tags (for subsequent Western blot analysis) were added by PCR to cloned P2X receptors using the Invertebrate P2X receptors were amplified using the Platinum® *Taq* DNA Polymerase High Fidelity (Life Technologies) enzyme mixture, according to section 2.4.5.2.2. A aepP2X cDNA was synthesised so as to reflect human codon usage of the HEK293 cell line in which it expressed (section 2.4.5.2.4). The hexahistidine tag and 5'/3' restriction sites are highlighted in underlined and bold text, respectively. 'For' and 'Rev' designations refer to forward and reverse primer sequences, repectively.

Table A6: adaptor primers used in 3' RACE of cloned invertebrate P2X receptors

Name	Forward sequence (5' to 3')	Reverse sequence (5' to 3')
$\mathbf{Q_t}$	CCA GTG AGC AGA TGT ACG AGG ACT CGA GCT CAA GCT TTT TTT TTT TTT TTT T	-
$\mathbf{Q_o}$	-	CCA GTG AGT AGA GTG ACG
$\mathbf{Q_i}$	-	GAG GAC TCG AGC TCA AGC

Adaptor primers were used in determining the 3' flanking region of aepP2X, *Dpu*P2XB, *Tad*P2XA and *Tad*P2XB receptor transcript sequences (section 2.4.5.2.3). 'For' and 'Rev' designations refer to forward and reverse primer sequences, repectively.

Table A7: gene-specific primers used in 3' RACE of cloned invertebrate P2X receptors

Receptor	Name	Sequence (5' to 3')	Length (nt)	T_m (°C)
Hydra vulgaris (AEP) P2X receptor	**GSP1**	GAC TTG ATG ATC CAG ATG CTC	21	45.6
	GSP2	GAT GCT CCA ATA TCT CCT GG	20	48.0
Daphnia pulex P2XB	**GSP1**	GAG CTG ATG ATC CGA ATA CCA	21	47.0
	GSP2	CTG GAA CTT TAG ACA CGC CA	20	47.0
Trichoplax adhaerens P2XA	**GSP1**	TGA AGC ATT GCA TGT ACG ATC C	22	45.5
	GSP2	CTT CAG AAG ACT TGA TGA CC	20	45.5
Trichoplax adhaerens P2XB	**GSP1**	ATT GCG ACT TAG ACT TTT GGC	21	45.0
	GSP2	CTC AGC ACA GAA CTT TGA CG	20	45.0

Gene-specific primer (GSP) sequences used in nested 3' RACE PCR to clone the 3' downstream sequence of P2X receptor mRNA in *H. vulgaris* (AEP), *D. pulex*, and *T. adhaerens*. 3' RACE was performed according to section 2.4.5.2.3.3. 'For' and 'Rev' designations refer to forward and reverse primer sequences, repectively.

Table A8: primers used in the attempted amplification of *Dpu*_p2xA from complementary DNA (cDNA) or genomic DNA template

	Primer	Sequence (5' to 3')	Length (nt)	Tm (°C)
FORWARD	**DaphA1F**	ATG GGT TGT TTA AAA AGC ATT TC	23	48
	DaphA2F	TGC ATT CAC GAA TAG TAC CAA C	22	51
	DaphA3F	CGG AAA TGG AGC CAT GAC TG	20	54
	DaphA4F	ACG AAA CAT CAT GGA AGA TGC	21	50
	DaphA5F	CCA ACA TCG CTC CT GTT GG	19	48
	DaphA6F	ACA ATT GT GTT TGC GAC TTC	20	48
	DaphA7R	TCT AAA AAC CCA TGA ACT TTC	22	47
	DaphA8F	TGA CGT CAC ATT TGA TAG TGC	21	50
	DpuP2XA_F	ATG GGT TGT TTA AAA GCA TTT TCT	24	49
	DapEx5F1	AGA GAT CCC TTC TGC CCT GT	20	54
	DapEx5F2	GAG ATC CCT TCT GCC CTG TA	20	54
	D1F1	CGT TAT GGT TTA CAA AAA CGG	21	49
	D1F2	GAA TAC TGG GAA GAT TTC TGC	21	50
	D1F3	TTT CTG CAG CTG TGT GTC C	19	51
	DaphAIF	GTG CTC ACT GCT CAG TGC	18	53
REVERSE	**DaphA2R**	TGT TGG TAC TAT TCG TGA ATG C	22	51
	DaphA3R	CAG TCA TGG CTC CAT TTC CG	20	54
	DaphA4R	CTG GAG ATA GGT TTT GTT AGC	21	50
	DaphA5R	CCA ACC AGG AGC GAT GTT GG	20	56
	DaphA6R	ATG AAG TCG CAA ACC ACA ATT G	22	51
	DaphA7R	CTA AAA ACC CAT GAA CTT TTC	21	47
	DpuP2XA_R	CTA AAA ACC CAT GAA CTT TTC ATT TAC	27	52
	DapEx5R1	CCA GGA GCG ATG TTG GTA TT	20	52
	DapEx5R2	GGA GCG ATG TTG GTA TTT GG	20	52
	D1R1	TAC CAT AAG ATT TGG ATG CG	20	48
	D1R2	CTT TTC ATT TAC CAC GTC AGC	21	50

PCR reactions using various combinations of primers (Appendix Table A9) were performed according to section 2.4.5.2.1 using Platinum® *Taq* DNA polymerase (Life Technologies).

Table A9: primers combinations (from Table 8) used in the attempted amplification of the candidate *Daphnia pulex* P2XA receptor subtype (*Dpu*_p2xA) from complementary DNA (cDNA) or genomic DNA (gDNA) template.

	gDNA template	*cDNA template*
Primer combination	**Predicted amplicon length (bp)**	**Predicted amplicon length (bp)**
DaphA1F + DaphA2R	1876	234
DaphA1F + DaphA3R	1155	457
DaphA1F + DaphA4R	1482	683
DaphA1F + DaphA5R	303	909
DaphA1F + DaphA6R	600	1086
DaphA1F + DaphA7R	966	1179
DaphA2F + DaphA3R	297	244
DaphA1F + D1R1	1379	970
DaphA1F + D1R2	1672	1164
DaphA2F + DaphA4R	643	470
DaphA2F + DaphA5R	889	696
DaphA2F + DaphA6R	1251	873
DaphA2F + DaphA7R	1344	966
DaphA3F + DaphA4R	363	246
DaphA3F + DaphA5R	592	472
DaphA3F + DaphA6R	954	649
DaphA3F + DaphA7R	1046	742
DaphA4F + DaphA5R	248	249
DaphA4F + DaphA6R	610	426
DaphA4F + DaphA7R	703	519
DaphA5F + DaphA6R	381	197
DaphA5F + DaphA7R	474	290
DaphA6F + DaphA7R	112	113
DaphA8F + DaphA2R	907	N/A
DaphA8F + DaphA3R	1204	N/A
DaphA8F + DaphA4R	1570	N/A
DaphA8F + DaphA5R	1796	N/A
DaphA8F + DaphA6R	2158	N/A
DaphA8F + DaphA7R	2251	N/A
DaphA8F + DaphA5R	2445	N/A
DaphA8F + DapEx5R1	2676	N/A
DaphA8F + DapEx5R2	1792	N/A
DaphA8F + D1R1	1983	N/A
DaphA8F + D1R2	2236	N/A
DaphA8F + DpuP2XA_R1	2445	N/A
DaphA8F + DpuP2XA_R2	2626	N/A
DpuP2XA_F1 + DpuP2XA_R1	2057	N/A
DpuP2XA_F1 + DpuP2XA_R2	1876	N/A
DapEx5F1 + DapEx5R1	202	203
DapEx5F1 + DapEx5R2	199	200
D1F1 + D1R1	1175	836
D1F1 + D1R2	1428	1030
D1F2 + D1R1	1259	888
D1F2 + D1R2	1550	1082
D1F3 + D1R1	1283	874
D1F3 + D1R2	1536	1068

Both genomic DNA (gDNA) and complementary DNA (cDNA) were used as a template in PCR reactions, where appropriate according to the position of primer pairs tested. Extension times of 1 min per kb length of nucleotide sequence were used. Extension temperatures of 60 and 72 °C were test for all primer pairs. When extension temperatures of 60 °C were used, extension times were increased by a further 15 seconds per kb to account for a reduced activity of Platinum® *Taq* polymerase (Life Technologies) at this lower temperature. Positions of primers (forward: red, reverse: blue) are indicated above the genomic sequence of *Dpu*_p2xA in Fig 5.2. Predicted amplicon (PCR product) size when using either gDNA or cDNA as a template are also indicated.

Table A10: Primers used in the amplification of 5' and 3' flanking regions for synthesis of *Hmp2xp-egfp* plasmid construct

Name	Sequence (5'-3')	For/rev	Length (nt)	Tm (°C)	Use
Hmp2xp_F_XbaI	ATA ATC TAG AGC GCA TGC TCT TAC ATT CTG	For	22	57	Amplification of 5' flanking region of predicted *H. magnipapillata p2x* receptor with 5' and 3' *Xba*I and *Sbf*I restriction sites
Hmp2xp_R_SbfI	ATA CCT GCA GGA TTC TTG CAA CAG TCG TTG	Rev	24	52	
Hmp2xt_F_AsiSI	ATA GCG ATC GCG AGG AGA AGA GTA GGC	For	22	47	Amplification of 3' flanking region of predicted *H. magnipapillata p2x* receptor with 5' and 3' *Asi*SI and *Spe*I restriction sites
Hmp2xt_R_SpeI	TAT AGC AGT TCT TTC GTG TTG TCA TGA GCC	Rev	23	55	

PCR reactions to amplify 5' and 3' flanking regions for transgenic construct synthesis were performed according to section 2.4.5.2.2 using Platinum® *Taq* DNA Polymerase High Fidelity (Life Technologies) enzyme mixture. 'For' and 'Rev' designations refer to forward and reverse primer sequences, repectively.

Table A11: primers used to sequence *Hmp2xp-egfp* plasmid construct

Name	Sequence (5'-3')	For/rev	Length (nt)	Tm (°C)	Use
GFP_F_SP6	CCC TTT CGA AAG ATC CCA AC	For	20	52	Sequencing of *Hmp2xp*-construct across 5' flanking region of predicted *H. magnipapillata p2x* receptor/*egfp* boundary
GFP_R_T7	AAC AAG AAT TGG GAC AAC TCC	Rev	21	50	Sequencing of *Hmp2xp*-construct across 3' flanking region of predicted *H. magnipapillata p2x* receptor/*egfp* boundary

Following synthesis of *Hmp2xp-efp* plasmid construct, sequencing reactions to confirm correct orientation of ligated regions were performed according to section 2.4.6.2. 'For' and 'Rev' designations refer to forward and reverse primer sequences, repectively.

Table A12: primers used in the amplification of *aepp2x* for synthesis of *actin-aepp2x::egfp* plasmid construct

Name	Sequence (5'-3')	For/rev	Length (nt)	Tm (°C)	Use
aepp2x_F_SbfI	CAT CCT GCA GGA ATG GCC AAC GAC TGT TGC AAG	For	22	57	Amplification of *H. vulgaris* (AEP) P2X (*aepP2X*) CDS with 5' and 3' *Sbf*I and *Pac*I restriction sites for upstream insertion of *egfp* casette
aepp2x_R_PacI	CAT TTA ATT AAA TGA TTG TCT TCA TCA TTC ATA TGG	Rev	24	52	

PCR reactions to amplify *aepp2x* coding region for use in a *H. vulgaris* (AEP) transgenic construct were performed according to section 2.4.5.2.2 using Platinum® *Taq* DNA Polymerase High Fidelity (Life Technologies) enzyme mixture. 'For' and 'Rev' designations refer to forward and reverse primer sequences, repectively.

Table A13: primers used to sequence *actin-aepp2x::egfp* plasmid construct

Name	Sequence (5'-3')	For/rev	Length (nt)	Tm (°C)	Use
ActP2X_seq	GCG TTC GTT ATT CAG AAG C	For	19	49	Sequencing of *actin-aepp2x::egfp* plasmid construct across 5' flanking *β-actin* sequence/*p2x* boundary
P2XGFP_seq	CGA GCG AGT CAA AAG TTG G	For	19	51	Sequencing of *actin-aepp2x::egfp* plasmid construct across *p2x-egfp* boundary
GFPact_seq	GAA GAT GGA AGC GTT CAA C	For	19	49	Sequencing of *actin-aepp2x::egfp* plasmid construct across 5' flanking *β-actin* sequence/*egfp* boundary

Following synthesis of *actin-aepp2x::egfp* plasmid construct, sequencing reactions to confirm correct orientation of ligated regions were performed according to section 2.4.6.2. 'For' and 'Rev' designations refer to forward and reverse primer sequences, repectively.